

**Proceedings of the Tenth Lomonosov  
Conference on Elementary Particle Physics**



# **FRONTIERS *of* PARTICLE PHYSICS**

Editor

**Alexander I Studenikin**

# **FRONTIERS *of* PARTICLE PHYSICS**

This page intentionally left blank

**Faculty of Physics of Moscow State University**



**INTERREGIONAL CENTRE  
FOR ADVANCED STUDIES**

Proceedings of the Tenth Lomonosov  
Conference on Elementary Particle Physics

# **FRONTIERS *of* PARTICLE PHYSICS**

Moscow, Russia

23 – 29 August 2001

Editor

**Alexander I Studenikin**

*Department of Theoretical Physics  
Moscow State University, Russia*



**World Scientific**

New Jersey • London • Singapore • Hong Kong

*Published by*

World Scientific Publishing Co. Pte. Ltd.

5 Toh Tuck Link, Singapore 596224

*USA office:* Suite 202, 1060 Main Street, River Edge, NJ 07661

*UK office:* 57 Shelton Street, Covent Garden, London WC2H 9HE

**British Library Cataloguing-in-Publication Data**

A catalogue record for this book is available from the British Library.

**FRONTIERS OF PARTICLE PHYSICS**

Copyright © 2003 by World Scientific Publishing Co. Pte. Ltd.

*All rights reserved. This book, or parts thereof, may not be reproduced in any form or by any means, electronic or mechanical, including photocopying, recording or any information storage and retrieval system now known or to be invented, without written permission from the Publisher.*

For photocopying of material in this volume, please pay a copying fee through the Copyright Clearance Center, Inc., 222 Rosewood Drive, Danvers, MA 01923, USA. In this case permission to photocopy is not required from the publisher.

ISBN 981-238-319-0

This book is printed on acid-free paper.

Printed in Singapore by Uto-Print

**Moscow State University  
Faculty of Physics  
Interregional Centre for Advanced Studies**



Mikhail Lomonosov  
1711-1765

**TENTH  
LOMONOSOV  
CONFERENCE  
ON  
ELEMENTARY  
PARTICLE  
PHYSICS**

**Sponsors**

Russian Foundation for Basic Research  
Ministry of Industries, Science and Technologies of Russia  
International Association for the promotion of co-operation  
with scientists from the New Independent  
States of the former Soviet Union (INTAS)

**Supporting Institutions**

Faculty of Physics of Moscow State University  
Interregional Centre for Advanced Studies  
Joint Institute for Nuclear Research (Dubna)  
Institute of Theoretical and Experimental Physics (Moscow)  
Institute for Nuclear Research (Moscow)

## **International Advisory Committee**

E.Akhmedov (Tech. Univ. of Muenchen & Kurchatov Inst.,Moscow),  
V.Berezinsky (LNGS, Gran Sasso)  
S.Bilenky (JINR, Dubna),  
G.Diambrini-Palazzi (Univ. of Rome),  
J.Dias de Deus (IST/CENTRA , Lisbon),  
V.Kadyshevsky (JINR, Dubna),  
A.Logunov (IHEP, Protvino),  
V.Matveev (INR, Moscow),  
L.Okun (ITEP, Moscow),  
V.Rubakov (INR, Moscow),  
J.Silk (Univ. of Oxford),  
A.Skrinsky (INP, Novosibirsk),  
A.Smirnov (INR, Moscow & ICTP, Trieste),  
P.Spillantini (INFN, Florence)

## **Organizing Committee**

V.Bagrov (Tomsk State Univ.),  
V.Belokurov (MSU), V.Braginsky (MSU),  
A.Egorov (ICAS, Moscow),  
R.Faustov (Russian Academy of Sciences & ICAS, Moscow),  
D.Galtsov (MSU),  
A.Kataev (INR, Moscow & CERN),  
P.Kashkarov (MSU),  
O.Khrustalev (MSU),  
D.Shirkov (JINR, Dubna),  
A.Mourao (IST/CENTRA, Lisbon),  
A.Nikishov (Lebedev Physical Inst., Moscow),  
N.Nikiforova (MSU) ,  
V.Ritus (Lebedev Physical Inst., Moscow),  
Yu.Popov (MSU) ,  
V.Savrin (MSU),  
Yu.Simonov (ITEP, Moscow),  
A.Sissakian (JINR,Dubna),  
A.Slavnov (MSU & Steklov Math. Inst., Moscow),  
A.Studenikin (MSU & ICAS, Moscow),  
V.Trukhin (MSU)

**Moscow State University  
Interregional Centre for Advanced Studies**

**FOURTH  
INTERNATIONAL  
MEETING  
ON PROBLEMS  
OF INTELLIGENTSIA  
“INTERNATIONAL  
COOPERATION  
OF INTELLECTUALS”**

**Presidium of the Meeting**

- V.A.Sadovnichy (MSU) - Chairman  
V.V.Alexandrov (MSU)  
J.Bleimaier (Princeton)  
G.Diambrini-Palazzi (Univ. of Rome)  
V.G.Kadyshevsky (JINR)  
S.P.Kapitza (Russian Academy of Sciences)  
V.V.Mikhailin (MSU)  
N.G.Nikolau (MSU)  
P.Nowosad (Univ. of San Paolo)  
A.I.Studenikin (MSU & ICAS) - Vice Chairman  
V.I.Trukhin (MSU)  
V.S.Volkov (MSU)  
A.A.Zinoviev (MSU)

This page intentionally left blank

## FOREWORD

The 10<sup>th</sup> Lomonosov Conference on Elementary Particle Physics was held at the Moscow State University (Moscow, Russia) on August 23-29, 2001.

The conference was organized by the Faculty of Physics of the Moscow State University and the Interregional Centre for Advanced Studies and supported by the Joint Institute for Nuclear Research (Dubna), the Institute of Theoretical and Experimental Physics (Moscow), and the Institute for Nuclear Research (Moscow). The Ministry of Industries, Science and Technologies of Russia, the Russian Foundation for Basic Research, and International Association for the promotion of co-operation with scientists from the New Independent States of the former Soviet Union (INTAS) sponsored the conference.

It was nineteen years ago when the first of the series of conferences (from 1993 called the "Lomonosov Conferences"), was held at the Department of Theoretical Physics of the Moscow State University (June 1983, Moscow). The second conference was held in Kishinev, Republic of Moldavia, USSR (May 1985).

After the four years break this series was resumed on a new conceptual basis for the conference programme focus. During the preparation of the third conference (that was held in Maykop, Russia, 1989) a desire to broaden the programme to include more general issues in particle physics became apparent. At subsequent meetings of this series (Minsk, Republic of Byelorussia, USSR, 1990; Yaroslavl, Russia, 1992) a wide variety of interesting things both in theory and experiment of particle physics, field theory, gravitation and astrophysics were included into the programmes. During the conference of 1992 in Yaroslavl it was proposed by myself and approved by numerous participants that these irregularly held meetings should be transformed into regular events under the title "Lomonosov Conferences on Elementary Particle Physics". It was also decided to enlarge the number of institutions that would take part in preparation of future conferences.

Mikhail Lomonosov (1711-1765), a brilliant Russian encyclopaedias of the era of the Russian Empress Catherine the 2nd, was world renowned for his distinguished contributions in the fields of science and art. He also helped establish the high school educational system in Russia. The Moscow State University was founded in 1755 based on his plan and initiative, and the University now bears the name of Lomonosov.

The 6<sup>th</sup> Lomonosov Conference on Elementary Particle Physics (1993) and all of the subsequent conferences of this series were held at the Moscow State University on each of the odd years. Publication of the volume "Particle Physics, Gauge Fields and Astrophysics" containing articles written on the basis of presentations at the 5<sup>th</sup> and 6<sup>th</sup> Lomonosov Conferences was supported by the Accademia Nazionale dei Lincei (Rome, 1994). Proceedings of the 7<sup>th</sup> and 8<sup>th</sup> Lomonosov Conference (entitled "Problems of Fundamental Physics" and "Elementary Particle Physics") were published by the Interregional Centre for Advanced Studies (Moscow, 1997 and 1999). Proceedings of the 9<sup>th</sup> Lomonosov

Conference ("Particle Physics at the Start of the New Millennium") were published by World Scientific Publishing Co. ( Singapore, 2001).

The physics programme of the 10<sup>th</sup> Lomonosov Conference on Elementary Particle Physics included review and original talks on wide range of items such as fundamental symmetries, electroweak theory, tests of standard model and beyond, heavy quark physics, non-perturbative QCD, neutrino physics, astroparticle physics, quantum gravity effects, physics at the future accelerators. Totally there were 79 talks including 22 review (40-45 min) talks, 14 session (30-25 min) reports and 43 brief (20 min) reports.

Following the tradition that has started in 1995, each of the Lomonosov Conferences on particle physics has been accompanied by a conference on problems of intellectuals. The 4th International Meeting on Problems of Intellectuals has been held during the last day of the 10<sup>th</sup> Lomonosov Conference. The subject of the Meeting was specified as follows: "International Co-operation of Intellectuals". During this meeting discussion on co-operation between scientists and intellectuals was organized. One of the talks was devoted to international collaboration on synchrotron radiation, there were also several talks on more general issues of international co-operation of scientists and the role of intellectuals in providing stable development of the human civilization. The two talks presented on this Meeting are also included into these proceedings.

On behalf of the Organizing Committee I should like to warmly thank the session chairpersons, the speakers and all of the participants of the 10<sup>th</sup> Lomonosov Conference and the 4<sup>th</sup> Meeting on Problems of Intellectuals.

We are grateful to the Rector of the Moscow State University, Victor Sadovnichy, the Dean of the Faculty of Physics of the Moscow State University, Vladimir Trukhin, the Director of the Joint Institute for Nuclear Research, Vladimir Kadyshevsky, the Director of the Institute of Theoretical and Experimental Physics, Mikhael Danilov, the Director of the Institute for Nuclear Research, Victor Matveev, and John Bleimaier (Princeton, USA) for the support in organizing these two conferences.

I should like to thank Lev Okun, Andrey Kataev and Yuri Simonov for their help in planning of the scientific programme of the meeting. Special thanks are due to Patrick Janot and Jan Nassalski for their valuable help in inviting speakers for the topical sessions of the conference.

Furthermore, I am very pleased to mention Andrey Egorov, the Scientific Secretary of the conference, and Alexey Illarionov for their very efficient work in preparing and running the meeting.

These Proceedings were prepared for publication and sponsored by the Interregional Centre for Advanced Studies with support by the Faculty of Physics of the Moscow State University, the Ministry of Industries, Science and Technologies of Russia, the Russian Foundation for Basic Research, the INTAS grant number 01-MO-194, and anonymous gift in memory of Mikhail Mikhailovich Okolodkoff (1854-1919), Colonel of the Russian Tsar Army.

Alexander Studenikin

## CONTENTS

Tenth Lomonosov Conference on Elementary Particle Physics - Sponsors and Committees	v
Fourth International Meeting on Problems of Intelligentsia - Presidium	vii
Foreword	ix
<b>Neutrino Physics and Astrophysics</b>	
Solar Neutrino Results from SAGE	1
<i>V.N.Gavrin</i>	
Neutrino Oscillation Measurements at SuperKamiokande	13
<i>Y.Fukuda</i>	
Resonant and Non-Resonant Neutrino Spin-Flavor Conversion in Static Solar Magnetic Field	25
<i>A.A.Bykov, O.G.Miranda, C.Peña-Garay, V.Yu.Popov, T.I.Rashba, V.B.Semikoz, J.W.F.Valle</i>	
Effect of Matter Motion and Polarization in Neutrino Flavour Oscillations	32
<i>A.Grigoriev, A.Lobanov, A.Studenikin</i>	
High-energy Neutrino from a Nascent Massive Black Hole	39
<i>V.S.Berezinsky, V.I.Dokuchaev</i>	
From the Extreme Universe Space Observatory (EUSO) to the Extreme Energy Neutrino Observatory	45
<i>S.Bottai, P.Spillantini</i>	
Detection of Ultra-High Energy Cosmic Rays with "Solar-Sail"-Type Detector	60
<i>V.A.Tsarev, V.A.Chechin, N.G.Polukhina</i>	
A Neutrino-induced Deuteron Disintegration Experiment at the Krasnoyarsk Nuclear Reactor	69
<i>Yu.V.Kozlov, S.V.Khaltourtsev, I.N.Machulin, A.V.Martemyanov, V.P.Martemyanov, A.A.Sabelnikov, V.G.Tarasenkov, E.V.Turbin, V.N.Vyrodov</i>	
Same-Sign Dilepton Production Via Heavy Majorana Neutrinos in Proton-Proton Collisions	74
<i>A.Ali, A.Borisov, N.Zamorin</i>	

**CP Violation and Rare Decays**

Situation with Test of CP,T and CPT Invariance <i>E.P.Shabalin</i>	80
The Precise Determination of $Re(\epsilon'/\epsilon)$ <i>M.Cirilli</i>	90
Rare Decays of Neutral Kaons with the NA48 Experiment <i>A.Bizzeti</i>	102
Study of $K^0_S$ , $K^\pm$ Decays at $\phi$ Resonance with the KLOE Detector <i>M.Martemianov</i>	114

**Hadron Physics**

Application of New Multiloop QCD Input to the Analysis of $xF_3$ Data <i>A.L.Kataev, G.Parente, A.V.Sidorov</i>	121
Heavy Quark Production near the Threshold in QCD <i>A.A.Pivovarov</i>	128
An Analysis of Unpolarized Structure Function Moments in $N^*$ Excitation Region <i>M.Osipenko, G.Ricco, M.Taiuti, S.Simula, M.Anghinolfi, M.Battaglieri, G.Fedorov, E.Golovach, R.De Vita, B.Ishkhanov, V.Mokeev, M.Ripani</i>	136
Pragmatic Approach to Description of $\pi\pi$ Scattering <i>E.P.Shabalin</i>	142
New Analytic Running Coupling in QCD <i>A.V.Nesterenko</i>	147
$QCD_2$ in the Axial Gauge Revisited <i>Yu.S.Kalashnikova, A.V.Nefediev</i>	153
Magnetic Moments of Charm Baryons in Chiral Perturbation Theory <i>V.S.Zamiralov</i>	159
Instanton in the Nonperturbative QCD Vacuum <i>N.O.Agasian, S.M.Fedorov</i>	165

Relativistic Model of Hadron-Hadron Interactions at Low and Intermediate Energies <i>A.N.Safronov, A.A.Safronov</i>	171
Quark-Gluon Plasma: Pro and Contra <i>Ilya I.Royzen</i>	177
Discovery of $\eta$ -Mesic Nuclei <i>G.A.Sokol, A.I.L'vov, L.N.Pavlyuchenko</i>	188
Exotic Mesons in E852 Experiment <i>V.L.Korotkikh</i>	197
Very High Multiplicity Physics <i>J.Manjavidze, A.Sissakian</i>	203
<b>Physics at Accelerators and Studies in SM and Beyond</b>	
Review of LEP2 Physics <i>P.M.Watkins</i>	213
Flavour Independent Higgs Searches at LEP-2 <i>P.Bambade</i>	223
Search for Supersymmetry at LEP2 <i>F.Mazzucato</i>	234
Anomalous Couplings at LEP2 <i>D.Fayolle</i>	243
Search for Single Top Quark Production at LEP <i>A.Leins</i>	250
Heavy Ion Collisions at CMS Experiment (LHC) <i>L.I.Sarycheva</i>	256
The Main Task of $B$ -meson Trigger at the LHC <i>N.Nikitine, L.Smirnova</i>	263
<b>Gravitation and Cosmology</b>	

Towards a Simultaneous Resolution of the Cosmological Constant and Fermion Families Problems <i>E.Guendelman, A.Kaganovich</i>	269
The Shape of the $K_\alpha$ Line as a Possible Indication of the Black Hole Existence <i>A.F.Zakharov, S.V.Repin</i>	278
Quantum Cosmological Model with Rotation <i>M.Fil'chenkov</i>	284
On the Influence of Einstein-Podolsky-Rosen Effect on the Domain Wall Formation During the Cosmological Phase Transitions <i>Yu.V.Dumin</i>	289
Possible EPR Experiment with Neutral Pseudo-Scalar Meson-Antimeson Correlated Pairs <i>A.Pompili, F.Selleri</i>	295
Violation of Parity in Space-Time of Dimension N+1 <i>S.V.Kopylov</i>	304
<b>New Developments in Quantum Field Theory</b>	
Renormalization-Group Flow in the 3D Georgi-Glashow Model <i>D.Antonov</i>	307
Noncommutative Field Theories and UV/IR Problem <i>A.S.Koshelev</i>	313
Exactly Solvable Potentials for the One-Dimensional Stationary Dirac Equation <i>V.G.Bagrov, A.A.Pecheritsyn, B.F.Samsonov</i>	319
<b>Problems of Intelligentsia</b>	
Intelligentsia - Singular or Plural <i>J.Bleimaier</i>	326
International Scientific Collaboration and Russian Physical Society <i>V.Mikhailin</i>	336
Conference Programme	341
List of Participants	347



This page intentionally left blank

# SOLAR NEUTRINO RESULTS FROM SAGE

Vladimir N.Gavrin <sup>a</sup>

*Institute for Nuclear Research RAS, 117312 Moscow, Russia  
For the SAGE Collaboration<sup>b</sup>*

*Abstract.* Since January of 1990, the Russian-American Solar neutrino Experiment has carried out measurements of the capture rate of solar neutrinos on metallic gallium in a radiochemical experiment at the Baksan Neutrino Observatory. The measured capture rate from the  $^{71}\text{Ge}$  K- and L-peak counting data through December 2000 is  $77.0 +7.1/-6.9$  SNU, where the uncertainties statistical and systematic, respectively. This result represents a 6 depression in the neutrino flux compared with predicted Standard Solar Model rates. The experimental procedures and data analysis are presented.

## 1 Introduction

Models describing the processes of nuclear fusion in the sun have been very successful in explaining numerous solar features. Although these models have had great success, the deficit in the solar neutrino flux relative to the predictions of the Standard Solar Model (SSM) still remains one of the outstanding problems. For 30 years the Homestake chlorine experiment [1] has consistently observed a flux 33% of that predicted by SSMs. In the mid 1980s, the water Cherenkov detector (Kamiokande) began its measurement of the solar neutrino flux that is 54% of the SSMs and recent results from SuperKamiokande are in agreement with its predecessor [2]. In the middle of 2001, results of measurements of high energy  $^8\text{B}$  neutrino flux from Sudbury Neutrino Observatory (SNO) - new high-rate real-time detector were presented [3]. The elastic scattering results of SuperKamiokande and the charge current results from SNO indicate that, in addition to electron neutrinos, active neutrinos of other flavors originate from the Sun. Since the Sun produces only electron neutrinos, these results are interpreted as strong evidence for neutrino oscillation in the solar sector. But despite this progress with the new generation of large water Cherenkov detectors, there has been no new information on the region of the solar neutrino spectrum below  $\sim 2$  MeV that contains the proton-proton (pp) and CNO continua as well as the  $^7\text{Be}$  and pep lines.

---

<sup>a</sup>e-mail: gavrin@adonis.iasnet.ru

<sup>b</sup>The SAGE Collaboration: J.N.Abdurashitov<sup>1</sup>, T.J.Bowles<sup>2</sup>, M.L.Cherry<sup>3</sup>, B.T.Cleveland<sup>4</sup>, R.Davis, Jr.<sup>5</sup>, S.R.Elliott<sup>4</sup>, V.N.Gavrin<sup>1</sup>, S.V.Girin<sup>1</sup>, V.V.Gorbachev<sup>1</sup>, P.P.Gurkina<sup>1</sup>, T.V.Ibragimova<sup>1</sup>, A.V.Kalikhov<sup>1</sup>, N.G.Khairnasov<sup>1</sup>, T.V.Knodel<sup>1</sup>, K.Lande<sup>5</sup>, I.N.Mirmov<sup>1</sup>, J.S.Nico<sup>6</sup>, A.A.Shikhin<sup>1</sup>, W.A.Teasdale<sup>2</sup>, E.P.Veretenkin<sup>1</sup>, V.M.Vermul<sup>1</sup>, D.L.Wark<sup>2\*</sup>, P.S.Wildenhan<sup>5</sup>, J.F.Wilkerson<sup>4</sup>, V.E.Yants<sup>1</sup>, and G.T.Zatsepin<sup>1</sup>, where

1.Institute for Nuclear Research RAS 117312 Moscow, Russia

2.Los Alamos National Laboratory, Los Alamos, NM 87545 USA

3.Louisiana State University, Baton Rouge, LA 70803 USA

4.University of Washington, Seattle, WA 98195 USA

5.University of Pennsylvania, Philadelphia, PA 19104 USA

6.J. S. Nico National Institute of Standards and Technology, Gaithersburg, MD 20899 USA

\*. Present Address: Oxford University, Dept. of Particle and Nuclear Physics, Oxford OX1 3RH, UK.

In the early 1990s the Russian-American Gallium Experiment (SAGE) [4] and the Gallium Experiment (GALLEX) [5] began measuring the low energy neutrinos from proton- proton (pp) fusion using Ga [6] as the target material. The reaction  $^{71}\text{Ga}(e^-, e^-)^{71}\text{Ge}$  provides the only feasible means at present to measure the predominant pp neutrinos as well as higher energy neutrinos produced by  $^8\text{B}$  and  $^7\text{Be}$ . Its 233 keV threshold for inverse beta decay is important since, exotic hypotheses aside, the rate of the pp reaction is directly related to the solar luminosity and is insensitive to alterations in the solar models. SSM calculations [7] show that the dominant contribution to the total expected capture rate in  $^{71}\text{Ga}$  ( $129 +8/-6$ ) SNU arises from the pp neutrinos and is 69.6 SNU, where 1 SNU = 1 interaction/s in a target that contains  $10^{36}$  atoms of the neutrino absorbing isotope. Contributions by  $^7\text{Be}$  and  $^8\text{B}$  neutrinos are 34.4 SNU and 12.4 SNU, respectively. The uncertainty to variation in the SSM for Ga is seen in the independently calculated result of 127.2 SNU [8] for the total capture rate.

### 1.1 *The SAGE Experiment*

The SAGE detector is situated in a specially built underground laboratory at the Baksan Neutrino Observatory in the Northern Caucasus Mountains. It is located 3.5 km from the entrance of a horizontal adit excavated into the side of Mount Andyrchi and has an overhead shielding of 4700 meters water equivalent. Up to 55.6 tons of Ga are contained in eight chemical reactors with approximately the same amount of Ga in each of them. The data span a ten year period during which many improvements to the experiment were made. As a result, the data naturally divide into three periods differentiated by experimental conditions. SAGE I refers to extractions on approximately 30 tons of Ga beginning in 1989 with backgrounds becoming low enough to begin solar neutrino extractions in 1990. In the summer of 1991, the extraction mass was increased to nearly 60 tons. The majority of those data were taken without digitized waveforms, and thus electronic noise levels were such that the L peak was inaccessible. After SAGE I completed, the experiment was greatly improved with respect to electronic noise, and the analysis of the L-peak region became tractable. The period of data taking from September 1992 through December 1994 is referred to as SAGE II. The majority of SAGE II data had waveform recording capability. Only extractions for which we have waveform data are analyzed in the L-peak region. Beginning in December of 1994, an experiment using a  $^{51}\text{Cr}$  source was undertaken; we refer to all data taken after January 1995 as SAGE III.

## 2 Experimental Procedures

Each measurement of the solar neutrino flux begins by adding to the gallium approximately 700 g of stable Ge carrier (distributed equally among all of the reactors) as a Ga-Ge alloy with known Ge content. The reactor contents are stirred thoroughly to disperse the carrier throughout the Ga metal. After a typical exposure interval of 4-6 weeks, the Ge carrier and any  $^{71}\text{Ge}$  atoms produced by solar neutrinos or background sources are chemically extracted from the Ga using procedures described elsewhere [4]. The final step of the chemical extraction procedure is the synthesis of

germane ( $\text{GeH}_4$ ), which is used as a proportional counter (PC) gas with an admixture of Xe. The total efficiency of extraction, now typically 90%, is determined by measuring the germane volume.

Once the  $^{71}\text{Ge}$  is isolated in the PC, it is placed in a well-type NaI detector within a passive shield and counted for a period ranging from 2 to 6 months. The decay is identified via electron capture to  $^{71}\text{Ga}$  with a half life of 11.43 d [9]. Low energy K- and L-shell Auger electrons and x-rays from electron shell relaxation produce a nearly point-like ionization in the counter gas, resulting in a fast rise time for the subsequent pulse. Most background events leave an extended trail of ionization, producing a slower rise time. A candidate  $^{71}\text{Ge}$  event must not only fall within an appropriate energy region, but it must also have a rise time consistent with point-like ionization. In addition, we remove all PC events in coincidence with the NaI detector. Since  $^{71}\text{Ge}$  has no gamma rays associated with its decay, this veto further eliminates potential backgrounds.

The data acquisition electronics have evolved over the course of SAGE. The first two years of data rely entirely on a hardware measure of the risetime. This amplitude of the differentiated pulse (ADP) technique suffices well in studies of the K- peak counter response but is inadequate for the L-peak, which is more sensitive to electronic drifts and where backgrounds are higher. In 1992 we implemented an 8-channel counting system with a 1 GHz digital oscilloscope, which permits off-line analysis of the event waveforms. The digitized pulse is fit to a functional form [10] providing a measure of the energy deposited during the event and TN, the time duration over which the ionization arrives at the anode wire of the PC. All of the L-peak data and the vast majority of the K peak data presented here use the waveform analysis.

Counters are calibrated with an  $^{55}\text{Fe}$  source immediately after filling. Typically, they are again calibrated with  $^{55}\text{Fe}$  after 3 days of operation and approximately every two weeks subsequently. Beginning with SAGE II, calibrations were usually made with a  $^{109}\text{Cd}$  source whenever an  $^{55}\text{Fe}$  calibration was done. The 88 keV Ag gamma rays from the  $^{109}\text{Cd}$  source have sufficient energy to penetrate the counter wall and fluoresce the length of the Fe cathode, thus giving the K x-ray peak from Fe at 6.4 keV. Beginning with the February 1993 extraction, a  $^{109}\text{Cd}+\text{Se}$  source was periodically used, producing peaks at 1.4 keV and 11.21 keV. These several calibration lines are useful for checking linearity and determining whether a correction for polymerization of the anode wire is necessary.

The measure of energy is the integral of the pulse waveform for 800 ns after pulse onset. The peak position is based on the  $^{55}\text{Fe}$  calibration, and the energy window is two full widths at half maximum (FWHM). If the calibration centroid shifts between two calibrations, there is an error made in the efficiency estimate. Typical gain shifts are of the order of a few percent, and the calculated uncertainty is 3.1% in the counting efficiency.

To verify the procedures for setting rise time windows, a PC with  $^{71}\text{GeH}_4$  was measured in each of the counting slots. All events inside the energy windows of the K- and L-peaks were selected, and the rise time of each event was calculated using the parameter TN from the extended pulse fit. The rise time values were arranged in ascending order and limits were set such that 5% of the events is excluded. We thus use K- and L-peak event selection limits on TN of 0.0 ns to 18.4 ns and 0.0

ns to 10.0 ns, respectively. The variation from counter fill and electronics channel is approximately 1.2 ns, which results in an uncertainty in the efficiency of about  $\pm 1\%$ .

### 3 Statistical Analysis

The selection criteria result in a group of events from each extraction that are candidate  $^{71}\text{Ge}$  decays. These events are fit to a maximum likelihood function [11] assuming that they originate from an undefined but constant rate background and the exponentially decaying rate of  $^{71}\text{Ge}$ . The production rate is corrected for the mass of gallium exposed in each extraction. In addition, a small correction (no greater than 3%) is made since the Earth-Sun distance varies due to the eccentricity of the Earth's orbit.

Two time cuts are made on the counting intervals to minimize the potential effects of radon and radon daughters, which can mimic pulses of  $^{71}\text{Ge}$ . To remove these false  $^{71}\text{Ge}$  events, we delete 2.6 h of counting time in the K- and L-peaks after any opening of the passive shield. It is also possible that the PC may have a small admixture of  $^{222}\text{Rn}$  that enters the counter during filling. Most Rn decays give slow pulses at a saturated energy beyond the  $^{71}\text{Ge}$  peaks, but approximately 8% of the pulses from Rn and its daughters make fast pulses that are indistinguishable from those of  $^{71}\text{Ge}$ . Since the radon decay chain takes on average only 50 min to reach a long-lived isotope, deleting 15 min before and 3 hours after each saturated pulse removes most of these internal Rn events. For each individual extraction, we determine the best estimate of the solar neutrino flux by maximizing the likelihood function. The uncertainty is determined by integrating the likelihood function over the background to provide a likelihood function of signal only and then locating the minimum range in signal which includes 68% of the area under that curve.

These individual results are plotted in Fig. 1. The overall result is deduced by taking the product the likelihood expressions for all extractions requiring that the production rate per unit mass of Ga be equivalent but allowing the background rate to fluctuate from extraction to extraction.

Combining the total data set over the three periods of SAGE, the statistical result of the 136 separate counting sets is  $77.0 +6.2/-6.2$  SNU. If one considers the K- peak and L- peak data independently, the results are  $82.8+7.9/-7.6$  SNU and  $66.5+10.2/-9.8$  SNU, respectively. The agreement between the two peaks serves as a strong check on the robustness of the event selection criteria. Fig. 2 illustrates the decay of the  $^{71}\text{Ge}$  signal by comparing the energy rise time histogram of all events during the first 30 days after extraction with an equal interval of time at the end of counting.

### 4 Systematic Effects

Table 1 summarizes the systematic effects that may affect the solar neutrino production rate. They fall into three main categories of extraction efficiencies, counting efficiencies, and backgrounds. Several of these systematics are discussed below.

An extensive series of measurements were performed on all the PCs used in SAGE counting to establish their efficiencies and the associated uncertainties. A series of three separate measurements using PCs filled with  $^{37}\text{Ar}$ ,  $^{71}\text{Ge}$ , and  $^{69}\text{Ge}$  was employed to establish the counter efficiencies. The uncertainties in the efficiencies are composed

of the volume efficiency, end effects, and gas efficiency. Adding the uncertainties from each of these effects in quadrature gives a  $\pm 2.8\%$  uncertainty due to the counters.

There exist contributions to the  $^{71}\text{Ge}$  signal by means other than solar neutrinos. Limits on the creation of Ge isotopes through (n,p) reaction on Ga and by cosmic ray muons come from measurements of both the fast neutron [12] and muon fluxes [13] in the Ga chamber.

In addition, the concentrations in the Ga of U and Th have been measured independently by low background counting in a Ge detector and by glow discharge mass spectrometry. No observable level of U or Th was found, and upper limits are given in Table 1.

The radon background is a problem for any low background experiment. Decays of radon and its daughters make false  $^{71}\text{Ge}$  pulses in proportional counters. To determine the influence of radon fell in the counting gas of the counters we carried out measurements with a counter with large amount of radon inside. On the base of the measurements one calculated pulse spectra from decays of each radon chain element in the counter. The initial from the influence on SAGE data we use time cut 15 min before and 3 hours after each overflow event. The probability of false  $^{71}\text{Ge}$  event from one radon decay in the counter after  $^{71}\text{Ge}$  pulse selection criteria is about  $4 \times 10^{-4}$  for L- and  $8 \times 10^{-4}$  for K-peak. Since the mean value of the overflow pulses per run assigned to  $^{222}\text{Rn}$  is 7.7 and the mean value of  $^{71}\text{Ge}$  events per run is 2.3 for L- and 2.8 for K-peak one finds that the relative systematic error due to radon is 0.1% for L- and 0.2% for K-peak. It corresponds to 0.2 SNU [4].

The contribution to the  $^{71}\text{Ge}$  signal from other germanium isotopes  $^{68}\text{Ge}$  and  $^{69}\text{Ge}$  was estimated using calculations on the base of measurements with muon beams and and neutron sources [4].

Table 1: A summary of systematic effects and their uncertainties in SNU. The values for extraction and counting efficiencies are based on a rate of 75.9 SNU.

Extraction Efficiency	Ge Carrier Mass	$\pm/- 1.4$
	Extracted Ge Mass	$\pm/- 1.7$
	Residual Carrier Ge	$\pm/- 0.5$
	Ga Mass	$\pm/- 0.2$
Counting Efficiency	Counter Effects	$\pm/- 1.9$
	Gain Shifts	+2.1
	Resolution	-0.3, +0.5
	Rise Time Limits	$\pm/- 0.7$
	Lead and Exposure Times	$\pm/- 0.5$
Backgrounds	Neutrons, U, Th, muons	-1.0
	Other Ge isotops	-0.6
	External radon	0.0
Internal Radon		-0.2
	Total	-3.0, +3.5

## 5 Results

If we combine SAGE I with SAGE II and SAGE III, the global best fit capture rate for the 136 separate counting sets is  $(77.0 +6.2/-6.2)$  SNU, where the uncertainty is statistical only. In the windows that define the L- and K-peaks there are 1594 counts with 360.7 assigned to  $^{71}\text{Ge}$  (the total counting live time is 30.99 years. The total systematic uncertainty is determined by adding in quadrature all the contributions given in Table 1 and is  $-3.0$ ,  $+3.5$  SNU. Our overall result is thus  $(77.0 +6.2/-6.2 +3.5/-3.0)$  SNU. If we combine the statistical and systematic uncertainties in quadrature, the result is  $77.0+7.1/-6.9$  SNU.

The validity of this result relies on the ability to extract, isolate, and count, all with well known efficiencies, a few atoms produced by neutrino interaction from many tonnes of the target material. In the case of 60 t of Ga, it is an isolation factor of about 1 part in  $10^{28}$ . To verify such a stringent requirement, we have performed several auxiliary measurements to confirm that the extraction efficiency is as anticipated.

An initial test was carried out in which Ge carrier doped with a known number of  $^{71}\text{Ge}$  atoms was added to a reactor holding 7 tons of Ga. Three successive extractions were carried out, and the number of  $^{71}\text{Ge}$  atoms in each extraction was determined by counting.

The insensitivity to variation in the SSM for Ga is seen in the independently calculated result. The result [4] indicates that the extraction efficiency of the natural Ge carrier and  $^{71}\text{Ge}$  track very closely.

A second experiment addressed the concern that the  $^{71}\text{Ge}$  atom from inverse beta decay may be created in an excited or ionized state which results in the  $^{71}\text{Ge}$  being tied up in a chemical form which we cannot efficiently extract. A set of measurements designed to test directly this question were carried out by observing the beta decay of radioactive Ga isotopes in liquid Ga. Results from measurements [4] show that the expected isotopes are formed in the amounts anticipated at the 10% level. Foremost, it has been understood since the outset that a test on the entire operation of the detector (i.e., its chemical extraction efficiency, the counting efficiency, and the analysis technique) with a known flux of neutrinos of the appropriate energy would constitute the most rigorous check on the integrity of the experiment. Such an experiment was performed using a 19.1 PBq (517 kCi)  $^{51}\text{Cr}$  neutrino source. The final result, expressed as a ratio of the measured  $^{71}\text{Ge}$  production to that expected due to the source strength, is  $0.95 \pm 0.12$  [14]. This value provides strong verification that the experimental efficiencies are as claimed and validates a fundamental assumption in radiochemical experiments that the extraction efficiency of atoms produced by neutrino interactions is the same as that of the natural carrier.

### 5.1 Evidence for $^{71}\text{Ge}$

The most direct visual evidence that we are really observing  $^{71}\text{Ge}$  is in Fig. 2. The expected location of the  $^{71}\text{Ge}$  L- and K-peaks is shown darkened on this figure. These peaks are apparent in the upper panel, but missing in the lower panel because the  $^{71}\text{Ge}$  has decayed away. Events outside the two peak regions occur at about the same rate in both panels because they are mainly produced by background processes.

A quantitative indication that  $^{71}\text{Ge}$  is being counted can be obtained by allowing the decay constant during counting to be a free variable in the maximum likelihood fit, along with the combined production rate and all the background rates. The best fit half-life to all selected events in both L- and K- peaks is then  $(10.2+1.6/-1.4)$  days, in good agreement with the measured value [9] of 11.43 days.

## 5.2 Consistency of the data with analysis hypotheses

### Energy and rise time window positions

To test whether or not the energy and rise time windows are properly set, the windows can be made wider and the data re-analyzed. If the rise time window for accepted events is increased by 30%, i.e., from 0 ns–10 ns to 0 ns–13 ns in the L - peak and from 0 ns–18.4 ns to 0 ns–24.0 ns in the K-peak, then the overall result of all runs of SAGE II and III that were counted in system 3 is 78.2 SNU. This change is entirely consistent with the increase in counting efficiency due to the increased size of the rise time acceptance window.

Similarly, if the energy window in both L and K peaks is opened from the usual 2 FWHM to 3 FWHM, then the overall result of all runs of SAGE II and III becomes 79.1 SNU. This increase from the value of 77.0 SNU in the 2 FWHM energy window is because some of the  $^{71}\text{Ge}$  decays occur at the ends of the counter and their detected energy is reduced from the full peak value. These results in an increase in the counting efficiency in the wider energy window of 2% to 3%. If this efficiency increase is included in the analysis, then the results in the two energy windows agree to better than 1%.

### Time sequence

A major analysis hypothesis is that the time sequence of observed events for each run consists of the superposition of events from the decay of a fixed number of  $^{71}\text{Ge}$  atoms plus background events which occur at a constant rate. The quantity  $Nw^2$  and the goodness of fit probability inferred from it provide a quantitative measure of how well the data fit this hypothesis (see [15] for the definition and interpretation of  $Nw^2$ ). These numbers are evaluated for each data set. There are occasional runs with rather low probability of occurrence, but no more of these are observed than are expected due to normal statistical variation. This method can also be used to determine the goodness of fit of the time sequence for any combination of runs.

These numbers are given in Table 2; for the combined time sequence of all L plus K events from all runs, this test yields  $Nw^2 = 0.048$ , with a goodness of fit probability of  $(79 \pm 5)\%$ . A visual indication of the quality of this fit is provided in Fig. 3 which shows the count rate for all events in the L and K peaks vs. time after extraction. As is apparent, the observed rate fits the hypothesis quite well.

Table 2: Results of combined analysis of various segments of SAGE data. The uncertainty in the probability is  $\sim 4\%$ .

Data segment	Peak	Data sets	Total events	Fit to $^{71}\text{Ge}$	Best fit (SNU)	68% conf. range (SNU)	$Nw^2$	Prob. (%)
SAGE I	K	16	157	41.2	81	63-101	0.097	24
SAGE II	L+K	33	342	85.5	79	66-92	0.105	32
SAGE III	L+K	87	1082	233.3	73.7	66-81	0.100	20
All	L	55	737	128.2	66.5	55-77	0.048	54
All	K	81	857	228.8	82.8	75-91	0.047	94
All	L+K	136	1594	360.7	77.0	71-83	0.048	79

## Production rate sequence

Another analysis hypothesis is that the rate of  $^{71}\text{Ge}$  production is constant in time. By examination of Fig. 1, it is apparent that, within the large statistical uncertainty for each run, there are no substantial long-term deviations from constancy.

To test quantitatively whether or not it is reasonable to assume that the production rate is constant, we can consider the three segments of SAGE data, whose results are given in Table 2. A test of the consistency of any data segment with the overall result of 77.0 SNU can be made using the cumulative distribution function of the production rate  $C(p)$ , defined as the fraction of data sets whose production rate is less than  $p$ . Fig. 4 shows this distribution for all data sets and the expected distribution from simulation, assuming a constant production rate of 77.0 SNU. The two spectra parallel each other closely and can be compared by calculating the  $Nw^2$  test statistic [11]. This gives  $Nw^2 = 0.325$ , whose probability is 12%.

## 6 Summary and Conclusions

Ten years of measurement of the solar neutrino flux give the capture rate result (77.0  $\pm$  6.2/-6.2) SNU, where the uncertainty is statistical only. Analysis of all known systematic effects indicates that the total systematic uncertainty is +3.5/-3.0 SNU, considerably smaller than the statistical uncertainty. Finally, we have examined the counting data and shown that there is good evidence that  $^{71}\text{Ge}$  is being counted, that the counting data fit the analysis hypotheses, and that the counting data are self-consistent.

The SAGE result of 77.0 SNU represents about 60 % [7, 8] of SSM predictions. Given the extensive systematic checks and auxiliary measurements that have been performed, especially the  $^{51}\text{Cr}$  neutrino source experiment [14], this 6 reduction in the solar neutrino flux compared to SSM predictions is very strong evidence that the solar neutrino spectrum below 2 MeV is significantly depleted, as was previously shown for the  $^8\text{B}$  flux by the Cl and Kamiokande experiments. If we take into account the results of all experiments, astrophysical solutions to the solar neutrino deficit can now nearly be excluded [16-18].

More credible explanations for the solar neutrino deficit involve either matter-enhanced Mikheyev-Smirnov-Wolfenstein (MSW) neutrino oscillations, in which the solar  $e$  oscillates into other flavor neutrinos or a sterile neutrino [20,22-24], or vacuum

oscillations [20, 25–27].

There are now very strong indications that the solar neutrino deficit has a particle physics explanation and is a consequence of neutrino mass. To fully unravel the solar neutrino story, however, will require more experiments, especially those with sensitivity to low-energy neutrinos or to neutrino flavor. SAGE continues to perform regular solar neutrino extractions every four weeks with approximately 50 tons of Ga and will continue to reduce its statistical and systematic uncertainties, thus further limiting possible solutions to the solar neutrino problem.

### Acknowledgments

We thank J. N. Bahcall, M. Baldo-Ceolin, P. Barnes, S. Brice, L. Callis, A. Dar, G. T. Garvey, W. Haxton, V. N. Kornoukhov, V. A. Kuzmin, V. A. Matveev, L. B. Okun, V. A. Rubakov, R. G. H. Robertson, N. Sapporo, A. Yu. Smirnov, A. A. Smolnikov, A. N. Tavkhelidze, and many members of GALLEX for their continued interest and for fruitful and stimulating discussions. We acknowledge the support of the Russian Academy of Sciences, the Institute for Nuclear Research of the Russian Academy of Sciences, the Russian Ministry of Industry, Science and Technology, the Division of Nuclear Physics of the U.S. Department of Energy, the U.S. National Science Foundation. This research was made possible in part by grants of the Russian Foundation of Fundamental Research No. 96-02-18399, 99-02-16110, 00-1596632 (this grant is supported by Council for Grants of the President of Russian Federation), in part by grant No. M7F000 from the International Science Foundation and grant No. M7F300 from the International Science Foundation and the Russian Government, and in part by the U.S. Civilian Research and Development Foundation awards No. RP2-159, RP2-2253.

### References

- [1] B.T. Cleveland et al., *Astrophys. J.* 496, 505 (1998).
- [2] Y. Fukuda et al., *Phys. Rev. Lett.* 81, 1158 (1998).
- [3] Q.R.Ahmad et al., *Phys. Rev. Lett.* 87, 071301 (2001).
- [4] J.N. Abdurashitov et al., *Phys. Lett. B* 328, 234 (1994) and J.N. Abdurashitov et al., *Phys. Rev. C* 60, 055801 (1999).
- [5] W. Hampel et al., *Phys. Lett. B* 447, 127 (1999).
- [6] V.A. Kuzmin, *Zh. Eksp. Teor. Fiz.* 49, 1532 (1965); *Sov. Phys. JETP* 22, 1051 (1966).
- [7] J.N. Bahcall, S. Basu, and M.H. Pinsonneault, *Phys. Lett. B* 433, 1 (1998).
- [8] A.S. Brun, S. Turck-Chi'eze, and P. Morel, *Astrophys. J.* 506, 913 (1998).
- [9] W. Hampel and L. Remsberg, *Phys. Rev. C* 31, 677 (1985).
- [10] S.R. Elliott, *Nucl. Instrum. Meth.* A290, 158 (1990).
- [11] B. T. Cleveland, *Nucl. Instrum. Meth. in Phys. Res.* 214, 451 (1983).
- [12] I.R. Barabanov, V.N. Gavrin, P.P. Prokopeva, and V. Yants, Institute for Nuclear Research of the Academy of Sciences of the USSR Report No. P-0559 (1987).

- [13] O.G. Ryazhskaya and G.T. Zatsepin, in Proc. Ninth International Conference on Cosmic Rays, London, Sept. 1965, (Inst. of Physics, London 1965), Vol. 2, p. 987.
- [14] J.N. Abdurashitov et al., Phys. Rev. Lett. 77, 4708 (1996) and J.N. Abdurashitov et al., Phys. Rev. C 59, 2246 (1999).
- [15] B. T. Cleveland, Nucl. Instrum. Meth. in Phys. Res. A416, 405 (1998).
- [16] V. Berezinsky, G. Fiorentini, and M. Lissia, Phys. Lett. B 365, 185 (1996).
- [17] V. Berezinsky, in Proc. of the 25th International Cosmic Ray Conference, Durban, South Africa, 28 July–8 August 1997, edited by M. S. Potgieter, B. C. Raubenheimer, and D.J. van der Walt, (World Scientific, Singapore, 1998), v. 8, p. 59.
- [18] Arnon Dar and Giora Shaviv, “Proc. of Conf. Astrophysical Plasmas: From Atomic Nuclei to Stars and Galaxies,” Haifa, Israel, 12–16 January 1998, Phys. Reports (in press).
- [19] J. N. Bahcall, Phys. Rev. C 56, (1997) 3391.
- [20] J. N. Bahcall, P. I. Krastev, and A. Yu. Smirnov, Phys. Rev. D, 096016 (1998).
- [21] K.M. Heeger and R.G.H. Robertson, Phys. Rev. Lett. 77, 3720 (1996)
- [22] D.O. Caldwell, Inter. J. Mod. Phys. A 13, 4409 (1998).
- [23] S. M. Bilenky, C. Giunti, and W. Grimus, hep-ph/9812360.
- [24] N. Hata and P. Lankacker, Phys. Rev. D 56, 6107 (1997).
- [25] P. I. Krastev and S. T. Petcov, Phys. Rev. D 53, 1665 (1996).
- [26] James M. Gelb and S. P. Rosen, Phys. Rev. D (to be published).
- [27] J.N. Abdurashitov et al., Phys. Rev. Lett., 83, 23, 4686 (1999).

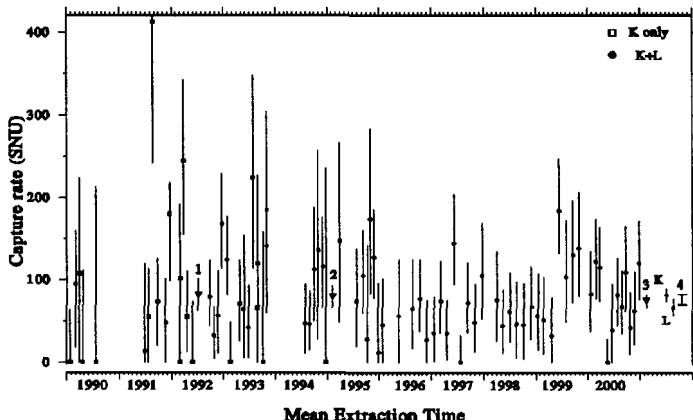


Figure 1: Capture rate for each extraction as a function of time. All uncertainties are statistical. The symbols 1, 2, and 3 show the combined result for SAGE I, II and III, respectively.

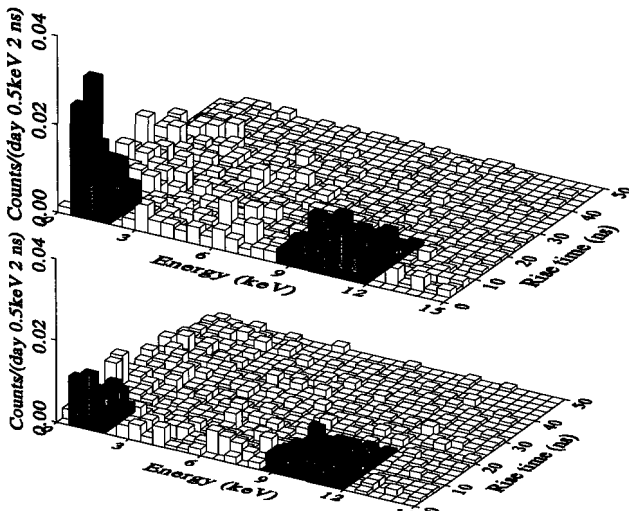


Figure 2: Upper panel shows the energy rise time histogram of all events observed during the first 30 days after extraction for all runs that could be counted in both K- and L-peaks (except May 96). The live time is 711.1 days. The expected location of the  $^{71}\text{Ge}$  decays is darkened. Lower panel shows the same histogram for all events that occurred during an equal live time interval at the end of counting.

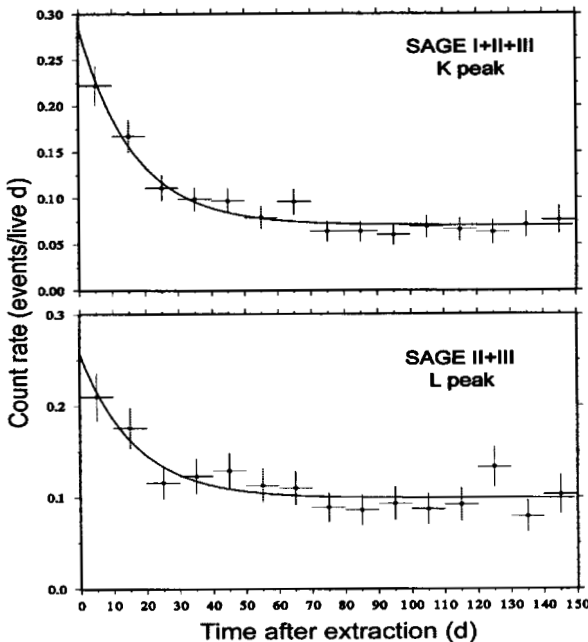


Figure 3: Count rate for all runs in L and K peaks. The solid line is a fit to the data points with the 11.4 day halflife of  $^{71}\text{Ge}$  plus a constant background. The vertical error bar on each point is proportional to the square root of the number of counts and is shown only to give the scale of the error. The horizontal error bar is  $\pm 5$  day, equal to the 10-day bin size.

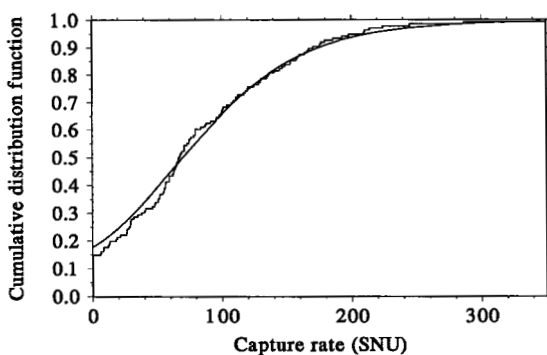


Figure 4: Measured capture rate for all SAGE data sets (jagged curve) and the expected distribution derived by 1000 Monte Carlo simulations of each set (smooth curve). The capture rate in the simulations was assumed to be 75.9 SNU.

# Neutrino Oscillation Measurements at SuperKamiokande

Y.Fukuda<sup>a</sup>

for SuperKamiokande Collaboration

*Kamioka Observatory, Institute for Cosmic Ray Research, University of Tokyo  
506-1205 Gifu, Japan*

*Abstract.* SuperKamiokande has observed solar and atmospheric neutrinos since 1996. We have found the evidence of neutrinos oscillation in the atmospheric neutrino data in 1998. Recently, concerning both results from SuperKamiokande and SNO, an another neutrino oscillation is naturally established in the  ${}^8\text{B}$  solar neutrino measurements. In this paper, recent updated data from both atmospheric and solar neutrino measurements will be reported. Also the recent result from K2K experiment will be included.

## 1 Introduction

Atmospheric neutrinos are produced by the decay products in hadronic shower due to the collision of primary cosmic ray with nuclei in the upper atmosphere. Production of muon and electron neutrino is dominated by the pion decay and muon decay. Therefore the ratio of electron and muon neutrino is almost 0.5 after fully decaying out. Of course, at higher energy region, this ratio goes small. SuperKamiokande has discovered the evidence of neutrino oscillation in 1998 [1] using  $\nu_e/\nu_\mu$  ratio anomaly and the distortion of the  $\nu_\mu$  zenith angle distribution in the atmospheric data. This indicates that muon neutrino oscillates to tau neutrinos or sterile neutrinos. The mass difference lays around  $10^{-3} \sim 10^{-2}\text{ eV}^2$ . On the other hands, solar neutrinos may also have a similar oscillation to solve the solar neutrino problem. Solar neutrinos are produced by the fusion reaction of light nuclei (pp-chain and CNO cycle) in a core of the Sun. All of neutrinos are purely  $\nu_e$ , and have low energy with a few keV up to 15 MeV. SuperKamiokande observes scattered electrons by induced neutrinos from  ${}^8\text{B}$   $\beta$ -decay with  $E_\nu \geq 5\text{ MeV}$ . The expected event rate 70 events per day. This high event rate makes us to measure the solar neutrino flux difference between daytime and nighttime, the time variations, and the precise energy spectrum. Concerning with the distance between the Earth and the Sun, we can investigate the neutrino oscillation with mass difference range of  $10^{-4} \sim 10^{-11}\text{ eV}^2$ .

## 2 Atmospheric neutrinos

The measurement of atmospheric neutrinos has started since 11st of May 1996. Total exposure period is 1289.4 days, which corresponds to 79.3 kton year. The sub-GeV sample has events with a visible energy less than 1.33 GeV and momentum for  $e$ -like and  $\mu$ -like event greater than 100 MeV/c and 200 MeV/c,

---

<sup>a</sup>e-mail: fukuda@icrr.u-tokyo.ac.jp

respectively. All of those events are fully contained (FC) events which means that the reconstructed vertex is inside of fiducial volume and the stopping point should be inside of inner tank. The multi-GeV sample has events with a visible energy greater than 1.33 GeV or partially contained (PC) events, which go out though the inner tank, even though the vertex is located inside of fiducial volume. Taking double ratio of  $\mu$ -like event and  $e$ -like event with data and Monte Carlo, the ratio is obtained by sub-GeV sample as;

$$\frac{(\mu/e)_{DATA}}{(\mu/e)_{MC}} = 0.652^{+0.019}_{-0.018} \pm 0.051,$$

where first and second error are statistical and systematic ones, respectively. On the other hands, for the multi-GeV sample, the ratio is obtained as;

$$\frac{(\mu/e)_{DATA}}{(\mu/e)_{MC}} = 0.675^{+0.034}_{-0.032} \pm 0.080.$$

Both results show us that  $\mu/e$  ratio is significantly small to the unity.

## 2.1 2-flavor oscillation analysis

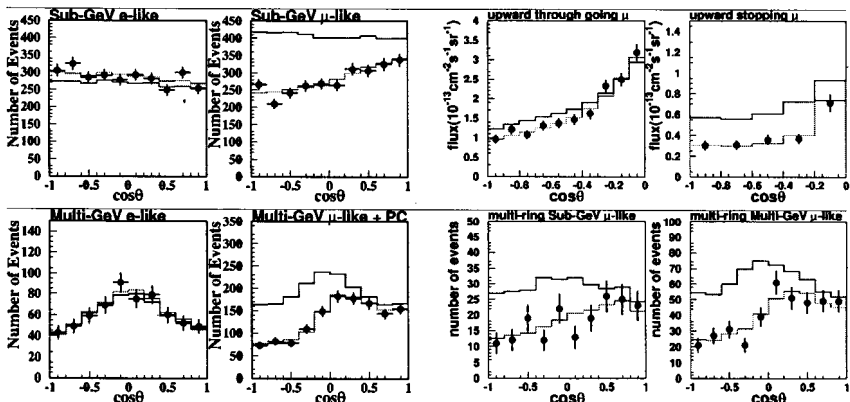


Figure 1: Zenith angle distribution of obtained atmospheric neutrino data. Red lines show the expected distribution from no oscillation and green lines show the expectation of best fit oscillation parameters assuming  $\nu_\mu \leftrightarrow \nu_\tau$  oscillation.

Figure 1 shows that the zenith angle distribution of (a) sub-GeV, (b) multi-GeV, (c) up going muon, and (d) multi-ring sample, respectively. Dotted and solid line show that the expected zenith angle distribution from no oscillation and from assuming  $\nu_\mu \leftrightarrow \nu_\tau$  oscillation with best fit parameter ( $\sin^2 2\theta = 1.0$ ,  $\Delta m^2 = 2.5 \times 10^{-3}$  eV $^2$ ). Obviously, in all samples,  $\mu$ -like events have a

strong distortion, especially the upward direction has smaller events than downward. Using these zenith angle distributions, we can obtain the allowed region on  $\sin^2 2\theta$  and  $\Delta m^2$  oscillation parameters. Figure 2 shows that the contour

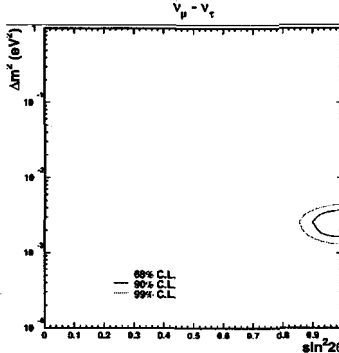


Figure 2: The 68 %, 90 %, and 99 % confidence level intervals are shown on  $\sin^2 2\theta$  and  $\Delta m^2$  oscillation parameter plane for  $\nu_\mu \leftrightarrow \nu_\tau$  oscillation based on 79.3 kton yr of SuperKamiokande data. The best fit parameter is obtained by  $\Delta m^2 = 2.5 \times 10^{-3} \text{ eV}^2$   $\sin^2 2\theta = 1.0$  with  $\chi^2 = 157.5/170$  d.o.f.

plots on oscillation parameters assuming  $\nu_\mu \leftrightarrow \nu_\tau$  oscillation. Obviously the finite allowed region can be found around  $\Delta m^2 = 1.6 \times 10^{-3} \sim 3.6 \times 10^{-3} \text{ eV}^2$  and  $\sin^2 2\theta \geq 0.9$ . Almost same allowed region can be also seen in a oscillation parameters assuming  $\nu_\mu \leftrightarrow \nu_s$  oscillation.

## 2.2 $\nu_\mu \leftrightarrow \nu_\tau$ or $\nu_\mu \leftrightarrow \nu_s$ ?

In order to distinguish those oscillation modes, the following analysis has done by using MSW effect in the Earth matter [2]. Assuming  $\nu_\mu \leftrightarrow \nu_s$  oscillation, muon neutrinos have an effective potential of neutral current, but no effect for sterile neutrinos. For very higher energy neutrinos ( $E_\nu = 30 \sim 100 \text{ GeV}$ ), the effective mixing angle in the matter becomes quite small, then  $\nu_\mu \leftrightarrow \nu_s$  oscillation should be suppressed. The atmospheric multi-ring neutral current enriched sample, the partially contained sample, and the upward through-going muon sample can be tested by above scenario. Figure 3 (a) shows the zenith angle distributions of those samples and the up/down (vertical/horizontal for upward going  $\mu$ ) asymmetry as a function of  $\Delta m^2$ . Solid and dashed lines in the zenith angle distribution show the expectation from Monte Carlo simulation assuming  $\nu_\mu \leftrightarrow \nu_\tau$  and  $\nu_\mu \leftrightarrow \nu_s$ , respectively. Fig.3 Also filled and blank circles in the asymmetry plots correspond to same oscillation modes, respectively. All data consistent with the  $\nu_\mu \leftrightarrow \nu_\tau$  oscillation. Figure 3 (b) shows the excluded region at 90 and 99 % C.L. assuming those oscillations. This result shows us that 99 % C.L. allowed regions assuming  $\nu_\mu \leftrightarrow \nu_s$  in FC single ring events

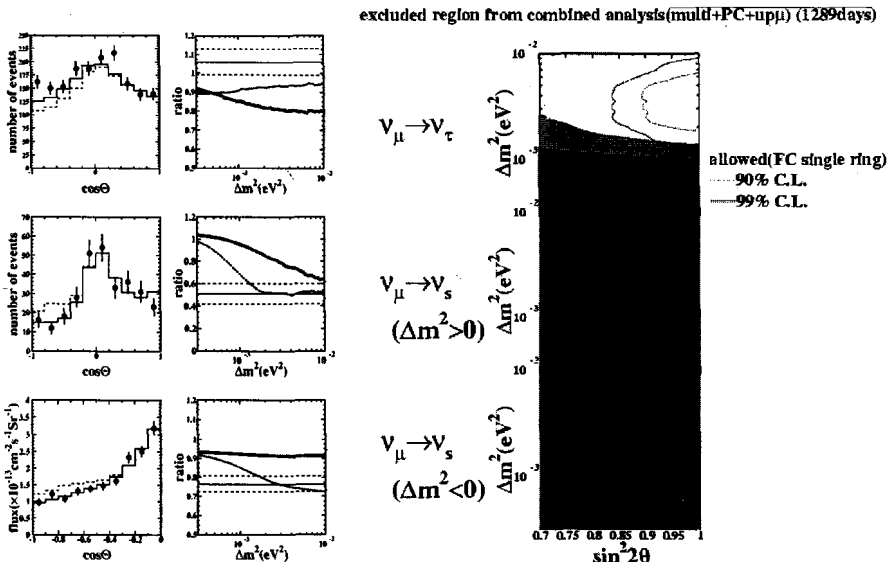


Figure 3: (a)Zenith angle plots and up/down (vertical/horizontal for upward going  $\mu$ ) for multi-ring NC enrich sample, PC sample, and upward through-going sample, respectively. Solid and dashed lines correspond to  $\nu_\mu \leftrightarrow \nu_\tau$  and  $\nu_\mu \leftrightarrow \nu_s$  oscillation, respectively. (b) Excluded regions assuming  $\nu_\mu \leftrightarrow \nu_\tau$  and  $\nu_\mu \leftrightarrow \nu_s$  oscillations on the allowed region which are obtained by FC single ring events. Solid and dotted lines are 99 and 90 % C.L. limits for both regions.

are disfavored by above analysis, on the other hands,  $\nu_\mu \leftrightarrow \nu_\tau$  is still alive. Therefore, the  $\nu_\mu \leftrightarrow \nu_s$  oscillation is completely disfavored by 99 % C.L. in the atmospheric data.

### 2.3 Search for $\tau$ appearance

According to the previous section. SuperKamiokande's results favors  $\nu_\mu \leftrightarrow \nu_\tau$  than  $\nu_\mu \leftrightarrow \nu_s$  oscillation. Assuming  $\nu_\mu \leftrightarrow \nu_\tau$  oscillation with  $\Delta m^2 = 3 \times 10^{-3} \text{ eV}^2$  and  $\sin^2 2\theta = 1.0$ , about 20  $\tau$  events are expected with 0.7 % S/N ratio. We tested three kinds of analysis methods independently to extract number of  $\tau$  events. They are (a) Likelihood analysis using "standard" SuperKamiokande variables, (b) Neural network method using "standard SuperKamiokande variables", and (c) Likelihood method using energy flow and event shape. For the case of (a), we used FC sample with  $E_{\text{vis}} \geq 1.33 \text{ GeV}$ , and restricted the event with most energetic ring assigned by e-like. Here, the S/N ratio becomes 3.5 %. Observed number of events is  $66 \pm 41(\text{stat.})^{+25}_{-18}(\text{syst.})$ . On the other hands, the

expected is 74. It is consistent with  $\nu_\mu \rightarrow \nu_\tau$  oscillation.

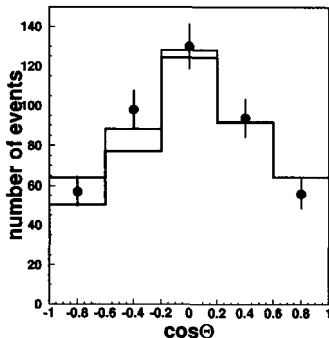


Figure 4: Zenith angle distribution of CC  $\nu_\tau$  enriched sample. Black and red solid line shows the background and background with  $\tau$  events for best fit. Expected number of  $\tau$  events is 32. On the other hands, the number of background is obtained by 399. Concerning the reduction efficiency, the obtained best fit number of  $\tau$  events is  $66 \pm 41(\text{stat.})^{+25}_{-18}(\text{syst.})$ .

### 3 Solar Neutrinos

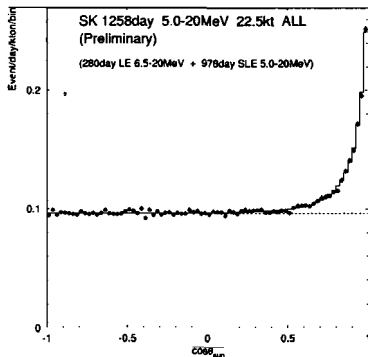


Figure 5: Angular distribution with respect to the solar direction based on 1258 days data. All events have an energy between 5.0 MeV to 20 MeV. Solid and dotted line show best fitted Monte Carlo expectation and background.

Solar neutrinos measurement has started since 31st of May 1996. We processed data analysis until 6th of October 2000, which corresponds to 1258 days in livetime. Figure 5 shows the angular distribution with respect to the solar direction. Observed solar neutrino flux with the energy range 5.0 to 20 MeV is  $2.32 \pm 0.03(\text{stat.})^{+0.08}_{-0.07}(\text{syst.}) \times 10^6 \text{ cm}^{-2} \text{ s}^{-1}$  [3]. Number of solar neutrinos is

extracted by  $18468 \pm 204$ . Taking ratio to the expectation of the standard solar model (SSM; here we used for the  $^8\text{B}$  flux from BP2000 [9] and new energy spectrum based on a recent measurement of  $^8\text{Be}$   $\alpha$  decay spectrum [10]) to the measured flux, the ratio is obtained by  $\frac{\text{Data}}{\text{SSM}_{BP98}} = 0.451 \pm 0.005(\text{stat.})^{+0.016}_{-0.014}(\text{syst.})$ . This flux is consistent with the observation of Kamiokande [8] and first observation of SuperKamiokande [5].

### 3.1 Recent results from the measurements

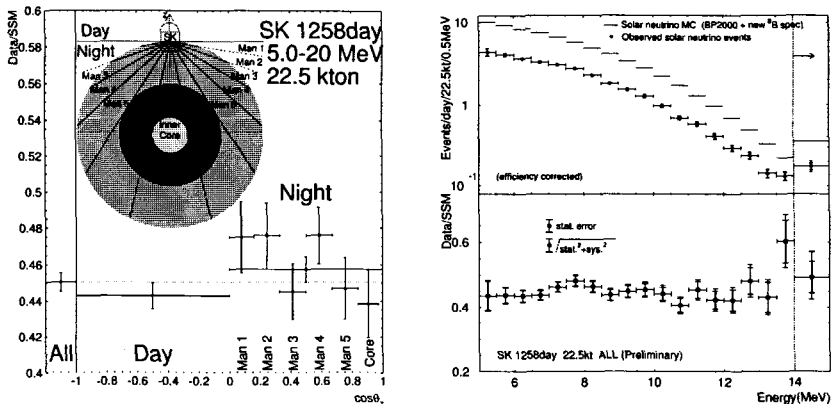


Figure 6: (a) Solar neutrino fluxes measured in daytime and nighttime. The nighttime is divided into 6 bins, man1,2,3,4,5 and core. Those are defined by the small figure. (b) Energy spectrum of recoiled electron based on 1258 days SuperKamiokande's data.

Solar neutrino fluxes obtained by daytime and nighttime, which is divided into 6 bins, are shown in Fig.6 (a). Assuming MSW matter oscillation [11], electron neutrinos may convert to muon (tau) neutrinos in the matter of the Sun by MSW effect, however, converted neutrinos may also re-convert to electron neutrinos by the matter in the Earth [6]. Therefore nighttime neutrino flux may be different from the daytime flux. The flux difference between day-night is obtained by  $\frac{N-D}{(N+D)/2} = 0.033 \pm 0.022(\text{stat.})^{+0.013}_{-0.012}(\text{syst.})$ . Significance of the day/night flux difference becomes 1.3 sigma [3]. Still we need more data to confirm this difference. The seasonal variation of solar neutrino fluxes were also measured. Within the experimental error, there is no seasonal variation in a present data.

The energy spectrum of observed neutrinos is shown in Fig.6 (b). Top and bottom figure show the event rate and the ratio to the expectation from SSM, respectively. The energy spectrum looks flat, and the confidence level is 39 %. Higher energy bins ( $E_e \geq 13 \text{ MeV}$ ) have a larger values than averaged flux.

Of course, we must consider carefully contribution from Hep neutrinos for this energy region, because Hep neutrino flux may have a large uncertainty. According to the extracting of solar neutrino events at 18 - 25 MeV, we obtained 90 % upper limit of Hep neutrino flux as  $4.3 \times \text{SSM}$ , if we assume no oscillation occurs.

### 3.2 Oscillation analysis and implication from SNO results

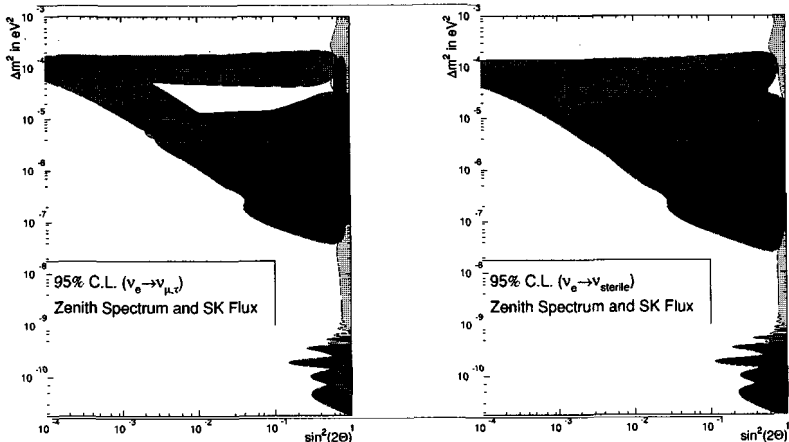


Figure 7: The 95 %, confidence level regions are shown. Green region is obtained by Global fit using obtained fluxes from Cl, Ga, and SuperKamiokande. Red regions correspond to 95 % C.L. excluded region by zenith spectrum without constraint of  ${}^8\text{B}$  neutrino flux. Blue regions are allowed by zenith spectrum with constraint of  ${}^8\text{B}$  flux. Left figure (a) is the case of fully 2 flavor active neutrino oscillation and right figure (b) is fully 2 flavor sterile neutrino oscillation.

Concerning both energy spectrum and day/6-night fluxes simultaneously, we can define the zenith spectrum ( $7$  zenith angle bin  $\times$   $6$  energy bin + day/night  $\times$   $2$  energy bin). The last  $2$  energy bins correspond to  $5.0\text{-}5.5\text{d MeV}$  and  $16\text{-}20\text{ MeV}$ . Those are divided into only day and night due to a poor statistics. Using zenith spectrum distribution, the oscillation parameters are constrained as shown in Fig.7 [4]. Here we take the Hep neutrino flux as a free parameter. Figure7 (a) shows the case of fully 2 flavor active neutrino oscillation, and (b) shows fully 2 flavor sterile neutrino oscillation. For former case, most of small mixing angle region and vacuum solution region allowed by global fit are excluded by zenith spectrum analysis even without constraint of  ${}^8\text{B}$  neutrino flux at 95 % C.L. The large mixing angle region and LOW (however it appears only 99 % C.L.) are preferred. On the other hands, the fully 2 flavor neutrino

sterile oscillation allowed by global fits is disfavored at 95% C.L by zenith spectrum analysis without flux constraint.

Recently Sudbury Neutrino Observatory published their first result based on the measurement from charged current reaction (CC) in heavy water and the elastic scattering in light water [12]. The obtained  ${}^8\text{B}$  solar neutrino flux from CC is  $1.75 \pm 0.07(\text{stat.})^{+0.12}_{-0.11}(\text{syst.}) \pm 0.05(\text{theo.}) \times 10^6 \text{cm}^{-2}\text{s}^{-1}$ , and then the difference of flux obtained by SuperKamiokande is 3.3 sigma with concerning both experimental and theoretical errors. At least, this difference comes from  $\nu_\mu$  or  $\nu_\tau$ , therefore we can establish the existence of neutrino oscillation in solar neutrinos. Assuming the difference is caused by  $\nu_\mu$  or  $\nu_\tau$ , the total active  ${}^8\text{B}$  solar neutrinos flux is consistent with the prediction of SSM. Using SNO rate into global fit, we can get allowed region as shown in Fig.8. According to this

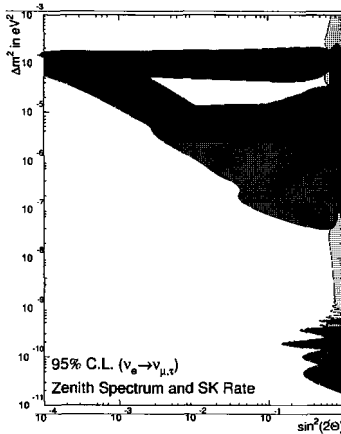


Figure 8: The 95 % confidence level regions are shown. Green region is obtained by Global fit using obtained fluxes from Cl, Ga, SuperKamiokande, and SNO. Red and blue regions are same as Fig.7.

figure, the SMA solution given by global fit is disfavored by zenith spectrum analysis by SuperKamiokande. Therefore, we can conclude the SMA region allowed by global fit is excluded by 3 sigma significance in case of 2 flavor active neutrino oscillation.

#### 4 Status of K2K experiment

K2K long base line neutrino experiment has started since January 1999. The muon neutrinos (99 %) beam with averaged energy 1.3GeV are produced by 10 GeV Proton Synchrotron at KEK, and emit them to the SuperKamiokande. The distance between SuperKamiokande and KEK is 250km, therefore we can

test a neutrino oscillation ( $\nu_\mu$  disappearance and  $\nu_e$  appearance) with  $\Delta m^2 \geq 2 \times 10^{-3} \text{ eV}^2$ . The accumulated proton on target is  $4.58 \times 10^{19}$  by 25th of April 2001.

Neutrino beam is monitored by the muon monitor in spill by spill, and the neutrino flux is measured by the front end detectors, which consist of 1kt Water Čerenkov detector, SCIFI with LEAD Glass, and the muon range detector (MRD) as shown in Fig.9 (a). To estimate neutrino flux and spectrum at the site of SuperKamiokande, the precise beam simulation is needed. It is calibrated by the pion monitor directly. Most important information to reduce the background or extract the neutrino event at SuperKamiokande is the GPS clock which is obtained at KEK and SuperKamiokande individually. The beam

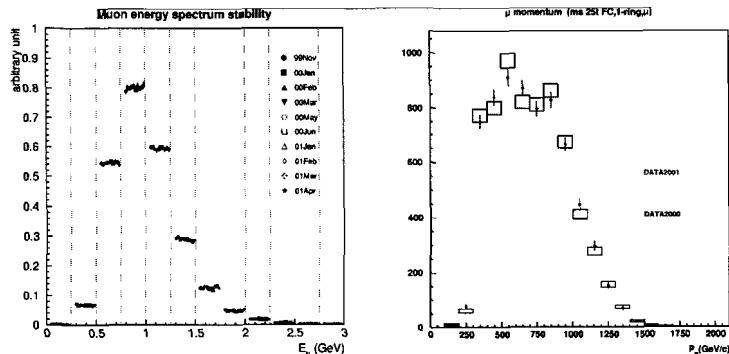
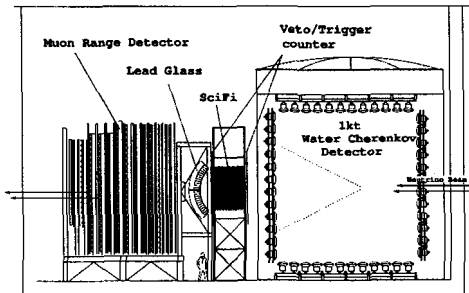


Figure 9: (a) Schematic view of front end detector in K2K experiment. Bottom figures show the beam stability, especially muon energy, monitored by (b) MRD and (c) 1kt water Čerenkov detector.

stability, especially energy of muons which are produced by induced muon

neutrinos, is monitored by the front end detectors. Figure 9 (b) and (c) show the energy stability monitored by MRD and 1kt Water Čerenkov detector, respectively.

Neutrino events related to the K2K experiment in SuperKamiokande are selected by using GPS timing as described above. The time difference between KEK and SuperKamiokande is about 1m second, so that it must be corrected to select candidates. Figure 10 shows that the number of events during  $\pm 500 \mu\text{sec}$  time window at several reduction steps. The events are required by no decay electron, HE trigger, the visible energy should be larger than 30 MeV, and fully contained of vertex. There are 44 events found in the 22.5 kton fiducial volume. The timing of those events are clustered within -0.2 to  $1.3 \mu\text{sec}$ . Expected backgrounds from atmospheric neutrinos are calculated by  $10^{-3}$  in the  $1.5 \mu\text{sec}$  window.

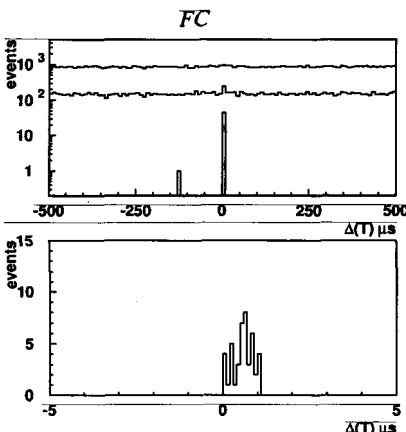


Figure 10: Top plot show that the number of events observed in SuperKamiokande at various reduction step within  $\pm 500 \mu\text{sec}$  difference between GPS timing. Finally 44 events are found in the fiducial volume.

Comparison of the observed and expected number of events is done by assuming both cases of no oscillation and several oscillation parameters. Table 1 shows the results from data taken during June 1999 to April 2001. It is clearly seen that the discrepancy between the observed number of events and the number of events assuming no oscillation. Concerning the errors, the probability of null oscillation is obtained by less than 3 %.

In order to confirm the neutrino oscillation parameter in K2K experiment, the energy spectrum of reconstructed neutrino should be measured. From Monte Carlo simulation, it has good sensitivity with low energy neutrinos for small  $\Delta m^2$  as shown in Fig.11 (a). Figure 11 (b) shows the observed energy spectrum and the expectation from Monte Carlo simulation without oscillation.

	Obs.	No osc.	$3 \times 10^{-3}$	$5 \times 10^{-3}$	$7 \times 10^{-3} \text{ eV}^2$
FC 22.5kt	44	$63.9^{+6.1}_{-8.6}$	41.5	27.4	23.1
1-ring	26	$38.4 \pm 5.5$	22.3	14.1	13.1
$\mu$ -like	24	$34.9 \pm 5.5$	19.3	11.6	10.7
e-like	2	$3.5 \pm 1.4$	2.9	2.5	2.4
multi-ring	18	$25.5 \pm 4.3$	19.3	13.3	10.0

Table 1: Summary of observed and expected number of events in K2K experiment

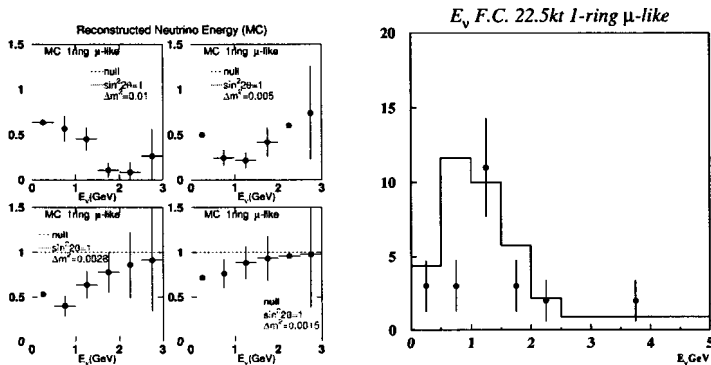


Figure 11: (a) Expected neutrino spectra at several  $\Delta m^2$ . The vertical axis shows the ratio of number of events obtained by oscillation case and null oscillation, and the horizontal shows the reconstructed neutrino energy. It looks that a good sensitivity with low energy neutrinos for small  $\Delta m^2$ . (b) Observed  $\nu$  reconstructed energy spectrum. Solid line corresponds to the expectation from the simulation without neutrino oscillation. Assuming  $\Delta m^2 = 3 \times 10^{-3} \text{ eV}^2$ , large deficit should be appeared around  $E_\nu = 600 \text{ MeV}$ . The error bar shows only statistical error.

It seems to be large deficit around 600 MeV, however, we still need to estimate the systematic error, because of only statistical error shown in Fig.11 (b).

## 5 Summary

In summary, SuperKamiokande disfavors  $\nu_\mu \leftrightarrow \nu_s$  oscillation in the atmospheric data at 99% C.L., and the extracted numbers of  $\tau$  events by three independent kind of analyses are consistent with the expected number using best fit oscillation parameter. SuperKamiokande also observed the  ${}^8\text{B}$  solar neutrino flux with  $2.32 \pm 0.03(\text{stat.})^{+0.08}_{-0.07}(\text{syst.}) \times 10^6 \text{ cm}^{-2} \text{ s}^{-2}$ , and Day/Night flux difference becomes about 3% with 1.3 sigma. Using zenith spectrum analysis, we can disfavor both SMA and VO solutions at 95% C.L. even without  ${}^8\text{B}$  flux constraint for 2 flavor active neutrino oscillation. Also fully 2 flavor sterile

neutrino oscillation is disfavored at 95 % C.L. In addition, combining the recent SNO rate in the global fit, SMA solution is disfavored at 3 sigma level in case of fully 2 flavor active neutrino oscillation. Finally, K2K experiment has accumulated the proton on target as  $4.58 \times 10^{19}$  by 25th of April 2001. The neutrino beam is monitored by muon/pion monitor and the front end detectors precisely, and is running very stably. They give us the expected number of events which should be observed at SuperKamiokande as  $63.9^{+6.1}_{-6.6}$  in case of null oscillation. The observed number of K2K event at SuperKamiokande is 44, therefore, the null oscillation is disfavored by 97 % C.L. The measurement of energy spectrum will give us more strong constraint on  $\nu_\mu \leftrightarrow \nu_\tau$  oscillation in K2K experiment.

### Acknowledgments

The authors acknowledge the cooperation of the Kamioka Mining and Smelting Company. The SuperKamiokande has been built and operated from funding by the Japanese Ministry of Education, Culture, Sports, Science and Technology, the U.S. Department of Energy, and the U.S. National Science Foundation

### References

- [1] Y.Fukuda *et al.*, *Phys. Rev. Lett.* **81**, 1562 (1998).
- [2] S.Fukuda *et al.*, *Phys. Rev. Lett.* **85**, 3999 (2000).
- [3] S.Fukuda *et al.*, *Phys. Rev. Lett.* **86**, 5651 (2001).
- [4] S.Fukuda *et al.*, *Phys. Rev. Lett.* **86**, 5656 (2001).
- [5] Y.Fukuda *et al.*, *Phys. Rev. Lett.* **81**, 1158 (1998).
- [6] Y.Fukuda *et al.*, *Phys. Rev. Lett.* **82**, 1810 (1999).
- [7] Y.Fukuda *et al.*, *Phys. Rev. Lett.* **82**, 2430 (1999).
- [8] Y.Fukuda *et al.*, *Phys. Rev. Lett.* **77**, 1683 (1996).
- [9] J.N.Bahcall *et al.*, astro-ph/0010346
- [10] C.E.Ortiz *et al.*, *Phys. Rev. Lett.* **85**, 2909 (2000)
- [11] S.P.Mikheyev and A.Y.Smirnov, *Sov. Jour. Nucl. Phys.* **42**, 913(1985); L.Wolfenstein, *Phys. Rev. D* **17**, 2369 (1978).
- [12] Q.R.Ahmad *et al.*, *Phys. Rev. Lett.* **87** 071301 (2001)

# RESONANT AND NON-RESONANT NEUTRINO SPIN-FLAVOR CONVERSION IN STATIC SOLAR MAGNETIC FIELD

A.A. Bykov<sup>1 a</sup>, O.G. Miranda<sup>2 b</sup>, C. Peña-Garay<sup>3 c</sup>, V.Yu. Popov<sup>1 d</sup>, T.I. Rashba<sup>4 e</sup>,  
V.B. Semikoz<sup>4 f</sup>, J.W.F. Valle<sup>3 g</sup>

<sup>1</sup>Physics Faculty of Moscow State University, 119899 Moscow, Russia

<sup>2</sup>Departamento de Física, Centro de Investigación y de Estudios Avanzados Apdo.  
Postal 14-740 07000 Mexico, DF, Mexico

<sup>3</sup>Instituto de Física Corpuscular – C.S.I.C., Universitat de València, Edificio  
Institutos, Apt. 22085, E-46071 València, Spain

<sup>4</sup>Institute of Terrestrial Magnetism, Ionosphere and Radio Wave Propagation of the  
Russian Academy of Sciences, 142190, Troitsk, Moscow region, Russia

*Abstract.* We perform the rates-only analysis of the spin-flavour precession solutions to the solar neutrino problem using the data of the chlorine, gallium experiments, the SNO charge-current measurement, the 1258-day Super-Kamiokande data and the LSD upper limit on solar anti-neutrinos. In a self-consistent magneto-hydrodynamics approach there are only 3 effective parameters:  $\Delta m^2$ ,  $\mu_\nu B_\perp$  and the neutrino mixing angle  $\theta$ . We obtain the well-known resonant spin-flavor precession solution and find new non-resonant spin-flavor solution in the so called “dark-side” region. We show for fixed  $\mu_\nu B_\perp$  that spin-flavour precession solutions are slightly favours over oscillations.

## 1 Introduction

In this paper we have reconsidered the spin-flavour precession solutions, based on non-zero transition magnetic moments of neutrinos [1]. These solutions are interesting on general theoretical grounds [2] because neutrinos are expected to be Majorana particles and the conversions induced by transition magnetic moments may be resonantly amplified in the matter [3]. We removed the arbitrariness in the choice of the magnetic field profile in the solar convective zone [4–6] in a self-consistent way from magneto-hydrodynamics theory [7].

We have generalized our previous work [7] to the case of non-zero neutrino mixing and found a genuinely new non-resonant spin-flavor precession solution in the so-called “dark-side” of the neutrino mixing parameter [8, 9]. It was shown that these solutions, both the resonant spin flavour precession solution (RSFP) as well as a new non-resonant one (NRSFP), provide excellent descriptions of the solar rates [10], including the recent SNO CC result [11]. We demonstrate that SFP solutions are in consistent with the non-observation of electron anti-neutrinos from the Sun [12, 13] in the results of the LSD experiment [14] as well as SuperKamiokande [15]. To simplify the presentation we considered here only the total rates of all solar neutrino

---

<sup>a</sup>e-mail: bykovzz@orc.ru

<sup>b</sup>e-mail: Omar.Miranda@fis.cinvestav.mx

<sup>c</sup>e-mail: pena@hal.ific.uv.es

<sup>d</sup>e-mail: popov@math380b.phys.msu.su

<sup>e</sup>e-mail: rashba@izmiran.rssi.ru

<sup>f</sup>e-mail: semikoz@orc.ru

<sup>g</sup>e-mail: valle@ific.uv.es

experiments and ignored spectral energy distribution and the day-night variations from the Super-Kamiokande data [10].

## 2 Neutrino Evolution

The Majorana neutrino evolution Hamiltonian in a magnetic field in the two-flavor case is [1],

$$i \begin{pmatrix} \dot{\nu}_{eL} \\ \dot{\bar{\nu}}_{eR} \\ \dot{\nu}_{\mu L} \\ \dot{\bar{\nu}}_{\mu R} \end{pmatrix} = \begin{pmatrix} V_e - c_2 \delta & 0 & s_2 \delta & \mu_\nu B_+(t) \\ 0 & -V_e - c_2 \delta & -\mu_\nu B_-(t) & s_2 \delta \\ s_2 \delta & -\mu_\nu B_+(t) & V_\mu + c_2 \delta & 0 \\ \mu_\nu B_-(t) & s_2 \delta & 0 & -V_\mu + c_2 \delta \end{pmatrix} \begin{pmatrix} \nu_{eL} \\ \bar{\nu}_{eR} \\ \nu_{\mu L} \\ \bar{\nu}_{\mu R} \end{pmatrix}, \quad (1)$$

where  $c_2 = \cos 2\theta$ ,  $s_2 = \sin 2\theta$ ,  $\delta = \Delta m^2/4E$ , assumed to be always positive, are the neutrino oscillation parameters;  $\mu_\nu$  is the neutrino transition magnetic moment;  $B_\pm = B_x \pm iB_y$ , are the magnetic field components which are perpendicular to the neutrino trajectory;  $V_e(t) = G_F \sqrt{2}(N_e(t) - N_n(t)/2)$  and  $V_\mu(t) = G_F \sqrt{2}(-N_n(t)/2)$  are the neutrino vector potentials for  $\nu_{eL}$  and  $\nu_{\mu L}$  in the Sun, given by the number densities of the electrons ( $N_e(t)$ ) and neutrons ( $N_n(t)$ ). When  $\theta \rightarrow 0$  we recover the RSFP case treated in [7] while as  $B \rightarrow 0$  we recover the pure neutrino oscillation case (OSC). In our calculations we use the electron and neutron number densities from the BP00 model [16] for the Sun and from the PREM [17] for Earth.

We adopt the analysis techniques which have already been presented in papers [18] using the theoretical BP00 standard solar model best-fit fluxes and estimated uncertainties from Ref. [16]. In addition to the solar data [10] we also use the reactor data [19] as well as the data on searches for anti-neutrinos from the Sun [14]. For the neutrino conversion probabilities we use the numerical solutions of the master equation 1.

We used the self-consistent magneto-hydrodynamics magnetic field profile (Fig. 1) which has been obtained and motivated in Ref. [7] for  $k = 6$  and  $r_0 = 0.6R_\odot$ . We assume a transition magnetic moment of  $10^{-11}$  Bohr magneton in accordance with present experimental limit and a magnetic field magnitude around 80 kGauss, allowed by helioseismological observations.

The resulting theoretical framework has therefore only 2 effective free parameters:  $\Delta m^2$ ,  $\tan^2 \theta$ . The remaining parameter  $\mu_\nu B_\perp$  characterizing the maximum magnitude of the magnetic field in the convective zone has been fixed at its optimum value.

In Fig. 2 we show a typical spin flavour precession survival probabilities both in the “light” ( $0 \leq \theta \leq \pi/4$ ) and “dark” ( $\pi/4 \leq \theta \leq \pi/2$ ) sides. For the case  $\cos 2\theta \approx 1$  we obtain the well-known resonant SFP solution (dotted curve), while the alternative  $\cos 2\theta \approx -1$  choice corresponds to our new NRSFP solution in the dark side (solid curve).

We present in Fig. 3 the allowed solutions for the two-flavor SFP case. These include the pure two-neutrino oscillation case, as well as the conventional RSFP and the new NRSFP solution. We find that in rates-only analysis both LMA and SMA oscillation solutions are recovered without an essential change in case of neutrino magnetic moment effect.

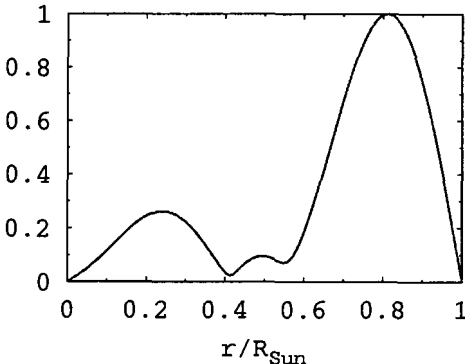


Figure 1: Magnetic field profile  $B_{\perp}(r)$  (details see in [7]).

Solution	$\Delta m^2$	$\tan^2(\theta)$	$\chi^2_{\min}$	g.o.f.
LMA	$2.1 \times 10^{-5}$	0.34	3.99	14%
SMA	$6.9 \times 10^{-6}$	$1.6 \times 10^{-3}$	5.25	7%
RSF	$8.9 \times 10^{-9}$	$1.1 \times 10^{-3}$	2.98	22%
NRSF	$4.0 \times 10^{-9}$	$3.5 \times 10^3$	3.83	15%

Table 1: Best-fit points and goodness-of-fit of oscillation and spin flavour solutions to the solar neutrino problem as determined from the rates-only analysis for  $\mu_{\nu} = 10^{-11} \mu_B$  and  $B_{\perp} = 84$  kGauss.

In the Fig. 3 we have fixed the value of  $\mu_{\nu} B_{\perp}$  to its best value (for  $\mu_{\nu} = 10^{-11}$  Bohr magneton it corresponds to  $B_{\perp} \sim 80$  kGauss). In case of the relatively large  $\mu_{\nu}$  value all large mixing solutions other than the LMA solution (LOW and VO) are forbidden because of the non-observation of the solar  $\bar{\nu}_e$  flux and over-suppression of  ${}^8B$  neutrino flux. The goodness of fit of the various solutions in Fig. 3 is given in Table 1. One notices that SFP solutions are slightly better against LMA, SMA and VO.

The main result presented in Fig. 3 is the appearance of two new solutions which are due to interaction of the neutrino magnetic moment and magnetic field. The known resonant small-mixing solution is recovered, after updating the solar data to the measurements from 1258 days of Super-Kamiokande data and SNO CC measurement [11]. One sees that this RSFP solution extends up to  $\tan^2 \theta$  values around  $10^{-2}$  or so. More important conclusion, one finds a genuinely new non-resonant (NRSFP) solution in the “dark-side” of the parameter space, for  $\tan^2 \theta > 1$ . The existence of these solutions can be easily understood on the basis of Fig. 2. Similarly one can understand the non-resonant nature of the new NRSFP solution. Non-observation of the solar anti-neutrinos [14] plays an important role in cutting the non-resonant RSF

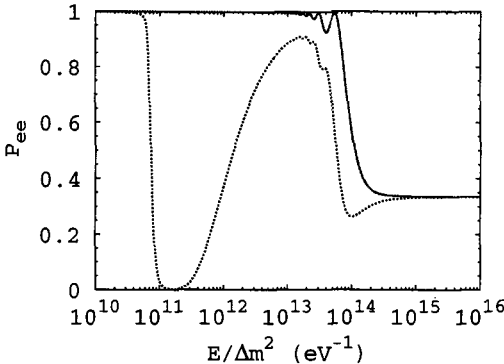


Figure 2: Neutrino spin flavour precession survival probabilities in “light” (dotted curve) and “dark” (solid curve) sides, for  $\mu_\nu = 10^{-11} \mu_B$  and  $B_\perp \sim 80$  kGauss.

solution to  $\tan^2 \theta$  values larger than about 30.

We now present in Fig. 4 the predicted day–night averaged spectral energy distribution for our two spin-flavour precession solutions.

Clearly both spin-flavor precession spectra are totally consistent with the SuperKamiokande data. We also present the predicted oscillation spectra, in solid that of the SMA solution and dashed the LMA solution. In contrast with the RSFP, NRSFP and LMA solutions, the SMA spectrum is in strong disagreement with the SuperKamiokande data.

### 3 Summary

In this paper we have re-considered the spin-flavour precession solutions and performed the rates-only analysis, based on non-zero transition magnetic moments of Majorana neutrinos taking into account the recent SNO CC result as well as the 1258-day solar neutrino data from Super-Kamiokande and chlorine and gallium experiments. We have took into account the upper limit on the solar anti-neutrino flux from the LSD experiment as well as the reactor neutrino data. We followed the self-consistent approach from magneto-hydrodynamics theory employed previously [7] in order to remove the arbitrariness associated to the magnetic field profile. We have generalized our previous work [7] to the case of non-zero neutrino mixing, performing the first “unified” study of solar neutrino data in the presence of a neutrino transition magnetic moment in “light-side” and “dark-side” cases. We have recovered the standard resonant spin-flavor small-mixing solution to the solar neutrino problem (RSFP) which remains as best solution to the solar neutrino problem and we have found a genuinely new non-resonant solution in the so-called “dark-side” of the neutrino mixing parameter. The NRSFP solution gives a very good fit of the present solar neutrino data.

## Acknowledgments

This work was supported by Spanish grants PB98-0693 and GV99-3-1-01, by the European Commission RTN network HPRN-CT-2000-00148 and by the European Science Foundation network grant N. 86. AAB, VYuP, VBS and TIR were supported by the RFBR grants 00-02-16271 and 01-02-06225. OGM was supported by the CONACyT-Mexico grants J32220-E and 35792-E. We would like to thank the Organizing Committee of the Conference for the warm and friendly atmosphere.

## References

- [1] J. Schechter and J. W. F. Valle, *Phys. Rev.* **D 24**, 1883 (1981); Erratum-ibid. **D 25**, 283 (1982).
- [2] J. Schechter and J. W. F. Valle, *Phys. Rev.* **D 22**, 2227 (1980).
- [3] E. K. Akhmedov, *Phys. Lett.* **B 213**, 64 (1988); C. Lim and W. J. Marciano, *Phys. Rev.* **D 37**, 1368 (1988).
- [4] E. K. Akhmedov and J. Pulido, *Phys. Lett.* **B 485**, 178 (2000) [hep-ph/0005173]; *Astropart. Phys.* **13**, 227 (2000) [hep-ph/9907399].
- [5] M. M. Guzzo and H. Nunokawa, *Astropart. Phys.* **12**, 87 (1999) [hep-ph/9810408]. H. Nunokawa and H. Minakata, *Phys. Lett.* **B 314**, 371 (1993).
- [6] J. Derkaoui and Y. Tayalati, *Astropart. Phys.* **14**, 351 (2001) [hep-ph/9909512].
- [7] O. G. Miranda, C. Pena-Garay, T. I. Rashba, V. B. Semikoz and J. W. F. Valle, *Nucl. Phys.* **B 595**, 360 (2001) [hep-ph/0005259].
- [8] G. L. Fogli, E. Lisi and D. Montanino, *Phys. Rev.* **D 54**, 2048 (1996) [hep-ph/9605273].
- [9] A. de Gouvea, A. Friedland and H. Murayama, *Phys. Lett.* **B 490**, 125 (2000) [hep-ph/0002064].
- [10] B.T. Cleveland *et al.*, *Astrophys. J.* **496** (1998) 505; K.S. Hirata *et al.* (Kamiokande Coll.), *Phys. Rev. Lett.* **77**, 1683 (1996); W. Hampel *et al.* (GALLEX Coll.), *Phys. Lett.* **B 447**, 127 (1999); D.N. Abdurashitov *et al.* (SAGE Coll.), *Phys. Rev. Lett.* **83**, 4686 (1999); *Phys. Rev.* **C 60**, 055801 (1999) [astro-ph/9907113]; V. Gavrin (SAGE Collaboration), *Nucl. Phys. Proc. Suppl.* **B 91**, 36 (2001); M. Altmann *et al.* (GNO Coll.), *Phys. Lett.* **B 490**, 16 (2000); E. Bellotti *et al.* (GNO Coll.), *Nucl. Phys. Proc. Suppl.* **B 91**, 44 (2001); Y. Fukuda *et al.* (SuperKamiokande Coll.), *Phys. Rev. Lett.* **81**, 1158 (1998); Erratum **81**, 4279 (1998); *Phys. Rev. Lett.* **82**, 1810 (1999); Y. Suzuki (SuperKamiokande Coll.), *Nucl. Phys. Proc. Suppl.* **B 91**, 29 (2001); S. Fukuda *et al.* (Super-Kamiokande Collaboration), *Phys. Rev. Lett.* **86**, 5651 (2001).
- [11] Q. R. Ahmad *et al.* [SNO Collaboration], nucl-ex/0106015.
- [12] R. Barbieri, G. Fiorentini, G. Mezzorani and M. Moretti, *Phys. Lett.* **B 259**, 119 (1991).
- [13] P. Vogel and J. F. Beacom, *Phys. Rev.* **D 60**, 053003 (1999) [hep-ph/9903554].
- [14] M. Aglietta *et al.*, *JETP Lett.* **63**, 791 (1996) [*Pisma Zh. Eksp. Teor. Fiz.* **63**, 753 (1996)].

- [15] C. Yanagisawa in *Proceedings of the EURESCO Conference on Frontiers in Particle Astrophysics and Cosmology, Spain, September, 2000, Nuclear Physics B*, Proceedings Supplements, 95 (2001)
- [16] <http://www.sns.ias.edu/~jnb/SNdata/Export/BP2000>; J.N. Bahcall, S. Basu and M.H. Pinsonneault, *Astrophys. J.* 529, 1084 (2000); *Astrophys. J.* 555, 990 (2001).
- [17] A. M. Dziewonski and D. L. Anderson, *Phys. Earth Planet. Inter.* 25, 297 (1981).
- [18] M. C. Gonzalez-Garcia, M. Maltoni, C. Pena-Garay and J. W. F. Valle, *Phys. Rev. D* 63, 033005 (2001) [hep-ph/0009350].
- [19] M. Apollonio *et al.* [CHOOZ Collaboration], *Phys. Lett. B* 466, 415 (1999) [hep-ex/9907037].

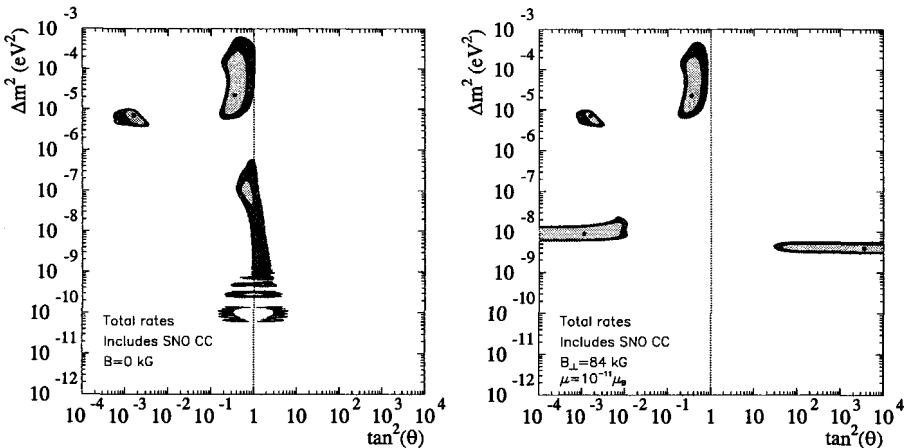


Figure 3: *Left panel:* Allowed (90% and 99% CL) solutions (SMA, LMA, LOW and VO) to the solar neutrino rates and reactor data for  $\mu_\nu, B_\perp = 0$ . *Right panel:* Allowed (90% and 99% CL) solutions (SMA, LMA, RSFP, NRSFP) to the solar neutrino rates and reactor data for  $\mu_\nu = 10^{-11} \mu_B$  and  $B_\perp = 84$  kGauss. The upper limit on the solar anti-neutrino flux according to LSD data is included.

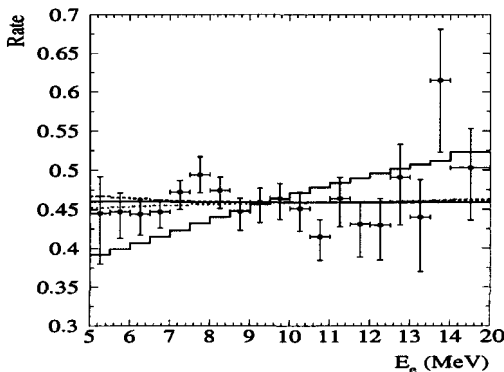


Figure 4: Predicted recoil energy spectra for spin flavour precession solutions. Solid sloping line is SMA solution, dashed line is LMA solution. Horizontal solid line is NRSFP solution, dash-dotted line is RSFP solution. Points are SuperKamiokande data.

# EFFECT OF MATTER MOTION AND POLARIZATION IN NEUTRINO FLAVOUR OSCILLATIONS

A. Grigoriev, A. Lobanov, A. Studenikin<sup>a</sup>

*Department of Theoretical Physics, Moscow State University,  
119992 Moscow, Russia*

*Abstract.* The Lorentz invariant formalism for description of neutrino flavour oscillations in moving and polarized matter is developed. It is shown that the neutrino effective potential, which determines the effective mass difference between neutrinos in matter can be significantly changed by relativistic motion of matter. In the case of matter motion parallel to neutrino propagation, matter effects in neutrino flavour oscillations are suppressed. In the case of relativistic motion of matter in the opposite direction substantial increase of effects of matter in neutrino oscillations is predicted. The dependence of the matter term in neutrino effective potential on the values and correlations of the three vectors, the neutrino and matter speeds and matter polarization, is discussed in detail.

The problem of neutrino propagation in matter, starting from the paper of Wolfenstein [1], is still under intensive study. One of the most famous results in this field was obtained by Mikheyev and Smirnov [2] who showed that there is a mechanism for resonance amplification of neutrino flavour oscillations in matter (the MSW effect). Now it is commonly believed that neutrino oscillations in matter can provide not only solutions for the solar and atmospheric neutrino puzzles but also have important applications in different astrophysical and cosmology environments (see, for example, [3]- [5] and references therein).

In this paper <sup>b</sup> we should like to discuss a new phenomenon in neutrino flavour oscillations in matter that have never been considered before neither in textbooks and monographs on neutrino physics nor in papers in research journals. We show below (see also [6]) that the matter Wolfenstein term in neutrino effective potential can be substantially increased or suppressed in the case of matter moving with relativistic speed. This effects can lead to interesting consequences for environments with neutrino propagating through relativistic jets of matter. As an example, we point out that astrophysical systems, such as quasars and microquasars, are believed to emit collimated relativistic jets of plasma. Another important application of the studied here effect can be found within several models of gamma-ray bursts ( see for a resent review [7]) where highly relativistic matter with Lorentz factor  $\gamma \sim 10^2 - 10^3$  is supposed to be accelerated in the fireball shocks.

In the frame of the Lorentz invariant approach (see [6], [8]- [11]) to description of the neutrino flavour and spin oscillations in matter we get below the effective neutrino potential which contributes to the Hamiltonian describing neutrino evolution in the case of matter motion with arbitrary (also relativistic) total speed. We show here that the matter motion could lead to sufficient change in the neutrino flavour oscillation probabilities and other neutrino oscillation parameters (like the effective mixing angle and oscillation length) if matter is moving with relativistic speed. In particular, in the case of matter moving parallel to the neutrino propagation, the Wolfenstein matter

---

<sup>a</sup>E-mail: studenik@srp.sinp.msu.ru

<sup>b</sup>This paper is published in Phys.Lett.B535 (2002) 187

term in the neutrino effective potential is suppressed. Contrary to this suppression effect, in the case of relativistic motion of matter in the opposite direction in respect to neutrino propagation, substancial increase of effects of matter in neutrino flavour oscillations is predicted. We also argue that effects of matter motion have to be accounted for in the resonance conditions for the neutrino flavour oscillations. Effects of matter polarization are also taken into account, and the dependence of the matter term in neutrino effective potential on the values and correlations of the three vectors, the neutrino and matter speeds and matter polarization, are discussed in detail.

It should be also noted here that effects of matter polarization in neutrino oscillations were considered previously in several papers ( see, for example, [12, 13] and references therein). However, the procedure used in refs. [12, 13] of accounting for the matter polarization effect does not enable one to study the case of matter motion with total relativistic speed. Within our approach we can reproduce corresponding results of [12, 13] in the case of matter which is slowly moving or is at rest.

Our goal is to investigate neutrino oscillations characteristics in the case of relativistic motion of matter which is composed of different charged and neutral background fermions,  $f = e, n, p, \mu, \tau, \nu_e, \nu_\mu, \nu_\tau$ , etc, accounting for possible effects of matter motion and polarization. In the general case each of the matter components is characterised by the number density  $n_f$ , the speed,  $\vec{v}_f$ , of the reference frame in which the mean momentum of the fermion  $f$  is zero, and fermion polarization  $\lambda_f^\mu$ . The fermion  $f$  current is determined as

$$j_f^\mu = (n_f, n_f \vec{v}_f). \quad (1)$$

If a component of the matter  $f$  is slowly moving or is at rest in the laboratory frame,  $v_f \approx 0$ , the fermion current equals

$$j_f^\mu = (n_f, 0, 0, 0). \quad (2)$$

The polarization of each of the matter components  $f$  is given by

$$\lambda_f^\mu = \left( n_f \vec{\zeta}_f \vec{v} 1_f, n_f \vec{\zeta}_f \sqrt{1 - v_f^2} + \frac{n_f \vec{v}_f (\vec{\zeta}_f \vec{v}_f)}{1 + \sqrt{1 - v_f^2}} \right). \quad (3)$$

Here vectors  $\vec{\zeta}_f$  ( $0 \leq |\vec{\zeta}_f|^2 \leq 1$ ) are the mean values of polarization vectors of background fermions  $f$  in the reference frame in which the mean momentum of fermions  $f$  is zero. These vectors are determined by the two-step averaging procedure described in ref. [10]. In the case of non-moving matter component  $f$ ,  $\vec{v}_f = 0$ , the fermion  $f$  polarization is

$$\lambda_f^\mu = (0, n_f \vec{\zeta}_f). \quad (4)$$

Let us suppose that at least one of the matter components  $f$  is moving as a whole with relativistic speed,  $v_f \approx 1$ . For simplicity, let us consider neutrino two-flavour oscillations, e.g.  $\nu_e \leftrightarrow \nu_\mu$ , in matter composed of only one component, electrons ( $f = e$ ), moving with relativistic total speed. Generalisation for the case of other types of neutrino conversions and different compositions and types of motion of matter is straightforward.

The matter effect in neutrino oscillations occurs as a result of elastic forward scattering of neutrinos on the background fermions. In our case the difference  $\Delta V$  between

the potentials  $V_e$  and  $V_\mu$  for the two-flavour neutrinos is produced by the charged current interaction of the electron neutrino with the background electrons. Note that the neutral current interaction is effective in oscillations between the active and sterile neutrinos. Concluding remarks of the paper are devoted to this type of neutrino oscillations. We do also account for effects of matter polarization which vanishes if there is no preferred spin orientation of electrons. Note that these effects were discussed in detail for neutrino flavour oscillations in non-moving matter [12] and also for neutrino spin oscillations in moving matter [10]. We neglect below the momentum dependence of the charged vector boson propagator. Then the corresponding part of the neutrino effective Lagrangian can be written in the following form (see [10] and also [14])

$$\mathcal{L}_{eff} = -f^\mu \left( \bar{\nu} \gamma_\mu \frac{1 + \gamma^5}{2} \nu \right), \quad (5)$$

where

$$f^\mu = \sqrt{2} G_F (j_e^\mu - \lambda_e^\mu). \quad (6)$$

This additional term in the Lagrangian modifies the Dirac equation:

$$(\gamma_0 E - \vec{\gamma} \vec{p} - m) \psi = (\gamma_\mu f^\mu) \psi. \quad (7)$$

Rearranging the terms we get the neutrino dispersion relation in matter in the following form,

$$E = \sqrt{(\vec{p} - \vec{f})^2 + m^2} + f_0. \quad (8)$$

The further simplification is found to occur in the limit of weak potential  $|\vec{f}| \ll p_0 = \sqrt{\vec{p}^2 + m^2}$ . Thus we get for the effective energy of the electron neutrino in the moving and polarized matter

$$E = \sqrt{\vec{p}^2 + m^2} + U \left\{ (1 - \vec{\zeta}_e \vec{v}_e) (1 - \vec{\beta} \vec{v}_e) + \sqrt{1 - v_e^2} \left[ \vec{\zeta}_e \vec{\beta} - \frac{(\vec{\beta} \vec{v}_e)(\vec{\zeta}_e \vec{v}_e)}{1 + \sqrt{1 - v_e^2}} \right] \right\} + O(\gamma_\nu^{-1}), \quad (9)$$

where  $\vec{\beta}$  is the neutrino speed,  $\gamma_\nu = (1 - \beta^2)^{-1/2}$ , and in the considered case of the two-flavour neutrino oscillations  $\nu_e \leftrightarrow \nu_\mu$  and one-component matter  $U = \sqrt{2} G_F n_e$ .

The effective electron neutrino energy in addition to the vacuum energy  $p_0$  contains the matter term which is proportional to the electron number density  $n_e$ . Let us underline that  $n_e$  is related to the invariant electron number density  $n_0$  given in the reference frame for which the total speed of electrons is zero,

$$n_e = n_0 / \sqrt{1 - v_e^2}. \quad (10)$$

There is no matter term in the muon neutrino effective energy in the case of matter composed of only electrons. If matter is slowly moving or is at rest,  $v_e \approx 0$ , eq. (9) includes the well known result for the Wolfenstein matter term [1].

The important new phenomenon, as it can be seen from eq. (9), is the matter term dependence on the value of the total speed  $\vec{v}_e$ , polarization  $\vec{\zeta}_e$  of background electrons, neutrino speed  $\vec{\beta}$  and correlations between these three vectors.

Now following the usual procedure for the two-flavour neutrinos,  $\nu_e$  and  $\nu_\mu$ , with mixing in the high-energy limit it is possible to get the constant-density solution for the neutrino oscillation problem. Thus, the probability of neutrino conversion  $\nu_e \rightarrow \nu_\mu$  can be written in the form

$$P_{\nu_e \rightarrow \nu_\mu}(x) = \sin^2 2\theta_{eff} \sin^2 \frac{\pi x}{L_{eff}}, \quad (11)$$

where  $x$  is the distance travelled by neutrino in moving and polarized matter. The effective mixing angle,  $\theta_{eff}$ , and the effective oscillation length,  $L_{eff}$ , are given by

$$\sin^2 2\theta_{eff} = \frac{\Delta^2 \sin^2 2\theta}{(\Delta \cos 2\theta - A)^2 + \Delta^2 \sin^2 2\theta}, \quad (12)$$

$$L_{eff} = \frac{2\pi}{\sqrt{(\Delta \cos 2\theta - A)^2 + \Delta^2 \sin^2 2\theta}}. \quad (13)$$

Here  $\Delta = \delta m_\nu^2 / 2|\vec{p}|$ ,  $\delta m_\nu^2 = m_2^2 - m_1^2$  is the difference of the neutrino masses squared,  $\vec{p}$  is the neutrino momentum,  $\theta$  is the vacuum mixing angle and

$$A = \sqrt{2}G_F \frac{n_0}{\sqrt{1 - v_e^2}} \left\{ (1 - \vec{\beta}\vec{v}_e)(1 - \vec{\zeta}_e\vec{v}_e) + \sqrt{1 - v_e^2} \left[ \vec{\zeta}_e\vec{\beta} - \frac{(\vec{\beta}\vec{v}_e)(\vec{\zeta}_e\vec{v}_e)}{1 + \sqrt{1 - v_e^2}} \right] \right\}. \quad (14)$$

One can see that the neutrino oscillation probability,  $P_{\nu_e \rightarrow \nu_\mu}(x)$ , the mixing angle,  $\theta_{eff}$ , and the oscillation length,  $L_{eff}$ , exhibit dependence on the total speed of electrons  $\vec{v}_e$ , correlation between  $\vec{\beta}$ ,  $\vec{v}_e$  and polarization of matter  $\vec{\zeta}_e$ . The resonance condition

$$\frac{\delta m_\nu^2}{2|\vec{p}|} \cos 2\theta = A, \quad (15)$$

at which the probability has unit amplitude no matter how small the mixing angle  $\theta$  is, also depends on the motion and polarization of matter and neutrino speed. We show below that the relativistic motion of matter could provide appearance of the resonance in the neutrino oscillations in certain cases when for the given neutrino characteristics,  $\delta m_\nu^2$ ,  $|\vec{p}|$  and  $\theta$ , and the invariant matter density at rest,  $n_0$ , the resonance is impossible.

Let us consider first unpolarized matter,  $\zeta_e \approx 0$ . Then the expression in the right hand side of eq. (15) is equal to the difference of the vector parts of neutrino  $\nu_e$  and  $\nu_\mu$  effective potentials (see also [6]),

$$V^V = \sqrt{2}G_F \frac{n_0}{\sqrt{1 - v_e^2}} (1 - \vec{\beta}\vec{v}_e). \quad (16)$$

The resonance condition (15) can be rewritten as

$$\frac{\delta m_\nu^2}{2|\vec{p}|} \cos 2\theta = \sqrt{2}G_F \frac{n_0}{\sqrt{1 - v_e^2}} (1 - \vec{\beta}\vec{v}_e). \quad (17)$$

Note that the value of  $n_0$  gives the matter density in the reference frame for which the total speed of matter is zero. It follows that the effect of matter motion in the resonance condition depends on the factor

$$a = \frac{1 - \vec{\beta} \vec{v}_e}{\sqrt{1 - v_e^2}}. \quad (18)$$

The appearance of the same factor in the matter term for neutrino spin oscillations was shown in [10].

If one estimates this factor for the ultra-relativistic neutrinos,  $\beta \approx 1$ , and matter moving along the direction of neutrino propagation with total speed  $v_e$ , then

$$\frac{1 - \vec{\beta} \vec{v}_e}{\sqrt{1 - v_e^2}} = \sqrt{\frac{1 - v_e}{1 + v_e}}. \quad (19)$$

Here we suppose that the condition  $\gamma_e \ll \gamma_\nu$  is valid,  $\gamma_e = (1 - v_e^2)^{-1/2}$ . For example, this condition in the case of the neutrino mass and energy to be equal to  $m_\nu \sim 2\text{eV}$  and  $E_\nu \sim 10\text{MeV}$  sets a limit on the total energy of the background electrons on the level of  $E_e < 2.5\text{TeV}$ . In the opposite case, when matter is moving against the direction to the neutrino propagation, we get

$$\frac{1 - \vec{\beta} \vec{v}_e}{\sqrt{1 - v_e^2}} = \sqrt{\frac{1 + v_e}{1 - v_e}}. \quad (20)$$

From these estimations it follows (see [6]) that: 1) the relativistic motion of matter,  $v_e \sim 1$ , along the neutrino propagation could provide the resonance increase of the oscillation probability if the matter density  $n_0$  is too high for the resonance appearance in non-moving matter, 2) the relativistic motion of matter in opposite direction to the neutrino propagation could provide the resonance increase of the oscillation probability if the matter density  $n_0$  is too low for the resonance appearance in non-moving matter.

Now let us discuss the case when the matter polarization effects are also important,  $\vec{\zeta}_e \neq 0$ . Consider the axial part of the difference of neutrino effective potentials. From the general expression, eq.(14), for  $A = V^V + V^A$  we find that the axial part is given by

$$V^A = \sqrt{2} G_F n_0 \left\{ \vec{\zeta}_e \vec{\beta} - \frac{(1 - \vec{\beta} \vec{v}_e)(\vec{\zeta}_e \vec{v}_e)}{\sqrt{1 - v_e^2}} - \frac{(\vec{\beta} \vec{v}_e)(\vec{\zeta}_e \vec{v}_e)}{1 + \sqrt{1 - v_e^2}} \right\}. \quad (21)$$

In the case of non-moving matter,  $v_e \sim 0$ , we find

$$V^A = \sqrt{2} G_F n_0 \vec{\zeta}_e \vec{\beta}. \quad (22)$$

This result coincides with the corresponding expression of ref. [12] if one follows approximation  $\vec{\beta} = \vec{k}_\nu$ , where  $\vec{k}_\nu = \vec{p}_\nu / |\vec{p}_\nu|$  is the unit vector in the direction of the neutrino momentum.

We get the same result, eq. (22), if electrons are polarized in the transverse plane,  $\vec{\zeta}_e \vec{v}_e = 0$ . Let us underline that due to the condition  $\vec{\zeta}_e \perp \vec{v}_e$  the axial potential  $V^A$  does not depend on the absolute value of matter speed  $v_e$ . In this case for the relativistic neutrino  $V^A$  is zero only if neutrino is also propagating in the perpendicular

direction to the matter polarization. Note that this statement is valid also for the case of the relativistic motion of matter (see below).

In an analogy with what have been found for the matter term in the neutrino spin oscillations [10], the potential  $V^A$  exhibits critical dependence on the correlation between the direction of the neutrino propagation,  $\vec{k}_\nu$ , and the direction of the matter motion given by the unit vector ( $\vec{k}_e = \vec{v}_e/v_e$ ). For these two particular cases,  $\vec{k}_\nu \cdot \vec{k}_e = \pm 1$ , from eq. (21) we get

$$V^A \Big|_{(\vec{k}_\nu \cdot \vec{k}_e)=1} = \sqrt{2} G_F n_0 \zeta_e \vec{k}_\nu \sqrt{\frac{1-v_e}{1+v_e}}, \quad (23)$$

and

$$V^A \Big|_{(\vec{k}_\nu \cdot \vec{k}_e)=-1} = \sqrt{2} G_F n_0 \zeta_e \vec{k}_\nu \sqrt{\frac{1+v_e}{1-v_e}}. \quad (24)$$

For the neutrino and matter motion along one line with respect to the sign of  $\vec{k}_\nu \cdot \vec{k}_e = \pm 1$  there can be a significant decrease (see also ref. [12]) and increase of matter term. Let us compare eqs. (23) and (24) with eq. (22) for the potential  $V^A$  which is also valid for the transversal polarization,  $\zeta_e \vec{v}_e = 0$ , and relativistic motion of matter,  $v_e \sim 1$ . It follows that in the relativistic case and transversal polarization of matter the potential  $V^A$  is zero not for any momenta of neutrinos (as it was claimed in [12]), but only when neutrino is also propagating in the transverse plane with respect to the matter polarization and in addition to  $\zeta_e \vec{v}_e = 0$  the condition  $\zeta_e \vec{k}_\nu = 0$  is valid.

The total potential  $A = V^V + V^A$  for arbitrary motion of matter in the direction of the neutrino propagation,  $\vec{k}_e \cdot \vec{k}_\nu = 1$ , as it follows from eqs. (16), (19) and (23), is

$$A = \sqrt{2} G_F n_0 \sqrt{\frac{1-v_e}{1+v_e}} (1 + \zeta_e \vec{k}_\nu). \quad (25)$$

The total potential  $A$  in the relativistic case has a general suppression factor  $(1-v_e)^{1/2} \ll 1$ , and is zero for the complete matter polarization  $\zeta_e \vec{k}_e = -1$ . In the case of opposite motion of matter and the neutrino,  $\vec{k}_e \cdot \vec{k}_\nu = -1$ , from eqs. (16), (20) and (24) we get for the total potential,

$$A = \sqrt{2} G_F n_0 \sqrt{\frac{1+v_e}{1-v_e}} (1 + \zeta_e \vec{k}_\nu). \quad (26)$$

It follows that the total potential can be substantially increased for the relativistic motion of matter due to the factor  $(1-v_e)^{-1/2} \gg 1$ , however in the case of the longitudinal polarization of matter,  $\zeta_e \vec{k}_e = 1$ , the potential is zero.

In conclusion it is worth noting that a similar analysis can be performed for any type of the neutrino flavour conversion and different matter composition. As it follows from the above considerations, there could be a decrease (increase) of the particular matter component contribution to the difference of neutrino potentials if the matter component is moving along (against) the direction of neutrino propagation. If different matter components move with different speeds, the difference of neutrino effective potentials in the general case depends on each of the speeds. As an example, let us

consider the case of electron neutrino  $\nu_e$  conversion into sterile neutrino  $\nu_s$  in the presence of matter composed of electrons, protons and neutrons. We also suppose that each of the matter components is characterised by its total speed  $\vec{v}_{e,p,n}$  and invariant number density  $n_0^{e,p,n}$ . For simplicity we consider the unpolarized matter components, then

$$A_{\nu_e \nu_s} = \frac{\sqrt{2}G_F}{2} \left\{ \frac{n_0^e(1+4\sin^2\theta_W)}{\sqrt{1-v_e^2}}(1-\beta\vec{v}_e) + \right. \\ \left. \frac{n_0^p(1-4\sin^2\theta_W)}{\sqrt{1-v_p^2}}(1-\beta\vec{v}_p) - \frac{n_0^n}{\sqrt{1-v_n^2}}(1-\beta\vec{v}_n) \right\}. \quad (27)$$

From this expression it follows that new phenomena are expected to appear in the case of moving matter which are absent if matter is at rest. For instance, it is easy to see that if  $\vec{v}_e \neq \vec{v}_p$ , then the neutral current contributions from the electron neutrino elastic forward scattering off the background electrons and protons does not cancel even in the case when the electron and proton invariant densities are equal  $n_e^{(0)} = n_p^{(0)}$ . This phenomenon can exist in the relativistically expanding fireballs which are predicted within several models of gamma-ray bursts [7] and in which the electron Lorentz factor may exceed that of the proton by a factor up to the ratio of the proton to the electron mass.

## References

- [1] L.Wolfenstein, Phys.Rev.D17 (1978) 2369.
- [2] S.Mikheyev, A.Smirnov, Sov.J.Nucl.Phys.42 (1985) 913.
- [3] G.Raffelt, Stars as Laboratories for Fundamental Physics, the Univ. of Chicago Press, Chicago and London, 1996.
- [4] E.Kolb, M.Turner, The Early Universe, Addison Wesley, 1993.
- [5] A.Dolgov, S.Hansen, S.Pastor, S.Petcov, G.Raffelt, D.Semikoz, hep-ph/0201287.
- [6] A.Grigoriev, A.Lobanov, A.Studenikin,hep-ph/0112304,hep-ph/0202276.
- [7] P.Mészáros, Theories of Gamma-Ray Bursts, astro-ph/0111170, to appear in Annu.Rev.Astron.Astrophys.40 (2002).
- [8] A.Egorov, A.Lobanov, A.Studenikin, in: New Worlds in Astroparticle Physics, ed. by A. Mourao, M. Pimenta, P. Sa, World Scientific, Singapore, p. 153, 1999; hep-ph/9902447.
- [9] A.Egorov, A.Lobanov, A.Studenikin, Phys.Lett.B491 (2000) 137, hep-ph/9910476.
- [10] A.Lobanov, A.Studenikin, Phys.Let.B515 (2001) 94; hep-ph/0106101.
- [11] M.Dvornikov, A.Egorov, A.Lobanov, A.Studenikin, in: Particle Physics at the Start of the New Millennium, ed. by A.Studenikin, World Scientific, Singapore, 2001, p. 178; hep-ph/0103015.
- [12] H.Nunokawa,V.Semikoz,A.Smirnov,J.W.F.Valle,Nucl.Phys.B501('97)17.
- [13] S.Bergmann, Y.Grossman, E.Nardi, Phys.Rev.D60 (1999) 093008.
- [14] P.Pal, Int.J.Mod.Phys. A 7 (1992) 5387.

# HIGH-ENERGY NEUTRINO FROM A NASCENT MASSIVE BLACK HOLE

V. S. Berezinsky<sup>†‡ a</sup>, V. I. Dokuchaev<sup>† b</sup>

<sup>†</sup>*Institute for Nuclear Research, Russian Academy of Sciences, Moscow, Russia*

<sup>‡</sup>*Laboratori Nazionali del Gran Sasso, INFN, Italy*

**Abstract.** It is described the astrophysical model of a short-lived and very powerful hidden source of high-energy neutrinos. This source is formed as a result of dynamical evolution of a galactic nucleus prior to its collapse into the massive black hole. A dense central stellar cluster in the galactic nucleus on the late stage of evolution consists of compact stars (neutron stars and stellar mass black holes) deep inside the massive gas envelope produced by destructive collisions of a primary stellar population. Frequent collisions of neutron stars result in a creation of an expanding rarefied cavity in the envelope. Particles are effectively accelerated in the cavity and, due to pp-collisions in the gas envelope, they produce high-energy neutrinos. High-energy neutrino signal can be detected by underground neutrino telescope with effective area  $S \sim 1 \text{ km}^2$ .

## 1 Introduction

High-energy (HE) neutrino radiation from astrophysical sources is accompanied by other types of radiation, most notably by the HE gamma-radiation. These HE gamma-radiation can be used to put upper limit on the neutrino flux emitted from a source. For example, if neutrinos are produced due to interaction of HE protons with low energy photons in extragalactic space or in the sources transparent for gamma radiation, the upper limit on diffuse neutrino flux  $I_\nu(E)$  can be derived from e-m cascade radiation (see e. g. [1]). However, there can be sources, where accompanying electromagnetic radiation, such as gamma and X-rays, are absorbed. They are called “hidden sources” [2]. Several models of hidden sources were discussed in the literature. *Young SN shells* [3] during time  $t_\nu \sim 10^3 - 10^4$  s are opaque for all radiation, but neutrinos. *The Thorne-Zytkow star* [4], the binary with a pulsar submerged into a red giant, can emit HE neutrinos while all kinds of e-m radiation are absorbed by the red giant component. *Cocooned massive black hole* (MBH) in AGN [5] is an example of AGN as hidden source: e-m radiation is absorbed in a cocoon around the massive black hole. *AGN with a standing shock* in vicinity of the MBH [6] can produce large flux of HE neutrinos with relatively weak X-ray radiation.

Here we describe our recent model [1] of a hidden source which can operate in galactic nucleus at pre-AGN phase, i.e. prior to MBH formation. MBH in AGN is produced as a result of the dynamical evolution of the central stellar cluster (see for review e. g. [7]). The first stage of this evolution is accompanied by collisions and destruction of normal stars in a relatively large volume, where virial velocities of the stars are large enough for the disruption. The compact stars (neutron stars and black holes) survive this stage and their population continue to contract, being surrounded by gas cloud from disrupted normal stars. Collisions of these stars result in formation of a rarefied cavity filled by the fireballs and shocks surrounded by slowly

---

<sup>a</sup>e-mail: berezinsky@lngs.infn.it

<sup>b</sup>e-mail: dokuchaev@inr.npd.ac.ru

expanding gas envelope. Particles accelerated in this cavity interact with the envelope gas, producing HE neutrinos. Accompanying gamma radiation can be fully absorbed in the case of thick envelope (matter depth  $X_{env} \sim 10^4 \text{ g/cm}^2$ ). The proposed source is short-lived (lifetime  $t_s \sim 10 \text{ years}$ ) and very powerful: neutrino luminosity exceeds the Eddington limit for e-m radiation.

## 2 The Model of Hidden Source

The dynamical evolution of dense central stellar clusters in the galactic nuclei is accompanied by the secular growth of the velocity dispersion of constituent stars  $v$  or, equivalently, by the growth of the central gravitational potential. On its way to the MBH formation the dense galactic nuclei inevitably proceed through the stellar collision phase of evolution [8]–[12], when all normal stars in the cluster are disrupted in mutual collisions of fast-moving constituent stars. The necessary condition for the collisional destruction of normal stars with mass  $m_*$  and radius  $r_*$  in the cluster of identical stars with a velocity dispersion  $v$  is  $v > v_p$ , where  $v_p = (2Gm_*/r_*)^{1/2} \simeq 6.2 \cdot 10^2 (m_*/M_\odot)^{1/2} (r_*/R_\odot)^{-1/2} \text{ km s}^{-1}$ . is an escape (parabolic) velocity from the surface of a constituent normal star. If  $v > v_p$ , the normal stars are eventually disrupted in mutual collisions or in collisions with the extremely compact stellar remnants: neutron stars (NSs) or stellar mass black holes (BHs).

Only compact stellar remnants, NSs or stellar mass BHs, survive through the stellar-destruction phase of evolution ( $v = v_p$ ) and form the self-gravitating core. We shall refer to this core as to the NS cluster. Meanwhile the remnants of disrupted normal stars form a gravitationally bound massive gas envelope in which the NS cluster is submerged. A virial radius of this envelope is

$$R_{env} = \frac{GM_{env}}{2v_p^2} = \frac{1}{4} \frac{M_{env}}{m_*} r_* \simeq 0.56 M_8 \left( \frac{m_*}{M_\odot} \right)^{-1} \left( \frac{r_*}{R_\odot} \right) \text{ pc}, \quad (1)$$

where  $M_{env} = 10^8 M_8 M_\odot$  is a corresponding mass of the envelope. The natural range for the total mass of the envelope is the same as the typical range for the mass of a central stellar cluster in the galactic nucleus,  $M_{env} = 10^7 - 10^8 M_\odot$ . A radius of the envelope  $R_{env}$  is fixed by the virial radius of the central cluster of the galactic nucleus at the moment of evolution when  $v = v_p$ . The mean number density of gas in the envelope is

$$n_{env} = \frac{3}{4\pi} \frac{1}{R_{env}^3} \frac{M_{env}}{m_p} \simeq 5.4 \cdot 10^9 M_8^{-2} \left( \frac{m_*}{M_\odot} \right)^3 \left( \frac{r_*}{R_\odot} \right)^{-3} \text{ cm}^{-3}, \quad (2)$$

where  $m_p$  is a proton mass. The column density of the envelope is

$$X_{env} = m_p n_{env} R_{env} \simeq 1.6 \cdot 10^4 M_8^{-1} \left( \frac{m_*}{M_\odot} \right)^2 \left( \frac{r_*}{R_\odot} \right)^{-2} \text{ g cm}^{-2}. \quad (3)$$

Such an envelope completely absorbs electromagnetic radiation and HE particles outgoing from the interior, except neutrinos and gravitational waves.

The dense NS cluster survives inside the massive envelope of the post-stellar-destruction galactic nucleus. The total mass of this cluster is  $\sim 1 - 10 \%$  of the

total mass of a progenitor galactic nucleus and so of the massive envelope, i. e.  $M \sim 0.01 - 0.1 M_{env}$ . We consider in the following an evolved ( $v > v_p$ ) central cluster of NSs with identical masses  $m = 1.4M_\odot$ . This evolved cluster of NSs is sunk deep into a massive gas envelope remaining after the previous evolution epoch of a typical normal galactic nucleus. Let  $N = M/m = 10^6 N_6$  is a total number of NSs stars in the cluster. The virial radius of this cluster is:

$$R = \frac{GNm}{2v^2} = \frac{1}{4} \left( \frac{c}{v} \right)^2 N r_g \simeq 1.0 \cdot 10^{13} N_6 (v/0.1c)^{-2} \text{ cm}, \quad (4)$$

where  $r_g = 2Gm/c^2$  is a gravitational radius of NS. For  $N \sim 10^6$  and  $v \sim 0.1c$  one has nearly collapsing cluster with the virial size of  $\sim 1$  AU. Characteristic times are the dynamical time  $t_{dyn} = R/v$  and the evolution (two-body relaxation) time of the NS cluster  $t_{rel} \simeq 0.1(N/\ln N)t_{dyn} \simeq 19N_6^2(v/0.1c)^{-3}$  years. This evolution time determines the duration of an active phase for the considered below hidden source, as  $t_s \sim t_{rel} \sim 10$  years.

The most important feature of our model is a secular growing rate of accidental NS collisions in the evolving cluster, accompanied by large energy release. The corresponding rate of NS collisions in the cluster (with the gravitational radiation losses taken into account) is [13]– [15]

$$\dot{N}_c = 9\sqrt{2} \left( \frac{v}{c} \right)^{17/7} \frac{c}{R} \simeq 4.4 \cdot 10^3 N_6^{-1} (v/0.1c)^{31/7} \text{ yr}^{-1}. \quad (5)$$

The time between two successive NS collisions is  $t_c = \dot{N}_c^{-1}$ . The energy of one fireball is  $E_0 = E_{52} 10^{52}$  ergs, and the total energy release in the form of fireballs during lifetime of the hidden source  $t_s \sim 10$  yr is  $E_{tot} \sim \dot{N}_c E_0 t_s \sim 4 \cdot 10^{56}$  ergs, where  $\dot{N}_c$  is the NS collision rate. The relevant parameter of a fireball is the total baryonic mass  $M_0 = E_0/\eta c^2 \simeq 5.6 \cdot 10^{-6} E_{52} \eta_3^{-1} M_\odot$ , where baryon-loading mass parameter  $\eta = 10^3 \eta_3$ . The maximum possible Lorentz factor of expanding fireball is  $\Gamma_f = \eta + 1$  during the matter-dominated phase of fireball expansion [16]. Fireball expands with  $\Gamma \gg 1$  up to the distance determined by the Sedov length

$$l_S = \left( \frac{3}{4\pi} \frac{E_0}{\rho_{env} c^2} \right)^{1/3} \simeq 1.2 \cdot 10^{15} n_9^{-1/3} E_{52}^{1/3} \text{ cm}. \quad (6)$$

Each fireball hitting the dense envelope is preceded by a shock. Propagating through envelope the shock sweeps up the gas ahead of it and decelerates. The swept up gas forms a thin shell with a density profile given by Sedov self-similar solution. The next fireball hits this thin shell when it decelerated to non-relativistic velocity. Moving in the envelope, the shell accumulates more gas, keeping the same density profile, and then it is hit by a new fireball again. The density perturbation in the envelope propagates as the shock until  $v_{sh}$  remains higher than sound speed  $v_s$ .

The rarefied cavity after swept out gas is filled by direct and reversed relativistic shocks from fireballs. The total number of fireballs existing in the cavity simultaneously can be estimated as  $N_f \sim R_{cav}/R_c$ , where  $R_c = ct_c$  is the repeating fireballs are ultrarelativistic inside the cavity and mildly relativistic in the envelope. Collisions of multiple shocks in the cavity, as well as inside fireballs, produce strongly turbulized

medium favorable for generation of magnetic fields and particle acceleration by Fermi II acceleration mechanism. We assume the existence of equipartition magnetic field in the cavity, induced by turbulence and dynamo mechanism. For the turbulent shell at the boundary between cavity and envelope, assuming mildly relativistic turbulence  $u_t \sim c$  and  $\rho \sim \rho_{env}$  we obtain  $H_{eq} = 4 \cdot 10^3$  G. The maximum acceleration energy is  $E_{max} = 2 \cdot 10^{21}$  eV, if the coherent length of magnetic field  $L_0$  is given by the Sedov length  $L_S$ , and the acceleration time is  $t_{acc} = 4 \cdot 10^4 E_{52}^{1/3} n_9^{-1/3}$  s. The typical time of energy losses, determined by  $pp$ -collisions, is much longer than  $t_{acc}$ , and does not prevent acceleration to  $E_{max}$  given above:

$$t_{pp} = \left( \frac{1}{E} \frac{dE}{dt} \right)^{-1} = \frac{1}{f_p \sigma_{pp} n_{env} c} \simeq 2 \cdot 10^6 n_9^{-1} \text{ s}, \quad (7)$$

where  $f_p \approx 0.5$  is the fraction of energy lost by HE proton in one collision,  $\sigma_{pp}$  is a cross-section of  $pp$ -interaction, and  $n_{env}$  is the gas number density in the boundary turbulent shell.

### 3 Neutrino Production and Detection

We assume that about half of the total power of the source  $L_{tot}$  is converted into energy of accelerated particles  $L_p \sim 7 \cdot 10^{47}$  erg/s. Taking into account the magnetic field, one concludes that accelerated protons loose in the dense envelope a substantial fraction of their energy. The charged pions, produced in  $pp$ -collisions, with Lorentz factors up to  $\Gamma_c \sim 1/(\sigma_{\pi N} n_{env} c \tau_\pi) \sim 4 \cdot 10^{13} n_9^{-1}$  freely decay in the envelope (here  $\sigma_{\pi N} \sim 3 \cdot 10^{-26}$  cm<sup>2</sup> is  $\pi N$ -cross-section,  $\tau_\pi$  is the lifetime of charged pion, and  $n_{env} = 10^9 n_9$  cm<sup>-3</sup> is the number density of gas in the envelope). We assume  $E^{-2}$  spectrum of accelerated protons  $Q_p(E) = L_p/\zeta E^2$ , where  $\zeta = \ln(E_{max}/E_{min}) \sim 20 - 30$ . About half of its energy protons transfer to high-energy neutrinos through decays of pions,  $L_\nu \sim (2/3)(3/4)L_p$ . So the production rate of  $\nu_\mu + \bar{\nu}_\mu$  neutrinos is  $Q_{\nu_\mu + \bar{\nu}_\mu}(> E) = (L_p/4\zeta)E^{-2}$ . Crossing the Earth, these neutrinos create deep underground the equilibrium flux of muons, which can be calculated as [17]:

$$F_\mu(> E) = \frac{\sigma_0 N_A}{b_\mu} Y_\mu(E_\mu) \frac{L_p}{4\xi E_\mu} \frac{1}{4\pi r^2}, \quad (8)$$

where the normalization cross-section  $\sigma_0 = 1 \cdot 10^{-34}$  cm<sup>2</sup>,  $N_A = 6 \cdot 10^{23}$ ,  $b_\mu = 4 \cdot 10^{-6}$  cm<sup>2</sup>/g is the rate of muon energy losses,  $Y_\mu(E)$  is the integral muon moment of  $\nu_\mu N$  interaction (see e. g. [2, 17]). The most effective energy of muon detection is  $E_\mu \geq 1$  TeV [17]. The rate of muon events in the underground detector with effective area  $S$  at distance  $r$  from the source is given by

$$\dot{N}(\nu_\mu) = F_\mu S \simeq 70 \left( \frac{L_p}{10^{48} \text{ erg s}^{-1}} \right) \left( \frac{S}{1 \text{ km}^2} \right) \left( \frac{r}{10^3 \text{ Mpc}} \right)^{-2} \text{ yr}^{-1}. \quad (9)$$

Thus, we expect about 10 muons per year from the source at distance  $10^3$  Mpc.

The duration of the active phase  $t_s$  is determined by relaxation time of the NS cluster:  $t_s \sim t_{rel} \sim 10 - 20$  yr. This stage appears only once during the lifetime of a

galaxy, prior to the MBH formation. If to assume that a galactic nucleus turns after it into AGN, the total number of hidden sources in the Universe can be estimated as

$$N_{HS} \sim \frac{4}{3}\pi(3ct_0)^3 n_{AGN} t_s / t_{AGN}, \quad (10)$$

where  $\frac{4}{3}\pi(3ct_0)^3$  is the cosmological volume inside the horizon  $ct_0$ ,  $n_{AGN}$  is the number density of AGNs and  $t_{AGN}$  is the AGN lifetime. The estimates for  $n_{AGN}$  and  $t_{AGN}$  taken for different populations of AGNs result in  $N_{HS} \sim 10 - 100$ .

#### 4 Conclusions

Dynamical evolution of the central stellar cluster in the galactic nucleus results in the stellar destruction of the constituent normal stars and in the production of massive gas envelope. The fast repeating fireballs caused by NS collisions inside this envelope create the rarefied cavity inside the massive envelope. Colliding fireballs and shocks produce the turbulence in the cavity, and particles are accelerated by Fermi II mechanism. All high-energy particles, except neutrinos, can be completely absorbed in the thick envelope. In this case the considered source is an example of a powerful hidden source of HE neutrinos.

In all cases the thickness of the envelope is much larger than the Thompson thickness ( $x_T \sim 3 \text{ g/cm}^2$ ), and this condition provides the absorption and X-rays and low energy gamma-rays.

A hidden source is to be seen as a bright quasar in optical region or as a bright IR source. A considered source is a precursor of most powerful AGN, and therefore most of these sources are expected to be at the same redshifts as AGNs. Moreover, for most of the hidden sources the distance cannot be determined, and thus they fall into category of faint non-identified IR sources or distant quasars.

The expected duration of neutrino activity for a hidden source is  $\sim 10 \text{ yr}$ , and the total number of hidden sources in the horizon volume ranges from a few up to  $\sim 100$ , within uncertainties of the estimates. Underground neutrino detector with an effective area  $S \sim 1 \text{ km}^2$  will observe  $\sim 10$  muons per year with energies  $E_\mu \geq 1 \text{ TeV}$  from this hidden source.

#### Acknowledgments

We are grateful to Bohdan Hnatyk for useful discussions. This work was supported in part by the INTAS through grant No. 99-1065.

#### References

- [1] V.S.Berezinsky, V.I.Dokuchaev, *Astrop.Phys.* 15, 87 (2001).
- [2] V.S.Berezinsky, S.V.Bulanov, V.A.Dogiel, V.L.Ginzburg, V.S.Ptuskin, *Astrophysics of Cosmic Rays*, North-Holland, Amsterdam, 1990.
- [3] V.S. Berezinsky, O.F. Prilutsky, *Astron. Astrophys.* 66, 325 (1987).
- [4] K.S.Thorne, A.N.Zytkow, *Astrophys.J.* 212, 832 (1977).
- [5] V.S.Berezinsky, V.L.Ginzburg, *Mon.Not.R.Astron.Soc.* 194, 3 (1981).

- [6] F.W.Stecker, C.Done, M.H.Salamon, P.Sommers, *Phys.Rev.Lett.* 66, 2697 (1991).
- [7] M.J. Rees, *Ann.Rev.Astron.Astrophys* 22, 471 (1984).
- [8] L.Spitzer, W.C.Saslaw, *Astrophys.J.* 143, 400 (1966).
- [9] S.A. Colgate, *Astrophys.J.* 150, 163 (1967).
- [10] R.H.Sanders, *Astrophys.J.* 162, 791 (1970).
- [11] L.Spitzer, *Galactic Nuclei*, ed by D.Q'Connel, North Holland, Amsterdam, p. 443, 1971.
- [12] V.I. Dokuchaev, *Mon.Not.R.Astron.Soc.* 251, 564 (1991).
- [13] C.D.Quinlan, S.L.Shapiro, *Astrophys.J.* 321, 199 (1987).
- [14] C.D.Quinlan, S.L.Shapiro, *Astrophys.J.* 356, 483 (1990).
- [15] V.I. Dokuchaev, Yu.N. Eroshenko, L.M. Ozernoy, *Astrophys.J.* 502, 192 (1998).
- [16] A.Shemi, T.Piran, *Astrophys.J.* 365, L55 (1990).
- [17] V. Berezinsky, *Nucl.Phys. B* (Proc. Suppl.) 19, 375 (1990).

# FROM THE EXTREME UNIVERSE SPACE OBSERVATORY (EUSO) TO THE EXTREME ENERGY NEUTRINO OBSERVATORY

S. Bottai<sup>a</sup>, P. Spillantini<sup>b</sup>

*University and INFN, Florence, Italy*

*Abstract.* The fluorescence light due to the Cosmic Rays of Extreme Energy showering in a huge mass of atmosphere, up to  $2\text{-}3 \times 10^{14}$  t, can be registered from a Low Earth Orbit (LEO: 400-1000 km of altitude). Using this technique a new field of fundamental research in Cosmology and in Astroparticle Physics can be explored. The physics of Cosmic Rays of Extreme Energy will be deeply investigated by the next generation of space detectors (EUSO, KLYPVE,...). For the Extreme Energy neutrino astronomy such detectors will probably exhibit a lack of statistics and a further increase of sensitivity will be necessary for this goal. The full coverage of the whole observable air mass from a LEO requires to cover a Field of View (FOV) of  $130^\circ\text{-}140^\circ$  by composing separate modules, each covering a smaller FOV. The ISS is the most suitable vehicle where those modules could be installed, or could be assembled in a co-flying complex. The ISS location also opens the possibility of a gradual realization of the full coverage, and a "technically evolving" approach: the optical system could be regarded as a permanent facility on board (or co-flying with) the ISS for observing the Earth surface in optical and near-optical wavelengths and different sensors could be alternated on its focal plane to meet the needs of different experiments or services. The missions currently under study can be the starting pieces for a full coverage facility.

## 1 Introduction

The discovery of cosmic ray particles with energy greater than  $10^{20}$  eV (Extreme High Energy Cosmic Rays -"EHECR") [1] has opened a new perspective for Astrophysics showing the existence of either unexpected extremely powerful acceleration mechanisms ("bottom-up") or more fundamental phenomena of emission/creation closely related to the primordial structure of the Universe ("top-down"). Furthermore if EHECR are hadrons or nuclei, the energy loss due to their interaction with the cosmic microwave background radiation (Greisen-Zatsepin-Kuzmin cut-off (GZK)) raises the fundamental question concerning the distance travelled by such particles. In case of uniform distribution of sources in the Universe, due to GZK cut-off, the observed spectrum should end around  $10^{20}$  eV. Among the possible EHECR proposed sources ("bottom-up") the most promising seem to be Active Galactic Nuclei (AGN), some types of Radio Galaxies and Gamma Ray Bursts, which also constitute some of the most interesting and mysterious objects ever observed. In general if sources yield hadronic EHECR, they produce as well photons and neutrinos of comparable energy. At present the few events observed with energy exceeding  $10^{20}$  eV [1] do not allow neither to identify the parent particles, nor the arrival

---

<sup>a</sup>e-mail: bottai@fi.infn.it

<sup>b</sup>e-mail: piero.spillantini@fi.infn.it

direction distribution and the details of the spectrum (i.e. the existence of a cut-off). The answers to these questions should clarify some fundamental issues in Astrophysics and Cosmology concerning the existence and the mechanisms of extreme energy accelerators or the possible role of topological defects. From an experimental point of view, an investigation deeper than the current ones is possible only with the realization of detectors whose acceptance is increased by several orders of magnitude with respect to present ground experiments. From the space it is possible to observe the fluorescence light emitted in the terrestrial atmosphere by the gigantic showers produced by extreme energy cosmic rays. Several experiment have been proposed for performing such an observation from orbiting spacecrafts (AIRWATCH concept) : TUS [2] on board of a Russian satellite, OWL [3] (proposed by NASA physicists) on board of two satellites in order to obtain a stereoscopic view of the shower, KLYPVE [2] on board of the Russian section of the International Space Station (ISS) and EUSO [6] as external payload attachment to the European module Columbus of the ISS. At the moment the most advanced project from a point of view of the official approval and financial support is the EUSO project, and in the following we will concentrate on it our attention. In section 2 the EUSO project will be shortly described while in sections 3,4 the EUSO parameters will be used as a "reference unit" for discussing the possibility of extending the AirWatch concept.

## 2 The EUSO project

The perspective of installing an adequate observing device on board of the ISS was suggested several years ago [4] and considered in the framework of the Airwatch concept [5]. The potentiality seemed very promising, given the enormous area of the terrestrial surface observable from the ISS. The mass of the air insisting on this surface is  $\approx 150 \cdot 10^{12}$  t, an enormous target not only for the study of extreme energy cosmic rays, but also sufficient for acting as an observatory for extreme energy neutrinos. At the end of 1999 the call for proposal issued by the European Space Agency (ESA) for the F2/F3 missions gave the occasion of proposing the EUSO experiment on board of a free flyer (as required by ESA). When, in February 2000, ESA selected the EUSO experiment for an accommodation study on board of the ISS, it was like a "return to the future", i.e. a return to the initial consideration of the ISS as a suitable vehicle for this kind of observations, with the perspective of a promising extension of the EUSO experimental approach in the future. EUSO is a space mission devoted to the investigation of EECRs and will observe the fluorescence signal looking downwards the dark Earth's atmosphere from 400 km altitude.

EUSO has been approved by the European Space Agency ESA for a Phase A study concerning its accommodation as external payload on the International

Space Station (ISS), with a goal for flight in 2008. The instrument consists of a UV telescope with large collecting area and wide field of view (FOV)  $60^\circ$  based on a double Fresnel lens system, a high segmented focal detector, and an on-board image processing acting as a trigger.

EUSO is a collaborating effort of many research groups from Europe, USA and Japan and it has been designed to operate for more than 3 years mission lifetime.

Fresnel lenses will be used for the main optics system which will provide the formation of the shower image on the focal plane (see fig. 1). An angular resolution of  $0.1^\circ$  and a full Field of View of  $60^\circ$  are the operational characteristics of the lens. The present detector design foresees a lens system with an entrance pupil diameter of 2m. The required angular resolution of  $0.1^\circ$  correspond to a ground spatial resolution of 0.8 km and yields the pixel diameter at about 5 mm. This figure leads to a total number of pixels of the order of  $2 \cdot 10^5$ . In order to prevent light of undesirable wavelengths from reaching the focal surface a band-pass filter in the wavelength comprises from 300 to 400 nm is planned for the instrument. A cover mechanism as a shutter or an iris, will be installed on the lens side to protect the optics elements and the focal surface in the diurnal orbit phase and from the pollution produced during the scheduled periodic Shuttle docking on the ISS. At present, the optical sensors that meets closely the requirements of pixel size, gain, fast response time, low weight and small dimension, has been identified in a couple of commercial multi-anode photomultiplier manufactured by Hamamatsu, series R7600-M64 (M16). These devices, which exhibit a very low cross talk and good response gain uniformity, are equipped with a bi-alkali photocatode and an UV transmitting window that assure an average Quantum Efficiency of 20% in the wavelength of interest.

The focal plane will be segmented in order to gain in modularity and adapt the detector unit to the curved focal plane. It will be constituted by about 100 macrocells each one formed by 6x6 multi-anode photomultipliers. The multi-anode photomultiplier exhibit a dead area close to 50% and hence demands a suitable light collector system to uniform the collecting area of the focal surface. A lens system, or a system made of a bundle of tapered light pipes, are the baselines solutions to this low collection problem.

In fig.2 it is reported the integral counting rate per year of EUSO, expected for the charged particle component (that here and in the following will be assumed to be constituted only by protons, for sake of simplicity) and for the  $\nu$ 's ( $\nu_e + \nu_\mu$ ) coming from the products of the interaction of the protons with the Cosmic Microwave Background (CMB) (the so called Greisen  $\nu$ 's). This is the "less un-probable" neutrino component expected at the extreme energies. To avoid to become "model dependent", no other neutrino sources will be considered, In fact, also if potentially supplying much more abundant neutrino fluxes (such as the neutrino's foreseen in the "Top-Down" processes,

or those connected in some models to the Gamma Ray Bursts (GRB's)), the previsions for their fluxes are much more uncertain. It is clear from fig.2 that EUSO, with several hundreds proton-originated events expected per year at  $E \geq 10^{20}$  eV, and several thousands per year in the  $10^{19}$ - $10^{20}$  eV range, is the adequate instrument for exploring the extreme energy region for the proton initiated showers (or whatever charged hadron primary would be). For the  $\nu$ -initiated showers EUSO can give a few Greisen  $\nu$  events, not sufficient for beginning a systematic neutrino astronomy. It must however be underlined the high discovery potential of EUSO for what concerns the Top-Down models of neutrino production.

### 3 Lowering of the energy threshold

Let's now assume EUSO on ISS as a starting point and a "unity" of measurement for discussing the potentiality of a detection system on board of the ISS that could cover the whole Field of View (FOV) from the Nadir up to the horizon observed from the ISS. Assuming the average altitude of the ISS at 400 km, the full coverage FOV is  $140.8^\circ$ , the area of the corresponding observed terrestrial surface  $\approx 15 \cdot 10^6$  km $^2$ , and the mass of the corresponding volume of air  $\approx 150 \cdot 10^{12}$  t, i.e.  $\approx 90$  times the air target observed by EUSO. For expanding EUSO in the direction of the realization of a neutrino observatory we can act in two directions: (a) going down in the energy threshold for the observation of the atmospheric showers, thus profiting of the expected increase of the rates in the lower energy region, where the flux is much higher; (b) and/or increasing the FOV for including in the observation as much as possible area of the terrestrial surface. In order to decrease the energy threshold we can both increase the diameter of the optical system collecting the fluorescence light, and the efficiency of the sensors in converting this light in an electric signal. In fig.2 it is indicated the effect on the annual counting rates by increasing the optics diameter for a factor 5, from the 3 m diameter of EUSO to 15 m. It is also indicated the additional effect by increasing the sensor efficiency from 25% (typical of good photomultiplier photocatodes) to 60% (typical of well matched solid state sensors). Appointing the attention on the annual rate of the Greisen  $\nu$ 's, it increases for about a factor 15, up to 22  $\nu$  events/year. The arrows reported in fig.2 indicate the approximate energy thresholds, considered at about 90% of the total integral counting rate. The approach of increasing the optics diameter is considered by the Mexican-Russian collaboration for the project KLYPVE. Also if its FOV is limited to  $15^\circ$ , it is planned of deploying in space a huge mirror, hung to an arm attached to the bottom part of the Russian segment of the ISS [7]. For sake of an easy comparison with the broken line of fig.2, suppose the diameter of the KLYPVE mirror be 15 m: the proton rate is very high in the whole  $10^{18}$ - $10^{21}$  eV energy range, while the Greisen  $\nu$  rate

remains insufficient for systematic neutrino observations (see fig.3).

#### 4 Increasing the FOV of the system

The approach of increasing as much as possible the FOV in order to increase the area of the observed terrestrial surface has been considered in the Airwatch/Owl collaboration, by combining seven independent optical systems in one device [8] reaching a total FOV of  $\approx 115^\circ$ . The expected rates are those reported in fig.4, showing that such an approach allows to start the neutrino astronomy at the extreme energies with about 100  $\nu$  events/year. Let's now put the question in general terms, forgetting about the design of a possible detection system. In Fig.5 is reported the area of the observable terrestrial surface from an altitude of 400 km as a function of the distance of the circumference of this surface from the Nadir direction (the scale is that at the right side, given both in  $10^6 \text{ km}^2$  and in "EUSO units"). In order to obtain the corresponding annual counting rates it must be taken into account several effects:

1) - The attenuation of the light signal due to the distance ' $d$ ' between the emission point and the detector. Because the length of the portion of shower seen in an angular pixel of the detector increases as  $d$ , while the signal attenuates as  $d^{-2}$ , the signal diminishes as  $d^{-1}$  (see in fig.5 the curve of the signal amplitude normalized to the amplitude at Nadir, the scale is that at left side).

2) - The absorption of the light by the atmosphere. At the Nadir the atmosphere transparency is  $\approx 0.56$ . By increasing the angle of view from the Nadir direction the thickness of the air to be crossed by the light increases. Due to the Earth curvature it increases much faster than for the observation of a flat surface. Furthermore, since it appears as power in an exponential function, the corresponding transparency of the atmosphere rapidly falls to zero. It is less than 2% already halfway between the Nadir and the horizon (the curve in fig.5 is normalized to the Nadir transparency; the scale is at the left side). The total transparency normalized to the Nadir is given by the product of the two above effects, and is reported in fig.5 on the same left side scale.

There are several other effects that should be taken into account and could further worsen the experimental situation at the increase of the distance from the Nadir direction. The most relevant are the signal/noise ratio, worsening as  $d^{-1}$ , and the increase of the terrestrial surface observed in a single angular pixel (it reaches  $4 \cdot 180 \text{ km}^2$  at the horizon) that could de-localize the position of the signal on the terrestrial surface and give difficulties for the corrections to be applied for the local atmospheric and light emission conditions. However, because these effects strongly depend by the detail of the detection system, they will not be considered in the following, living to the real project how to take care of them. We can now obtain the annual rate of detectable Greisen

$\nu$ 's as a function of the area of the covered terrestrial surface, in the hypothesis of having considered all possible actions for minimizing the energy threshold, i.e. increase of the optics diameter up to 15 m and of the sensor efficiency up to 60%. The result is reported in fig.6, while in fig.7 is reported the energy threshold of the system, considered at 90% of the total integral counting rate. In order to reach a conclusion it is necessary to add a further consideration. To the total number of detectable Greisen  $\nu$ 's per year it must be applied the efficiency for recognizing the  $\nu$ -originated showers in the huge sea of the proton-originated showers. Not taking into account the experimental difficulties in the observations, such as the local atmospheric conditions that can blind portion of the shower (and of whom it could be taken into account in a careful analysis), about two third of the  $\nu$ -originated showers can be distinguished by their deeper origin in the atmosphere, with a neglegible contamination from the proton-originated showers. Of the remaining one third, about half should be originated by  $\nu_e$  and should show a maximum at the depth typical of hadronic showers, and an other maximum (in general more intense) at a depth two times deeper, due to the LPM effect that expands the length of the very high energy electromagnetic shower originated by the electron produced in the  $\nu_e$  interaction. The other half of the not deeply originated  $\nu$  showers are due to  $\nu_\mu$  interactions, originating a high energy  $\mu$  and a hadronic shower indistinguishable from a proton-originated shower. The total efficiency for distinguishing a  $\nu$ -originated shower is therefore not more than 0.8. Correspondly, the number of Greisen  $\nu$ 's detectable from the ISS is not more 280, 170 of them originated by  $\nu_e$  interactions and 110 by  $\nu_\mu$  interactions. However, it must be noted that a further reduction factor could be introduced, by considering the different efficiency of the instrument for detecting  $\nu$ -induced showers with respect to p-induced showers. This difference is being evaluated by the EUSO collaboration, and it mainly depends by the shorter path available to deeply originated  $\nu$  showers [9].

## 5 Conclusions

It cannot be a priori decided if the about 300 Greisen  $\nu$ 's per year could be considered an adequate figure for a possible neutrino observatory, and it will strongly depend from the results of the EUSO observations and of other similar devices and of the possible their extensions. Here we limit ourselves to two considerations:

1) - The area of the total observed terrestrial surface can be increased by increasing the altitude of the detection system. This can be still obtained starting from the ISS, by assembling on board the whole system, and launching it from the ISS equipped by a suitable free flyer module. Afterward it would be possible to raise the altitude of the orbit: in fact the mass of the fuel needed for increasing the height of the orbit is not enormous, about 30 kg per t of mass

for doubling the height of the orbit from 400 km up to 800 km. However for the same FOV, from a 800 km altitude the total rate of detectable Greisen  $\nu$ 's increases much less than the 4 geometric factor respect to the ISS orbit, but only by a 1.6 factor, because of the increase of the energy threshold due to the light attenuation for the longer distance.

2) - A number of identical wide FOV systems could be assembled on board of the ISS and launched on its same orbit, what could present several advantages:

2a) - the results from the first detection system will teach about the opportunity of increasing the gathering of  $\nu$  events by launching other devices;

2b) - the following on devices could have general structure (optics + mechanics) identical to the first one, greatly decreasing the needed work, the realization time and possibly the prices;

2c) - since the temporal distance between two subsequent launches could not be in any case short, the sensor and trigger efficiency could be improved from one launch to the following up;

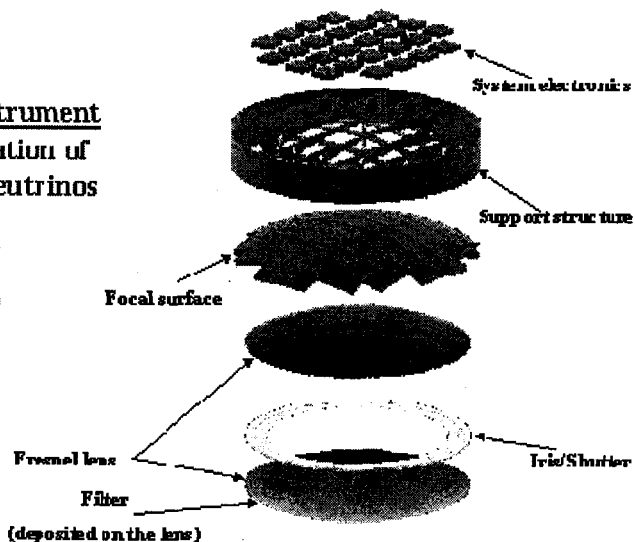
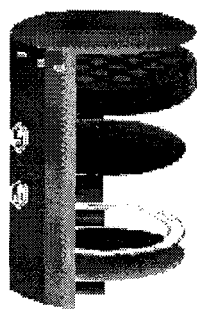
2d) - the attitude of two sufficiently near systems (e.g. distant less than 1000 km) could be adjusted for obtaining a partial overlap of the observed portions of the terrestrial surface, allowing the inter-calibration of the systems.

With N systems, the rate should therefore be N times larger than that obtainable by the first system alone.

## THE EUSO TELESCOPE

### OVERVIEW

A compact instrument  
for the observation of  
EECRs and Neutrinos



EUSO : Extreme Universe Space Observatory

Figure 1: Schematic view of the EUSO instrument.

**EUSO = INTEGRAL RATE ( $E^{-\infty}$ )/YEAR**

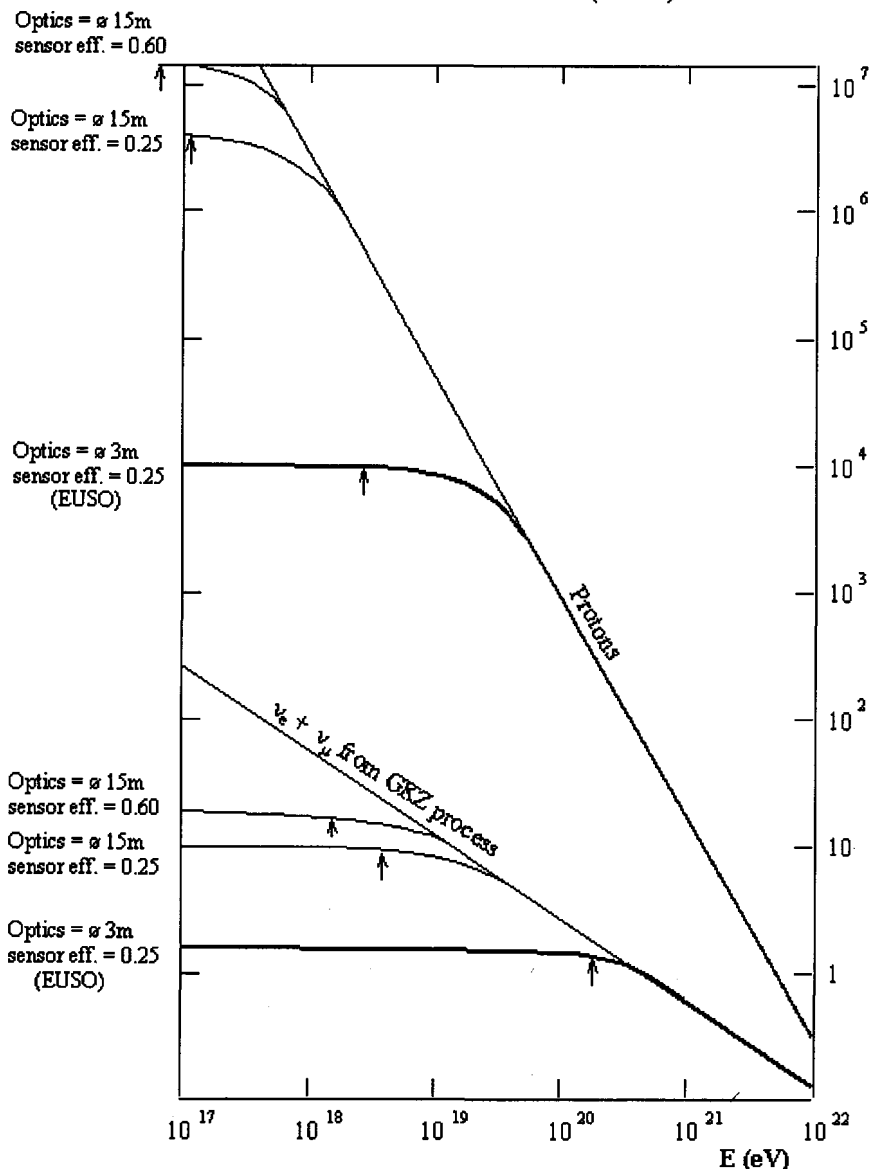


Figure 2: Expected integral counting rate per year for EUSO in case of protons and Greisen-neutrinos. Also the curves relative to increased optics diameter and sensor efficiency are reported. Arrows indicate the energy threshold.

**KLYPVE = INTEGRAL RATE ( $E \div \infty$ )/YEAR**

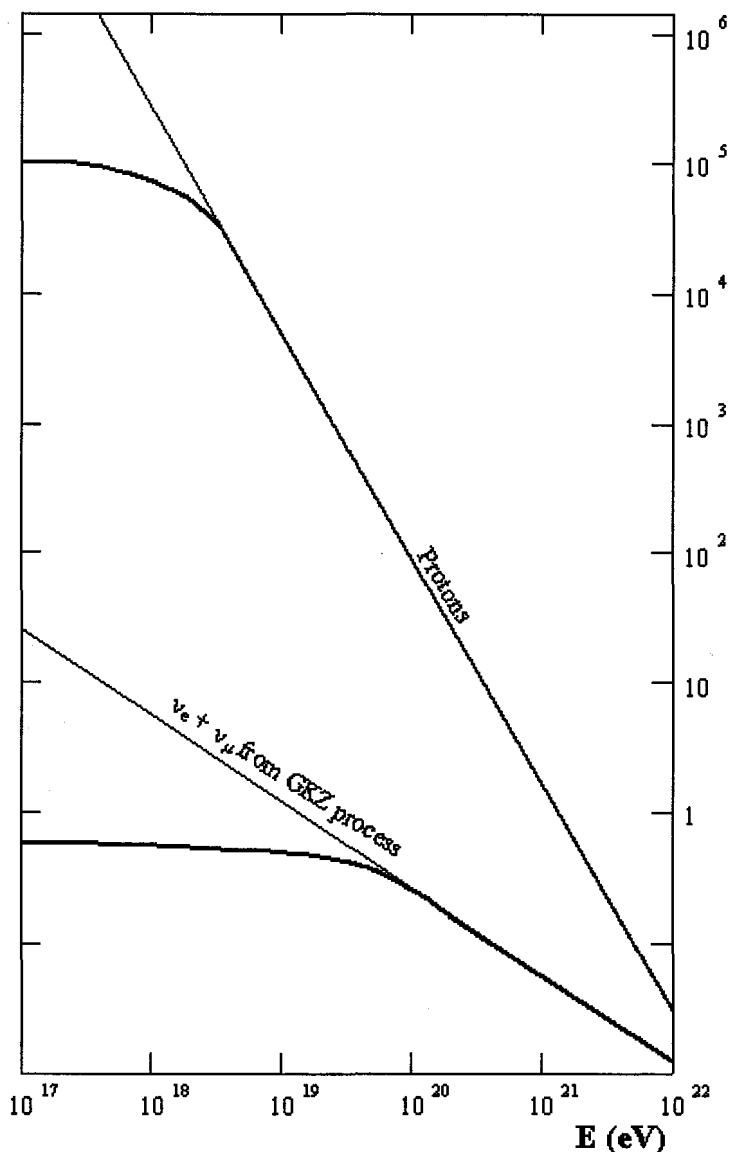


Figure 3: Expected integral counting rate per year for KLYPVE in case of protons and Greisenneutrinos.

'GODS' = INTEGRAL RATE ( $E \div \infty$ )/YEAR

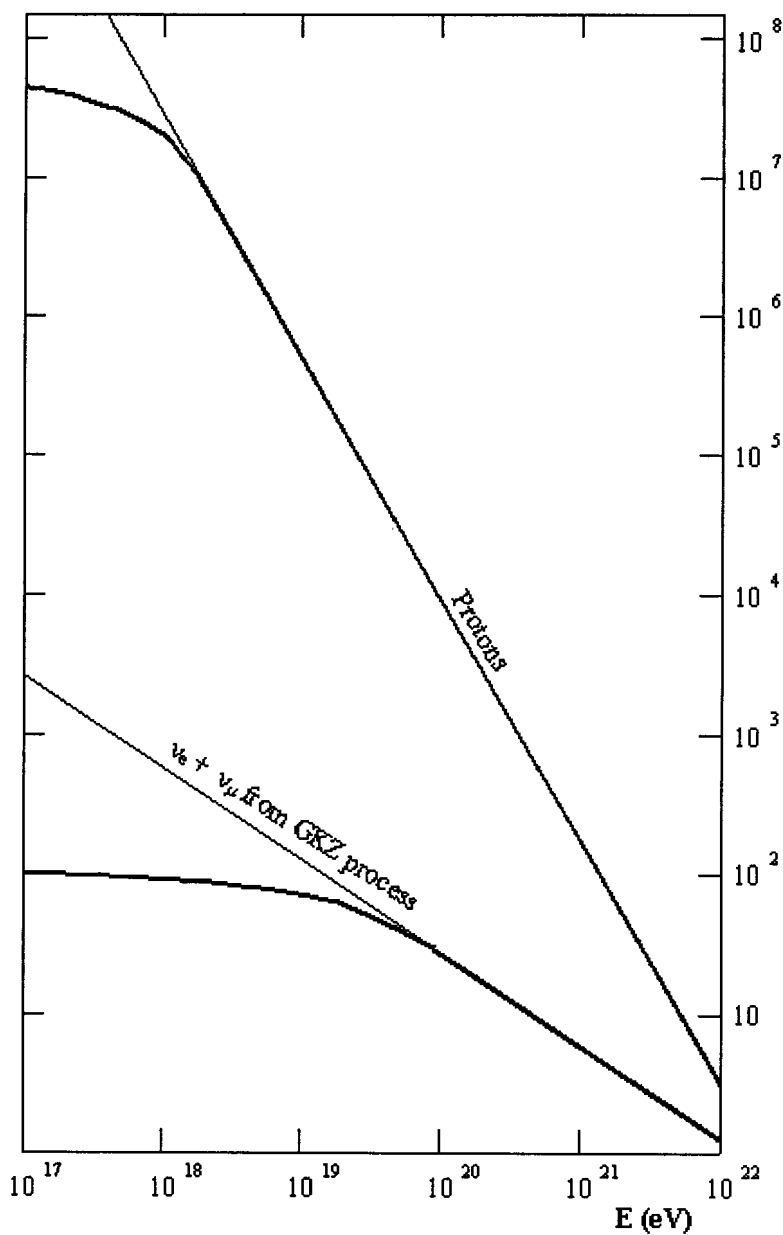


Figure 4: Expected integral counting rate per year for GODS in case of protons and Greisen-neutrinos.

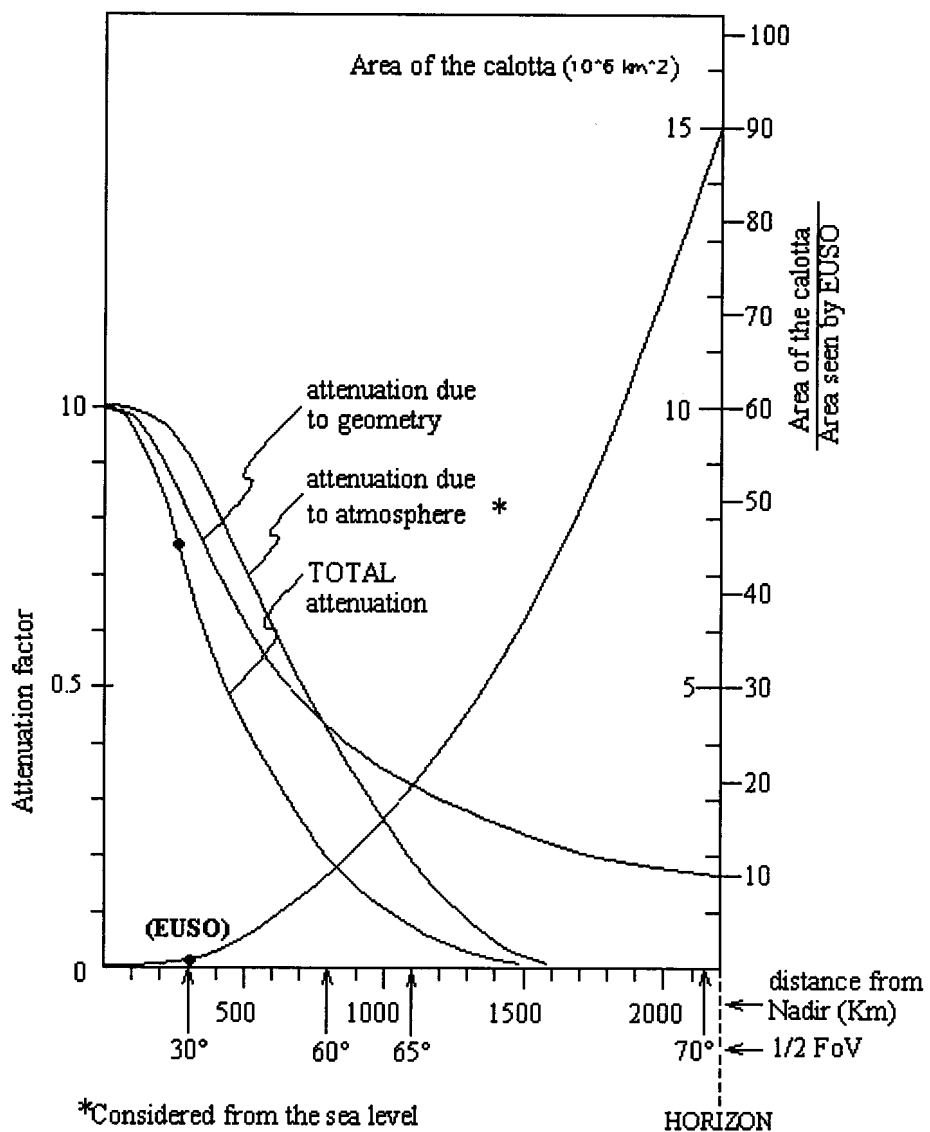


Figure 5: Attenuation factors normalized at Nadir (left scale). Area of the observable terrestrial surface from an altitude of 400 km as a function of the distance of the circumference of this surface from the Nadir direction (right scale).

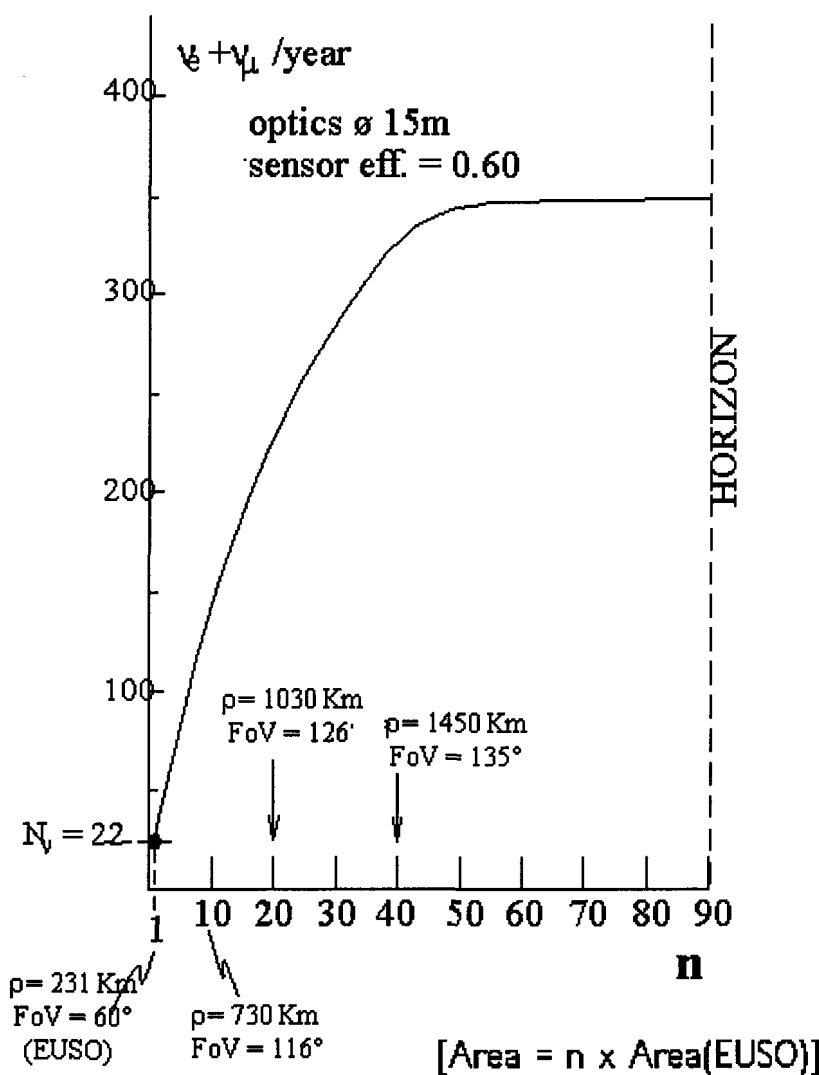


Figure 6: Annual rate of detectable Greisen  $\nu$ 's as a function of the ratio  $n = \frac{\text{Area of the calotta}}{\text{Area observed by EUSO}}$  in case of 15 m optics diameter and 60% sensor efficiency.

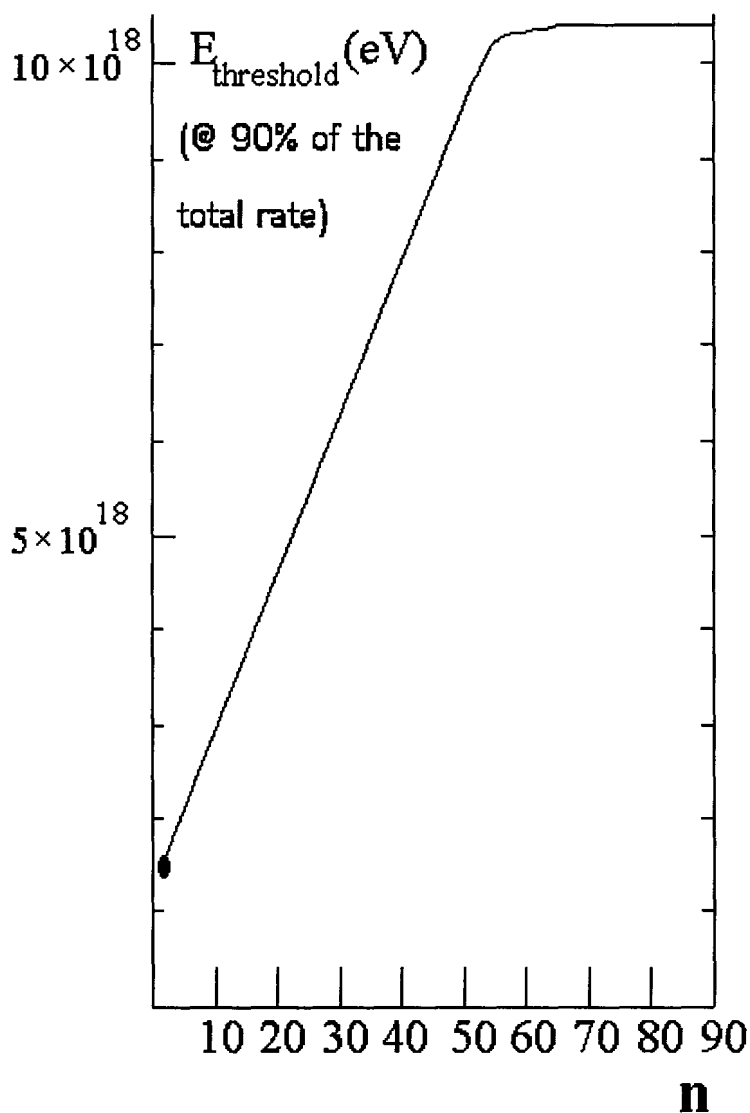


Figure 7: Energy threshold of the system in fig 5 as a function of theratio  $n = \frac{\text{Area of the calotta}}{\text{Area observed by EUSO}}$ ,considered at 90% of the total integral counting rate.

## References

- [1] D. J. Bird et al.: Phys. Rev. Lett. 71 (1993) 3401; N. Hayashida et al.: Phys. Rev. Lett. 73 (1994) 3491. M. Takeda et al. Phys. Rev. Lett. 81 (1998) 1163
- [2] B.A. Khrenov et al. "Space program KOSMOPETL ...." Metepec 2000, Observing ultrahigh energy cosmic rays from space and earth 57-75
- [3] R.E. Streitmatter for the OWL collaboration. "Orbiting Wide Angle Light-Collectors (OWL) : Observing Cosmic Rays from Space" College Park 1997, Observing giant cosmic ray air showers 95-107.
- [4] P. Spillantini, 'First International Symposium on Airwatch', Catania, Jan.30-Febr.2, 1997.
- [5] J. Linsley et al., "Space Air Watch: Observation of the Earth Atmosphere from ISSA Space Station", 25-th International Cosmic Ray Conference, Durban 1997, proc. OG.10.6.20
- [6] L. Scarsi et al., "Extreme Universe Space Observatory", proposal to ESA for the F2/F3 missions ; ESA and EUSO Team, "Extreme Universe Space Observatory - Report on the accommodation of EUSO on the Columbus Exposed Payload Facility" ESA/MSM-GU/2000.462/AP/RDA December 2000
- [7] G.K. Garikov et al., "Russian plans for ISS", AIP Conf. Proc., 433 (1998) 108-116; "Camera for detection of Cosmic Rays of energy more than 10 EeV on the ISS orbit", AIP Conf. Proc., 433 (1988) 403-417.
- [8] O. Catalano et al., "GODS for EUSO: A Grand Observatory Deployed from the Space Station for the Extreme Universe Space Observatory", International Workshop on 'Space Factory on International Space Station', Tsukuba Space Center of NASDA, June 7-9, 1999, proc. Pag.7.
- [9] Marco Valerio Tognetti, Florence University, thesis, June 2000.

# DETECTION OF ULTRA-HIGH ENERGY COSMIC RAYS WITH "SOLAR-SAIL"-TYPE DETECTOR

V. A. Tsarev <sup>a</sup>, V. A. Chechin <sup>b</sup>, N. G. Polukhina <sup>c</sup>

*P. N. Lebedev Physical Institute, Russian Academy of Sciences, Leninskii pr. 53,  
Moscow, 117333 Russia*

*Abstract.* We propose to detect radio emission from nearly horizontal EAS initiated by ultra-high energy cosmic rays with radio antennas on satellites. The signal amplitude is calculated and compared with background. The event rate for  $E \geq 10^{20}$  eV is estimated as a few events per day.

## 1 INTRODUCTION

Currently in Russia, USA, and Europe, work is underway toward the construction of a "solar-sail boat", i.e., a space vehicle with a "solar sail" of an area of a few hectares, which is propelled by the sun light pressure. This work stimulates the development of technology for production and unfolding in space of large-area thin-film constructions (we shall call them "astrophysical film constructions, AFC). Recently, several Russian organizations (Lebedev Physical Institute, Babakin Research Center, Moscow State University, Joint Institute for Nuclear Research, S.-P. Physical-Technical Institute) proposed a project [1], which involves a wide program of astrophysical studies based on the AFC. The program includes the following lines of investigations: (a) Detection of Ultra-High Energy Cosmic Rays; (b) Search for massive charged particles of "Dark Matter"; (c) Measurement of variations of cosmic ray nuclei, including exotic and radioactive ones; (d) Measurement of magnetic field in space; (e) Micrometeorite-stream monitoring.

In this talk, we'll concentrate on some aspects of the first problem. Since, at the present stage, the AFC-technology development is mainly related to the realization of the "Solar Sail", it seems appropriate to say a few words on this idea.

The first experimental measurements of the light pressure were carried out by P. N. Lebedev (1899). The idea to use the light pressure for acceleration of space vehicles, which left behind its time, was proposed in 1924 by F. A. Tsander (see [2]). Technological possibilities for realizing this, in due time fantastic, Tsander's idea appear only today. Recently, the "Solar-Sail" idea has drawn attention of general public in the context of the proposed Solar-Sail-Space-Vehicle regatta on the Earth-Moon-Mars route to celebrate the 500th anniversary of the discovery of America (1993), and using "Solar Sail" for exploration of the Galley comet (1985-1986). Unfortunately, neither the "Solar Sail" regatta nor the flight to the Galley comet were realized. Nevertheless, a wealth of technological experience was gained. The most appreciable steps forward in the "Solar Sail" program appeared to be done to date in Russia. A solar-sail prototype was unfolded from the space vehicle "Progress-M" (February 4, 1993). The first vehicle with "Solar Sail", designed and manufactured by Babakin Research Center, is scheduled for testing in orbit for the beginning of the next year. These achievements provide the basis for realizing the AFC program.

---

<sup>a</sup>e-mail: tsarev@x4u.lpi.ruhep.ru

<sup>b</sup>e-mail: chechin@x4u.lpi.ruhep.ru

<sup>c</sup>e-mail: poluhina@sci.lebedev.ru

## 2 ULTRA-HIGH ENERGY COSMIC RAYS

Over the past 40 years, a few tens of events have been detected by the largest cosmic ray (CR) detectors which testify that the CR flux includes particles with macroscopic energies ( $> 5 \cdot 10^{19} \text{ eV} \approx 8 \text{ J}$ ), the so-called Ultra-High Energy Cosmic Rays (UHECR). These observations pose fundamental questions on sources of these particles, mechanisms of their production and propagation, that remain to be answered, and could be a signal of a new physics and / or astrophysics (see reviews [3]). The Greisen-Zatsepin-Kuzmin (GZK) cutoff [4] (due to interaction of CR with the cosmic microwave background) means that if the UHECR are due to the known stable particles, they must be produced at distances less than 100 Mpc. Since, at the ultra high energies, the bending in the galactic and extragalactic magnetic fields is weak, one can expect that reconstructed incident directions of these particles should point toward their sources (within a few degrees). However, no astrophysical objects, which, according to the existing ideas, could give UHECR, are visible in the directions from where they come. Thus, to explain the EHECR, there is a need either to change the traditional ideas on astrophysical sources of ultra-high energy particles (see, for example, [5]) or to assume existence of decaying super-massive particles, or something else (see [3, 6]).

For an extensive investigation of the UHECR and checking various models proposed for their explanation, there is a need to considerably increase the statistics and advance to higher energies. However, the UHECR flux is extremely low:

$$J(E > E_0) \approx (E_0/10^{19} \text{ eV})^{-2} (km^2 \cdot sr \cdot year)^{-1}.$$

Thus, for  $E \geq 10^{20} \text{ eV}$  the flux is about one particle per  $km^2$  per century. For obtaining a statistically significant sample of events within a reasonable time, there is a need of detectors with very large aperture. The typical value is  $S \cdot T = 10^4 km^2 \cdot sr \cdot year$ , which could provide 100 events per year at  $E \geq 10^{20} \text{ eV}$ . Currently, such detectors are planned or are under construction. They are oriented to the detection of either charged (shower) particles or photons (fluorescent light) produced in Extended Air Showers (EAS), initiated by the UHECR in the atmosphere. The typical size of the controlled area is  $6000 \text{ km}^2$  in the ground-based "Auger observatory" [7] or about  $10^5 \text{ km}^2$  for detection of fluorescent light from a satellite [8].

In the present project, it is proposed to use radio antennas on satellites for detecting radio emission from nearly horizontal EAS initiated by ultra-high energy particles [9]. Metallized AFC surface can serve as a reflector focusing radio waves to feeders (incidentally, a balloon with part of its surface metallized can be also used for a pilot experiment). The antenna can have good directionality and high gain which can be useful for efficient noise suppression. From technical point of view, the radio-method seems to be easier than the optical one. A highly developed radio technique makes it possible to detect pulses even in the presence of heavy noise. We hope also to benefit from powerful methods of radio pulse analysis.

## 3 EAS RADIOEMISSION

The radio emission from electromagnetic showers was predicted by G. Askaryan (1962) [10], and J. V. Jelly (1965) [11] was the first who experimentally observed radio pulses

correlated with EAS. Later on, work in this field was carried out at many laboratories, and radio pulses were detected in a wide frequency interval from a few MHz to a few hundreds of MHz. In particular, a possibility to work only with radio antennas (without coincidence with a shower array or other tradition EAS-detecting technique) was demonstrated [12]. However, up to now, the radio method does not become an efficient method of EAS detection similar to the Cherenkov optical method. The main problem here seems to be as follows. When passing from optics to radio frequencies, one loses 6-8 orders of magnitude in the radiation intensity  $W$ , because  $W \propto \nu \cdot d\nu$  for radiation by negative charge excess [10] or  $\nu^2 \cdot d\nu$  for dipole radiation [13] (optics:  $\lambda \approx 4 \cdot 10^{-7}$  m; radio:  $\lambda \approx 1 \div 10$  m);  $d\nu$  is also reduced. However, the coherent nature of radiation at long (radio) wavelengths results in increasing the radiation intensity. If the total number of coherently radiating particles in EAS is  $N_{coh}$ , the amplification of the amplitude by coherence is a factor  $N_{coh}$  too.  $N_{coh}$  increases proportional to  $E_{EAS}$ . For large  $N_{coh}$ , the effect of coherence  $W \propto N_{coh}^2 \propto E_{EAS}^2$  may compensate the smallness caused by going to low frequencies. It is estimated (see, for example, [13]) that  $N_{coh} \approx (0.1 \div 0.2) \cdot N_{max}$ , where  $N_{max} \approx E_{EAS}/10^9$  eV is the total number of electrons and positrons in the EAS maximum. Then, it is easy to find that the ratio  $W(\text{coherent radio}) / W(\text{Cherenkov radiation})$  can be greater than unity for EAS with energy  $E_{EAS} \geq 10^{18}$  eV. Thus, for being able to produce a sizeable radio signal that can be reliably detected, the EAS must be very large. But such very high energy EAS are extremely rarely coming, and detectors with huge apertures are needed for their recording. It is hoped that the problem of the EAS radio detection could be solved on the way proposed in the present project, i.e., by means of observing EAS from space. It will be shown that the controlled area may be as large as  $10^6$  km<sup>2</sup> and more in this case; thus, detection of EAS with  $E \geq 10^{20}$  eV becomes statistically possible. We shall see in the next sections that the signal from these ultra-high energy EAS is high enough to be reliably detected on the satellite and be separated from background.

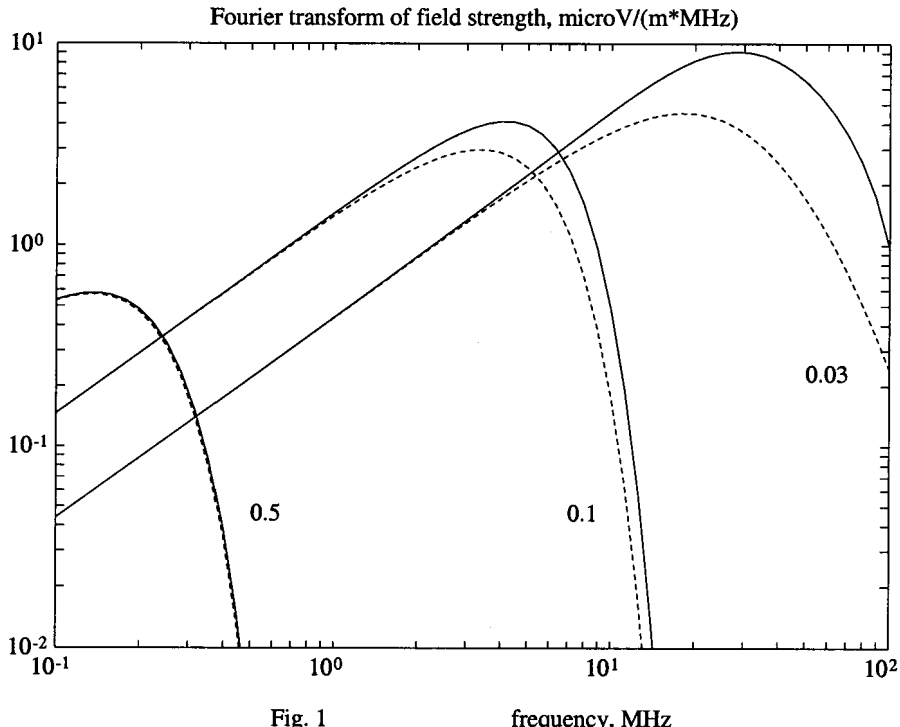
#### 4 ESTIMATE OF THE EAS RADIO SIGNAL AT EXTREMELY HIGH ENERGIES

Two main mechanisms are responsible for the EAS coherent radio emission [13]. One of them is related to the electro-negative excess produced by the shower-particle interaction with atomic electrons:

$$\gamma + e_{at}^- \rightarrow \gamma + e^-, e^+ + e_{at}^- \rightarrow e^+ + e^-, e^+ + e_{at}^- \rightarrow \gamma + \gamma, e^- + e_{at}^- \rightarrow e^- + e^-.$$

The magnitude of the excess  $\eta = (N_- - N_+)/N_- + N_+$  is estimated as  $\eta = 0.1 \div 0.2$  [13]. The other source of radiation is related to a separation of positively and negatively charged particles in an EAS caused by geomagnetic field, which results in the EAS acquiring a transversal electric dipole (and current). Motion of this dipole (and current) through the atmosphere (with the refractive index  $n=1.0003$ ) generates Cherenkov-type radiation even in the absence of the charge excess. The calculations with these two mechanisms taken into account, as applied to the conditions of the signal detection at high distances on a satellite, were carried out recently [9], and the results are presented briefly below.

Consider, for definiteness, an EAS with  $E = 10^{20} \text{ eV}$ . In this case the total number of particles in the shower maximum is about  $N_{\max} = E/10^9 \text{ eV} = 10^{11}$ , the corresponding number of excessive electrons is  $N_{-\max} = \eta \cdot N_{\max} = 2 \cdot 10^{10}$  (we assume  $\eta = 0.2$ ). Fig. 1 shows the calculated [9] frequency dependence of the Fourier component of electric field for observation angles  $\theta = 0.03, 0.1$ , and  $0.5$  at distance  $R=1000 \text{ km}$ . The solid lines show results with the geomagnetic separation effect taken into account; the dashed lines correspond to results obtained without this separation. For definiteness, it was assumed that the direction of the separation lies in the observation plane. (In the actual experiment, this direction can be found by measurement of the radiation polarization). The dipole contribution is seen to be prevailing (see also [13]). The frequency dependence of radiated power is shown in Fig. 2 for the same angles  $\theta$ . In the small-angle region ( $\theta \leq 0.1$ ), within the frequency interval  $\nu \approx 30 \div 50 \text{ MHz}$ , the spectral density of power flux is  $dW / dSd\nu \approx 10^{-11} \div 10^{-13} \text{ W} / m^2 \text{ MHz}$ . Radio pulses of such magnitude can be easily detected by modern radio receivers. (For comparison, typical magnitudes of signals detected in the radio astronomy are as low as 1 Jansky =  $10^{-20} \text{ W} / m^2 \text{ MHz}$ ).



The above results were obtained in the long-wavelength approximation, where an EAS can be considered as a continuous moving volume charge. For a more accurate consideration, one must take into account that a shower represents not continuous distribution of a volume charge but an aggregate of a finite number of moving charged particles subjected to multiple scattering. However, as was shown in [9], the multiple scattering effect results only in a minor modification of the radiated field in the chosen frequency interval  $\nu \approx 30 \div 50$  MHz.

It is seen from Figs. 1 and 2 that the radiation is strongly dependent on the radiation angle. To reconstruct the EAS energy from measured value of the field intensity or radiation power one needs to know at what angle  $\theta$  to the EAS axis the detected radio waves were radiated. This angle can be found using additional information on duration of the pulse as a function of the angle  $\tau(\theta)$  (see Fig. 3). As far as the distance between an EAS and satellite is concerned, it can be found from the geometry of the horizontal EAS detection and the orbit height with an accuracy of about  $1/2(h/H)^{1/2}$ , where  $h$  is conventional boundary of atmosphere, and  $H$  is satellite orbit altitude. It should be also emphasized that the direct calibration of the radio detector on satellite can be done using proton bunches from high-energy proton accelerators, which are sent to the atmosphere. These bunches will produce showers and their radio pulses will imitate that of ultra-high energy EAS with the energy  $E \approx N \cdot E_p$ , where  $N$  is the number of protons in a bunch and  $E_p$  is the energy of individual protons in the bunch. This procedure will be similar to that used in the recent SLAC experiment with radio waves generated by electron beams [14].

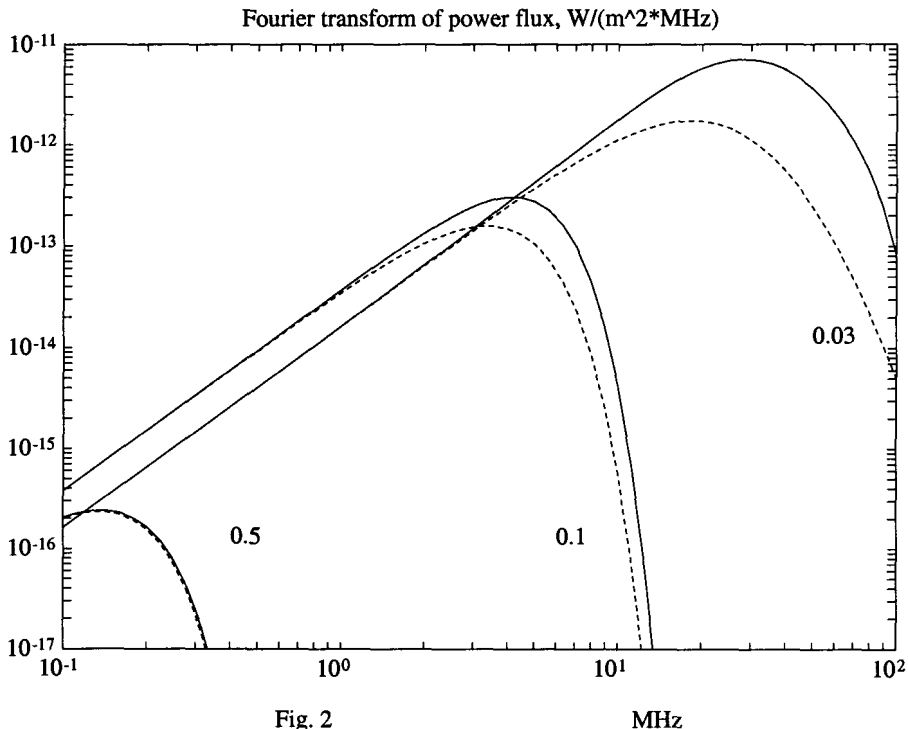


Fig. 2

MHz

Notice that the frequency interval  $\nu \approx 30 \div 50$  MHz is the most appropriate for the EAS-pulse detection from a satellite. It is determined, on the one hand, by the lower boundary of the atmosphere transparency for radio waves (caused by the wave reflection from the ionosphere,  $\lambda_{max} \approx 15 \div 20$  m,  $\nu_{min} \approx 20 \div 15$  MHz) and, on the other hand, by decreasing the signal at high frequencies  $\nu \geq 100$  MHz.

## 5 BACKGROUNDS FOR THE EAS RADIODETECTION

The isolation of the desired signal from a background is one of the key problems in the EAS detection by radio method. It is customary to recognize the following radio-background sources: (1) Natural: radio emission of the atmosphere and ionosphere; radio emission of the sky (galactic, extragalactic, radio-sun); (2) Artificial: man-made radiation; (3) Receiver intrinsic noise. We consider the first two briefly.

Natural "terrestrial" radio pulses could be produced both by instabilities of the magnetosphere and ionosphere and by the wave exposure coming from the Earth surface, mainly from lightning discharges. It is significant that all "terrestrial" natural types of radiation lie mainly in the low-frequency region (1-100 kHz) and are not a threat to detection within the chosen interval 30-50 MHz.

The Sun is the brightest radio-source in the sky. In our operating region of 30-50 MHz, the "quiet" Sun produces background flux of the order of  $10^{-16}$  W/m<sup>2</sup>·MHz, whereas "perturbed" Sun can radiate as much as  $10^{-12}$  W/m<sup>2</sup>·MHz. We can see that

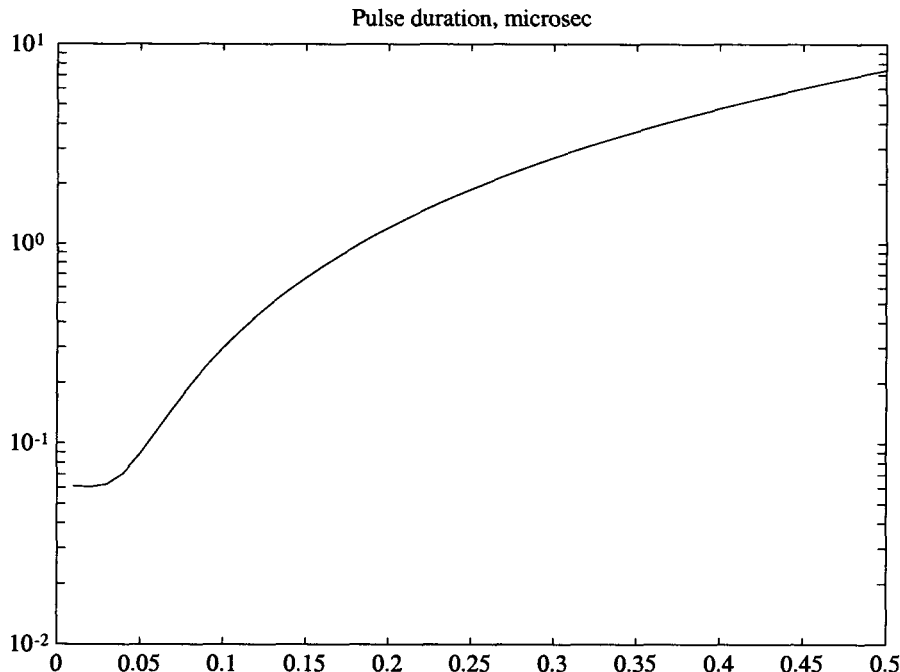


Fig. 3                          angle

the expected signal will exceed the background from the most powerful natural source, the Sun, when it is quiet, by a few orders of magnitude; however, measurements during the periods when the Sun is perturbed may be difficult. The characteristic very short duration of the EAS signal ( $10^{-7} \div 10^{-6}$  s), which is much shorter than that for signals from natural radio sources, and the signal polarization measurements can be also used for the background rejection.

The highest background is produced by man-made sources owing to operation of broadcasting stations. For estimating this background, we use the results of the analysis of the "global radio-pollution" over the short-wavelength [15] and the compilation of satellite data [16]. From comparison of the expected signal and the background level, we can conclude that the desired signal for  $E \geq 10^{20}$  eV and small radiation angles  $\theta \leq 0.1$  (even without the antenna gain taken into account) exceeds the background level for radio-loud regions (say, in the Southern hemisphere, above ocean area, where it is at the level of  $\leq 10^{-14}$  W/m<sup>2</sup>·MHz) by two or three orders of magnitude.

## 6 ESTIMATE OF THE EVENT RATE

We estimate now the expected event rate  $dN / dt = J \cdot S_{eff} \cdot \Delta\Omega$ . Here,  $J$  is the UHECR flux, which is on the order of  $10^{-2}$  event per km<sup>2</sup> per year for  $E \geq 10^{20}$  eV,  $S_{eff}$  is the effective area of the atmosphere from which the UHECR can be detected from a given satellite position, and  $\Delta\Omega$  is a solid angle of the UHECR incidence for which the

signal can be detected. We shall assume that radio waves are focused at the antenna feeders by a "paraboloid-type" reflecting surface [17] (which could be manufactured from a metallized AFC). In this case, all azimuthal angles are accepted, and the signal can be received from a circular atmospheric layer of a width  $L \approx (2Rh)^{1/2}$  and a radius  $R_l \approx (2RH)^{1/2}$ , i.e.,  $S_{eff} \approx 4\pi(Hh)^{1/2}$ . Here,  $R$  is the Earth's radius,  $H$  is the satellite orbit height, and  $h$  is the effective atmosphere thickness. Taking  $R = 6000$  km,  $H = 500$  km, and (very conservatively)  $h = 10$  km, we find

$$S_{eff} = 5 \cdot 10^6 \text{ km}^2.$$

Based on the above background consideration, we can take that the signal can be separated from the background at  $\theta \leq 0.1$ . Then, finally, we have the following estimate

$$\frac{dN}{dt} \approx 4 \text{ events per day for } E \geq 10^{20} \text{ eV.}$$

Thus, for a year of operation, about 1500 of events can be collected, which will increase the existing UHECR statistics by about two orders of magnitude and extend the measured energy interval by one or two orders of magnitude.

## 7 CONCLUSION

(1) The radio signal produced in the atmosphere by UHECR is high enough for reliable detection from a distance of several thousands km and can be detected by a satellite-based detector.

(2) The background for such detection is below the expected signal in the quiet regions and does not present a serious problem for the signal detection.

(3) Simultaneous measurement of the signal magnitude and pulse duration allows for finding EAS energy.

(4) The controlled area is expected to be as high as  $5 \cdot 10^6 \text{ km}^2$ ; the corresponding event rate could be as high as a few events per day at  $E \geq 10^{20} \text{ eV}$ .

(5) The method proposed provides a mean for greatly increasing the UHECR statistics and reaching higher energies.

## Acknowledgments

The authors are grateful to E. L. Feinberg for reading the manuscript and making useful remarks.

## References

- [1] Research and development works of the Federal space program "FUTURE" for 2002-2004 years.
- [2] F. A. Tsander, "*A problem of flight with jet apparatus, Collection of papers*" (Ed. by L. V. Korneev, Oborongiz, Moscow) 1961.
- [3] A. V. Olinto, *Phys. Rept.* **333**, 329 (2000);  
X. Bertou, M. Baratov, and A. Letessier-Selvon, *Int. J. Mod. Phys. A* **15**, 2182 (2000).

- [4] G. T. Zatsepin and V. A. Kuzmin, *JETP Letters*, **4**, 78 (1966); ;  
K. Greisen, *Phys. Rev. Lett.* **16**, 748 (1966).
- [5] N. S. Kardashev, *MNRAS*, **276**, 515 (1995);  
A. V. Uryson, *Kratkie soobsh. po fizike*, 2001, in press.
- [6] V. S. Berezinsky, A. Vilenkin, *Phys. Rev. Lett.* **79**, 5202 (1997);  
V. A. Kuzmin, V. A. Rubakov *Yad. Fiz.* **276**, 1122 (1998).
- [7] J. W. Cronin, *Rev. Mod. Phys.* **71**(2), S165 (1999).
- [8] J. F. Ormes et al., (Proc. 25th ICRC), Durban, **5**, 273 (1997).
- [9] K. M. Pichkhadze, V. G. Sysoev, V. A. Tsarev, V. A. Chechin, *Kratkie soobsh. po fiz.* **12**, 9 (2000);  
V. A. Tsarev, V. A. Chechin, *Kratkie soobsh. po fiz.* **4**, 42 (2001);  
V. A. Tsarev, V. A. Chechin, *DAN*, 2001, in press;
- [10] G. A. Askaryan, *JETP* **41**, 616 (1961); **48**, 988 (1965).
- [11] J. V. Jelley et al., *Nature* **205**, 327 (1965).
- [12] D. J. Fegnan et al., *Canadian J. of Phys.* **46**, S250 (1968).
- [13] H. R. Allan, in *Progress in Elementary Particles and Cosmic Ray Physics*, v. **10**, edited by J. G. Wilson and S. G. Wouthuysen (North-Holland, Amsterdam, 1971), p. 171.
- [14] D. Saltzberger et al., arXiv:hep-ex/0011001, 1 No. 2000.
- [15] A. G. Kolesnik and S. A. Kolesnik, *Geomagnetizm i Aeronomiya* **36**, 59 (1996).
- [16] <http://www.atnf.csiro.au/SKA/intmit/database.html>
- [17] N. Z. Gogitidze, V. A. Tsarev, V. A. Chechin, *NIM A* **248**, 186 (1986).

# NEUTRINO-INDUCED DEUTERON DISINTEGRATION EXPERIMENT AT THE KRASNOYARSK NUCLEAR REACTOR

Yu. V. Kozlov, S. V. Khaltourtsev, I. N. Machulin, A. V. Martemyanov, V. P. Martemyanov, A.A.Sabelnikov V. G. Tarasenkov, E. V. Turbin, V. N. Vyrodov.<sup>a</sup>

*Russian Research Center "Kurchatov Institute, 123182 Moscow, Russia*

**Abstract.** The investigation of antineutrinos interactions with the nucleus of Deuteron (CCD&NCD reactions) and Hydrogen (CCP) at the Krasnoyarsk underground reactor using "Deuteron" detector are presented. As a result the cross section for NCD&CCD were measured with the 9% precision. For the CCP precision is 3%.

$$\sigma_{exp}^{ncd} = (3.35 \pm 0.31) \times 10^{-44} \text{ cm}^2/\text{fission} \quad ^{235}\text{U}$$

$$\sigma_{exp}^{ccd} = (1.08 \pm 0.09) \times 10^{-44} \text{ cm}^2/\text{fission} \quad ^{235}\text{U}$$

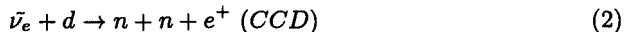
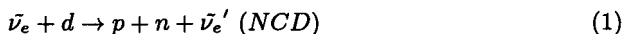
$$\sigma_{exp}^{ccp} = (6.39 \pm 0.19) \times 10^{-43} \text{ cm}^2/\text{fission} \quad ^{235}\text{U}$$

The precision of the experimental results is close to the theoretical one and is in a good agreement with the other experiments. The limit on the antineutrino oscillation parameters into the sterile state was done:  $\Delta m^2 \leq 4.7 \times 10^{-2} \text{ eV}^2$ ,  $\sin^2(2\Theta) = 1$ . (68%CL). The comparison of the measured and theoretical cross section gives us the value of the neutron-neutron scattering length as a  $a_{nn}(S) = -17 \pm 6 [\text{fm}]$  in the approach of zero momentum transition. The weak neutral current constant is in a good agreement with the prediction of SM:  $G_A^{nc} = G_A^{cc}/0.932 \pm 0.056$ .

## 0.1 Introduction

This report presents the results of the experiments, which carried out at the neutrino underground laboratory of the Krasnoyarsk nuclear plant.

The interaction of antineutrinos ( $\bar{\nu}_e$ ) with a Deuteron occurs via two channels, Neutral Current on Deuteron (NCD) and Charged Current on Deuteron (CCD),



These reactions were investigated in the experiments [1], [2], [3], [4] and investigated theoretically by Yu. Gaponov [5].

The study of these reactions can give the information about:

- Weak constants for charged and neutral currents;
- A length of neutron-neutron scattering;
- Neutrino oscillation.

## 0.2 Detector design

The modernized detector "Deuteron" ( see details [6] ) is situated in the underground laboratory at a distance 34.0 m from the reactor, the neutrino flux is about a few units to  $10^{12} \bar{\nu}/\text{cm}^2$

<sup>a</sup>e-mail: vyrodov@dnuc.polyn.kiae.su

The target volume is 513 l of  $D_2O(H_2O)$  placed in a stainless tank, which is surrounded by 30 cm of Teflon for neutron reflection, 0.1 cm of Cd, 8 cm of steel shots, 20 cm of graphite and 16 cm of boron polyethylene ( $CH_2 + 3\%B$ ) for gamma and neutron shielding. The whole installation is pierced to make 169 holes (81 holes pass through the Tank and Teflon, the others through the Teflon only). These holes house 169 proportional  $^3He$  neutron counters with a reduced intrinsic alpha background. These counters are used for neutron registration. They are located in a square lattice with a side of 10 cm. The active shielding covers the main assembly, against cosmic muons.

An efficiency of the detector was calculated using Monte-Carlo method as for inverse beta decay reaction as for antineutrino-deuteron reaction. Also calculations have been made for  $^{252}Cf$  source and this result was checked experimentally. The difference (less 1%) between the calculation and experimental data shows good reliability of MC calculations. To make the MC calculation more confidence the special calibration procedure was made. Using the  $^{238}Pu - Li$  neutron source, which has the neutron spectrum very close to one from CCD, NCD reactions the space distribution inside the tank was measured. From this distribution and measured efficiency in the center of the detector one can obtain the experimental efficiency for NCD&CCD reactions. The neutron efficiency, neutron lifetime and measured efficiency for  $D_2O & H_2O$  target are shown in the Table 1.

Table 1

Parameters/Target	$H_2O$	$D_2O$
Efficiency of one neutron registration by tank counters only	$(27.5 \pm 0.3)\%$	$(56.2 \pm 0.1)\%$
Efficiency of double neutron registration by all counters	$(9.9 \pm 0.1)\%$	$(41.7 \pm 0.1)\%$
Neutron live time	$138 \pm 2\mu s$	$203 \pm 2\mu s$

A special attention was given to the correlated background for NCD channel connected with the antineutrino interaction with proton ( $H_2$  atoms), because the cross section for such process is relatively large. The construction of the detector allowed us to decrease the efficiency neutron registration from a boron polyethylene up to 0.003% (0.25 events/day). We estimate the correlated background ( $N_{cor}$ ) as 0.69 events/day due to the concentration  $H_2O(0.15\%)$  in heavy water.

### 0.3 Target $H_2O$

The inverse beta decay on the proton reaction

$$\bar{\nu}_e + p \rightarrow n + e^+ \text{ (CCP)} \quad (3)$$

is used for checking and improving of some parameters of the detector. In this case detector was filed with water  $H_2O$ . The exposure time is  $115 \times 10^5$  s. or about 133 days. Four sets of measurement with different background condition have been made. As a result the CCP cross section was

$$\sigma_{exp}^{ccp} = (6.39 \pm 0.19) \times 10^{-43} \text{ cm}^2/\text{fission} \quad ^{235}U$$

This result is in a good agreement with theoretical cross section of (V-A theory). The ratio is (68% C.L.):

$$R = \frac{\sigma_{exp}^{ccp}}{\sigma_{V-A}}(^{235}U) = 1.00 \pm 0.04$$

#### 0.4 Target $D_2O$

From the beginning of 1997 and up to February 2001 the experimental data were collected during 718.4 days reactor "on" and 208 days reactor "off". Fourteen sets of the measurements were done. The different sets mean different conditions of the experiment (some improvement of the VETO system, increasing passive shielding or changing some counters). Taking into account both "wall" effect and time rejection for double neutron events and amplitude selection, we have the next neutron registration efficiencies:

$$\varepsilon_2^{ncd} = 0.354 \pm 0.003$$

$$\varepsilon_1^{ncd} = 0.514 \pm 0.005$$

After correction of the registration probability of NCD channel events corresponded CCD channel and correlated CCP background:

$$N^{ncd}(NCD) = 20.0 \pm 1.8 \quad (4)$$

$$N^{ccd}(CCD) = 4.35 \pm 0.36 \quad (5)$$

One can obtain the cross section for NCD & CCD reactions:

$$\sigma_{exp}^{ncd} = (3.35 \pm 0.31) \times 10^{-44} \text{ cm}^2/\text{fission} \quad ^{235}U$$

$$\sigma_{exp}^{ccd} = (1.08 \pm 0.09) \times 10^{-44} \text{ cm}^2/\text{fission} \quad ^{235}U$$

These results are in good agreement with theory (Table 2).

Table 2

	$\sigma \times 10^{44} \text{ cm}^2/\text{fission}$	
	NCD	CCD
Experiment		
For real mixture of fuel U-235, Pu-249, U238	$3.38 \pm 0.31$	$1.09 \pm 0.09$
Experiment corrected for U-235	$3.35 \pm 0.31$	$1.08 \pm 0.09$
Theory		
for real mixture of fuel $U - 235, Pu - 249, U - 238^{*)}$	$3.20 \pm 0.16$	$1.90 \pm 0.06$
Theory for $U - 235^{**})$	$3.17 \pm 0.16$	$1.08 \pm 0.06$
Theory for $U - 235^{**})$	$3.16 \pm 0.16$	$1.12 \pm 0.06$
Ratio (exp/theory <sup>*)</sup> )	$1.06 \pm 0.11$	$1.0 \pm 0.10$

<sup>\*)</sup> K.Schreckenbach antineutrino spectrum, K.Kubodera antineutrino deuteron cross section [8]

<sup>\*\*)</sup>  These are theoretical values of the cross sections taken from the paper of Yu.Gaponov and V.Vladimirov for the K.Schreckenbach reactor antineutrino spectrum.

### 0.5 n-n scattering length

The comparison of the measured and theoretical cross section gives us the value of the neutron-neutron scattering length as a  $a_{nn}(S) = -17 \pm 6(fm)$  in the approach of zero momentum transfers is presented in the Table 3.

Table 3

$a_{nn}(S), (fm)$	$\langle \sigma_c c \rangle \times 10^4 4, (cm^2/fiss)$
-16.6	1.077
-17.0	1.084
-18.5	1.112
-23.7( $= a_{np}$ )	1.179

### 0.6 Neutral weak constant

From the experimental ratio ( $\sigma_{\text{exper}}^{\text{CCD}} / \sigma_{\text{exper}}^{\text{NCD}}$ ) which is proportional to

$$(G_A^{\text{NC}} / G_A^{\text{CC}})^2 = (\cos(\Theta_C))^{-2}$$

it is easy to obtain the experimental value of  $G_A^{\text{NC}}$ . The weak neutral current constant is in a good agreement with the prediction of SM:  $G_A^{\text{NC}} = G_A^{\text{CC}} / 0.932 \pm 0.056$ .

### 0.7 Neutrino oscillation

The experimental data for the NCD and CCD gives an unique possibility to obtain the limit on the neutrino oscillation parameters  $\Delta m^2, \sin^2(2\Theta)$  into into the sterile state, using the ratio of ratios construction

$$R = \frac{\sigma_{\text{exp}}^{\text{CCD}} / \sigma_{\text{exp}}^{\text{NCD}}}{\sigma_{\text{theory}}^{\text{CCD}} / \sigma_{\text{theory}}^{\text{NCD}}} = 0.95 \pm 0.11$$

This is possible because of the threshold of the CCD & NCD reactions are different (4.0 MeV and 2.2MeV respectively) and NCD reaction is more sensitive to oscillation of neutrino with lower energy because of it has the lower threshold of reaction. The limit on the oscillations parameters of the reactor antineutrinos into the sterile state is presented in the Fig 1.

### Acknowledgments

This work was supported by grants RFBR 99-15-96640 and 98-02-16313. We would like to thank the staff of Krasnoyarsk reactor for constant help, Ac. S.T. Belayev and Dr. Yu.V.Gaponov for very useful discussions and the theoretical group headed by E.A. Gomin for the adaptation of MC program to the neutrino purposes.

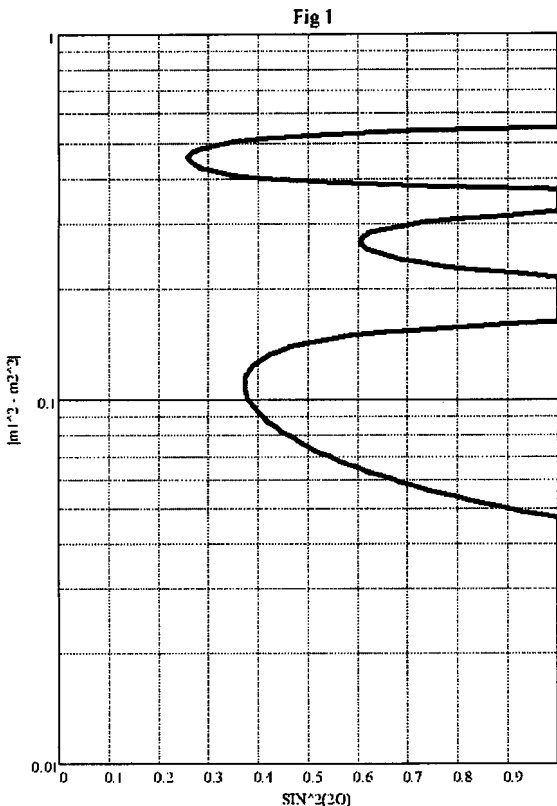


Figure 1: Limit on the neutrino oscillation parameters.

## References

- [1] E. Pasierb et al., *Phys.Rev.Lett.*, vol. 43., 96 (1979)
- [2] Yu. Kozlov et al., *JETF Lett.*, vol. 51., 245 (1990)
- [3] Yu. Vershinsky et al., *JETF Lett.*, , vol. 53., 489, (1991)
- [4] S.P. Riley et al., *Phys.Rev. C* vol.59, 3 (1999)
- [5] Yu. Gaponov at al. *J.Nuc.Phys.* vol. 49, 902 (1989)
- [6] V. Vydrov et al., *Jadernaja Fizika* , vol. 61., 844 (1998)
- [7] K. Schreckenbach et al., *Phys.Let. B*, vol.160, 325 (1985), K. Schreckenbach et al.,*Phys.Let. B*, vol.218, 365 (1989),
- [8] K. Kubodera et al., *J.Mod.Phys. E*, vol.3., 101 (1994)

# SAME-SIGN DILEPTON PRODUCTION VIA HEAVY MAJORANA NEUTRINOS IN PROTON-PROTON COLLISIONS

A. Ali<sup>a</sup>

*Deutsches Elektronen Synchrotron DESY, Hamburg, Germany*

A.V. Borisov<sup>b</sup>, N.B. Zamorin

*Physics Faculty of Moscow State University, 119899 Moscow, Russia*

**Abstract.** We discuss same-sign dilepton production mediated by Majorana neutrinos in high-energy proton-proton collisions  $pp \rightarrow \ell^+ \ell'^+ X$  for  $\ell, \ell' = e, \mu, \tau$  at the LHC energy  $\sqrt{s} = 14$  TeV. Assuming one heavy Majorana neutrino of mass  $m_N$ , we present discovery limits in the  $(m_N, |U_{\ell N} U_{\ell' N}|)$  plane where  $U_{\ell N}$  are the mixing parameters. Taking into account the present limits from low energy experiments, we show that at LHC for the nominal luminosity  $L = 100 \text{ fb}^{-1}$  there is no room for observable same-sign dilepton signals. But after increasing the luminosity to a value about  $3200 \text{ fb}^{-1}$  one will have sensitivity to heavy Majorana neutrinos up to a mass  $m_N \lesssim 1.5$  TeV only in the dilepton channel  $\mu\mu$ , other dilepton states will not be detectable due to the already existing strong constraints.

## 1 Introduction

While impressive, and providing so far the only evidence of new physics, the solar and atmospheric neutrino experiments do not probe the nature of the neutrino masses, i.e., they can not distinguish between the Dirac and Majorana character of the neutrinos. The nature of neutrino mass is one of the main unsolved problems in particle physics and there are practically no experimental clues on this issue [1].

If neutrinos are Majorana particles then their mass term violates lepton number by two units  $\Delta L = \pm 2$  [2]. If present, it can lead to a large number of processes violating lepton number by two units, of which neutrinoless double beta decay ( $\beta\beta_{0\nu}$ ) is a particular example. The seesaw models [3] provide a natural framework for generating a small Majorana neutrino mass which is induced by mixing between an active (light) neutrino and a very heavy Majorana sterile neutrino of mass  $M_N$ . The light state has a naturally small mass  $m_\nu \sim m_D^2/M_N \ll m_D$ , where  $m_D$  is a quark or charged lepton mass. There is a heavy Majorana state corresponding to each light (active) neutrino state. Typical scale for  $M_N$  in Grand unified theories (GUT) is of order the GUT-scale, though in general, there exists a large number of seesaw models in which both  $m_D$  and  $M_N$  vary over many orders of magnitude, with the latter ranging somewhere between the TeV scale and the GUT-scale [4].

If  $M_N$  is of order GUT-scale, then it is obvious that there are essentially no low energy effects induced by such a heavy Majorana neutrino state. However, if  $M_N$  is allowed to be much lower, or if the light (active) neutrinos are Majorana particles, then the induced effects of such Majorana neutrinos can be searched for in a number of rare processes. Among them neutrinoless double beta decay, like-sign dilepton states

---

<sup>a</sup>e-mail: ali@x4u2.desy.de

<sup>b</sup>e-mail: borisov@ave.phys.msu.su

produced in rare meson decays and in hadron-hadron, lepton-hadron, and lepton-lepton collisions have been extensively studied. (See, e.g., the papers:  $\beta\beta_{0\nu}$  [5–8],  $K^+ \rightarrow \pi^- \mu^+ \mu^+$  [9–11],  $pp \rightarrow \ell^\pm \ell^\pm X$  [12],  $pp \rightarrow \ell^\pm \ell^\pm W^\mp X$  [13],  $e^\pm p \rightarrow \overset{(-)}{\nu_e} \ell^\pm \ell'^\pm X$  [14, 15].)

Of the current experiments which are sensitive to the Majorana nature of neutrino, the neutrinoless double beta decay, which yields an upper limit on the  $ee$  element of the Majorana mass matrix, is already quite stringent [5]. Likewise, precision electroweak physics experiments severely constrain the mixing elements [16–18].

Taking into account these constraints, we obtain discovery limits for heavy Majorana neutrinos involved in the process of same-sign dilepton production in the proton-proton collision:

$$pp \rightarrow \ell^+ \ell'^+ X \quad (1)$$

with  $\ell, \ell' = e, \mu, \tau$  at the LHC energy  $\sqrt{s} = 14$  TeV.

## 2 Dilepton production in high-energy $pp$ collisions

We have calculated the cross section for the process (1) at high energies,

$$\sqrt{s} \gg m_W, \quad (2)$$

via an intermediate heavy Majorana neutrino  $N$  in the leading effective vector-boson approximation [19] neglecting transverse polarizations of  $W$  bosons and quark mixing. We use the simple scenario for neutrino mass spectrum

$$m_{N_1} \equiv m_N \ll m_{N_2} < m_{N_3}, \dots,$$

and single out the contribution of the lightest Majorana neutrino assuming

$$\sqrt{s} \ll m_{N_2}.$$

The cross section for the process in question is then parameterized by the mass  $m_N$  and the corresponding neutrino mixing parameters  $U_{\ell N}$  and  $U_{\ell' N}$ :

$$\sigma(pp \rightarrow \ell^+ \ell'^+ X) = \frac{G_F^4 m_W^6}{8\pi^5} \left(1 - \frac{1}{2}\delta_{\ell\ell'}\right) |U_{\ell N} U_{\ell' N}|^2 F(E, m_N), \quad (3)$$

with

$$F(E, m_N) = \left(\frac{m_N}{m_W}\right)^2 \int_{z_0}^1 \frac{dz}{z} \int_z^1 \frac{dy}{y} \int_y^1 \frac{dx}{x} p(x, xs) p\left(\frac{y}{x}, \frac{y}{x}s\right) \times h\left(\frac{z}{y}\right) w\left(\frac{s}{m_N^2} z\right). \quad (4)$$

Here,  $z_0 = 4m_W^2/s$ ,  $E = \sqrt{s}$ , and

$$w(t) = 2 + \frac{1}{t+1} - \frac{2(2t+3)}{t(t+2)} \ln(t+1)$$

is the normalized cross section for the subprocess  $W^+W^+ \rightarrow \ell^+\ell'^+$  (in the limit (2) it is obtained from the well-known cross section for  $e^-e^- \rightarrow W^-W^-$  [20] using crossing symmetry). The function  $h(r)$  defined as

$$h(r) = -(1+r)\ln r - 2(1-r)$$

is the normalized luminosity (multiplied by  $r$ ) of  $W^+W^+$  pairs in the two-quark system [19], and

$$p(x, Q^2) = x \sum_i q_i(x, Q^2) = x(u + c + t + \bar{d} + \bar{s} + \bar{b})$$

is the corresponding quark distribution in the proton.

In the numerical calculation of the cross section (3) the CTEQ6 Fortran codes for the parton distributions [21] have been used. We assume the mixing constraints obtained from the precision electroweak data [17]

$$\begin{aligned} \sum |U_{eN}|^2 &< 6.6 \times 10^{-3}, & \sum |U_{\mu N}|^2 &< 6.0 \times 10^{-3} (1.8 \times 10^{-3}), \\ \sum |U_{\tau N}|^2 &< 1.8 \times 10^{-2} (9.6 \times 10^{-3}). \end{aligned} \quad (5)$$

The bound on the mixing matrix elements involving fermions depends on the underlying theoretical scenario. There are the single limit and joint limit [17, 18], obtained by allowing just one fermion mixing to be present or allowing simultaneous presence of all types of fermion mixings, respectively. In our analysis, we have used the conservative constraints for the joint limit case.

We must also include the constraint from the double beta decay  $\beta\beta_{0\nu}$ , mentioned above. For heavy neutrinos,  $m_N \gg 1$  GeV, the bound is [20]

$$\left| \sum_{N(\text{heavy})} U_{eN}^2 m_N^{-1} \right| < 5 \times 10^{-5} \text{ TeV}^{-1}. \quad (6)$$

In calculating the cross sections for the  $\ell\tau$  and  $\tau\tau$  processes, we have used the effective value

$$|U_{\tau N}|_{\text{eff}}^2 = B_{\tau\mu} |U_{\tau N}|^2 < 3.1 \times 10^{-3} \quad (7)$$

with  $B_{\tau\mu} = \text{Br}(\tau^- \rightarrow \mu^- \bar{\nu}_\mu \nu_\tau) = 0.1737$  [22], as this  $\tau$ -decay mode is most suitable for the like-sign dilepton detection at LHC (see, e.g., [15]).

Combining the constraints of Eqs. (5), (7), and (6) and taking a nominal luminosity  $L = 100 \text{ fb}^{-1}$ , we obtain  $\sigma L < 1$  for all  $\ell\ell'$  channels. Therefore at the LHC there is no room for observable signals for same-sign dilepton processes  $pp \rightarrow \ell\ell' X$  ( $\ell, \ell' = e, \mu, \tau$ ) due to the existing constraints for the mixing elements  $|U_{\ell N}|^2$  from the precision electroweak data and neutrinoless double beta decay.

Let us take into account a recent proposal to increase the instantaneous LHC luminosity  $\mathcal{L}$  to a value of  $10^{35} \text{ cm}^{-2}\text{s}^{-1}$  [23], i.e., a total luminosity  $L = \mathcal{L} \times 1 \text{ year} \simeq 3200 \text{ fb}^{-1}$ .

Using the upgraded LHC luminosity and demanding  $n = 1, 3$  events for discovery (i.e.,  $\sigma L > n$ ), we present the two-dimensional plot for the discovery limits in Fig. 1

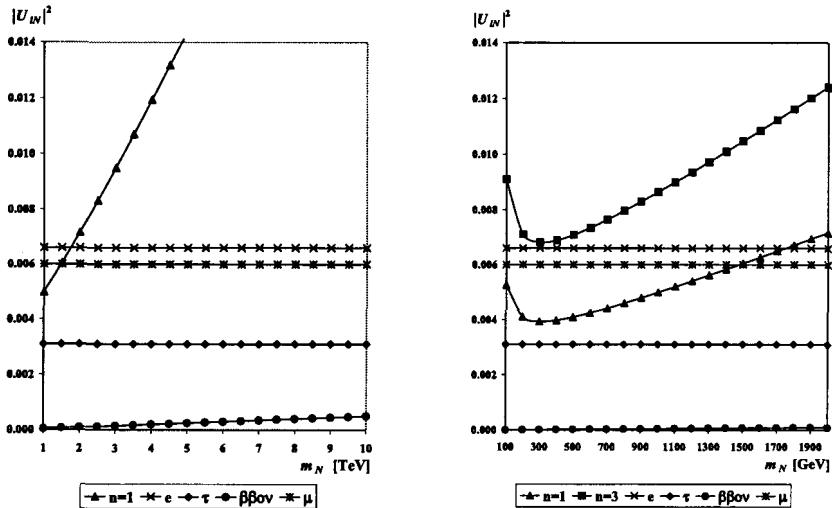


Figure 1: *Left:* Discovery limits for  $pp \rightarrow \ell^+\ell^+X$  as functions of  $m_N$  and  $|U_{\ell N}|^2$  for  $E = 14$  TeV,  $L = 3200 \text{ fb}^{-1}$  and various values of  $n$ , the number of events. We also superimpose the experimental limit from  $\beta\beta_{0\nu}$  (Eq.(6)), as well as the experimental limits on  $|U_{\ell N}|^2$  [horizontal lines for  $\ell = e, \mu$  (Eq. (5)), and  $\tau$  (Eq. (7))]. *Right:* The same as the left figure but for lighter Majorana neutrinos.

for the case of identical same-sign leptons ( $\ell = \ell'$ ). Discovery limits for the case of distinct same-sign leptons,  $\ell\ell' = e\mu, e\tau, \mu\tau$ , are shown in Fig. 2.

From Figs. 1 and 2 we see that the existing strong constraints for the mixing elements  $|U_{\ell N}|^2$  allow a possibility to observe only the same-sign  $\mu\mu$  process after increasing the nominal LHC luminosity  $L = 100 \text{ fb}^{-1}$  by a factor of about 30. For this case, LHC experiments will have a sensitivity to heavy Majorana neutrinos of mass  $m_N \lesssim 1.5$  TeV.

### 3 Conclusion

In conclusion, same-sign dilepton production at LHC will provide non-trivial constraints on the Majorana mass matrix only after increasing a nominal luminosity of  $100 \text{ fb}^{-1}$  at least by one order.

### Acknowledgments

We thank Christoph Greub, David London and Enrico Nardi for helpful discussions and communication, Dmitri Zhuridov for correcting a coefficient in Eq. (3), Dmitri Peregoudov for help in numerical calculations. A.V.B. thanks DESY for its hospitality and partial support.

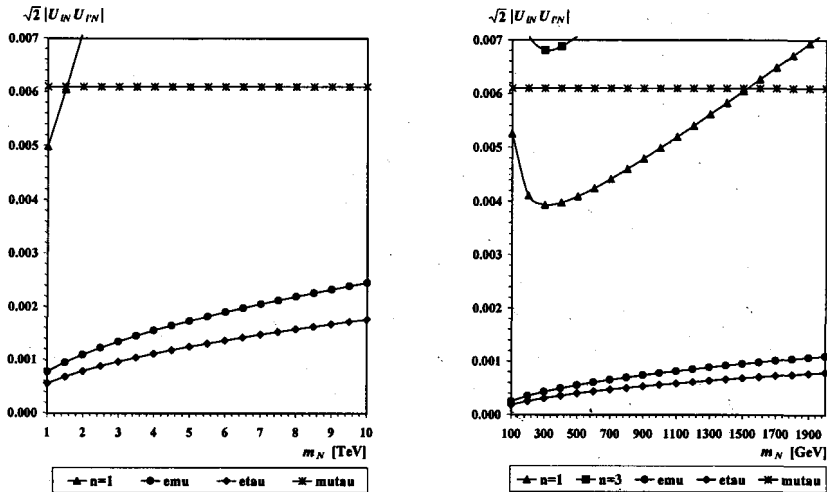


Figure 2: *Left:* Discovery limits for  $pp \rightarrow \ell^+ \ell'^+ X$ ,  $\ell \ell' = e\mu$ ,  $e\tau$ ,  $\mu\tau$ . We also superimpose the limits on  $\sqrt{2} |U_{\ell N} U_{\ell' N}|$  obtained from the experimental limits [Eqs. (6), (5), and (7)]. *Right:* The same as the left figure but for lighter Majorana neutrinos.

## References

- [1] For a review, see K. Zuber, *Phys. Rep.* **305**, 295 (1998); B. Kayser, preprint hep-ph/0104147; S.M. Bilenky, preprint hep-ph/0110306.
- [2] B. Kayser, F. Gibrat-Debu, F. Perrier, “*The Physics of the Massive Neutrinos*” (World Scientific, Singapore) 1989.
- [3] M. Gell-Mann, P. Ramond, R. Slansky, in “*Supergravity*”, eds. D. Freedman, P. van Nieuwenhuizen (North Holland, Amsterdam) 315, 1979; T. Yanagida, in *Proceedings of the Workshop on Unified Theory and Baryon Number in the Universe*, eds. O. Sawada, A. Sugamoto (KEK, Tsukuba, Japan) 1979; R.N. Mohapatra and G. Senjanovic, *Phys. Rev. Lett.* **44**, 912 (1980).
- [4] See, for example, P. Langacker, *Nucl. Phys. B (Proc. Suppl.)* **100**, 383 (2001).
- [5] L. Baudis et al., *Phys. Rev. Lett.* **83**, 411 (1999).
- [6] A. Faessler, F. Simkovic, *J. Phys. G* **24**, 2139 (1998).
- [7] H.V. Klapdor-Kleingrothaus, *Springer Tracts in Modern Physics* **163**, 69 (2000); preprint hep-ph/0102277.
- [8] R.N. Mohapatra, *Phys. Rev. D* **34**, 909 (1986).
- [9] L.S. Littenberg, R.E. Shrock, *Phys. Lett. B* **491**, 285 (2000).
- [10] K. Zuber, *Phys. Lett. B* **479**, 33 (2000).
- [11] C. Dib, V. Gribanov, S. Kovalenko, I. Schmidt, *Phys. Lett. B* **493**, 82 (2000).
- [12] H. Tso-hsiu, C. Cheng-rui, T. Zhi-jian, *Phys. Rev. D* **42**, 2265 (1990); A. Datta, M. Guchait, D.P. Roy, *Phys. Rev. D* **47**, 961 (1993); A. Ferrari et al., *Phys. Rev. D* **62**, 013001 (2000).

- [13] F.M.L. Almeida Jr, Y.A. Coutinho, J.A. Martins Simões, M.A.B. do Vale, *Phys. Rev.* **D 62**, 075004 (2000).
- [14] W. Buchmüller, C. Greub, *Nucl. Phys.* **B 363**, 345 (1991).
- [15] M. Flanz, W. Rodejohann, K. Zuber, *Phys. Lett.* **B 473**, 324 (2000) (Erratum, *Phys. Lett.* **B 480**, 418 (2000)).
- [16] W. Buchmüller, C. Greub, H.-G. Kohrs, *Nucl. Phys.* **B 370**, 3 (1992).
- [17] E. Nardi, E. Roulet, D. Tommasini, *Phys. Lett.* **B 344**, 225 (1995); E. Nardi, private communication.
- [18] E. Nardi, E. Roulet, D. Tommasini, *Phys. Lett.* **B 327**, 319 (1994).
- [19] S. Dawson, *Nucl. Phys.* **B 249**, 42 (1985); M. Chanowitz, M.K. Gaillard, *Phys. Lett.* **B 142**, 85 (1984); G.L. Kane, W.W. Repko, W.B. Rolnik, *Phys. Lett.* **B 148**, 367 (1984); I. Kuss, H. Spiesberger, *Phys. Rev.* **D 53**, 6078 (1996).
- [20] G. Bélanger, F. Boudjema, D. London, H. Nadeau, *Phys. Rev.* **D 53**, 6292 (1996); D. London, preprint hep-ph/9907419.
- [21] J. Pumplin, D.R. Stump, J. Huston, H.L. Lai, P. Nadolsky, W.K. Tung, preprint hep-ph/0201195.
- [22] D.E. Groom et al. (PDG Collaboration), *Eur. Phys. J. C* **15**, 1 (2000).
- [23] F. Gianotti, M.L. Mangano, T. Virdee et al., preprint hep-ph/0204087.

# SITUATION WITH TEST OF CP, T AND CPT INVARIANCE

E.P.Shabalin <sup>a</sup>

*State Research Center Institute of Theoretical and Experimental Physics, Moscow,  
Russia*

*Abstract.* A purpose of this overview is to describe the general situation with test  
of the fundamental symmetries in particle physics.

## 1 What is known on P,C,CP violation and CPT invariance

### 1.1 General remarks

The modern quantum field theory of the elementary particles is automatically invariant under CPT transformation [1], that is, invariant under product of C, P and T transformations. Here C is the operator of charge conjugation, P is operator of space reflection and T is time reversal operator.

Historically, during a long time, the elementary particles theory was constructed in such a way that it was invariant under separate C, P and T transformations. But beginning from 1957 we know that the weak interactions do not conserve P-parity [2] and C-parity [3].

In the proposed thereupon V-A theory of weak interaction [4], P and C invariances were violated at 100 % level, but the CP invariance was conserved in agreement with the Landau's hypothesis [5] on existence of the combined CP invariance.

In 1964, it was discovered [6] that the CP invariance also is not exact symmetry. The CP symmetry breakdown was observed in decay of CP-odd state  $K_2^0 = \frac{1}{\sqrt{2}}(K^0 - \bar{K}^0)$  into  $2\pi$  state with  $CP=+1$ .<sup>b</sup>

In the experiments with  $K^0(\bar{K}^0)$  mesons, this breakdown turned out to be of order 0.2 %. But in general, CP violation in weak processes may be both considerably smaller and considerably larger than that in  $K_2^0 \rightarrow 2\pi$  decay. Thus, for the rare decays  $K_L \rightarrow \pi^0 l^+ l^-$ ,  $K_L \rightarrow \pi^0 \nu \bar{\nu}$  and for some decays of the system  $\{B^0, \bar{B}^0\}$  mesons, the theory predicts CP-effects of order 1.

We have introduced above the  $K_L$  state instead of  $K_2^0$  state. A reason is that in presence of CP violation, the physical states with a definite mass and lifetime are

$$K_S = (K_1 + \varepsilon K_2)/\sqrt{1 + |\varepsilon|^2}, \quad K_L = (K_2 + \varepsilon K_1)/\sqrt{1 + |\varepsilon|^2} \quad (1)$$

where the parameter  $\varepsilon$  characterizes a strength of so-called indirect CP violation.

In the Standard Model (SM) CP violation is originated by some complex coupling constants  $V_{ji}$  in the interaction of weak  $W^\pm$  bosons with quarks

$$W_\mu^- \bar{q}_{Uj} V_{ji} \gamma_\mu (1 + \gamma_5) q_{Di} + H.c \quad (2)$$

where  $q_{Uj} = u, c, t$ ;  $q_{Di} = d, s, b$  — "up" and "down" quarks. The form of matrix

<sup>a</sup>e-mail: shabalin@heron.itep.ru

<sup>b</sup>The another CP eigenstate of  $\{K^0, \bar{K}^0\}$  system with  $CP=+1$  is  $K_1^0 = \frac{1}{\sqrt{2}}(K^0 + \bar{K}^0)$ .

$V$  proposed by Kobayasi and Maskawa [7] is

$$V = \begin{pmatrix} c_1 & -s_1c_3 & -s_1s_3 \\ s_1c_2 & c_1c_2c_3 - s_2s_3e^{i\delta} & c_1c_2s_3 + s_2c_3e^{i\delta} \\ s_1s_2 & c_1s_2c_3 + c_2s_3e^{i\delta} & c_1s_2s_3 - c_2c_3e^{i\delta} \end{pmatrix}, \quad (3)$$

where  $s_i = \sin \theta_i$ ,  $c_i = \cos \theta_i$  and the phase  $\delta$  bears the name of the authors of ref. [7]. We shall name this phase sometimes by  $\delta_{KM}$ .

Another widely used form of  $V$  was proposed by Wolfenstein [8]

$$V \approx \begin{pmatrix} 1 - \lambda^2/2 & \lambda & A\lambda^3(\rho - i\eta) \\ -\lambda & 1 - \lambda^2/2 & A\lambda^2 \\ A\lambda^3(1 - \rho - i\eta) & -A\lambda^2 & 1 \end{pmatrix}, \quad (4)$$

where  $\lambda = s_1c_3$  and  $A, \rho, \eta$  are the real numbers of order 1.

The matrix  $V$  is called the Cabibbo-Kobayasi-Maskawa (CKM) matrix.

### 1.2 CP violation in $K_L$ decays

In the  $\{K^0, \bar{K}^0\} \rightarrow 2\pi$  decays, the following CP-odd quantities were measured

$$\eta_{+-} = \frac{A(K_L \rightarrow \pi^+ \pi^-)}{A(K_S \rightarrow \pi^+ \pi^-)} = \varepsilon + \varepsilon', \quad \eta_{00} = \frac{A(K_L \rightarrow \pi^0 \pi^0)}{A(K_S \rightarrow \pi^0 \pi^0)} = \varepsilon - 2\varepsilon'. \quad (5)$$

where the parameter  $\varepsilon'$  characterizes the direct CP violation in the decay amplitude.

$$\varepsilon' = \frac{A(K_2^0 \rightarrow 2\pi, I=2)}{A(K_1^0 \rightarrow 2\pi, I=0)} \quad (6)$$

Experimentally [9],

$$\varepsilon = \frac{2}{3}\eta_{+-} + \frac{1}{3}\eta_{00} = 2.28 \cdot 10^{-3} \cdot \exp(i44^\circ) \quad (7)$$

and  $\varepsilon' \ll \varepsilon$ . Theoretically

$$\varepsilon \sim s_2s_3 \sin \delta, \quad \varepsilon' \sim \frac{\omega}{16\pi^2} s_2s_3 \quad (8)$$

where  $\omega = \langle 2\pi; I=2 | K_S \rangle / \langle 2\pi; I=0 | K_S \rangle \approx 1/22$ .

The exact magnitude of the ratio  $\varepsilon'/\varepsilon$  depends of the prescription how to transform the 4-quark operators describing the nonleptonic transitions into the amplitudes for the physical mesons and also on a choice of magnitude of  $m_s(q^2)$ . Because of these reasons, the theoretical results for  $\varepsilon'/\varepsilon$  are rather uncertain

$$(\varepsilon'/\varepsilon)^{th} = 10^{-4} \left\{ \begin{array}{ll} 6.7 \pm 0.7 & [10] \\ 3.1 \pm 2.5 & [11] \\ 17^{+14}_{-10} & [12] \\ 1.5 - 31.6 & [13] \end{array} \right. \quad (9)$$

The experiments give

$$(\varepsilon'/\varepsilon)^{exp} = 10^{-3} \begin{cases} 2.30 \pm 0.65 & [14] \\ 0.6 \pm 0.7 & [15] \\ 2.8 \pm 0.41 & [16] \\ 1.85 \pm 0.75 & [17] \end{cases} \quad (10)$$

These data exclude the models where  $\varepsilon' = 0$ , in particular, the model of superweak interaction [18], as the only mechanism of CP violation.

It should be noted that other hypothetical sources of CP violation also could contribute to  $\varepsilon'$ . In particular, a value  $\varepsilon'/\varepsilon \sim (2 - 3)10^{-3}$  could be generated in a theory with extended Higgs sector [19–21] and in the supersymmetric extensions of SM [22].

One more CP-odd effect in  $K_L$  decays is the charge asymmetry in semileptonic decays

$$\delta_L = \frac{\Gamma(K_L \rightarrow l^+ \nu \pi^-) - \Gamma(K_L \rightarrow l^- \bar{\nu} \pi^+)}{\Gamma(K_L \rightarrow l^+ \nu \pi^-) + \Gamma(K_L \rightarrow l^- \bar{\nu} \pi^+)} \approx 2Re\varepsilon. \quad (11)$$

Experimentally,  $\delta_L = (3.33 \pm 0.14)10^{-3}$ . A value of  $2Re\varepsilon$  determined from  $K_L \rightarrow 2\pi$  decays is  $3.29 \cdot 10^{-3}$ .

### 1.3 CP effects in $K^\pm \rightarrow \pi^\pm \pi^\pm \pi^\mp$ decays

In these decays, the direct CP violation is the only possible one. The CP effects are

$$\Delta\Gamma = \frac{\Gamma(K^+ \rightarrow \pi^+ \pi^+ \pi^-) - \Gamma(K^- \rightarrow \pi^- \pi^- \pi^+)}{\Gamma(K^+ \rightarrow \pi^+ \pi^+ \pi^-) + \Gamma(K^- \rightarrow \pi^- \pi^- \pi^+)}, \quad (12)$$

and

$$\Delta g = \frac{g^{(+)} - g^{(-)}}{g^{(+)} + g^{(-)}} \quad (13)$$

where the slope parameters  $g^{(\pm)}$  are defined by the expression

$$|M(K^\pm(k) \rightarrow \pi^\pm(p_1)\pi^\pm(p_2)\pi^\mp(p_3))|^2 \sim 1 + g^{(\pm)}(s_3 - s_0)/m_\pi^2 + \dots \quad (14)$$

where  $s_3 = (k - p_3)^2$ ,  $s_0 = \frac{1}{3}m_K^2 + m_\pi^2$ .

In the leading  $p^2$  approximation CP-odd effects turn out to be small:  $\Delta\Gamma \sim 10^{-7}$  [23]. In the papers [24], it was declared that the next  $p^2$  corrections enlarge CP-odd effects by one-two orders. But this conclusion was not confirmed. According to the estimates in [25]  $\Delta g \sim 2 \cdot 10^{-6}$  and  $\Delta\Gamma \sim 6 \cdot 10^{-8}$ . The calculations taking into account  $p^4$  corrections gave

$$\begin{aligned} \Delta g &\leq 3 \cdot 10^{-5} \sin \delta & [26] \\ \Delta\Gamma &\leq 2.5 \cdot 10^{-6} \sin \delta & [27]. \end{aligned} \quad (15)$$

These values are smaller than the ones in [24] by 30 times at  $\delta = \pi/2$ .

If CP violation takes place in the extended Higgs sector of the electroweak theory, some enlargement of CP-odd effects in  $K^\pm \rightarrow 3\pi$  decays is possible [28].

### 1.4 CP violation in the rare kaon decays

In the decays  $K_L \rightarrow \pi^0 e^+ e^-$ ,  $K^+ \rightarrow \pi^+ \nu \bar{\nu}$  and  $K_L \rightarrow \pi^0 \nu \bar{\nu}$ , CP-odd parts of the amplitudes turn out to be comparable with or even larger than the CP-even parts.

In  $K_L \rightarrow \pi^0 e^+ e^-$  decay

$$\begin{aligned} Br(K_L \rightarrow \pi^0 e^+ e^-)_{CP\text{-even}} &\leq 4 \cdot 10^{-12} & [29] \\ Br(K_L \rightarrow \pi^0 e^+ e^-)_{CP\text{-odd}}^{\text{indirect}} &= (1.6 - 6) 10^{-12} & [30] \\ Br(K_L \rightarrow \pi^0 e^+ e^-)_{CP\text{-odd}}^{\text{direct}} &= (5 \pm 2) 10^{-12} & [31] \end{aligned} \quad (16)$$

At present, experimentally

$$Br(K_L \rightarrow \pi^0 e^+ e^-)^{\text{exp}} < 4.3 \cdot 10^{-8} \quad (17)$$

A probability of  $K^+ \rightarrow \pi^+ \nu \bar{\nu}$  decay is proportional to

$$|V_{td}|^2 = a^2 \lambda^6 [(1 - \rho)^2 + \eta^2] \quad (18)$$

and the branching ratio of this decay is expected at the level  $10^{-10}$  [32]. At present, only one event of such decay was observed that means that

$$Br(K^+ \rightarrow \pi^+ \nu \bar{\nu}) = (1.5^{+3.5}_{-1.3}) 10^{-10} \quad [33]. \quad (19)$$

The most interesting decay is  $K_L \rightarrow \pi^0 \nu \bar{\nu}$ . Practically, it is pure CP-odd decay because its amplitude is proportional to

$$< \pi^0 |V_{ts} V_{td}^* (\bar{s}d)_{V-A} - V_{ts}^* V_{td} (\bar{d}s)_{V-A}| K_L > \sim (V_{td}^* - V_{td}) \sim 2ia\lambda^3\eta \quad (20)$$

where  $\eta$  is the CP-odd CKM parameter. The relative probability of this decay is expected at the level  $(3.1 \pm 1.3) 10^{-10}$  [32]. An observation of this decay will allow to define more precisely the CKM parameters. The correspondent experiments are planned [34].

CP violation and as a consequence — T violation was observed in  $K_L \rightarrow \pi^+ \pi^- e^+ e^-$  decay [35]. The measured T-odd asymmetry turned out to be equal to the expected in SM [36].

### 1.5 T violation in kaon decays

A test of T invariance implies a comparison of the direct and inverse reaction. Such a test was realised for the first time by CPLEAR Collaboration in 1998 [37]. A magnitude of observed T-odd asymmetry turned out to be the same as was expected in SM.

A search for T-odd transverse polarization of muon in  $K^+ \rightarrow \pi^0 \mu^+ \nu$  decay belonging to the processes where the final-state interaction is negligible small [38] gave

$$P_\perp^\mu = (4.2 \pm 4.9 \pm 0.9) 10^{-3} \quad [39]$$

An observation of  $P_\perp^\mu \gg 10^{-6}$  would be an evidence of existance of other sources of CP violation. In particular,  $P_\perp^\mu \leq 1.2 \cdot 10^{-2}$  could arise in the models with CP violation in the extended sector of Higgs fields [40, 41].

### 1.6 CP violation in decays of D mesons

A phenomenology of CP violation in decays of the  $\{D^0, \bar{D}^0\}$  system is the same as for  $\{K^0, \bar{K}^0\}$  system and  $\varepsilon_D \sim s_2 s_3 \sin \delta \sim |\varepsilon_K| \sim 10^{-3}$ . But contrary to the case of neutral kaons, the life-times of  $D_1$  and  $D_2$  are very close one to another and very short ( $\sim 4 \cdot 10^{-13}$  s). This makes an observation of CP effects very difficult. And though  $\varepsilon_D \sim \varepsilon_K$ , CP violation in decay of  $\{D^0, \bar{D}^0\}$  system was not observed until now. For more details see [41]. The results of the experimental study are summed in [42]. For the meanwhile, the mean values of the asymmetries are of order 1-8 %, but the error bars are of the same order.

### 1.7 CP violation in decays of B mesons

As it was noted above, a smallness of CP violation in decays of  $K$  and  $D$  mesons has an accidental character. It was associated with the dependence

$$|\varepsilon_K| \sim |\varepsilon_D| \sim s_2 s_3 \sin \delta \sim 10^{-3}$$

For the  $\{B^0, \bar{B}^0\}$  system,  $\varepsilon_B$  is also small, but CP-odd parts of the subprocesses

$$b \rightarrow c\bar{c}s, \quad b \rightarrow u\bar{d}d$$

are large and governed by "tree" diagrams. For this reason, the *time-dependent* CP asymmetry

$$A_B(\tau) = \frac{\Gamma(B_{t=0}^0 \rightarrow f_{t=\tau}) - \Gamma(\bar{B}_{t=0}^0 \rightarrow f_{t=\tau})}{\Gamma(B_{t=0}^0 \rightarrow f_{t=\tau}) + \Gamma(\bar{B}_{t=0}^0 \rightarrow f_{t=\tau})}$$

where  $f$  is the CP-eigenstate, can be of order 1 in some processes, in particular, in decays

$$\{B^0, \bar{B}^0\} \rightarrow J/\psi K_S, \quad \{B^0, \bar{B}^0\} \rightarrow \pi^+ \pi^-$$

In the "tree" approximation, for the integral asymmetry, it was expected [43]

$$A_B(J/\psi K_S) \approx -0.47 \sin 2\beta = -0.47 \frac{2\eta(1-\rho)}{\eta^2 + (1-\rho)^2} \quad (21)$$

where  $\beta$  is an angle of the so-called unitarity triangle (see [9] p.112). A measurement of this asymmetry allows to improve our knowledge on CKM matrix. At present, there are few experimental results on  $\sin 2\beta$ , but an accuracy is not high:

$$\sin 2\beta = \begin{cases} 0.79^{+0.43}_{-0.42} & [44] \\ 0.99 \pm 0.14 \pm 0.06 & [45] \\ 0.59 \pm 0.14 \pm 0.05 & [46] \end{cases} \quad (22)$$

For the decays of charged B mesons, the CP-odd asymmetries are expected at the level of few percents or smaller [47].

In the semileptonic decays, the expected asymmetries are even smaller:

$$A_{Bd}(l^\pm \nu X) \leq (1-3)10^{-3}, \quad A_{Bs}(l^\pm \nu X) \leq O(10^{-4}), \quad [48]. \quad (23)$$

### 1.8 $T$ and $CP$ effects in the flavour-conserving processes

No one of the general principles does not forbid to add to well known QCD lagrangian the so-called  $\theta$  term [49]

$$\Delta L = -\theta \frac{g_s^2}{64\pi^2} \epsilon_{\mu\nu\alpha\beta} G_{\mu\nu}^a G_{\alpha\beta}^a \quad (24)$$

This term can violate CP invariance in flavour-conserving processes. The theory does not limit a magnitude of  $\theta$ , but the data on the electric dipole moment (EDM) of the neutron also generated by  $\theta$  term say us that

$$\theta < 3 \cdot 10^{-10} \quad (25)$$

Theoretically,

$$|d_n/e| = (2 - 3.6) 10^{-16} |\theta| \text{cm} \quad [50] \quad (26)$$

Though the parameter  $\theta$  is extremely small, the upper bounds on the effects generated by  $\theta$  term are larger in the flavor-conserving processes than that produced by the KM phase  $\delta$ . Thus,

$$\begin{aligned} d_n/e &\sim 10^{-32} \text{cm} & [51, 52] \\ d_e/e &\sim 10^{-40} \text{cm} & [53] \end{aligned} \quad (27)$$

Experimentally,

$$\begin{aligned} (d_n/e)^{\text{exp}} &< 6 \cdot 10^{-26} \text{cm} & [54] \\ (d_e/e)^{\text{exp}} &< 4 \cdot 10^{-27} \text{cm} & [55] \end{aligned} \quad (28)$$

This many-order difference between the  $d_{n,e}$  expected in SM and the experimental upper bounds for these quantities allows to search for the sources of CP violation beyond SM. The mechanisms of CP violation appearing in a theory with extended Higgs sector could give  $d_{n,e}$  close to their experimental bounds [41, 56, 57, 58]. The same is predicted in the supersymmetric generalization of SM [59] as well as for many other models (see refs. in [41]). Therefore, the experimental searches for EDM of the elementary particles are very actual.

## 2 CPT test with kaons and beyond

If any of the claims concerning the lagrangian density of the standard field theory is drawn off, a proof of the CPT theorem becomes not possible. The hypothetical sources of CPT violation are listed in [41]. But the realistic models allowing to calculate the effects starting from the first principles are absent. For this reason, it remains only to study the phenomenological consequences of CPT breakdown.

If CP is violated, but T invariance is conserved, that is, CPT is violated, the wave functions of  $K_{L,S}$  become of the form

$$K_S = [K_1 + (\varepsilon + \Delta) K_2] / \sqrt{1 + |\varepsilon + \Delta|^2}, \quad K_L = [K_2 + (\varepsilon - \Delta) K_1] / \sqrt{1 + |\varepsilon - \Delta|^2} \quad (29)$$

where  $\Delta$  describes the CPT-odd part of the wave functions.

Besides, if CP and CPT are violated in the direct transition of  $\{K^0, \bar{K}^0\}$  system into the final states, a set of additional parameters arises:

$$a = A(K_2^0 \rightarrow 2\pi; I = 0)/A(K_1^0 \rightarrow 2\pi : I = 0), \quad a \neq 0 \quad \rightarrow CPT = -1 \quad (30)$$

$$\frac{1 - y_l}{1 + y_l} = \frac{A(K^0 \rightarrow l^+ \nu \pi^-)}{A^*(\bar{K}^0 \rightarrow l^- \bar{\nu} \pi^+)}, \quad y \neq 0 \quad \rightarrow CPT = -1. \quad (31)$$

For the semileptonic Kaon decays, an inequality of the  $\Delta Q = -\Delta S$  parameters

$$x_l = \frac{A(\bar{K}^0 \rightarrow l^+ \nu \pi^-)}{A(K^0 \rightarrow l^+ \nu \pi^-)}, \quad \bar{x}_l = \frac{A^*(K^0 \rightarrow l^- \bar{\nu} \pi^+)}{A^*(\bar{K}^0 \rightarrow l^- \bar{\nu} \pi^+)} \quad (32)$$

also would be a signal of CPT violation.

As a result, for the parameters  $\eta_{+-}$  and  $\eta_{00}$  defined by eq.(6) one obtains

$$\eta_{+-} \cong \varepsilon - \Delta + \varepsilon' + a, \quad (33)$$

$$\eta_{00} \cong \varepsilon - \Delta - 2\varepsilon' + a \quad (34)$$

and the charge asymmetry parameter  $\delta_L$  (see (14)) becomes of the form

$$\delta_L \cong 2Re(\varepsilon - \Delta) - 2Rey_l - Re(x_l - \bar{x}_l). \quad (35)$$

These formulae show that the data on  $K_L^0$  decays only does not allow to separate CP and CPT violating parts of the wave functions. The data on  $K_S^0$  decays are necessary. In particular, the charge asymmetry  $\delta_S$ :

$$\delta_S = \frac{\Gamma(K_S \rightarrow l^+ \nu \pi^-) - \Gamma(K_S \rightarrow l^- \bar{\nu} \pi^+)}{\Gamma(K_S \rightarrow l^+ \nu \pi^-) + \Gamma(K_S \rightarrow l^- \bar{\nu} \pi^+)} \cong 2Re(\varepsilon + \Delta) - 2Rey_l + Re(x_l - \bar{x}_l). \quad (36)$$

In SM with the known quark contents, the  $\Delta Q = \Delta S$  rule is violated in second order in weak constant  $G_F$ . So that, the upper limit on  $Re(x_l - \bar{x}_l) < G_F m_K^2 \sim 2 \cdot 10^{-6}$ . Neglecting such small value we find

$$Re\Delta = \frac{1}{4}(\delta_S - \delta_L) \quad (37)$$

The first estimates of  $Re\Delta$  and  $Im\Delta$  for the case  $Rey_l \neq 0$  were obtained in [60] using the old data on  $K_{e3}^0$  decay:

$$Re\Delta = 0.018 \pm 0.020, \quad Im\Delta = 0.021 \pm 0.037 \quad (38)$$

The recent measurements [61] gave

$$Re\Delta = (2.4 \pm 2.8)10^{-4}, \quad Im\Delta = (-1.5 \pm 2.3)10^{-2} \quad (39)$$

For the other CPT-odd parameters, it was found [62]

$$Rey_l = (0.3 \pm 3.1)10^{-3}, \quad Imx_l = (-2.0 \pm 2.7)10^{-3}, \quad Re\bar{x}_l = (-0.5 \pm 3.0)10^{-3}. \quad (40)$$

It should be noted that a limit on  $Im\Delta$  can be lowered considerably using the Bell-Steinberger unitarity relation [63]. Then, according to [61]

$$Im\Delta = (2.4 \pm 5.0)10^{-5} \quad (41)$$

Let's consider now the CPT violating  $m_{K^0} - m_{\bar{K}^0}$  difference. It is defined by the relation [64]

$$m_{K^0} - m_{\bar{K}^0} = 2(m_L - m_S)(Re\Delta - Im\Delta \cdot \tan^{-1}\Phi_{SW}) \quad (42)$$

Using the above results one comes to

$$|m_{K^0} - m_{\bar{K}^0}|/m_K \leq 1.2 \cdot 10^{-17}, \quad [65]. \quad (43)$$

This result is one order less restrictive than in ref.[9] where the the possible contribution of the direct CPT violation characterized by parameter  $a$  was neglected. Taking into account such contribution it becomes possible to estimate a magnitude of  $|a| \leq 8 \cdot 10^{-4}$ . It follows from the above results that the upper limit on CPT violating parameters in decays of  $\{K^0, \bar{K}^0\}$  system is lower by 3 times than the parameter  $\eta_+$  characterizing a strength of CP violation.

A precise test of CPT invariance can be realized in the antihydrogen where a comparison of the frequency of  $(1s - 2s)2\gamma$  transition with the frequency of corresponding transition in hydrogen is possible with the accuracy  $10^{-15} - 10^{-18}$  [66]. If an equality of the charges of particles and their antiparticles is supposed, such a measurement would allow to reduce a limit on the combination

$$\frac{m_e - m_{e+}}{m_e} + \frac{m_e}{m_p} \cdot \frac{m_p - m_{\bar{p}}}{m_p}$$

to the level  $10^{-15} - 10^{-18}$ . The present upper limit for this combination is  $8 \cdot 10^{-9}$ .

One more precise test of CPT invariance is possible, if there is an interaction performing the neutron in antineutron. At  $m_n - m_{\bar{n}} \equiv \Delta m_{n\bar{n}} \leq 1/t$  where  $t$  is the life-time of the neutron beam in vacuum, an observation of the  $n \rightarrow \bar{n}$  transitions could give  $\Delta m_{n\bar{n}} \leq (10^{-22} - 10^{-23})m_n$  [67]. Until now, such transitions were not observed at the level  $\tau_{n\bar{n}} > 0.86 \cdot 10^8$  s [68].

## References

- [1] J.Schwinger, *Phys.Rev.* **82** 914 (1941); G.Luders, *Dansk.Mat.Fys.Medd.* **28** 17 (1954); G.Gravert,G.Luders and Rollnik, *Fortsch.Physik* **7** 291 (1959).
- [2] E.Amblor et al., *Phys.Rev.* **104** 1413 (1957).
- [3] B.L.Ioffe, L.B.Okun and A.P.Rudik, *JETP* **32** 396 (1957).
- [4] E.C.G.Sudarshan and R.E.Marshak, Proc.Int.Conf.*Mesons and Recently Discovered Particles* Padova-Venezia, 1957; R.P.Feynman and M.Gell-Mann, *Phys.Rev.* **109** 193 (1958); J.J.Sakurai, *Nuovo Cimento* **7** 649 (1958).
- [5] L.D.Landau, *Nucl.Phys.* **3** 138 (1957).
- [6] J.H.Christenson et al., *Phys.Rev.Lett.* **13** 138 (1964).
- [7] M.Kobayashi and T.Maskawa, *Prog.Theor.Phys.* **49** 652 (1973).
- [8] L.Wolfenstein, *Phys.Rev.Lett.* **51** 1945 (1983).
- [9] Particle Data Group, *Eur.Phys.J. C* **15** 1 (2000).
- [10] A.Buras, M.Jamin and M.E.Lautenbacher, *Nucl.Phys. B* **408** 209 (1993).
- [11] M.Ciuchini et al., *The Second DAPHNE Physics Handbook* Ed.L.Maiani, G.Panzeri and N.Paver, INFN-LNF , 1995 , p.27 .

- [12] S.Bertolini et al., *Nucl.Phys.* **B** **514** 93 (1998).
- [13] T.Hambye et al., *Nucl.Phys.* **B** **564** 391 (2000).
- [14] G.D.Barr et al.,(NA31 Collab.CERN) *Phys.Lett.* **317** 233 (1993).
- [15] L.K.Gibbons et al.,(E731 Collab.FNAL), *Phys.Rev.Lett.* **70** 1203 (1993).
- [16] A.Alavi-Harati et al.,(KTeV Collab. FNAL), *Phys.Rev.Lett.* **83** 22 (1999).
- [17] V.Fanti et al.,(NA48 Collab. CERN), *Phys.Lett.* **B** **465** 335 (1999).
- [18] L.Wolfenstein, *Phys.Rev.Lett.* **13** 569 (1964).
- [19] C.Jarlskog and E.Shabalin, *Phys.Rev.* **D** **52** 6327 (1995).
- [20] E.Shabalin, *Workshop on K Physics*, Orsay, France, 30 May-June 4, 1996, p.71.
- [21] E.Shabalin , *Phys.Reports* **320** 355 (1999).
- [22] A.Masiero and H.Murayama, *Phys.Lett.* **83** 907 (1999) ; S.Khalil, T.Kobayashi, A.Masiero , *Phys. Rev.* **D** **60** 075003 (1999); S.Khalil and T.Kobayashi, *Phys.Lett.* **B** **460** 341 (1999) ; K.S.Babu, B.Dutta and R.N.Mohapatra, , hep-ph/9907572, 1999; R.Barbieri, R.Contino and A.Strumia, hep-ph/9908255, 1999; A.J.Buras et al., hep-ph/9908371.
- [23] B.Grinstein, S.Rey and M.B.Wise, *Phys.Rev.* **D** **33** 1495 (1986); H.-Y.Cheng , *Phys.Rev.* **D** **44** 919 (1991); G.D'Ambrosio, G.Isidori and N.Paver, *Phys.Lett.* **B** **273** 497 (1991); E.Shabalin, preprint ITEP 6-92, 1992.
- [24] A.A.Bel'kov et al., *Phys.Lett.* **B** **232** 118 (1989) ; A.A.Bel'kov et al., *Phys.Lett.* **B** **300** 283 (1993).
- [25] L.Maiani and N.Paver, *The Second DAPhNE Physics Handbook*, Ed. L.Maiani, G.Pancheri and N.Paver, INFN-LNF 1995, p.51.
- [26] E.P.Shabalin , *Nucl. Phys.* **B** **409** 87 (1993).
- [27] E.P.Shabalin , *Phys.Atomic Nucl.* **61** 1372 (1998).
- [28] E.P.Shabalin, *Phys.Atomic Nucl.* **62** 1552 (1999).
- [29] A.G.Cohen, G.Ecker and A.Pich, *Phys.Lett.* **B** **304** 347 (1993).
- [30] B.Winstein and L.Wolfenstein , *Rev.Mod.Phys.* **65** 1113 (1993).
- [31] A.J.Buras et al., *Nucl.Phys.* **B** **423** 349 (1994).
- [32] G.Buchalla and A.J.Buras , *Nucl.Phys.* **B** **548** 309 (1999).
- [33] T.Sato, Proc.*III Int. Workshop on Physics and Detectors for DAPhNE*, Frascati , November 16-19, 1999, p.159.
- [34] D.Bryman, Proc.*III Int. Workshop on Physics and Detectors for DAPhNE*, Frascati, November 16-19, 1999, p.189; *ibid.* R.E.Ray , p.179.
- [35] Alavi-Harati et al., (KTeV Collab., FNAL) *Phys.Rev.Lett.* **84** 408 (2000).
- [36] P.Heiliger and L.M.Sehgal, *Phys.Rev.* **D** **48** 9 (1993); L.M.Sehgal and J.Lensen, *Phys.Rev.Lett.* **83** 4933 (1999).
- [37] A.Angelopoulos et al., (CPLEAR Collab., CERN), *Phys.Lett.* **B** **444** 43 (1998).
- [38] A.R.Zhitnitskii, *Yad.Fiz.* **31** 1024 (1980).
- [39] M.Abe et al., Abstr.of XV Particle and Nuclei Int. Conf. PANIC'99, Uppsala, Sweden, June 10-16, 1999, p.511.
- [40] G.Belanger and C.O.Geng, *Phys.Rev.* **D** **44** 2789 (1991).
- [41] E.P.Shabalin, *Usp.Fiz.Nauk* **171** 951 (2001).
- [42] J.A.Appel, Proc.Int.Conf. *Physics and Detectors for DAPhNE* , Frascati, November 16-19, 1999,p.231.

- [43] H.M.Nelson , Proc. *XX SLAC Summer Institute on Particle Physics*, SLAC-Report-412, 1992, p.47.
- [44] C.A.Blocker , (CDF Collab.), Proc.Int.Conf. *Physics and Detectors for DAPhNE*, Frascati, November 16-19, 1999, p.248.
- [45] K.Abe et al., *Phys.Rev.Lett.* **87** 091802-1 (2001).
- [46] B.Aubert et al., *Phys.Rev.Lett.* **87** 091801-1(2001).
- [47] H.Simma, G.Eliam and D.Wyler , *Nucl.Phys.* **B 352** 367 (1991).
- [48] I.Bigi et al., in *CP Violation*, Ed. C.Jarlskog (World Scientific, Singapore), 1988.
- [49] G.t'Hooft , *Phys.Rev.Lett.* **37** 8 (1976).
- [50] V.Baluni , *Phys.Rev.* **D 19** 2227 (1979); R.J.Crewter et al., *Phys.Lett.* **B 88** 123 (1979).
- [51] E.P.Shabalin , *Yad.Phys.* **28** 151 (1978).
- [52] E.P.Shabalin , *Sov.Phys.Usp.* **26**(4) 297 (1983).
- [53] I.B.Khriplovich , Proc. *XV Int.Conf. on Particles and Nuclei (PANIC'99)*, Uppsala, Sweden, June 10-16, 1999, p. 147c.
- [54] P.G.Harris et al., *Phys.Rev.Lett.* **82** 904 (1999).
- [55] E.D.Commins et al., *Phys.Rev.* **A 50** 2960 (1994).
- [56] S.M.Barr and A.Zee , *Phys.Rev.Lett.* **65** 21 (1990).
- [57] A.Das and C.Kao , *Phys.Lett.* **B 372** 106 (1996).
- [58] A.Bramon and E.Shabalin , *Phys.Lett.* **B 404** 115 (1997).
- [59] J.Ellis , S.Ferrara and D.V.Nanopoulos, *Phys.Lett.* **B 114** 231 (1982); J.Polchinski and M.B.Wise , *Phys.Lett.* **B 125** 393 (1983); F.del Aguila et al., *Phys.Lett.* **B 126** 71 (1983); M.Dugan , B.Grinstein and L.Hall, *Nucl.Phys.* **B 255** 413 (1985).
- [60] V.Demidov , K.Gusev and E.Shabalin, *Phys.Atomic Nucl.* **58** 968 (1995).
- [61] A.Angelopoulos et al.(CPLEAR Collab.), *Phys.Lett.* **B 444** 52 (1998).
- [62] A.Apostolakis et al.(CPLEAR Collab.), *Phys. Lett.* **B 456** 297 (1999).
- [63] J.S.Bell and J.Steinberger, Proc.Int.Conf. on Elementary Particles, Oxford 1965 (Chilton, Rutherford High Energy Lab.), 1966, p.193.
- [64] V.V.Barmin et al., *Nucl.Phys.* **B 247** 293 (1984).
- [65] E.Shabalin, *Phys.Lett.* **B 369** 335 (1996).
- [66] J.Eades and F.J.Hartmann, *Rev.Mod.Phys.* **71** 373 (1999).
- [67] Yu.G.Abov, F.S.Djeparov and L.B.Okun , *JETP Lett.* **39** 493 (1984); L.B.Okun, Proc. *Workshop on K Physics*, Orsay, 30 May- June 4, 1996, p.419.
- [68] M.Baldo-Ceolin et al., *Z.Phys.* **C 63** (1994) 409.

# The precise determination of $\Re(\epsilon'/\epsilon)$

M.Cirilli <sup>a</sup>

*University of Rome and INFN, I-00185, Rome, Italy*

*Abstract.*  $\mathcal{CP}$  violation in the neutral kaon system is known to be dominated by the mixing of  $K^0$  and  $\bar{K}^0$ . Direct  $\mathcal{CP}$  violation in the 2 pion decays of neutral kaons has been a controversial subject over the last decade. A strong experimental effort has been devoted to the precise measurement of the direct  $\mathcal{CP}$  violation parameter  $\Re(\epsilon'/\epsilon)$ . After 10 years of detector development, data collection and analysis, the NA48 experiment at CERN and the KTeV experiment at Fermilab have now established direct  $\mathcal{CP}$  violation as a fact. Both KTeV and NA48 use the same experimental principle, measuring the double ratio of long lived and short lived neutral kaons to two charged and two neutral pions. However, their experimental and analysis techniques differ in important ways, and I will extensively discuss the two approaches. I will also present the latest results on  $\Re(\epsilon'/\epsilon)$  from both experiments, which were announced just a few months ago.

## 1 Introduction

The violation of  $\mathcal{CP}$  symmetry was first reported in 1964 by J.H. Christenson, J.W. Cronin, V. Fitch and R. Turlay, who detected a clean signal of  $\mathcal{CP}$  violating  $K_L^0 \rightarrow \pi^+ \pi^-$  decays [1].  $\mathcal{CP}$  conservation implies that the  $K_S^0$  and  $K_L^0$  particles are pure  $\mathcal{CP}$  eigenstates and that  $K_L^0$  decays only into  $\mathcal{CP} = -1$  and  $K_S^0$  into  $\mathcal{CP} = +1$  final states. The observed signal of the forbidden  $K_L^0 \rightarrow \pi\pi$  decays ( $\mathcal{CP} = +1$ ) indicates that  $\mathcal{CP}$  is not a conserved symmetry.

$\mathcal{CP}$  violation can occur via the mixing of  $\mathcal{CP}$  eigenstates, called *indirect*  $\mathcal{CP}$  violation, represented by the parameter  $\epsilon$ .  $\mathcal{CP}$  violation can also occur in the decay process itself, through the interference of final states with different isospins. This is represented by the parameter  $\epsilon'$  and is called *direct*  $\mathcal{CP}$  violation. L. Wolfenstein in 1964 [2] proposed a super-weak force responsible for  $\Delta S = 2$  transitions, so that all observed  $\mathcal{CP}$  violation phenomena come from mixing and  $\epsilon' = 0$ . In 1973, Kobayashi and Maskawa proposed a matrix representation of the coupling between fermion families [3]. In the case of three fermion generations, both direct and indirect  $\mathcal{CP}$  violation are naturally accommodated in their model, via an irreducible phase.

The parameters  $\epsilon$  and  $\epsilon'$  are related to the amplitude ratios

$$\eta_{+-} = \frac{A(K_L^0 \rightarrow \pi^+ \pi^-)}{A(K_S^0 \rightarrow \pi^+ \pi^-)} = \epsilon + \epsilon'$$

and

$$\eta_{00} = \frac{A(K_L^0 \rightarrow \pi^0 \pi^0)}{A(K_S^0 \rightarrow \pi^0 \pi^0)} = \epsilon - 2\epsilon'$$

---

<sup>a</sup>e-mail: Manuela.Cirilli@cern.ch

which represent the strength of the  $\mathcal{CP}$  violating amplitude with respect to the  $\mathcal{CP}$  conserving one, in each mode. By the mid-1970s, experiments had demonstrated that  $\mathcal{CP}$  violation in the neutral kaon system is dominated by mixing, with the limit  $\Re(\epsilon'/\epsilon) \leq 10^{-2}$  [4]. On the other hand, theoretical work showed that direct  $\mathcal{CP}$  violation in the Standard Model could be large enough to be measurable [5]. This stimulated experimental effort with sophisticated detectors to measure  $\Re(\epsilon'/\epsilon)$ . The first evidence for the existence of a direct component of  $\mathcal{CP}$  violation was published in 1988 [6]. In 1993, two experiments published their final results without a conclusive answer on the existence of this component. NA31 [7] measured  $\Re(\epsilon'/\epsilon) = (23.0 \pm 6.5) \times 10^{-4}$ , indicating a  $3.5\sigma$  effect. The result of E731 [8],  $\Re(\epsilon'/\epsilon) = (7.4 \pm 5.9) \times 10^{-4}$ , was instead compatible with no effect.

The controversial results from NA31 and E731 called for the realization of more precise experiments, to measure  $\Re(\epsilon'/\epsilon)$  with a precision of  $\mathcal{O}(10^{-4})$ . Presently, there are three experiments in different laboratories working on the precise measurement of  $\Re(\epsilon'/\epsilon)$ : two of these, namely NA48 [9] at CERN and KTeV [10] at Fermilab, represent the “evolution” of NA31 and E731 respectively; the third one is KLOE [11] at the Laboratori Nazionali di Frascati and its conceptual design is radically different from the other experiments.

This paper is devoted to a comparative presentation of KTeV and NA48, since these experiments have already published results. Detector designs and analysis techniques will be discussed, together with the results announced just recently from these two collaborations [12] [13].

## 2 The experimental method

Experimentally, it is convenient to measure the double ratio  $\mathcal{R}$ , which is related to the ratio  $\Re(\epsilon'/\epsilon)$ :

$$\mathcal{R} = \frac{\Gamma(K_L^0 \rightarrow \pi^0 \pi^0)}{\Gamma(K_S^0 \rightarrow \pi^0 \pi^0)} / \frac{\Gamma(K_L^0 \rightarrow \pi^+ \pi^-)}{\Gamma(K_S^0 \rightarrow \pi^+ \pi^-)} \approx \infty - \propto \Re(\epsilon'/\epsilon) \quad (1)$$

The double ratio  $\mathcal{R}$  is experimentally measured by *counting* the number of decays detected in each of the four modes in equation 1. The statistical error is dominated by the events collected in the most suppressed decay, namely  $K_L^0 \rightarrow \pi^0 \pi^0$  ( $BR \sim 0.09\%$ ). The value  $\mathcal{R}_{true}$  is then deduced correcting the measured value  $\mathcal{R}_{meas}$  for the kaon beam fluxes, detector acceptances, trigger efficiencies, backgrounds evaluations, etc., i.e. for all the possible biases in the counting process. It is now evident that the difficulty of  $\Re(\epsilon'/\epsilon)$  measurements lies in the necessity to disentangle the  $\mathcal{CP}$  violating  $K_L^0$  modes from the dominant environment of  $\mathcal{CP}$  conserving 3-body decays of both  $K_L^0$  and  $K_S^0$ .

## 2.1 Advantages of the double ratio technique

The main advantage of the double ratio measurement, when performed under the adequate data taking conditions, is that the corrections to  $\mathcal{R}_{meas}$  can cancel out at first order. Let us consider the beam fluxes and trigger/reconstruction efficiencies corrections as an example:

- **Beam fluxes:** the knowledge of the kaon flux in the  $K_S^0$  and  $K_L^0$  beams is a priori needed for normalization purposes. However, if the charged and neutral decay modes of either the  $K_S^0$  or the  $K_L^0$  are simultaneously collected, then the ratio of  $\pi^+\pi^-$  and  $\pi^0\pi^0$  events in each beam is independent from the absolute flux. Hence, under these conditions, beam fluxes cancel out in the double ratio at first order.
- **Efficiencies:** the trigger scheme is conceived to minimise any loss of good events. However, a small correction usually has to be applied to  $\mathcal{R}_{meas}$  to account for trigger inefficiencies. A first order cancellation of this correction can be achieved for the charged/neutral trigger efficiency if both  $K_L^0$  and  $K_S^0$  decays into the charged/neutral final state are simultaneously collected. The same principle also holds for any instability of a given detector, which could affect the reconstruction efficiency of the charged or neutral modes.

The best strategy to exploit the cancellation of eventual biases is to collect all the four modes simultaneously. This allows to evaluate only second order effects to get the true value  $\mathcal{R}_{true}$  from  $\mathcal{R}_{meas}$ . Even in this ideal situation, there will still be some leftover corrections that do not cancel out. This is the case for the physical background, which comes only from  $K_L^0$  decays and is clearly final-state-dependent. Also, acceptance corrections do not a priori cancel out in the four modes: this is related to the huge lifetime difference between  $K_L^0$  and  $K_S^0$ , which causes very different longitudinal decay vertex distributions for the two beams, and to the different topologies of  $\pi^0\pi^0 \rightarrow 4\gamma$  and  $\pi^+\pi^-$  events. Both the physical background and the acceptance correction must be carefully studied, and different solutions can be envisaged to handle them.

All the above considerations have been thoroughly taken into account while conceiving KTeV and NA48. The design of the experiments and the analysis methods focus on making the inevitable systematic biases in the event counting symmetric between at least two of the four components of the double ratio. In this way, most of the important systematic effects cancel to first order, and only the differences between two components need to be considered in detail in the analysis. This allows the systematic uncertainties to be kept sufficiently low.

### 3 KTeV and NA48: overview

Both KTeV and NA48 are fixed target experiments designed to simultaneously collect all the four decay modes in 1. Measuring  $\Re(\epsilon'/\epsilon)$  to a precision of  $\sim 10^{-4}$  requires several millions of  $K_L^0$  and  $K_S^0 \rightarrow \pi\pi$  decays: this implies taking data with high-intensity kaon beams and running for several years to achieve the desired statistics. A number of challenges had to be faced during the design phase. Stable detectors were needed to sustain the long data taking periods. The trigger electronics had to be fast enough to cope with the high flux of particles in the decay region and a powerful data acquisition was needed to handle the high trigger rates. The overwhelming  $3\pi^0$  background set the requirement of an extremely precise electromagnetic calorimeter. The whole detector had to be radiation-hard, to cope with the beam intensities. Long R&Ds were necessary to meet these very demanding requirements, and this effort has also been profitable in view of future experiments in high-intensity environments (*e.g.*, the Tevatron and LHC).

KTeV collected  $\sim 7M$  events in the most suppressed channel  $K_L^0 \rightarrow \pi^0\pi^0$  during the 96, 97 and 99 runs. A first  $\Re(\epsilon'/\epsilon)$  measurement [14] was announced in February, 1999, based on 10% of the total sample. In June, 2001, KTeV presented a new result on the 97 data sample, together with an update of the already published result: the combined measurement [13] is obtained from  $\sim 50\%$  of the available data. NA48 took data in 97, 98 and 99, collecting almost 4M events in the neutral  $K_L^0$  decay mode. The first  $\Re(\epsilon'/\epsilon)$  measurement [15] was reported in June, 1999, and was based on the statistics collected during the 97 run; a preliminary result on the 98 sample was presented in February, 2000. The final result on the 98 and 99 data [12] was announced in May, 2001. A slight increase in statistics for NA48 is expected from the data collected in the 2001 run.

#### 3.1 KTeV: Detector and beam lines

A schematic view of KTeV detectors and beams is shown in figure 1. KTeV exploits the 800 GeV proton beam delivered by the Tevatron: two nearly parallel kaon beams are produced by the protons hitting a 50 cm long beryllium target at 4.8 mrad angle. The beams are cleaned up and let fly for roughly 120 m, so that only the  $K_L^0$  component survives. The beams direction defines the longitudinal  $z$  axis. The decay region begins at the end of the last collimator; here the two beams are 10 cm apart, and one of them hits a 1.8 m long regenerator made of plastic scintillators. The regenerator beam is a coherent superposition  $K_L^0 + \rho K_S^0$  of long- and short-lived kaons. The regenerated fraction  $\rho$  is proportional to the amount of matter traversed by the previously pure  $K_L^0$  beam, and its value 0.03 is sufficient to ensure that the regenerator  $2\pi$  decays are dominated by  $K_S^0 \rightarrow \pi\pi$ . The regenerator technique ensures that

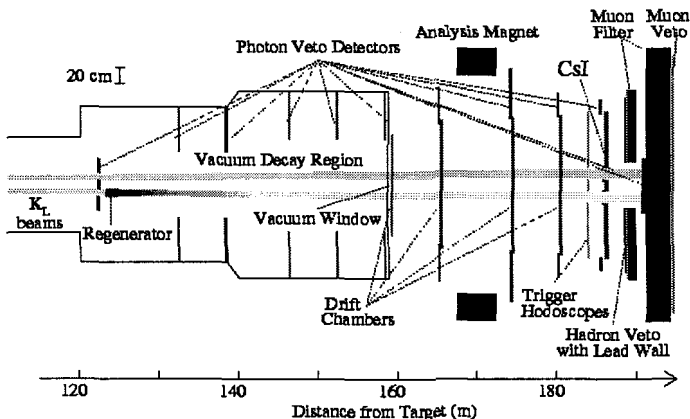


Figure 1: Top view of KTeV detector and beam lines.

the  $K_S^0$  are produced with an energy spectrum similar to that of  $K_L^0$ . The decay region extends up to 159 m from the primary target.

A distinctive feature of KTeV is the fact that the two beams are parallel and hit the detectors at separate points (left and right). This allows to easily identify  $K_L^0$  and  $K_S^0$  decays reconstructing the transverse decay vertex position and comparing it with the known regenerator position. The regenerator is fully instrumented, and switches beam line once per minute, in order to reduce the effects of possible left-right asymmetries of the detectors.

Charged kaon decays are detected by a spectrometer consisting of a central magnet with a 411 MeV/c kick in the horizontal plane and of four drift chambers with wires along the  $x$  and  $y$  directions. The spectrometer has a position resolution of  $100\mu\text{m}$  and a momentum resolution  $\sigma_p/p = 0.17\% \oplus [0.008 \times p]\%$ , where  $p$  is in GeV/c units.

Neutral decays are detected by a crystal calorimeter [16] consisting of 3100 pure CsI blocks. The crystals cover  $27X_0$  in length (50 cm) and have a transverse section of  $2.5 \times 2.5\text{cm}^2$  in the central region, where the density of photons is higher; in the outer region of the calorimeter, the granularity is of  $5 \times 5\text{cm}^2$ . The main advantage of this calorimeter lies in its excellent stochastic term in the energy resolution, which allows to reach an overall resolution of 0.7% for a 15 GeV photon (as shown in figure 2 left). The longitudinal light collection is equalised within 5% by means of a meticulous crystal wrapping. In addition, the stability of the response for each crystal is continuously checked using a  $\text{Cs}^{137}$  source for calibration. The overall energy response is linear within 0.4%.

The main apparatus is surrounded by circular vetoes to detect escaping pho-

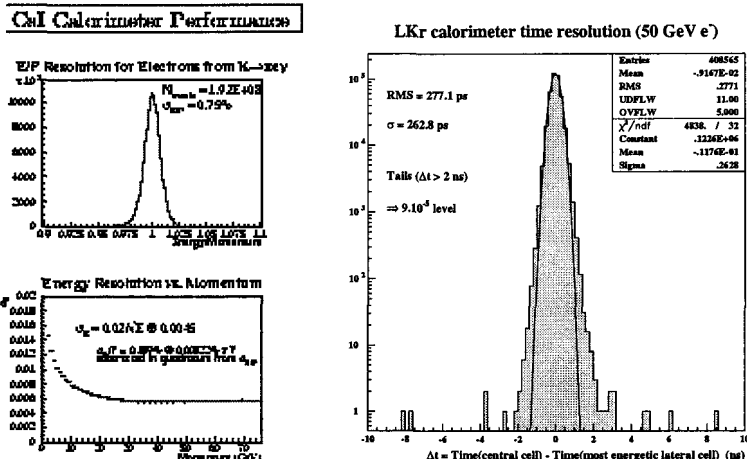


Figure 2: Performances of KTeV CsI crystal calorimeter (left) and of the NA48 LKr ionization calorimeter (right)

tons, and a muon veto placed at the end of the line is used to identify  $K_{\mu 3}$  decays.

### 3.2 NA48: Detector and beam lines

A schematic view of the NA48 beam lines is given in figure 3. The primary 450 GeV proton beam is delivered from the SPS and impinges on a 40 cm beryllium target with an incidence angle of 2.4 mrad relative to the  $K_L^0$  beam axis. The charged component of the outgoing particles is swept away by bending magnets, while the neutral beam component passes through three stages of collimation. The fiducial region starts at the exit of the “final” collimator, 126 m downstream of the target. At this point, the neutral beam is dominated by long-lived kaons. The non-interacting protons from the  $K_L^0$  target are directed onto a mechanically bent mono-crystal of silicon. A small fraction ( $10^{-5}$ ) of protons satisfies the conditions for channelling and is deflected following the crystalline planes. Use of the crystal allows a deflection of 9.6 mrad to be obtained in only 6 cm length, corresponding to a bending power of 14.4 Tm. The transmitted protons pass through the tagging station (or *tagger*), which precisely registers their time of passage. They are then deflected back onto the  $K_L^0$  beam axis, transported through a series of quadrupoles and finally directed to the  $K_S^0$  target (same size as  $K_L^0$ ) located 72 mm above the  $K_L^0$  beam axis. A combination of collimator and sweeping magnet defines a neutral beam at 4.2 mrad to the incoming protons. The decay spectrum of kaons at the exit of the collimator is similar to that in the  $K_L^0$  beam, with an average energy of

110 GeV. The fiducial region begins 6 m downstream of the  $K_S^0$  target, such that decays are dominated by short lived particles. At this point, the  $K_S^0$  and  $K_L^0$  beams emerge from the aperture of the final collimators into the common decay region. The whole  $K_S^0$  target and collimator system is aligned along an axis pointing to the centre of the detector 120 m away, such that the two beams intersect at this point with an angle of 0.6 mrad.

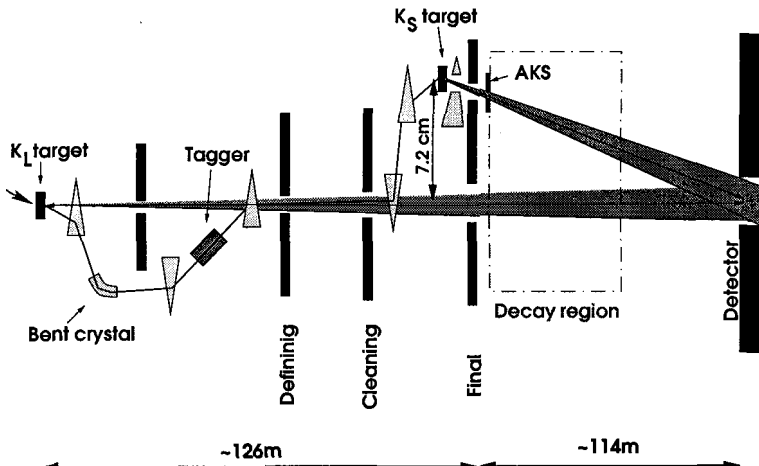


Figure 3: Schematic view of NA48 beam lines (not to scale).

Since the two beams are not separated at the detector position, as it is in KTeV, the identification of  $K_L^0$  and  $K_S^0$  decays must be accomplished in a different way. This is done using the tagging station, which consists of two scintillator ladders, crossing the beam horizontally and vertically. The coincidence between the proton time and the event time in the detectors assigns the decay to the  $K_S^0$  beam. Two close pulses can be resolved down to 4–5 ns.

The reconstruction of charged decays is performed by a magnetic spectrometer, with a central magnet giving a 250 MeV/c transverse kick and four chambers with plane wires oriented along four different directions  $x$ ,  $y$ ,  $u$  and  $v$ . The redundancy of the planes allows to resolve the possible track ambiguities.

NA48 has chosen a liquid Krypton ionization calorimeter with a depth of  $27X_0$ , corresponding to 125 cm. The read-out is performed by Cu-Be-Co ribbons defining  $\sim 13\,000$  cells, in a structure of longitudinal projective towers pointing to the centre of the decay region. The cross section of a cell is about  $2\text{ cm} \times 2\text{ cm}$ , and the electrodes are guided longitudinally through precisely machined holes in five spacer plates. The planes also apply a  $\pm 48$  mrad zig-zag to the electrodes, in order to maintain the mechanical stability and to decrease the sensitivity of the energy resolution to the impact position. Good energy

response is further guaranteed by the initial current readout technique which also provides a high rate capability. The overall energy resolution is 1.5% at 10 GeV. The energy response is linear to about 0.1% in the range 5–100 GeV. A precise time measurement is mandatory for the NA48 calorimeter, since it must be used together with the proton time from the tagger to distinguish  $K_S^0$  from  $K_L^0$ . The neutral event time is reconstructed with a precision of  $\sim 220$  ps.; tails coming from misreconstructed times are below the level of  $10^{-4}$  (see figure 2 right).

A muon veto system is used to reject muons from  $K_{\mu 3}$  decays.

## 4 KTeV and NA48: analysis techniques

Once the events are collected, all corrections that do not cancel in the double ratio must be applied. The long list of residual effects that must be studied includes physical backgrounds,  $K_S^0 - K_L^0$  misidentifications, trigger efficiencies, Monte Carlo correction, geometrical acceptances, detector biases (calorimeter energy scale, drift chamber alignment, etc.), accidental effects. In the following, I will focus on just a few of these effects, highlighting the important differences between KTeV and NA48 approach.

### 4.1 Selection of the $\pi^+\pi^-$ sample

Both experiments use the magnetic spectrometer to reconstruct the kaon mass, vertex and momentum. The resolution on the kaon mass in the charged mode is 1.5 MeV in KTeV and 2.5 MeV in NA48. The better KTeV resolution is due to the higher transverse kick of their magnet and to the choice of having only  $x$  and  $y$  planes in the drift chambers. This choice implies lighter chambers with respect to NA48, and so a lower multiple scattering term in the resolution. However, having only two views reduces the capability of resolving ambiguities in the track reconstruction: for this reason, KTeV needs additional information from the calorimeter to perform a reliable reconstruction of  $\pi^+\pi^-$  events.

Background to $K^0 \rightarrow \pi^+\pi^-$			
Background source	KTeV (vac)	KTeV (reg)	NA48 $K_L^0$
$K_{\mu 3} + K_{e3}$	$0.9 \times 10^{-3}$	$0.03 \times 10^{-3}$	$1.69 \times 10^{-3}$
Collimator scatt.	$0.10 \times 10^{-3}$	$0.10 \times 10^{-3}$	-
Regenerator scatt.	-	$0.73 \times 10^{-3}$	-

Table 1: Summary of background fractions in the charged mode.

$K_{\mu 3}$  decays are rejected using the identified muon in the dedicated vetoes, while electrons from  $K_{e3}$  events are identified comparing the track momentum in the spectrometer with the corresponding energy in the calorimeter.

Additional cuts are imposed on the reconstructed mass and transverse momentum. The leftover background contributions are then evaluated studying high-statistics samples of the identified 3-body decays. The background fractions in the two experiments are summarized in table 1, including the components due to scattering in the collimator and (only for KTeV) regenerator.

#### 4.2 Selection of the $\pi^0\pi^0$ sample

Both experiments base the reconstruction of neutral events on the information from the electromagnetic calorimeter. In addition to the energies and positions of the four photons, a mass constraint must be imposed in order to reconstruct the decay vertex position. KTeV method imposes the  $\pi^0$  mass to all photon pairs combinations, computing the vertex position for each pairing; only the two closest solutions are kept, and they are combined to produce the most probable value for the kaon decay vertex. NA48 method imposes the kaon invariant mass on the  $4\gamma$  event, thus constraining the decay vertex position. The two  $\pi^0$  are reconstructed choosing the best of all the possible pairings between the photons.

Background to $K^0 \rightarrow \pi^0\pi^0$			
Background source	KTeV (vac)	KTeV (reg)	NA48 $K_L^0$
$K_L^0 \rightarrow 3\pi^0$	$1.1 \times 10^{-3}$	$0.3 \times 10^{-3}$	$0.59 \times 10^{-3}$
Collimator scatt.	$1.2 \times 10^{-3}$	$0.9 \times 10^{-3}$	$0.96 \times 10^{-3}$
Regenerator scatt.	$2.5 \times 10^{-3}$	$11.3 \times 10^{-3}$	-
Regenerator had. int	-	$0.1 \times 10^{-3}$	-

Table 2: Summary of background fractions in the neutral mode.

Both experiment define a  $\chi^2$  variable that states the compatibility of each event with the  $K^0 \rightarrow \pi^0\pi^0$  hypothesis. Background events from  $K_L^0 \rightarrow 3\pi^0$  decays with lost or merged photons have a high value of the  $\chi^2$  and are rejected. The amount of remaining background is evaluated from a high-statistic sample of  $3\pi^0$  events. Background fractions for KTeV and NA48 are summarized in table 2.

#### 4.3 $K_S^0$ and $K_L^0$ identification

As already described in sections 3.1 and 3.2, the two experiments use different techniques to distinguish  $K_S^0$  from  $K_L^0$ . KTeV takes advantage of having two parallel beams: the 10 cm separation allows to disentangle  $K_S^0$  and  $K_L^0$  by looking at the reconstructed decay vertex position in the transverse plane, in the case of charged events. In the case of neutral events, the energy centroid of the four photons is used, as shown in figure 4 left. The halo surrounding one of the two beams is due to events scattered in the regenerator before decaying:

this effect is accurately studied in the  $p_T^2$  distribution of charged events, and is then introduced into a detailed simulation to evaluate the contribution in the neutral case.

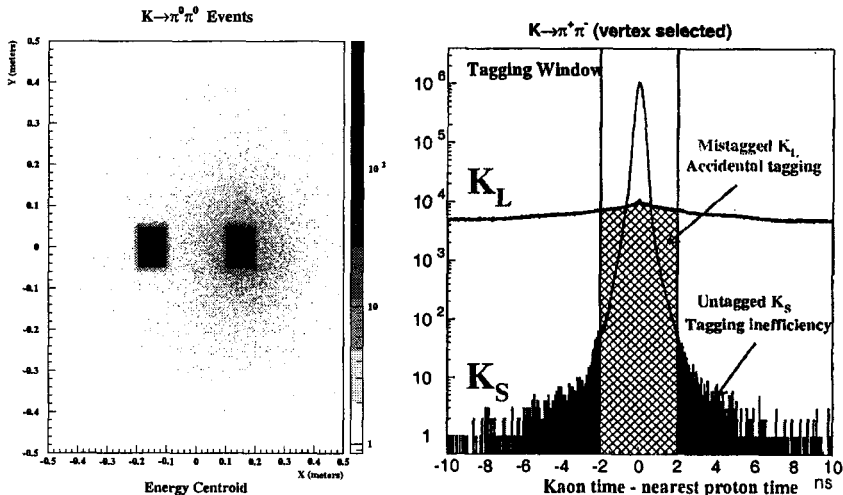


Figure 4: tagging

NA48 uses the tagging method: a decay is identified as  $K_S^0$  if its event time is within a  $\pm 2$  ns coincidence with a proton time measured by the tagger. The principle can be clearly illustrated for charged events, which can be identified as  $K_S^0$  or  $K_L^0$  also on the basis of the vertical separation between the two beams at the drift chamber position. This is shown in figure 4 right, where the difference between the event time and the time of the nearest proton in the tagger is plotted. It is evident that the inefficiencies in identifying true  $K_S^0$  decays is very small ( $10^{-4}$  level). On the other hand, there is a sizeable mistagging probability in the case of  $K_L^0$ : the high rate of events in the  $K_L^0$  beam causes accidental coincidences, and it turns out that  $\sim 10\%$  of the true  $K_L^0$  events are misidentified as  $K_S^0$ . The final data samples are corrected for both inefficiency and accidental tagging.

#### 4.4 From event counting to $\mathcal{R}$

Having identified  $K_S^0$  and  $K_L^0$ , as well as charged and neutral decays, both experiments end up with four samples of events. In the case of KTeV, the samples correspond to the Vacuum beam ( $K_L^0$  decays) and to Regenerator beam (mostly  $K_S^0$ ) into  $π^+π^-$  and  $π^0π^0$  final modes. The striking difference in the decay vertex distributions for  $K_S^0$  and  $K_L^0$  translates in a large acceptance correction,

which therefore must be precisely known. The correction is implemented using a highly detailed Monte Carlo simulation which includes all known effects, as trigger and detector efficiencies, regeneration,  $K_S^0 - K_L^0$  interference, detector apertures, etc. The value of  $\Re(\epsilon'/\epsilon)$  is then obtained fitting the data in 10 GeV bins in the kaon energy, in order to minimise residual differences in the energy spectra.

NA48 has two charged/neutral samples of tagged events (essentially  $K_S^0$ ) and two other charged/neutral samples of untagged events ( $K_L^0$  with a  $\sim 10\%$  contamination of  $K_S^0$ ). All samples are corrected for mistagging and trigger inefficiencies. The final result is computed by dividing the data into 20 bins of kaon energy from 70 to 170 GeV, and calculating the double ratio for each bin. To cancel the contribution from the different lifetimes to the acceptance,  $K_L^0$  events are weighted with the  $K_S^0$  lifetime as a function of the reconstructed proper decay time. After weighting, the  $K_L^0$  and  $K_S^0$  decay distributions become nearly identical and the size of the acceptance correction is drastically reduced. The weighting technique avoids the need of an extremely sophisticated simulation, although it results in a  $\sim 35\%$  increase of the statistical error on  $R$ . All corrections are applied to each bin separately, and the results are averaged using an unbiased estimator.

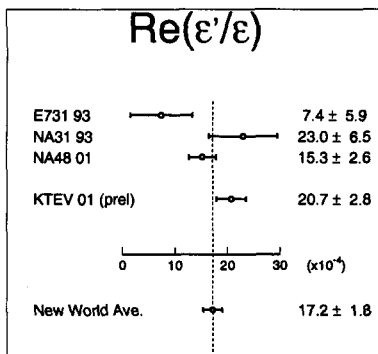


Figure 5: result

## 5 Results from KTeV and NA48

The latest results from KTeV [13] and NA48 [12] are summarized in figure 5, together with the final results from NA31 and E731. The new world average value of  $\Re(\epsilon'/\epsilon)$  is  $(17.2 \pm 1.8) \times 10^{-4}$ . This result confirms the existence of direct  $\mathcal{CP}$  violation in the neutral kaon system. Whether the measured size of  $\Re(\epsilon'/\epsilon)$  is compatible with Standard Model expectations or is a hint that

new physics is at work, this is still matter of debate: theoretical calculations suffers from big uncertainties in the determination of the hadronix mass matrix elements, thus their predictive power on  $\varepsilon'/\varepsilon$  is rather poor.

Establishing beyond doubt the existence of the direct  $\mathcal{CP}$  violation mechanism has been a long experimental adventure. Both KTeV and NA48 have still other data samples to analyse, and hopefully KLOE will provide also its measurement of  $\Re(\varepsilon'/\varepsilon)$  with a different method. We recently witnessed the first observation of  $\mathcal{CP}$  violation in a system other than the neutral kaon system, namely in  $B^0 - \bar{B}^0$  oscillations.  $\mathcal{CP}$  violation studies are also being performed in the sector of B and K rare decays. Considering all these constraints together, there is reasonable hope that a deeper understanding of the  $\mathcal{CP}$  violation mechanism will be achieved in the forthcoming years.

## Acknowledgements

I would like to warmly thank the organisers of the 10<sup>th</sup> Lomonosov Conference on Elementary Particle Physics for the interesting meeting.

## References

- [1] J.H. Christenson et al., Phys. Rev. Lett. **13**, 138 (1964)
- [2] L. Wolfenstein, Phys. Rev. Lett. **13**, 562 (1964).
- [3] M. Kobayashi and K. Maskawa, Prog. Theor. Phys. **49**, 652 (1973).
- [4] M. Holder et al., Phys. Lett. B **40**, 141 (1972); M. Banner et al., Phys. Rev. Lett. **28**, 1957 (1972).
- [5] J. Ellis, M.K. Gaillard and D.V. Nanopoulos, Nucl. Phys. B **109**, 213 (1976); F.J. Gilman and M.B. Wise, Phys. Lett. B **83**, 83 (1979).
- [6] H. Burkhardt et al., Phys. Lett. B **206**, 169 (1988).
- [7] G. Barr et al., Phys. Lett. B **317**, 233 (1993).
- [8] L.K. Gibbons et al., Phys. Rev. Lett. **70**, 1203 (1993).
- [9] G. D. Barr et al., CERN/SPSC/90-22 (1990).
- [10] K. Arisaka et al., FN-580 (1992).
- [11] The KLOE Collaboration, LNF-93/002 (1993).
- [12] A. Lai et al. [NA48 Collaboration], CERN-EP-2001-067.
- [13] J. Graham [KTeV Collaboration], FNAL Seminar; R. Kessler, hep-ex/0110020.
- [14] A. Alavi et. al., [KTeV Collaboration], Phys. Rev. Lett. **83**, 22 (1999).
- [15] V. Fanti et al., Phys. Lett. B **465**, 335-348 (1999).
- [16] R. S. Kessler et. al., Nucl. Instr. Meth. A **368**, 653 (1996).
- [17] G. Barr et. al., Nucl. Instr. Meth. Phys. Res. A **370**, 413 (1996).

# RARE DECAYS OF NEUTRAL KAONS WITH THE NA48 EXPERIMENT

A. Bizzeti

*Università di Modena e Reggio Emilia - Dipartimento di Fisica,  
via G. Campi 213/A, I-41100 Modena, Italy*

*INFN - Sezione di Firenze, via G. Sansone 1, Sesto F.no, Firenze, Italy  
e-mail: andrea.bizzeti@fi.infn.it*

representing the NA48 Collaboration:

*Cagliari, Cambridge, CERN, Dubna, Edinburgh, Ferrara, Firenze,  
Mainz, Orsay, Perugia, Pisa, Saclay, Siegen, Torino, Vienna, Warsaw*

**Abstract.** New and recent results by the NA48 collaboration on neutral kaons rare decays are presented. Future programs to search for very rare  $K_S$  and  $\Xi^0$  decays and for direct CP violation in charged kaons are discussed.

## 1 Introduction

The NA48 experiment at CERN SPS has been designed to measure [1, 2] the direct CP violation parameter  $\Re(\epsilon'/\epsilon)$  in two-pion decays of neutral kaons. However, the quality of its simultaneous  $K_L$  and  $K_S$  beams [3], high resolution detectors [4], fast trigger and performing data acquisition system allows to investigate, at the same time, rare decays of neutral kaons and neutral hyperons.

Rare decay data have been collected during 1997-1999  $\Re(\epsilon'/\epsilon)$  runs, as well as during dedicated runs with a high intensity  $K_S$  and hyperon beam in 1999 and 2000.

In this paper some recent NA48 results on rare decays of neutral kaons are presented, together with an outlook on NA48 future program. The experimental apparatus is described in section 2. Section 3 reports NA48 preliminary results on  $K_L$  and  $K_S$  decays into the  $\pi^+\pi^-e^+e^-$  final state, confirming a recently discovered effect [5] of indirect CP violation in  $K_L$  decays. Final results on the decay  $K_L \rightarrow \pi^0\gamma\gamma$  are discussed in section 4. Sections 5 and 6 describe two extensions [6, 7] of NA48 experimental activity, already approved by CERN Research Board, to search for very rare  $K_S$  and hyperon decays in 2002 and for CP violation in the decays of charged kaons starting in 2003. Conclusions are given in section 7.

## 2 Beams and detector

### 2.1 The neutral kaon beams

The NA48 experiment uses two simultaneous neutral beams [3]. They are produced from CERN SPS 450 GeV/c protons interacting on two separate targets, located 126 m and 6 m upstream of the beginning of the decay fiducial region, respectively (fig. 1).

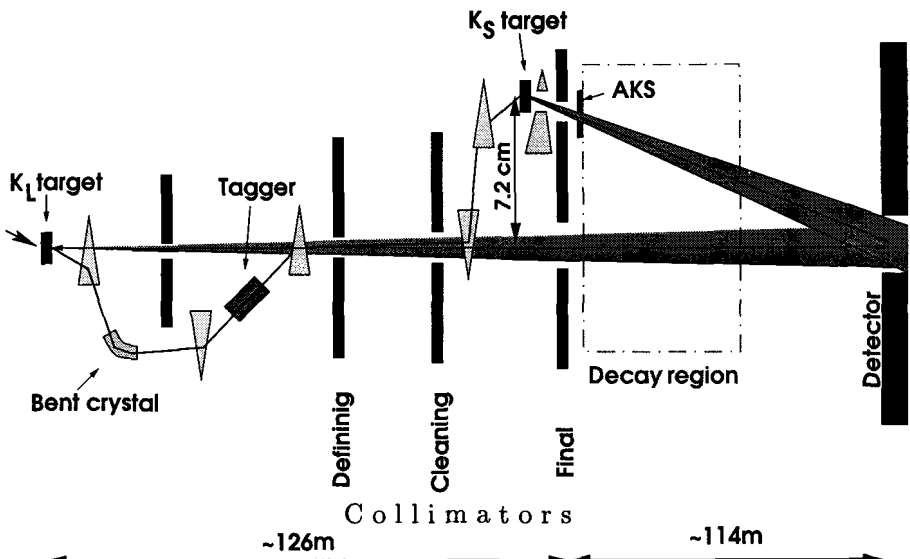


Figure 1: A schematic view of the beam line (not to scale).

During normal NA48 runs, for each SPS pulse (2.4 s spill every 14.4 s)  $1.5 \cdot 10^{12}$  protons hit the  $K_L$  production target, originating an intense neutral secondary beam. Due to the different mean decay length of  $K_L$  and  $K_S$  (3.4 km and 5.9 m, respectively, at the average kaon momentum of 110 GeV/c) almost all  $K_L$  within the acceptance of the three-stage collimation system reach the decay region, while nearly all  $K_S$  and other short-lived particles decay long before.

A small fraction of the non-interacting protons is deflected by channelling in a mechanically bent silicon mono-crystal [8] to produce a collimated beam of  $3 \cdot 10^7$  protons per pulse. This beam is transported to the  $K_S$  production target, where it generates a neutral beam entering the fiducial region 6 m downstream of the target, such that the decays are dominated by short-lived particles ( $K_S$ ,  $\Lambda$  and  $\bar{\Lambda}$ ). The protons transported to the  $K_S$  target are detected by an array of plastic scintillators ("tagger") [9], used to tag  $K_S$  decays. An event is defined a  $K_S$  ( $K_L$ ) decay based on the presence (absence) of a proton in coincidence with the event.

At the exit of the  $K_S$  collimator a photon converter [10] followed by three plastic scintillators ("AKS") is used to veto  $K_S$  decays occurring upstream and to provide an accurate definition of the beginning of the fiducial region.

The fiducial decay region is contained in an evacuated ( $\sim 5 \cdot 10^{-5}$  mbar) 90 m long tank, closed at its end by a thin ( $3 \cdot 10^{-3} X_0$ ) composite polyamide (Kevlar) window. It is followed by a 16 cm diameter beam pipe transporting the intense neutral beam to the beam dump downstream of all detector elements.

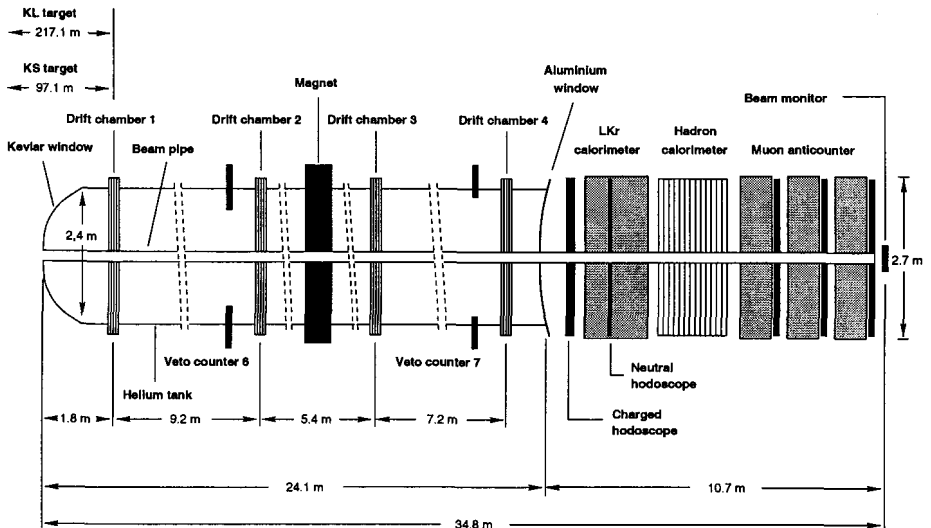


Figure 2: Schematic drawing of the NA48 detector.

## 2.2 The detector

The NA48 detector, described in detail elsewhere [2, 4] is shown in figure 2. Seven annular veto counters (“AKL”) are located around the decay region to detect photons escaping the acceptance of the main detector.

Directions and momenta of charged particles are measured by a magnetic spectrometer consisting of four drift chambers [11] and a dipole magnet giving a horizontal momentum kick of 265 MeV/c. Downstream of the spectrometer a scintillator hodoscope provides a precise time measurement of charged events.

A 127 cm ( $27X_0$ ) long liquid Krypton electromagnetic calorimeter [12] with projective tower readout is used to measure the photons from neutral decays. It is also used, together with a subsequent iron-scintillator hadron calorimeter, to measure the total visible energy for triggering purposes.

Downstream of the calorimeters three planes of scintillators interleaved with 80 cm thick iron walls are used for muon identification.

The intensity of the beams is monitored by two beam counters. One of them (“ $K_L$  monitor”) is located at the end of the  $K_L$  beam line, the other (“ $K_S$  monitor”) close to the  $K_S$  production target.

## 3 $K_L, K_S \rightarrow \pi^+ \pi^- e^+ e^-$

### 3.1 $K_L \rightarrow \pi^+ \pi^- e^+ e^-$

The  $\pi^+ \pi^- e^+ e^-$  decays of neutral kaons are expected to proceed through an intermediate state involving a virtual photon [13, 14]:  $K_{L,S} \rightarrow \pi^+ \pi^- \gamma^* \rightarrow$

$\pi^+\pi^-e^+e^-$ . The main components of the  $K_L \rightarrow \pi^+\pi^-e^+e^-$  decay amplitude come from CP-odd magnetic dipole (M1) direct photon emission and from the decay to the CP-even state  $\pi^+\pi^-$  with inner bremsstrahlung. An interesting effect of the interference between these amplitudes is the appearance of a large CP-violating asymmetry in the distribution of the angle  $\varphi$  from the  $e^+e^-$  plane to the  $\pi^+\pi^-$  plane (right-handed with respect to the direction of the total momentum of charged pions) in the kaon rest frame:

$$\frac{d\Gamma}{d\varphi} = \Gamma_1 \cos^2(\varphi) + \Gamma_2 \sin^2(\varphi) + \Gamma_3 \sin(\varphi) \cos(\varphi),$$

where the third term gives a dependence of  $d\Gamma/d\varphi$  on the sign of the CP-odd and T-odd variable  $\sin(\varphi) \cos(\varphi)$ , which constitutes a clear signature of CP violation. The CP-violating asymmetry

$$\mathcal{A} \equiv \frac{N_{\sin(\varphi) \cos(\varphi) > 0} - N_{\sin(\varphi) \cos(\varphi) < 0}}{N_{\sin(\varphi) \cos(\varphi) > 0} + N_{\sin(\varphi) \cos(\varphi) < 0}} = \frac{N_{0 < \varphi < \pi/2} - N_{\pi/2 < \varphi < \pi}}{N_{0 < \varphi < \pi/2} + N_{\pi/2 < \varphi < \pi}}$$

is predicted by theory [13, 14] to be  $|\mathcal{A}(K_L)| \approx 14\%$ . The value  $\mathcal{A}(K_L) = (13.6 \pm 2.5_{stat} \pm 1.2_{syst})\%$  recently measured by KTeV [5] is in good agreement with theoretical predictions.

During 1998 and 1999 run periods more than 1300 good  $K_L \rightarrow \pi^+\pi^-e^+e^-$  events have been selected using a dedicated four-track trigger [15]. The events are selected requiring a good 4-track vertex; electrons and pions are identified by their different interactions in the calorimeter. Electrons from photon conversions in the material before the spectrometer are eliminated by requiring a 2 cm minimum separation between the  $e^+$  and  $e^-$  tracks in the first chamber, while  $\pi^+\pi^-e^+e^-$  events from two overlaid  $K_{e3}$  decays are rejected by time constraints. The large background from  $K_L \rightarrow \pi^+\pi^-\pi_D^0 \rightarrow \pi^+\pi^-e^+e^-\gamma$  decays is strongly suppressed using a kinematic cut on the variable [16]

$$P_0'^2 = \frac{(M_K^2 - M_{\pi^0}^2 - M_{\pi\pi})^2 - 4M_{\pi^0}^2 M_{\pi\pi}^2 - 4(P_T^2)_{\pi\pi} M_K^2}{4[M_{\pi\pi}^2 + (P_T^2)_{\pi\pi}]}$$

which is greater than zero for  $K_L \rightarrow \pi^+\pi^-\pi_D^0$  but is mostly negative for  $K_L \rightarrow \pi^+\pi^-e^+e^-$  events.

The invariant mass distribution of the  $K_L \rightarrow \pi^+\pi^-e^+e^-$  candidate events passing all analysis cuts is plotted in fig. 3(a) together with the expected background.

For the determination of the  $K_L \rightarrow \pi^+\pi^-e^+e^-$  branching fraction the decay  $K_L \rightarrow \pi^+\pi^-\pi_D^0 \rightarrow \pi^+\pi^-e^+e^-\gamma$  is used as normalization channel. The correction for the detector acceptance is determined using a model by Heiliger and Sehgal [14] with the inclusion of a form factor in the M1 direct emission amplitude:

$$F_{M1} = \tilde{g}_{M1} \left[ 1 + \frac{a_1/a_2}{(M_\rho^2 - M_K^2)c^2 + 2M_K(E_{e^+} + E_{e^-})} \right].$$

Using the values  $\bar{g}_{M1} = 1.35^{+0.20}_{-0.17}$  and  $a_1/a_2 = (-0.720 \pm 0.029)$  (GeV/c)<sup>2</sup> measured by KTeV [5] we obtain the preliminary result  $B(K_L \rightarrow \pi^+\pi^-e^+e^-) = (3.1 \pm 0.1 \pm 0.2) \cdot 10^{-7}$ , in fair agreement with the KTeV preliminary result [17] of  $(3.63 \pm 0.11 \pm 0.14) \cdot 10^{-7}$ .

The  $\sin(\varphi)\cos(\varphi)$  distribution of  $K_L \rightarrow \pi^+\pi^-e^+e^-$  events after acceptance correction is shown in fig. 3(b). Our preliminary result on the observed asymmetry is  $\mathcal{A}(K_L) = (13.9 \pm 2.7 \pm 2.0)\%$ , in good agreement with theoretical predictions [14] and the recently published KTeV value [5].

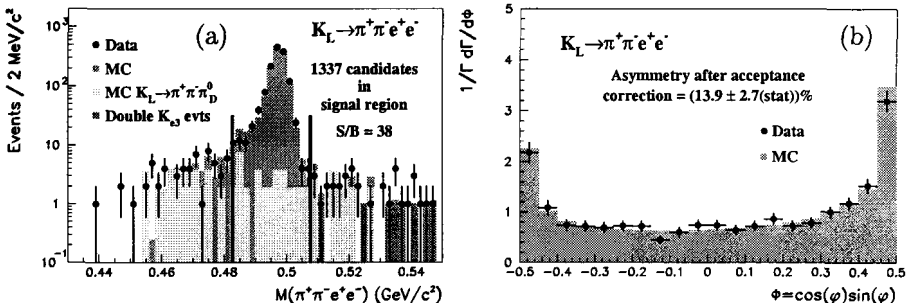


Figure 3: (a) Invariant mass distribution and (b) acceptance corrected  $\sin(\varphi)\cos(\varphi)$  distribution of  $K_L \rightarrow \pi^+\pi^-e^+e^-$  candidate events.

### 3.2 $K_S \rightarrow \pi^+\pi^-e^+e^-$

The  $K_S \rightarrow \pi^+\pi^-e^+e^-$  decay amplitude is largely dominated by the CP-even inner bremsstrahlung process, therefore no CP-violating asymmetry is expected in this case.

The first observation of this decay mode with a clean sample of 56 events selected from 1998 data has been recently published [15] by NA48.

In 1999 two days of run were dedicated to the investigation of rare decays of  $K_S$  and neutral hyperons. During this run the  $K_L$  beam was switched off, the AKS converter at the beginning of the fiducial volume was removed and the proton beam intensity on the  $K_S$  target was increased by about a factor 200. During this short test run a large amount of rare decay events was collected, equivalent to several years of operation with the standard beam setup.

Fig. 4(a) shows the invariant mass distribution of  $K_S \rightarrow \pi^+\pi^-e^+e^-$  candidate events from the full 1998+1999 data sample, together with the background expected from  $\pi^+\pi^-\pi^0$  decays of  $K_L$  originating from the  $K_S$  target. The  $\sin(\varphi)\cos(\varphi)$  distribution of these events is plotted in fig. 4(b), together with Monte Carlo prediction with no asymmetry. The measured value of the CP-violating asymmetry  $\mathcal{A}(K_S) = (-0.2 \pm 3.4 \pm 1.4)\%$  is consistent with zero. Our preliminary result on the branching fraction is  $B(K_S \rightarrow$

$\pi^+\pi^-e^+e^-) = (4.3 \pm 0.2 \pm 0.3) \cdot 10^{-5}$ . This value can be used to evaluate the inner bremsstrahlung contribution to the  $K_L$  decay, obtaining  $B(K_L^{IB} \rightarrow \pi^+\pi^-e^+e^-) = (1.3 \pm 0.1) \cdot 10^{-7}$ , in good agreement with theoretical predictions [13, 14].

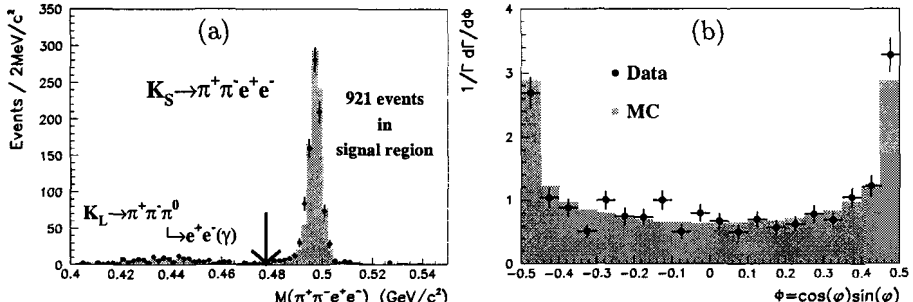


Figure 4: (a) Invariant mass distribution and (b) acceptance corrected  $\sin(\phi)\cos(\phi)$  distribution of  $K_S \rightarrow \pi^+\pi^-e^+e^-$  candidate events.

#### 4 $K_L \rightarrow \pi^0\gamma\gamma$

The decay  $K_L \rightarrow \pi^0\gamma\gamma$  is interesting in two ways. Firstly, it allows to test the predictions of models based on Chiral Perturbation Theory ( $\chi$ PT); secondly, it is related to the CP-conserving amplitude of the  $K_L \rightarrow \pi^0e^+e^-$  decay, which is expected to have also a CP-violating component.

$\chi$ PT calculations at one loop ( $O(p^4)$ ) predict a decay rate [18] which is only 1/3 of the measured one [19, 20]. Calculations to  $O(p^6)$  [21], including a Vector Meson Dominance (VMD) contribution (parametrized by a coupling constant  $a_v$ ), can account for the measured rate. Contrary to  $O(p^4)$  ones,  $O(p^6)$  calculations also predict a tail at low values of the two-photon invariant mass  $m_{\gamma\gamma}$ . A measurement of this tail allows to extract the amplitude of the VMD contribution, from which the CP-conserving amplitude in the  $K_L \rightarrow \pi^0e^+e^-$  decay can be derived.

The  $K_L \rightarrow \pi^0\gamma\gamma$  decays are detected as a 4 photon final state. They are therefore triggered with high efficiency by the same trigger used to select  $K_L \rightarrow \pi^0\pi^0$  decays for  $\Re(\epsilon'/\epsilon)$  measurement. The data sample used in this measurement comes from 1998 and 1999  $\Re(\epsilon'/\epsilon)$  data sets. It contains a large amount of  $K_L \rightarrow \pi^0\pi^0$  decays, which are used as a normalization channel. Due to the similar topology of the two decay channels, selected by the same trigger, most systematic uncertainties cancel in the ratio.

The candidate events are triggered by an energy deposited in the electromagnetic calorimeter of at least 50 GeV, with a center of gravity within 15 cm from the beam axis and less than 6 peaks in each of the two transverse projections. The trigger system also requires the second moments of the energy distribution

in the electromagnetic calorimeter to be consistent with a  $K_L$  decay occurring within the first 5  $K_S$  decay lengths from the beginning of the fiducial volume.

Triggered events with four photon candidates, no hits in the drift chambers or in the  $K_L$  vetoes and no proton detected in the tagger within  $\pm 2$  ns from the event time are then selected to be used in the analysis.

The main backgrounds to the  $K_L \rightarrow \pi^0 \gamma\gamma$  decay channel come from  $K_L \rightarrow 2\pi^0$  and  $K_L \rightarrow 3\pi^0$  decays, the latter with two photons lost (outside of the electromagnetic calorimeter acceptance) or one photon lost and other two overlapping in the calorimeter.

In order to reject the  $2\pi^0$  background, invariant masses of  $\gamma\gamma$  pairs are calculated under a  $K_L$  invariant mass constraint for the complete event. For each of the three combinations of  $\gamma\gamma$  pairs a  $\chi^2$  variable is calculated:

$$\chi^2 = \left[ \frac{(m_{12} + m_{34})/2 - m_{\pi^0}}{\sigma_+} \right]^2 + \left[ \frac{(m_{12} - m_{34})/2}{\sigma_-} \right]^2$$

where  $m_{12}$  and  $m_{34}$  are the invariant masses of the two photon pairs and  $\sigma_{\pm}$  are the experimental resolutions on  $(m_{12} \pm m_{34})/2$ . The event is then rejected if the lowest of the three  $\chi^2$  values is below 300 or if one of the  $\gamma\gamma$  invariant masses is within  $\pm 3$  MeV/c<sup>2</sup> from the nominal  $\pi^0$  mass  $m_{\pi^0}$  and the other one is inside the window 110–160 MeV/c<sup>2</sup>.

The large  $3\pi^0$  background is strongly suppressed by combinatorial cuts based on the fact that the decay vertex is correctly calculated, using an invariant mass constraint, for  $\pi^0 \rightarrow \gamma\gamma$  but not for  $K_L$  in case of lost photons. In addition, the cluster width of each photon candidate is required to be compatible with that of a single electromagnetic shower.

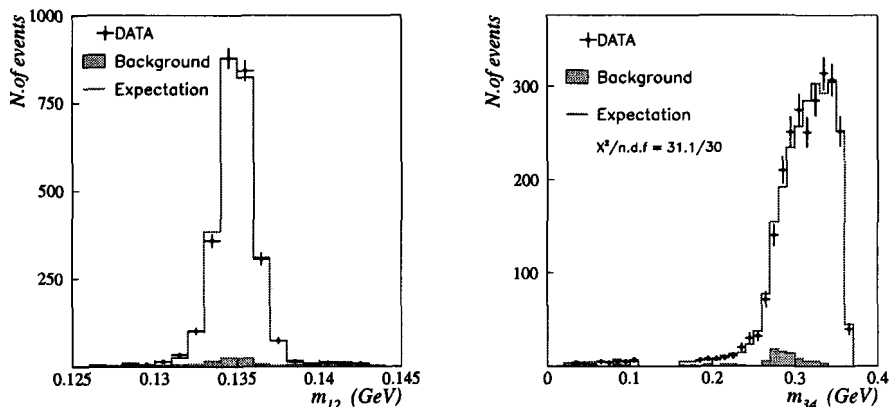


Figure 5: Invariant mass distribution of the two photons from  $\pi^0$  decay ( $m_{12}$ ) and of the other two photons ( $m_{34}$ ).

The  $\gamma\gamma$  invariant mass distribution of the two photons associated to the  $\pi^0$  ( $m_{12}$ ) and that of the other two photons ( $m_{34}$ ) are plotted in fig. 5, together

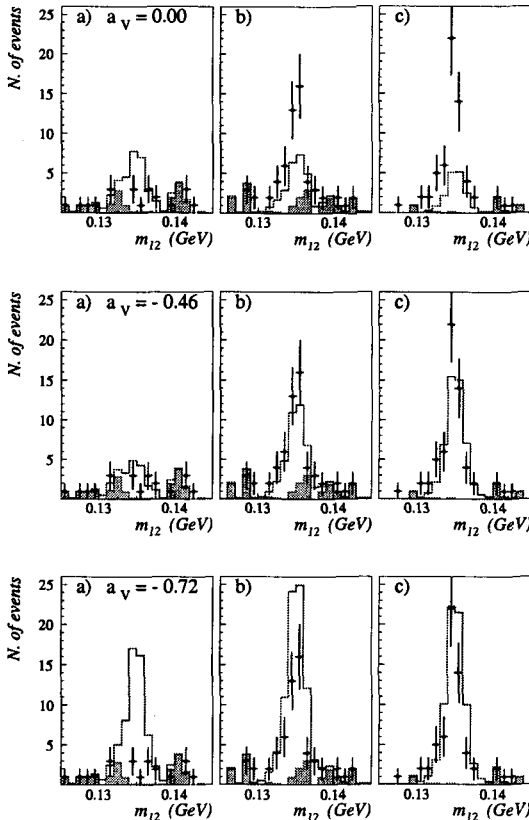


Figure 6: Invariant mass distribution of the two photons from  $\pi^0$  decay ( $m_{12}$ ) in three different regions of the low- $m_{34}$  tail: (a)  $<135 \text{ MeV}/c^2$ ; (b)  $135\text{--}240 \text{ MeV}/c^2$ ; (c)  $240\text{--}280 \text{ MeV}/c^2$ . Measured values (points) are compared to Monte Carlo predictions (histogram), including background (shaded histogram), obtained with three different values of  $a_V$ .

with the expected residual background (mainly from  $3\pi^0$  decays). The tail at small  $m_{34}$  provides a clear evidence for contributions beyond  $O(p^4)$  with a non-zero value of  $a_V$ .

In order to understand the sensitivity of the invariant mass distributions to the value of  $a_V$ , three regions in  $m_{34}$  have been chosen and, for each of them, the measured  $m_{12}$  has been plotted. Fig. 6 shows these plots, together with Monte Carlo predictions for  $a_V=0, -0.46$  and  $-0.72$ , corresponding to no VMD contribution, to our best fit and to KTeV result [20], respectively. While a zero value of  $a_V$  underestimates the number of events in the  $240\text{--}260 \text{ MeV}/c^2$  invariant mass region, the large  $-0.72$  value overestimates the number of events in the lowest mass region.

The final value obtained from NA48 data is  $a_V = -0.46 \pm 0.03_{(\text{stat})} \pm 0.03_{(\text{syst})} \pm$

$0.02_{(theo)}$ . The branching fraction of the decay  $K_L \rightarrow \pi^0 \gamma\gamma$  is determined to be  $B(K_L \rightarrow \pi^0 \gamma\gamma) = (1.36 \pm 0.03_{(stat)} \pm 0.03_{(syst)} \pm 0.03_{(norm)}) \cdot 10^{-6}$ . A publication of this result is in preparation.

## 5 Future plans on $K_S$ and $\Xi^0$ rare decays: NA48/1

After completion of  $\Re(\epsilon'/\epsilon)$  program in 2001, the NA48 experiment will take data in 2002 with a modified  $K_S$  beam line in order to investigate  $K_S$  and neutral hyperon rare decays with high sensitivities [6].

The improved beam duty cycle (already operational in 2001), together with the upgraded drift chamber and electromagnetic calorimeter readout systems, will allow to increase the primary proton flux to  $2 \cdot 10^{10}$  protons per pulse, producing about  $6 \cdot 10^{10}$   $K_S$  decays per year in the fiducial volume and a large number of neutral hyperon decays.

One of the main goals of this experimental program is the search for the  $K_S \rightarrow \pi^0 e^+ e^-$  decay, whose branching fraction can be used to determine the indirect CP-violating component of the  $K_L \rightarrow \pi^0 e^+ e^-$  decay:

$$B(K_L \rightarrow \pi^0 e^+ e^-)_{ind.CPV} = |\epsilon|^2 \frac{\tau_L}{\tau_S} B(K_S \rightarrow \pi^0 e^+ e^-) \simeq 3.0 \cdot 10^{-3} B(K_S \rightarrow \pi^0 e^+ e^-)$$

An upper limit  $B(K_S \rightarrow \pi^0 e^+ e^-) < 1.4 \cdot 10^{-7}$  (90% C.L.) has been recently measured by NA48 [22], improving by an order of magnitude the limit previously measured by NA31 [23]. In one year of operation we expect to reach a single event sensitivity (SES) of  $2 \cdot 10^{-10}$  on the  $K_S \rightarrow \pi^0 e^+ e^-$  rare decay.

The  $K_S \rightarrow \pi^0 \mu^+ \mu^-$  decay will also be searched for, although its branching fraction is expected to be about five time smaller.

The  $K_S \rightarrow \pi^0 \pi^0 \pi^0$  rare decay is expected to occur with a very small branching fraction through CP violation in the  $K^0 - \overline{K^0}$  mixing. The experimental search of this decay mode will be performed by measuring the interference term in the proper time distribution of  $K^0, \overline{K^0} \rightarrow \pi^0 \pi^0 \pi^0$  decays:

$$N_{000}(t) \propto e^{-t/\tau_L} + |\eta_{000}|^2 e^{-t/\tau_S} + 2D|\eta_{000}|e^{-\frac{t}{2}(\frac{1}{\tau_S} + \frac{1}{\tau_L})} \cos(\Delta m \cdot t + \phi_{000})$$

where  $\eta_{000} = |\eta_{000}|e^{i\phi_{000}} \equiv \frac{A(K_S \rightarrow \pi^0 \pi^0 \pi^0)}{A(K_L \rightarrow \pi^0 \pi^0 \pi^0)}$  and  $D \equiv \frac{N(K^0) - N(\overline{K^0})}{N(K^0) + N(\overline{K^0})} \approx 0.3$  for NA48. This measurement should allow to reach an upper limit of about  $10^{-2}$  on  $\eta_{000}$ .

The sensitivity of the NA48 experiment should also allow the observation of the rare decays  $K_S \rightarrow \pi^0 \pi^0 \gamma\gamma$ ,  $K_S \rightarrow e^+ e^- \gamma$  and  $K_S \rightarrow \mu^+ \mu^- \gamma$ .

The  $\beta$  decay of the  $\Xi^0$  hyperon ( $B = (2.7 \pm 0.4) \cdot 10^{-4}$ ) [24], reconstructed through the decay chain  $\Xi^0 \rightarrow \Sigma^+ e^- \bar{\nu}$ ,  $\Sigma^+ \rightarrow p \pi^0$ , will be studied in detail with an expected statistics of about 50,000 events.

The  $\Xi^0 \rightarrow \Lambda\gamma$  and  $\Xi^0 \rightarrow \Sigma^0\gamma$  radiative decays will also be investigated, with a statistics two orders of magnitude higher than in our previous measurements [25]. The high resolution of NA48 photon detector already allowed to perform the up to now most precise measurement of the  $\Xi^0$  mass [25]. With 2002 data it should be possible to further reduce its uncertainty to 0.1 MeV, at the level of the current experimental error on the  $\Xi^-$  mass [26].

The second order weak decay  $\Xi^0 \rightarrow p\pi^-$  with double strangeness change ( $\Delta S = 2$ ) will be searched for, improving the present upper limit [27] on the branching fraction ( $< 4 \cdot 10^{-5}$  at 90% C.L.) by two orders of magnitude.

## 6 Search for CP violation in Charged Kaons decay: NA48/2

Direct CP violation has been observed up to now only in  $K^0 \rightarrow 2\pi$  decays. This effect has been recently confirmed with high accuracy by NA48 [2]. The observation of direct CP violation in other processes would provide important informations in order to understand the origin of this effect.

The NA48 collaboration proposed [7] to look for direct CP violation in  $K^\pm \rightarrow (3\pi)^\pm$  decays using an extended experimental setup. This proposal has been approved by CERN Research Board and we plan to start data taking in 2003.

The Dalitz plot distribution of  $K^\pm \rightarrow (3\pi)^\pm$  decays can be parametrized [28] by the following formula:  $|M(u, v)|^2 \propto 1 + gu + hv^2 + kv^2$ , where  $u = (s_3 - s_0)/m_\pi^2$ ,  $v = (s_1 - s_2)/m_\pi^2$ ,  $s_0 = \frac{1}{3}(s_1 + s_2 + s_3)$ ,  $s_i = (P_K - P_i)^2$ ,  $P_K$  and  $P_i$  are the four-momenta of the kaon and pion ( $i = 3$  for the odd pion), respectively, and  $m_\pi$  is the mass of the charged pion.

The coefficients  $g$ ,  $h$  and  $k$  must be the same for  $K^+$  and  $K^-$  decays if CP is conserved. As a measure of CP violation, the asymmetry  $A_g \equiv (g^+ - g^-)/(g^+ + g^-)$  is considered, where  $g^+$  and  $g^-$  correspond to the  $g$  coefficients for the  $K^+$  and  $K^-$  decays, respectively. Several theoretical predictions [30–32] exist for  $A_g$ , ranging between  $10^{-6}$  and a few  $10^{-4}$ . The best measurement done up to now [29] gives  $A_g = (-7.0 \pm 5.3) \cdot 10^{-3}$ .

The value of  $A_g$  can be determined by measuring the ratio of the integrated Dalitz plot distributions:

$$R(u) \equiv \frac{\int dv |M^+(u, v)|^2}{\int dv |M^-(u, v)|^2} \approx 1 + (g^+ - g^-) \cdot u$$

Simultaneous  $K^+$  and  $K^-$  beams from the same target will be used, with a central momentum value of 60 GeV/c and a momentum spread of  $\pm(10 \div 20)\%$ . Both beams will be selected with the same geometrical acceptance and directed towards the NA48 detector along a common axis. The detection system will be upgraded by adding a TRD to improve  $e/\pi$  separation and a small beam spectrometer to measure the position and momentum of beam particles.

With a proton beam intensity of  $1 \cdot 10^{12}$  on the production target, NA48 should collect  $10^{10} K^\pm \rightarrow \pi^+ \pi^- \pi^\pm$  decays per year and measure  $A_g$  with a precision better than  $10^{-4}$ .

CP violation effects will be looked for also in the decay  $K^\pm \rightarrow \pi^\pm \pi^0 \pi^0$ , with a precision in the asymmetry of about  $2 \cdot 10^{-4}$ , and in the decay  $K^\pm \rightarrow \pi^\pm \pi^0 \gamma$ .

The use of intense charged kaon beams will allow to study the  $\pi^+ \pi^-$  interaction at low energy from the final state rescattering in the  $K^\pm \rightarrow \pi^+ \pi^- e^\pm \nu(\bar{\nu})$  decays ( $B = 3.9 \cdot 10^{-5}$  [33]). As no other hadron is present in the final state, the  $\pi^+ \pi^-$  scattering lengths  $a_0^0$  and  $a_2^0$  can be extracted in a clean way. A precise measurement of  $a_0^0$  to better than 0.01 will constitute an important input to the understanding of QCD vacuum and of the spontaneous chiral symmetry breaking mechanism.

## 7 Conclusions

Several rare decays of neutral kaons have been investigated by NA48 concurrently with the measurement of direct CP violation in  $K^0$  decays.

A recently discovered CP violating asymmetry in the  $K_L \rightarrow \pi^+ \pi^- e^+ e^-$  decay has been confirmed, while a careful study of the  $K_S \rightarrow \pi^+ \pi^- e^+ e^-$  decay shows no such effect.

$K_L \rightarrow \pi^0 \gamma\gamma$  branching fraction has been measured, together with the  $\gamma\gamma$  invariant mass spectrum. The significant tail at low  $m_{\gamma\gamma}$  provides evidence for a VMD contribution to the decay amplitude, which allows to predict the CP-conserving contribution to  $K_L \rightarrow \pi^0 e^+ e^-$  decay.

More results on rare and very rare  $K_S$  and  $\Xi^0$  decays are expected from a dedicated run in 2002; a search for direct CP violation in charged kaon decays with simultaneous  $K^+$  and  $K^-$  beams is planned for 2003.

## References

- [1] V. Fanti et al., *Phys. Lett. B* 465, 335-348 (1999).
- [2] A. Lai et al., *Eur. Phys. J. C* 22, 231-254 (2001).
- [3] C. Biino et al., *CERN-SL-98-033(EA)* and in "Proceedings of the 6th European Particle Accelerator Conference", Stockholm, Sweden, 22-26 June 1998; ed. by S. Myers, L. Liljeby and C. Petit-Jean-Genaz; IOP, Bristol, 2100 (1999).
- [4] V. Fanti et al., "The beam and detector for a precision CP violation experiment, NA48", to be published.
- [5] A. Alavi-Harati et al., *Phys. Rev. Lett.* 84, 408 (2000).
- [6] R. Batley et al., "A high sensitivity investigation of  $K_S$  and neutral hyperon decays using a modified  $K_S$  beam", CERN/SPSC 2000-002, CERN/SPSC/P253 add.2 (19 December 1999).

- [7] R. Batley et al., "Precision Measurement of Charged Kaon Decay Parameters with an Extended NA48 Setup", CERN/SPSC 2000-003, CERN/SPSC/P253 add.3 (16 January 2000).
- [8] N. Doble, L. Gatignon, P. Grafström, *Nucl. Instr. Meth.* **B**119, 181 (1996).
- [9] P. Grafström et al., *Nucl. Instr. Meth.* **A** 344, 487 (1994);  
H. Bergauer et al., *Nucl. Instr. Meth.* **A** 419, 623 (1998).
- [10] R. Moore et al., *Nucl. Instr. Meth.* **B** 119, 149 (1996).
- [11] D. Béderède et al., *Nucl. Instr. Meth.* **A** 367, 88 (1995);  
I. Augustin et al., *Nucl. Instr. Meth.* **A** 403, 472 (1998).
- [12] G. D. Barr et al., *Nucl. Instr. Meth.* **A** 370, 413 (1993).
- [13] L. M. Sehgal and M. Wanninger, *Phys. Rev.* **D** 4610351992;  
*ibid.* 46, 5209(E) (1992).
- [14] P. Heiliger and L. M. Sehgal, *Phys. Rev.* **D** 48, 4146 (1993);  
*ibid.* 60, 079902(E) (1999).
- [15] A. Lai et al., *Phys. Lett.* **B** 496, 137 (2000).
- [16] D. Leurs et al., *Phys. Rev.* **B** 133, 1276 (1964);  
A. Carroll et al., *Phys. Rev. Lett.* 44, 525 (1980);  
J. Adams et al., *Phys. Rev.* **D** 80, 4123 (1998).
- [17] K. Senyo, in "Proc. Int. Europhysics Conference on High Energy Physics", Tampere, Finland, 15-21 July 1999; ed. by K. Huitu, H. Kurki-Suonio and J. Maalampi; IOP, Bristol, 2000.
- [18] G. Ecker, A. Pich and E. De Rafael, *Phys. Lett.* **B** 189, 363 (1987).
- [19] G. D. Barr et al., *Phys. Lett.* **B** 328, 528 (1994).
- [20] A. Alavi-Harati et al., *Phys. Rev. Lett.* 83, 917 (1999).
- [21] A. G. Cohen, G. Ecker and A. Pitch, *Phys. Lett.* **B** 304, 347 (1993); P. Heiliger and L. M. Sehgal, *Phys. Rev.* **D** 47, 4920 (1993);  
J. F. Donoghue and F. Gabbiani, *Phys. Rev.* **D** 51, 2187 (1995);  
G. D'Ambrosio and J. Portolès, *Nucl. Phys.* **B** 492, 417 (1997).
- [22] A. Lai et al., *Phys. Lett.* **B** 514, 253 (2001).
- [23] G. Barr et al., *Phys. Lett.* **B** 304, 381 (1993).
- [24] A. Affolder et al., *Phys. Rev. Lett.* 82, 3751 (1999).
- [25] V. Fanti et al., *Eur. Phys. J.* **C** 12, 69 (2000).
- [26] Particle Data Group, *Eur. Phys. J.* **C** 15, 786 (2000)
- [27] C. Geweniger et al., *Phys. Lett.* **B** 57, 193 (1975).
- [28] Particle Data Group, *Eur. Phys. J.* **C** 15, 503 (2000)
- [29] Ford et al., *Phys. Rev. Lett.* 25, 1370 (1970).
- [30] A. Belkov et al., *Phys. Lett.* **B** 232, 118 (1989); *Phys. Lett.* **B** 300, 283 (1993); *Phys. Part. Nucl.* 26, 239 (1995).
- [31] L. Maiani and N. Paver, *The second DAPHNE physics handbook*, INFN, LNF, Vol. 1, 51 (1995).
- [32] G. D'Ambrosio, G. Isidori and G. Martinelli, *hep-ph/9911522* (1999).
- [33] V. V. Barmin et al., *Sov. J. Nucl. Phys.* 48, 1032 (1988).

# STUDY OF $K_S^0$ , $K^\pm$ DECAYS AT $\phi$ RESONANCE WITH THE KLOE DETECTOR

The KLOE collaboration\*, presented by M. Martemianov\*\*

LNF-INFN, I-00044 Frascati, Italy

*Abstract.* The status of the KLOE experiment at the DAFNE  $\phi$ -factory in Frascati is presented. To the summer of year 2001 the integrated luminosity consisted of about  $80 \text{ pb}^{-1}$ . The  $\phi(1020)$  meson is a good source of neutral and charged kaons decays in flight detected with complete reconstruction in the KLOE detector. Latest analysis of these decays are presented in this paper.

---

A. Aloisio<sup>g</sup>, F. Ambrosino<sup>g</sup>, A. Antonelli<sup>c</sup>, M. Antonelli<sup>c</sup>, C. Bacci<sup>n</sup>, G. Barbiellini<sup>g</sup>, F. Bellini<sup>n</sup>, G. Bencivenni<sup>c</sup>, S. Bertolucci<sup>c</sup>, C. Bini<sup>k</sup>, C. Bloise<sup>c</sup>, V. Bocci<sup>k</sup>, F. Bossi<sup>c</sup>, P. Branchini<sup>n</sup>, S. A. Bulychjov<sup>f</sup>, G. Cabibbo<sup>k</sup>, R. Caloi<sup>k</sup>, P. Campana<sup>c</sup>, G. Capon<sup>c</sup>, G. Carboni<sup>m</sup>, M. Casarsa<sup>g</sup>, V. Casavola<sup>e</sup>, G. Cataldi<sup>e</sup>, F. Ceradini<sup>n</sup>, F. Cervelli<sup>j</sup>, F. Cevenini<sup>g</sup>, G. Chieffari<sup>g</sup>, P. Ciambrone<sup>c</sup>, S. Conetti<sup>r</sup>, E. De Lucia<sup>k</sup>, G. De Robertis<sup>a</sup>, P. De Simone<sup>c</sup>, G. De Zorzi<sup>k</sup>, S. Dell'Agnello<sup>c</sup>, A. Denig<sup>c</sup>, A. Di Domenico<sup>k</sup>, C. Di Donato<sup>g</sup>, S. Di Falco<sup>d</sup>, A. Doria<sup>g</sup>, M. Dreucco<sup>c</sup>, O. Erriquez<sup>a</sup>, A. Farilla<sup>n</sup>, G. Felici<sup>c</sup>, A. Ferrari<sup>n</sup>, M. L. Ferrer<sup>c</sup>, G. Finocchiaro<sup>c</sup>, C. Forti<sup>c</sup>, A. Franceschi<sup>c</sup>, P. Franzini<sup>k,i</sup>, C. Gatti<sup>j</sup>, P. Gauzzi<sup>k</sup>, A. Giannasi<sup>j</sup>, S. Giovannella<sup>c</sup>, E. Gorini<sup>e</sup>, F. Grancagnolo<sup>e</sup>, E. Graziani<sup>n</sup>, S. W. Han<sup>c,b</sup>, M. Incagli<sup>j</sup>, L. Ingrosso<sup>c</sup>, W. Kluge<sup>e</sup>, C. Kuo<sup>d</sup>, V. Kulikov<sup>f</sup>, F. Lacava<sup>k</sup>, G. Lanfranci<sup>c</sup>, J. Lee-Franzini<sup>c,o</sup>, D. Leone<sup>k</sup>, F. Luc<sup>c,b</sup>, M. Martemianov<sup>c,f</sup>, M. Matsyuk<sup>f</sup>, W. Mei<sup>c</sup>, A. Menicucci<sup>m</sup>, L. Merola<sup>g</sup>, R. Messi<sup>m</sup>, S. Miscetti<sup>c</sup>, M. Moulson<sup>c</sup>, S. Müller<sup>d</sup>, F. Murtas<sup>c</sup>, M. Napolitano<sup>g</sup>, A. Nedosekin<sup>c,f</sup>, F. Nguyen<sup>n</sup>, M. Palutan<sup>n</sup>, L. Paoluzi<sup>m</sup>, E. Pasqualucci<sup>k</sup>, L. Passalacqua<sup>c</sup>, A. Passeri<sup>n</sup>, V. Patera<sup>l,c</sup>, E. Petrolo<sup>k</sup>, D. Picca<sup>k</sup>, G. Pirozzi<sup>g</sup>, L. Pontecorvo<sup>k</sup>, M. Primavera<sup>e</sup>, F. Ruggieri<sup>a</sup>, P. Santangelo<sup>c</sup>, E. Santovetti<sup>m</sup>, G. Saracino<sup>g</sup>, R. D. Schamberger<sup>o</sup>, B. Sciascia<sup>k</sup>, A. Sciubba<sup>l,c</sup>, F. Scuri<sup>g</sup>, I. Sfiligoi<sup>c</sup>, J. Shan<sup>c</sup>, P. Silano<sup>k</sup>, T. Spadaro<sup>k</sup>, E. Spiriti<sup>n</sup>, G. L. Tong<sup>c,b</sup>, L. Tortora<sup>n</sup>, E. Valente<sup>k</sup>, P. Valente<sup>c</sup>, B. Valeriani<sup>d</sup>, G. Venanzoni<sup>j</sup>, S. Veneziano<sup>k</sup>, A. Ventura<sup>e</sup>, Y. Wu<sup>c,b</sup>, G. Xu<sup>c,b</sup>, G. W. Yu<sup>c,b</sup>, P. F. Zema<sup>j</sup>, Y. Zhou<sup>c</sup>

\* Dipartimento di Fisicadell'Università e Sezione INFN, Bari, Italy.

<sup>b</sup> Permanent address: Institute of High Energy Physics of Academica Sinica, Beijing, China.

<sup>c</sup> Laboratori Nazionali di Frascati dell'INFN, Frascati, Italy.

<sup>d</sup> Institut für Experimentelle Kernphysik, Universität Karlsruhe, Germany.

<sup>e</sup> Dipartimento di Fisicadell'Università e Sezione INFN, Lecce, Italy.

<sup>f</sup> Permanent address: Institute for Theoretical and Experimental Physics, Moscow, Russia.

<sup>g</sup> Dipartimento di Scienze Fisiche dell'Università e Sezione INFN, Napoli, Italy.

<sup>i</sup> Physics Department, Columbia University, New York, USA.

<sup>j</sup> Dipartimento di Fisica dell'Università e Sezione INFN, Pisa, Italy.

<sup>k</sup> Dipartimento di Fisica dell'Università "La Sapienza" e Sezione INFN, Roma, Italy.

<sup>l</sup> Dipartimento di Energetica dell'Università "La Sapienza", Roma, Italy.

<sup>m</sup> Dipartimento di Fisica dell'Università "Tor Vergata" e Sezione INFN, Roma, Italy.

<sup>n</sup> Dipartimento di Fisica dell'Università "Roma Tre" e Sezione INFN, Roma, Italy.

<sup>o</sup> Physics Department, State University of New York at Stony Brook, USA.

<sup>q</sup> Dipartimento di Fisica dell'Università e Sezione INFN, Trieste, Italy.

<sup>r</sup> Physics Department, University of Virginia, USA.

\*\*e-mail: martem@lnf.infn.it

## 1 Introduction

The DAFNE  $\phi$ -factory built in the Laboratori Nazionali di Frascati, Italy is an  $e^+e^-$ -collider at the region of the  $\phi(1020)$  meson resonance. The KLOE detector was designed with a main goal to measure direct CP violation in  $K^0$  decays with a sensitivity  $\approx 10^{-4}$  in  $\text{Re}(\epsilon'/\epsilon)$  using the double ratio method [1]. The design philosophy is based on the possibility to achieve the required luminosity  $5 \times 10^{32} \text{ cm}^{-2} \text{ sec}^{-1}$  by filling the machine with a large number of bunches (up to 120). The KLOE physics data taking was started in April 1999 and collected about  $80 \text{ pb}^{-1}$  up to summer 2001.

The  $\phi$  mesons predominantly decay into pairs of slow monochromatic kaons ( $K^+ - K^-$  49% and  $K_S^0 - K_L^0$  34%). This rather high kaon flux and very small hadronic background give unique possibility to study various problems of kaon physics. This paper presents a status of  $K_S^0$  and  $K^\pm$  decay channels. The measurement of the ratio of the  $K_S^0$  branching fractions into two charged and neutral pions is presented. It is one of the two factors which enter into the definition of the double ratio. Next part of this report is a measurement of the branching ratio of  $K_S^0 \rightarrow \pi^\pm e^\mp \nu$ ; in the present analysis the determination of the branching ratio is done with higher statistics than world average and at lower background. The investigation of charged kaons has concerned the ratio of the main branching modes of  $K^\pm$  decays. This result shows a good performance of the KLOE detector and demonstrates the possibility of a precision measurement useful for the chiral perturbation theory.

## 2 The KLOE detector

KLOE (KLOngExperiment) [2] is a typical  $e^+e^-$  detector with solenoidal geometry. It consists of a large drift chamber (DC), a hermetical electromagnetic calorimeter (EMC) and superconductive magnet surrounding the detector. The EMC includes a barrel part and two endcap parts; 98 % total coverage of the solid angle is achieved. The side view of the KLOE detector is shown on Fig.1.

The KLOE drift chamber [3] has a cylindrical structure with alternated stereo views. The sensitive volume has 0.5 m inner and 4 m outer diameters and length of 3.7 m. It is filled with 12582 almost square cells arranged in 58 circular layers. In order to improve the acceptance of  $K_S^0$  decays, the 12 inner layers consist of  $2 \times 2 \text{ cm}^2$  cells while the outer layers are made of  $3 \times 3 \text{ cm}^2$  cells. To minimize multiple scattering of charged particles and  $K_L$  regeneration the drift chamber is filled with a low-Z, Helium based gas mixture (90% Helium, 10% Isobutane). The radiation length of the DC (gas + wires) amounts to about 900 m. A spatial resolution  $\sigma_{r\phi} \leq 200 \mu\text{m}$  and  $\sigma_z \leq 2 \text{ mm}$  was obtained. The momentum resolution for 510 MeV/c electrons and positrons from Bhabha scattering events is 1.3 MeV/c.

The electromagnetic calorimeter [4] is a sampling one made of lead and scintillating fibers. It is divided on 24 barrel 4.3 m long, 23 cm thick and 32 end-cap modules 0.7 to 3.9 m long and 23 cm thick corresponding to 15  $X_0$ . The modules are constructed from interleaved layers of 0.5 mm thick lead foil and 1 mm diameter scintillating fibers. The calorimeter was designed to detect with high efficiency photons with energy as low as 20 MeV. The best process to study the performance of the EMC in a wide energy range is radiative Bhabha scattering  $e^+e^- \rightarrow e^+e^-\gamma$ , where the photon energy

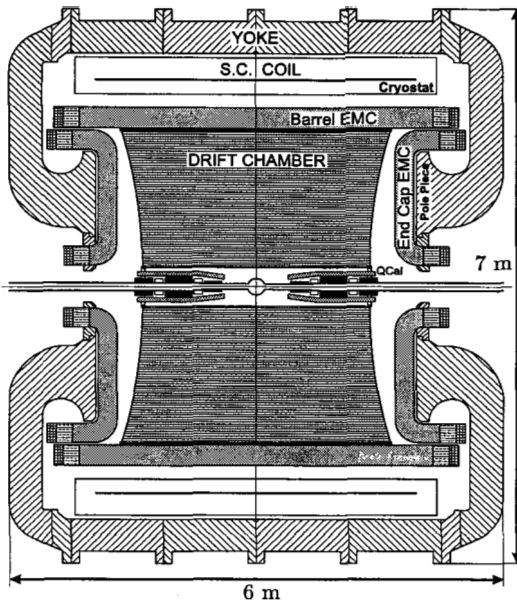


Figure 1: The KLOE detector

is determined by missing momentum (measured in DC with two charged tracks). It gives  $\sigma_E/E = 5.7\%/\sqrt{E(\text{GeV})}$  energy and  $\sigma_t = 54 / \sqrt{E(\text{GeV})} \otimes 50 \text{ ps}$  time resolution.

The beam pipe surrounding the interaction point has a spherical shape (10 cm radius). It consists of 0.5 mm thick Aluminium-Beryllium alloy to minimize multiple scattering and energy losses for charged kaons. The KLOE trigger system [5] uses both chamber and calorimeter information, it has near 100 % efficiency on the processes under study. The two level system contains two specific vetos for Bhabha and cosmic ray events. The DAQ system [6] handles 23000 FEE channels and can acquire up to 10000 events per second. The digitization time is  $2\mu\text{s}$  and the bandwidth is 50 MByte/s (at 5 kBByte/event).

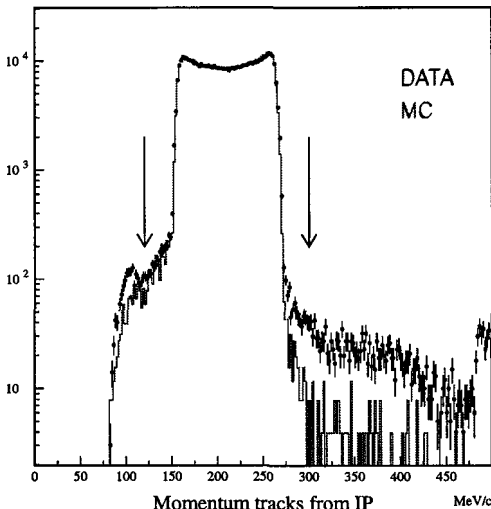


Figure 2: Momentum distribution for the tracks from the interaction point (IP) for selection  $K_S^0 \rightarrow \pi^+ \pi^-$  decay

### 3 Neutral kaon study

#### 3.1 $K_S^0 \rightarrow \pi^+ \pi^-$ and $K_S^0 \rightarrow \pi^0 \pi^0$ decays

$K_L$  from  $\phi$  decay into  $K_L$ - $K_S$  pairs can be used for a clear identification of  $K_S$ . More than half of  $K_L$  reach the calorimeter before decay. Normally  $K_L$  interacts in the EMC with a signal compatible with a slow moving ( $\beta \approx 0.22$ ) neutral particle. The presence (tag) of a  $K_S$  is therefore inferred by the detection of a  $K_L$  in the opposite hemisphere ( $K_{\text{crash}}$ ).

The  $K_S^0 \rightarrow \pi^0 \pi^0$  decays are selected requiring four  $\gamma$ -clusters in the calorimeter with energy larger than 20 MeV. The selection of  $K_S^0 \rightarrow \pi^+ \pi^-$  requires two opposite charged tracks from interaction point with polar angle in the region  $30^\circ < \theta < 150^\circ$  and measured momenta  $120 \text{ MeV}/c < p < 300 \text{ MeV}/c$  (see Fig.2). On this plot tracks with  $p > 300 \text{ MeV}/c$  correspond to machine background, while the peak around 100 MeV/c is due to the contamination of  $\phi \rightarrow K^+ K^-$  decay.

From an integrated luminosity of about  $17 \text{ pb}^{-1}$  the following value was obtained the value of the ratio of the branching fractions [7]:

$$B(K_S^0 \rightarrow \pi^+ \pi^-)/B(K_S^0 \rightarrow \pi^0 \pi^0) = 2.23 \times (1 \pm 0.35 \times 10^{-2} (\text{stat}) \pm 1.5 \times 10^{-2} (\text{syst}))$$

This result should be compared with the current PDG value:

$$2.197 \times (1 \pm 1.2 \times 10^{-2} (\text{stat}) \pm 1.5 \times 10^{-2} (\text{syst}))$$

The main contribution to systematics is due to residual uncertainties in the photon

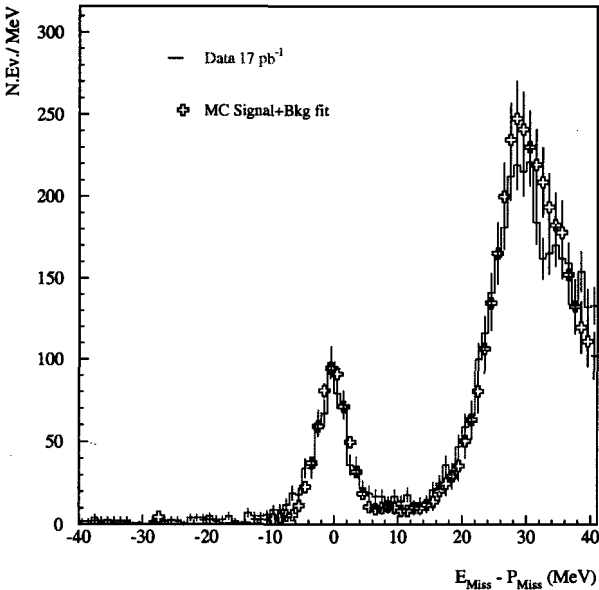


Figure 3: Distribution of the difference between missing energy and missing momentum for  $K_S^0 \rightarrow \pi^\pm e^\mp \nu$

measurements. Presently studies to reduce the systematic error are under way.

### 3.2 $K_S^0 \rightarrow \pi^\pm e^\mp \nu$ decay

The measurement of  $K_S^0 \rightarrow \pi^\pm e^\mp \nu$  was performed on the statistics of  $17 \text{ pb}^{-1}$  collected in the year 2000. Initial selection of  $K_S^0$  candidates requires a  $K_{\text{crash}}$  cluster in the calorimeter and two tracks of opposite charge and extrapolated to the center of the detector. For both charged tracks an association with the clusters in the calorimeter is required

The residual background due to  $K_S^0 \rightarrow \pi^+ \pi^-$  was rejected using electron identification by time of flight. The time of flight differences  $\Delta t$  for the two charged particles in  $e - \pi$  and  $\pi - \pi$  hypothesis are computed and events are accepted if  $|\Delta t(\pi - \pi)| > 1.5 \text{ ns}$ ,  $|\Delta t(\pi - e)| < 1 \text{ ns}$  and  $|\Delta t(e - \pi)| > 3 \text{ ns}$ .

After this the missing energy and momentum of  $K_S^0 - \pi - e$  system,  $E_{\text{miss}}$  and  $P_{\text{miss}}$ , are computed using the  $K_{\text{crash}}$  cluster direction and the  $\phi$  - meson boost. The distribution of  $E_{\text{miss}} - P_{\text{miss}}$  is shown in Fig.3. The signal events cluster in the peak around zero; data and MC spectra are in good agreement.

The measured yield of  $K_S^0 \rightarrow \pi^\pm e^\mp \nu$  is  $627 \pm 30$  events. Under these conditions about  $1.6 \times 10^6$   $K_S^0$  decay into  $\pi^+ \pi^-$  mode were selected. These events were used as normalization factor. The corresponding branching ratio was then found to be  $B(K_S^0 \rightarrow \pi^\pm e^\mp \nu) = (6.8 \pm 0.3 \text{ (stat)}) \times 10^{-4}$  [9]. The result improves the mea-

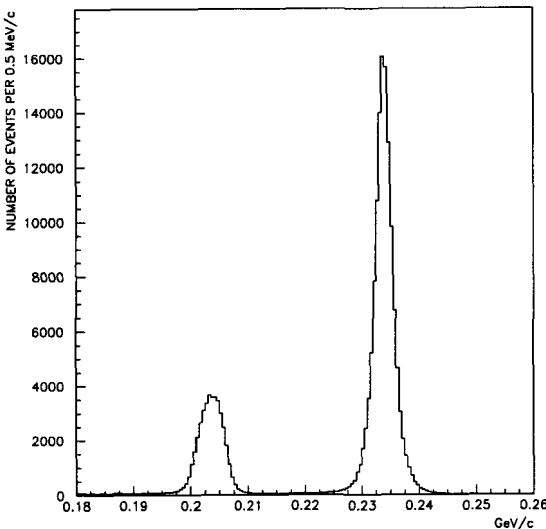


Figure 4: Momentum spectrum of charged secondaries from  $K^\pm$  decay (in rest frame of  $K^\pm$ ).

surement performed by the CMD-2 Collaboration at VEPP-2M ( $75 \pm 13$  observed events) [8]:  $B(K_S^0 \rightarrow \pi^\pm e^\mp \nu) = (7.2 \pm 1.2) \times 10^{-4}$ . Assuming (according to the  $\Delta S = \Delta Q$  rule)  $\Gamma(K_L^0 \rightarrow \pi^\pm e^\mp \nu) = \Gamma(K_S^0 \rightarrow \pi^\pm e^\mp \nu)$ , the expected value of the branching ratio is  $B(K_S^0 \rightarrow \pi^\pm e^\mp \nu) = 6.70 \pm 0.07 \times 10^{-4}$

#### 4 Charged kaon study

##### 4.1 $K^\pm \rightarrow \pi^\pm \pi^0$ and $K^\pm \rightarrow \mu^\pm \nu$ decays

The charged kaons with 130 MeV/c momentum from  $\phi$  decays have 95 cm mean decay length. Most of the charged kaons decays inside the KLOE drift chamber. Fig.4 presents the momentum spectrum of charged secondary particles from  $K^\pm$  decay calculated in the rest frame of charged kaon. Peaks from the two-body decays  $K^\pm \rightarrow \pi^\pm \pi^0$  (at pion momentum = 205 MeV/c) and  $K^\pm \rightarrow \mu^\pm \nu$  (at muon momentum = 235 MeV/c) dominate the spectrum. The tagging strategy includes selection of mode  $K^\pm \rightarrow \pi^\pm \pi^0$  by momenta in the window  $195 \text{ MeV}/c < p < 215 \text{ MeV}/c$  of one charged kaon at least to obtain a high trigger efficiency.

Using number of events in the peaks the following preliminary value for the ratio has been obtained:

$$R_{\pi\mu} = \Gamma(K^\pm \rightarrow \pi^\pm \pi^0) / \Gamma(K^\pm \rightarrow \mu^\pm \nu) = 0.3300 \pm 0.0013 \text{ (stat)}$$

This value for the ratio was corrected for Monte Carlo efficiency and radiative con-

tribution of  $K^\pm \rightarrow \mu^\pm \nu \gamma$  (the corresponding radiative decay of the pions is negligible) [10, 11]. Residual small contributions from other kaon decays and the relative trigger efficiencies for the two decaying modes are obtained from Monte Carlo. The corresponding result of ratio  $R_{\pi\mu} = 0.3306 \pm 0.0012$  (stat) can be compared with the one listed in PDG tables  $R_{\pi\mu} = 0.3316 \pm 0.0032$ . We hope that systematic errors, presently under study, can be kept on the level of our statistic uncertainties.

### Acknowledgments

The work has been supported in part by the grant INTAS 00-0037.

### References

- [1] J.Lee-Franzini, "The Second DAFNE Physics Handbook", 761, 1995.
- [2] The KLOE Collaboration "The KLOE detector, Technical Proposal", LNF-93/002, 1993.
- [3] M.Adinolfi et al., *Nucl.Instrum.Meth.* **A** 461, 25 (2001).
- [4] M.Adinolfi et al., *Nucl.Instrum.Meth.* **A** 461, 355 (2001).
- [5] M.Adinolfi et al., *Nucl.Instrum.Meth.* **A** 461, 465 (2001).
- [6] The KLOE Collaboration, "The KLOE data acquisition system", LNF-95/014, 1995.
- [7] G.Cabibo, Ph.D. Thesis, Università di Roma La Sapienza, 2000.
- [8] R.Akhmetshin et al., *Phys.Lett.* **B** 456, 90 (1999).
- [9] T.Spadaro, C.Gatti, KLOE Memo 256, 2001.
- [10] T.Usher et al., *Phys.Rev.* **D** 45, 3961 (1992).
- [11] A.Weissenberg et al., *Nucl.Phys.* **B** 115, 55 (1977).

# APPLICATION OF NEW MULTILOOP QCD INPUT TO THE ANALYSIS OF $xF_3$ DATA

A.L. Kataev<sup>a</sup>

*Institute for Nuclear Research of the Academy of Sciences of Rusia,  
117312 Moscow, Russia*

G. Parente<sup>b</sup>

*Department of Particle Physics, University of Santiago de Compostela,  
15706 Santiago de Compostela, Spain*

A.V. Sidorov<sup>f</sup>

*Bogoliubov Laboratory of Theoretical Physics,  
Joint Institute for Nucle Research,  
141980 Dubna, Russia*

**Abstract.** The new theoretical input to the analysis of the experimental data of the CCFR collaboration for  $F_3$  structure function of  $\nu N$  deep inelastic scattering is considered. This input comes from the next-to-next-to-leading order corrections to the anomalous dimensions of the Mellin moments of the  $F_3$  structure function and  $N^3\text{LO}$  corrections to the related coefficient functions. The QCD scale parameter  $\Lambda_{MS}^{(4)}$  is extracted from higher-twist independent fits. The results obtained demonstrate the minimization of the influence of perturbative QCD contributions to the value of  $\Lambda_{MS}^{(4)}$ .

## 1 Introduction

One of the most important current problems of symbolic perturbative QCD studies is the analytical evaluation of the next-to-next-to-leading order (NNLO) QCD corrections to the kernels of the DGLAP equations [1] for different structure functions of the deep-inelastic scattering (DIS) process. In this note we will apply the related information for the fixation of definite uncertainties of the NNLO analysis [2, 3] of experimental data for  $F_3$  structure function (SF) data of  $\nu N$  DIS, provided by the CCFR collaboration [4] at the Fermilab Tevatron and present preliminary results of our improved fits which will be described elsewhere [5].

## 2 Methods of analysis of DIS data

There are several methods of analysis of the experimental data of DIS in the high orders of perturbation theory. The traditional method is based on the solution of the DGLAP equation, which in the case of the  $F_3$  SF has the following form:

$$Q^2 \frac{d}{dQ^2} F_3(x, Q^2) = \frac{1}{2} \int_x^1 \frac{dy}{y} \left[ V_{F_3}(y, A_s) + \beta(A_s) \frac{\partial \ln C_{F_3}(y, A_s)}{\partial A_s} \right] F_3\left(\frac{x}{y}, Q^2\right) \quad (1)$$

<sup>a</sup>Supported by RFBI (Grants N 99-00091, 00-02-17432)  
and State Support of Leading Scientific Schools (grant 00-15-96626)

<sup>b</sup>Supported by Xunta de Galicia (RGIDT00PX2061PR)  
and CICYT (AEN99-0589-C02-02)

<sup>c</sup>Supported by RFBI (Grants N 99-01-00091, 00-02-17432) and by INTAS call 2000  
(project N 587)

where  $A_s = \alpha_s/(4\pi)$ ,  $\mu \partial A_s / \partial \mu = \beta(A_s)$  is the QCD  $\beta$ -function and  $C_{F_3}(y, A_s)$  is the coefficient function, defined as

$$C_{F_3}(y, A_s) = \sum_{n \geq 0} C_{F_3, n}(y) \left( \frac{\alpha_s}{4\pi} \right)^n \quad (2)$$

and  $V_{F_3}(z)$  is the DGLAP kernel, related to a non-singlet (NS)  $F_3$  SF. The solution of Eq.(1) is describing the predicted by perturbative QCD violation of scaling [6] or automedeling [7] behaviour of the DIS SFs by the logarithmically decreasing order  $\alpha_s$ -corrections.

The coefficient function we are interested in has been known at the NNLO for quite a long period. The term  $C_{F_3, 2}(y)$  was analytically calculated in Ref. [8]. The results of these calculations were confirmed recently [9] using a different technique.

The kernel  $V_{F_3}(z, \alpha_s)$  is analytically known only at the NLO. However, since there exists a method of symbolic evaluation of multiloop corrections to the renormalization group functions in the  $\overline{MS}$ -scheme [10] and its realization at the FORM system, it became possible to calculate analytically the NNLO corrections to the  $n = 2, 4, 6, 8, 10$  Mellin moments of the NS kernel of the  $F_2$  SF [11]. They have the following expansion:

$$-\int_0^1 z^{n-1} V_{NS, F_2}(z, \alpha_s) dz = \sum_{i \geq 0} \gamma_{NS, F_2}^{(i)}(n) \left( \frac{\alpha_s}{4\pi} \right)^{i+1} \quad (3)$$

and are related to the anomalous dimension of NS renormalization group (RG) constants of  $F_2$  SF<sup>d</sup>:

$$\mu \frac{\partial \ln Z_n^{NS, F_2}}{\partial \mu} = \gamma_{NS, F_2}^{(n)}(\alpha_s) \quad . \quad (4)$$

These results were used in the process of the fits of Refs. [2, 3] of the CCFR data for the  $F_3$  SF with the help of the Jacobi polynomial method [13]. It allows the reconstruction of the SF  $F_3$  from the finite number of Mellin moments  $M_{j, F_3}(Q^2)$  of the  $x F_3$  SF:

$$F_3^{N_{max}}(x, Q^2) = w \sum_{n=0}^{N_{max}} \Theta_n^{\alpha, \beta}(x) \sum_{j=0}^n c_j^{(n)}(\alpha, \beta) M_{j+2, F_3}^{TMC}(Q^2) \quad (5)$$

where  $w = w(\alpha, \beta) = x^{\alpha-1}(1-x)^\beta$ ,  $\Theta_n^{\alpha, \beta}$  are the orthogonal Jacobi polynomials and  $c_j^{(n)}(\alpha, \beta)$  is the combination of Euler  $\Gamma$ -functions, which is factorially increasing with increasing of  $N_{max}$  and thus  $n$ .

The expressions for  $M_{j+2, F_3}^{TMC}(Q^2)$  include the information about Mellin moments of the coefficient function

$$C_{n, F_3}(Q^2) = \int_0^1 x^{n-1} C_{F_3}(x, \alpha_s) dx = \sum_{i \geq 0} C^{(i)}(n) \left( \frac{\alpha_s}{4\pi} \right)^i \quad (6)$$

where  $C^{(0)}(n) = 1$ .

---

<sup>d</sup>The method of renormalization group was originally developed in [12].

The target mass corrections, proportional to  $(M_N^2/Q^2)M_{j+4,F_3}(Q^2)$ , are also included into the fits. Therefore, the number of the Jacobi polynomials  $N_{max} = 6$  corresponds to taking into account the information about RG evolution of 10 moments, and  $N_{max} = 9$  presumes that the evolution of  $n = 13$  number of Mellin moments is considered.

The procedure of reconstruction of  $F_3(x, Q^2)$  from the finite number of Mellin moments and the related fits of the experimental data were implemented in the form of FORTRAN programs. The details of the fits of the CCFR data, based on RG evolution of 10 moments, are described in Refs. [2,3] (for the brief review see Ref. [14]). In the process of these analyses the following approximations were made: a) it was assumed that for a large enough number of moments,  $\gamma_{NS,F_3}^{(n)}(\alpha_s) \approx \gamma_{NS,F_2}^{(n)}(\alpha_s)$ ; b) since the odd NNLO terms of  $\gamma_{NS,F_2}^{(n)}$  are explicitly unknown, they were fixed using the smooth interpolation procedure proposed in Ref. [15]. It was known that the additional contributions, proportional to the  $d^{abc}d^{abc}$  structure of the colour gauge group  $SU(N_c)$  are starting to contribute to the coefficients of  $\gamma_{NS,F_3}^{(n)}(\alpha_s)$  from the NNLO [3]. In the process of the analysis of Refs. [2,3] it was assumed that they were not dominating and therefore were not taken into account.

### 3 New inputs for the fits

After recent explicit analytical evaluation of the NNLO coefficients of  $\gamma_{NS,F_3}^{(n)}(\alpha_s)$  at  $n = 3, 5, 7, 9, 11, 13$  (see Ref. [16]) it became possible to fix this uncertainty (it is worth noting that the NNLO contribution to  $\gamma_{NS,F_2}^{(n)}(\alpha_s)$  for  $n = 12$  was analytically evaluated in Ref. [16] also). To estimate the NNLO terms of  $\gamma_{NS,F_3}^{(n)}(\alpha_s)$  at  $n = 4, 6, 8, 10, 12$  we applied the smooth interpolation procedure, identical to the one used to estimate the odd NNLO terms of  $\gamma_{NS,F_2}^{(n)}(\alpha_s)$ , while the numerical value of  $\gamma_{NS,F_3}^{(2)}(2)$  was fixed with the help of an extrapolation procedure, where we have not used the value at  $n = 1$ . The justification and more details of this procedure will be given elsewhere [5].

The used numerical results of the NNLO contributions  $\gamma_{NS,F_3}^{(2)}(n)$  with and without  $d^{abc}d^{abc}$ -factors are presented in Table 1, where we marked in parenthesis the estimated even terms. The expressions for the NNLO contributions to the NS anomalous dimensions terms  $\gamma_{NS,F_2}^{(2)}(n)$  are also given for comparison. They include the numerical results of the explicit analytical calculations of Refs. [11,16], normalized to  $f = 4$  numbers of active flavours, and the results of the smooth interpolation procedure, in parenthesis, applied for estimating explicitly uncalculated odd terms. The satisfactory agreement between the numbers in the second and third columns supports the assumptions a) and b) mentioned above.

In Table 2 the numerical expressions for the coefficients of Eq.(6) for  $f = 4$  numbers of active flavours are given. They include the results of explicit calculations of  $N^3LO$  corrections of odd moments [16], supplemented with the information about the coefficients of the Gross-Llewellyn Smith sum rule [17,18], defined by the  $n = 1$  Mellin moment of the  $xF_3$  SF. The numbers in parenthesis are the results of the interpolation procedure. In the last column we present the values of  $C^{(3)}(n)$ , obtained with the help of the [1/1] Padé estimates approach. One can see that the agreement of

$n$	$\gamma_{NS,F_3}^{(2)}(n)$	$d^{abc}d^{abc}$ neglected in $\gamma_{NS,F_3}^{(2)}(n)$	$\gamma_{NS,F_2}^{(2)}(n)$
2	(631)	(585)	612.06
3	861.65	836.34	(838.93)
4	(1015.37)	(1001.42)	1005.82
5	1140.90	1132.73	(1135.28)
6	(1247)	(1241.21)	1242.01
7	1338.27	1334.32	(1334.65)
8	(1420)	(1416.73)	1417.45
9	1493.47	1491.13	(1492.02)
10	(1561)	(1558.85)	1559.01
11	1622.28	1620.73	(1619.83)
12	(1679.81)	(1677.70)	1678.40

Table 1: The numerical expressions of the NNLO coefficients of anomalous dimensions of the  $n$ -th NS moments of the  $F_3$  and  $F_2$  SFs at  $f = 4$ . The numbers in parenthesis are the estimated results.

$n$	$C^{(1)}(n)$	$C^{(2)}(n)$	$C^{(3)}(n)$	$C^{(3)}(n)_{[1/1]}$
1	-4	-52	-644.35	-676
2	-1.78	-47.47	(-1127.45)	-1268
3	1.67	-12.72	-1013.17	97
4	4.87	37.12	(-410.66)	283
5	7.75	95.41	584.94	1175
6	10.35	158.29	(1893.58)	2421
7	12.72	223.90	3450.47	3940
8	14.90	290.88	(5205.39)	5679
9	16.92	358.59	7120.99	7602
10	18.79	426.44	(9170.21)	9677
11	20.55	494.19	11332.82	11884
12	22.20	561.56	(13590.97)	14205
13	22.76	628.45	15923.91	17353

Table 2: The numerical expressions for the coefficients of the coefficient functions for  $n$ -th Mellin moments of the  $F_3$  SF up to N<sup>3</sup>LO and their [1/1] Padé estimates.

	$N_{max}$	$\Lambda_{MS}^{(4)}$ (MeV)
result of Ref. [3]: NLO	6	$339 \pm 36$
	7	$340 \pm 37$
	8	$343 \pm 37$
	9	$345 \pm 37$
	10	$339 \pm 36$
	NNLO 6	$326 \pm 35$
NNLO results with inclusion of NNLO terms of $\gamma_{NS,F_3}^{(n)}$	6	$325 \pm 35$
	7	$326 \pm 31$
	8	$329 \pm 36$
	9	$332 \pm 36$
$N^3$ LO approximate results with inclusion of the interpolated values of $C^{(3)}(n)$ -terms	6	$324 \pm 33$
	7	$322 \pm 33$
	8	$325 \pm 34$
	9	$326 \pm 33$

Table 3: The results of the fits of the CCFR data for  $xF_3$  SF, taking into account the NNLO approximation for  $\gamma_{F_3,NS}^{(n)}$ . The initial scale of RG evolution is  $Q_0^2=20$  GeV $^2$ .

Padé estimates with the used  $N^3$ LO results is good in the case of the Gross–Llewellyn Smith sum rule (this fact was already known from the considerations of Ref. [19]). In the case of  $n = 2$  and  $n \geq 6$  moments the results are also in satisfactory agreement. Indeed, one should keep in mind that the difference between the results of column 3 and 4 of Table 2 should be devided by the factor  $(1/4)^3$ , which comes from our definition of expansion parameter  $A_s = \alpha_s/(4\pi)$ . Note, that starting from  $n \geq 6$  the results of application of [0/2] Padé approximants, which in accordance with analysis of Ref. [20] are reducing scale-dependence uncertainties, are even closer to the the results of the interpolation procedure (for the comparison of the estimates, given by [1/1] and [0/2] Padé approximants in the case of moments of  $xF_3$  SF see Ref. [3], while in Ref. [21] the similar topic was analysed within the quantum mechanic model). For  $n=3,4$  the interpolation method gives completely different results. The failure of the application of the Padé estimates approach in these cases might be related to the irregular sign structure of the perturbative series under consideration.

#### 4 Some results of the fits

In Table 3 we present the comparison of the results of the determination of the  $\Lambda_{MS}^{(4)}$  parameter, made in Ref. [3], with the new ones, obtained by taking into account more definite theoretical information. Since NNLO corrections to the anomalous dimensions and  $N^3$ LO contributions to the coefficient functions of odd moments of the  $xF_3$  SF are now known up to  $n=13$ , it became possible to study the dependence of the results of the fits from the value of  $N_{max}$ , which we can now vary from  $N_{max}=6$  to  $N_{max}=9$ . It should be mentioned that for  $N_{max}=6$  the new NNLO result and its  $Q_0^2$  dependence are in agreement with the results of Ref. [3]. However, the incorporation of higher number of moments, and thus the increase of  $N_{max}$ , make the

NNLO (and approximate N<sup>3</sup>LO) results almost independent from the variation of  $Q_0^2$  in the interval 5 GeV<sup>2</sup>–100 GeV<sup>2</sup>. This is the welcome feature of including into the fits the results of the new analytical calculations of the NNLO corrections to anomalous dimensions and N<sup>3</sup>LO corrections to the coefficient functions of odd moments of the  $xF_3$  SF [16]. Comparing now the central values of the results of the stable NLO fits of Ref. [3] with the new NNLO and N<sup>3</sup>LO results, we observe the decrease of the theoretical uncertainties and, probably, the saturation of the predictive power of the corresponding perturbative series at the 4-loop level. More detailed results of our fits, including extraction of  $\alpha_s(M_Z)$ , its scale dependence and the information about the behaviour of twist-4 corrections at the NNLO and N<sup>3</sup>LO, in the case of  $N_{max} = 9$ , are described elsewhere [5].

### Acknowledgements

This work and the essential part of Ref. [5] were done during the appointment of one of us (ALK) at Theoretical Physics Division of ERN. He is grateful to his colleagues for pleasant atmosphere.

We wish to thank G. Altarelli, S. Catani, A.V. Kotikov, S.A. Larin, A.Peterman, A.N. Tavkhelidze and F. J. Yndurain for their interest to our work.

- [1] V. N. Gribov, and L. N. Lipatov , *Sov. J. Nucl. Phys.* **15** 438 (1972); L. N. Lipatov, *Sov. J. Nucl. Phys.* **20** 94 (1975);  
G. Altarelli, and G. Parisi, *Nucl. Phys.* **B126** 298 (1977);  
Yu. L. Dokshitzer, *Sov. Phys. JETP* **B126** 641 (1977).
- [2] A.L. Kataev, A.V. Kotikov, G. Parente, and A.V. Sidorov, *Phys. Lett.* **B417** 374 (1998).
- [3] A.L. Kataev, G. Parente, and A.V. Sidorov, *Nucl. Phys.* **B 573** 405 (2000).
- [4] CCFR-NuTeV Collab., W.G. Seligman et al., *Phys. Rev. Lett.* **79** 1213 (1997).
- [5] A.L. Kataev, G. Parente, and A.V. Sidorov, CERN-TH/2001-58 [hep-ph/0106221].
- [6] J.D. Bjorken, *Phys. Rev.* **179** 1547 (1969).
- [7] N. N. Bogolyubov, V. S. Vladimirov, A. N. Tavkhelidze , *Teor. Mat. Fiz.* **12** 3 (1972).
- [8] E.B. Zijlstra, and W.L. van Neerven, *Phys. Lett.* **B297** 377 (1992).
- [9] S. Moch S., and J.A.M. Vermaseren, *Nucl. Phys.* **B573** 853 (2000).
- [10] F.V. Tkachov, *Phys. Lett.* **B100** 65 (1981);  
K.G. Chetyrkin, and F.V. Tkachov, *Nucl. Phys.* **B192** 159 (1981).
- [11] S. A. Larin, T. van Ritbergen, and J. A. M. Vermaseren, *Nucl. Phys.* **B427** 41 (1994) 41; S. A. Larin, P. Nogueira, T. van Ritbergen, and J. A. M. Vermaseren, *Nucl.Phys.* **B492** 338 (1997).
- [12] E.C.G. Stueckelberg and A. Petermann, *Helv. Phys. Acta* **26** 499 (1953); M. Gell-Mann and F. E. Low, *Phys. Rev.* **95** 1300 (1954); N. N. Bogoliubov and D.V. Shirkov D. V., *Nuov. Cim.* **3** 845 (1956).
- [13] G. Parisi and N. Sourlas, *Nucl. Phys.* **B151** 421 (1979); I.S. Barker , C. B. Langiensiepen, and G. Shaw , *Nucl. Phys.* **B186** 61 (1981);  
J. Chýla and J. Rames , *Z. Phys.* **C31** 151 (1986); V.G. Krivokhizhin et al., *Z. Phys.* **C36** 51 (1987); *ibid.* **C48** 347 (1990).
- [14] A. L. Kataev, G. Parente and A. V. Sidorov, Preprint DTP/00/02 [hep-ph/0001096]; Proceedings of Bogolyubov Conference “Problems of Theoretical

- and Mathematical Physics”, October 1999; *Phys. Part. Nucl. (Fiz. Elem. Chast. Atom. Yadra)*, **31** part7b, 29 (2000) Eds. V.G. Kadyshevskij and A.N. Sissakian ; S. Catani et al., *QCD* Preprint CERN-TH-2000-131 [hep-ph/0005025]; in *Proceedings of the Workshop on Standard Model (and more) at the LHC*, Eds. G. Altarelli and M.L. Mangano; CERN Yellow Report 2000-004 (2000).
- [15] G. Parente, A.V. Kotikov, and V.G. Krivokhizhin, *Phys. Lett.* **B333** 190 (1994).
  - [16] A. Retey, and J.A.M. Vermaseren, *Nucl. Phys.* **B604** 281 (2001). [hep-ph/0007294]
  - [17] S. G. Gorishny, and S. A. Larin, *Phys.Lett.* **B172** 109 (1986).
  - [18] S. A. Larin, and J. A. M. Vermaseren, *Phys. Lett.* **B259** 345 (1991).
  - [19] M.A. Samuel, J. Ellis, and M. Karliner, *Phys.Rev.Lett.* **74** 4380 (1995).
  - [20] E. Gardi, *Phys. Rev.* **D56** 68 (1997) [hep-ph/9611453].
  - [21] A.A. Penin and A.A. Pivovarov, *Phys. Lett.* **B367** 342 (1996) [hep-ph/9506370].

# HEAVY QUARK PRODUCTION NEAR THE THRESHOLD IN QCD

A.A.Pivovarov <sup>a</sup>

*Institut für Physik, Johannes-Gutenberg-Universität,  
Staudinger Weg 7, D-55099 Mainz, Germany  
and*

*Institute for Nuclear Research of the Russian Academy of Sciences,  
Moscow 117312, Russia*

*Abstract.* Theoretical results for the cross section of heavy quark production near the threshold at NNLO of NRQCD are briefly overviewed.

## 1 Introduction

The heavy quark production near thresholds will be thoroughly investigated at future accelerators, e.g. [1]. One can study the  $q\bar{q}$  systems near threshold in  $e^+e^-$  annihilation [2, 3] and  $\gamma\gamma$  collisions [4, 5]. In  $e^+e^-$  annihilation the production vertex is local (the electromagnetic current in case of photon and/or neutral weak current in case of  $Z$ -boson), the basic observable is a production cross section which is saturated by S-wave (for the vector current). In  $\gamma\gamma$  collisions the production vertex is nonlocal and both S- and P-waves can be studied for different helicity photons, the number of observables is larger (cross sections  $\sigma_S$ ,  $\sigma_P$ , S-P interference). In  $e^+e^-$  annihilation high precision data are already available for  $b\bar{b}$  and expected for  $t\bar{t}$ . The  $\gamma\gamma \rightarrow q\bar{q}$  experiments are planned.

## 2 Features of theoretical description

Heavy quarks near the production threshold moves slowly that justifies the use of the nonrelativistic quantum mechanics for their description [6–8]. Being much simpler than the comprehensive relativistic treatment of the bound state problem with Bethe-Salpeter amplitude [9], the nonrelativistic approach allows one to take into account exactly such an essential feature of the near-threshold dynamics as Coulomb interaction [10]. For unstable heavy quarks with a large decay width it is possible to compute the cross section near threshold point-wise in energy because the large decay width suppresses the long distance effects of strong interaction [11]. The  $t\bar{t}$ -pair near the production threshold is just a system that satisfies the requirement of being nonrelativistic. Therefore the description of  $t\bar{t}$ -system near the production threshold  $\sqrt{s} \approx 2m_t$  ( $\sqrt{s}$  is a total energy of the pair,  $m_t$  is the top quark mass) is quite precise within nonrelativistic QCD (NRQCD). Reasons for this accuracy are related to the large mass of the top:

- The top quark is very heavy  $m_t = 175$  GeV [12] and there is an energy region of about 8–10 GeV near the threshold where the nonrelativistic approximation for the kinematics is very precise. For  $\sqrt{s} = 2m_t + E$  with  $|E| < 5$  GeV the

---

<sup>a</sup>e-mail: aapiv@ms2.inr.ac.ru

quark velocity is small

$$v = \sqrt{1 - \frac{4m_t^2}{s}} = \sqrt{1 - \frac{4m_t^2}{(2m_t + E)^2}} \simeq \sqrt{\frac{E}{m_t}} < 0.15 \ll 1. \quad (1)$$

Relativistic effects are small and can be taken into account perturbatively in  $v$  (even in  $v^2$ ).

- The strong coupling constant at the high energy scale is small  $\alpha_s(m_t) \approx 0.1$  that makes the perturbative mapping of QCD onto the low energy effective theory (NRQCD) numerically precise.
- The decay width of top quark is large,  $\Gamma_t = 1.43$  GeV; infrared (small momenta) region is suppressed and PT calculation for the cross section near the threshold is reliable point-wise in energy.

Because  $\alpha_s \sim v$  and the ratio  $\alpha_s/v$  is not small, the Coulomb interaction is enhanced. The ordinary perturbation theory for the cross section (with free quarks as the lowest order approximation) breaks down and all terms of the order  $(\alpha_s/v)^n$  should be summed. The expansion for a generic observable  $f(E)$  in this kinematical region has the form

$$f(E) = f_0(\alpha_s/v) + \alpha_s f_1(\alpha_s/v) + \alpha_s^2 f_2(\alpha_s/v) + \dots \quad (2)$$

where  $f_i(\alpha_s/v)$  are some (not polynomial) functions of the ratio  $\alpha_s/v$ ,  $f_0(\alpha_s/v)$  is a result of the pure Coulomb approximation (or a kind of its improvement). The expansion in  $\alpha_s$  in eq. (2) takes into account the perturbative QCD corrections to the parameters of NRQCD and relativistic corrections (in the regime  $v \sim \alpha_s$ ).

For the  $e^+e^- \rightarrow t\bar{t}$  process mediated by the photon the NNLO analysis is well known. The basic quantity is the vacuum polarization function

$$\Pi(E) = i \int \langle T j_{em}(x) j_{em}(0) \rangle e^{iqx} dx, \quad q^2 = (2m_t + E)^2. \quad (3)$$

Near the threshold (for small energy  $E$ ) NRQCD is used. The cross section is saturated with S-wave scattering. In this approximation the polarization function near the threshold to the NNLO accuracy in NRQCD is given by

$$\Pi(E) = \frac{2\pi}{m_t^2} C_h(\alpha_s) C_O(E/m_t) G(E; 0, 0). \quad (4)$$

The pole mass definition is used for  $m_t$  (e.g. [13]),  $\alpha_s$  is the strong coupling constant.  $C_h(\alpha_s)$  is the high energy coefficient.  $G(E; 0, 0)$  is the nonrelativistic Green function (GF). The quantity  $C_O(E/m_t)$  describes the contributions of higher dimension operators within the effective theory approach. These contributions have, in general, a different structure than the leading term. To the NNLO of NRQCD the contribution of higher dimension operators can be written as a total factor  $C_O(E/m_t)$  for the leading order GF,  $C_O(E/m_t) = 1 - 4E/3m_t$ . The polarization function near the threshold (4) contains expansions in small parameters  $\alpha_s$  and/or  $v$ , cf. eq. (2). The leading order approximation of the low energy part is the exact Coulomb solution for the Green function.

The nonrelativistic Green's function  $G(E) = (H - E)^{-1}$  is determined by the nonrelativistic Hamiltonian

$$H = \frac{p^2}{m_t} + V(r) \quad (5)$$

describing dynamics of the  $t\bar{t}$ -pair near the threshold. The most complicated part of Hamiltonian (5) to find is the heavy quark static potential  $V_{pot}(r)$  entering into the potential  $V(r)$ . The static potential  $V_{pot}(r)$  is computed in perturbation theory and can be written in the form

$$V_{pot}(q) = -\frac{4\alpha_v(r)}{3r} \quad (6)$$

that gives a definition of the effective charge  $\alpha_v$  related to the  $\overline{\text{MS}}$ -scheme coupling constant

$$\alpha_v(\mu) = \alpha_s(\mu)(1 + a_1\alpha_s(\mu) + a_2\alpha_s(\mu)^2). \quad (7)$$

Coefficients  $a_{1,2}$  are known [14–16]. The effective coupling  $\alpha_v$  is nothing but a coupling constant in some special subtraction scheme. The coefficient  $a_2$  allows one to find the effective  $\beta$ -function  $\beta_v$  for the evolution of the coupling  $\alpha_v$  at NNLO.

High energy coefficient  $C_h(\alpha_s)$  is given by the expression

$$C_h(\alpha) = 1 - \frac{16}{3} \frac{\alpha_s}{\pi} + \left( \frac{\alpha_s}{\pi} \right)^2 \left( -\frac{140}{27} \pi^2 \ln \frac{\mu_f}{m_t} + c_2 \right). \quad (8)$$

The NLO result for  $C_h(\alpha_s)$  has been known since long ago [17–19]. At NNLO there appears a term proportional to the logarithm of the factorization parameter  $\mu_f$  that separates long and short distances (or large and small momenta) within the effective theory approach. The finite ( $\mu_f$  independent) coefficient  $c_2$  is known [20, 21]. An explicit dependence of high and low energy quantities on the factorization scale  $\mu_f$  is a general feature of effective theories which are valid only for a given region of energy. Physical quantities are factorization scale independent. In NRQCD the  $\mu_f$  dependence cancels between Green's function and the high energy coefficient  $C_h$ .

The main dynamical quantity in description of the  $t\bar{t}$  system near the threshold is the nonrelativistic Green's function  $G = (H - E)^{-1}$ . The Hamiltonian is represented in the form [22–24]

$$H = H_C + \Delta H, \quad H_C = \frac{p^2}{m_t} - \frac{4\alpha_s}{3r} \quad (9)$$

with  $\Delta H$  describing high order corrections. Constructing the Green's function is straightforward and can be done analytically within perturbation theory near Coulomb Green's function  $G_C(E)$  or numerically for complex values of  $E$  that can be used to describe the production of particles with nonzero width [25–33].

The analytical solution for Green's function is perturbative in  $\Delta H$

$$G = G_C - G_C \Delta H G_C + G_C \Delta H G_C \Delta H G_C - \dots \quad (10)$$

Results are presented basically as an expansion in consecutive orders

$$G = G_0 + \Delta G_1 + \Delta G_2 \quad (11)$$

to check the convergence of the approximations. The leading order is given by Coulomb approximation,  $G_0 = G_C$ . At NLO the quantity  $\Delta G_1$  takes into account

the corrections from the static potential  $V_{pot}(r)$  related to  $a_1$  coefficient in eq. (7). At the NNLO the quantity  $\Delta G_2 \sim O(\alpha_s^2)$  in a sense of eq. (2) accounts for  $\alpha_s^2$  terms in the static potential  $V_{pot}(r)$  ( $a_2$  coefficient in eq. (7)) and relativistic  $v^2$  corrections. It also contains a second iteration of the  $O(\alpha_s)$  term from  $V_{pot}(r)$ . The  $\overline{\text{MS}}$ -scheme for the static potential  $V_{pot}(r)$  is mainly used in the solution. The numerical results for GF obtained by different authors agree with each other [34].

### 3 Physical results

For the  $b\bar{b}$  system an accurate description of the spectrum in terms of moments

$$\mathcal{M}_n = \int_{4m_b^2}^{\infty} \frac{\rho(s)ds}{s^n}$$

is obtained in the near-threshold Coulomb PT calculations. This analysis gave the best determination of the numerical value for the  $b$  quark mass

$$m_b = 4.80 \pm 0.06 \text{ GeV}.$$

For the  $t\bar{t}$  system the top quark width  $\Gamma_t$  plays a crucial role in the calculation of the production cross section near the threshold. At the formal level the width is taken into account by a shift of the energy variable  $E$ . The mass operator of the top quark is approximated by the expression  $M = m_t - i\Gamma_t/2$ . Then the kinematical variable  $s - 4m_t^2$  relevant to the near-threshold dynamics is substituted with  $s - 4M^2$  ( $\sqrt{s} = E + 2m_t$ ) and one finds

$$s - 4M^2 = 4m_t(E + i\Gamma_t) + E^2 + \Gamma_t^2.$$

Neglecting higher orders in  $E$  and  $\Gamma_t$  one obtains a recipe for taking into account the width  $\Gamma_t$  by the shift  $E \rightarrow E + i\Gamma_t$ . The dispersion relation for the vacuum polarization function  $\Pi(E)$  has the form

$$\Pi(E) = \int \frac{\rho(E')dE'}{E' - E}.$$

With the shift recipe one finds

$$\sigma(E) \sim \text{Im } \Pi(E + i\Gamma_t) = \text{Im} \int \frac{\rho(E')dE'}{E' - E - i\Gamma_t} = \Gamma_t \int \frac{\rho(E')dE'}{(E' - E)^2 + \Gamma_t^2}. \quad (12)$$

Because the point  $E + i\Gamma_t$  lies sufficiently far from the positive semiaxis (and the origin) in the complex energy plane the cross section eq. (12) is calculable point-wise in energy. The hadronic cross section  $\sigma(E)$  was obtained by many authors [34]. The normalized cross section for typical values  $m_t = 175$  GeV,  $\Gamma_t = 1.43$  GeV,  $\alpha_s(M_Z) = 0.118$  has the characteristic points which are usually considered as basic observables. They are:  $E_p$  – the position of the peak in the cross section and  $H_p$  – its height. In the limit of the small  $\Gamma_t$  (at least for  $\Gamma_t$  that is smaller than the spacing between the first two Coulomb poles) one would have  $E_p \sim E_0$  and  $H_p \sim |\psi_0(0)|^2$ . The actual value of  $\Gamma_t = 1.43$  GeV is larger than the spacing  $|E_0 - E_1| \sim m_t \alpha_s^2 / 3 \approx 0.6$  GeV

therefore the peak position and height are not determined by the first resonance only. The convergence for  $E_p$  and  $H_p$  in the consecutive orders of perturbation theory near the Coulomb solution is not fast in the  $\overline{\text{MS}}$ -scheme. For the typical numerical values of the theoretical parameters  $m_t$ ,  $\Gamma_t$  and  $\alpha_s(M_Z)$  one finds [31]

$$\begin{aligned} E_p &= E_0(1 + 0.58 + 0.38 + \dots) \\ H_p &= H_0(1 - 0.15 + 0.12 + \dots) \end{aligned} \quad (13)$$

(see also [35, 36]). Important contributions that affect the quality of convergence are the local term ( $\sim \alpha_s V_0 \delta(\vec{r})$  which is related to  $1/r^2$  non-Abelian term [37]) and higher order PT corrections to  $V_{\text{pot}}(r)$ .

#### 4 Discussion and conclusion

Slow convergence for the peak characteristics of the cross section given in eq. (13) has been actively discussed. The suggestions of the redefinition of the top quark mass have been made (e.g. [34, 38, 39]) as the use of the pole mass for a description of the cross section near the threshold is criticized on the ground of its infrared instability [40]. This approach is based on introduction of an effective mass that partly accounts for interaction [41–43]. In this talk I only discuss some possible ways of optimizing the convergence for the Green's function with the pole mass as a theoretical parameter. Actual calculations near the threshold have been performed within the pole mass scheme. For optimizing the convergence one can use methods of exact summation of some contributions in all orders and renormalization scheme invariance of PT series e.g. [25]. The Hamiltonian can be written in the form

$$H = H_{LO} + \Delta V_{PT} + \alpha_s V_0 \delta(\vec{r}), \quad V_0 = -\frac{70\pi}{9m_t^2} \quad (14)$$

where corrections are given by the perturbation theory corrections to  $V_{\text{pot}}(r)$  ( $\Delta V_{PT}$ -part) and by the local term ( $\alpha_s V_0 \delta(\vec{r})$ -part). The  $\delta(\vec{r})$ -part is a separable potential and can be taken into account exactly [44]. The solution reads

$$G(E; 0, 0) = \frac{G_{ir}(E; 0, 0)}{1 + \alpha_s V_0 G_{ir}(E; 0, 0)} \quad (15)$$

with

$$G_{ir}(E) = (H_{LO} + \Delta V_{PT} - E)^{-1} \quad (16)$$

being the irreducible Green's function. The PT expansion of the static potential in NRQCD is important for getting stable results for the cross section near the threshold because the static potential is the genuine quantity which is computed in high order of PT in the strong coupling constant [45]. The convergence in the  $\overline{\text{MS}}$  scheme is not fast which reflects the physical situation that the observables represented by the cross section curve (for instance,  $E_p$  and  $H_p$ ) are sensitive to different scales. The finite-order perturbation theory expansion of the static potential cannot handle several distinct scales with the same accuracy. Indeed, the PT expansion of the static potential is done near some (arbitrary) scale (or distance) which can be considered simply as a normalization point. The farther a given point lies from this normalization

point the worse the precision of the PT expansion for the static potential is. The PT expressions in the  $\overline{\text{MS}}$  scheme are not directly sensitive to physical scales because subtractions are made in a mass independent way (for instance, massive particles do not decouple automatically in the  $\overline{\text{MS}}$  scheme e.g. [46, 47]). One can rewrite the static potential through some physical parameters which is similar to the use of the momentum subtraction scheme instead of the  $\overline{\text{MS}}$ -scheme

$$V_{\text{pot}}(r) = -\frac{4\alpha_0}{3r} \left( 1 + \alpha_0 b_1 \ln r/r_0 + \alpha_0^2 (b_1^2 \ln^2 r/r_0 + b_2' \ln r/r_0 + c) \right). \quad (17)$$

Here  $r_0$  and  $c$  are the parameters of the renormalization scheme freedom in NNLO and  $\alpha_0$  is the corresponding coupling in the  $\{r_0, c\}$ -scheme [48]. They parameterize the center of the expansion (a normalization point) and the derivative (respective  $\beta$ -function) of the static potential. The parameters  $(r_0, c)$  can be chosen such in order to minimize the higher order corrections to a particular observable (e.g. [25] where NLO analysis has been done). In such a case  $r_0$  can be understood as a typical distance to which a chosen observable is sensitive. Note that the best approximation of the static potential  $V_{\text{pot}}(r)$  for different scales would be provided by the use of the running coupling constant  $\alpha_s(r)$ . The analytical calculation of GF becomes technically impossible in this case. The numerical calculation of GF requires some regularization at large distances where the IR singularity (Landau pole) can occur in  $\alpha_s(r)$ . The singularity can be dealt with if an IR fixed point appears in the evolution for the effective coupling constant (e.g. [49]) or with some nonPT regularization for the potential (e.g. [50]). For the top quark production the contribution of the large  $r$  region into the cross section is small because of the large decay width of the top quark. In the finite-order PT analysis the parameters  $r_0$  and  $c$  can be chosen to minimize higher order corrections either to  $E_p$  or to  $H_p$  but not to both simultaneously because  $E_p$  and  $H_p$  are sensitive to different distances. One finds the difference of scales minimizing corrections to the first Coulomb resonance in NLO to be

$$\ln(r_E/r_\psi) = \frac{1}{3} + \frac{\pi^2}{9}. \quad (18)$$

Because of the large top quark width many states contribute into the position and height of the peak in the cross section. Therefore the characteristic distance estimates are not so transparent (the NNLO peak position, for instance, is not exactly the ground state energy in the zero width limit). The relation (18) can serve just as a basic guide. In practical analysis one can choose the particular numerical values for the parameters  $(r_0, c)$  which stabilize either  $E_p$  or  $H_p$ .

### Acknowledgments

I thank J.G.Körner for kind hospitality at Mainz University where the paper was completed. The work is supported in part by Russian Fund for Basic Research under contracts 99-01-00091 and 01-02-16171, by INTAS and DFG grants.

### References

- [1] E.Accomando *et al.*, Phys.Rep. **299**(1998)1.

- [2] W.Kwong, Phys.Rev. **D43**(1991)1488;  
M.J.Strassler and M.E.Peskin, Phys.Rev. **D43**(1991)1500.
- [3] M.Jezabek, J.H.Kühn and T.Teubner, Z.Phys. **C56**(1992)653;  
Y.Sumino *et al.*, Phys.Rev. **D47**(1993)56.
- [4] V.S.Fadin and V.A.Khoze, Yad.Fiz. **93**(1991)1118;  
I.I.Bigi, V.S.Fadin and V.A.Khoze, Nucl.Phys. **B377**(1992)461;  
I.I.Bigi, F.Gabbiani and V.A.Khoze, Nucl.Phys. **B406**(1993)3.
- [5] J.H.Kühn, E.Mirkes and J.Steegborn, Z.Phys. **C57**(1993)615.
- [6] W.E.Caswell and G.E.Lepage, Phys.Lett. **B167**(1986)437.
- [7] G.E.Lepage *et al.*, Phys.Rev. **D46**(1992)4052.
- [8] G.T.Bodwin, E.Braaten and G.P.Lepage, Phys.Rev. **D51**(1995)1125.
- [9] E.E.Salpeter, H.A.Bethe, Phys.Rev. **84**(1951)1232.
- [10] M.B.Voloshin, Nucl.Phys. **B154**(1979)365;  
H.Leutwyler, Phys.Lett. **B98**(1981)447.
- [11] V.S.Fadin and V.A.Khoze, Pis'ma Zh.Eksp.Teor.Fiz. **46**(1987)417;  
Yad.Fiz. **48**(1988)487.
- [12] C.Caso *et al.*, Eur.Phys.J. **C3**(1998)1.
- [13] R.Tarrach, Nucl.Phys. **B183**(1981)384.
- [14] W.Fisher, Nucl.Phys. **B129**(1977)157;  
A.Billoire, Phys.Lett. **B92**(1980)343.
- [15] M.Peter, Phys.Rev.Lett. **78**(1997)602; Nucl.Phys **B501**(1997)471.
- [16] Y.Schröder, Phys.Lett. **B447**(1999)321.
- [17] R.Karplus and A.Klein, Phys.Rev. **87**(1952)848;  
G.Källen and A.Sarby, K.Dan.Vidensk.Selsk.Mat.-Fis.Medd. **29**(1955)1;  
R.Barbieri *et al.*, Phys.Lett. **B57**(1975)535.
- [18] I.Harris and L.M.Brown, Phys.Rev. **105**(1957)1656;  
R.Barbieri *et al.*, Nucl.Phys. **B154**(1979)535.
- [19] B.M.Chibisov and M.V.Voloshin, Mod.Phys.Lett. **A13**(1998)973.
- [20] A.Czarnecki and K.Melnikov, Phys.Rev.Lett. **80**(1998)2531.
- [21] M.Beneke, A.Signer and V.A.Smirnov, Phys.Rev.Lett. **80**(1998)2535.
- [22] A.I.Achieser and V.B.Berestezki,  
Quantum electrodynamics, Moscow 1959.
- [23] L.D.Landau and E.M.Lifshitz, Relativistic Quantum Theory, Part 1  
(Pergamon, Oxford, 1974).
- [24] I.G.Halliday, P.Suranyi, Phys.Rev. **D21**(1980)1529.
- [25] J.H.Kühn, A.A.Penin and A.A.Pivovarov,  
Nucl.Phys. **B534**(1998)356.
- [26] A.H.Hoang and T.Teubner, Phys.Rev. **D58**(1998)114023.
- [27] A.A.Penin and A.A.Pivovarov, Phys.Lett. **B435**(1998)413;  
Phys.Lett. **B443**(1998)264; Nucl.Phys. **B549**(1999)217.
- [28] K.Melnikov and A.Yelkhovsky, Nucl.Phys. **B528**(1998)59.
- [29] M.Beneke, A.Signer and V.A.Smirnov, Phys.Lett. **B454**(1999)137.
- [30] T.Nagano, A.Ota and Y.Sumino, Phys.Rev. **D60**(1999)114014.
- [31] A.A.Penin and A.A.Pivovarov, Phys.At.Nucl. **64**(2001)275;  
hep-ph/9904278.
- [32] O.Yakovlev, Phys.Lett. **B457**(1999)170.

- [33] A.H.Hoang and T.Teubner, Phys.Rev. **D60**(1999)114027.
- [34] A.H.Hoang *et al.*, Eur.Phys.J.direct **C3**(2000)1.
- [35] A.Pineda and F.J.Yndurain, Phys.Rev. **D58**(1998)094022.
- [36] F.J.Yndurain, FTUAM-00-14, Jul 2000. 13pp. hep-ph/0007333.
- [37] S.N.Gupta and S.F.Radford, Phys.Rev. **D24**(1981)2309;  
Phys.Rev. **D25**(1982)3430 (Erratum); S.N.Gupta, S.F.Radford and  
W.W.Repko, Phys.Rev. **D26**(1982)3305.
- [38] K.G.Chesterkin, M.Steinhauser, Phys.Rev.Lett. **B83**(1999)4001.
- [39] S.Groote and O.Yakovlev, hep-ph/0008156.
- [40] M.Beneke and V.M.Braun, Nucl.Phys. **B426**(1994)301;  
I.I.Bigi *et al.*, Phys.Rev. **D50**(1994)2234.
- [41] R.P.Feynman, Phys.Rev. **97**(1955)660.
- [42] H.D.Politzer, Nucl.Phys. **B117**(1976)397.
- [43] N.V.Krasnikov and A.A.Pivovarov, Russ.Phys.J. **25**(1982)55.
- [44] A.A.Pivovarov, Phys.Lett. **B475**(2000)135.
- [45] M.Jezabek, J.H.Kühn, M.Peter, Y.Sumino and T.Teubner,  
Phys.Rev. **D58**(1998)014006.
- [46] K.G.Chesterkin, B.A.Kniehl, M.Steinhauser,  
Phys.Rev.Lett. **79**(1997)2184.
- [47] T.Appelquist and J.Carazzone, Phys.Rev. **D11**(1975)2856.
- [48] P.M.Stevenson, Phys.Rev. **D23**(1981)2916.
- [49] A.A.Penin and A.A.Pivovarov, Phys.Lett. **B401**(1997)294;  
N.V.Krasnikov and A.A.Pivovarov, Mod.Phys.Lett. **A11**(1996)835;  
Phys.Atom.Nucl. **64**(2001)1500; hep-ph/9512213.
- [50] J.L.Richardson, Phys.Lett. **B82**(1979)272.

# AN ANALYSIS OF UNPOLARIZED STRUCTURE FUNCTION MOMENTS IN $N^*$ EXCITATION REGION

M. OSIPENKO<sup>1, a</sup>, G. RICCO<sup>2, b</sup>, M. TAIUTI<sup>2, c</sup>, S. SIMULA<sup>3, d</sup>,  
M. ANGHINOLFI<sup>2, e</sup>, M. BATTAGLIERI<sup>2, f</sup>, G. FEDOTOV<sup>1, g</sup>,  
E. GOLOVACH<sup>4, h</sup>, R. DE VITA<sup>2, i</sup>, B. ISHKHANOV<sup>1,4, j</sup> V. MOKEEV<sup>4, k</sup>  
M. RIPANI<sup>2, l</sup>

<sup>1</sup> Physics Faculty of Moscow State University, 119899 Moscow, Russia

<sup>2</sup> Istituto Nazionale di Fisica Nucleare, Sezione di Genova, e Dipartimento di Fisica dell'Università, 16146 Genova, Italy

<sup>3</sup> Istituto Nazionale di Fisica Nucleare, Sezione Roma III, 00146 Roma, Italy

<sup>4</sup> Nuclear Physics Institute of Moscow State University, 119899 Moscow, Russia

*Abstract.* The main goal of the present analysis is the direct evaluation of the moments of the structure function  $F_2$ , which implies numerical integration of the experimental data over  $x$  at fixed  $Q^2$ , in whole available  $Q^2$  range. This experimental information will allow to extract the contribution of the higher twists related to multiparton correlation effects. Moreover the comparison with theoretical predictions either based on first-principle calculations, like lattice QCD simulations, or obtained from models of the nucleon structure may represent an important test of the nonperturbative QCD regime.

## 1 Introduction

The analysis of inelastic electron scattering experiments in GeV region shows some interesting features:

1. At high  $W$  ( $> 3$  GeV), proton and deuteron data exhibit precocious scaling around photon mass scale 1-2 GeV<sup>2</sup>; the experimental cross section approaches the perturbative behavior, as determined by the nucleon structure functions, with remaining discrepancy still compatible with the so called “power corrections”, as predicted in PQCD framework [1]. At lower  $W$  the resonances and the underlying continuous cross section show a very similar  $Q^2$  evolution (local duality) [2]. This effect, up to now poorly understood, seems to be quite general [3] and casts some doubt on the consistency of commonly followed separation procedures between the two components in data analysis or phenomenological models.

---

<sup>a</sup>e-mail: osipenko@depni.npi.msu.su

<sup>b</sup>e-mail: ricco@ge.infn.it

<sup>c</sup>e-mail: taiuti@ge.infn.it

<sup>d</sup>e-mail: simula@roma3.infn.it

<sup>e</sup>e-mail: anghi@ge.infn.it

<sup>f</sup>e-mail: batta@ge.infn.it

<sup>g</sup>e-mail: fedotov@depni.npi.msu.su

<sup>h</sup>e-mail: golovach@depni.npi.msu.su

<sup>i</sup>e-mail: devita@ge.infn.it

<sup>j</sup>e-mail: BSI@depni.npi.msu.su

<sup>k</sup>e-mail: mokeev@depni.npi.msu.su

<sup>l</sup>e-mail: ripani@ge.infn.it

2. Data on nuclei show the influence of nuclear matter on nucleon excitation both at high  $W$  (EMC effect) and in resonance region, where  $P_{33}$  and  $D_{13}$  transition form factors have been reported to decrease with increasing  $Q^2$  faster than in the free nucleon [4].

These physics issues, presented in more detail in the following two sections force us to undertake an effort to a systematic analysis of inclusive inelastic cross section in proton and nuclei using data measured at CLAS. In section 4 the reliability of inclusive CLAS data, from preliminary analysis, and the covered kinematic range will be discussed.

## 2 The Proton

The Operator Product Expansion (OPE) of the virtual photon-nucleon scattering amplitude leads to a description of the complete  $Q^2$  evolution for the moments of the nucleon structure functions:

$$M_n^{CN}(Q^2) = \int_0^\infty dx x^{(n-2)} F_2(x, Q^2) = \sum_{\tau=2k}^\infty E_{n\tau}(\mu, Q^2) O_{n\tau}(\mu) \left( \frac{\mu^2}{Q^2} \right)^{\frac{1}{2}(\tau-2)} \quad (1)$$

where  $k = 1, 2, \dots$ ,  $M_n^{CN}(Q^2)$  is the  $n$ -th Cornwell-Norton moment of the (asymptotic) structure function for a “massless” nucleon  $F_2(x, Q^2)$ ;  $\mu$  is the renormalization scale (about 1 GeV),  $O_{n\tau}(\mu)$  is the reduced matrix element of operators with definite spin  $n$  and twist  $\tau$  (dimension-spin), related to the nonperturbative structure of the target;  $E_{n\tau}(\mu, Q^2)$  is a dimensionless coefficient function describing small distance behavior, which can be perturbatively expressed as a power expansion of the running coupling constant  $\alpha_s(Q^2)$ .

At  $Q^2$  values comparable with the proton mass  $M_p$ , the experimental structure function still contains non negligible mass dependent terms that produce in Eq. 1 further  $M_p^2/Q^2$  power corrections (kinematic twists). To avoid these terms, the  $M_n^{CN}(Q^2)$  of the “massless”  $F_2$  have to be replaced in Eq. 1 by the corresponding Nachtmann [5] moments  $M_n^N(Q^2)$  of the measured structure function  $F_{2_{exp}}(x, Q^2)$  since:

$$M_n^{CN}(F_2(x, Q^2)) = M_n^N(F_{2_{exp}}(x, Q^2)) \quad (2)$$

For leading twist  $\tau = 2$  one ends up in LO or NLO with the well known perturbative logarithmic  $Q^2$  evolution of singlet and non singlet  $F_2$  moments. In order to estimate possible higher order terms in the  $\alpha_s$  perturbative expansion, which completely defines  $E_n$ , one can use two different techniques. One of those is so called infrared renormalon phenomenology [5] and second represented by recently developed soft gluon resummation technique [10].

For higher twist,  $\tau > 2$ , power terms  $O_{n\tau}(\mu)$  are related to quark-quark and quark-gluon (multiparton) correlations, as illustrated by Fig. 1, and should become important at large  $x$  and small  $Q^2$ .

For an analysis of data on the transverse structure function  $F_2$  Eq. 1 can be written [6] in the simplified form, limited to twist 4 and 6:

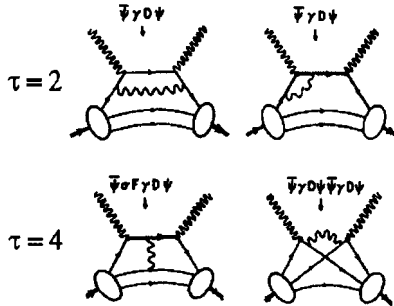


Figure 1: Twist diagrams.

$$M_n^T(Q^2) = \mu_n^T(Q^2) + \mu_n^{T(RS)}(Q^2) + a_n^{(4)} \left[ \frac{\alpha_s(Q^2)}{\alpha_s(\mu^2)} \right]^{\gamma_n^{(4)}} \frac{\mu^2}{Q^2} + a_n^{(6)} \left[ \frac{\alpha_s(Q^2)}{\alpha_s(\mu^2)} \right]^{\gamma_n^{(6)}} \frac{\mu^4}{Q^4} \quad (3)$$

where  $\mu_n^T(Q^2)$  is the leading twist evaluated at next-to-leading order (NLO) in the running coupling constant,  $\mu_n^{T(RS)}(Q^2)$  is the contribution of the rest of perturbative series, estimated either by infrared renormalon phenomenology or in the frame of soft gluon resummation technique; this term is aimed to describe high-order radiative effects beyond the NLO approximation, and the parameters  $a_n^{(4)}$ ,  $\gamma_n^{(4)}$ ,  $a_n^{(6)}$ ,  $\gamma_n^{(6)}$  should be related to multiparton correlation effects.

A systematic analysis of the  $Q^2$  dependence of the experimental Nachtmann moments  $M_n^N(F(x, Q^2))$  in the intermediate  $Q^2$  range ( $0.5 < Q^2 < 10 \text{ GeV}^2$ ) should therefore allow separation of twist two and higher twist terms in the structure function of nucleon and nuclei.

The preliminary work in this direction lead to a few conclusions:

1. The lowest  $n = 2$  transverse moment (related to the average  $x$  dependence of the  $F_2$  structure function) at  $Q^2 > 1 \text{ GeV}^2$  seems to be well reproduced by NLO twist 2 calculation, the contribution of higher orders of perturbative series and higher twists being almost negligible in this moment.
2. For higher  $n = 4, 6, 8$  moments, related to  $F_2$  data at large  $x$ , the twist 4 and twist 6 contributions have opposite sign [7], producing therefore, to some extent, compensating effects on the structure function  $F_2(x, Q^2)$ .

These illustrate in moments space the well known "local duality" of the transverse structure function and corresponding precocious scaling often observed in low  $Q^2$  experiments [2, 3].

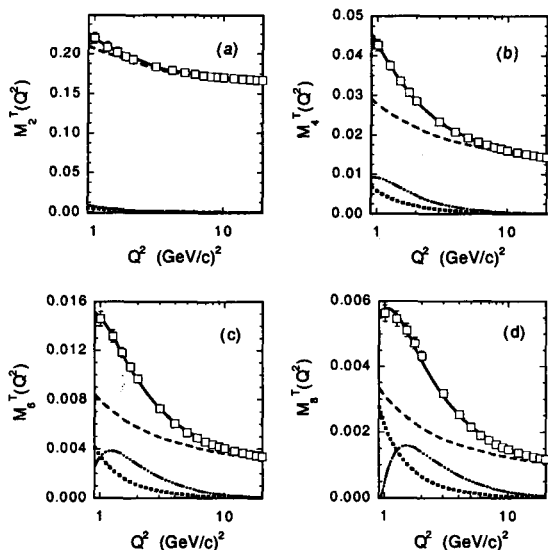


Figure 2: Twist analysis of the proton transverse moments  $M_n^T(Q^2)$  for  $n = 2, 4, 6$  and  $8$ , including both phenomenological higher twists originating from multiparton correlations and the power corrections arising from the IR-renormalon model. The solid lines are the results fitted by the least- $\chi^2$  procedure to the pseudo-data (open squares); the dashed lines are the twist-2 contribution, while the dotted and dot-dashed lines correspond to the IR-renormalon and multiparton correlation contribution, respectively.

### 3 Nuclei

Despite the fact that experimental data in interesting  $Q^2$  domain ( $0.5 < Q^2 < 10$  GeV $^2$ ) are still too sparse for quantitative evaluations, a preliminary analysis [8] for nuclei around mass 12, seems to provide some evidence that scaling in complex nuclei may be even more precocious than observed in proton.

The obtained from data the minimum momentum transfer  $Q_0^2$  at which measured moments of the structure function  $F_2$  are still compatible with the leading twist contribution for the proton and nuclei (see Tab. 1) exhibit a much faster convergence of the twist series from r.h.s. of Eq. 3 in nuclei with respect to the case of proton.

Table 1: The minimum momentum transfer  $Q_0^2$  where the moments are consistent with the leading twist behaviour for different target particles.

	$Q_0^2(M_2)$	$Q_0^2(M_4)$	$Q_0^2(M_6)$
Proton	$1.6 \pm 0.2$	$1.5 \pm 0.1$	$1.6 \pm 0.1$
Deuteron	$1.6 \pm 0.1$	$1.5 \pm 0.1$	$1.5 \pm 0.1$
Nuclei	$0.8 \pm 0.1$	$1.0 \pm 0.2$	$1.2 \pm 0.1$

This point suggests the occurrence of the dominance of twist 2 operators for  $Q^2$  values above the onset  $Q_0^2$  reported in Tab. 1. This further precocity of local duality in nuclei, if confirmed, can be justified by different arguments like for instance:

1. Partial quark deconfinement due to change of mass scale  $\mu$  in nuclear matter; this assumption might also account for the faster decrease, respect to the deuteron, of  $P_{33}$  and, perhaps,  $D_{13}$  resonance transition form factors observed [4] in light nuclei in a limited  $Q^2$  range, as well as for the behaviour of the higher  $x$  part of EMC effect [9].
2. A quenching of higher twists in nuclear matter; this assumption which is not for the moment supported by any theoretical predictions, remains however an interesting speculation.

### 4 CLAS Data Analysis

The Thomas Jefferson National Accelerator Facility (TJNAF) provides an experimental information on the nucleon structure functions in the resonance region with an unprecedented accuracy. Existing data, measured in Hall-C [11] with a record energy resolution, do not allow a full integration of experimental values of the structure function  $F_2(x, Q^2)$  over  $x$  at fixed  $Q^2$ . Approaches for an evaluation of moments using different models of  $F_2$ , performed first in [7] with the SLAC function [12] and recently repeated, according to the new fit [13], contain unknown systematic uncertainties generated by their model dependence. Moreover, in case of nuclei, where few data exist and the  $Q^2$  dependence of the structure function is completely unknown in the interesting kinematic domain ( $0.1 < x < 1$  and  $1 < Q^2 < 5$  GeV $^2$ ), the result of such a technique would be very uncertain. CLAS data, which continuously cover whole the bidimensional kinematic region accessible at TJNAF, as shown in

Fig. 3, allow us to extract moments based on experimental points over most of the integration range.

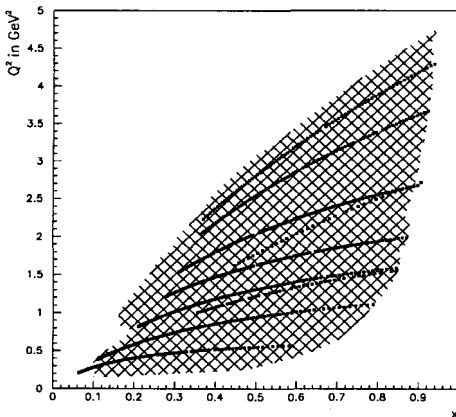


Figure 3: The kinematic range covered by CLAS data: the hatched area represents preliminary CLAS data, points show Hall-C TJNAF data [11].

A direct evaluation of the  $n > 2 F_2$  Nachtmann moments on the proton and nuclei from data in the  $0.5 < Q^2 < 5 \text{ GeV}^2$  region, as possible using CLAS with the present and upgraded TJNAF beam, will be a necessary complement to the existing data analysis for a systematic understanding of large  $x$  parton physics in inclusive experiments.

## References

- [1] R. Roberts, "The structure of the proton", (Cambridge U.P.), 1993.
- [2] E. Bloom and F. Gilman, *Phys. Rev. D* 4, 2901 (1971).
- [3] C. Carlson and M. Mukhopadhyay, *Phys. Rev. D* 47, 1737 (1993).
- [4] M. Anghinolfi *et al.*, *Nucl. Phys. A* 602, 405 (1996).
- [5] M. Beneke, CERN TH/98-233 (1998).
- [6] A. De Rujula, H. Georgi and H. Politzer, *Ann. Phys.* 103, 315 (1977).
- [7] G. Ricco *et al.*, *Nucl. Phys. B* 555, 306 (1999).
- [8] G. Ricco *et al.*, *Phys. Rev. C* 57, 356 (1998).
- [9] R. Jaffe, *Phys. Rev. Lett.* 50, 228 (1983).
- [10] S. Simula, *Phys. Lett. B* 493, 325 (2000).
- [11] I. Niculescu, *Ph.D. Thesis*, (Hampton University), 1999.
- [12] A. Bodek *et al.*, *Phys. Rev. D* 20, 1471 (1979).
- [13] C. S. Armstrong *et al.*, *Phys. Rev. D* 63, 094008 (2001).

# PRAGMATIC APPROACH TO DESCRIPTION OF $\pi\pi$ SCATTERING

E.P.Shabalin <sup>a</sup>

*State Research Center Institute of Theoretical and Experimental Physics, Moscow,  
Russia*

*Abstract.* The  $\pi\pi$ -scattering in the energy region  $\sqrt{s} < 1$  GeV is described quite successfully by the pole diagrams with the low-mass intermediate particles of the spins 0, 1 and 2 if the properties of these particles and their interactions are determined proceeding from the principle of maximal resemblance between the properties of QCD and mesonic world objects.

## 1 Introduction

The Quantum Chromodynamics (QCD) used for the description of the processes at high energy does not work in the low-energy region because of rapid increasing of the coupling constant leading to non-applicability of the perturbation theory. For this reason, the low-energy hadronic processes are described basing on the effective lagrangians, more or less reflecting the fundamental properties of QCD, or using the effective lagrangian containing all possible covariant combinations of the pseudoscalar fields and their derivatives up to some fixed order in momenta of these fields. The last approach is realized in the so-called Chiral Perturbation Theory (ChPT), the mesonic lagrangian of which to the order  $p^4$  contains 10 terms [1] with the coefficients predominantly determined from a comparison of such theory predictions with the experimental data. This approach, however, is not free from some substantial disadvantages. The part of  $L^{eff}$  of order  $p^6$  contains 143 terms [2] and is useless for practical calculations. Besides, the energy range of ChPT applicability is limited by  $\sqrt{s} < m_K$ , because the power expansion  $ap^2 + bp^4 + \dots$  can not describe the energy behavior produced by appearing at larger  $\sqrt{s}$  resonances. In addition, ChPT theory says nothing on the properties of the low-energy scalar resonances.

If for  $\sqrt{s} > m_K$  incorporation of the resonances is inevitable, the question arise - would it be possible to describe the low-energy  $\pi\pi$  scattering in terms of the pole contributions only. An answer is YES, if solving this problem one will use the Principle of Maximal Resemblance (PMR) between the QCD and real world objects. Then, the amplitude of  $\pi\pi$  scattering can be approximated by set of the pole diagrams with intermediate resonances

$$R = \sigma_{\eta'}(700), f_0(980), \rho(770), f_2(1270), \sigma_\eta(1370)$$

and the diagram corresponding to point-like  $\pi\pi$  interaction. But the contribution corresponding to this last interaction is cancelled by the momentum-independent part of the diagrams with  $R = \sigma_{\eta',\eta}$ .

---

<sup>a</sup>e-mail: shabalin@heron.itep.ru

## 2 What kind of a low-energy theory reflects adequately the properties of QCD.

The QCD lagrangian

$$L^{QCD} = -\frac{1}{4}G_{\mu\nu}^a G_{\mu\nu}^a + \sum_q \bar{q}[i\gamma_\mu(\partial_\mu + i\frac{g}{\sqrt{2}}G_\mu^a t^a) - m_q]q \quad (1)$$

in the chiral symmetry limit  $m_q=0$ , is invariant under independent global transformation of "left" and "right" quark fields

$$q_L \rightarrow q_L \exp(-i\hat{\varepsilon}_L/\sqrt{2}), \quad q_R \rightarrow q_R \exp(-i\hat{\varepsilon}_R/\sqrt{2}) \quad (2)$$

where  $\hat{\varepsilon}_{L,R}$  are independent  $3 \times 3$ -matrices in the flavour space

$$\hat{\varepsilon}_{L,R} = \varepsilon_{L,R}^a t^a, \quad t^0 = \frac{1}{\sqrt{3}}\mathbf{1}, \quad t^{1-8} = \frac{1}{\sqrt{2}}\lambda^{1-8} \quad (3)$$

and  $\varepsilon_{L,R}^a$  are *c*-numbers.

The simplest QCD quark constructions corresponding to the spinless states are  $\bar{q}_R t^a q_L$  and its Hermitian conjugate. Therefore, to reflect the properties of QCD, the mesonic lagrangian must be built in terms of non-self-conjugate matrix incorporating the fields of opposite parity:

$$\hat{U} = \sigma^a t^a + i\pi^a t^a \quad (4)$$

where  $\sigma^a$  and  $\pi^a$  are the scalar and pseudoscalar members of the spin-0 fields. In accordance with (2), the transformation properties of  $U$  under chiral rotation of "left" and "right" quarks are defined by the relation

$$\hat{U} \rightarrow \exp(i\hat{\varepsilon}_R/\sqrt{2})\hat{U}\exp(-i\hat{\varepsilon}_L/\sqrt{2}) \quad (5)$$

This transformation converts the scalars into pseudoscalars and vice versa and does not change the number of quarks. Therefore, QCD dictates a necessity of existence of diquarks scalar states which are the chiral partners of the pseudoscalar ones. These scalar mesons can be identified with the known scalar resonances.

The effective Lagrangian of the system of  $0^\pm$  fields written in terms of matrix  $U$  in the form (4) is given in [3] - [6]. It takes into account the effects of spontaneous and explicit breakdown of chiral symmetry and effects of mixing the isosinglet scalar and pseudoscalar quark-antiquark states with the corresponding gluonic states [5, 6].

The characteristics of  $0^+$  mesons including  $\sigma_{\eta'}$  and  $\sigma_\eta$  which are the mixtures of  $\sigma_0$ ,  $\sigma_8$  and the scalar gluonic field were found in [6, 7].

The scalar  $\sigma_{\eta',\eta}$  mesons exchange together with the point-like interaction  $\pi^4(x)$  containing in the effective lagrangians [3] - [6] lead to the amplitude

$$T_\sigma = <\pi_k(p'_1)\pi_l(p'_2)|\pi_i(p_1)\pi_j(p_2)>_\sigma = \sum_{n=\eta',\eta} \left[ \delta_{ij}\delta_{kl}G_n(s)\frac{s-\mu^2}{m_{\sigma_n}^2-s} + \delta_{ik}\delta_{jl}G_n(t)\frac{t-\mu^2}{m_{\sigma_n}^2-t} + \delta_{il}\delta_{jk}G_n(u)\frac{u-\mu^2}{m_{\sigma_n}^2-u} \right], \quad (6)$$

where it has been taken into account that the vertex  $\sigma(q^2)\pi\pi$  contains the form factor depending on  $q^2$ . Our theory says nothing on this form factor. We shall employ the form factor given by

$$G_n(x) = G_n(x = \mu^2) \exp[-k(x - \mu^2)], \quad k > 0. \quad (7)$$

The magnitudes of  $G_n(\mu^2)$  are presented in [7].

The resonance  $f_0(980)$  can not be treated as the one corresponding to simple  $\bar{q}q$  configuration. The chiral theory requires that this resonance would be coupled to the derivatives of the pion fields

$$\langle \pi^a(p_1)\pi^b(p_2) | f_0(q) \rangle = -\frac{g_{f_0}}{M_{f_0}} p_{1\mu} p_{2\mu} \delta^{ab} \quad (8)$$

The contribution of  $f_0$  exchange to  $\pi\pi$  scattering is given in [7].

### 3 The spin 1 fields and their interactions

A conventional way to incorporate the spin 1 fields into chiral theory is described in [8]. Within this approach, the Hermitian fields  $A_\mu^{L,a}$  and  $A_\mu^{R,a}$  are related to Hermitian quark currents

$$i\bar{q}_L \gamma_\mu \frac{\lambda^a}{2} q_L, \quad i\bar{q}_R \gamma_\mu \frac{\lambda^a}{2} q_R. \quad (9)$$

But these currents do not satisfy the conditions

$$k_\mu V_\mu^\alpha(k) = 0, \quad k_\mu A_\mu^\alpha(k) = 0 \quad (10)$$

excluding the spin-0 component from the vector and axial-vector fields. Quark constructions that satisfy the above conditions are given by

$$A_\nu^a \sim i \frac{\partial}{\partial x_\mu} \bar{q}_R \sigma_{\mu\nu} \lambda^a q_L, \quad A_\nu^{a\dagger} \sim (-i) \frac{\partial}{\partial x_\mu} \bar{q}_L \sigma_{\mu\nu} \lambda^a q_R \quad (11)$$

and it means that the physical vector and axial-vector mesonic fields are the divergences of the tensor and pseudotensor quark currents. An assumption that the fields of spin 1 could be the divergences of the tensor currents was uttered long time ago [9] - [11]. But our statement is based on the different arguments, namely, on the idea of necessity of one-to-one correspondence of the properties of the physical objects and constructions built from quarks and gluons. The remarkable property of the relation (11) consists in the turning to zero of the  $\rho\pi\pi$  coupling at  $q_\rho^2 = 0$  [11]. Taking into account this circumstance we come to

$$T_\rho = \langle \pi_k(p'_1)\pi_l(p'_2) | \pi_i(p_1)\pi_j(p_2) \rangle_\rho = \frac{1}{M_\rho^2} \left( \delta_{ij} \delta_{kl} [g^2(u) \frac{(s-t)u}{M_\rho^2 - u} + g^2(t) \frac{(s-u)t}{M_\rho^2 - t}] \right. \\ \left. + \delta_{ik} \delta_{jl} [g^2(s) \frac{(t-u)s}{M_\rho^2 - s} + g^2(u) \frac{(t-s)u}{M_\rho^2 - u}] + \delta_{il} \delta_{jk} [g^2(s) \frac{(u-t)s}{M_\rho^2 - s} + g^2(t) \frac{(u-s)t}{M_\rho^2 - t}] \right), \quad (12)$$

At  $g(s) = g(t) = g(u) = g_\rho = \text{const}$ , the same expression for  $T_\rho$  arises in the other approaches to evaluation of the  $\rho$  exchange contribution to  $\pi\pi$  scattering amplitude [12, 13]. But for  $g(s) \neq g(t) \neq g(u)$  our expression leads to different results.

Dependence of  $g$  of momentum transfer is not fixed by our theory and we shall use the form

$$g(x) = g_\rho \exp \left( 0.7855 \left[ \frac{x}{2M_\rho^2} - \left( \frac{x}{2M_\rho^2} \right)^2 \right] \right) \quad (13)$$

solving a few problems at once (see [7]). In particular, it gives  $g(0) = 5$  and  $g(M_\rho^2) = 6.85$  in accordance with the observations.

#### 4 The spin 2 field and its interactions

The gauge-invariant form of interaction of the spin 2 field  $\varphi$  with two pions satisfying Adler's self-consistency condition [14] is presented in [7]. The  $\pi\pi$  scattering amplitude generated by spin-2 meson exchange can be found in the same reference. Again, we replaced the coupling constant  $g_T$  by the form factor

$$g_T(x) = g_T(M_T^2) \cdot \frac{1 + M_T^4/m^4}{1 + x^2/m^4} \quad (14)$$

#### 5 The results for phase shifts

The results for the phase shifts are presented in Figs.1-4 and Table 2 in [7], where the formalism for description of the phase shifts and the unitarization procedure had been described. We send off the reader to [7] because of the limitations for a volume of conference presentation that do not allow to show the Figs. and Tables. Here we stress only that the theoretical curves in [7] for phase shifts  $\delta_0^0(s), \delta_0^2(s), \delta_1^1(s)$  reproduced very good the experimental data borrowed from [15], [16] and [17] respectively. The phase shifts  $\delta_2^0, \delta_2^2$  calculated in [7] also are in agreement with those calculated using Roy's dispersion relations [18]. And this was achieved without introduction of the so-called mysterious "repulsive core", as it was done, for example, in [19]. The correspondent part arose naturally from the exchange by resonances  $R$  in  $t$ - and  $u$ -channels.

#### References

- [1] J.Gasser and H.Leutwyler, *Ann.Phys.* **158**, 142 (1984); *Nucl.Phys.* **B 250** 465;517;539 (1985).
- [2] H.W.Fearing and S.Scherer, *Phys.Rev.* **D 53** 315 (1996).
- [3] C.Rosenzweig, J.Schechter and G.Trahern, *Phys.Rev.* **D 21** 3388 (1980); P.Di Vecchia and C.Veneziano, *Nucl.Phys.* **B 171** 253 (1980).
- [4] J.Schechter, *Phys.Rev.* **D 21** 3393 (1980).
- [5] E.Shabalin, *Nucl.Phys.* **B 409** 87 (1993).
- [6] E.Shabalin, *Yad.Fiz.* **49** 588 (1989). [*Sov.J.Nucl.Phys.* **49** 365(1989)].
- [7] E.Shabalin, *Phys.Atomic Nucl.* **63** 594 (2000).
- [8] B.W.Lee and H.T.Nieh, *Phys.Rev.* **166** 1507 (1968); A.K.Bhargava and T.Dass, *Phys.Rev.* **D 1** 649 (1970); D.P.Majumdar, *Phys.Rev.* **D 1** 684 (1970).
- [9] W.Krolikowski, *Nuovo Cim.* **42A** 435 (1966).
- [10] M.Ademolo et al., *Phys.Lett.* **22** 521 (1966).

- [11] D.G.Caldi and H.Pagels, *Phys.Rev.* **D 14** 809 (1976).
- [12] S.Weinberg, *Phys.Rev.* **166** 1568 (1986).
- [13] M.Bando ,T.Kugo and K.Yamawaki, *Phys. Reports* **164** 218 (1988).
- [14] S.L.Adler, *Phys.Rev.* **137** B1022 (1965).
- [15] V.Bernard, N.Kaiser and U.-G.Meissner, *Nucl.Phys.* **B 364** 283 (1991).
- [16] S.Ishida et al., *Prog.Theor.Phys.* **98** 1005 (1997).
- [17] E.A.Alekseeva et al., *Zh.Eksp.Teor Fis.* **82** 1007 (1982).
- [18] J.L.Basdevant ,C.D.Froggat and J.L.Petersen, *Nucl.Phys.* **B 72** 413 1974.
- [19] S.Ishida et al. *Prog.Theor.Phys.* **95** 745 (1966).

# NEW ANALYTIC RUNNING COUPLING IN QCD

A. V. Nesterenko<sup>a</sup>

*Department of Physics, Moscow State University,  
Vorobiyovy Gory, Moscow, 119899, Russian Federation*

*Abstract.* As an elaboration of the analytic approach to Quantum Chromodynamics (QCD), a new model for the QCD analytic running coupling is proposed. A self-evident advantage of the new analytic running coupling (NARC) is that it incorporates the infrared enhancement and the ultraviolet asymptotic freedom in a single expression. It is essential that additional parameters are not introduced in the theory. The absence of unphysical singularities in the physical region  $q^2 > 0$  and a fairly well loop and scheme stability are the remarkable features of the NARC. By making use of practically the same values of  $\Lambda_{\text{QCD}}$  in the approach developed, one succeeded in description of various physical phenomena, from quark confinement to the  $\tau$  lepton decay. This undoubtedly implies that the new analytic running coupling substantially involves both the nonperturbative and the perturbative behavior of Quantum Chromodynamics.

## 1 Introduction

The discovering of the asymptotic freedom phenomenon in Quantum Chromodynamics (QCD) led to the wide using of the perturbation theory. The latter gives good results in the ultraviolet (UV) region, but the perturbation theory is absolutely unapplicable in the infrared (IR) region. So, for the description of a number of physical phenomena one needs to use the nonperturbative methods. The current consideration relies on the analytic approach to QCD.

The analytic approach to Quantum Field Theory (QFT) is a nonperturbative method which is based solely on the first principles of the local QFT. First it was formulated on the example of Quantum Electrodynamics in the late 1950's in the papers [1, 2]. The basic idea of this approach is the explicit imposition of the causality condition, which implies the requirement of the analyticity in the  $q^2$  variable for the relevant physical quantities. This approach has recently been extended to QCD [3] and applied to the "analytization" of the perturbative series for the QCD observables [4]. The term "analytization" means the recovering of the proper analytic properties in the  $q^2$  variable by making use of the Källén–Lehmann spectral representation

$$\left\{ A(q^2) \right\}_{\text{an}} \equiv \int_0^\infty \frac{\varrho(\sigma)}{\sigma + q^2} d\sigma, \quad (1)$$

where the spectral density is determined by the initial (perturbative) expression for some quantity  $A(q^2)$ :

$$\varrho(\sigma) \equiv \frac{1}{2\pi i} \lim_{\epsilon \rightarrow 0_+} \left[ A(-\sigma - i\epsilon) - A(-\sigma + i\epsilon) \right], \quad \sigma \geq 0. \quad (2)$$

---

<sup>a</sup>E-mail: nesterav@thsun1.jinr.ru

## 2 New Analytic Running Coupling

First of all, let us consider the renormalization group (RG) equation for the invariant charge  $g(\mu)$

$$\frac{d \ln [g^2(\mu)]}{d \ln \mu^2} = \beta(g(\mu)). \quad (3)$$

In accordance with the perturbative approach one expands the  $\beta$  function on the right hand side of Eq. (3) as a power series

$$\beta(g(\mu)) = - \left\{ \beta_0 \left[ \frac{g^2(\mu)}{16\pi^2} \right] + \beta_1 \left[ \frac{g^2(\mu)}{16\pi^2} \right]^2 + \dots \right\}, \quad (4)$$

where  $\beta_0 = 11 - 2n_f/3$ ,  $\beta_1 = 102 - 38n_f/3$ , and  $n_f$  is the number of active quarks. Introducing the standard notations  $\alpha_s(\mu^2) = g^2(\mu)/(4\pi)$  and  $\tilde{\alpha}_s(\mu^2) = \alpha(\mu^2)\beta_0/(4\pi)$ , one can reduce the RG equation at the  $\ell$ -loop level to the form

$$\frac{d \ln [\tilde{\alpha}_s^{(\ell)}(\mu^2)]}{d \ln \mu^2} = - \sum_{j=0}^{\ell-1} \beta_j \left[ \frac{\tilde{\alpha}_s^{(\ell)}(\mu^2)}{\beta_0} \right]^{j+1}. \quad (5)$$

It is well-known that the solution to this equation has unphysical singularities at any loop level. So, there is the ghost pole at the one-loop level, and the account of the higher loop corrections just introduces the additional singularities of the cut type into the expression for the running coupling. But we know from the first principles that the QCD running coupling must have the correct analytic properties in the  $q^2$  variable, namely, there should be the only left cut-off along the negative semiaxis of  $q^2$ .

So, what is missing in the  $\beta$  function perturbative expansion? How one could try to improve the situation? This objective can be achieved by involving into consideration the analytic properties in the  $q^2$  variable of the RG equation. The perturbative expansion of the  $\beta$  function as a power series (4) leads to the violation of the correct analytic properties of the RG equation (3). Thus, one can improve the  $\beta$  function perturbative expansion by applying the analytization procedure to it [5]. This results in the equation

$$\frac{d \ln [{}^N\tilde{\alpha}_s^{(\ell)}(\mu^2)]}{d \ln \mu^2} = - \left\{ \sum_{j=0}^{\ell-1} \frac{\beta_j}{\beta_0^{j+1}} \left[ \tilde{\alpha}_s^{(\ell)}(\mu^2) \right]^{j+1} \right\}_{\text{an}}, \quad (6)$$

which solution is by definition [5,6] the  $\ell$ -loop new analytic running coupling,  ${}^N\alpha_{\text{an}}^{(\ell)}(q^2)$ . In fact, the solution to Eq. (6) is determined up to a constant factor, but this ambiguity can easily be avoided by imposing the physical condition of the asymptotic freedom  ${}^N\alpha_{\text{an}}^{(\ell)}(q^2) \rightarrow \alpha_s^{(\ell)}(q^2)$ , when  $q^2 \rightarrow \infty$ . At the one-loop level Eq. (6) can be integrated explicitly with the result

$${}^N\alpha_{\text{an}}^{(1)}(q^2) = \frac{4\pi}{\beta_0} \frac{z-1}{z \ln z}, \quad z = \frac{q^2}{\Lambda^2}. \quad (7)$$

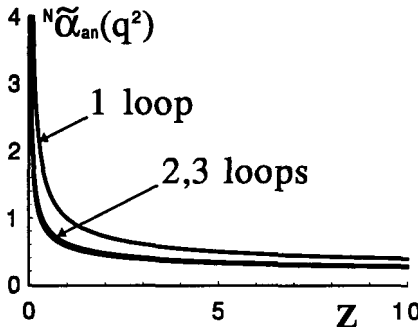


Figure 1: The new analytic running coupling at different loop levels,  $z = q^2/\Lambda^2$ .

At the higher loop levels there is only the integral representation for the new analytic running coupling (NARC). So, at the  $\ell$ -loop level we have

$${}^N\alpha_{\text{an}}^{(\ell)}(q^2) = \frac{4\pi}{\beta_0} \frac{z-1}{z \ln z} \exp \left[ \int_0^\infty \Delta\mathcal{R}^{(\ell)}(\sigma) \ln \left( 1 + \frac{\sigma}{z} \right) \frac{d\sigma}{\sigma} \right], \quad (8)$$

where

$$\mathcal{R}^{(\ell)}(\sigma) = \frac{1}{2\pi i} \lim_{\epsilon \rightarrow 0+} \sum_{j=0}^{\ell-1} \frac{\beta_j}{\beta_0^{j+1}} \left\{ \left[ \tilde{\alpha}_s^{(\ell)}(-\sigma - i\epsilon) \right]^{j+1} - \left[ \tilde{\alpha}_s^{(\ell)}(-\sigma + i\epsilon) \right]^{j+1} \right\}, \quad (9)$$

and  $\Delta\mathcal{R}^{(\ell)}(\sigma) = \mathcal{R}^{(\ell)}(\sigma) - \mathcal{R}^{(1)}(\sigma)$ . The Figure 1 shows the NARC (8) at the one-, two-, and three-loop levels. It is clear from this figure that NARC possesses the higher loop stability. The brief description of the properties of the NARC is given in the next section.

### 3 Properties of the New Analytic Running Coupling

One of most important features of the new analytic running coupling is that it incorporates both the asymptotic freedom behavior and the IR enhancement in a single expression. It was demonstrated [7] that such a behavior of the invariant charge is in agreement with the Schwinger–Dyson equation. It is worth noting here that the additional parameters are not introduced in the theory.

The consistent continuation of the new analytic running coupling to the timelike region has been performed recently [6]. By making use of the function  $N(a)$  (see Eq. (14) in Ref. [8]) the running coupling (7) was presented in the renorminvariant form and the relevant  $\beta$  function was derived:

$${}^N\tilde{\beta}_{\text{an}}^{(1)}(a) = \frac{d \ln a(\mu^2)}{d \ln \mu^2} = \frac{1 - N(a)/a}{\ln [N(a)]}, \quad a(\mu^2) \equiv {}^N\alpha_{\text{an}}^{(1)}(\mu^2). \quad (10)$$

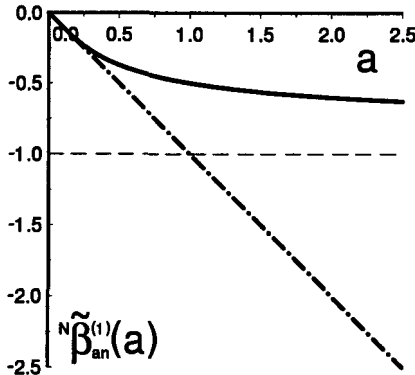


Figure 2: The  $\beta$  function corresponding to the one-loop new analytic running coupling (solid curve). The perturbative result is shown as the dot-dashed line.

Figure 2 shows the  $\beta$  function (10) and the perturbative result corresponding to the one-loop perturbative running coupling  $\tilde{\alpha}_s^{(1)}(q^2) = 1/\ln z$ . The  $\beta$  function (10) coincides with the perturbative result  $\tilde{\beta}_s^{(1)}(a) = -a$  in the region of small values of invariant charge and tends to  $-1$  at large  $a$ . This results in the IR enhancement of the running coupling, namely,  $\alpha(q^2) \sim 1/q^2$  when  $q^2 \rightarrow 0$ . At the higher loop levels the  $\beta$  function has the same asymptotics. Thus the NARC possesses the universal IR and UV behavior at any loop level. The  $\beta$  function (10) in the region of small  $a$  acquires the form  $N\tilde{\beta}_{an}^{(1)}(a) = \tilde{\beta}_s^{(1)}(a) + O[a^{-1} \exp(-a^{-1})]$ , which reveals its intrinsically nonperturbative nature. The detailed description of the properties of the NARC can be found in Ref. [8].

#### 4 Applications of the New Analytic Running Coupling

For verification of the consistency of the model proposed one should turn to the applications. Since we are working in the framework of a nonperturbative approach, the study of nonperturbative phenomena is of a primary interest. The most exciting problem here is the quark confinement.

It has been shown [5, 9] that the new analytic running coupling (7) explicitly leads to the rising at large distances static quark-antiquark potential *without invoking any additional assumptions*:

$$N V(r) \sim \frac{8\pi}{3\beta_0} \Lambda \frac{1}{2} \frac{\Lambda r}{\ln(\Lambda r)}, \quad r \rightarrow \infty. \quad (11)$$

For the practical purposes it is worth using the approximating function  $U(r)$  for the interquark potential (see Eq. (31) in Ref. [5]). The comparison of  $U(r)$  with the Cornell phenomenological potential  $C V(r) = -4a/(3r) + \sigma r$ ,  $a = 0.39$ ,  $\sigma = 0.182 \text{ GeV}^2$ , as well as with the lattice data [10] shows their almost complete coincidence.

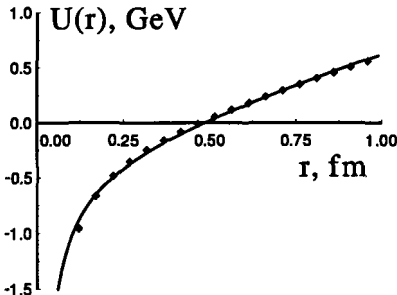


Figure 3: Comparison of the potential  $U(r)$  (solid curve) with the Cornell potential ( $\circ$ );  $\Lambda = 600$  MeV,  $n_f = 3$ .

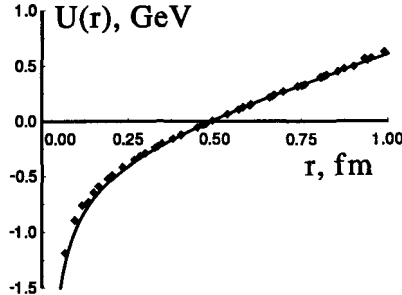


Figure 4: Comparison of the potential  $U(r)$  (solid curve) with the lattice data ( $\circ$ );  $\Lambda = 580$  MeV,  $n_f = 3$ .

It should be mentioned here that the normalization [10]  $U(r_0) = 0$ ,  $r_0 = 0.49$  fm was used, so that  $\Lambda_{\text{QCD}}$  was the only varied parameter here.

By making use of the one-loop new analytic running coupling the estimation of the parameter  $\Lambda_{\text{QCD}}$  has been performed recently by calculation of the value of gluon condensate  $K \simeq (0.36 \text{ GeV})^4$ . This gave  $\Lambda = (650 \pm 50)$  MeV, which is close to the previous estimation.

It turns out that the new analytic running coupling being applied to the standard perturbative phenomena provides the similar values of the parameter  $\Lambda$ . So, the tentative estimations are the following. The  $e^+e^- \rightarrow \text{hadrons}$  annihilation gives  $\Lambda = 490 \pm 80$  MeV, and the  $\tau$  lepton decay gives  $\Lambda = 520 \pm 65$  MeV (light quark mass  $m \simeq [2.5 \div 6.0]$  MeV is used here). These values of  $\Lambda$  correspond to the one-loop level with three active quarks.

Thus, there is a consistent estimation of the parameter  $\Lambda_{\text{QCD}}$  in the framework of the approach developed:  $\Lambda \simeq 550$  MeV (one-loop level,  $n_f = 3$ ). This testifies that the new analytic running coupling combines in a consistent way both nonperturbative and perturbative behavior of QCD.

## 5 Conclusions

A new model for the QCD analytic running coupling has been proposed [5]. It was presented explicitly in the renorminvariant form and the relevant  $\beta$  function was derived [8]. The consistent continuation of the NARC to the timelike region is performed [6]. The NARC possesses a number of appealing features. Namely, there are no unphysical singularities at any loop level. The IR enhancement and the UV asymptotic freedom are incorporated in a single expression. At any loop level the universal IR behavior ( $\alpha \sim 1/q^2$ ) is reproduced. The additional parameters are not introduced in the theory. This approach possesses a good loop and scheme stability. The confining static quark-antiquark potential is derived *without invoking any additional assumptions* [5, 9]. There is a consistent estimation of the parameter  $\Lambda_{\text{QCD}}$  in the framework of the current approach. All this implies that the new analytic running coupling substantially incorporates in a consistent way perturbative and nonperturbative behavior of Quantum Chromodynamics.

### Acknowledgments

The partial support of RFBR (Grant No. 00-15-96691) is appreciated.

### References

- [1] P. J. Redmond, *Phys. Rev.* **112**, 1404 (1958).
- [2] N. N. Bogoliubov, A. A. Logunov, and D. V. Shirkov, *Zh. Eksp. Teor. Fiz.* **37**, 805 (1959) [*Sov. Phys. JETP* **37**, 574 (1960)].
- [3] D. V. Shirkov and I. L. Solovtsov, *Phys. Rev. Lett.* **79**, 1209 (1997); hep-ph/9704333.
- [4] I. L. Solovtsov and D. V. Shirkov, *Theor. Math. Phys.* **120**, 482 (1999); hep-ph/9909305.
- [5] A. V. Nesterenko, *Phys. Rev. D* **62**, 094028 (2000); hep-ph/9912351.
- [6] A. V. Nesterenko, *Phys. Rev. D* (to be published); hep-ph/0102124.
- [7] A. I. Alekseev and B. A. Arbuzov, *Mod. Phys. Lett. A* **13**, 1747 (1998); hep-ph/9704228.
- [8] A. V. Nesterenko, *Mod. Phys. Lett. A* **15**, 2401 (2000); hep-ph/0102203.
- [9] A. V. Nesterenko, in *Proc. Int. Conf. Confinement IV, Vienna, Austria, 2000*, ed. W. Lucha (to be published); hep-ph/0010257.
- [10] G. S. Bali *et al.*, *Phys. Rev. D* **62**, 054503 (2000); hep-lat/0003012.

## QCD<sub>2</sub> IN THE AXIAL GAUGE REVISITED

Yu.S.Kalashnikova <sup>a</sup>

*ITEP, 117218, B.Cheremushkinskaya 25, Moscow, Russia*

A.V.Nefediev <sup>b</sup>

*ITEP, 117218, B.Cheremushkinskaya 25, Moscow, Russia*

*and*

*Centro de Física das Interacções Fundamentais (CFIF)*

*Departamento de Física, Instituto Superior Técnico*

*Av. Rovisco Pais, P-1049-001 Lisboa, Portugal*

*Abstract.* The 't Hooft model for the two-dimensional QCD in the limit of infinite number of colours is studied in the axial gauge. The mass-gap and the bound-state equations are derived using the two consequent Bogoliubov-like transformations. Chiral properties of the model are studied in the Hamiltonian and matrix approaches to the latter. Special attention is payed to the explicit pionic solution of the bound-state equation.

The model for the two-dimensional QCD in the limit of infinite number of colour was suggested in 1974 [1] and it is a marvelous playground for testing methods and approaches used in QCD<sub>4</sub>. It is described by the Lagrangian

$$L(x) = -\frac{1}{4}F_{\mu\nu}^a(x)F_{\mu\nu}^a(x) + \bar{q}(x)(i\gamma_\mu\partial_\mu - gA_\mu^a t^a\gamma_\mu - m)q(x), \quad (1)$$

whereas the large  $N_C$  limit implies that  $\gamma \equiv \frac{g^2 N_C}{4\pi}$  remains finite, so that a nontrivial set of diagrams (planar diagrams) appear to be of the same order in  $N_C$  and should be summed.

Following [2, 3] we consider the model (1) in the axial gauge  $A_1^a(x_0, x) = 0$  and use the principal-value prescription to regularize the infrared divergences. We also define the dressed quark field

$$q_{\alpha i}(t, x) = \int \frac{dk}{2\pi} e^{ikx} [b_\alpha(k, t)u_i(k) + d_\alpha^+(-k, t)v_i(-k)], \quad (2)$$

$$\{b_\alpha(t, p)b_\beta^+(t, q)\} = \{d_\alpha(t, -p)d_\beta^+(t, -q)\} = 2\pi\delta(p - q)\delta_{\alpha\beta}, \quad (3)$$

$$u(k) = T(k) \begin{pmatrix} 1 \\ 0 \end{pmatrix}, \quad v(-k) = T(k) \begin{pmatrix} 0 \\ 1 \end{pmatrix}, \quad T(k) = \exp \left[ -\frac{1}{2}\theta(k)\gamma_1 \right], \quad (4)$$

where the Bogoliubov angle  $\theta(p)$  is the solution to the mass-gap equation. To derive the latter, we organize the normal ordering of the Hamiltonian in the new basis,

$$H = L N_C \mathcal{E}_v + :H_2:+:H_4:, \quad (5)$$

and demand that the quadratic part be diagonal in terms of the dressed-quark creation and annihilation operators. This implies that  $\theta$  is a solution to the following equation:

$$p \cos \theta(p) - m \sin \theta(p) = \frac{\gamma}{2} \int \frac{dk}{(p - k)^2} \sin[\theta(p) - \theta(k)], \quad (6)$$

---

<sup>a</sup>e-mail: yulia@heron.itep.ru

<sup>b</sup>e-mail: nefediev@heron.itep.ru

and the dressed-quark dispersive law is

$$E(p) = m \cos \theta(p) + p \sin \theta(p) + \frac{\gamma}{2} \int \frac{dk}{(p-k)^2} \cos[\theta(p) - \theta(k)]. \quad (7)$$

An alternative way to derive the mass-gap equation (6) is to minimize the vacuum energy (the first term on the r.h.s. in (5)),

$$\mathcal{E}_v = \int \frac{dp}{2\pi} \text{Tr} \left\{ \gamma_5 p \Lambda_-(p) + \frac{\gamma}{4\pi} \int \frac{dk}{(p-k)^2} \Lambda_+(k) \Lambda_-(p) \right\}, \quad (8)$$

with the projectors being  $\Lambda_{\pm}(p) = T(p) \frac{1 \pm \gamma_5}{2} T^+(p)$ .

In the meantime, one should be extremely careful with the divergences which show up in the second term of (8). Indeed, defining the difference between the vacuum energy of a nontrivial vacuum and the free-theory one,

$$\Delta \mathcal{E}_v[\theta] = \mathcal{E}_v[\theta] - \mathcal{E}_v[\theta_{\text{free}}], \quad \theta_{\text{free}}(p) = \frac{\pi}{2} \text{sign}(p), \quad (9)$$

one can use the following trick [4]. If  $\theta(p)$  is the function which provides the minimum of the vacuum energy (9), then the function with the same profile, but stretched with an arbitrary parameter  $A$ ,  $\theta(p) \rightarrow \theta(p/A)$ , should enlarge the energy. A simple analysis demonstrates, that this is, indeed, the case, since  $\Delta \mathcal{E}_v$  has the following behaviour as a function of  $A$ :

$$\Delta \mathcal{E}_v = \frac{1}{2} C_1 A^2 - \gamma C_2 \ln A + \gamma C_3 \quad (10)$$

with  $C_{1,2,3}$  being positive constants. The logarithm in the second term on the r.h.s. of (10) is due to the infrared divergence of the integral in (8), and the constant  $C_3$  contains the logarithm of the cut-off. The function (10) has a minimum for a nonzero  $A$  and, what is more, there is no minimum for  $A = 0$  provided  $\gamma \neq 0$ . The latter fact means that there is no phase of the theory with the angle  $\theta = \frac{\pi}{2} \text{sign}(p)$  found in [2], which leads to zero chiral condensate and unbroken chiral symmetry. Thus the 't Hooft model has the only nontrivial vacuum which provides spontaneous breaking of the chiral symmetry and which is defined by the numerical solution of equation (6) found in [5]. Formula (10) can be written in a more physically transparent form if one notices that the chiral condensate transforms linearly under the above-mentioned transformation ( $\Sigma \equiv \langle \bar{q}q \rangle \rightarrow A\Sigma$ ), so that one can use  $\Sigma$  instead of  $A$ :

$$\Delta \mathcal{E}_v = C'_1 \left[ \frac{1}{2} (\Sigma/\Sigma_0)^2 - \ln |\Sigma/\Sigma_0| \right] + \gamma C'_3 \quad (11)$$

with  $\Sigma_0$  being the real condensate of the model which will be discussed below.

From the original paper [1] it is known that the "physical" degrees of freedom of the model are the quark-antiquark mesons. The operators creating and annihilating mesonic states can be defined via the dressed quark states as [6]

$$m_n = \int \frac{dq}{2\pi\sqrt{N_C}} \left\{ d_i(P-q) b_i(q) \varphi_+^n(q, P) + b_i^+(q) d_i^+(P-q) \varphi_-^n(q, P) \right\}, \quad (12)$$

where the two wave function appeared for each meson. The "+" function describes the motion of the  $q\bar{q}$  pair in meson forward in time, whereas the "-" one describes the backward motion. The orthogonality and completeness conditions for  $\varphi$ 's contain the negative sign between the "+" and the "-" parts, e.g.,

$$\begin{aligned} \int \frac{dp}{2\pi} (\varphi_+^n(p, Q)\varphi_+^m(p, Q) - \varphi_-^n(p, Q)\varphi_-^m(p, Q)) &= \delta_{nm}, \\ \int \frac{dp}{2\pi} (\varphi_+^n(p, Q)\varphi_-^m(p, Q) - \varphi_-^n(p, Q)\varphi_+^m(p, Q)) &= 0. \end{aligned} \quad (13)$$

This sign is a consequence of the second Bogoliubov-like transformation which is to be performed in the theory to find the form (12) of the mesonic operators, so that the two components of the mesonic wave function play the role of the standard Bogoliubov amplitudes  $u$  and  $v$  [6]. The Hamiltonian of the model takes the diagonal form in the new basis,

$$H = LN_C \mathcal{E}'_v + \sum_{n=0}^{+\infty} \int \frac{dP}{2\pi} P_n^0(P) m_n^+(P) m_n(P) + O\left(\frac{1}{\sqrt{N_C}}\right), \quad (14)$$

if the wave functions obey the bound-state equation in the form of a system of two coupled equations [2, 3]:

$$\begin{cases} [K(p, P) - P_0]\varphi_+(p, P) = \gamma \int \frac{dk}{(p-k)^2} [C\varphi_+(k, P) - S\varphi_-(k, P)] \\ [K(p, P) + P_0]\varphi_-(p, P) = \gamma \int \frac{dk}{(p-k)^2} [C\varphi_-(k, P) - S\varphi_+(k, P)], \end{cases} \quad (15)$$

with  $K(p, P) = E(p) + E(P-p)$ ,  $C = \cos \frac{\theta(p)-\theta(k)}{2} \cos \frac{\theta(P-p)-\theta(P-k)}{2}$  and  $S = \sin \frac{\theta(p)-\theta(k)}{2} \sin \frac{\theta(P-p)-\theta(P-k)}{2}$ . Note that the system (15) can be written in the form of a Dirac-type equation in the Hamiltonian form,

$$\hat{\mathcal{H}}\psi = Q_0\psi, \quad \hat{\mathcal{H}} = \begin{pmatrix} K - \hat{C} & \hat{S} \\ -\hat{S} & -K + \hat{C} \end{pmatrix} = \gamma_0(K - \hat{C}) + \gamma_1\hat{S}, \quad (16)$$

where for an arbitrary function  $F(p, P)$  operators  $\hat{S}$  and  $\hat{C}$  act as

$$\hat{C}(\hat{S})F(p, P) \equiv \gamma \int \frac{dk}{(p-k)^2} C(S)(p, k, P) F(k, P). \quad (17)$$

The operator  $\hat{\mathcal{H}}$  is not Hermitian, and the distorted form of the norm (13) is a remnant of this fact. Nevertheless the positiveness of its eigenvalues can be proved explicitly [7].

Using the Hamiltonian approach to the model developed above, one can study its chiral properties, among which we mention

- The chiral pion — the exact massless (in the chiral limit) solution of the bound-state equation (15) [7]:

$$\varphi_\pm^\pi(p, Q) = \sqrt{\frac{\pi}{2Q}} \left( \cos \frac{\theta(Q-p) - \theta(p)}{2} \pm \sin \frac{\theta(Q-p) + \theta(p)}{2} \right). \quad (18)$$

- The pion decay constant, which can be defined for the above-mentioned state ( $|\Omega\rangle$  is the vacuum annihilated by mesonic operators (12)):

$$\langle\Omega|\bar{q}(x)\gamma_\mu\gamma_5 q(x)|\pi(Q)\rangle = f_\pi Q_\mu \frac{e^{-iQx}}{\sqrt{2Q_0}}, \quad f_\pi = \sqrt{\frac{N_C}{\pi}}. \quad (19)$$

- Partial conservation of the axial-vector current, which holds true in the operator form,

$$J_\mu^5(x) = i f_\pi \partial_\mu \Psi_\pi(x), \quad f_n = f_\pi \delta_{n\pi}. \quad (20)$$

- The chiral condensate,

$$\langle\bar{q}q\rangle(m=0) = -N_C \int_{-\infty}^{+\infty} \frac{dp}{2\pi} \cos\theta(p) = -0.29 N_C \sqrt{2\gamma}. \quad (21)$$

- The Gell-Mann-Oakes-Renner relation,

$$f_\pi^2 M_\pi^2 = -2m\langle\bar{q}q\rangle, \quad (22)$$

which can be checked explicitly.

Now we turn to the properties of currents in the 't Hooft model. The conservation laws can be derived for both, vector and axial-vector, currents in the chiral limit, which read:

$$V_\mu^M(P) = \langle\Omega|\bar{q}\gamma_\mu q|M, P\rangle, \quad P_0^M V_0^M - PV^M = 0, \quad (23)$$

$$A_\mu^M(P) = \langle\Omega|\bar{q}\gamma_\mu\gamma_5 q|M, P\rangle, \quad P_0^M A_0^M - PA^M = 0. \quad (24)$$

For the current-quark-antiquark vertices one has the vector and the axial-vector Ward identities [3, 7, 8]

$$-iP_\mu v_\mu(p, P) = S^{-1}(p) - S^{-1}(p - P), \quad (25)$$

$$-iP_\mu a_\mu(p, P) = S^{-1}(p)\gamma_5 + \gamma_5 S^{-1}(p - P), \quad (26)$$

and, as a result, the following conservation laws:

$$(P_\mu - P'_\mu)\langle M, P|v_\mu|M', P'\rangle = 0, \quad (27)$$

$$(P_\mu - P'_\mu)\langle M, P|a_\mu|M', P'\rangle = 0. \quad (28)$$

In derivation of the latter formulae the matrix approach to the model was used [7,8], in which an effective diagrammatic technique is defined containing the matrix form of the wave function obeying the matrix bound-state equation, the dressed quark propagator  $S(p)$ , the dressed meson-quark-antiquark vertex  $\Gamma$  ( $\bar{\Gamma}$  for outgoing meson), the dressed quark-quark scattering amplitude, and, finally, the effective coupling constant  $-i\gamma/\sqrt{N_C}$ , which is to be prescribed to each meson-quark-antiquark vertex. For example, for the pion one can find the following vertex function:

$$\Gamma_\pi(p, P) = S^{-1}(p)(1 + \gamma_5) - (1 - \gamma_5)S^{-1}(p - P), \quad (29)$$

which can be easily identified with the divergences of the vector and axial-vector currents (25) and (26):

$$\Gamma_\pi(p, P) = -iP_\mu v_\mu(p, P) - iP_\mu a_\mu(p, P). \quad (30)$$

It is not surprise that the pion couples to both, the vector and the axial-vector currents, since in two dimensions the two currents are dual to one another. The interested reader can find details of the approach in the review paper [3].

As a next application of the Hamiltonian and the matrix approaches discussed above, let us study hadronic decays in this theory. If meson  $A$  decays into mesons  $B$  and  $C$ , then the amplitude of such a process can be found in two ways: in the Hamiltonian technique,

$$M(A \rightarrow B + C) = \langle B(P_B)C(P_C) | \Delta H | A(P_A) \rangle, \quad (31)$$

or using the matrix approach, directly from the corresponding decay diagrams:

$$M(A \rightarrow B + C) = -\frac{i\gamma^3}{\sqrt{N_C}} \int \frac{d^2 k}{(2\pi)^2} Sp[\Gamma_A(k + P_B, P_A) S(k - P_C) \times \bar{\Gamma}_C(k, P_C) S(k) \bar{\Gamma}_B(k + P_B, P_B) S(k + P_B)] + (B \leftrightarrow C). \quad (32)$$

Both equations, (31) and (32), lead to one and the same 6-term form of the amplitude (see [3, 7] for details), which possesses contributions of both components of the wave function for each meson. If one of the final states is the pion and the chiral limit is used, then the explicit form of the vertex (29) can be substituted into (32) that immediately leads to the result that the amplitude vanishes,

$$M(A \rightarrow \pi + C) \equiv 0, \quad (33)$$

which also follows from the identification (30) and the vector and axial-vector conservation laws.

The result (33) could be anticipated, since the pion decay constant is dimensionless in the 't Hooft model. As a result, the Adler selfconsistency condition for the amplitudes with pions involved [9] has to hold true for any pion momentum.

In conclusion let us say, that the two-dimensional 't Hooft model possesses many features which are known to be inherent to QCD<sub>4</sub> and it can be used as a test laboratory to see how all these beautiful properties may appear.

## Acknowledgments

Financial support of RFFI grants 00-02-17836 and 00-15-96786, INTAS-RFFI grant IR-97-232 and INTAS CALL 2000-110 is gratefully acknowledged. One of the authors (A.N.) is also supported via RFFI grant 01-02-06273.

## References

- [1] G.'t Hooft, *Nucl.Phys.* **B** 75, 461 (1974)
- [2] I.Bars and M.B.Green, *Phys.Rev.* **D** 17, 537 (1978)

- [3] Yu.S.Kalashnikova and A.V.Nefediev, review paper, in press
- [4] P.Bicudo, A.V.Nefediev and E.Ribeiro, in preparation.
- [5] Ming Li, *Phys.Rev.* **D** 34, 3888 (1986); Ming Li, L.Wilets and M.C.Birse, *J.Phys.* **G** 13, 915 (1987)
- [6] Yu.S.Kalashnikova, A.V.Nefediev and A.V.Volodin, *Phys.Atom.Nucl.* **63**, 1623 (2000); A.V.Nefediev, in *Proceedings of the XVII International School of Physics "QCD: Perturbative or Nonperturbative,"*, ed. by L.S.Ferreira, P.Nogueira and J.I.Silva-Marcos, World Scientific 2000
- [7] Yu.S.Kalashnikova, A.V.Nefediev, *Phys.Lett.* **B** 487, 371 (2000)
- [8] M.B.Einhorn, *Phys.Rev.* **D** 14, 3451 (1976)
- [9] S.L.Adler, *Phys. Rev.* **139B**, 1638 (1965)

# MAGNETIC MOMENTS OF CHARM BARYONS IN CHIRAL PERTURBATION THEORY

V.S.Zamiralov <sup>a</sup>

*D. V. Skobeltsyn Institute of Nuclear Physics, Moscow State University, 119899  
Moscow, Russia*

*Abstract.* Magnetic moments of the 1/2 charm baryons are reevaluated in framework of Heavy Hadron Chiral Perturbation Theory (HHCPT). NRQM and broken  $SU(4)$  unitary symmetry model are used at the tree level. Calculations of one-loop contributions to magnetic moments are performed in terms of the  $SU(4)$  couplings of charm baryons to Goldstone bosons. The relation between HHChPT results and those of NRQM and unitary symmetry model is discussed. One-loop corrections are shown to have the same structure as the tree-level formulae for the magnetic moments of the charm baryons in the  $SU(4)$  model.

## 1 Introduction

Magnetic moments of charm baryons were described first in the quark model with four flavors [1] and  $SU(4)_f$  unitary symmetry model [2]. Later when a specific role of heavy quark inside heavy hadron were realized [3–5] in an approach based on the heavy quark effective theory and chiral perturbation theory leading long-distance contribution to magnetic moments of the charm antitriplet were computed in [6]. Recently in a similar approach magnetic moments of heavy baryons were analyzed [7]. One-loop corrections (OLC) were calculated and relations are obtained between magnetic moments of sextet charm and beauty baryons [7]. In order to make a more direct comparison of magnetic moments of charm baryons with those of the octet baryons I reevaluate here magnetic moments of the charm baryons following approach of [8–10] and taking into account OLC within the HHCPT in terms of  $SU(4)$  coupling constants for charm baryons and Goldstone bosons.

## 2 Elements of the HHCPT Formalism

In a framework of Heavy Hadron Chiral Perturbation Theory (HHCPT) chiral expansion of the heavy (charm in our case) baryon Lagrangian is written in terms of the velocity-dependent fields  $B_v(x)$  constructed in order to remove free momentum dependence in Dirac equation,

$$B_v(x) = \exp(iM_B \vec{v} \cdot \vec{x}) B(x).$$

Here  $B(x)$  is a charm baryon 1/2 field with central mass  $M_B$ . The 20<sub>4</sub>-plet  $B_v(x)$  is given by 3rd-rank tensor ( $B_{\beta\gamma}^{\alpha} = -B_{\gamma\beta}^{\alpha}$ ,  $B_{\alpha\beta}^{\alpha} = 0$ ). The ordinary octet  $8_3$  with  $C = 0$  is given by terms  $B_{b4}^a$ ,  $a, b = 1, 2, 3$ . Charm baryons of the sextet  $6_3$  and antitriplet  $3_3^*$  with  $C = 1$  are given by tensors  $B_{bc}^a$  and  $B_{b4}^4$ ,  $a, b, c = 1, 2, 3$ , In NRQM the 6<sub>3</sub>-plet charm baryons are all  $\Sigma(qq', c)$ -like with two light quarks in a symmetrical state and the charm quark apart. Instead 3<sub>3</sub><sup>\*</sup>-plet charm baryons are all

The 3/2 6<sub>3</sub>-plet charm baryons  $T_{\mu}^{ab4}$ ,  $a, b = 1, 2, 3$ , are part of the  $SU(4)_f$  20<sub>4</sub>-plet and in NRQM have all quarks in a symmetric state:

---

<sup>a</sup>e-mail: zamir@depni.npi.msu.su

Goldstone bosons appearing are identified with the pseudoscalar octet which couples to the baryon fields via the vector and axial vector currents

$$V^\mu = \frac{1}{2}(\xi \partial^\mu \xi^\dagger + \xi^\dagger \partial^\mu \xi), \quad A^\mu = \frac{i}{2}(\xi \partial^\mu \xi^\dagger - \xi^\dagger \partial^\mu \xi),$$

where  $\xi = \exp(iP/f)$  and  $\xi \rightarrow L\xi R^\dagger$ , with  $L, R \in SU(3)_{L,R}$  and  $f = f_\pi \approx 93\text{ MeV}$  being the pseudoscalar decay constant in the chiral limit.

The lowest order Lagrangian (in notations of [8–10]) reads

$$L = L^{1/2} + L^{3/2 \rightarrow 1/2} + L^{3/2} + \frac{f_\pi^2}{4} \text{Tr}(\partial^\mu \Sigma^\dagger \partial_\mu \Sigma)$$

with  $\Sigma = \exp(2iP/f) \equiv \xi^2$  and  $L^{1/2}, L^{3/2 \rightarrow 1/2}, L^{3/2}$  written below. I write formally vector and axial-vector baryon currents and their couplings to the Goldstone bosons in terms of the  $SU(4)$  unitary symmetry model:

$$\begin{aligned} L^{1/2} &= i\text{Tr}(\bar{B}_v v \cdot \mathcal{D} B_v) + 2(-F + D)(\bar{B}_v^{\alpha\beta} S_v^\mu A_\mu^\rho B_v^\gamma{}_{\rho\beta} \\ &\quad 2(F + D)(\bar{B}_v^{\alpha\beta} S_v^\mu B_v^\gamma{}_{\alpha\beta}) A_\mu^\rho{}_\gamma, \quad \mathcal{D}_\mu B_v = \partial_\mu B_v + [V_\mu, B_v], \end{aligned} \quad (1)$$

$$L^{3/2 \rightarrow 1/2} = \mathcal{C}(\epsilon_{\beta\gamma\rho\sigma} \bar{B}_v^\beta{}_\alpha T_v^\mu{}^{\alpha\rho\tau} A_\mu^\delta{}_\beta + \epsilon^{\beta\gamma\rho\delta} A_\delta^\mu{}^\beta), \quad (2)$$

$$\begin{aligned} L^{3/2} &= \bar{T}_v^\mu{}_{\alpha\rho\eta} v \cdot \mathcal{D} T_v^{\alpha\rho\delta} + 2\mathcal{H}\bar{T}_v^\mu{}_{\alpha\rho\eta} S_v{}_\nu A_\beta^\nu{}^\delta T_v^{\alpha\rho\beta}, \\ \mathcal{D}^\nu T_v^{\alpha\rho\delta} &= \partial^\nu T_v^{\alpha\rho\delta} + (V^\nu)_\beta^\alpha T_v^{\beta\rho\delta} + (V^\nu)_\beta^\rho T_v^{\alpha\beta\delta} + (V^\nu)_\beta^\delta T_v^{\alpha\rho\beta}. \end{aligned} \quad (3)$$

and then take the part involving interaction of the charm baryons with the light Goldstone bosons  $P_b^a$ ,  $a, b = 1, 2, 3$ . Extracting from Eqs.(1,2,3)  $SU(3)$  octet and decuplet baryons, one arrives at the effective Lagrangians used in [9] for the OLC with the same constants  $F, D, \mathcal{C}, \mathcal{H}$ .

### 3 Tree-level magnetic moments

#### 3.1 Nonrelativistic Quark Model

In the 4-flavor NRQM all the moments can be expressed in terms of the 4 quark magnetons  $\mu_{u,d,s}$  and  $\mu_c$ . The 6-plet charm baryon magnetic moments are [1]:

$$\mu_{\Sigma(qq',c)} = \frac{2}{3}\mu_q + \frac{2}{3}\mu_{q'} - \frac{1}{3}\mu_c, \quad q, q' = u, d, s. \quad (4)$$

In the HHPCT a natural scale of the leading order contributions to the magnetic moments would be  $\mathcal{O}(1/\Lambda_\chi)$  for  $\mu_{u,d,s}$  and  $\mathcal{O}(1/m_c)$  for  $\mu_c$  [7, 10]. The following relations are valid:

$$\begin{aligned} \mu_{\Sigma_c^{++}} + \mu_{\Sigma_c^0} &= 2\mu_{\Sigma_c^+}, \quad \mu_{\Sigma_c^{++}} + \mu_{\Omega_c^0} = 2\mu_{\Xi_c'{}^+}, \\ \mu_{\Sigma_c^+} + 2\mu_{\Xi_c'{}^0} &= \mu_{\Sigma_c^0} + 2\mu_{\Xi_c'{}^+}. \end{aligned} \quad (5)$$

The  $3^*$ -plet charm baryon magnetic moments are all equal [1]:

$$\mu_{\Lambda_c^+} = \mu_{\Xi_c^+} = \mu_{\Xi_c^0} = \mu_c. \quad (6)$$

### 3.2 Unitary Symmetry Model

Magnetic moments of the charm baryons at the tree level can be evaluated in the framework of the  $SU(4)_f$  model [2]. Electromagnetic baryon current is constructed to have symmetry breaking terms due to strangeness and charm:

$$\begin{aligned} J_\mu^{el-mag} = & (g_1 \bar{B}_\gamma^{1\beta} \gamma_\mu B_{1\beta}^\gamma + g'_1 \bar{B}_\gamma^{4\beta} \gamma_\mu B_{4\beta}^\gamma + h_1 \bar{B}_\gamma^{3\beta} \gamma_\mu B_{3\beta}^\gamma) + \\ & \frac{1}{2} (g_2 \bar{B}_1^{\alpha\beta} \gamma_\mu B_{\alpha\beta}^1 + g'_2 \bar{B}_4^{\alpha\beta} \gamma_\mu B_{\alpha\beta}^4 + h_2 \bar{B}_3^{\alpha\beta} \gamma_\mu B_{\alpha\beta}^3) - \\ & \frac{1}{3} (g_1 + g_2 + g'_1 - 2g_0 - 3h_1) Sp(\bar{B} \gamma_\mu B) \end{aligned} \quad (7)$$

With  $g_1 = g'_1 = -\frac{1}{2}\mu_x$ ,  $g_2 = g'_2 = -\frac{1}{2}\mu_y$ ,  $h_1 = h_2 = 0$   $SU(4)_f$ -symmetric electromagnetic current given in [2].

The 6-plet magnetic moments are given by Eq.(7) as:

$$\mu_{\Sigma(qq',c)} = e_q \mu_F + e_{q'} \mu'_F + e_c (\mu_F^c - \mu_D^c).$$

with  $g_{1,2} = \mp \mu_F + \mu_D$ ,  $h_{1,2} = \mp \mu_F^s + \mu_D^s$ ,  $g_0 = -g'_1$  and  $3g'_{1,2} = (\mp \mu_F + \mu_D) + 2(\mp \mu_F^c + \mu_D^c)$ .

The magnetic moments  $\Lambda$ -like hyperons are given by

$$\mu_{\Lambda(qq'c)} = e_q (\mu_F - \frac{2}{3} \mu_D) + e_{q'} (\mu'_F - \frac{2}{3} \mu'_D) + e_c (\mu_F^c + \frac{1}{3} \mu_D^c). \quad (8)$$

Results of the broken  $SU(4)$  symmetry for the charm sextet can be matched to those of the quark model by relations

$$\begin{aligned} \mu_F = & \frac{2}{3} (\mu_u - \mu_d), \quad \mu_F^s = \frac{2}{3} (\mu_u + 2\mu_d - 3\mu_s), \\ 2(\mu_F^c - \mu_D^c) = & \frac{4}{3} \mu_u + \frac{8}{3} \mu_s - \mu_c. \end{aligned} \quad (9)$$

## 4 One-Loop Corrections in HHCPT

An expression for the charm baryon magnetic moments in the HHCPT and the non-analytic corrections arising from the one-loop diagrams, involving  $\pi$  and  $K$  loops with charm baryon insertions. OLC were evaluated in [6, 7] through effective Lagrangians involving directly sextet 1/2, 3/2 and 3\* 1/2 charm baryon fields. But in order to relate it to the case of the octet baryons I treat 1/2 and 3/2 spinors separately [8–10].

I write magnetic moments of the charm baryons in the form similar to those of the octet [8–10]

$$\mu_B = \mu_B^0 + \frac{\pi}{\Lambda_\chi^2} \sum_{X=\pi,K} (\beta_B^X + \tilde{\beta}_B^X) m_X \equiv \mu_B^0 + U(B), \quad (10)$$

where  $\mu_B^0$  are tree-level magnetic moments of the order  $\mathcal{O}(1/\Lambda_\chi)$  and/or  $\mathcal{O}(1/m_c)$ , earlier.

The  $\beta_B^{\pi,K}$ 's and  $\tilde{\beta}_B^{\pi,K}$ 's are the contributions from the pion and kaon loops from Fig.1 with respectively [8].

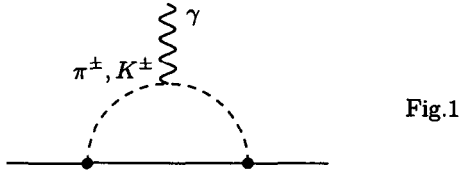


Fig.1

The detailed evaluation of all coefficients is given similar to reevaluation of the Ha results [9] for the octet baryons in [14]. All masses of the charm 1/2 and 3/2 baryons are taken to be degenerated.

#### 4.1 The 6-plet Charm Baryon Magnetic Moments

I describe in a few words calculation of the contribution into  $\Sigma_c^{++}$  magnetic moment. There are 6 diagrams, four of them with the 1/2 and 3/2 6-plet baryons in the loops ( $\pi$ -loops with  $\Sigma_c^+$  and  $\Sigma_c^{*+}$  insertions and  $K^+$ -loop with  $\Xi_c^{*+}$  and  $\Xi_c^{*0}$  insertions) and two last diagrams with the 1/2 3\*-plet baryons in the loop ( $\pi$ -loop with  $\Lambda_c^+$  insertion and  $K^+$ -loop with  $\Xi_c^+$  insertion). The coupling constants of the Goldstone bosons to the charm baryons in these diagrams are given by the Lagrangians (1) and (2)

The corresponding contribution upon taking account of the factors arriving from integration (see [8–10]) is written as<sup>b</sup>:

$$\begin{aligned} U(\Sigma_c^{++}) &= \frac{\pi}{\Lambda_x^2} [-2F^2 - \frac{2}{3}D^2 + \frac{2}{36}\mathcal{C}^2](m_\pi + m_K) \\ &\equiv 2\kappa \cdot (m_\pi + m_K) \Rightarrow -\frac{4}{3}\frac{\pi}{\Lambda_x^2}(m_\pi + m_K)D^2 \end{aligned}$$

In a similar way OLC's to other sextet 1/2 magnetic moments can be evaluated to yield:

$$\begin{aligned} \mu_{\Sigma_c^{++}} &= \mu_{\Sigma_c^{++}}^0 + 2\kappa(m_\pi + m_K), \quad \mu_{\Sigma_c^+} = \mu_{\Sigma_c^+}^0 + \kappa m_K, \\ \mu_{\Sigma_c^0} &= \mu_{\Sigma_c^0}^0 - 2\kappa m_\pi, \quad \mu_{\Omega_c^0} = \mu_{\Omega_c^0}^0 - 2\kappa m_K, \\ \mu_{\Xi_c^{*+}} &= \mu_{\Xi_c^{*+}}^0 + \kappa m_\pi, \quad \mu_{\Xi_c^{*0}} = \mu_{\Xi_c^{*0}}^0 - \kappa(m_\pi + m_K). \end{aligned}$$

OLC considered in [7] and in this work do not change the relations (6).

#### 4.2 The 3\*-plet Charm Baryon Magnetic Moments

I briefly describe diagrams for calculation of the OLC to  $\Lambda_c^+$  magnetic moment. There are 7 diagrams, four of them with the 1/2 and 3/2 6-plet baryons in the  $\pi^{-,+}$ -loop, (with  $\Sigma_c^{++,0}$ ,  $\Sigma_c^{*++,0}$  insertions), two more with the 1/2 and 3/2 6-plet in the  $K^+$ -loop (with  $\Xi_c^{*0}$  and  $\Xi_c^{*0}$  insertions) and the last one in the  $K^+$ -loop. Upon using Eqs.(1) and (2):

$$U(\Lambda_c^+) = \frac{\pi}{\Lambda_x^2} [-\frac{1}{3}D^2 - (F - \frac{2}{3}D)^2 + \frac{1}{12}\mathcal{C}^2]m_K \Rightarrow 0.$$

---

<sup>b</sup>⇒ means the QM limit  $F = 2/3D$ ,  $\mathcal{C} = -2D$ ,  $\mathcal{H} = -3D$ .

There is a non-zero contribution of the diagram with the  $\Xi_c^0$ -insertion proportional to the factor  $(F - \frac{2}{3}D)^2$  which disappears in the quark model limit with  $F = \frac{2}{3}D$ . The remaining part of the OLC also disappears in this limit, but only because degenerated masses of the  $3^* 1/2$  and sextet baryons are taken here. These diagrams gives a non-zero contribution with nondegenerate masses [6, 7]. OLC's yield the following expressions for the magnetic moments of antitriplet  $1/2$ :

$$\begin{aligned}\mu_{\Lambda_c^+} &= \mu_{\Lambda_c^+}^0 + \alpha m_K, \\ \mu_{\Xi_c^+} &= \mu_{\Xi_c^+}^0 + \alpha m_\pi, \quad \mu_{\Xi_c^0} = \mu_{\Xi_c^0}^0 - \alpha(m_\pi + m_K).\end{aligned}\quad (11)$$

## 5 Results and discussion

The tree-level formulae for the magnetic moments of the sextet charm baryons in the quark model (see Eq.(4)) remain essentially the same with the account of the OLC's considered if one renormalizes effectively the light quark magnetic moments:

$$\mu_q \rightarrow \mu_q - (3/2)\kappa \cdot m^{(q)},$$

$m^{(u)} = (m_\pi + m_K)$ ,  $m^{(d)} = m_\pi$ ,  $m^{(s)} = m_K$ . Analogous conclusion is valid for results obtained in [7]. One can proceed in a similar way in the unitary symmetry model, renormalizing  $\mu_{D,F}$ 's upon using Eq.(9).

The OLC's to the  $3^*$ -plet disappear in the quark model limit ( $F = \frac{2}{3}D$ ,  $C = -2D$ ). Instead in the unitary symmetry model the OLC's can be hidden into the constants  $\mu_{D,F}$ ,  $\mu_{D,F}^{s,c}$  of the Eq.(8) by an obvious renormalization procedure.

Thus for the magnetic moments of the sextet  $1/2$  baryons with the OLC's the old-fasion NRQM picture unitary symmetry model effectively emerges. The one-to-one correspondence between HHChPT results proved here is a rather unexpected result and is not valid for octet and decuplet baryons [8–10].

As for the magnetic moments of the  $3^* 1/2$  charm baryons an eventual deviation from the quark model prediction [1] could be connected either with the or with the high-order corrections, as those considered in [6] or [7].

A more general picture which embraces octet and eventually decuplet baryon magnetic moments would one-loop within the chiral perturbation theory.

## Acknowledgments

I am grateful to J.Bernabeu, V.M.Dubovik, F.Hussain and G.Thompson for discussions.

I would like to thank Professor S.Randjbar-Daemi and the High Energy Section of the Abdus Salam ICTP (Trieste, Italy) where the main part of this work was done for the hospitality extended to me.

The financial support of the Abdus Salam International Centre for Theoretical Physics (Trieste, Italy) is gratefully acknowledged.

## References

- [1] R.J. Johnson and M. Shah-Jahan, *Phys.Rev.D* **16**, 1400 (1977).

- [2] A.I.Choudhury, V.Joshi,*Phys.Rev.D***13**, 3115 (1976); *ibid.*,3120.
- [3] N.Isgur and M.B.Wise,*Phys.Lett.B***232**,113 (1989);*Nucl.Phys.B***348**, 276 (1991).
- [4] H.Georgi,*Phys.Lett.B***240**, 447 (1990);*Nucl.Phys.B***348**,293(1991).
- [5] F.Hussain, J.G.Körner, G.Thompson, *Ann.Phys.***206**, 334 (1991).
- [6] M.J.Savage,*Phys.Lett.***326**,303 1994).
- [7] M.C.Banuls, I.Scimemi,J.Bernabeu, V.Gimenez, and A.Pich, *Phys.Rev.D***61**,074007 (2000).
- [8] E.Jenkins, M.Luke, A.Manohar and M.J.Savage, *Phys.Lett.B***302**, 482 (1993); *ibid.*, **B388**, 866 (1996)(E).
- [9] P.Ha and L.Durand,*Phys.Rev.D***58**,093008 (1998); L.Durand and P.Ha,*ibid.*, 013010(1998); P.Ha,*ibid.*, 113003 (1998).
- [10] S.J.Puglia and M.J.Ramsey-Musolf,*Phys.Rev.D***62**, 034010 (2000).
- [11] E.Jenkins and A.Manohar, *Phys.Lett.B***255**, 558(1991).
- [12] S.Coleman, S.L.Glashow,*Phys.Rev.Lett.***6**, 423 (1961).
- [13] E.N.Bukina, V.M.Dubovik, V.S.Zamiralov, *Vestnik.Mosk.Universiteta*.**2**,3(2000); E.N.Bukina,*J.Mod.Phys.A*,**14**,2525(1999).
- [14] V.S.Zamiralov, NPI MSU Preprint 2001-8/648,Nuclear Physics Institute, Moscow State University, 119899 Moscow, Russia.

# INSTANTON IN THE NONPERTURBATIVE QCD VACUUM

N.O. Agasian <sup>a</sup>, S.M. Fedorov <sup>b</sup>

*Institute of Theoretical and Experimental Physics,  
117218, Moscow, B.Cheremushkinskaya 25, Russia*

*Abstract.* The influence of nonperturbative fields on instantons in quantum chromodynamics is studied. Effective action for instanton is derived in bilocal approximation and it is demonstrated that stochastic background gluon fields are responsible for IR stabilization of instantons. It is shown that instanton size in QCD is of order of 0.25 fm. Comparison of obtained instanton size distribution with lattice data is made.

1. Instantons were introduced in 1975 by Polyakov and coauthors [1]. These topologically nontrivial field configurations are essential for the solution of some problems of quantum chromodynamics. Instantons allow to explain anomalous breaking of  $U(1)_A$  symmetry and the  $\eta'$  mass [2, 3], spontaneous chiral symmetry breaking (SCSB) [4]. Taking into account instantons is of crucial importance for many phenomena of QCD (see [5] and references therein).

At the same time, there is a number of serious problems in instanton physics. The first is IR inflation of instanton, i.e. divergence of integrals over instanton size  $\rho$  at big  $\rho$ . Second, quasiclassical instanton anti-instanton vacuum lacks confinement.

The most popular model of instantons is the model of "instanton liquid", which was phenomenologically formulated by Shuryak [6]. It states that average distance between pseudoparticles is  $\bar{R} \sim 1$  fm and their average size is  $\bar{\rho} \sim 1/3$  fm. Thus,  $\bar{\rho}/\bar{R} \simeq 1/3$  and vacuum consists of well separated, and therefore not very much deformed, instantons and anti-instantons. However, the mechanism for the suppression of large-size instantons in the ensemble of topologically non-trivial fields is still not understood.

On the other hand, QCD vacuum contains not only quasiclassical instantons, but other nonperturbative fields as well. In this talk we will demonstrate that instanton can be stabilized in nonperturbative vacuum and exist as a stable topologically non-trivial field configuration against the background of stochastic nonperturbative fields, which are responsible for confinement, and will find quantitatively its size. In this way, we will follow the analysis performed in [7].

2. Standard euclidian action of gluodynamics has the form

$$S[A] = \frac{1}{2g_0^2} \int d^4x \text{tr}(F_{\mu\nu}^2[A]) = \frac{1}{4} \int d^4x F_{\mu\nu}^a[A] F_{\mu\nu}^a[A], \quad (1)$$

where  $F_{\mu\nu}[A] = \partial_\mu A_\nu - \partial_\nu A_\mu - i[A_\mu, A_\nu]$  is the strength of gluon field and we use the Hermitian matrix form for gauge fields  $A_\mu(x) = g_0 A_\mu^a(x)t^a/2$  and  $\text{tr } t^a t^b = \delta^{ab}/2$ . We decompose  $A_\mu$  as  $A_\mu = A_\mu^{\text{inst}} + B_\mu + a_\mu$ , where  $A_\mu^{\text{inst}}$  is an instanton-like field configuration with a unit topological charge  $Q_T[A^{\text{inst}}] = 1$ ;  $a_\mu$  is quantum field and  $B_\mu$  is nonperturbative background field (with zero topological charge), which can be parametrized by gauge invariant nonlocal vacuum averages of gluon field strength<sup>c</sup>.

---

<sup>a</sup>e-mail: agasian@heron.itep.ru

<sup>b</sup>e-mail: fedorov@heron.itep.ru

<sup>c</sup>In operator product expansion method and in QCD sum rules nonperturbative field is characterized by a set of local gluon condensates  $\langle G^2 \rangle, \langle G^3 \rangle, \dots$

In general case effective action for instanton in NP vacuum takes the form

$$Z = e^{-S_{\text{eff}}[A^{\text{inst}}]} = \int [D a_\mu] \langle e^{-S[A^{\text{inst}} + B + a]} \rangle, \quad (2)$$

where  $\langle \dots \rangle$  implies averaging over background field  $B_\mu$ .

Integration over  $a_\mu$  and  $B_\mu$  corresponds to averaging over fields that are responsible for the physics at different scales. Integration over  $a_\mu$  takes into account perturbative gluons and describes phenomena at small distances, while averaging over  $B_\mu$  (formally interaction with gluon condensate) accounts for phenomena at scales of confinement radius. Therefore averaging factorizes  $Z = \langle Z_1 \rangle \langle Z_2 \rangle$  (see [7] for details) and effective action appears to be sum of two terms, "perturbative" and "nonperturbative". Perturbative fluctuations were considered in [8, 9], and it was shown that in NP vacuum standard perturbation theory for instantons changes, which results in "freezing" of effective coupling constant. The perturbative part of effective instanton action in stochastic vacuum  $S_{\text{eff}}^P[A^{\text{inst}}]$  was shown to be

$$S_{\text{eff}}^P(\rho) = \frac{b}{2} \ln \frac{1/\rho^2 + m_*^2}{\Lambda^2} \quad (3)$$

Here  $m_* \simeq 0.75m_{0++} \sim 1\text{GeV}$ , where  $0^{++}$  is the lightest glueball.

Thus, we have for effective instanton action

$$S_{\text{eff}}[A^{\text{inst}}] = S_{\text{eff}}^P[A^{\text{inst}}] + S_{\text{eff}}^{\text{NP}}[A^{\text{inst}}] \quad (4)$$

$$S_{\text{eff}}^{\text{NP}}[A^{\text{inst}}] = -\ln \langle Z_2(B) \rangle = -\ln \langle \exp\{-S[A^{\text{inst}} + B] + S[A^{\text{inst}}]\} \rangle \quad (5)$$

**3.** We consider effect of NP fields on instanton, i.e. we evaluate  $\langle Z_2 \rangle$ . In this work we make use of the method of vacuum correlators, introduced in works of Dosch and Simonov [10]. NP vacuum of QCD is described in terms of gauge invariant vacuum averages of gluon fields (correlators)

$$\Delta_{\mu_1 \nu_1 \dots \mu_n \nu_n} = \langle \text{tr } G_{\mu_1 \nu_1}(x_1) \Phi(x_1, x_2) G_{\mu_2 \nu_2}(x_2) \dots G_{\mu_n \nu_n}(x_n) \Phi(x_n, x_1) \rangle,$$

where  $G_{\mu\nu}$  is gluon field strength, and  $\Phi(x, y) = \text{Pexp} \left( i \int_y^x B_\mu dz_\mu \right)$  is a parallel transporter, which ensures gauge invariance. In many cases bilocal approximation appears to be sufficient for qualitative and quantitative description of various physical phenomena in QCD. Moreover, there are indications that corrections due to higher correlators are small [11].

Tensor structure of bilocal correlator follows from antisymmetry in Lorentz indices. It is parametrized by two functions  $D(x - y)$  and  $\overline{D}(x - y)$ :

$$\begin{aligned} \langle g^2 G_{\mu\nu}^a(x, x_0) G_{\rho\sigma}^b(y, x_0) \rangle &= \langle G^2 \rangle \frac{\delta^{ab}}{N_c^2 - 1} \times \\ &\times \left\{ \frac{D(z)}{12} \delta_{\mu\rho} \delta_{\nu\sigma} + \frac{\overline{D}(z)}{6} (n_\mu n_\rho \delta_{\nu\sigma} + n_\nu n_\sigma \delta_{\mu\rho}) - (\mu \leftrightarrow \nu) \right\}, \end{aligned} \quad (6)$$

where  $G_{\mu\nu}(x, x_0) = \Phi(x_0, x)G_{\mu\nu}(x)\Phi(x, x_0)$ ,  $n_\mu = z_\mu/|z| = (x - y)_\mu/|x - y|$  is the unit vector,  $\langle G^2 \rangle \equiv \langle g^2 G_{\mu\nu}^a G_{\mu\nu}^a \rangle$  and, as it follows from normalization,  $D(0) + \bar{D}(0) = 1$ .

Bilocal correlator was measured on the lattice (see [12] and references therein), and functions  $D(z)$  and  $\bar{D}(z)$  were found to be exponentially decreasing  $D(z) = A_0 \exp(-z/T_g)$ ,  $\bar{D}(z) = A_1 z \exp(-z/T_g)/T_g$ , where  $T_g$  is the gluonic correlation length. Besides, according to lattice measurements  $A_1 \ll A_0$  ( $A_1 \sim A_0/10$ ). Lattice data are presented in Table 1.  $SU(3)$  full stands for chromodynamics with 4 quarks, while  $SU(2)$  and  $SU(3)$  quenched mean pure  $SU(2)$  and  $SU(3)$  gluodynamics, respectively.

Table 1: Lattice data [12] for bilocal correlator

	$\langle G^2 \rangle$ , GeV <sup>4</sup>	$T_g$ , fm
$SU(2)$ quenched	13	0.16
$SU(3)$ quenched	5.92	0.22
$SU(3)$ full	0.87	0.34

To evaluate  $S_{\text{eff}}^{\text{NP}}$  we use the cluster expansion:

$$\langle \exp(x) \rangle = \exp \left( \langle x \rangle + \frac{\langle x^2 \rangle - \langle x \rangle^2}{2!} + \dots \right) \quad (7)$$

In bilocal approximation we find  $S_{\text{eff}}^{\text{NP}} = S_{\text{dia}} + \frac{1}{2}S_{\text{dia}}^2 + S_{\text{para}} + S_1 + S_2$ , where

$$S_{\text{dia}} = -\frac{1}{2g^2} \int d^4x \langle \text{tr} \left[ ([A_\mu, B_\nu] - [A_\nu, B_\mu])^2 \right] \rangle \quad (8)$$

$$S_{\text{para}} = -\frac{1}{2g^4} \int d^4x d^4y \langle \text{tr} (F_{\mu\nu}(x)G_{\mu\nu}(x)) \text{tr} (F_{\rho\sigma}(y)G_{\rho\sigma}(y)) \rangle \quad (9)$$

$$S_1 = \frac{2}{g^4} \int d^4x d^4y \left\langle \text{tr} (F_{\mu\nu}[A_\mu, B_\nu])_x \text{tr} (F_{\rho\sigma}[A_\rho, B_\sigma])_y \right\rangle \quad (10)$$

$$S_2 = \frac{2i}{g^4} \int d^4x d^4y \left\langle \text{tr} (F_{\mu\nu}G_{\mu\nu})_x \text{tr} (F_{\rho\sigma}[A_\rho, B_\sigma])_y \right\rangle \quad (11)$$

We use notations  $S_{\text{dia}}$  (diamagnetic) and  $S_{\text{para}}$  (paramagnetic) for contributions (8) and (9) into interaction of instanton with background field. Next,  $S_{\text{eff}}^{\text{NP}}$  can be expressed through bilocal correlator (see [7] for details), for instance

$$S_{\text{dia}} = \frac{\langle G^2 \rangle}{12} \frac{N_c}{N_c^2 - 1} \int d^4x \int_0^1 \alpha d\alpha \int_0^1 \beta d\beta x^2 (A_\mu^a(x))^2 \times \quad (12)$$

$$\times [D((\alpha - \beta)x) + 2\bar{D}((\alpha - \beta)x)] \quad (13)$$

#### 4. We use standard form for instanton field configuration

$$A_\mu^{\text{inst}} = 2t^b R^{b\rho} \bar{\eta}_{\mu\nu}^\beta \frac{(x - x_0)_\nu}{(x - x_0)^2} f \left( \frac{(x - x_0)^2}{\rho^2} \right), \quad (14)$$

where matrix  $R^{b\beta}$  ensures embedding of instanton into  $SU(N_c)$  group,  $b = 1, 2, \dots, N_c^2 - 1$ ;  $\beta = 1, 2, 3$ ,  $\bar{\eta}_{\mu\nu}^\alpha$  are 't Hooft symbols. In singular gauge profile function  $f(z)$  satisfies boundary conditions  $f(0) = 1$ ,  $f(\infty) = 0$  and the classical solution has the form  $f(z) = 1/(1 + z^2)$ . Of course, real instanton profile in NP vacuum is different. The problem of asymptotic behavior of instanton solution far from the center  $|x| \gg \rho_c$  was studied in detail in Refs. [13–15]. Our numerical analysis shows that the value of  $\rho_c$  is almost not affected by the asymptotic of classical instanton solution provided that condensate  $\langle G^2 \rangle$  and correlation length  $T_g$  have reasonable values.

Numerical calculations show that  $S_{\text{dia}}(\rho)$  is a growing function of  $\rho$ , and it ensured IR stabilization of an instanton. Numerical results for instanton size distribution  $d\rho/d^4z d\rho \sim \exp(-S_{\text{eff}})$  and corresponding lattice data [16] are presented in Fig. 1. All graphs are normalized to the commonly accepted instanton density  $1 \text{ fm}^{-4}$ . Different lattice groups roughly agree on instantons size within a factor of two, e.g.  $\bar{\rho} = 0.3 \dots 0.6 \text{ fm}$  for  $SU(3)$  gluodynamics. There is no agreement at all concerning the density  $N/V$ . As a tendency, lattice studies give higher density and larger instantons than phenomenologically assumed.

Using our model we find for  $\langle G^2 \rangle = 5.92 \text{ GeV}^4$  and  $T_g = 0.22 \text{ fm}$  that  $\rho_c \simeq 0.15 \text{ fm}$ , which is less than phenomenological ( $\sim 0.3 \text{ fm}$ ) and lattice results (in full QCD we find  $\rho_c \simeq 0.25 \text{ fm}$ ). However, we can present physical arguments to explain these deviations. Lattice calculations include cooling procedure, during which some lattice configurations of gluon field are discarded. This procedure can result in a change in gluon condensate  $\langle G^2 \rangle$ , and thus instanton size distribution is calculated at a value of gluon condensate  $\langle G^2 \rangle_{\text{cool}}$  which is smaller than physical value  $\langle G^2 \rangle$ . Therefore, lattice data for average instanton size  $\bar{\rho}$  should be compared with our calculations for  $\rho_c$ , performed at smaller values of  $\langle G^2 \rangle$ . We show dependence of  $\rho_c$  on  $\langle G^2 \rangle$  for several values of  $T_g$  in Fig. 2. One can see that increase of  $\langle G^2 \rangle$  results in decrease of instanton size, and that effect is a result of nonlocal "diamagnetic" interaction of instanton with NP fields.

We did not go beyond bilocal approximation in this work. As mentioned above, this approximation is good enough not only for qualitative, but also for quantitative description of some phenomena in nonperturbative QCD. In the problem under consideration there are two small parameters. These are  $1/g^2(\rho_c) \sim 0.15 \dots 0.25$  and  $1/N_c$ , and there powers grow in each term of cluster expansion. Moreover, we made an estimate for the sum of leading terms in cluster expansion [17], and found that IR stabilization stays intact ( $\rho_c$  appears to be a little smaller). Thus, proposed model describes physics of single instanton stabilization in NP vacuum, not only qualitatively, but also quantitatively with rather good accuracy.

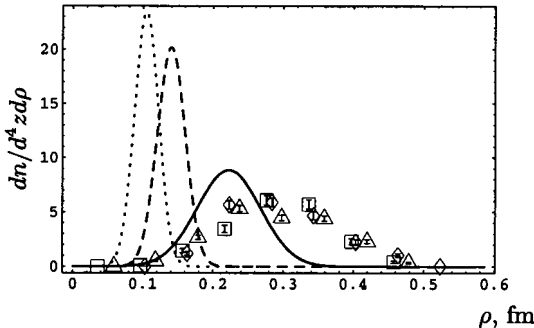


Figure 1: Instanton density  $dn/d^4z d\rho$  and lattice data [16].  $SU(3)$  full (solid line),  $SU(2)$  quenched (dotted line) and  $SU(3)$  quenched (dashed line)

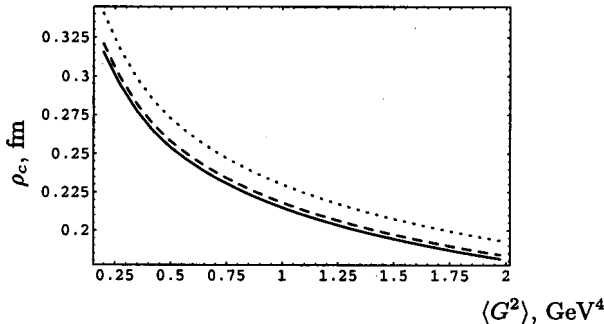


Figure 2: Instanton size as a function of gluon condensate ( $N_c = 3$ ,  $N_f = 4$ ) at  $T_g = 0.2$  fm (dotted line),  $T_g = 0.3$  fm (dashed line),  $T_g = 0.34$  fm (solid line)

### Acknowledgments

We are grateful to Yu.A. Simonov for helpful discussions and comments. The financial support of RFFI grant 00-02-17836 and INTAS grant CALL 2000 N 110 is gratefully acknowledged.

### References

- [1] A. M. Polyakov, *Phys. Lett.* **B59** (1975) 79; A. A. Belavin, A. M. Polyakov, A. S. Shvarts and Y. S. Tyupkin, *Phys. Lett.* **B59** (1975) 85.
- [2] G. 't Hooft, *Phys. Rev. Lett.* **37** (1976) 8.
- [3] E. Witten, *Nucl. Phys.* **B149** (1979) 285; G. Veneziano, *Nucl. Phys.* **B159** (1979) 213.
- [4] D. Diakonov and V. Y. Petrov, *Nucl. Phys.* **B272** (1986) 457.
- [5] T. Schafer and E. V. Shuryak, *Rev. Mod. Phys.* **70** (1998) 323 [hep-ph/9610451].
- [6] E. V. Shuryak, *Nucl. Phys.* **B203** (1982) 93.
- [7] N. O. Agasian and S. M. Fedorov, hep-ph/0111208.
- [8] N. O. Agasian and Yu. A. Simonov, *Mod. Phys. Lett.* **A10** (1995) 1755.
- [9] N. O. Agasian, *Phys. Atom. Nucl.* **59** (1996) 297.
- [10] H. G. Dosch, *Phys. Lett.* **B190** (1987) 177; H. G. Dosch and Yu. A. Simonov, *Phys. Lett.* **B205** (1988) 339; Yu. A. Simonov, *Nucl. Phys.* **B307** (1988) 512.
- [11] A. Di Giacomo, H. G. Dosch, V. I. Shevchenko and Yu. A. Simonov, hep-ph/0007223.
- [12] A. Di Giacomo, hep-lat/0012013.
- [13] D. Diakonov and V. Y. Petrov, *Nucl. Phys.* **B245** (1984) 259.
- [14] A. B. Migdal, N. O. Agasian and S. B. Khokhlachev, *JETP Lett.* **41** (1985) 497; N. O. Agasian and S. B. Khokhlachev, *Sov. J. Nucl. Phys.* **55** (1992) 628, 633; N. O. Agasian, hep-ph/9803252; hep-ph/9904227.
- [15] A. E. Dorokhov, S. V. Esaibegian, A. E. Maximov and S. V. Mikhailov, *Eur. Phys. J.* **C13** (2000) 331 [hep-ph/9903450].
- [16] A. Hasenfratz and C. Nieter, *Phys. Lett.* **B439** (1998) 366 [hep-lat/9806026].
- [17] N.O. Agasian and S.M. Fedorov, ITEP-PH-6/2001

# RELATIVISTIC MODEL OF HADRON-HADRON INTERACTIONS AT LOW AND INTERMEDIATE ENERGIES

A.N.Safronov <sup>a</sup>, A.A.Safronov <sup>b</sup>

<sup>a</sup> *Institute of Nuclear Physics, Moscow State University, 119899 Moscow, Russia*

<sup>b</sup> *Moscow State Institute of Radioengineering, Electronics and Automation, 117454 Moscow, Russia*

**Abstract.** The relativistic model of hadron-hadron interactions at low and intermediate energies taking into account the meson and quark-gluon degrees of freedom is proposed. It is assumed that the quark-gluon compound states are formed when two hadrons draw together at the distances of order 0.3 fm. We formulate the modified N/D-equations to calculate the partial-wave hadron-hadron scattering amplitudes taking into account the meson exchange mechanisms, formation of the quark-gluon compound states and influence of the inelastic channels. The model is applied to description of the energy dependence of the  $^1S_0$  and  $^3S_1$  partial-wave  $NN$  scattering amplitudes at the kinetic energies  $0 < T \leq 2.5$  GeV of incident nucleon in the laboratory system.

## 1 Introduction

It is now widely believed that quantum chromodynamics (QCD) is the fundamental theory of strong interactions which necessitates inclusion of the quark-gluon degrees of freedom in few-particle and nuclear physics at intermediate energies. Keeping in mind that a significant gap still exists in implementing QCD in the non-perturbative, low energy regime, it is natural to employ the mesonic theory for description of hadron-hadron interactions at large distances. Meson-exchange models for the nucleon-nucleon interaction are originated with Yukawa's basic hypothesis that the nuclear force is mediated by the exchange of massive particle [1]. However, the mesonic theories [2, 3] are unsatisfactory at small distances where quark-gluon picture is more adequate and asymptotic freedom prevails. The theoretical interpretation of the new nucleon-nucleon [4, 5] and other hadron-hadron scattering data at energies of order a few GeV is very important for understanding of the mechanisms of strong interactions. The investigation of this problem is able to clarify the status of the meson-exchange theories of nuclear forces and it can shed light on the role of quark-gluon degrees of freedom in the dynamics of strong interactions at low and intermediate energies.

## 2 Mechanisms of strong interactions

We follow the conception according to which the quark-gluon matter can be characterized by two distinctive configurations. In configurations of the first type the hadrons keep their individualities although they could interact with each other by exchange processes as in usual mesonic theories. In the configuration of the second type the hadrons lose their individualities turning into one of the quark-gluon compound states (QGCS) which are coupled with hadron-hadron scattering channels and so

---

<sup>a</sup>e-mail: safron@srn.sinp.msu.ru

<sup>b</sup>e-mail: mirea@mirea.ac.ru

they are not realized as asymptotic states. QGCS are treated as quasiparticles which effectively take into account the quark-gluon degrees of freedom at small distances. However, if the coupling of QGCS with scattering channels is sufficiently small then they can be revealed as genuine (multi-quark) resonances in the scattering processes.

The system is described in the framework of the relativistic light-front Hamilton dynamics (see, for example [6]). We start with the mass operator of the form  $M^2 = M_0^2 + U_m + U_c$ , where  $M_0$  is the mass operator of a free particles,  $U_m$  is the meson part of the invariant interaction operator and  $U_c$  describes creation (destruction) of QGCS. Using the method of unitary transformation [7] we perform the renormalization of the operator  $M$  and obtain in the subspace of two physical (dressed) hadrons effective mass operator  $M_a^2(s) = M_{a0}^2 + W(s)$ , depending on the spectral parameter  $s$  (square of energy in the center of mass system), where the effective interaction operator is given by

$$W(s) = U_e + \sum_n \int \frac{U_c |\chi_n(\mathbf{p}_n)\rangle \langle \chi_n(\mathbf{p}_n)| U_c}{s - \mu_n^2} \frac{d\mathbf{p}_n}{2p_{n+}}, \quad (1)$$

$U_e$  is meson-exchange part of effective interaction operator,  $\mu_n$  and  $\mathbf{p}_n = (p_{n+}, \mathbf{p}_\perp)$  are the mass and light-front momentum of QGCS respectively.

### 3 Equations for partial-wave amplitudes

It is convenient to introduce the generalized scattering operator by definition

$$A(s, \bar{s}) = W(\bar{s}) + W(\bar{s})G(s, \bar{s})W(\bar{s}),$$

where  $G(s, \bar{s}) = (s - M^2(\bar{s}))^{-1}$  is the Green operator, which depend on two spectral parameters. Taking into account that  $G(s, \bar{s})W(\bar{s}) = G_{a0}(s)A(s, \bar{s})$ , where  $G_{a0}(s) = (s - M_{a0}^2)^{-1}$ , we obtain the equation for operator  $A(s, \bar{s})$

$$A(s, \bar{s}) = W(\bar{s}) + W(\bar{s})G_{a0}(s)A(s, \bar{s}). \quad (2)$$

Note that in consequence of Poincare-invariance the matrix elements of operators  $W(s)$  and  $A(s, \bar{s})$  in light-front dynamics depend on relative momentum of particles only. As a result in case of uncoupled scattering channel Eq.(2) leads to integral equation for partial-wave amplitude of the form

$$A_l(\nu', \nu; s, \bar{s}) = W_l(\nu', \nu; \bar{s}) + \frac{1}{\pi} \int_{s_0}^{\infty} \frac{W_l(\nu', \xi; \bar{s}) A_l(\xi, \nu; s, \bar{s})}{\xi - s} \rho(\xi) d\xi, \quad (3)$$

where  $\rho(\xi) = 2q(\xi)/\sqrt{\xi}$ ,  $s_0 = (m_1 + m_2)^2$ ,  $m_i$  ( $i = 1, 2$ ) are masses and  $q(\xi)$  is relative momentum of particles;

$$W_l(\nu', \nu; s) = W_l^{(e)}(\nu', \nu) + W_l^{(c)}(\nu', \nu; s)$$

is partial-wave matrix element of effective interaction operator  $W(s)$  (see Eq. (1)), where  $W_l^{(e)}(\nu', \nu)$  is contribution of meson-exchange mechanisms and

$$W_l^{(c)}(\nu', \nu; s) = \sum_i \frac{g_{li}(\nu') g_{li}(\nu)}{s - \mu_{li}^2} \quad (4)$$

is conditioned by the coupling of the partial-wave scattering channel with the QGCS;  $g_{li}(\nu)$  is the form factor which determines the transition matrix element between  $i$ -th QGCS and the scattering state with orbital momentum  $l$ .

The solution of Eq. (3) can be represented in the form

$$A_l(\nu', \nu; s, \tilde{s}) = \frac{N_l(\nu', \nu; s, \tilde{s})}{D_l(s, \tilde{s})}, \quad (5)$$

where functions  $N_l(\nu', \nu; s, \tilde{s})$  and  $D_l(s, \tilde{s})$  are determined by the Fredholm series

$$N_l(\nu', \nu; s, \tilde{s}) = \sum_{n=0}^{\infty} \frac{(-1)^n}{n!} \prod_{i=1}^n \frac{1}{\pi} \int_{s_0}^{\infty} d\nu_i \frac{\rho(\nu_i)}{\nu_i - s} \langle \nu'_1 \dots \nu'_n | W_{n+1}^l(\tilde{s}) | \nu_1 \dots \nu_n \rangle, \quad (6)$$

$$D_l(s, \tilde{s}) = \sum_{n=0}^{\infty} \frac{(-1)^n}{n!} \prod_{i=1}^n \frac{1}{\pi} \int_{s_0}^{\infty} d\nu_i \frac{\rho(\nu_i)}{\nu_i - s} \langle \nu_1 \dots \nu_n | W_n^l(\tilde{s}) | \nu_1 \dots \nu_n \rangle, \quad (7)$$

where

$$\langle \nu'_1 \dots \nu'_n | W_n^l(\tilde{s}) | \nu_1 \dots \nu_n \rangle = \det_{(i,j)} \|W_l(\nu'_i, \nu_j; \tilde{s})\|. \quad (8)$$

Using Eqs. (6) and (7) on the energy shell (at  $\nu' = \nu = s$ ) we obtain the equation

$$D_l(s, \tilde{s}) = 1 - \frac{1}{\pi} \int_{s_0}^{\infty} \frac{N_l(s', \tilde{s})}{s' - s} \rho(s') ds', \quad (9)$$

where  $N_l(s, \tilde{s}) = N_l(s, s; s, \tilde{s})$ . Now we modify the "elastic" unitarity condition to include the effects of the inelastic channels  $Im A_l^{-1}(s) = -\sigma_l(s)$ , where  $A_l(s) = A_l(s, s)$ ,  $\sigma_l(s) = \rho(s)(1 + \eta_l(s))$  and  $\eta_l(s) \geq 0$  is the function which take into account the influence of inelastic scattering channels. As result we obtain the generalized version of Eq. (8)

$$D_l(s, \tilde{s}) = 1 - \frac{1}{\pi} \int_{s_0}^{\infty} \frac{N_l(s', \tilde{s})}{s' - s} \sigma_l(s') ds'. \quad (10)$$

If we suppose for simplicity that  $g_{li}(s) = \kappa_{li} g_l(s)$ , then  $W_l^{(c)}(\nu', \nu; s) = \lambda_l(s) g_l(\nu') g_l(\nu)$ , where

$$\lambda_l(s) = \sum_i \frac{\kappa_{li}^2}{\mu_{li}^2 - s}. \quad (11)$$

The function  $N_l(s, \tilde{s})$  can be represented in the form  $N_l(s, \tilde{s}) = N_l^{(c)}(s, \tilde{s}) + \tilde{N}_l(s, \tilde{s})$ , where  $N_l^{(c)}(s, \tilde{s}) = F_l(s) \lambda_l(\tilde{s})$ ,  $F_l(s) = g_l^2(s)$  and  $\tilde{N}_l(s, \tilde{s})$  is the function which has the dynamical (left) cuts  $C_L$  conditioned by meson-exchange mechanisms. The discontinuities of the function  $\tilde{N}_l(s, \tilde{s})$  across the dynamical cuts  $C_L$  are determined by the equation  $disc \tilde{N}_l(s, \tilde{s}) = disc A_l(s) D_l(s, \tilde{s})$  and as a result for  $N_l(s, \tilde{s})$  we obtain the expression

$$N_l(s, \tilde{s}) = F_l(s) \lambda_l(\tilde{s}) + \frac{1}{\pi} \int_{C_L} \frac{disc A_l(s') D_l(s', \tilde{s})}{s' - s} ds'. \quad (12)$$

Finally, inserting Eq. (10) into right hand side of Eq. (12), we find the closed equation for the function  $N_l(s, \tilde{s})$

$$N_l(s, \tilde{s}) = F_l(s)\lambda_l(\tilde{s}) + L_l(s) + \frac{1}{\pi} \int_{C_L} \frac{L_l(s') - L(s)}{s' - s} N_l(s', \tilde{s}) \sigma_l(s') ds', \quad (13)$$

where

$$L_l(s) = \frac{1}{\pi} \int_{C_L} \frac{\text{disc} A_l(s')}{s' - s} ds'$$

is the potential function which is determined by discontinuities of the partial-wave amplitude across dynamical cuts. Equations (10), (13) are the generalized N/D-equations which take into account the meson-exchange mechanisms, the formation of the quark-gluon compound systems in intermediate s-channel states and influence of the effects of inelasticity.

#### 4 Application to $NN$ -scattering

As example let us discuss the energy dependence of the  $S$ -wave  $NN$ -scattering amplitudes ( $^1S_0$  and  $^3S_1$ ) in the region of energies  $0 < T \leq 2.5$  GeV. It follows from very general physical principles (such as Poincare-invariance, unitarity and analyticity which reflects the requirement of causality) that  $\lambda_l(s)$  must be increasing function of  $s$ , if of course our suggestion about CGCS formation is true and if the meson-exchange contributions are taken into account correctly. The function  $g_0(s)$  was chosen in the form  $g_0(s) = \exp[-q^2(s)/4\Lambda^2]$  which corresponds to the Gauss form factor in coordinate representation  $g(r) \sim \exp(-\Lambda^2 r^2)$ . Thus the parameter  $\Lambda$  determines the effective radius  $r_0 = 1/\Lambda$  of interaction of the  $NN$ -scattering channel with CGCS. Using the available data [4] and taking into account the meson mechanisms in framework of the one-boson-exchange model we extract the information about the energy dependence of the functions  $\lambda_0(s)$  in the  $^1S_0$  and  $^3S_1$   $NN$ -scattering channels. Potential function in one boson exchange model can be represented in the form  $L_0(s) = \sum_\alpha L_{0\alpha}(s)$ , where

$$L_{0\alpha}(s) = \frac{1}{\pi} \int_{s_\alpha}^{s_{0\alpha}} \frac{\text{Im} A_{0\alpha}(s')}{s' - s} ds'$$

are contributions of mesons  $\alpha = (\pi, \rho, \omega, \eta, a_0, \sigma)$ ,  $s_{0\alpha} = 4m_N^2 - m_\alpha^2$ ,  $s_\alpha = 4m_n^2(1 - \gamma_\alpha^2)$ ,  $m_N$  and  $m_\alpha$  are masses of nucleon and mesons respectively,  $\gamma_\alpha$  are the cutoff parameters. The  $\sigma$ -meson approximates the contributions from correlated  $\pi\pi$ -pair exchange in t-channel with angular momentum  $J = 0$  and isospin  $I = 0$ . The meson coupling constants, masses of mesons and cut-off parameters are shown in Table 1. The information about parameters of inelasticity  $\eta_0(s)$  in  $^1S_0$  and  $^3S_1$  channels has been taken from energy-dependent analyses [4]. We conclude that the inverse functions  $\lambda_0^{-1}(s)$  are really decreasing functions of  $s$ , as predicted by theory, and at  $T \geq 550$  MeV they are approximated sufficiently well by straight lines  $\lambda_0^{-1}(s) = a - bs$ , where  $a = 0.126$  (0.062),  $b = 0.029$  (0.018)  $\text{GeV}^{-2}$  for  $^1S_0$  ( $^3S_1$ ) channel at  $\Lambda = 809$  MeV. Solutions of the equations (10), (13) with these parameters and meson-nucleon coupling constants in Table 1 result in the  $^1S_0$  and  $^3S_1$  phase shifts shown in Table 2.

Table 1. Meson coupling constants, masses and cutoff parameters.

	$\pi$	$\rho$	$\omega$	$\eta$	$a_0$	$\sigma$
$\frac{g_{NN\alpha}^2}{4\pi} \left[ \frac{f_{NN\rho}^T}{g_{NN\rho}} \right]$	14.0	0.83 [6.0]	5.3	1.6	2.5	12.0
$m_\alpha$ , MeV	138.03	769	782	548.8	983	550
$\gamma_\alpha$	1	1	1	1	1	1.55

Table 2.  ${}^1S_0$  and  ${}^3S_1$  NN-scattering phase shifts are calculated using Eqs. (10), (13); energy-dependent solution ( ED ) and single energy values ( SE ) are taken from Ref. [4].

T, MeV	$\delta({}^1S_0)$ , degree			$\delta({}^3S_1)$ , degree		
	Eqs.(10),(13)	ED	SE	Eqs.(10),(13)	ED	SE
200	8.04	7.68	8.55	22.85	20.61	20.98
400	-18.32	-15.08	-15.39	-5.27	-3.44	-3.61
800	-43.79	-44.90	-44.32	-34.05	-33.92	-35.70
1000	-50.78	-53.14	-61.06	-43.61	-43.85	-46.71
1800	-60.93	-59.81	-65.41	-65.20	-66.79	-
2400	-48.16	-48.62	-63.88	-63.14	-56.83	-

## 5 Conclusion

The proposed model describes the energy dependence of the  ${}^1S_0$  and  ${}^3S_1$  NN-scattering phase shifts in the region  $0 < T \leq 2.5$  GeV. We conclude that only one quark-gluon compound state is coupled with  ${}^1S_0$  ( or  ${}^3S_1$  ) NN-scattering channel and effective radius of this interaction is equal  $\sim 0.23$  fm. We use approximately the same meson-nucleon coupling constants as modern models of the  $\pi N$ -scattering [8]. The mesonic theories of nuclear forces [2,3] require considerably greater value of coupling constant  $g_{NN\omega}$  ( $g_{NN\omega}^2/4\pi \sim 20$ ). This is necessary to describe the repulsive part of the  $NN$ -interaction at small distances in the meson-exchange models. In our approach the nature of the short range repulsion is different. It is conditioned by the formation mechanism of the quark-gluon compound states. We note in conclusion that the idea of formation of the quark-gluon systems in hadron-hadron interactions is considered before in the framework of the  $P$ -matrix formalism [9], the quark compound model [10] and dispersion approach [11, 12]. All these approaches generalize the conception of the boundary condition model [13]. They were used to describe the  $NN$ -interaction at energies  $T \leq 1$  GeV. It was obtained that the effective radius of interaction  $r_0$  of the  $NN$ -scattering channel with quark bags is equal  $\sim 1$  fm. The present model has been used up to energies  $T \sim 2.5$  GeV and it is consistent with the small  $r_0(\sim 0.3$  fm).

## Acknowledgments

This work is supported by the Ministry of Education of Russian Federation, Scientific Program "Universities of Russia" ( Project N 01200006448 ).

**References**

- [1] H.Yukawa, *Proc.Phys.Math.Soc.Jpn.* 17, 48 (1935).
- [2] M.Lacombe, B.Loiseau, J.M.Richard, e.a., *Phys.Rev.* **D** 12, 1495 (1975).
- [3] R.Machleidt, K.Holinde,Ch.Elster, *Phys.Rep.* 149, 1 (1987).
- [4] R.A.Arndt, e.a., *Phys.Rev.* **C** 56, 3005 (1997); <http://said-hh.desy.de>.
- [5] M.Matsuda, *Nucl.Phys.* **A** 631, 436 (1998).
- [6] M.G.Fuda, Y.Zhang, *Phys.Rev.* **C** 51, 23 (1995).
- [7] S.Okubo, *Prog. Theor.Phys.* 12, 603 (1954).
- [8] O.Krehl, e.a., *Phys.Rev.* **C** 62, 025207 (2000).
- [9] R.L.Jaffe, F.E.Low, *Phys.Rev.* **D** 19, 2105 (1979).
- [10] Yu.A.Simonov, *Phys.Lett.* **B** 107, 1 (1981).
- [11] A.N.Safronov, *Phys.Lett.* **B** 124, 149 (1983).
- [12] A.N.Safronov , *Phys.of Elem.Particles and Atom.Nuclei* 21, 1187 (1990).
- [13] H.Feshbach, E.L.Lomon, *Ann. of Phys.* 29, 19 (1964).

# QUARK-GLUON PLASMA: PRO AND CONTRA

Ilya I. Royzen <sup>a</sup>

*Lebedev Physical Institute of RAS, 117924 Moscow, Russia*

*Abstract.* The current status and perspectives of QCD production and identification are discussed. The great endeavors which were made and difficulties we are in face of along carrying out the relevant programs are outlined.

## 1 General Motivation and Problems

A great majority of physicists believe, in principle, in existence of QGP, the (almost) chirally symmetrical phase of current quarks and gluons, as a possible state of the matter, just like solid, liquid, gaseous and ordinary plasma ones. Their belief is based on treatment of the light-flavor quark constituent masses as being acquired due to the color confinement. Thus, these quarks are expected to lose their masses (except of the very small current masses), when color screening length scales down to become considerably shorter than the confinement radius, in other words, when the mean quark spacing becomes sufficiently short. Such a configuration could be achieved by increase of temperature and/or pressure. That is why QGP has had to be inherent in the early Universe at the proper stage of its evolution ( $\sim$  from 40 up to 80  $\mu s$  after Big Bang). Much less is the number of those, who believe that one can produce QGP artificially in the lab's. Still lower part of them believe that we are able to detect it unambiguously, even being successful in producing it for a short instant. And, nevertheless, there is plenty of us, who do believe in all that.

Let me start with some most general features of the sub-hadronic matter. In fact, it is not necessarily to be QGP. The variety of possibilities suggested by the first principles (QCD lattice calculations) is illustrated by mapping the  $(\mu, T)$  plane [1] shown in Fig. 1. where  $\mu$  and  $T$  are baryon chemical potential and temperature of nuclear medium under consideration, respectively. The most significant points are:

- two phases of subhadronic matter are expected to exist: QGP and (massive?) quark (diquark) matter. No QGP can exist in a certain bottom-right sector of  $(\mu, T)$  plane.
- these phases transform into each other either by undergoing a phase transition or more smoothly, i.e., passing through a crossover intermediate state which occupies a certain rather extended domain (not a line!) in the phase plane.
- the type of phase transition between hadronic matter (HM) and sub-hadronic matter depends on  $\mu$ : being the first order one at large values of  $\mu$ , it evolves (as  $\mu$  decreases) to become, firstly, the second order one (critical point E in Fig. 1) and, then, to transform into a crossover instead of a conventional phase transition <sup>b</sup>.

In what follows, I concentrate on HM and QGP only.

## 2 QGP Fireball: Creation and Evolution

---

<sup>a</sup>e-mail: royzin@lpi.ru

<sup>b</sup>The physical meaning of this pattern seems quite transparent: at large baryon density, a large number of frozen degrees of freedom are getting alive as quarks become unleashed, whereas both this density and this number decrease alongside.

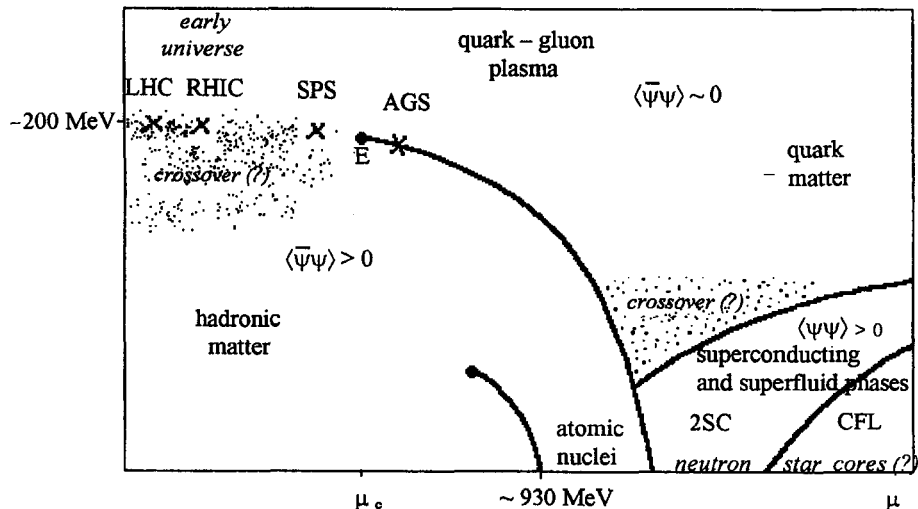


Fig. 1

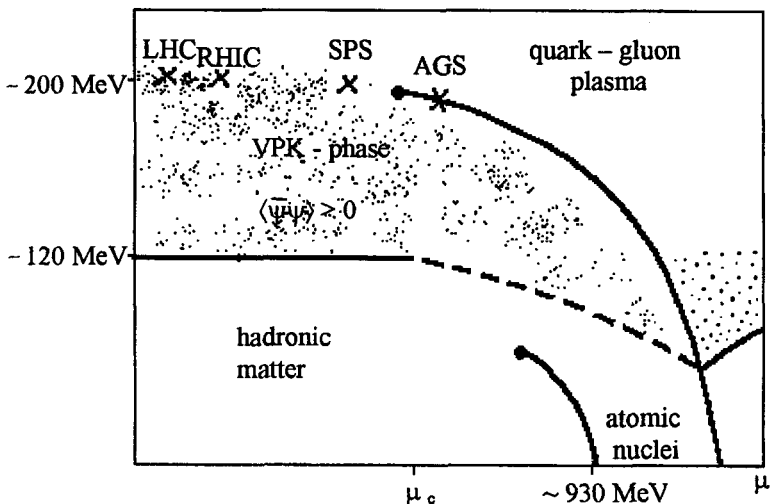


Fig. 1\*

Fig. 1.  $(\mu - T)$  phase diagram as it is emerged from lattice calculations. Here  $\langle \bar{\psi} \psi \rangle$  and  $\langle \psi \psi \rangle$  are the  $\bar{q}q$  and  $qq$  condensate densities; 2SC denotes a superconducting state made by pairing of two light flavors and CFL denotes an all-flavor-color-locked superfluid state. For the experimental facilities see Table 1.

Fig. 1\*. Modified bottom-left corner of Fig. 1, allowing for the VPK-phase.

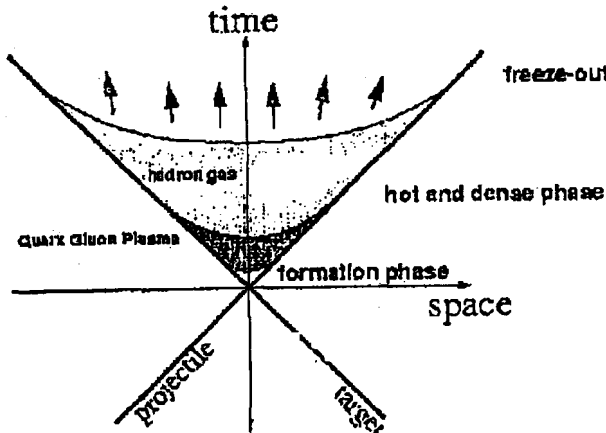


Fig. 2. Space-time evolution of fireball.

The only conceivable way of producing QGP artificially is making the proper heavy ions to come into head-on (central) collision. In course of such a collision, some number of nucleons break through the dense nuclear matter to move rapidly in opposite directions, preserving their color singlet structure, whereas the remainders are ruined dramatically and disintegrate into colored partons - quarks and gluons - which are stopped due to multiple collisions. As a result, a large amount of energy is deposited within a small volume (fireball), what results in numerous production of  $q\bar{q}$  pairs. Thus, a mean color field is set in where the color screening length is sufficiently small for allowing free propagation of colored particles, what, in turn, is just necessary to bring the matter to form the QGP state<sup>c</sup>. In course of fireball expansion and cooling down, the average spacing (or color screening length) between colored particles scales up to become in a some time about the confinement radius. Then, the dominant degrees of freedom are no longer quarks but hadrons themselves, quarks being locked within them, and the corresponding phase transition (or crossover) takes place. As the hadrons diverge sufficiently to stop interacting, they become "frozen out" to scatter away as free particles. The relevant space-time evolution scheme is shown in Fig. 2.

The higher is the colliding ion energy, the lower are the typical values of  $\mu$  at the same  $T$ . This is because the number of stopped and disintegrated nucleons (the net baryon number) becomes smaller (the so-called stopping power falls down as the energy increases). The available now and forthcoming facilities are listed in Table 1. Of course, the values of the initial energy density within fireball given in the rightmost

<sup>c</sup>This is necessary, but not sufficient, since for chiral symmetry restoration inherent in QGP one has still to make quarks "undressed". Otherwise, a mixed quark-hadronic state might be produced instead. What would it happen really is regulated by  $\mu - T$  relation, see Fig.s 1 and 1\*.

Machine	Start	Type	Beam	$\sqrt{s}$ [GeV/A]	$e_0^{AB}$ [GeV/fm <sup>3</sup> ]
BNL - AGS	1986	Fixed Target	<sup>28</sup> Si	5	0.7
CERN - SPS	1986	Fixed Target	<sup>16</sup> O, <sup>32</sup> S	19	1.6
BNL - AGS	1992	Fixed Target	<sup>197</sup> Au	5	1.5
CERN - SPS	1994	Fixed Target	<sup>208</sup> Pb	17	3.7
BNL - RHIC	2000	Collider	<sup>197</sup> Au	200	7.6
CERN - LHC	~ 2005	Collider	<sup>208</sup> Pb	5000	13

Table 1: Experimental facilities for high energy nuclear collisions; the light ion beam results are for heavy ( $A = 200$ ) targets, the others for symmetric ( $A - A$ ) collisions.

column of this Table are calculated theoretically under certain assumptions and thus their accuracy may be as poor as about 50%.

The above scenario is to be verified by some experimental evidences. However, the direct "visiting cards" of QGP can be either washed out in course of subsequent evolution or mimicked by similar processes within the hadronic matter. The problem is complicated additionally because of the lack of our knowledge about the properties of hot and dense HM<sup>d</sup> which takes a whole epoch in fireball evolution (in the relevant time scale).

Meanwhile, an alternative scenario could be proposed [2], in which the cooling QGP is suggested to transform first into an equilibrium three-component (VPK) gas composed from *unleashed* massive constituent quarks, so-called valons (the dominant fraction,  $\sim (75 \div 80)\%$ ), pions ( $\sim 20\%$ ) and kaons (small fraction,  $\sim (4 \div 5)\%$ )<sup>e</sup>. Pions and kaons can survive under relevant conditions because their *spontaneous* decays into the proper *massive* quarks is strongly forbidden by the energy conservation law, in contrast to other hadron species which are stable against immediate disintegration into massive quarks due to color confinement only (lost in this phase). At small values of  $\mu$ ,  $\mu < \mu_c$  in Fig. 1, one could consider this phase to be a certain concrete realization of the crossover, since it incorporates both the color singlet and color octet particles, see Fig. 1\*. If so, then allowing for this phase at  $\mu > \mu_c$  is nothing but extension of the crossover pattern of  $\text{HM} \leftrightarrow \text{QGP}$  to all values of  $\mu$ , in contrast to what is suggested by lattice calculations. Within this approach, one gets rid of the necessity to deal with a rather obscured state of very dense and hot hadronic matter. The obvious weakness of the approach is seeming failure of the endeavors [4] to derive rigorously the massive constituent quarks as some quasi-particles inherent in the general QCD field theory. However, this notion was widely and fruitfully exploited before QCD was developed as a consistent field theory. Besides, till now QCD remains actually a quite workable theory of hard processes and suffers from the lack of even qualitative results for the processes at low and intermediate energies, i.e., just for those ones which proceed within nuclear matter below the chiral breaking temperature. Thus, maybe, embedding of massive constituent quarks unambiguously into the body of QCD is still waiting for its turn.

### 3 Signals of QCD

At times some ideas were put forward on what experimental signal could bring a decisive evidence that QGP does appear in course of heavy ion collisions. However, after more careful analysis, all they were found to be model dependent, and now the common opinion is that the eventual decision is rather to be made "on the all strength of evidence", what is rather juridical than scientific way of doing. Let me turn now

<sup>d</sup>Of course, no gaseous treatment of this HM is admissible, because the hadronic wave functions overlap strongly under such a conditions.

<sup>e</sup>Due to sufficiently small size of valons,  $r_v \simeq 0.3 \text{ fm}$  [3], this three-component state was shown [2] to be well subjected to gaseous treatment. The content of different components is regulated by thermodynamics or by the detailed balancing relation between them [2].

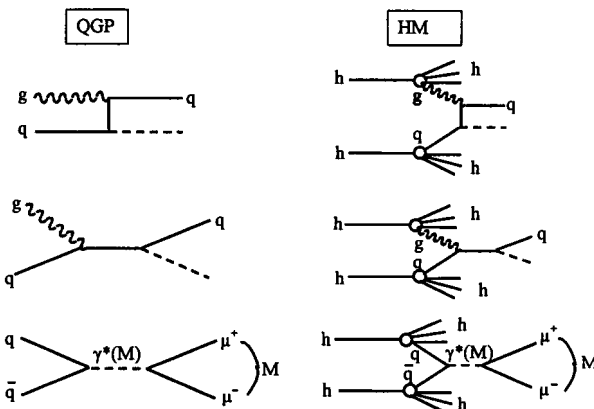


Fig. 3. Typical competing processes in QGP (thermal ones) and in HM (predominantly, DY-ones), responsible for direct photon and dimuon production.

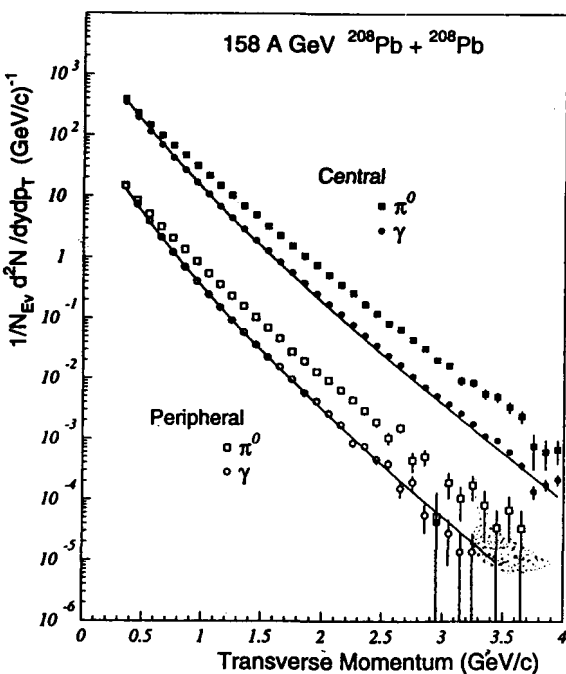


Fig. 4. The inclusive photon (circles) and  $\pi^0$  (squares) transverse momentum distributions. Only statistical errors are shown.

to consideration of the specific signals which are being analyzed in this connection<sup>f</sup>.

- *Direct photons and dimuons*

The idea is that, being produced within QGP, these electromagnetically interacting particles escape the fireball, remaining unperturbed by subsequent interactions and thus carrying the direct information on QGP phase. In particular, their (high temperature) thermal spectrum is expected to be enhanced substantially at large transverse momenta as compared to that emerged from ("low temperature") HM. No doubt, this is true, however the non-thermal processes, predominantly of DY-type (see Fig. 3), caused by hadronic interactions also fit the available experimental data fairly well [5, 6], see Fig. 4<sup>g</sup> and Fig. 5.

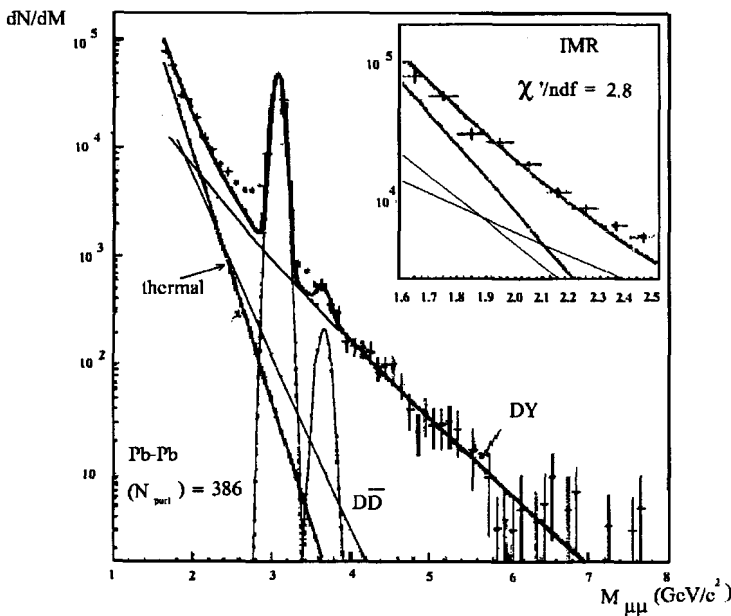


Fig. 5. Data on dimuon yield versus theoretical predictions, coming from DY+mesonic decay analysis.

- *Jet quenching*

<sup>f</sup>There is no room here for the comprehensive analysis, so I select the signals which seem to be most promising.

<sup>g</sup>One can take notice here of a hint on a signal coming from the direct photons with transverse momenta  $p_T > 1.5$  GeV in central collisions. To take this signal seriously, one has to be sure, however, that observed small excess ( $\leq 10 \div 20\%$ ) over the  $\pi^0$ -induced photons is not caused by some interplay of the collective transverse flow and  $\gamma$ -producing decays of other mesons. Otherwise, one has to wait for a more unambiguous signal.

Within sufficiently hot and dense QGP, the Landau-Pomeranchuk-Migdal (LPM) mechanism [7] of coherent scattering from many centers is suggested [8] to come into play, what may result in substantial increase of energy losses along with propagation of initially very hard jets and thus in quenching the jet spectrum at high transverse momenta. The basic relation to be exploited in this connection reads:

$$\frac{dE}{dx} \propto -\alpha_s \mu^2 \frac{L}{\lambda}$$

at  $L \leq L_{cr} \equiv \mu^{-1} \sqrt{\lambda E}$ , where  $\mu$  is the screening-mass scale and  $\lambda$  is the mean free path within QGP. Thus, the energy loss over the path  $L_{cr}$  just after the jet production is proportional to  $E$ ,

$$-\Delta E \propto L_{cr}^2 \propto E,$$

instead of being independent of  $E$ , what is the case for the incoherent single-center scattering within HM. This mechanism may be relevant for understanding the jet quenching observed at RHIC [9], see Fig. 7, as a signal of QGP. Unfortunately, the estimates one has for today are rather qualitative. Moreover, there is still one puzzling point: why the transverse momentum quenching is observed unambiguously in the  $\pi^0$ -spectrum only?

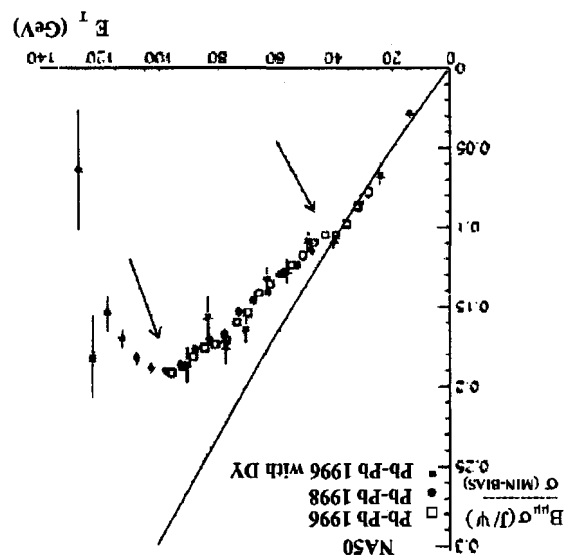
- *J/ $\Psi$  suppression in junction with the proper D-meson enhancement*

This would be a serious test of QGP. Indeed, the small spatial scale of color screening within high temperature QGP (in contrast to HM) is favorable for scattering away of charmed (anti)quarks  $c\bar{c}$  just after their production at a quite small distance ( $r \simeq m_c^{-1}$ ). Thus,  $J/\Psi$ - and  $D(\bar{D})$ -meson outcomes from QGP are expected to be correlated as follows: the first one should be suppressed, whereas the second one should be enhanced, correspondingly, in the central heavy ion collisions as compared to the peripheral ones and to  $pA$  collisions. The first half of this expectation is already proved to be true [10], see Fig. 8, while the second half remains still to be the challenging experimental task.

- *The critical point*

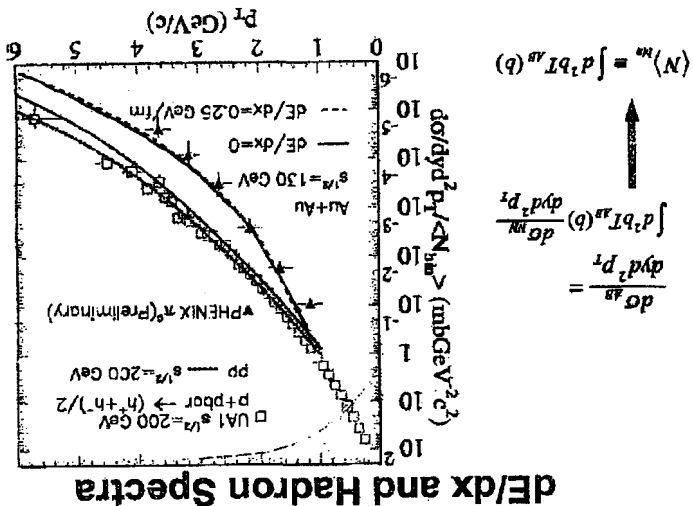
Identification of this point (see Fig's. 1 and 3) would be apparently the model independent signal of phase transition between QGP and another phase because the attendant manifestations - substantially larger fluctuations, than the statistical ones, in event-by-event analyses of all the observables - are predicted by the general theory of the 2nd order phase transitions. Thus, this would be, firstly, confirmation of the phase transition itself and, secondly, an evidence in support of lattice calculations which are not sufficiently reliable themselves. Unfortunately, being the most indisputable, this signal is also the most difficult for searching. Indeed, for doing this, one has to scan over the colliding ion energies for catching the proper value of  $\mu$  which, in turn, depends not only on this energy (say, on centrality of a collision as well). This is a very hard hunting!

Fig. 7.  $\bar{J}/\Psi$ -suppression versus "centrality" (transverse energy  $E_T$ ) collisions.



$\bar{J}/\Psi$ /Minimum Bias as a function of  $E_T$

Fig. 6. Possible modelling of jet quenching by allowing for some effective LPM energy losses.



#### 4 Hadronic Yields

This point is related rather to the problems of thermalization of the nuclear matter obtained in course of heavy ion collisions and of particle interaction within fireball, than to the QGP itself. While being thermalized, this matter would produce different hadron species in the accordance with the black body radiation law, if the final state interaction of produced hadrons is insignificant. It has been noticed [?, 11] that the relative hadron yields observed at "old" accelerators are compatible with the assumption that the hadrons are originated due to coalescence of the proper quark combinations and become chemically frozen <sup>h</sup> to form an ideal hadronic gas at the temperatures  $T_c \simeq 170, 110$  and  $60$  MeV for SPS, AGS and SIS, respectively. One can easily notice the obvious weakness of this hadronization assumption: at these temperatures (especially, for SPS), the ideal hadronic gas would be so dense that wave functions of neighboring hadrons would overlap essentially and thus no gaseous approximation seems to be selfconsistent. All the more, one can not disregard the subsequent interhadronic interaction (especially, baryon-antibaryon one [?]), what makes the approach rather controversial.

On the other hand, one can assume that QGP (if it is really formed initially) transforms firstly into a mixed VPK phase (see section 2 and Fig. 1\*) which lasts to meet hadronization at considerably lower temperatures ( $\sim 100$ - $130$  MeV). This approach enables to escape (to a large extent) two unpleasant difficulties: owing to small size of valons, VPK phase is subjected to (ideal?) gas treatment, and corrections caused by hadronic final-state interaction are reasonably expected to be much smaller, since the gap between the temperatures of hadronization and thermal freeze-out <sup>i</sup> ( $\sim 100$  MeV) is substantially contracted. This approach is shown [2] to be equally compatible with all measured hadronic yields and provides many other predictions for RHIC and LHC. Thus, the hadronic yield analysis itself is hardly an effective tool for the diagnostics of QGP.

#### 5 Instead of Conclusion

In view of said above, one can characterize the modern status of the problem under consideration by some winged phrases from the conference QUARK MATTER 2001.

##### PESSIMISTIC

- "Theoretical uncertainties are bigger, than experimental error bars" /K. Eskola/
- "Almost all signals available now are signalling almost equally in favor and disfavor of QGP" /H.G. Specht/

##### PRAGMATIC

- "We have to be more concerned about the theoretical content of models: an ill-defined model which fits the data is quite useless" /K. Werner/

---

<sup>h</sup>This means that then no changes in the relative content of different species take place.

<sup>i</sup>Below this temperature hadrons stop interacting and then scatter away as free particles.

- "Transverse energy measurements will be more efficient model killer" /K. Eskola/

### OPTIMISTIC

- "Absence of evidence is not evidence of absence" /V.H. Koch/

*Everybody is free to make his own choice!*

The author is deeply thankful to O.A. Langer and N.G. Polukhina for the invaluable help in composing the figures.

This work is supported by the Russian Foundation for Basic Researches, grants Nos. 96-15-96798 and 00-02-17250.

- [1] See, e.g., K. Rajagopal, in *Proc. of the 14th Int. Conf. on Ultra-Relativistic Nucleus-Nucleus collisions*, p.150c, Torino, Italy, 10-15 May, 1999, Ed. L. Riccati, M. Masera and E. Vercellin, and ref.s therein; S. Hands, *Contemporary Phys.*, 2001, vol.42, p. 4; and ref.s therein.
- [2] O.D. Chernavskaya, E.L. Feinberg, I.I. Royzen, Sov. Nucl. Phys., 2002, vol. 65, p. 1 and 2002, to be published; hep-ph/0101063; and ref.s therein.
- [3] V.V. Anisovich *et al.*, Sov. Phys. Uspekhi, 1984, vol. 27, p. 901; B.L. Ioffe and V.A. Khose, *Hard Processes*, vol. 1, North Holland, Amsterdam, 1984.
- [4] K.G. Wilson, Phys.Rev.D, 1974, vol. 10, p. 2245.
- [5] M.M. Aggarwal *et al.* (WA98 Collab.), Phys. Rev. Lett, 2000, vol. 85, p. 3595.
- [6] L. Capelly, *Talk at the Int. Conf. QUARK MATTER 2001, Stony Brook, USA, 15-20 January, 2001*.
- [7] See, e.g., M.L. Ter-Mikhaelyan, *High-Energy Electromagnetic Processes in Condensed Media*, Wiley Interscience, New York, 1972, and ref.s therein.
- [8] See, e.g., D. Schiff, *Talk at the Int. Conf. From the Smallest to the Largest Distances*, Moscow, Russia, 24-26 May, 2001.
- [9] X.N. Wang, *Talk at the Int. Conf. QUARK MATTER-2001, Stony Brook, USA, 15-20 January, 2001*.
- [10] P. Bordalo, *Talk at the Int. Conf. QUARK MATTER-2001, Stony Brook, USA, 15-20 January, 2001*.
- [11] P. Braun-Munzinger, I. Heppe, J. Stachel, nucl-th/9903010 v2
- [12] J. Cleymans, K. Redlich, Nucl. Phys. 1999 vol. A661, p. 379; nucl-th/9903063.
- [13] R. Rapp and E.V. Shuryak, hep-ph/0008326 v3.

## DISCOVERY OF $\eta$ -MESIC NUCLEI.

G.A. Sokol <sup>a</sup>, A.I. L'vov, L.N. Pavlyuchenko.

*Lebedev Physical Institute, RAS, Moscow, Russia*

*Abstract.* The first experimental results confirmed the existence of eta-mesic nuclei are represented. The experiment was performed at 1 GeV electron synchrotron of LPI. The correlated ( $\pi^+n$ ) pairs from  $^{12}\text{C}$ -target were detected by two TOF scintillation spectrometers placed oppozite both transversly to  $\gamma$ -beam. It was used two value of top energies of bremsstrahlung beam: 650 and 850 MeV (below and above of the photoproduction threshold of  $\eta$ -meson on nucleon.) The received results are allowed to speak about of the creation of eta-mesic nuclei at intermediate state of the studied reaction.

### 1 Introduction

Modern view on atomic nuclei structure as a system of protons and neutrons has appeared in 30th years of 20th century after discovery of a neutron. The second half of 20th century was marked by discovery of many new particles and its resonance states. In 60th years the quark conception was developed. From this point of view the question was arised on possible existence of nuclear bound system including new particles apart from protons and neutrons (nucleons). In 50th years hypernuclei - a new kind nuclei contained of  $\Lambda$  - or  $\Sigma$ -hyperons apart from nucleons were discovered. The  $\Lambda$  and  $\Sigma$  hyperons are close analogues of the nucleons as masses as for their quark content. Their masses only  $\sim 200$  MeV are been more then mass of nucleons ( $\sim 940$  MeV) and they consist of 3 constituent quarks as nucleons but one of them being the strange (s) quark.

### 2 $\eta N$ interaction and $\eta$ -nuclei

The idea that a bound state of the  $\eta$ -meson and a nucleus (the so-called  $\eta$ -mesic nucleus) can exist in Nature was put forward long ago by Peng [1]. The  $\eta$ -meson does not have an open strangeness. It consist of 2 quarks (more exactly, a quark and antiquark with the total isospin 0) of different flavors, of which  $\approx 50\%$  is an  $s\bar{s}$  pair. The mass of  $\eta$  is 547,5 MeV i.e. about 1/2 of the nucleon mass. Suggestion of J.C. Peng based on the first estimate of the  $\eta N$  scattering length  $a_{\eta N}$

$$a_{\eta N} = (0, 27 + i \cdot 0, 22) \text{ fm} \quad (1)$$

derived by Bhalerao and Liu [2] from a coupled-channel analysis of the reactions  $\pi N \rightarrow \pi N$ ,  $\pi N \rightarrow \eta N$  and  $\pi N \rightarrow \pi\pi N$ . Owing to  $\text{Re}a_{\eta N} > 0$ , there is an average attractive s-wave potential between a slow  $\eta$  and a nucleon. For extended nuclei, such an attraction should be sufficient for making the  $\eta$ -meson bound, provided the life-time of the  $\eta$ -meson in the nucleus is not too short. A quantum-mechanical consideration done Liu and Haider [3] and based on the  $\eta N$  potential corresponding to Eq. (1) predicted that bound states of the  $\eta$ -meson and a nucleus A must exist for  $A \geq 11$ . Later on, this conclusion was strengthen. More sophisticated coupled-channel analysis [4,5] taking into account both resonance and nonresonance contributions

---

<sup>a</sup>e-mail: gsokol@sgi.lpi.msk.su

arrived to very different results, giving a scattering length  $Rea_{\eta N}$  about 3 times larger than the very first estimate (1) [5]:

$$a_{\eta N} = (0, 75 + i \cdot 0, 29) fm \quad (2)$$

For such  $a_{\eta N}$ ,  $\eta$ -mesic nuclei should exist for all nuclei with  $A \geq 4$ . With slightly larger  $a_{\eta N}$ ,  $\eta$ -bound states would be possible for  $A=3$  and even for  $A=2$  [6]. It is worth to emphasize that elementary  $\eta N$  scattering amplitudes are theoretically derived from other reactions like  $\pi N \rightarrow \pi N$  and  $\pi N \rightarrow \eta N$  through extrapolations based on a factorization [2] or, in the latest works, on unitarity constraints [4,5]. Since, however, not all important channels are involved into these extrapolations (missing are e.g.  $\pi N \rightarrow K\Lambda$  and  $\eta N \rightarrow K\Lambda$ ), it is not clear how reliable are the obtained results. A difference between Eqs (1) and (2) may give a hint about real uncertainties. Therefore, experimental studies of bound states of various  $\eta A$  systems would greatly contribute to learning elementary  $\eta N$  scattering. The real part of the  $\eta N$  scattering

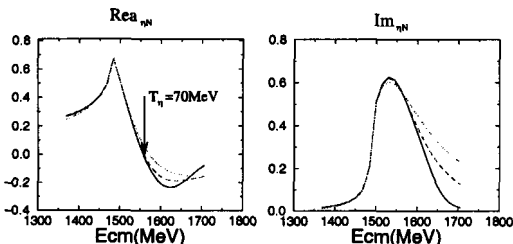


Figure 1: Energy dependence of  $Rea_{\eta N}$  and  $Im{a}_{\eta N}$  for the process  $\eta N \rightarrow \eta N$  [5].

amplitude  $f_{\eta N}$ , the threshold value of which is just equal to the scattering length  $a_{\eta N}$ , remains positive up to kinetic energies of  $\eta$  below 70 MeV [5] (fig.1). This means that the effective  $\eta A$  attraction exists in a wide near-threshold energy region  $\Delta E_\eta \approx 0 \div 70$  MeV. The attractive forces in the final state should lead to a near threshold enhancement in the total and differential cross section of real  $\eta$  production by different beams. Such an enhancement was indeed observed in several reactions including  $p(d, {}^3 He)\eta$  [7,8] and  $d(d, {}^4 He)\eta$  [9,10], thus supporting the existence of the  $\eta A$  attraction even for the lightest nuclei. Nevertheless, all these experiments which have deal with  $\eta$  in the final state cannot directly prove that bound  $\eta A$  states do really exist. A well-known counter example is provided by the NN system in the  $S_0$  state, which has a virtual, not real level described by a negative, not positive scattering length.

### 3 A previous experiences

Two attempts to discover  $\eta$ -nuclei in the missing mass spectrum of the reaction  $\pi^+ A \rightarrow pX$  were performed at BNL [11] and LAMPF [12] soon after the first theoretical suggestions [1,2]. Both the experiments failed to find a signal of  $\eta$ -nuclei, perhaps owing to their bigger width than then expected.

In 1994 the experiment was started at the Lebedev Physical Institute 1 GeV electron synchrotron to search on  $\eta$ -meson and nucleus bound states in photoreactions. In 1998 the first experimental data were obtained [13] indicating that a bound state  $\eta$ -meson and nucleus system exists.

#### 4 Experiment at LPI

The present work is aimed detailed discription of the  $\eta$ -meson and nucleus bound state identification method used in [13], the procedure of measurements and handling experimental data.

Using of a photon beam for  $\eta$ -nuclei formation seems to be preferable than using of pion beam due to the next reasons:

- gamma interacts with a nucleon throughout the hole nucleus volume but pion interacts strongly with the superficial nucleons only.
- gamma flux rates are  $10^9 - 10^{10}$  photons per second in the energy range of  $\Delta E \simeq 200$  MeV and that provides adequate high reaction yield.

#### 5 Method of identification of $\eta$ -mesic nuclei

The most important of the work [13] was employing the  $\eta$ -nuclei identification method of  $\pi N$ -pairs registration arising from  $S_{11}(1535)$  resonance decay inside a nucleus [14]. Mechanism of  $\eta$ -nuclei production and decay in photoreactions is schematically shown on the fig.2. First of all incoming photon produces slow  $\eta$ -meson and fast nucleon

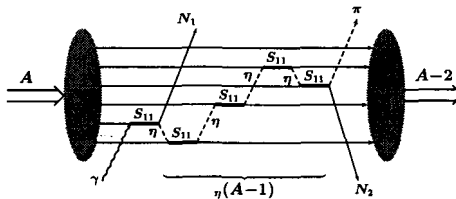


Figure 2: Mechanism of creation and decay of  $\eta$ -mesic nucleus into a  $(\pi N)$ -pair in photoreaction.

that outgoes from nucleus. Then in nuclear medium  $\eta$ -meson passes multifold elastic scattering off nucleons ( $\eta N \rightarrow S_{11} \rightarrow \eta N$ ). At last  $\eta$ -meson annihilates by interaction with a nucleon and  $\pi N$  pair outgoing from nucleus is generated ( $\eta N \rightarrow S_{11} \rightarrow \pi N$ ). The  $S_{11}(1535)$  resonance plays fundamental role in this dynamics. It provides production and annihilation of  $\eta$ -meson and it also clearly designates  $\eta$ -meson coupling in nucleus due to strongly attractive  $\eta N$  interaction. A chain of elastic processes  $\eta N \rightarrow S_{11} \rightarrow \eta N \rightarrow \dots S_{11}$  in nucleus medium is resulted in averaging of  $S_{11}(1535)$  resonance and  $\eta$ -meson characteristics. Fermi motion of nucleons is important for this averaging because  $\eta$ -meson scatters on moving nucleons with different velocities and directions. The most important result of the averaging is isotropy angular distribution of decaying  $S_{11}(1535)$  resonance and small momentum of  $S_{11}(1535)$  resonance. It means directional isotropy of a  $\pi N$ -pair and that average outgoing angle  $\Theta_{\pi N}$

is about  $180^\circ$ . This is base of the  $\eta$ -nuclei identification method suggested in [14]. Method consists in detection and energy measurement of  $\pi N$ -pair components from  $S_{11}$ -resonance decay in nucleus medium. Note that the  $\pi^+ n$  pairs flying transversely to the photon beam cannot be produced via the one step reaction  $\gamma p \rightarrow \pi^+ n$  in the nucleus. It is need to emphasize that using of the bremsstrahlung  $\gamma$ -rays, kinematics of  $\eta$ -meson photoproduction and fermi-motion of nucleons into nuclei are guaranteed of appearing the  $S_{11}$ -resonance into nucleus for all possible its mass or exciting energies.

## 6 Simulation of $\pi N$ -events

Theoretical estimation [15] show that the binding effects lead a full dominance of the reaction mechanism related with the multiple rescattering of  $\eta$  and a formation of the intermediate  $\eta$ -nucleus over a mechanism of non-resonance background production of the  $\pi N$  pairs in the subthreshold invariant-mass region  $\sqrt{S_{\pi N}} < m_\eta + m_N$  of the subprocess  $\eta + N \rightarrow \pi + N$ . A peak in the mass distribution of  $\pi N$  is theoretically expected in this region. This is illustrated in fig.3 where the spectral function  $S(E)$

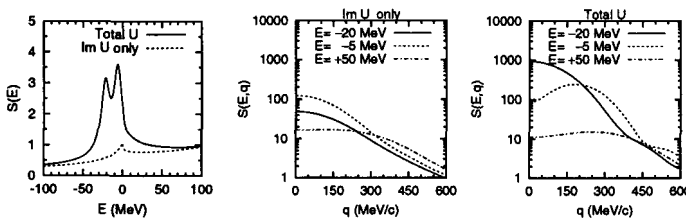
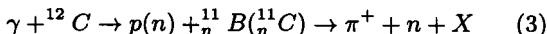


Figure 3: Spectral functions  $S(E)$  and  $S(E, q)$  (in arbitrary units) of the kinetic energy  $E$  and momentum  $q$  of  $\eta$  in the nucleus. They are found with a rectangular-well optical potential simulating the nucleus  $^{12}\text{C}$ . For a comparison results obtained with dropping out the attractive (i.e. real) part of the  $\eta A$  potential  $U$  are also shown.

of the (kinetic) energy  $E$  of  $\eta$  in the nucleus is shown which is proportional to the number of  $\eta N$  collisions which the  $\eta$  experiences when travels through the nucleus. Another spectral function,  $S(E, q)$ , shows a distribution of the produced  $\pi N$  pairs over their total energy ( $E + m_\eta + m_N$ ) and momentum  $q$ . The presence of the  $\eta N$  attractive potential produces strong enhancements in the spectral functions in the energy -momentum region corresponding to the bound  $\eta A$  states.

## 7 Experimental setup and procedure of measurements

The reaction was studied in our work:



in which energy-momentum correlations of  $\pi^+$  and  $n$  take place. We choosed  $(\pi^+ n)$  pair from the four possible  $\pi^+ n, \pi^- p, \pi^0 p, \pi^0 n$  pairs of  $S_{11}(1535)$  resonance decay

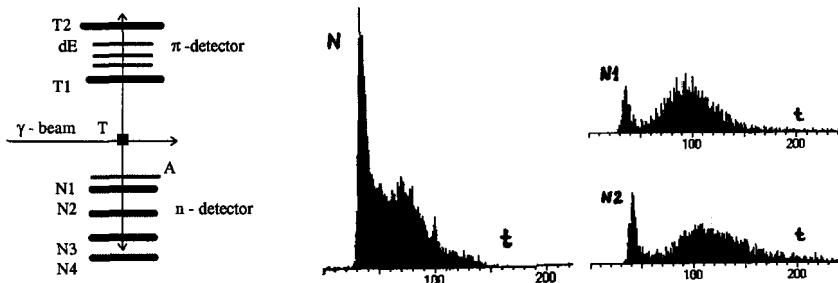


Figure 4: Layout of the experimental setup. Shown also time-of-flight spectra in the  $\pi$  (left) and  $n$  (right) spectrometers.

channels. The choice was determined as follows:

- registration of  $\pi^0$ -decay channels are more expensive due that requires using of  $4\pi$  geometry  $\gamma$ -spectrometer.
- registration of  $\pi^- p$  pair with average proton energy of 100 MeV required using of enough thin targets that reduces expected yield.

At the same time the selected decay channel of  $\pi^+ n$  pair registration provides enough thick target and very simple setup. Average energies of  $\pi n$  pair components are  $\langle E_\pi \rangle = 300$  MeV,  $\langle E_n \rangle = 100$  MeV. The setup was consisted of two arms time of flight (TOF) scintillator spectrometers (fig. 4). The pion spectrometer was contained of two scintillator plates with dimentions  $50 \times 50 \times 2 \text{ cm}^3$  and  $50 \times 50 \times 5 \text{ cm}^3$ . The neutron spectrometer was contained of anti-coincidence scintillator detector with dimentions  $50 \times 50 \times 2 \text{ cm}^3$  and four scintillator detectors with dimentions  $50 \times 50 \times 10 \text{ cm}^3$ . Efficiency of anti-coincidence (veto) detector was equal not more than 90%. Efficiency of neutron detecting was about  $8 \div 10\%$ . Each scintillator detector has four photomultipliers FEU-63 on the edges of scintillator plate which were used for determining of the coordinates passed through detector particle by difference on the time of flight of light on FEU. Accuracy of determining of the coordinaters was about  $\Delta x, \Delta y = \pm 1,5 \text{ cm}$ . Accuracy of determing of the time was about  $\Delta t = \pm 250 \text{ psec}$ . The measurement procedure of three different run types was used for the experiment. For the "calibration" run both spectrometers are positioned into angles of  $\langle \Theta_\pi \rangle = +50^\circ$  and  $\langle \Theta_n \rangle = -50^\circ$  relating to a  $\gamma$ -beam and the top bremsstrahlung beam energy  $E_{\gamma max} = 650$  MeV was used. This position is suitable for a quasi-elastic single pion photoproduction ( $\gamma p \rightarrow \pi^+ n$ ) on nucleus target protons. It was used for final testing of the setup both arms since detected particles energies were close to expected energies of ( $\pi^+ n$ ) pairs arising from the  $S_{11}(1535)$  resonance decay. For the "background" run the angles were  $\langle \Theta_\pi \rangle = +90^\circ$  and  $\langle \Theta_n \rangle = -90^\circ$  and the beam energy was 650 MeV. This position is out of single pion production kinematics, so detected events mostly related to a quasi-elastic double pion photoproduction ( $\gamma N \rightarrow \pi \Delta \rightarrow \pi \pi N$ ).

For the expected  $\eta$ -nuclei excitation "effect + background" run the beam energy of 850 MeV was fixed but the setup position was kept the same as for the "background"

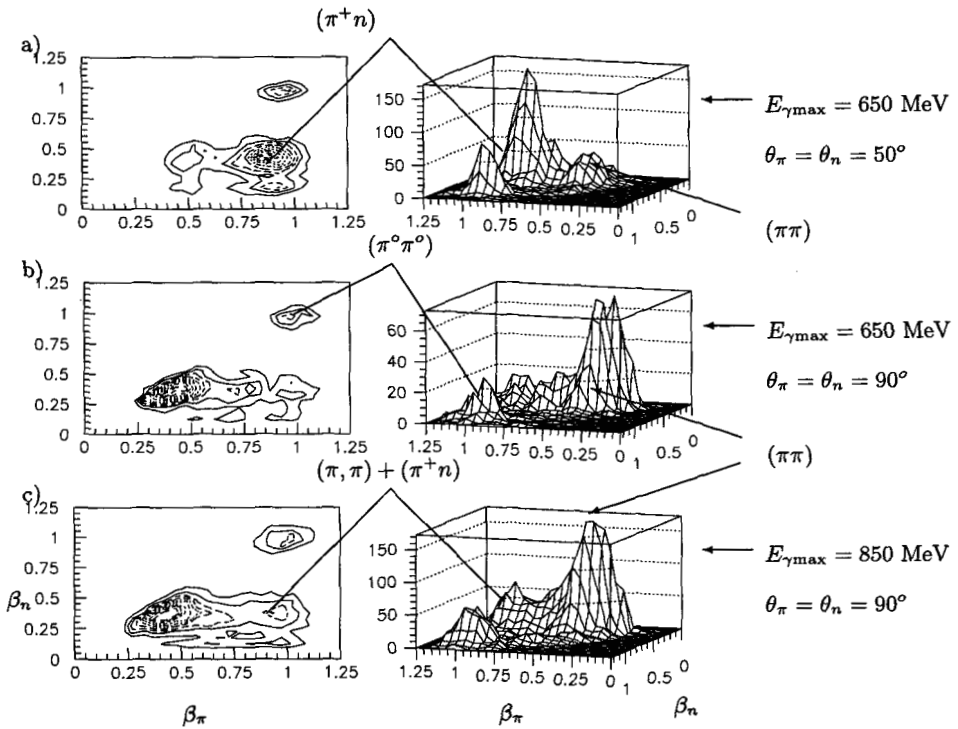


Figure 5: Raw  $\pi^+ n$  event distributions over the particle velocities  $\beta_n$  and  $\beta_\pi$  for the "calibration" (a), "background" (b) and "effect + background" (c) runs.

run.

## 8 Handling of experimental data and results

Fig. 5 shows a two dimensional spectrum of detected particle velocities for all three runs.

The velocities ( $\beta_i = L_i/ct_i$ ) are subject to fluctuations stemming from errors  $\delta t_i$  and  $\delta L_i$  in the time-of-flight  $t_i$  and the flight base  $L_i$  measured in the experiment. Such fluctuations are clearly seen in the case of the relativistic ( $\pi^0 \pi^0$ ) events detecting which have experimentally observed velocities close but not equal to 1. (see fig. 5). Therefore, an experimental  $\beta$ -resolution of the setup can be directly inferred from the fast-fast ( $\pi^0 \pi^0$ ) events. Then, using this information and applying an inverse problem statistical method described in [16], one can unfold the experimental spectrum, obtain a smooth velocity distribution in the physical region  $\beta_i \leq 1$  (fig. 6) and eventually find a distribution of the particles kinetic energies  $E_i = M_i[(1 - \beta_i^2)^{-1/2} - 1]$ . Finding  $E_i$

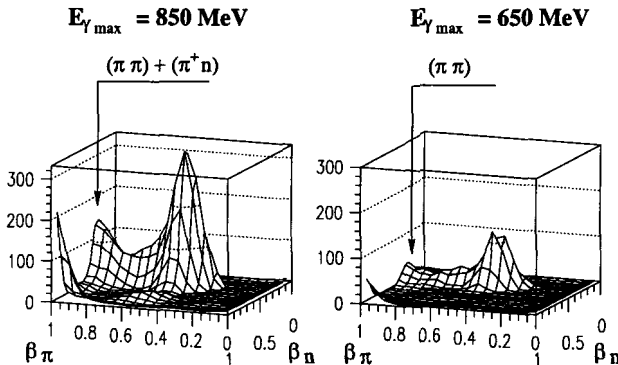


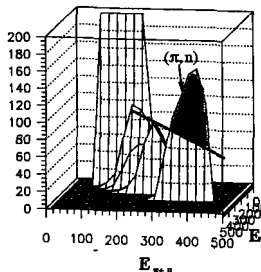
Figure 6: Corrected two dimensional distributions over the velocities  $\beta$  of the  $(\pi^+ n)$  events with the end-point energy of the bremsstrahlung spectrum  $E_{\gamma max} = 850$  and  $650$  MeV.

we introduced corrections related with average energy losses of particles in absorbers and in the detector matter. Fig.7 shows a two dimensional energy distribution of  $(\pi^+ n)$  pairs obtained by a data processing for two runs at beam energies of 650 and 850 MeV. At 650 MeV the figure shows a smooth decrease of a  $\pi^+ n$  pairs number with an energy. At 850 MeV a resonant structure is observable in the region of a  $S_{11}(1535)$  resonance decay. We believe that such a structure is directly related to  $\eta$ -nuclei formation and decay.

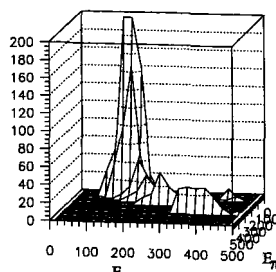
Of the most interest is the distribution of the  $\pi^+ n$  events over their total energy  $E_{tot} = E_n + E_\pi$ . Subtracting a smooth background (fig. 7) we have found a 1-dimensional energy distribution of the  $\pi^+ n$  events presumably coming from bound  $\eta$  decaying in the nucleus (fig. 8). The experimental width of this distribution is about 150 MeV. Its center lies by  $\Delta E \approx 90 \pm 15$  MeV below the position of the  $S_{11}(1535)$  resonance and even below the threshold energy  $m_\eta + m_N = 1485$  MeV, thus indicating a presence of binding effect, for  $S_{11}$ -resonance into nucleus.

## 9 Perspectives

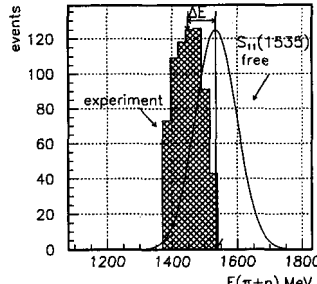
In prospect, studies of the  $\eta$ -mesic nuclei lying at the intersection of the nuclear physics and physics of hadrons promise to bring a new information important for both the fields. The  $\eta$ -mesic nuclei provide a unique possibility to learn interactions of  $\eta$ -mesons with nucleons and nucleon resonances in the nuclear matter. Data of the self energy of  $S_{11}(1535)$  in the medium interpreted in the frame work of the chiral-symmetry models, can shed more light on the problem of masses of free and bound hadrons [17].



$$E_{\gamma\max} = 850 \text{ MeV}$$



$$E_{\gamma\max} = 650 \text{ MeV}$$



$$E_{\gamma\max} = 850 \text{ MeV}$$

Figure 7: Distribution over the total kinetic energy of the  $(\pi^+, n)$  pairs for the "effect + background" run (left panel) and for the "background" run (right panel) obtained after unfolding raw spectra.

Figure 8: Distribution over the total energy of the  $(\pi^+, n)$  pairs after a subtraction of the background. A distribution corresponding to a decay of a free  $S_{11}(1535)$  resonance is shown for a comparison.

## 10 Address of organization

Department of Nuclear Physics and Astrophysics,  
Lebedev Physical Institute Russian Academy of Science,  
117924 Leninski pr, 53, Moscow, Russia  
Tel (007-095)334-01-19; fAX (007-095)334-07-85  
e-mail: gsokol@sgi.lpi.msk.su

## Acknowledgements

This work was supported the Russian Foundation for Basic Research, grant N 99-02-18224.

## References

- [1] J.C. Peng, AIP Conference Proceedings 133, (1985), 255.
- [2] R.S. Bhalerao, L.C. Liu, Phys. Rev. Lett. 54, (1985), 865.
- [3] L.C. Liu, Q. Haider, Phys. Rev. C 34, (1986), 1845.
- [4] M. Batinic et al., Phys. Rev. C 57, (1998), 1004.
- [5] A.M. Green, S. Wycech, Phys. Rev. C 55, (1997) R2167.
- [6] J. Kulpa, S. Wycech, A.M. Green, Preprint nucl-th /9807020.
- [7] J. Berger et al., Phys. Rev. Lett. 61 (1988), 919.
- [8] N. Willis et al., Phys. Lett. B 406, (1997), 14.
- [9] B. Mayer et al., Phys. Rev. C 53, (1996), 2068.

- [10] L. Kondratyuk et al., Proc. Int. Conf. "Mesons and Nuclei at Intermediate Energies", Dubna, 1994 (World Scient. Singapore, Eds. M. Khankhasaev, Zn. Kurmanov, 1995, p.714).
- [11] R.E. Chrien et al., Phys. Rev. Lett. 60 (1988), 2595.
- [12] B.J. Lieb, L.C. Liu, LAMPF Progress Report, LA-11670 PR(1988).
- [13] G.A. Sokol et al., Fizika B 8, (1998), 81.
- [14] G.A. Sokol, V.A. Tryasuchev, Kratk. Soobsch. Fiz. [Sov. Phys. Lebedev Institute Reports] 4 (1991), 23.
- [15] A.I. Lvov "Mesons and Light Nuclei" 98, World Scintific, Eds. J. Adam et al., p. 469; nucl-th/9810054.
- [16] V.P. Pavlyuchenko, Vopr. Atom. Nauki i Tekh., ser. Thekh. Fiz. Eksp. 1/13 (1982), 39.
- [17] T. Hatsuda, T. Kunihiro, Phys. Rep. 247 (1999), 241.

# EXOTIC MESONS IN E852 EXPERIMENT

V.L. Korotkikh <sup>a</sup>

*Scobeltsyn Institute of Nuclear Physics,  
Moscow State University,  
119899 Moscow, Russia*

*Abstract.* The main results of Exotic mesons study in the  $\pi^- p$  interaction at 18GeV/c are presented. Some problems and questions on Exotic meson physics are discussed. The particular attention is given to the discrepancy between theory and experiment and to the interpretation of experimental data.

## 1 Introduction

Not many physicists doubt that other forms of hadronic matter with gluonic degrees of freedom can exist. More than 170 cites are devoted to so called "Non  $q\bar{q}$  candidates" (see PDG [1]). A  $q\bar{q}$  meson with orbital momentum  $l$  and total spin  $s$  has a parity  $P = (-1)^{l+1}$  and a charge conjugation  $C = (-1)^{l+s}$ . This excludes states with  $J^{PC} = 0^{--}, 0^{+-}, 1^{-+}, 2^{+-}$  etc. Resonances with these exotic quantum numbers could be Hybrids (bound state of quark, antiquark and gluon) or multiquark states. The lightest state is expected to be a  $1^{-+}$  state. The last years give the experimental evidence of two such states at mass 1.4 GeV/c<sup>2</sup> and 1.6 GeV/c<sup>2</sup> [2-8].

Experiment E852 was conducted at the Alternating Gradient Synchrotron at BNL (USA) with the Multi-Particle Spectrometer (MPS) augmented by additional detectors. The experimental apparatus [9] is shown in Fig. 1. A Cherenkov tagged  $\pi^-$  beam of momentum 18.3 GeV/c and 30 cm liquid hydrogen target were used. The target was placed at the center of the MPS magnet with a field of 1 Tesla. The target was surrounded by a four-layer cylindrical drift chamber (TCYL), used to trigger on the charged recoil particles, and a 198-element cylindrical thallium-doped cesium iodide array (CsI) to reject events with soft photons. The downstream part of the magnet was equipped with 6 seven-plane drift chamber modules (DM1-6) for charged-particle tracking. A large two-plane drift chamber (TDX4) was added to improve the momentum resolution. Triggering on the multiplicity of forward charged tracks was allowed by three proportional wire chambers (TPX1-3). Photon hermicity was ensured by a window-frame lead scintillator photon veto counter (DEA) in combination with an upstream segmented scintillator counter to identify charged tracks entering DEA. Non-interacting beam and elastic scattering events were rejected with the help of two forward scintillator counters (Beam Veto). Forward photons were detected by a 3000-element lead glass electromagnetic calorimeter (LGD) [10], which was built with an active MSU group participation. The trigger included a requirement on the total energy or invariant mass of all signals registered in the LGD. We don't describe here a Cherenkov counter, which was placed before LGD for distinguishing charged kaons from pions. The data acquisition system typically accepted about 700 events per second.

The experiment took data in 1994 ( $2.47 \times 10^6$  triggers), 1995 ( $8.12 \times 10^6$  triggers), 1997 ( $2.56 \times 10^6$  triggers) and 1998 ( $6.23 \times 10^6$  triggers).

---

<sup>a</sup>e-mail: VLK@LAV01.SINP.MSU.RU.

## 2 Results

### 2.1 Mass and Width of Exotic $J^{PC} = 1^{-+}$ states

Four experimental group are more active in Exotic state study last time. The results on the  $1^{-+}$  exotics of BNL (6 USA and 2 Russian institutions), VES (IHEP, Russia), GAMS (IHEP, Russia) and Crystall Barrel (CERN) are demonstrated in Table 1.

Table 1  
Evidence for  $J^{PC} = 1^{-+}$  exotics

Experiment	Mass (MeV/c <sup>2</sup> )	Width (MeV/c <sup>2</sup> )	Decay mode	Reaction
$\pi_1(1400)$				
BNL-94 [2]	$1370 \pm 16^{+50}_{-30}$	$385 \pm 40^{+65}_{-105}$	$\eta\pi^-$	$\pi^- p \rightarrow \eta\pi^- p$
CBar [3]	$1400 \pm 20 \pm 20$	$310 \pm 50^{+50}_{-30}$	$\eta\pi^-$	$\bar{p}n \rightarrow \pi^-\pi^0\eta$
CBar [4]	$1360 \pm 25$	$220 \pm 90$	$\eta\pi^0$	$\bar{p}p \rightarrow \pi^0\pi^0\eta$
GAMS [5]	1370 fixed	$300 \pm 125$	$\eta\pi^0$	$\pi^- p \rightarrow \eta\pi^0 n$
$\pi_1(1600)$				
BNL [6]	$1593 \pm 8^{+29}_{-47}$	$168 \pm 20^{+160}_{-12}$	$\rho\pi^-$	$\pi^- p \rightarrow \pi^+\pi^-\pi^- p$
BNL [7]	$1597 \pm 10^{+45}_{-10}$	$340 \pm 40 \pm 50$	$\eta'\pi^-$	$\pi^- p \rightarrow \eta'\pi^- p$
VES [8]	$1610 \pm 20$	$290 \pm 30$	$\rho\pi, \eta'\pi, b_1\pi$	$\pi^- Be \rightarrow \rho\pi(\eta'\pi, b_1\pi)X$

The results of the experiments of the various reactions, on the different targets and at the different beam energies are remarkably coincident. It removes such kind of questions as the correct calculation of the different apparatus acceptance, some distinctions of partial wave analysis, the different background contributions. So the evidences of  $1^{-+}$  exotic states at mass 1.4 GeV/c<sup>2</sup> ( $\pi_1(1400)$ ) and 1.6 GeV/c<sup>2</sup> ( $\pi_1(1600)$ ) are very weighable.

### 2.2 Different t-dependence of $\pi_1(1600)$ and $a_2(1320)$

Let's discuss here one of the last BNL-E852 work [7]. The E852 collaboration studied 6040 events of the reaction  $\pi^- p \rightarrow \eta'(959)\pi^- p$  where  $\eta'(959) \rightarrow \eta\pi^+\pi^-$  and  $\eta \rightarrow \gamma\gamma$ . Two significant properties differ  $\eta'\pi^-$  data from  $\eta\pi^-$  [2] and  $\rho\pi^-$  [6] data. The first, the  $P^+$  wave, which includes the exotic  $1^{-+}$  state, is comparable with and even larger than the  $D^+$  wave (fig.2). Remind that in the previous cases the  $P^+$  wave was 2–4% of  $D^+$  wave. So, the contribution of  $\pi_1(1600)$ , according to the mass-dependent fit (solid lines in fig.2c-2d), is larger than 50%.

The second, there is a clear evidence of different t-dependence of the  $P^+$  wave and the  $D^+$  wave (fig.3). A slope parameter of  $a_2(1320)$  t-dependence is about  $b = 5(GeV^2/c^2)^{-1}$  [2]. Here for all waves (fig.2a), where  $P^+$  wave is dominant, it is smaller,  $b = 2.93 \pm 0.02(GeV^2/c^2)^{-1}$ . Fig.3 shows that the ratio of the rate for  $\pi_1(1600)$  to that for  $a_2(1320)$  production changes with  $|t|$ . The production rate of  $a_2(1320)$  decreases faster with  $|t|$  than the production rate of the exotic state.

Since the  $|t|$  distribution is correlated with production mechanism for peripheral production, we conclude that exotic meson production proceeds via a different production mechanism than that for production of the  $q\bar{q}$   $a_2(1320)$  meson. It can be an additional signature of exotic mesons. Besides it is important for the theory, which has to describe the different t-dependence of  $\pi_1(1600)$  and  $a_2(1320)$ .

### 3 Problems and Questions

#### 3.1 Theory and experiment discrepancy

On the other hand the theoretical predictions (see review [11] and numerical cites in it) are indeterminate because the nonperturbative effects are very strong for light mesons. More exact QCD lattice gauge theory (LGT) predicts lightest hybrid masses between  $1.7 \text{ GeV}/c^2$  and  $2.1 \text{ GeV}/c^2$ . The estimations of famous flux-tube model (FTM) are close to LGT. The lightest gluonic hybrid  $J^{PC} = 1^{-+}$  has a mass around  $1.9 \text{ GeV}/c^2$ . It is larger than the experimental values for  $J^{PC} = 1^{-+}$  (Table 1). Other models such as a bag model, a diquark cluster model, QCD sum rules (see cites in [11]) predict the mass of  $1^{-+}$  hybrid in large mass range  $1.4$  to  $2.0 \text{ GeV}/c^2$ . The theoretical predictions are very strong model dependent. So, the first problem is that the theory gives larger value of  $1^{-+}$  meson mass or the accuracy of theoretical predictions is lower than the experimental ones. The second problem is the discrepancy concerning the branching ratio. For example, the FTM predicts that  $J^{PC} = 1^{-+}$  exotic state has a dominant  $b_1\pi$  decay with  $\rho\pi$  weak and  $\eta\pi$  and  $\eta'\pi$  very small decay branching [11]. VES result [12] on the decay branching of  $\pi_1(1600) \rightarrow b_1\pi, \eta'\pi, \rho\pi$  are  $1.0, 1.0 \pm 0.3, 1.6 \pm 0.4$ , correspondingly. Either these three modes are not all due to a hybrid exotic, or our understanding of hybrid decay is inaccurate.

There is another question concerning to the  $1^{-+}$  exotic decay. The state  $\pi_1(1400)$  decays to  $\eta\pi$  and not to  $\eta'\pi$  (Table 1). The state  $\pi_1(1600)$  decays quite invert.  $\pi$  and  $\eta$  belong to an octet and  $\eta'$  is a singlet of SU(3). E.Klempt [13] showed that  $J^{PC} = 1^{-+}$  state cannot decay into two octet pseudoscalar mesons in the limit of flavor symmetry. But it is possible the  $1^{-+}$  octet to decay to  $\eta'\pi$ . So,  $\pi_1(1600)$  may be the octet state and  $\pi_1(1400)$  must be a multiplet of higher order. The easiest choice is a decuplet, which can describe  $(q\bar{q} + q\bar{q})$  states. The decuplet cannot possible be a hybrid: gluonic excitations do not contribute to the flavor. The strange phenomenon that the  $\pi_1(1600)$  does not decay into  $\eta\pi$  thus provides the clue for the interpretation of the  $\pi_1(1400)$  as decuplet state [13]. The  $\eta-\eta'$  mixing can destroy this rule. So, S.U. Chung [14] suggested that  $\pi_1(1400)$  could be a complicated mixture  $(q\bar{q} + \text{gluon})$  hybrid and a  $(q\bar{q} + q\bar{q})$  state .

#### 3.2 Data Interpretation. Background.

Are the exotic mesons the new physical effects or is it a background display? The people ask this question because the data background and exotic signal is comparable in  $\eta\pi^-$ ,  $\rho\pi^-$  and  $\eta\pi^0$  systems. The situation is more better in  $\eta'\pi^-$  system because here the  $\pi_1(1600)$  contribution is comparable with  $a_2(1300)$  [7]. The ground answer is that the PWA is studying an interference effect of weak (say  $P$ -wave) with a strong wave ( $D$ -wave). And the interference contribution is larger than the background. But the questions are remained. Let not to discuss here the incoherent isotropical background  $B_{INC}(m)$ , which adds to common distribution

$$W(m, \Omega) = |D(m)I_D(\Omega) + P(m)I_P(\Omega)|^2 + B_{INC}(m). \quad (1)$$

Here  $m$  is a mass of meson system,  $\Omega$  are particle decay angles.  $I_D(\Omega)$  and  $I_P(\Omega)$  is a wave decay amplitudes. Each wave has its own background:

$$\begin{aligned} D(m) &= f_{BW}^{(D)}(m) + B_{COH}^{(D)}(m); \\ P(m) &= f_{BW}^{(P)}(m) + B_{COH}^{(P)}(m). \end{aligned} \quad (2)$$

The authors [2] used the real and mass independent background  $B_{COH}^{(D)}$  and no background in  $P$ -wave. The description of experimental intensities and relative phase is good with Breit-Wigner (BW) amplitudes  $f_{BW}^{(D)}(m)$  and  $f_{BW}^{(P)}(m)$ . Such simplest model is used in other works [2, 5–8]. The remain questions are the next. Can we describe data without resonant BW in  $P$ -wave, but with the complex background  $B_{COH}^{(D)}$  in  $D$ -wave and with some mass dependence phase of this background? How it could be interpreted? What is the contribution  $B_{COH}^{(P)}(m)$  in the  $P$ -wave and has it the mass dependent phase? Theory could help, but it has to suggest description of two wave simultaneously at least.

The authors [15] suggested a new interpretation of  $\pi_1(1400)$ . They used  $K$ -matrix approach, which connects various channels of reaction. Model has many free parameters. It describes approximately the peak at  $m = 1.4 \text{ GeV}/c^2$  by the interference of a Deck-type background with a real hybrid at  $m = 1.6 \text{ GeV}/c^2$ . But such kind of approach cannot describe the Exotics of the Crystal Barrel experiment (Table 1) in the annihilation  $\bar{p}p$  and  $\bar{p}n$ .

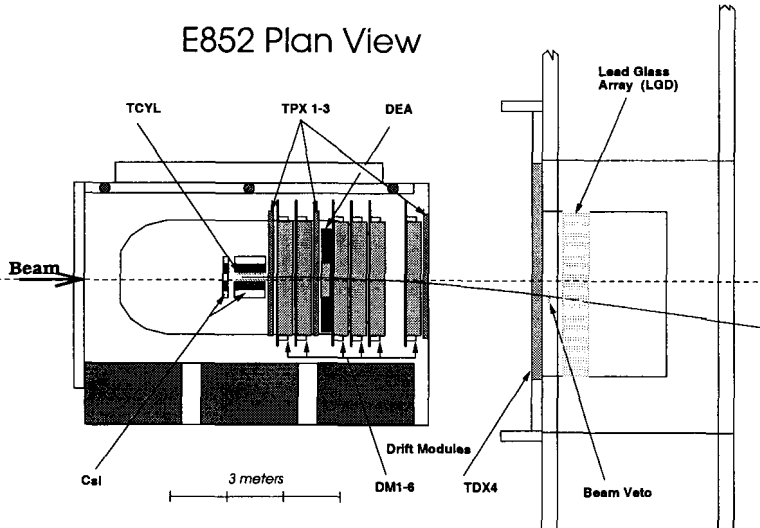


Figure 1

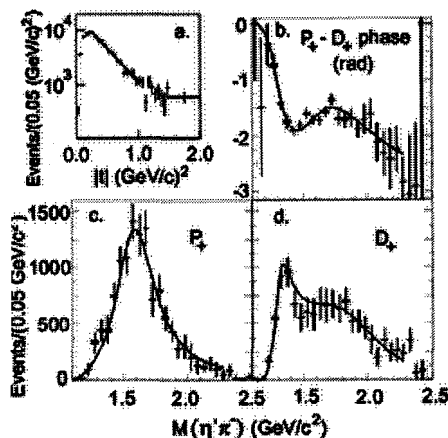


Figure 2

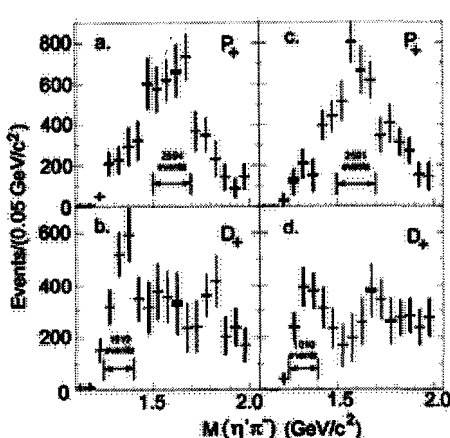


Figure 3

## FIGURES

**Figure 1:** Diagram of the experimental apparatus.

**Figure 2:** E852 results on the reaction  $\pi^- + p \rightarrow \eta'\pi^- + p$  at  $18\text{GeV}/c$ . (a) The acceptance corrected  $|t|$  distribution fitted with the function  $f(t) = \text{const} * e^{-b|t|}$  (solid line). (b),(c),(d) The results of the mass-independent PWA (horizontal lines with error bars) and a mass-dependent fit (solid line). (b) The  $(P_+ - D_+)$  phase difference. (c) The intensity distribution of the  $P_+$  partial wave. (d) The intensity distribution of the  $D_+$  partial wave. The solid curves in (b),(c),(d) show a mass-dependent fit to the  $P^+$  and  $D^+$  waves intensities and  $(P^+ - D^+)$  phase difference. The fit parameters of  $1^{-+}$  resonant state in the  $P^+$  wave for  $\eta'\pi^-$  are in Table.1.

**Figure 3:** a) and b): Mass-independent PWA for  $0.090 < |t| < 0.293 \text{ GeV}^2/c^2$ ; c) and d): Mass-independent PWA for  $0.293 < |t| < 3.0 \text{ GeV}^2/c^2$ . Numbers (a)2594, (c)2591, (b)1610, (d)1010 in figure are the numbers of events in the interval of the  $\pi_1(1600)$  (a,c) and  $a_2(1320)$  (b,d) resonance widths. They don't change with  $|t|$  for  $\pi_1(1600)$  and change for  $a_2(1320)$ .

**References**

- [1] D.E. Groom e. a. (PDG), Eur. Phys. J. C 15 (2000) 1.
- [2] S.U. Chung e. a. (E852), Phys. Rev. D 60 (1999) 092001.
- [3] A. Abele e. a. (CBar), Phys. Lett. B 423 (1998) 175.
- [4] A. Abele e. a. (CBar), Phys. Lett. B 446 (1999) 349.
- [5] S.A. Sadobsky, Nucl. Phys. A 655 (1999) 131c.
- [6] G.S. Adams e. a. (BNL), Phys. Rev. Lett. 81 (1998) 5760.
- [7] E.I. Ivanov e. a. (BNL), Phys. Rev. Lett. 86 (2001) 3977.
- [8] Y.V. Khokhlov, (VES), Nucl. Phys. A 663 (2000) 596.
- [9] S. Teige, e. a. (E852), Phys. Rev. D 59 (1999) 012001.
- [10] R.R. Grittenden e. a. (E852), Nucl. Instrum. Methods Phys. Res., Sect. A 387 (1997) 377.
- [11] T. Barnes, Exotic Mesons, Theory and Experiment, hep-ph/00072296, 1999 and this conference.
- [12] V. Dorofeev, New results from VES, hep-ex/9905002, 1999.
- [13] E. Klempt, Meson Spectroscopy: Glueballs, Hebrids, and  $q\bar{q} + q\bar{q}$  Mesons, hep-ex/0101031, 2001.
- [14] S.U. Chung, On SU(3) Representation of  $q\bar{q} + q\bar{q}$  mesons, BNL-QGS-00-501, 2000.
- [15] A. Donnachie and P. Page, Interpretation of Experimental  $J^{PC}$  Exotic Signal, preprint CEBAF, JLAB-THY-98-20, 1998.

# VERY HIGH MULTIPLICITY PHYSICS

J.Manjavidze <sup>a</sup>, A.Sissakian <sup>b</sup>

*Joint Institute for Nuclear Research, Dubna, Russia*

*Abstract.* We concentrate an attention on the problem: may one attain complete description of the high energy hadron multiple production process. Considering this inelastic reaction as the typical process of energy dissipation (into the produced particle masses), we consider a possibility to use the statistical method. Adaptation of this approach is crucial since only it may allow to describe considered processes completely. Our aim is to formulate the controllable in accelerator experiments condition when such description is available. It will be shown at the end that the statistical approach is actually acceptable, at least in the theoretically very high multiplicity domain.

## 1 Introduction

The physics of multiple production is still under intensive investigations in spite of the almost one century old history. We guess that the reasons of such longevity of the problem consist in following circumstances.

(i) *The mixture of various multiple production mechanisms obscure one another.*

Let us remind that the hadron production process includes two subprocess: quarks production and theirs subsequent confinement into the hadrons. Last process may give influence on the produced particle spectrum, i.e. deform the effective phase space volume into which particles are produced, though the widely used parton-hadron duality [1] assumes that this deformation is negligible on the level of present theory accuracy. Nevertheless, considering production of the very high multiplicity (VHM) state this effect may be neglected: because of the energy-momentum conservation law the energy of particles can not be large and the phase space deformation in this condition is actually negligible.

The quark production process in present theory includes the “short-distance” perturbative QCD mechanism [2], see also [3] and the “large-distance” non-perturbative one [4] of quarks “evaporation” from the vacuum. It should be underlined that the status of existing hadron theory compel us to distinguish this two sizeable overlapped mechanisms, despite a resulting remarkable confusion.

We are able to estimate more or less correctly first mechanism [2, 5], yet exist a well-founded opinion that it can not describe completely existing experimental data.

At the same time, we did not know much about the second, i.e. “large-distance”, mechanism of quarks production despite the built powerful methods [6]. So, for instance, it is offered obviously to take into account a possibility that the strong (color) electric field is able to produce the quark-antiquark pair from the vacuum (it is so called mechanism of Schwinger of the particle production in strong electric fields [4]). But we should assume for this purpose that the strong enough fields are arose in the process of hadron interaction. Just the corresponding mechanism of strong fields formation in form of the tube (i.e. of the “QCD string”) remains quantitatively unclear.

---

<sup>a</sup>e-mail: joseph@nusun.jinr.ru

<sup>b</sup>e-mail: sisakian@jinr.ru

(ii) *Many degrees of freedom are involved in the high energy process of the many-particle states production.*

For instance, the  $n$  particle production amplitude should depend on the  $(3n - 4)$  variables. Presence of the large number of variables is not important if exist enough number of connections between particles. One may introduce the corresponding correlation functions to formulate this question quantitatively. So, the particle number correlation function  $K_k$ ,  $k = 1, 2, \dots$  is defined through the equality [7]:

$$K_k(E) = \left. \frac{\partial^k}{\partial z^k} \ln T(z, E) \right|_{z=1}$$

where  $T(z, E)$  is the sum:

$$T(z, E) = \sum_n z^n \sigma_n(E) / \sigma_{tot}(E).$$

If all  $K_k(E) = 0$  for  $k > 1$  then the multiple production cross section  $\sigma_n(E)$  is described by the Poisson distribution. This reflects production of uncorrelated particles. Therefore, the deviation of  $\ln T(z, s)$  from straight line over  $z$  defines the rate of correlation. It is seen from Fig.1 that  $K_k$  with  $k \geq 1$  are important at high multiplicity and theirs value increase with energy. Notice that positive  $K_k$ ,  $k > 1$ , would lead to widening of the multiplicity distribution.

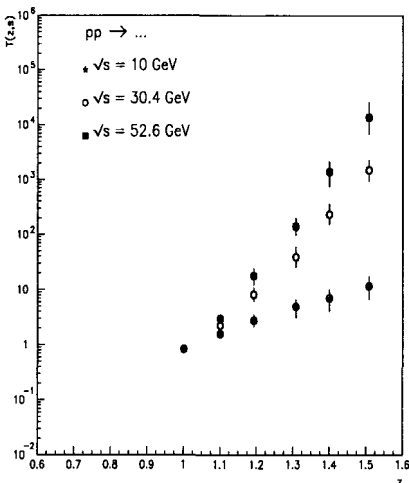


Figure 1: The generating function for various energies.

Moreover, one may simplify picture proposing [8], for instance, that

$$K_k(s) = c_k (C_1(s))^k, \quad (1)$$

with arbitrary constants  $c_k$ . This assumption leads to the well established KNO-scaling. Nevertheless, it is remarkable that the KNO-scaling is broken in the VHM region.

We would like to stress in result that, at all evidence, since  $C_k$  with all  $k > 1$  are important at high energies, it is impossible to formulate the *complete* multiple production theory, which is able to describe the experiment with high enough accuracy. It is noticeable also (a) existence of a few Pomeron-like objects [9], (b) observed uncertainty in the Pomeron intersection  $\alpha_P(0) > 1$  and necessity to include into consideration the multi-Pomeron screening effects [10], (c) existence of the nontrivial intermittency index [11]. For this reason, the existing multiple production models, assigned for not VHM events description, may have only heuristic value and the approach of “generator of events” of PYTHIA-like seems having a perspective.

At the same time, the inelastic channels provide main contribution into the total cross section [12]. For this reason, the sizeable background to the investigated processes<sup>f</sup> by the multiple production process always exist and we should be able to extract it for the reason of practical necessity. Having in mind the idea that no exact general theory of multiple production can be built, the ultimate aim of our investigations is construction of theory in the VHM domain and after that to extend it into the region of less values of the multiplicity.

The common sense suggests to start consideration from mostly simple picture of multiple production. We will start from the model proposed by the couple Ehrenfest [13] to explain why the very high multiplicity (VHM) production processes are so “simple” that we hope to construct the complete theory of them. In Sec.3 production of the VHM will be considered to demonstrate existence of the regime where the thermodynamical description becomes available. Using this experience, we outline in Sec.4 the possible future to be studied.

## 2 The Ehrenfest model

At the beginning of 20-th century couple Ehrenfest had offered the model appealed to help understanding the irreversibility phenomena in the Boltzmann statistical physics (so called *H*- theorem of Boltzmann). Exist a definite opinion that this model adequately resembles the irreversibility phenomenon. The complete description of the model one may find in the book of M.Kac [14].

The “toy” verse of the model is following. Let us consider two box *a* and *b* with  $N_a$  and  $N_b$  numerated ball in them. The total number of balls is  $N$  and the label of balls is run from 1 to  $N$ . The process is realized by *random* choice of the label and putting of the ball with this label into the another box. This operation may be repeated arbitrary times  $M$ . If  $\Delta t$  is the time needed for one operation then  $t = M\Delta t$  is the total time of experiment. One may start from initial condition when all balls are in the box *a*. Then the number of “produced” particles will be  $N_b$ .

The MC simulation of the Ehrenfest model with  $N = 2000$  is shown in Fig.2.

It was shown four independent series of MC simulation. One can see coincidence of this series up to  $t \cong t_0 = 1000$  ( $(N_a - N_b) \cong 750$ ). This means absence of

---

<sup>f</sup>For instance, to the production of Higgs meson

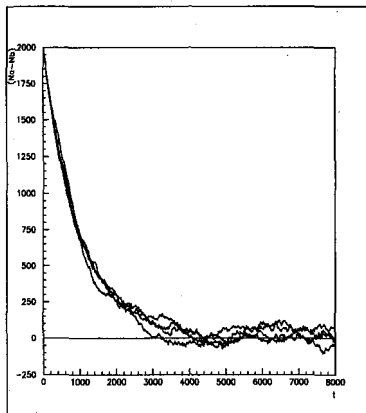


Figure 2:  $(N_a - N_b)$  as function of the ‘time’.

fluctuations on the early stage of the process of decay of the highly nonequilibrium state ( $N_b(t = 0) = 0$  in our example).

It should be noted also fastness of the balls “production” in the box  $b$  on this early stage,  $(N_a - N_b) = 2N_a - t$ , see Fig.2. This means that if the initial state is far from the equilibrium then there is the “flow” toward the equilibrium and its fluctuation, i.e. the “back process”, is small.

So, we can conclude that the highly nonequilibrium processes are “cleared up” from the fluctuations and for this reason they would be extremely simple. The VHM processes, where the initial and final states were far away, are just of this kind.

The number of particles in the  $b$  box  $N_b$  rise with “time”  $t$  and in the time asymptotics the equilibrium culminated: the difference  $(N_a - N_b)$  is fluctuate in vicinity of zero. It is noticeable that the (equilibrium) fluctuations in vicinity of  $(N_a - N_b) = 0$  are comparatively large.

One may ask also what a time is necessary to repeat initial state (with  $N_b = 0$ ) , when all balls return to the box  $a$ . The calculation [14] gives this time  $t_r$  extremely large:

$$\ln t_r \simeq 2N_b = 2000.$$

It is so called Poincare recurrence time. For the time periods  $t \ll t_r$  one should expect that  $N_b$  fluctuates near  $N_a$ .

There is the question: what means the “equilibrium” quantitatively. In the Ehrenfest model the “equilibrium” situation means that the flow of particles from  $a$  to  $b$  is compensated in average by the flow from  $b$  to  $a$ . So, absence of the macroscopic flows of, for instance, particles number is the natural condition of equilibrium. The term “macroscopic” means that the process is considered a sufficiently long time.

To be more quantitative in definition of the notion of “flow”, one may introduce the correlation functions. So, having a particles number macroscopic flow, there should be non-zero correlation among particles number. Indeed, otherwise the flow would not conserved, i.e. would disappeared.

The first particles number correlation function  $K_1$  is the mean multiplicity and it can not be small. The second correlation function  $K_2$  is the dispersion, i.e. defines fluctuation in vicinity of  $K_1$  and also can not be small. So, starting from the three-point correlation  $K_3$  one may hope that the correlations are small. Noting that  $K_2$  is the dispersion, i.e. defines the scale of fluctuations, smallness of macroscopic flow should mean that

$$|K_3|^{2/3} \ll K_2. \quad (1)$$

Fig.3 shows the time dependence of  $K_1$ ,  $K_2$  and  $K_3$ . We would like to note that

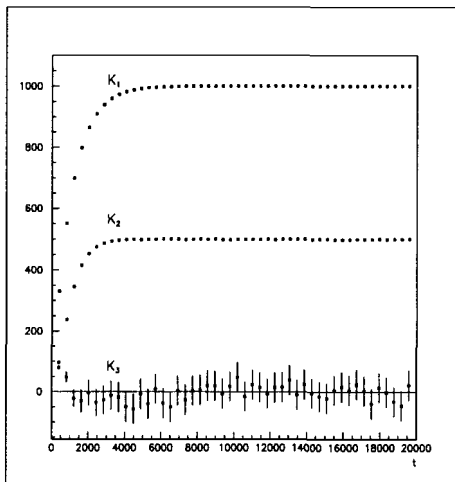


Figure 3: Three correlation function versus ‘time’.

described above condition reflects well known in statistics principle of “vanishing correlations”, introduced by N.Bogolyubov. It means that if we want to use some fluctuating parameter as the measurable quantity then the fluctuations in vicinity of its mean value should be Gaussian. In other words, corresponding higher correlation functions should be small in comparisons with characteristic fluctuations of this parameter.

This figure, where the initial stage,  $t \leq t_0$ , is shown, shows that our interpretation of the Fig.2 is rightful. Indeed, at the initial stage  $|K_3|^{2/3} \geq K_2$  but later the condition (1) is satisfied.

Then, one may consider balls label as the “charge” of particles in the Ehrenfest model. Then one may investigate the equilibrium over charge. The mean value of third “charge” correlation function  $D_3$  in comparison with  $D_2$  is shown on the Fig.5. It is readily seen absence of equilibrium over this “charge”. Therefore, one may expect the equilibrium over one parameter and absence of the equilibrium over other parameters.

In particle physics one may investigate the equilibrium over energy of produced

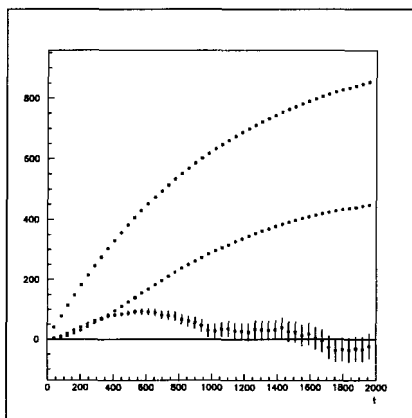


Figure 4: The same as on previous figure in larger scale.

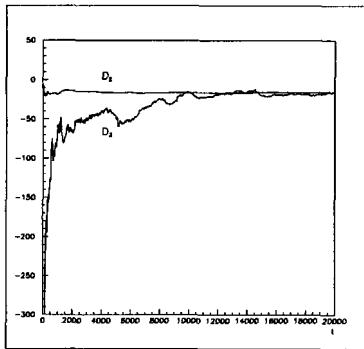


Figure 5: Ball labels correlation functions.

particles. If the mean value of at least third energy correlation function is small:

$$|K_3(E, n)|^{2/3} << K_2(E, n) \quad (2)$$

then one may use the thermal description, i.e. one would have a right to introduce the temperature of *interacting* particles. It is the *S*-matrix analogue of the N.N.Bogolyubov's "correlations relaxation" principle [15]. In this inequality  $E$  is the total energy and  $n$  is the multiplicity. The Ehrenfest model prompts to assume that (2) should be satisfied in the VHM domain.

### 3 Thermodynamical limit

Discussed above tendency to equilibrium is the general law of arbitrary many-particle system (known as the thermodynamics second law) and it should be satisfied independently of the mechanism (model) of particles interactions. And if the model did not satisfy this general law then this model is wrong and should be rejected.

It is not hard to show that the system of massive particles produced in the arbitrary energy collision without fail should come to the thermal equilibrium in the VHM region of multiplicities. The "thermal equilibrium" means that no macroscopic energy flow appears in the considered system (of interacting fields)<sup>d</sup>. Quantitatively this assumes that at least third energy central moment  $K_3$  should be small enough, see (2) [7].

To demonstrate this statement, let us consider the ordinary definition of the topological cross section:

$$\sigma_n(E) = \int d\Omega_n(p) \delta(p_a + p_b - p_1 - p_2 - \dots - p_n) |a_n(p_a, p_b, p_1, \dots, p_n)|^2, \quad (1)$$

where the interaction of particles  $a$  and  $b$  is considered and  $a_n(p_a, p_b, p_1, \dots, p_n)$  is the  $n$ -particle, with momenta  $p_1, p_2, \dots, p_n$ , production amplitude. Integration is performed over all momenta:

$$d\Omega_n(p) = \frac{d^3 p_1}{(2\pi)^3 2\varepsilon(p_1)} \frac{d^3 p_2}{(2\pi)^3 2\varepsilon(p_2)} \dots \frac{d^3 p_n}{(2\pi)^3 2\varepsilon(p_n)}, \quad \varepsilon(p) = \sqrt{p^2 + m^2}. \quad (2)$$

We will assume that  $m \neq 0$ .

The energy-momentum conservation law, fixed by the  $\delta$ -function in (2), defines the boundary value of hadron multiplicity

$$n \leq n_{max}(s) = \sqrt{s}/m, \quad (3)$$

where  $\sqrt{s}$  is the CM total energy,  $m \approx 0.2$  Gev is the characteristic hadron mass. If the energy of fastest particle is  $\varepsilon_{max}$  then the energy conservation law gives:

$$n \geq E/\varepsilon_{max}, \quad (4)$$

where  $E$  is the total energy in the given frame:  $E = \sqrt{s}$  in the CM frame.

---

<sup>d</sup>As was shown in [7], one may imagine the interacting fields system as the ordinary statistical system in some environment to simulate the dissipation, i.e. the process of production.

Let us consider now the ‘thermodynamical limit’, when  $n \rightarrow n_{max}$ . The momenta of produced particles, as follows from (4), becomes small in this limit

$$|p_i| \ll m, \quad i = 1, 2, \dots, n \quad (5)$$

One may estimate the cross sections for such multiplicity [16]:

$$\sigma_n \sim \{(n_{max} - n)\}^n, \quad (6)$$

i.e. the cross sections would be extremely small and for this reason considered limit may have the theoretical interest only.

One may assume that in this limit the multiple production amplitude have the low momentum expansion:

$$a_n(\varepsilon_1, \varepsilon_2, \dots, \varepsilon_n) = a_n^0 + n|p_{max}|a_n^1 + O((n|p_{max}|)^2), \quad (7)$$

where  $a_n^0, a_n^1$  are some constants. One should assume that the momentum of fastest particle  $p_{max}$  should be sufficiently small:

$$np_{max} \rightarrow 0 \quad (8)$$

in our limit to have the possibility neglect momentum dependence of amplitudes<sup>e</sup>.

So, assuming that (8) is satisfied, with  $O(n|p_{max}|)$  accuracy,

$$\sigma_n(E) = |a_n^0|^2 \int d\Omega_n(p) \delta(p_a + p_b - p_1 - p_2 - \dots - p_n). \quad (9)$$

To calculate the remaining integral, one may use following trick. Let us consider the CM frame and write  $\sigma_n$  in the form:

$$\sigma_n(E) = \int \frac{d\beta}{2\pi} e^{\beta E} \rho_n(\beta), \quad (10)$$

where, having (9),

$$\rho_n(\beta) = |a_n^0|^2 \left\{ \int d\omega(\beta) \right\}^n \quad (11)$$

and

$$d\omega(\beta) = \frac{d^3 p e^{-\beta \epsilon(p)}}{(2\pi)^3 2\epsilon(p)}. \quad (12)$$

The integral (10) may be estimated in vicinity of the solution  $\beta_c$  of the equation (of state)

$$E = \frac{\partial}{\partial \beta} \ln \rho_n(\beta). \quad (13)$$

Using (11) it is not hard to find that

$$\beta_c(n, E)m = \frac{3}{2} \frac{n}{n_{max} - n}. \quad (14)$$

---

<sup>e</sup>The identity of particles was assumed deriving decomposition (7).

Using the low temperature expansion:  $\epsilon(p) \simeq m + p^2/2m$ , one may find from (12) that  $\beta p^2/2m \leq 1$  are essential. We can assume therefore that

$$|p|n \leq n(2m/\beta_c)^{1/2} \sim m(n(n_{max} - n))^{1/2} \rightarrow 0, \quad (15)$$

i.e. the assumption (8) may be satisfied with arbitrary high accuracy. Then one can find that

$$\int d\Omega(\beta) = C \frac{e^{-\beta_c m}}{(\beta_c m)^{3/2}} \quad (16)$$

where  $C$  is the insufficient constant.

We can define the energy central moment  $K_l$  by the equality:

$$K_l(n, E) = \frac{\partial}{\partial \beta_c} \ln \rho(\beta_c). \quad (17)$$

It is evident from (13) that

$$K_1(n, E) = E \quad (18)$$

Inserting (16) into (11) it is easy find that:

$$K_2(n, E) = \frac{3n}{2\beta_c^2} = \frac{2(n_{max} - n)^2}{3m^2 n} \rightarrow 0. \quad (19)$$

Noting that  $K_2$  defines dispersion, the result (19) means that fluctuations will rise if  $n \rightarrow n_{max}$ . Nevertheless

$$K_3(n, E) = -\frac{3n}{\beta_c^3}. \quad (20)$$

and

$$(|K_3|^{2/3}/K_2) \sim n^{-1/3} \rightarrow 0. \quad (21)$$

So, the inequality (2) means that we should have:

$$n \gg 1. \quad (22)$$

#### 4 Conclusion

We must to note that the constraint (22) is rather week and the inequality:

$$n|p_{max}| |a_n^1| << |a_n^0| \quad (1)$$

is much more important since it reflects the dynamics. On other hand, our result shows that always exist such values of the multiplicity  $n$  where the multiple production final state may be considered thermodynamically and may be described introducing its temperature. The question can this situation be distinguishable experimentally will be considered later.

We would like to note here that the QCD prediction in the frame leading-log philosophy deny this possibility. For this reason the experimental investigation of the complete thermalization phenomena would have fundamental consequences. First of all, in this case we have a chance to find a complete description of the system produced in the high energy hadron collision.

In addition, production of the equilibrium states on experiment is extremely important since this will allow to use a reach baggage of equilibrium statistical physics. For instance, to observe various collective phenomena (i.e., the phase transition phenomena).

## Acknowledgments

Authors would like to take the opportunity to thank J. A. Budagov, G. A. Chelkov, I. A. Golutvin, P. Jenni, V. G. Kadyshevski, E. A. Kuraev, E. M. Levin, L. N. Lipatov, L. Maiani, V. A. Matveev, V. A. Nikitin, A. G. Olchevski, N. A. Russakovich, V. I. Savrin, A. N. Tavkhelidze, E. Sarkisian, S. Tapprogge, O. I. Zavialov, G. Zinovyev for valuable discussions and important comments. The scientific communications with them on the various stages were important. We acknowledged also to members of the scientific seminars of the V. P. Dzelepov Laboratory of nuclear problems, of the ATLAS experiment community for a number of important discussions. We would like also to thank N. Shubitidze for the help in the formulation of the Monte Carlo simulation programs and for the discussions. One of us (J.M.) was supported in part by Georgian Academy of Sciences.

## References

- [1] V.N.Gribov, Moscow 1 ITEP school, 1, 65 (1973)
- [2] Yu.L.Dokshitser, D.I.Dyakonov and S.I.Troyan, Phys. Rep., 58, 211 (1980)
- [3] V.A.Matveev, R.M.Muradyan and A.N.Tavkhelidze, Lett. Nuovo Cim., 7 (1973) 719;  
S.Brodski and C.Farrar, Phys. Rev. Lett., 31 (1973) 1153
- [4] A.Casher, H.Neuberger and S.Nassinov, Phys. Rev., D20, 179 (1979)
- [5] E.Kuraev, L.Lipatov and V.Fadin, JETP, 44, 443 (1976), G.Altarelli and G.Parisi, Nucl. Phys., B 126, 298 (1977)
- [6] R.Feynman, Phys. Rev. Lett., 23 (1969) 1415;  
A.A.Logunov and M.A.Mestvirishvili, CERN TH/1659;  
A.A.Logunov, M.A.Mestvirishvili, Nguen Van Hieu, Phys. Lett., 25B (1967) 611;  
A.A.Logunov and M.A.Mestvirishvili, CERN, TH-1707, 1973
- [7] J.Manjavidze and A.Sissakian, Phys. Rep., (2001)
- [8] Z.Koba, H.Nielsen and P.Olesen, Nucl. Phys., B40, 317 (1972)
- [9] E.Levin, hep-ph/ 9710546, hep-ph/9808483
- [10] P.V.Landshoff, Nucl.Phys., B 25, 129 (1992)
- [11] E.A.De Wolf, I.M.Dremin and W.Kittel, Phys. Rep., 270, 1 (1996)
- [12] D.E.Groom et al, European Phys. J., C15, 1 (2000)
- [13] P.Ehrenfest and T.Ehrenfest, Phys. Z., 8, 311 (1907),
- [14] M.Kac, in: Probability and Related Topics (Intersciens Publ., London, New York, 1957)
- [15] N.N.Bogolyubov, Studies in Statistical Mechanics, (North-Holland, Amsterdam, 1962)
- [16] E.Byuckling and K.Kajantie, Particles Kinematics (John Wiley and Sons, London, 1973)

## REVIEW OF LEP2 PHYSICS

P.M.Watkins<sup>a</sup>

*School of Physics and Astronomy, University of Birmingham, Edgbaston,  
Birmingham, UK*

*Abstract.* In this short review I summarise some of the current results obtained by the ALEPH, DELPHI, L3 and OPAL experiments using data taken at LEP2 at collision energies between 160 and 209 GeV.

### 1 Introduction

This is a review of results obtained by the ALEPH, DELPHI, L3 and OPAL experiments using data recorded at energies above the threshold for WW production between 1996 and 2000 at the LEP2 accelerator at CERN. There were other talks at this conference describing LEP2 searches for Higgs and SUSY particles, anomalous gauge couplings and single top production. Recent results on fermion-pair production, W and Z pair production and measurement of the W boson mass form the main topics for this talk. A few results on other topics have been included to illustrate the wide range of physics that can be studied with the LEP2 data. The combined results from all four LEP experiments were presented where available. Most of these results were preliminary and had been prepared for the 2001 summer conferences. At LEP2 the collision energy was regularly increased up to a maximum of 209 GeV. In the last year of data-taking the delivered luminosity was very high even though the LEP design energy had been exceeded. This was an outstanding achievement by the LEP machine group.

### 2 Fermion-pair production

In fermion-pair production at collision energies above the Z mass, initial state radiation plays an important role. These final states include non-radiative events at the full collision energy with back to back fermions. There are also radiative collisions at a range of lower collision energies including a radiative return peak due to the large cross-section at the Z mass. The value of the collision energy is reconstructed from the measured angles of the final state fermions or from kinematic fits to the measured final states.

The fermion-pair channels are detected with high efficiency and relatively low background which is predominantly from four fermion and two photon processes. Precise measurement of the cross-sections and angular distributions for all fermion-pair channels have been made at all LEP2 energies by the four experiments and compared to the predictions of the Standard Model (SM). This comparison for the hadronic and lepton-pair cross-sections is shown in Fig. 1. There is generally good agreement between the data and the predictions. The measured forward-backward asymmetries of lepton pairs also shows good agreement with SM predictions up to the highest LEP2 energy as shown in Fig. 1.

---

<sup>a</sup>e-mail: pmw@hep.ph.bham.ac.uk

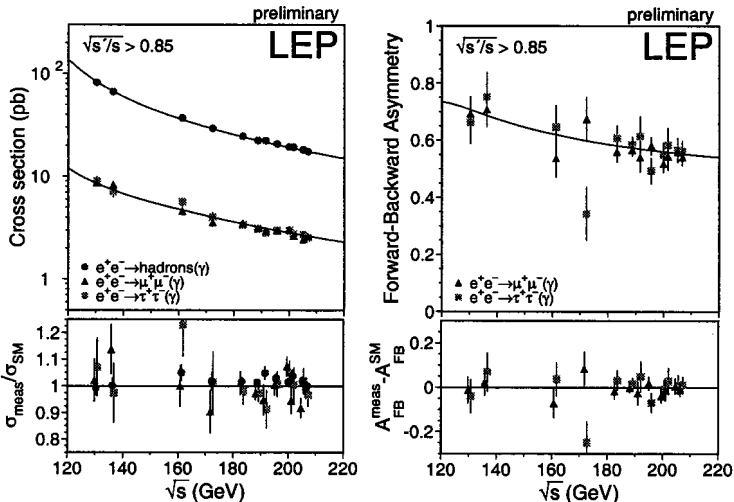


Figure 1: (a) LEP averaged cross-sections for  $q\bar{q}$ ,  $\mu^+\mu^-$  and  $\tau^+\tau^-$  final states as a function of energy [1]. (b) LEP averaged forward-backward asymmetries for  $\mu^+\mu^-$  and  $\tau^+\tau^-$  as a function of energy [1]. The curves on both figures are SM predictions.

Many possible contributions to physics beyond the Standard Model eg extra Z bosons, lepto-quarks, contact interactions and hidden dimensions could modify these two-fermion cross-sections and angular distributions. The level of the agreement between the data and the SM predictions can therefore be used to place strong constraints on some of these models. The LEP-wide constraints on additional Z bosons produce lower mass limits which range from 0.45 to 2.1 TeV and lepto-quark lower mass limits range from 0.17 to 1.1 TeV. Limits extracted from the LEP2 data for the smallest allowed energy scale for various forms of new lepton-lepton contact interactions are summarised in Fig. 2. These limits, which depend on the type of coupling assumed, are typically around 10 TeV or above.

### 3 QED, QCD and two photon physics

Many new QED, QCD and two photon measurements have been made at LEP2 and a few examples are included here. The angular distribution of photons from the reaction  $e^+e^- \rightarrow \gamma\gamma(\gamma)$  can be predicted from QED calculations and compared to the experimental measurements as shown in Fig. 3. The difference between the predicted and measured distribution has been parameterised in terms of a cutoff scale  $\Lambda$  which defines the energy scale at which a new interaction may contribute. The lower limit on  $\Lambda$  from the data currently exceeds 300 GeV for a single LEP experiment.

At each of the LEP energies the jet production rates and event shape variables in multi-hadronic events have been used to determine  $\alpha_s$ . These results, together

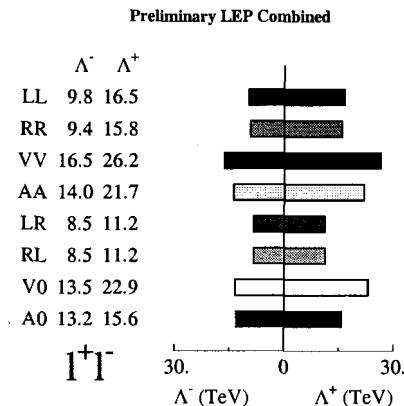


Figure 2: Contact interaction lepton-lepton limits from the combined LEP results [1].

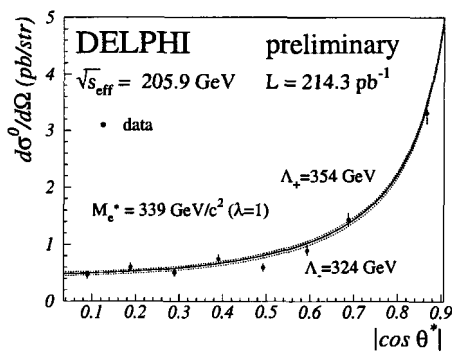


Figure 3: Two photon angular distribution from the DELPHI experiment

with others from lower energies, are shown in Fig. 4 and show clear evidence for the running of  $\alpha_s$  with energy. The observed variation is in very good agreement with the predictions of NLLA QCD which is also shown on this figure.

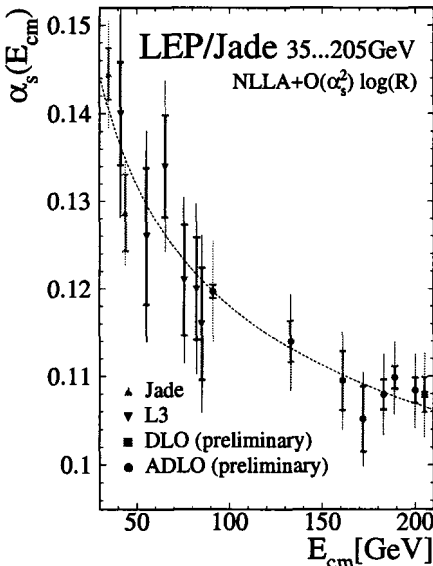


Figure 4: Variation of  $\alpha_s$  with energy as measured by the listed experiments [2] together with the QCD predictions in the Next to Leading Log approximation (NLLA) at second order in  $\alpha_s$ .

Two photon processes, where the two photons are radiated by the beam particles, produce the highest cross-sections at LEP2. Measurements allow the extraction of photon structure functions as a function of  $x$  and  $Q^2$  and these are summarised in Fig. 5. These data show clear evidence for scaling violation consistent with the leading order predictions of QCD [4].

#### 4 WW and ZZ production

A primary reason for the construction of LEP2 was to allow a precise measurement of the W boson properties, particularly its mass, which is a crucial input to the SM precision electroweak fits. The cross-section and production and decay angular distributions of W pairs also provide a direct measurement of the triple gauge coupling which is predicted by the SM. At LEP2  $W^+W^-$  pairs are expected to be produced by a mixture of s channel  $\gamma/Z$  and t channel  $\nu$  exchange diagrams. The W bosons can decay into a charged lepton and a  $\nu$  or a quark and antiquark with decay branching ratios of 1/3 and 2/3 respectively. This leads to three classes of  $W^+W^-$  final states

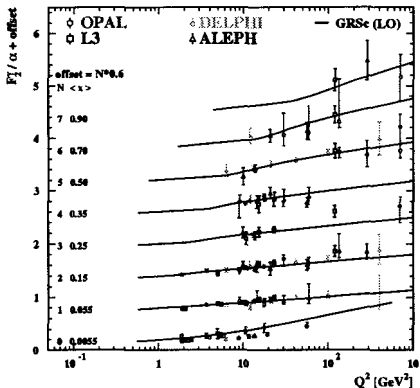


Figure 5: The photon structure function as measured by the LEP experiments [3] as a function of  $Q^2$  for various  $x$  ranges together with the leading order QCD predictions [4].

being observed in the detectors namely fully leptonic (1/9), fully hadronic (4/9) and finally a leptonic and hadronic decay (4/9). The detection efficiency and background levels for these events vary somewhat for the different lepton species and between the different experiments. However the typical detection efficiency exceeds 80 % and increases to 90 % for events where at least one of the W decays is leptonic. The fully leptonic channel is very pure but because of the two missing neutrinos and its low production rate it has only limited impact on the W mass measurement.

The events with fully hadronic final states contain at least four jets and there can be pairing ambiguities in the reconstruction of the two W bosons. In addition as the two W bosons decay when they are separated by much less than one fermi, there is the possibility of final state interactions between the decay products of different W bosons. These colour reconnection and Bose-Einstein effects could in principle influence the W mass measurement and need to be carefully studied. The  $W^+W^-$  events with one hadronic and one leptonic decay are the cleanest and most useful sample. In this case the single missing neutrino can be reconstructed from energy and momentum conservation in a constrained fit.

The measured WW cross-section as a function of energy is shown in Fig. 6 together with the predictions of the RacoonWW [5] and YFSWW [6] Monte Carlo programmes. These include full order  $\alpha$  corrections to the W pair production diagrams. The other curves on this figure, which are clearly excluded by the data, indicate the dramatic increase in the cross-section that would be predicted if the contributions from various diagrams with triple gauge couplings were removed. For the WW cross-section measurement the W decay branching ratios from the SM have been assumed. However these can also be determined from the LEP data and these measurements,

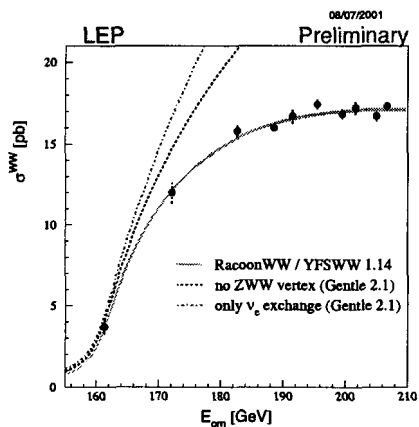


Figure 6: The LEP averaged WW cross-section as a function of energy [7]. The solid curve shows the SM prediction [5] [6]. The other curves show the effect of removing various triple gauge coupling contributions.

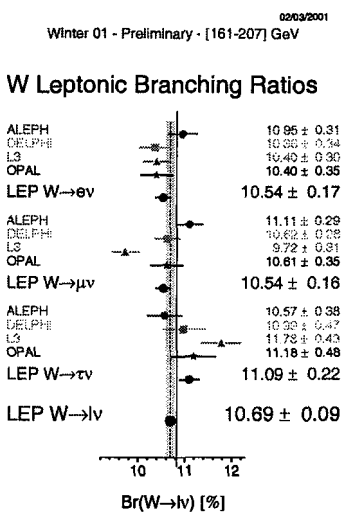


Figure 7: The W boson leptonic branching ratio measurements from the four LEP experiments [7].

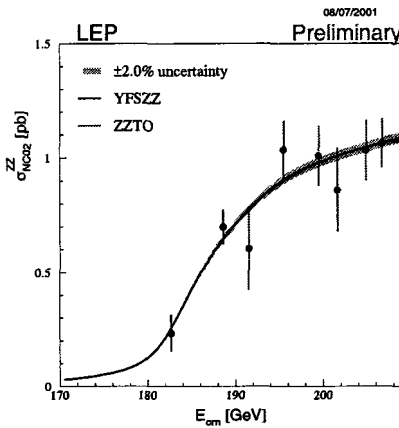


Figure 8: The LEP averaged ZZ cross-section as a function of energy [7]. The curves indicate the range of current SM predictions [8].

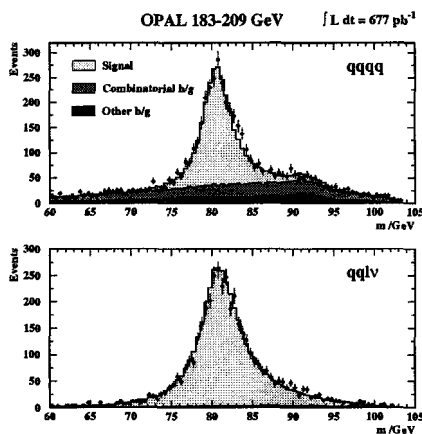


Figure 9: (a) Mass plot for preliminary data on qq pairs from the qqqq channel in the OPAL experiment. (b) Corresponding plot for qq pairs from the qqlv channel. In both plots the fitted curve is superimposed and the predicted background contributions are indicated.

which are more precise than current measurements from hadron colliders, are shown in Fig. 7. These agree well with the SM predictions.

The CKM matrix element  $V_{cs}$ , which is poorly known, has been directly measured at LEP from W decays into hadrons by using charm tagging of the jets. A much more precise indirect measurement of  $V_{cs}$  can be extracted from the LEP2 data by measuring the ratio of W decays to hadrons and leptons and by assuming the PDG values for all other CKM elements. From this approach a value of  $V_{cs} = 0.996 \pm 0.013$  has been obtained without any direct unitarity assumptions.

The measured W decay angular distributions have also been used to verify the SM predictions for the helicity fractions and the production rate of longitudinally polarised W bosons. The most important measurements of triple gauge couplings are made by measuring the production and decay properties of the W boson in WW production as described in a separate talk at this conference. However the production rate for single W bosons can also be used to constrain the charged triple gauge coupling as the incoming beams can exchange a W and a photon which then interact to produce the detected W boson. The LEP combined cross-section for single W production has a large statistical error but it agrees with the SM prediction.

At the higher LEP2 energies the production of Z pairs is also possible although the cross-section is much lower than for W pairs. These events are more difficult to isolate than  $W^+W^-$  events but the use of neural networks and likelihood methods allow a sample of such events to be selected. The ZZ production proceeds via both t channel electron exchange and s channel neutral triple gauge coupling diagrams. The energy dependence and size of this cross-section is well reproduced by theoretical predictions as shown in Fig. 8 .

## 5 W mass measurement

The first W mass measurements at LEP2 were extracted by measuring the cross-section for W pair production close to threshold. Although the statistics were very limited this yielded a W mass value of  $80.40 \pm 0.22$  GeV which was the most precise measurement available at that time. At higher LEP2 energies the W mass is extracted from direct reconstruction of the events. Some examples of the observed quark-quark mass distributions for the qqqq and qql $\nu$  final states are shown in Fig. 9. For the qqqq channel the predicted contributions from background processes and events where the wrong jet pairing has been chosen are also indicated on the plot. The background in the qqln $\nu$  channel is also shown but it is negligible.

Various methods are adopted by the collaborations to extract the W mass but all involve the use of constrained kinematic fits to improve the mass resolution. The W mass can then be calculated from direct Breit-Wigner fits or by performing likelihood or convolution fits to the mass distribution. These fits all require input from the Monte Carlo for the detector resolution but in the convolution fits the dependence on other features of the Monte Carlo is reduced. The preliminary results for the W mass and width extracted by the four LEP experiments are shown in Fig. 10.

These LEP2 results for the W mass are used to make a comparison between the direct and indirect measurements of the W and top quark masses in Fig. 11. These results are consistent with each other and favour a low mass Higgs boson within the

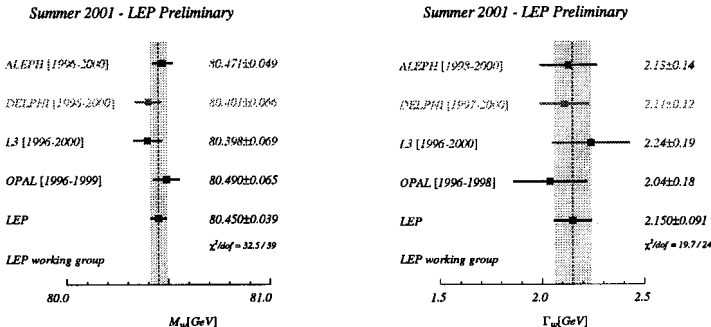


Figure 10: (a) The W mass as measured by the four LEP experiments [9]. (b) The W width as measured by the four LEP experiments.

context of the SM. The W mass measurements are also used together with many other precision electroweak measurements, performed at LEP and by SLD, CDF, D0, NuTeV and others as a function of the Higgs-boson mass assuming the Standard Model. The  $\Delta\chi^2$  curve derived from these precision electroweak measurements is shown in Fig. 11 and this favours a relatively low mass Higgs. Some of this low mass region, up to a mass of 115 GeV, has been excluded by direct searches at LEP2 as also shown on this figure. As LEP running has now been completed the search for the Higgs boson at higher masses is being continued at FNAL and the LHC.

The LEP experiments continue to make a number of precise measurements which provide direct experimental tests of the predicted radiative corrections of the Standard Model. Currently much effort is going into converting the mainly preliminary LEP2 results presented here into final publications. The excellent working relationship between the accelerator staff and the experimental collaborations has contributed significantly to the final precision of these measurements. The LEP combined working groups have also been a very successful way of optimising the physics extracted from the many different measurements performed by the four experiments. It has been a pleasure to be a part of this venture over the past decade and more.

## Acknowledgments

I am very grateful to many colleagues from the LEP experiments and the LEP combined working groups for their help in preparing this talk. I would particularly like to thank Alan and Nigel Watson for their help. Finally I would like to thank the organisers for an interesting conference and a very enjoyable stay in Moscow.

## References

- [1] LEPEWWG  $f\bar{f}$  subgroup, note LEP2FF/01-02

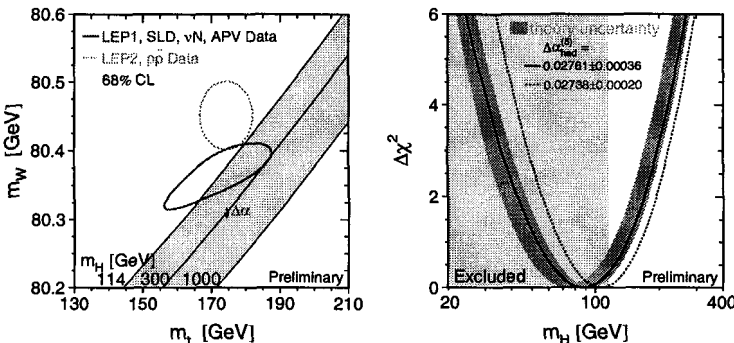


Figure 11: (a) A comparison between the direct and indirect measurements of the W and top quark masses. The predictions of the SM for a range of Higgs boson masses are also shown. (b) The  $\Delta\chi^2$  curve derived from the precision electroweak measurements, performed at LEP and by SLD, CDF, D0, NuTeV and others, as a function of the Higgs-boson mass, assuming the Standard Model. The shaded band shows an estimate of the theoretical uncertainty. The light shaded region has been excluded by direct searches.

- [2] The combined LEPQCD working group web page at CERN  
<http://lepqcd.web.cern.ch/LEPQCD/annihilations>
- [3] The combined LEP two photon working group web page at CERN  
[http://lepqcd.web.cern.ch/LEPQCD/gamma\\_gamma/Welcome.html](http://lepqcd.web.cern.ch/LEPQCD/gamma_gamma/Welcome.html)
- [4] M. Gluck, E. Reya, and I. Schienbein, Phys. Rev. **D** 60, 054019 (1999), Erratum, Phys. Rev. **D** 62, 019902 (2000).
- [5] A.Denner, S.Dittmaier, M.Roth and D.Wackerlo, Nucl Phys **B** 587 (2000) 67
- [6] S.Jadach et al., Comput. Phys. Commun. **140** (2001) 432
- [7] The LEP collaborations and the LEP WW Working Group, note LEPEWWG/XSEC/2001-03
- [8] S.Jadach, W.Placzek and B.F.L.Ward Phys Rev **D** 56 (1997) 6939; G.Passarino, in hep-ph/0005309
- [9] The LEP collaborations and the LEP W Working Group, note LEPEWWG/MASS/2001-02

# FLAVOUR INDEPENDENT HIGGS SEARCHES AT LEP-2

P.Bambade <sup>a</sup>

LAL, Université Paris-Sud, Bâtiment 200, B.P. 34, F-91898 Orsay Cédex, France

*Abstract.* Searches for hadronically decaying neutral Higgs bosons, conducted at LEP-2 in the framework of the Standard and Minimal SuperSymmetric Models, strongly exploit the information from its  $b\bar{b}$  decays. However, although this signature dominates the accessible mass range in these models, there are special cases of extended models with suppressed  $h \rightarrow b\bar{b}$  couplings. Recently, complementary searches, performed without relying on  $b$ -quark identification, have enabled to reduce the model-dependence of the results, for both  $hZ$  and  $hA$  production mechanisms. The preliminary results obtained by the four LEP collaborations are presented. No evidence for a signal was found. *Flavour independent* bounds on Higgs boson production are given, and used to constrain specific scenarios.

## 1 Introduction

There are extensions of the Standard Model (SM) in which Higgs bosons have suppressed couplings into  $b$ -quarks. This can occur for specific parameters of the Two Higgs Doublet Model (2HDM) [1], or of the Minimal SuperSymmetric Model (MSSM) [2], as well as for some composite models [3]. Searches for SM and MSSM neutral Higgs bosons, produced through  $e^+e^- \rightarrow hZ, hA$  processes, would have reduced sensitivities in such cases, because of their strong reliance on the identification of  $b$ -quarks from the Higgs boson decays to maximize the separating power [4–6]. It is very important to also cover such scenarios experimentally, with dedicated searches not exploiting the *b-tagging*, to reduce the model-dependence of the results.

All LEP collaborations have developed versions of their Higgs searches without *b*-tagging in recent years. The data collected in 1998, 1999 and 2000, at centre-of-mass energies near 189 GeV, and in the ranges 192–202 and 204–208 GeV, respectively, were analysed. No evidence for a signal was found. Results were given in terms of cross-section or mass exclusions, independent of the flavour of the Higgs boson decays [7–10, 13, 14], and were also combined with results from other Higgs boson searches to constrain specific models [6, 11, 12, 15].

In this report, the main features of these new analyses are described, highlighting aspects specific to the flavour independent hypothesis. The obtained results are presented, and model independent interpretations, as well as applications to specific scenarios, are discussed.

## 2 Search for $hZ$ production

### 2.1 Analysis

The data collected by the four LEP experiments at the highest energies were used to search for  $hZ$  production in the flavour independent hypothesis. The analysis methods were adapted from existing LEP-2 searches or measurements performed in

---

<sup>a</sup>e-mail: bambade@lal.in2p3.fr

the four-jet ( $q\bar{q}q\bar{q}$ ), missing energy ( $q\bar{q}\nu\bar{\nu}$ ) and leptonic ( $q\bar{q}l^+l^-$ ) topologies<sup>b</sup>. In all channels except four-jets, events were selected exactly, or almost exactly, as in the corresponding SM Higgs boson search, removing the  $b$ -tagging from the final selection. In the four-jet channel, on the other hand, all collaborations used dedicated test-mass dependent selections, to exploit maximally the specific kinematic features and the mass reconstruction. This was necessary to reduce dominant backgrounds from  $WW$  and  $ZZ$  production and from QCD multi-jet processes, without using  $b$ -tagging information.

ALEPH [7] used the data collected in 1998–2000, clustered in seven energy bins in the last year. In the four-jet channel, a dedicated search based on a neural network method was developed. The compatibility of the data with the signal hypothesis was tested in the Higgs boson mass range from 60 up to 115 GeV/c<sup>2</sup>, in 5 GeV/c<sup>2</sup> steps, interpolating the final discriminant variable for intermediate values. DELPHI [8] used the data collected in 1999–2000, clustered in two energy bins in the last year. The compatibility of the data with the signal hypothesis was tested in the Higgs boson mass range from 50 up to 110 GeV/c<sup>2</sup>, in 5 GeV/c<sup>2</sup> steps. A small reduction in performance was introduced in the final evaluation, between each test mass, to account for mass resolution effects. L3 [9] used the data collected in 1999–2000, clustered in five energy bins in the last year. OPAL [10] used the data collected in 1998–2000, clustered in a single energy bin in the last year. In L3, and for the four-jet channel in OPAL, test-masses were chosen in the Higgs boson mass range from 60 up to 115 GeV/c<sup>2</sup>, in 1 GeV/c<sup>2</sup> steps. All topologies corresponding to possible decay products of the  $Z$  boson were analysed by all collaborations, except, in the case of DELPHI,  $q\bar{q}\tau^+\tau^-$ .

Even though  $b$ -tagging was not used, every experiment did find some variation in performance between the possible decay products of the Higgs boson, arising from differences in mass resolution and jet structure<sup>c</sup>. In order to enable quoting genuinely flavour independent results, the samples used for the final evaluation were therefore conservatively chosen as those which gave the weakest expected performance in each channel, and for each value of the Higgs boson mass.

In general, because these searches were developed recently, they were up to now less optimised, slightly less comprehensive, and used more simplifying assumptions to extract the results than corresponding searches for SM or MSSM Higgs bosons. Also, although potential biases to the results were studied by individual experiments, there was no consideration yet of systematic effects in the common evaluation. All results presented here are preliminary.

## 2.2 Results

No evidence for a signal was found in any of the topologies analysed by the four collaborations. The information from all topologies and collaborations was combined to compute flavour independent bounds on  $hZ$  production as a function of the Higgs bo-

---

<sup>b</sup>Throughout the paper, the notation  $q$  stands for both primary quarks or gluons produced in Higgs boson decays.

<sup>c</sup>For instance, Higgs boson decays into gluon pairs have larger multiplicities, but at the same time coarser dijet mass resolution, than decays into light quarks.

son mass [14]. The standard statistical procedures based on the Modified Frequentist approach and using the likelihood ratio technique [16] were applied as in the other combinations performed by the LEP working group for Higgs boson searches [5]. The observed and expected confidence levels for the signal,  $CL_s$ , and background-only,  $CL_b$  hypotheses, obtained for each of the four collaborations, using two independent implementations of the combination software [17,18], were very consistent with results obtained within each collaboration. The calculations of the observed and expected 95% CL lower limits on the mass of the Higgs boson, assuming production cross-sections equal to those in the SM and 100 % hadronically decaying Higgs bosons, are shown from one of the implementations [18] in Table 1, together with the combined results using the data from all four collaborations<sup>d</sup>. The combined observed and median expected limits were 112.9 and 113.0  $\text{GeV}/c^2$ , respectively.

Collaboration	Obs. limit ( $\text{GeV}/c^2$ )	Exp. median limit ( $\text{GeV}/c^2$ )
ALEPH	109.3	108.4
DELPHI	109.6	108.8
L3	111.6	109.3
OPAL	109.4	108.5
<b>LEP</b>	<b>112.9</b>	<b>113.0</b>

Table 1: Flavour independent observed and expected 95% CL lower limits on the mass of the Higgs boson, assuming production cross-sections equal to those in the SM and 100 % hadronically decaying Higgs bosons. Systematic uncertainties were not included.

The confidence levels  $CL_s$  and  $CL_b$  obtained from the full combination in the signal and background-only hypotheses are shown as a function of the mass in Figure 1. Good overall agreement can be seen between the observation and expectation in the absence of a signal. The slightly lower values for  $1 - CL_b$  for masses below 80  $\text{GeV}/c^2$  reflect an excess of data in this region, and may be the result of some systematic effect. An investigation is in progress. A 5 sigma discovery corresponds to a value of  $1 - CL_b$  of  $5.7 \cdot 10^{-7}$ , as indicated by the horizontal line. The sensitivity for such a discovery is reached for an assumed Higgs boson mass of 107  $\text{GeV}/c^2$ , when this line is intersected by the expected median confidence in the background-only hypothesis.

Upper limits on the production cross-section as a function of mass were also determined for each individual collaboration, and combined using the data from all four collaborations. Typically, cross-sections larger than about 10-60 % of the expected SM value were excluded at 95% CL in the mass range 60-100  $\text{GeV}/c^2$ , by each collaboration alone. The combined exclusion from the four collaborations is shown as a function of the mass in Figure 2. In the same mass range, it is possible to exclude cross-sections larger than about a few to 30 % of the expected SM value with the full LEP-2 data set. Good overall agreement between the observation and expectation

<sup>d</sup>Because the evaluations performed did not include systematic uncertainties, the values obtained differ in some cases from those quoted by the individual collaborations which included them in their evaluations. This is most notably the case for the OPAL results [10].

# ADLO PRELIMINARY

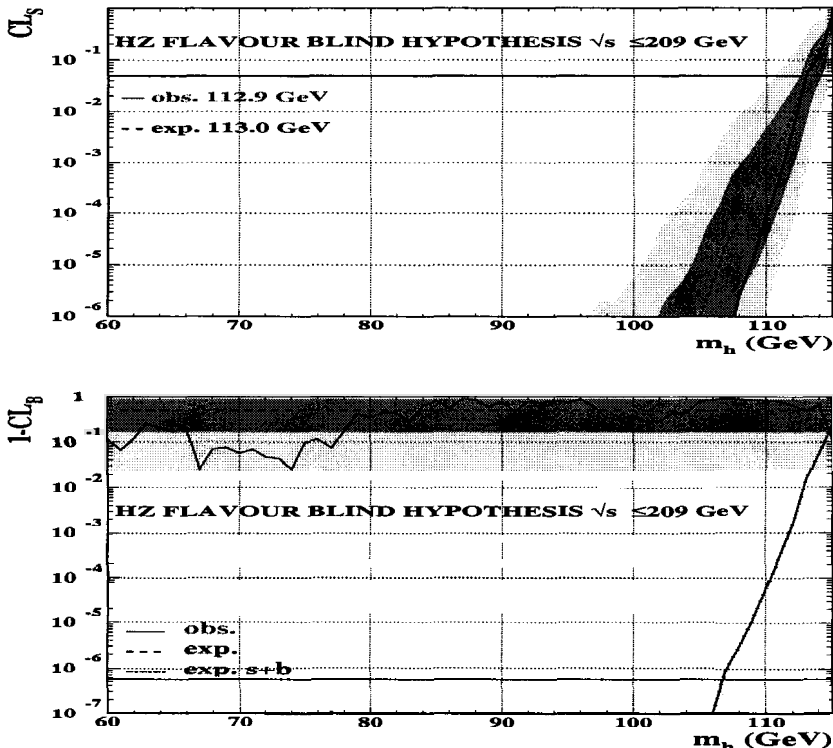


Figure 1: Combined LEP confidence levels as a function of the Higgs boson mass in the flavour independent hypothesis, assuming production cross-sections equal to those in the SM and 100 % hadronically decaying Higgs bosons. The confidence levels for the signal and background-only hypotheses are shown in the upper and lower plots, respectively. The curves are the observed (solid) and expected median (dashed) confidences from background-only experiments, and the bands are the corresponding 68.3 and 95 % confidence intervals. In the lower plot, the dot-dashed line shows the expected median confidence from experiments including an expected signal of mass given in abscissa.

can be seen also here, except in the lower mass range, where the weaker observed limit is resulting from some excesses of data in this region, as was already noted.

### 3 Search for $hA$ production

The search for  $hA$  production used hadronic final states [8, 11, 12], associated or not with  $\tau^+\tau^-$  leptons [13]. No signal was found. Flavour independent results were

# ADLO PRELIMINARY

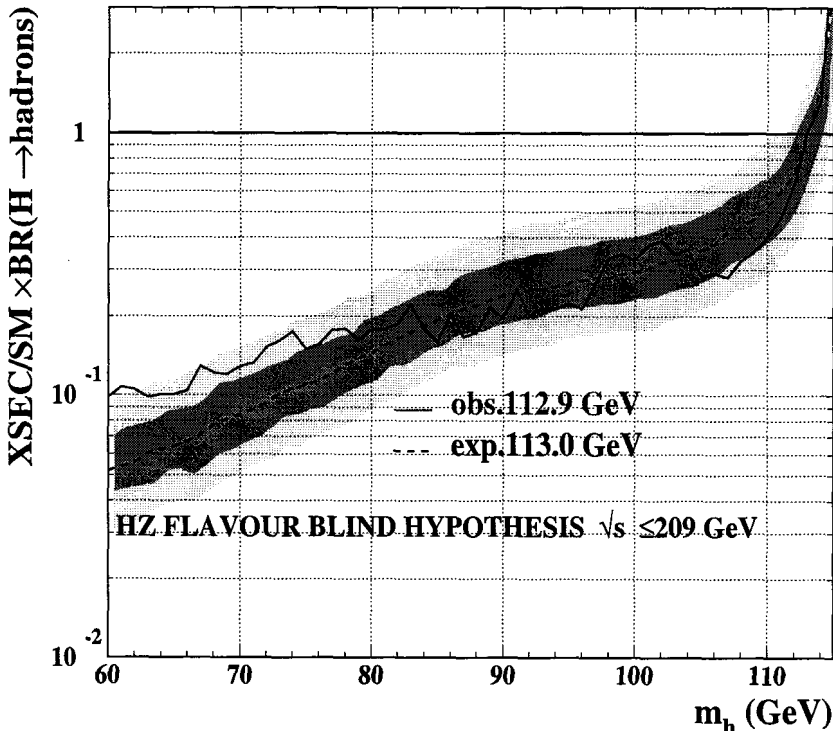


Figure 2: Combined flavour independent LEP observed and expected 95 % CL upper limits on the production cross-section as a function of the Higgs boson mass, normalised to the expected SM values, computed assuming 100 % hadronically decaying Higgs bosons. The curves are the observed (solid) and expected median (dashed) excluded ratios, and the bands correspond to 68.3 and 95 % confidence intervals from the background-only experiments.

obtained separately by each collaboration, in terms of excluded ranges for  $h$  and  $A$  masses, for different assumptions on production cross-sections [8, 13]. Only part of the available data was used so far, and systematic effects were not considered in all the studies. Moreover, some selections used were not fully optimised. No LEP-wide combination of results was performed yet. All results except [12] are preliminary. Applications to constrain specific models, through combination [6, 11, 12, 15] with other Higgs boson searches, both standard and flavour independent, are discussed in the following two sections.

### 3.1 DELPHI [8]

The DELPHI flavour independent  $hA$  search used most of the data collected in 1998–2000. Only fully hadronic ( $q\bar{q}q\bar{q}$ ) final states were analysed. In order to cover a wide range of masses (in the range  $m_h, m_A > 15 \text{ GeV}/c^2$  and  $40 < m_h + m_A < 180 \text{ GeV}/c^2$ ) three complementary analysis streams were defined, for four-jet, three-jet and three-jet-with-high-thrust topologies. A test-mass dependent discriminant variable based on the mass reconstruction was obtained in each stream. Signal samples were generated in  $10 \text{ GeV}/c^2$  steps for  $m_h$  and  $m_A$ , if both masses were above  $30 \text{ GeV}/c^2$ , and  $5 \text{ GeV}/c^2$  if one was below. In the final evaluation, the discriminant variable was interpolated to test intermediate values, using  $2 \text{ GeV}/c^2$  steps, and the overlap between analysis streams was removed by choosing the strongest one, based on expected performance. The efficiencies obtained were checked to be flavour independent at the 3 % level. The procedure described in [19] was applied to compute 95 % CL exclusions in the  $(m_h, m_A)$  plane (see Figure 3), assuming maximal  $ZhA$  couplings<sup>e</sup> and 100 % hadronically decaying  $h$  and  $A$  bosons.

### 3.2 L3 [13]

The L3 flavour independent  $hA$  search used the data collected in 1998–1999, focussing on the range  $m_h, m_A > 50 \text{ GeV}/c^2$ . Both  $q\bar{q}q\bar{q}$  and  $q\bar{q}\tau\bar{\tau}$  final states were analysed. Test-mass dependent selections were constructed, based on kinematics and mass reconstruction, to compute 95 % CL exclusions in the  $(m_h, m_A)$  plane, for several assumptions on the  $hA$  production cross-section.

### 3.3 OPAL [11, 12]

The OPAL flavour independent  $hA$  search used the data collected in 1998. Only fully hadronic ( $q\bar{q}q\bar{q}$ ) final states were analysed. A test-mass dependent discriminant variable based on kinematics and mass reconstruction was used to evaluate the compatibility of data and simulation for a fixed set of mass hypotheses in the range  $m_h, m_A > 30 \text{ GeV}/c^2$ . Final selection efficiencies were interpolated to test intermediate values, using the most conservative final-state flavour assignment. The results were not expressed directly in terms of bounds on  $hA$  production, but combined with other Higgs boson searches to provide general limits in the context of the 2HDM (see the next section).

## 4 Constraints on Two Higgs Doublet Models of Type II

The popular 2HDM [1] provides an attractive framework for improving the SM because it features the simplest possible extension of the Higgs sector satisfying the constraints of  $\rho \simeq 1$  and the absence of tree-level flavour changing neutral currents<sup>f</sup>,

---

<sup>e</sup>The  $e^+e^- \rightarrow hA$  production cross-sections were computed with the HZHA generator [20], taking into account the kinematical suppression in the phase-space from the  $p$ -wave threshold behaviour, and effects from initial state radiation, but specifying  $\cos^2(\beta - \alpha) = 1$  in the expression of the  $ZhA$  coupling (see section 4 for a description of couplings in the 2HDM).

<sup>f</sup>If Higgs-fermion couplings are appropriately chosen.

# DELPHI PRELIMINARY

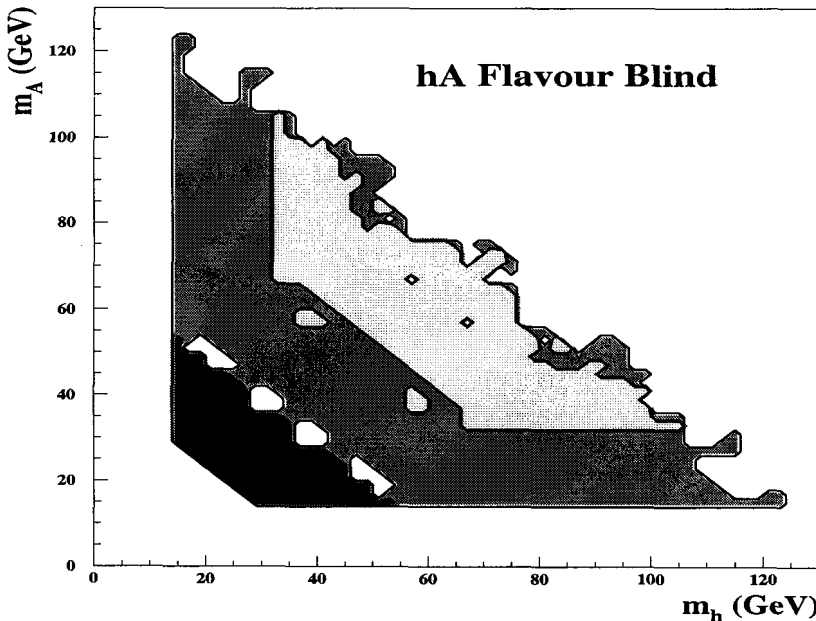


Figure 3: Flavour independent 95 % CL excluded ranges in the  $(m_h, m_A)$  plane, assuming maximal  $Z h A$  couplings and 100 % hadronically decaying  $h$  and  $A$  bosons, shown using lighter to darker grey for the four-jet, three-jet and three-jet-with-high-thrust streams, respectively. The unexcluded region near the  $m_h + m_A = 70 \text{ GeV}/c^2$  line is due to the transition between three-jet and three-jet-with-high-thrust streams, which is still being optimised.

and has few new parameters. In 2HDMs, tree-level production cross-sections for neutral Higgs bosons  $h$  and  $A$  are related to SM expressions via

$$\sigma_{hZ} = \sin^2(\beta - \alpha) \sigma_{HZ}^{SM} \quad \text{and} \quad \sigma_{hA} = \cos^2(\beta - \alpha) \lambda \sigma_{HZ}^{SM},$$

where the phase-space factor  $\lambda$  accounts for the  $p$ -wave threshold behaviour,  $\alpha$  is the Higgs mixing angle, and  $\tan\beta$  the ratio of vacuum expectation values for the two Higgs superfields. Couplings to fermions specify the type of 2HDM. In *Type II* 2HDMs, the first Higgs doublet couples only to *down*-type fermions, and the second only *up*-type fermions. In this case, tree-level couplings between neutral Higgs bosons

$h$ ,  $A$  and fermions are related to SM couplings through the factors

$$h\bar{c}\bar{c} : \frac{\cos \alpha}{\sin \beta}, \quad h\bar{b}\bar{b} : -\frac{\sin \alpha}{\cos \beta}, \quad A\bar{c}\bar{c} : \cot \beta \quad \text{and} \quad A\bar{b}\bar{b} : \tan \beta.$$

The MSSM is a physically strongly motivated *Type II* 2HDM. New particles and specific constraints on model parameters arise in this case from the introduction of supersymmetry, and also once specific schemes for its breaking are added.

However, if full generality is sought, no such constraints can be invoked, and parameters such as  $\alpha, \beta, m_h, m_A$  are entirely free. In large regions of the  $(\alpha, \beta)$  parameter space, suppressed production of either  $h$  or  $A$  can occur, together with suppressed decay rates into  $b\bar{b}$ , for values of  $m_h, m_A$  kinematically accessible at LEP-2. General model-independent bounds can in this context only be obtained from broad scans of the  $(\alpha, \beta, m_h, m_A)$  parameter space, by combining results from standard and flavour independent  $hZ$  and  $hA$  searches.

This has been done by OPAL [11, 12]. The best illustration of the results is shown in Figure 4, where 95 % CL excluded ranges in the  $(m_h, m_A)$  plane are given for almost any  $\alpha, \beta$ . Although weaker than in more constrained scenarios [6], the excluded mass ranges obtained are significant given their high level of generality. Even if full exclusion remains out of reach in this approach, specific hypotheses (theoretically motivated or driven by independent observations), corresponding to scenarios or ranges of parameters of the *Type II* 2HDM, can be tested.

## 5 Constraints on MSSM large $\mu$ scenarios [2]

Higgs bosons can also have suppressed couplings to  $b$ -quarks in the MSSM once higher order loop corrections are included. This was shown to occur for large values of  $\tan \beta$  and of the Higgs mixing parameter,  $\mu$ . A specific example was designed as an illustration in the LEP-2 context, and was proposed as one of three benchmark scenarios to be tested. For any choice of  $m_A$  or  $\tan \beta$  with the parameters specified<sup>g</sup>, one of the two neutral CP-even Higgs bosons always had a mass  $\leq 108$  GeV/c<sup>2</sup> within kinematic reach at LEP-2, and a sizeable production cross-section, but could have a strongly suppressed coupling to  $b$ -quarks. Thanks to the bounds provided by the flavour independent  $hZ$  search described in section 2, this particular scenario is excluded<sup>h</sup> [6].

## 6 Conclusions and prospects

Searches for neutral Higgs bosons performed without exploiting  $b$ -tagging have enabled to reduce the model-dependence of the results in important ways, by not re-

---

<sup>g</sup>In the specified "large  $\mu$ " benchmark scenario, model parameters were scanned setting  $M_{SUSY} = 400$  GeV/c<sup>2</sup>,  $\mu = 1$  TeV/c<sup>2</sup>,  $M_2 = 400$  GeV/c<sup>2</sup>,  $m_{\tilde{g}} = 200$  GeV/c<sup>2</sup>,  $4 \leq m_A \leq 400$  GeV/c<sup>2</sup> and  $X_t = -300$  GeV/c<sup>2</sup>.

<sup>h</sup>It should be noted, however, that this result can probably not be considered as a general exclusion of MSSM scenarios with suppressed Higgs boson couplings to  $b\bar{b}$  in the mass range accessible to LEP-2, as sets of model parameters different from those chosen here could lead to larger than 108 GeV/c<sup>2</sup> and/or smaller production rates. A more general parameter scan would be required to identify potentially remaining unexcluded zones.

## OPAL PRELIMINARY

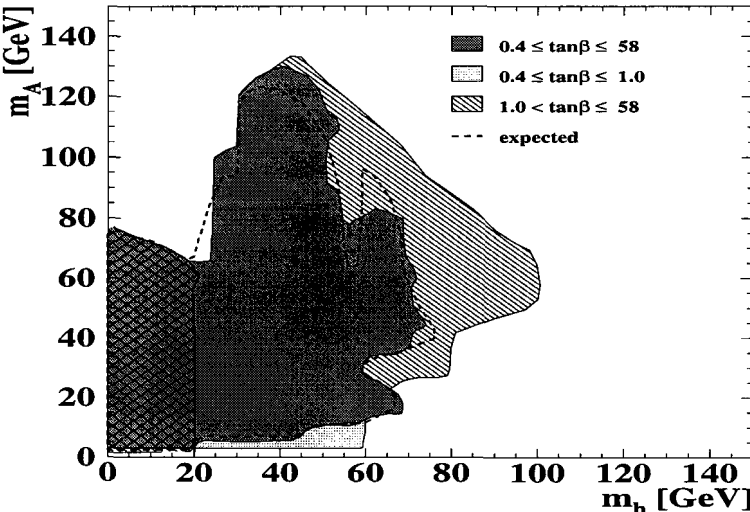


Figure 4: Regions excluded at 95 % CL in the  $(m_h, m_A)$  plane, for any  $\alpha$ , and  $\beta$ , in the ranges  $0.4 \leq \tan \beta \leq 58.0$  (dark grey area),  $0.4 \leq \tan \beta \leq 1.0$  (light grey area) and  $1.0 \leq \tan \beta \leq 58.0$  (hatched area). Constraints from direct Higgs boson searches at  $\sqrt{s} = M_Z$  [21], and from the total  $Z$  boson width determination [22] are used in the combination. The exclusion from applying only these two constraints is shown in the cross-hatched region. The expected exclusion corresponding to the dark grey area is shown as a dashed line.

stricting their applicability to models with standard SM or MSSM-like Higgs boson couplings to  $b$ -quark pairs.

In the search for  $hZ$  production, the combined flavour independent bounds, although preliminary and not fully optimised, were almost as strong as in the corresponding SM search. This was a surprise given the strong emphasis given to  $b$ -tagging in Higgs boson searches throughout the LEP-2 period, but can be understood in retrospect, from the lower background present once the  $Z$  boson mass range (populated by the very signal-like  $ZZ$  component) is overcome, something which was not anticipated to be easy at the start of LEP-2.

In the search for  $hA$  production, although all the data have yet to be exploited and combined, results obtained so far by individual collaborations allowed to improve significantly the exclusion in the kinematically accessible mass range, and, by combining with results from other Higgs boson searches, to provide very general constraints on *Type II* 2HDMs.

Several applications of these searches to specific scenarios with suppressed  $BR(h \rightarrow b\bar{b})$  were also possible. Composite models of the kind described in [3], although not covered in detail here, can for instance be excluded by the flavour independent bounds

on  $hZ$  production obtained, over the full mass range in which Higgs boson decays into gluon pairs are dominating in this model (i.e. up to  $m_h \simeq 110$  GeV/c $^2$ ). The particular "large- $\mu$ " MSSM scenario, proposed to be tested at LEP-2 as a benchmark to illustrate cases giving rise to Higgs bosons with suppressed couplings to  $b\bar{b}$  (together with masses and production rates well within reach at LEP-2) could also be excluded.

In year 2002, the final performance and full combination of this set of searches will be pushed, to maximize the sensitivity for all tested Higgs masses kinematically accessible at LEP-2, in as model independent a way as possible.

### Acknowledgments

This presentation was given on behalf of the ALEPH, DELPHI, L3 and OPAL collaborations, and the LEP Higgs Working Group (LHWG). I would like to thank members of the flavour independent Higgs search teams in the four collaborations for the material and help provided, and for the efficient work done recently within the LHWG sub-group responsible for flavour independent combinations. I would also like to thank Pamela Ferrari, Marcel Stanitzki and Ivo van Vulpen for useful comments on this write-up.

### References

- [1] J. F. Gunion *et al.*, *The Higgs Hunter's Guide*, Addison-Wesley Publishing Company, 1990
- [2] M. Carena *et al.*, Suggestions for improved benchmark scenarios for Higgs-boson searches at LEP2, hep-ph/9912223.  
M. Carena *et al.*, Phys. Rev. D **60** (1999) 075010  
W. Loinaz and J. D. Wells, Phys. Lett. B **445** (1998) 178  
M. Carena *et al.*, Nucl. Phys. **B586** (2000) 92
- [3] X. Calmet and H. Fritzsch, Phys. Lett. B **496** (2000) 190
- [4] P. Colas, *Twelve Years of Higgs Hunting at LEP*, These Proceedings.
- [5] The LEP Working Group for Higgs Boson searches, *Search for the Standard Model Higgs bosons at LEP*, Contribution to the EPS conference in Budapest, Hungary, 2001, ALEPH 2001-066, DELPHI 2001-113, L3 Note 2699, OPAL PN-479, LHWG note 2001-03.
- [6] The LEP Working Group for Higgs Boson searches, *Search for the neutral Higgs boson of the MSSM: Preliminary combined results using LEP data collected up to 209 GeV*, Contribution to the EPS conference in Budapest, Hungary, 2001, ALEPH 2001-057, DELPHI 2001-114, L3 Note 2700, OPAL TN-699, LHWG note 2001-04.
- [7] ALEPH Collaboration, *A flavour independent search for the Higgsstrahlung process in e+e- collisions at centre-of-mass energies from 189 to 209 GeV*, Contribution to the EPS conference in Budapest, Hungary, 2001, ALEPH 2001-021.
- [8] DELPHI Collaboration, *Generalised search for hadronic decays of Higgs bosons with the DELPHI detector at LEP-2*, Contribution to the EPS conference in Budapest, Hungary, 2001, DELPHI 2001-070.

- [9] L3 Collaboration, *Flavour Independent Search for Hadronically Decaying Higgs Boson in Higgs-strahlung Process at  $\sqrt{s}$  up to 209 GeV*, Contribution to the EPS conference in Budapest, Hungary, 2001, L3 Note 2693.
- [10] OPAL Collaboration, *Searches for Higgs Bosons in Extensions to the Standard Model in  $e+e-$  Collisions at the Highest LEP Energies*, OPAL PN-472,  
OPAL Collaboration, *Model Independent Searches for Scalar Bosons with the OPAL Detector at LEP*, OPAL PN-449.
- [11] OPAL Collaboration, *Two Higgs Doublet Model Interpretation of Neutral Higgs Boson Searches up to the Highest LEP Energies*, OPAL PN-475.
- [12] OPAL Collaboration, Eur. Phys. J. C18 (2001) 425-445.
- [13] L3 Collaboration, *Search for Production of Neutral Higgs Scalars in  $e^+e^-$  Annihilations at LEP*, Contribution to the ICHEP conference in Osaka, Japan, 2000, L3 Note 2576.
- [14] The LEP Working Group for Higgs Boson searches, *Flavour Independent Search for Hadronically Decaying Neutral Higgs Bosons at LEP*, Contribution to the EPS conference in Budapest, Hungary, 2001, ALEPH 2001-058, DELPHI 2001-118, L3 Note 2703, OPAL TN-700, LHWG note 2001-07.
- [15] D. Zer-Zion, *Beyond the Standard Model Higgs Searches at LEP (part A)*, Proceedings of the EPS conference in Budapest, Hungary, 2001, PRHEP-hep2001/144.
- [16] A. L. Read, in CERN Report 2000-005, p. 81 (2000).
- [17] A. Raspereza, Private Communication.
- [18] T. Junk, Nucl. Inst. Meth. A434 (1999) 435-443.
- [19] V.F. Obraztsov, Nucl. Instr. Meth. A316 (1992) 388.
- [20] P. Janot, in CERN Report 96-01, Vol. 2, p. 309.
- [21] OPAL Collaboration, Phys. Lett. B268 (1991) 122.
- [22] The LEP Collaborations ALEPH, DELPHI, L3 and OPAL, the LEP Electroweak Working Group and SLD Heavy Flavour and Electroweak Groups, for Higgs Boson searches, CERN-EP-021 (2001).

# SEARCH FOR SUPERSYMMETRY AT LEP2

F.Mazzucato <sup>a</sup>

*DPNC, 24 quai Ernest-Ansermet, Geneva , Switzerland*

*Abstract.* The search for Supersymmetry (SUSY) performed by the four LEP collaborations ALEPH [1], DELPHI [2], L3 [3] and OPAL [4] at centre of mass energies from 136 to 208 GeV is reviewed.

## 1 Framework

### 1.1 LEP Data Sets

The results presented below refer to about  $700 pb^{-1}$  of data collected, at centre-of mass energies ( $\sqrt{s}$ ) from 136 GeV to 209 GeV, by the LEP collaborations from 1996 to 2000.

### 1.2 Supersymmetry

Today Supersymmetry is the most fashionable way of extending the Standard Model (SM) of particle physics. It is a symmetry between fermions and bosons which foresees the existence, for each known SM particle, of a SUSY companion with identical quantum numbers. Supersymmetry is a broken symmetry, as no SUSY partner was ever observed, but it has very appealing features: it solves in an elegant way the hierarchy problem of the Higgs mass; it foresees gauge couplings unification at a Grand Unified Theory (GUT) energy scale; it is compatible with Electro-Weak (EW) fits; it is foreseen by string theories etc..

The details of SUSY phenomenology depend on the model considered. In the following the Minimal Supersymmetric Extension of the SM (MSSM) is used, as it introduces the minimal number of new particles and free parameters. Non minimal extensions were also proposed in the literature and studied, but are not addressed here. Table 1 summarises the particle spectrum of the MSSM. One should note that the SUSY partners of EW gauge bosons and Higgses with same charge, mix into mass eigenstates called Charginos ( $\tilde{\chi}_1^\pm, \tilde{\chi}_2^\pm$ ) and Neutralinos ( $\tilde{\chi}_1^0, \tilde{\chi}_2^0, \tilde{\chi}_3^0, \tilde{\chi}_4^0$ ).

The results presented here are also based on the conservation of a multiplicative quantum number called R-parity<sup>b</sup> which has important phenomenological consequences, namely: the Lightest Supersymmetric Particle (LSP) is stable, SUSY particles are pair produced at LEP and in the decay chain of each SUSY particle at least one LSP is produced. R-parity violating (RPV) models will be briefly discussed in section 4.

The final element to specify the phenomenology is the SUSY breaking mechanism, that can be introduced through different types of interaction. In the following the most popular scenarios are discussed: gravity and gauge mediated SUSY breaking.

---

<sup>a</sup>e-mail: Federica.Mazzucato@cern.ch

<sup>b</sup>R-parity is defined for each particle as  $R = (-1)^{3(B-L)+2S}$  where B and L are the Barion and Lepton numbers of the particle and S is its spin, so that  $R_{SM} = +1$ ,  $R_{SUSY} = -1$

SM		SUSY		
		Gauge	Mass	
leptons	$l_{L,R} \nu_{L,R}$	sleptons	$\tilde{l}_{L,R} \tilde{\nu}_{L,R}$	$\tilde{l}_{1,2} \tilde{\nu}_{1,2}$
quarks	$q_{L,R}$	squarks	$\tilde{q}_{L,R}$	$\tilde{q}_{1,2}$
Higgs bosons	$h_0 H_0 A_0 H_\pm$	higgsinos	$H_0^1 H_0^2 \tilde{H}^\pm$	
EW gauge bosons	$W^\pm W^0 B^0$	gauginos	$\tilde{W}^\pm \tilde{B}^0$	$\tilde{\chi}_1^\pm \tilde{\chi}_2^\pm$ $\tilde{\chi}_1^0 \tilde{\chi}_2^0 \tilde{\chi}_3^0 \tilde{\chi}_4^0$
gluons	$g$	gluinos	$\tilde{g}$	
graviton	$G$	gravitino	$\tilde{G}$	

Table 1: SM particles and their SUSY partners in the MSSM.

## 2 Gravity-mediation

### 2.1 Search strategy

In gravity mediation  $\tilde{\chi}_1^0$  is the LSP. It's a massive particle having only EW interactions with matter and therefore it escapes detection giving a characteristic signal of missing energy in the detector and acoplanar final states.

The search strategy depends first of all on the final state topology generated by the pair production of the SUSY particle considered and its dominant decay pattern(s). Sfermions decay in the corresponding fermion and the LSP .Squarks and sleptons therefore leads respectively to a pair of acoplanar jets and leptons in the final state. Charginos decay in a pair of fermions ( $SU(2)_L$  doublet) and one LSP. If both charginos decay hadronically (leptonically) the final states consists of 4 jets (2 acoplanar leptons). Mixed decays leads to a golden channel for SUSY discovery: a pair of jets plus one lepton and missing energy, which has very low SM background. For neutralinos the lightest detectable state is the associated production  $\tilde{\chi}_1^0 \tilde{\chi}_2^0$  followed by the decay of  $\tilde{\chi}_2^0$  in  $\tilde{\chi}_1^0$  plus a fermion-antifermion pair. Acoplanar pairs of leptons or quarks are then expected in the final state. Typical cross section values for these processes are:  $\sigma(\tilde{\chi}_1^\pm \tilde{\chi}_1^\pm) \sim O(5pb)$ ,  $\sigma(\tilde{\chi}_1^0 \tilde{\chi}_2^0) \sim O(pb)$ ,  $\sigma(\tilde{f}\tilde{f}) \sim O(0.1pb)$ . One should note that, even if the same topology appears in many searches (eg. acoplanar lepton pairs), the analyses were designed and optimised separately for each particle as the kinematic is very different.

The second relevant parameter in the searches definition is the mass difference ( $\Delta m$ ) between the SUSY particle and the  $\tilde{\chi}_1^0$  which defines the visible energy in the detector and therefore the main SM background. If  $\Delta m < 25GeV$  two photon interactions,  $\sigma \sim O(10^5 pb)$ , are the dominant SM process but they can be rejected as they have forward activity and low missing transverse energy. For  $25 < \Delta m < 100GeV$  the leading two fermion backgrounds,  $\sigma \sim O(10^2 pb)$ , can be suppressed as they have low acoplanarity and missing energy. Above  $\Delta m \sim 100GeV$  four-fermion final states,  $\sigma \sim O(20pb)$ , need more sophisticated techniques as likelihood or neural networks to be rejected down to the irreducible component that sets the final LEP reach in cross section limits. In the degenerate region ( $\Delta m < 5GeV$ ) special searches were designed as the decay products of the SUSY particle become

too soft to trigger the detector. For example for degenerate charginos the interaction  $e^+e^- \rightarrow \gamma \tilde{\chi}_1^{\pm} \tilde{\chi}_1^{\mp}$  was looked for where the energetic Initial State Radiation photon was used to trigger and one or two additional soft tracks from chargino decays were required to identify the process over the huge two photon background. If  $\Delta m$  is so small (below  $O(\text{MeV})$ ) that charginos acquire a sizable lifetime and fly through the detector before decaying, they were searched for as heavy ionising particles with anomalous energy losses in the Time Projection Chambers or, in the case of DELPHI, also thanks to the Cherenkov detectors. SM events in these channel are negligible and the main background is due to cosmic rays or detector noise.

## 2.2 Searches results

In none of the search channels studied deviations from the SM predictions were observed so limits on the production cross section of the different SUSY particles were computed at 95 % CL.

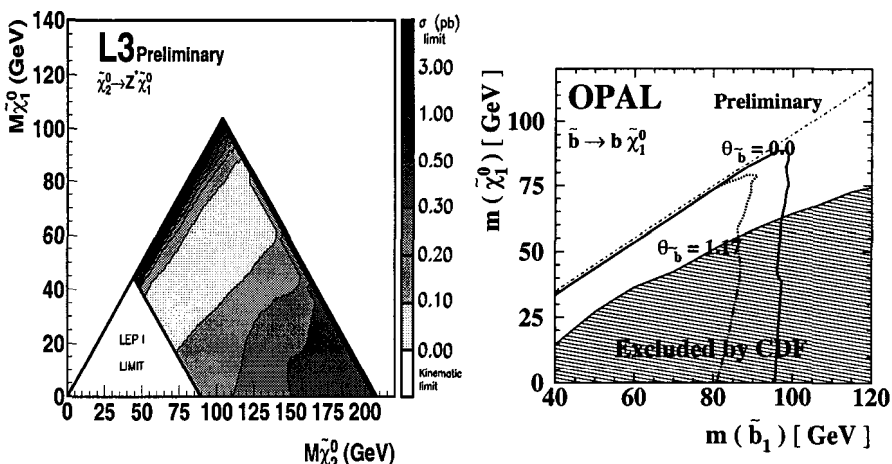


Figure 1: Left: Neutralino cross section limits. Right: excluded regions in sbottom searches for different mixing angles

As the signal selection efficiency depends on the masses of the LSP and the SUSY particle considered, limits are presented in the plane  $(m_{\text{LSP}}, m_{\text{susy}})$  as can be seen in the right plot of fig. 1 for neutralinos. Regions outside the triangle are kinematically forbidden. The plot combines, using  $\text{BR}(Z_0)$ , the results of all neutralino search channels and the typical cross section reach is of the order of hundreds fb. Similarly the charginos cross section is constrained below few tenths of fb in most of the mass ranges. The LEP SUSY working group, combining the data collected by the four LEP collaborations at the highest energies excluded chargino with masses below 103.5 GeV (in the heavy sfermion scenario).

The cross section for sfermion production depends not only on the masses but also on the mixing angle between left and right sfermions. However this dependence is

not too heavy as can be seen in the right plot of fig. 1 that shows, for sbottom, the regions excluded in the mass plane ( $m_{LSP}, m_b$ ) for the two extreme cases of mixing, corresponding to maximal and minimal cross section. One should note the complementarity between searches at Tevatron which exclude higher masses and searches at LEP which close smaller  $\Delta m$  differences.

### 2.3 Constraints on the parameter space and LSP mass limit

The informations of different searches were combined to derive constraints on the parameters of the model. This was not affordable in the most general MSSM, which has 124 free parameters, so it was usually assumed that some of the masses or/and couplings would unify at GUT scale following the renormalisation group equations. In the Constrained MSSM (CMSSM) the additional assumptions are that all sfermion masses unify at GUT scale to a common value ( $m_0$ ) and that all gaugino masses unify to a common value. Results can then be expressed in terms of  $m_0$  and one of the gaugino masses at EW scale,  $M_2$ . The other free parameters of the model are the trilinear couplings which determine the mixing for each sfermion flavour plus  $\mu$  and  $\tan \beta$ , respectively the higgs mixing parameter and ratio of higgs vacuum expectation values. More constrained models were also studied but are not addressed here.

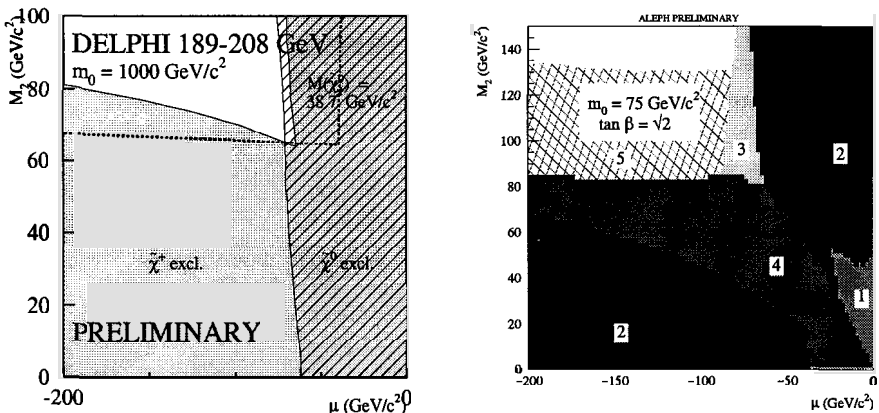


Figure 2: Left: for the high  $m_0$  scenario, chargino (neutralino) exclusion regions in the plane ( $\mu, M_2$ ) are shown in yellow (shaded). Right: the plot shows for the low  $m_0$  scenario exclusion limits in the plane ( $\mu, M_2$ ) from LEP1 searches (1), charginos (2), neutralinos (3), sleptons (4). The fifth region can be excluded from the negative results of higgs searches.

In the CMSSM if sfermions are heavy (high  $m_0 > O(200\text{GeV})$ ) charginos have the highest cross section and exclusion power in most of the parameter space accessible at LEP2, as illustrated by the yellow region in the left plot of fig. 2. High values of  $M_2$  are excluded by the degenerate chargino search. Neutralinos searches allow to extend the exclusion in the dashed band which is beyond the chargino kinematic reach. If

sfermions are light (low  $m_0$ ), charginos and neutralinos production proceed not only via an s-channel  $Z/\gamma$  exchange (as for high  $m_0$ ) but also via a t-channel through a sfermion. The interference of the two diagrams is negative (positive) for charginos (neutralinos). For  $m_0$  down to  $O(100\text{GeV})$  the drop in chargino cross section and exclusion power is compensated by the increase in the neutralino ones. For lower  $m_0$  values sfermions affect also the decay patterns of chargino and neutralino, and might lead to undetectable final states. In this case however sleptons are sufficiently light to be directly produced at LEP2, so the corresponding searches can be used to cover the blind spots in the chargino/neutralino exclusions as illustrated in the right plot of fig. 2.

Particle	Neutralino	Chargino	Selectron	Sneutrino
Mass Limit (GeV)	45.6	84.7	77.	95.

Table 2: Mass limits of SUSY particles in the CMSSM

A scan of the un-excluded parameter regions established the lower allowed values, at 95% CL, for the masses of the different SUSY particles. Results are summarised in table 2. The limit of 45.6 GeV on the mass of the LSP is particularly relevant for cosmology as the lightest neutralino is an ideal candidate for dark matter.

### 3 Gauge-mediation

#### 3.1 Search strategy

In Gauge mediation (GMSB) the LSP is an almost massless Gravitino. The search topologies are defined by the Next to Lightest Susy Particle (NLSP) which can be the lightest neutralino or a slepton. A  $\tilde{\chi}_1^0$  ( $\tilde{l}$ ) NLSP decays in the LSP plus a photon (lepton) generating a pair of acoplanar photons (leptons) in the final state. More complicated topologies arising from cascade decays of heavier SUSY particles were also studied but are not addressed here.

The characteristic feature in GMSB is that the NLSP can have a sizable lifetime ( $\lambda_{NLSP}$  is proportional to  $m_{\tilde{g}}$ ). NLSP with short lifetimes have prompt decays and were searched for similarly to the gravity mediation case. For long lifetimes the NLSP decays outside the detector, therefore a slepton NLSP was searched as an heavy ionising particles in the TPC while a neutralino NLSP is undetectable. For intermediate lifetimes the NLSP decays inside the detector volume and generates particles with large impact parameter (ip) or kinks in the tracks. In this case the background is typically very low and comes from events with badly reconstructed particles, cosmic rays or detector noise.

#### 3.2 Results

For  $\tilde{\chi}_1^0$  NLSP, neither the search for acoplanar pairs of photons nor the search for a single photon with large ip showed deviations from the SM predictions. These results were combined to obtain cross section limits at 95% CL on neutralino pair production as a function of the neutralino mass and lifetime, as can be seen in the left plot of fig.

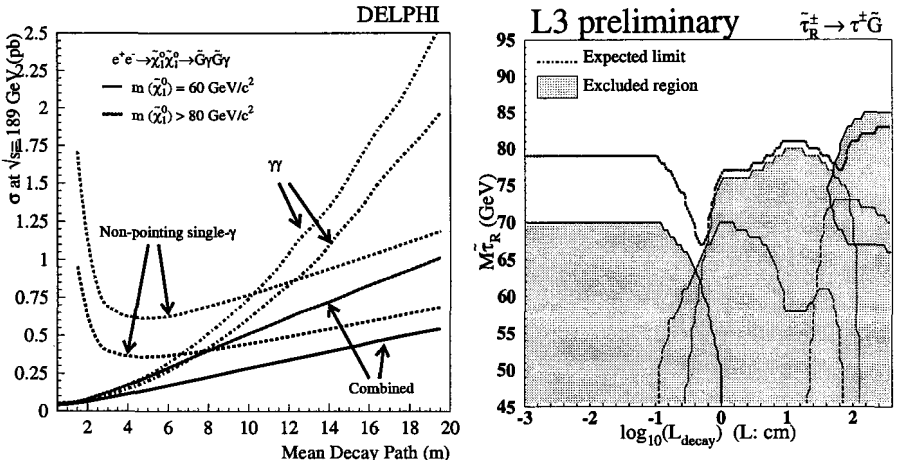


Figure 3: Left: Neutralino cross section limits as a function of the neutralino mean decay lengths for  $\tilde{\chi}_1^0$  NLSP. Right: excluded regions in the  $(m_{\tilde{l}}, m_{\tilde{g}})$  plane for  $\tilde{l}$  NLSP

3. One should note that the search for large ip photons gives an essential contribution for decay lengths longer than 8m. For short lived neutralino cross section of the order of 10-50fb are typically excluded up to neutralino masses of 100 GeV.

No deviations from the SM prediction were observed in the searches for sleptons NLSP and the excluded regions in the plane  $(m_{\tilde{g}}, m_{\tilde{l}})$  were computed, as shown in the right plot of fig.3. One should keep in mind that the gravitino mass is proportional to the slepton lifetime: gravity mediation like searches for acoplanar lepton pairs excluded sleptons with short lifetimes, kinks and large ip searches excluded intermediate lifetimes and searches for heavy ionising particles excluded sleptons with long lifetime. Sleptons NLSP are typically excluded in the mass range below 90GeV for all lifetimes.

### 3.3 NLSP mass limit

Within a minimal GMSB model the combination of the results from various channels was used to extract a lower limit on the NLSP mass. The left plot of fig. 4 shows the excluded regions in the plane  $(m_{NLSP}, m_{\tilde{g}})$  coming from different searches for short lifetimes. The regions below the diagonal, when a slepton is the NLSP, were excluded in the case of short or intermediate lifetimes by searches with leptons in the final state and for long lifetimes by searches for heavy ionising particles. The region above the diagonal, when the neutralino is the NLSP, was excluded in the case of short or intermediate lifetimes by searches in photonic final states while for long lifetimes the only coverage was achieved by searches for chargino cascade decays as a long lived neutralino is invisible. The lower limit, at 95% CL, on the NLSP mass was found to be 54 GeV in the region where a long lived neutralino is the NLSP.

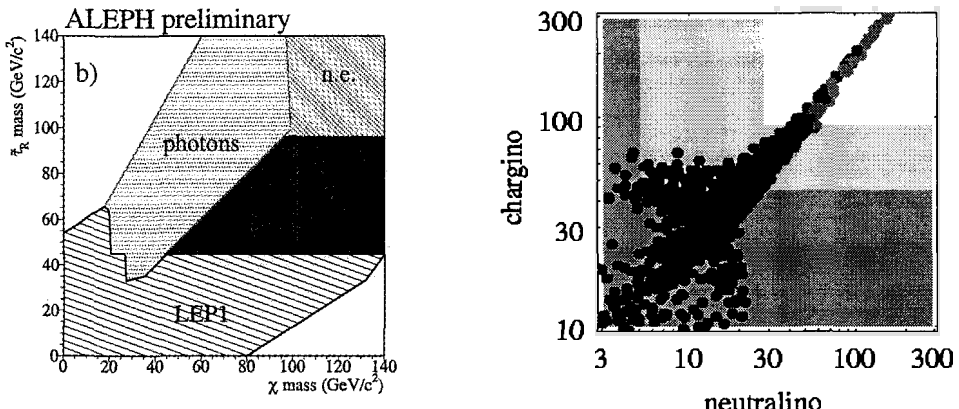


Figure 4: Left: excluded regions in the plane slepton versus neutralino mass for all gmsb searches for NLSP with short lifetimes. Right: distribution of natural susy points from [5]

#### 4 Other frameworks

All the searches presented so far in the R-parity conserving framework were repeated in case of R-parity violation with the additional complication that there is no stable LSP and a single SUSY particle can be created in resonant production. One of the main interests of RPV is that it leads to new final states topologies with a high number of jets and/or leptons which are very different from what predicted by R-parity conserving models. RPV can be introduced in the MSSM via three types of Yukawa couplings (only one of which can be non zero at time to avoid proton decay) called  $\lambda, \lambda', \lambda''$ . Depending on the SUSY particle production considered, 2 to 6 leptons are expected in the final state from a non zero  $\lambda$  coupling, 1-4 leptons plus 4 to 8 jets from  $\lambda'$  and 6 to 10 jets from  $\lambda''$ . In none of the channels considered deviations from the SM prediction were observed, therefore limits were derived on the production cross section and masses of the various SUSY particles as well as exclusion regions in the parameter space. These are of the same order of what was found for the R-parity conserving case, eg a lower limit on the neutralino mass between 40 and 45 GeV was found for all RPV couplings.

Many unconventional scenarios were also studied by the LEP collaborations, as for example the possibility of a gluino LSP. A pair of stable and light gluinos could be produced at LEP by the decay of a gluon or a squark. In all cases the signature consist of jets accompanied by R-hadrons generated in the hadronisation of the gluino. R-hadrons could be identified by anomalous energy losses in the TPC or in the calorimeters. No deviations from the SM expectations were observed.

## 5 Conclusions

Supersymmetry was searched for at LEP2 in a very wide set of models and signatures and dedicated analyses were designed for difficult cases or unconventional scenarios. No significant deviations from the SM were observed in any of the channels considered. The results were used to derive model independent limits on the production cross sections and on the masses of the SUSY particles. Typically the LEP2 sensitivity achieved was  $O(10\text{-}100\text{fb})$  for cross sections and  $O(100 \text{ GeV})$  for mass limits. In addition the combination of the different searches was used to exclude regions in the parameter space of more constrained models. In the CMSSM the absolute limit on the LSP mass was found to be 45.6 GeV.

The right plot of 4 was produced in [5] and tries to give a global (though not compelling) evaluation on supersymmetry after the LEP era. It shows, in the plane mass of the chargino versus mass of the neutralino the distribution of all SUSY points in the MSSM parameter space which do not need an unnatural fine-tuning to be compatible with the present experimental observations. The gray bands correspond to limits set from LEP1 and LEP2 direct searches the dark grey points are excluded by higgs searches. According to this picture, susy points still allowed after LEP2 (light gray) represent only 5% of the total. This means that after LEP2 a natural and minimal Supersymmetry is extremely constrained, but also that if it exists it must be just around the corner and Tevatron and LHC have the potential to discover it.

## Acknowledgments

I want to thank professors A.Clark and A.Blondel for supporting my stay in Moscow. My gratitude also to Prof. A.Blondel, F.Gianotti and L.Pape for the usefull suggestions in the preparation of the talk.

## References

- [1] ALEPH collaboration, contributed papers to ICHEP 2001:  
 ALEPH 2000-065 CONF (CONFERENCE) 2000-043  
 ALEPH 2001-012 CONF (CONFERENCE) 2001-009  
 ALEPH 2001-004 CONF (CONFERENCE) 2001-001  
 ALEPH 2001-011 CONF (CONFERENCE) 2001-008  
 ALEPH 2001-010 CONF (CONFERENCE) 2001-007  
 ALEPH 2001-009 CONF (CONFERENCE) 2001-006  
 ALEPH 2001-005 CONF (CONFERENCE) 2001-002  
 ALEPH 2000-061 CONF (CONFERENCE) 2001-040  
 ALEPH 2001-018 CONF (CONFERENCE) 2001-015  
 ALEPH 2000-019 CONF (CONFERENCE) 2000-016  
 and references therein.
- [2] DELPHI collaboration, contributed papers to ICHEP 2001:  
 DELPHI-2001-074 CONF502  
 DELPHI-2001-075 CONF503  
 DELPHI-2001-082 CONF510

DELPHI-2001-083 CONF511

DELPHI-2001-085 CONF513

and references therein.

- [3] L3 collaboration, contributed papers to ICHEP 2001:

L3 note 2707

L3 note 2704

and references therein.

- [4] OPAL collaboration, contributed papers to ICHEP 2001:

OPAL note PN470

OPAL note PN464

OPAL note PN478

and references therein.

- [5] Giusti,Romanino,Strumia, hep-ph/9811386

## ANOMALOUS COUPLINGS AT LEP2

D.Fayolle <sup>a</sup>

*Laboratoire de Physique Corpusculaire*

*Université Blaise Pascal IN2P3/CNRS*

*24 avenue des Landais, 63177 Aubière Cedex, France*

*Abstract.* In its second phase, LEP has allowed to study four fermion processes never observed before. Results are presented on the charged triple gauge boson couplings (TGC) from the  $W$ -pair, Single  $W$  and Single  $\gamma$  production. The anomalous quartic gauge couplings (QGC) are constrained using production of  $WW\gamma$ ,  $\nu\bar{\nu}\gamma\gamma$  and  $Z\gamma\gamma$  final states. Finally, limits on the neutral anomalous gauge couplings (NGC) using the  $Z\gamma$  and  $ZZ$  production processes are also reported. All results are consistent with the Standard Model expectations.

### 1 Introduction

The Large Electron-Positron (LEP) collider has been running above the  $W$ -pair production threshold since 1996 until the LEP stopped in 2000, at centre-of-mass energies between 161 GeV and 208 GeV. This has allowed each of the four experiments ALEPH, DELPHI, L3 and OPAL to collect nearly  $700 pb^{-1}$  of data.

The non-abelian structure of the Standard Model (SM) leads to three and four charged gauge boson vertices of which the couplings are specified in the bosonic part of the lagrangian. The self-interactions of these bosons correspond to the vertices  $\gamma WW$ ,  $ZWW$  and four quartic  $WWXX'$ , where  $XX'$  is either  $WW$ ,  $\gamma\gamma$ ,  $ZZ$  or  $Z\gamma$ . Even though the SM is experimentally so reliable, there are still some theoretical problems if one looks at higher energies. One way to cope with this is to consider the SM as an effective theory and assume that New Physics (NP) exists at an higher energy scale, inducing deviations of physical observable values from the SM predictions. The anomalous gauge boson couplings are thus introduced in the upper-dimensional lagrangian.

The study of the charged TGCs is presented in the next section, and the constraints on QGCs are reported in section 3. The NGCs are described in section 4. Conclusions are given in section 5.

### 2 Charged TGCs

#### 2.1 $W^+W^-$ channel

One of the most important SM process at LEP2 energies is the  $W^+W^-$  production because it allows to measure the  $W$  mass and the charged triple gauge boson couplings.

In addition to the  $t$ -channel  $\nu$ -exchange,  $W$ -pair production in  $e^+e^-$  annihilation involves the triple gauge boson vertices  $WW\gamma$  and  $WWZ$  which are present in the SM due to its non-abelian nature. The most general Lorentz invariant lagrangian which describes the triple gauge boson interaction involving  $W$  bosons has fourteen independent terms, seven describing each  $WWV$  vertex, with  $V = Z, \gamma$ . Assuming electromagnetic gauge invariance, C, P and CP conservation, a total of five couplings

---

<sup>a</sup>e-mail: fayolle@clermont.in2p3.fr

remain, which are  $\Delta g_1^Z$ ,  $\Delta\kappa_\gamma$ ,  $\lambda_\gamma$ ,  $\Delta\kappa_Z$  and  $\lambda_Z$  [1]<sup>b</sup>. At the tree level in the SM,  $g_1^Z = \kappa_\gamma = \kappa_Z = 1$ , while  $\lambda_\gamma = \lambda_Z = 0$ . Requiring  $SU(2)_L \times U(1)_Y$  leads to three independent couplings<sup>c</sup>,  $\Delta g_1^Z$ ,  $\Delta\kappa_\gamma$  and  $\lambda$ , related through  $\Delta\kappa_Z = \Delta g_1^Z - \Delta\kappa_\gamma \tan^2 \theta_W$  and  $\lambda_Z = \lambda_\gamma$ .

Anomalous TGCs affect both the total cross-section and the production angular distributions. Moreover, the relative contributions of each helicity state would be modified, which in turn affect the angular distributions of the  $W$  decay products.

All the four collaborations use the event rate information in the three decay channels (hadronic, semileptonic and fullyleptonic) to measure the values of the TGCs, together with the event shape. Different methods are used to analyse  $WW$  events in order to extract the TGCs<sup>d</sup>: multidimensional phase-space fit or optimal observables [2]. Then the distributions are compared with the expectations relative to different values of the parameters, as obtained from fully simulated  $WW$  Monte Carlo events. A new method consists in the Spin Density Matrix (SDM) of which the elements (see figure 1) are observables directly related to the polarisation of the  $W$  [3]. The comparison of the SDM elements with the theoretical predictions allows a model independent test of the TGCs.

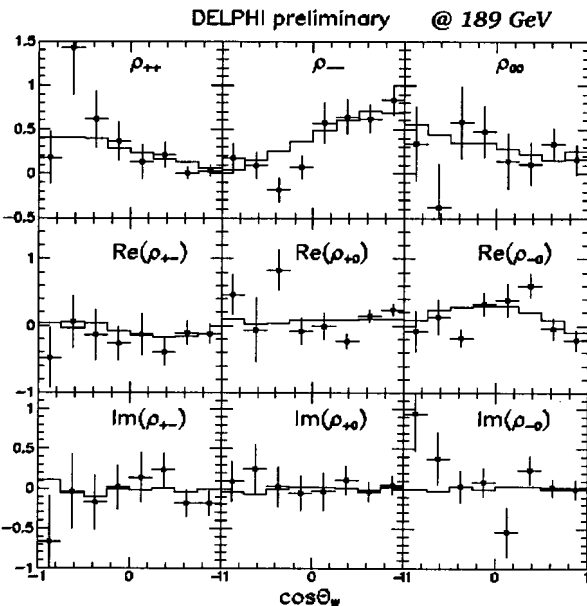


Figure 1: The SDM elements for the  $W^+W^-$  production.

There is no LEP combination since last summer because the experiments are waiting for a new  $WW$  generator including higher order corrections. With respect to

<sup>b</sup>  $\Delta$  denotes the difference of these couplings with respect to the SM value.

<sup>c</sup> The common set used includes  $g_5^Z$  which is C- and P-violating.

<sup>d</sup> The LEP experiments are also computing the CP-violating TGCs.

the old generators,  $\mathcal{O}(\alpha)$  Monte Carlos predict a lower  $WW$  cross-section (2.5%) and a sizeable change in the slope of the  $\cos\theta_W$  distributions (2%). Only ALEPH has preliminary results [4], listed in table 1, including these higher order corrections.

coupling	$\Delta g_1^Z$	$\Delta \kappa_\gamma$	$\lambda_\gamma$
fit result	$0.015^{+0.035}_{-0.032}$	$-0.020^{+0.078}_{-0.072}$	$-0.001^{+0.034}_{-0.031}$

Table 1: ALEPH charged current TGC results including  $\mathcal{O}(\alpha)$  corrections.

## 2.2 Other channels

The Single  $W$ , that is  $We\nu$  final state, also gives information on the  $WW\gamma$  vertex. The signature is one electron lost in the beam pipe and missing transverse momentum coming from the neutrino. The  $We\nu$  channel has the same sensitivity to  $\Delta\kappa_\gamma$  than the  $WW$  channel and is also sensitive to  $\lambda$ .

The Single  $\gamma$ , that is  $\nu\bar{\nu}\gamma$ , concerns the  $WW\gamma$  vertex only. The signature is a high energy photon isolated in the detector. The sensitivity to the couplings is about ten times lower than the  $WW$  sensitivity.

## 3 Quartic gauge couplings

Four quartic gauge boson vertices are predicted in the SM with fixed couplings,  $W^+W^-W^+W^-$ ,  $W^+W^-Z^0Z^0$ ,  $W^+W^-Z^0\gamma$  and  $W^+W^-\gamma\gamma$ , but their contributions to processes studied at LEP2 are negligible. On the other hand, anomalous contributions to effective QGCs arising from physics beyond the SM could lead to measurable effects.

The formalism of anomalous QGCs involving at least one photon leads to the “genuine” QGC operators of dimension 6 after neglecting operators leading to triple gauge couplings. Three anomalous QGCs,  $a_0$ ,  $a_c$  and  $a_n$  are considered.  $a_0$  and  $a_c$  are CP-conserving and contribute to the  $WW\gamma\gamma$  and  $ZZ\gamma\gamma$  vertices [5], whereas  $a_n$  is CP-violating and contributes to the  $WWZ\gamma$  vertex only [6].

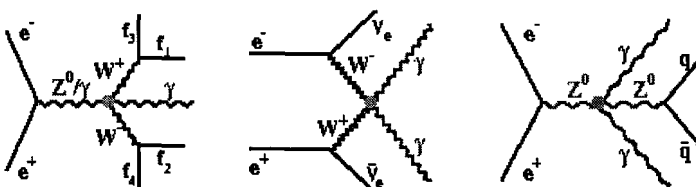


Figure 2: The three anomalous vertices  $WWZ\gamma$ ,  $WW\gamma\gamma$  and  $ZZ\gamma\gamma$ .

Limits on  $a_i/\Lambda^2$  ( $i = 0, c, n$ ), with  $\Lambda$  the energy scale where this new physics is supposed to appear, are obtained by comparing the cross-section (see figure 3) and

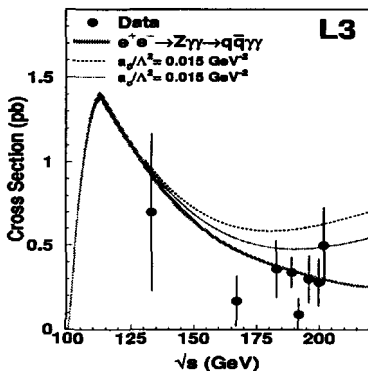


Figure 3:  $Z\gamma\gamma$  cross-section with anomalous contributions from  $a_0$  and  $a_c$ .

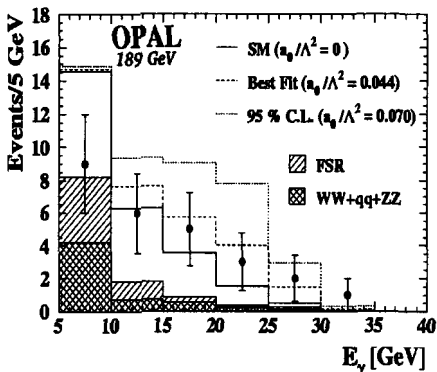


Figure 4: Energy distribution of the photon for the  $WW\gamma$  channel.

kinematic distributions (see figure 4) of the  $WW\gamma$ ,  $\nu\bar{\nu}\gamma\gamma$  and  $Z\gamma\gamma$  final states with the SM predictions. The results are listed in table 2 [7].

The  $WW\gamma$  channel is analysed in the semileptonic and hadronic channels where the standard  $WW$  selection is applied in addition to the search of a high energy and isolated photon. A cut on low polar angles for the photon reduces the initial state radiations and a sharp mass window for the dijet reduces the final state radiations. The  $W$  radiations are negligible.

The second charged anomalous QGC comes from the  $\nu\bar{\nu}\gamma\gamma$  channel where two acoplanar photons are expected. A cut on missing mass is used to reduce the  $Z\gamma\gamma$  background.

The analysis concerning the neutral process leading to the  $Z\gamma\gamma$  channel<sup>f</sup> is based on the search of high energy and isolated photons in hadronic events.

parameter [ $\text{GeV}^{-2}$ ]	vertex	95% CL
$a_0^W/\Lambda^2$	$WW\gamma + \nu\bar{\nu}\gamma\gamma$	[ -0.018 , 0.018 ]
$a_c^W/\Lambda^2$	$WW\gamma + \nu\bar{\nu}\gamma\gamma$	[ -0.033 , 0.047 ]
$a_n/\Lambda^2$	$WW\gamma$	[ -0.17 , 0.15 ]

Table 2: 95% CL combined LEP QGC results.

<sup>e</sup>There is no combination of neutral and charged QGCs because under more general theoretical hypothesis, effects in neutral QGCs may be different from charged QGCs ( $a_i^Z \neq a_i^W$ ).

<sup>f</sup>The  $Z\gamma\gamma$  channel is not combined because the different generators used give different predictions.

## 4 Neutral TGCs

The SM does not predict any direct coupling between the neutral gauge bosons themselves, but there are two possible anomalous vertices in the neutral sector [8]. Each vertex is parametrized by the most general Lorentz and  $U(1)_{em}$  invariant lagrangian plus Bose symmetry and requiring only one off-shell boson<sup>9</sup>. These  $ZZZ$ ,  $ZZ\gamma$  and  $Z\gamma\gamma$  vertices are all forbidden at tree level in the SM and have unobservably small values through loops.

$Z\gamma$  final states are sensitive to possible contributions from anomalous  $Z\gamma\gamma$  and  $Z\gamma Z$  vertices which are parametrized by height couplings:  $h_1^V$ ,  $h_2^V$  (CP-violating) and  $h_3^V$ ,  $h_4^V$  (CP-conserving) with  $V = Z^*, \gamma^*$ .  $Z\gamma$  events are investigated in  $q\bar{q}\gamma$  and  $\nu\bar{\nu}\gamma$  decay products where a hard visible photon and two jets or large missing energy and momentum for the neutrinos are searched for. The  $h_i^V$  couplings are fitted from the event rate (see figure 5), the angular and energy distributions of the photon. The results are shown in table 3 [7] and figure 6.

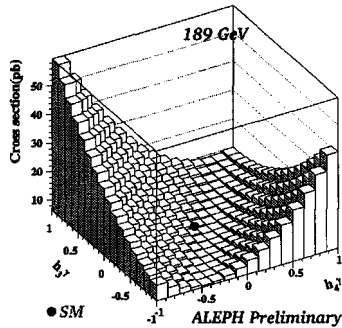


Figure 5: Variation of the  $Z\gamma$  cross-section with respect to  $(h_3^V, h_4^V)$ .

Similarly to  $Z\gamma$ ,  $Z$ -pairs can be used to constrain couplings related to the anomalous  $ZZ\gamma$  and  $ZZZ$  vertices. There are four couplings:  $f_4^V$  (CP-violating) and  $f_5^V$  (CP-conserving) with  $V = Z^*, \gamma^*$ . The five visible decay channels are investigated:  $Z \rightarrow q\bar{q}q\bar{q}$ ,  $Z \rightarrow q\bar{q}\nu\bar{\nu}$ ,  $Z \rightarrow q\bar{q}l^+l^-$ ,  $Z \rightarrow l^+l^-\nu\bar{\nu}$  and  $Z \rightarrow l^+l^-l^+l^-$  with an expected branching ratio of 49%, 28%, 14%, 4% and 1% respectively. The  $Z$ -pair event rate, as well as angular distributions (mainly  $\cos\theta_Z$ ) are used to constrain the values of the  $f_i^V$  couplings. The results are summarized in table 3 [7] and figure 6.

$h_i^V$	95% CL	$h_i^Z$	95% CL	$f_i^V$	95% CL
$h_1^V$	[-0.056, 0.055]	$h_1^Z$	[-0.128, 0.126]	$f_4^V$	[-0.17, 0.19]
$h_2^V$	[-0.045, 0.025]	$h_2^Z$	[-0.078, 0.071]	$f_4^Z$	[-0.31, 0.28]
$h_3^V$	[-0.049, 0.008]	$h_3^Z$	[-0.197, 0.074]	$f_5^V$	[-0.36, 0.40]
$h_4^V$	[-0.002, 0.034]	$h_4^Z$	[-0.049, 0.124]	$f_5^Z$	[-0.36, 0.39]

Table 3: 95% CL combined LEP neutral current TGC results.

<sup>9</sup>DELPHI is also looking at off-shell couplings [9], canceling the condition of two outgoing on-shell bosons. This leads to 44 new couplings that are related to the  $f_i^V$  and  $h_i^V$  couplings.

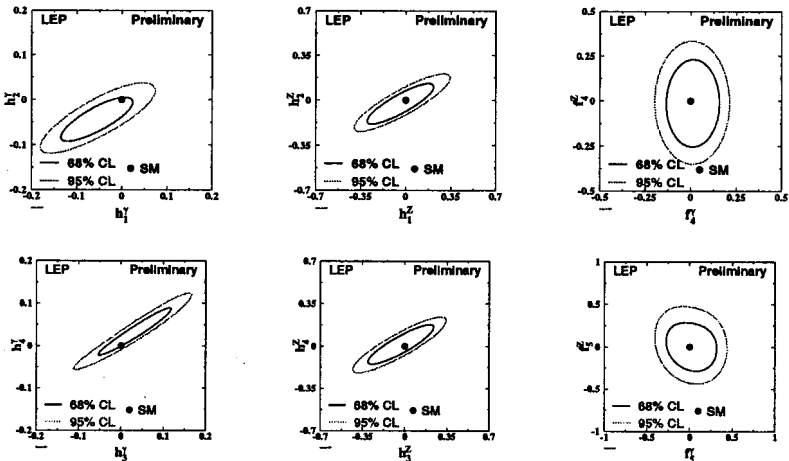


Figure 6: 2D fit contours for combined LEP neutral current TGC.

## 5 Conclusions

Values and limits for anomalous triple and quartic gauge couplings in  $e^+e^-$  collisions at centre of mass energies up to 208 GeV have been presented. The Standard Model predictions are in well agreement with data. The precision in the measurement of the gauge boson couplings has exceeded the expectations prior to the LEP2 startup. The full potential of the LEP2 data is not yet fully exploited everywhere and future improvements of the combined LEP results can be expected.

## Acknowledgments

I would like to thank my ALEPH colleagues for interesting discussions about the physics of  $W$  and  $Z$  bosons. Moreover, the warm hospitality of the 10th Lomonosov Conference has been well appreciated.

## References

- [1] Physics at LEP2, ed. by G. Altarelli, T. Sjostrand and F. Zwirner, CERN 96-01 Vol. 1, 525.
- [2] M. Diehl *et al.*, *Z. Phys.* **C62**, 397 (1994).
- [3] G. Gounaris *et al.*, *Int. J. Mod. Phys.* **A19**, 3285 (1993).
- [4] The ALEPH Collaboration, ALEPH 2001-060, CONF 040.
- [5] G. Bélanger *et al.*, *Eur. Phys. J.* **C13**, 283 (2000).
- [6] O. J. P. Eboli *et al.*, *Nucl. Phys.* **B411**, 381 (1994).
- [7] The LEP Collaboration ALEPH, DELPHI, L3, OPAL, and the LEP GC Working Group, "Combined Preliminary Results on Electroweak Gauge Coupling

*Measurements by the LEP Experiments*", LEPEWWG/TGC/2001-03, and references therein, [http://lepww.web.cern.ch/lepww/tgc/bp01/gc\\_main.ps.gz](http://lepww.web.cern.ch/lepww/tgc/bp01/gc_main.ps.gz)

- [8] K.Hagiwara *et al*, *Nucl.Phys.* **B282**, 253 (1987).
- [9] G.J.Gounaris *et al*, *Phys.Rev.* **D62**, 073012 (2000).

# SEARCH FOR SINGLE TOP QUARK PRODUCTION AT LEP2

A.Leins<sup>a</sup>

Ludwig-Maximilians-Universität München, Sektion Physik, Am Coulombwall 1,  
D-85748 Garching, Germany

*Abstract.* A search for single top quark production via flavour changing neutral current (FCNC) was performed with  $\approx 2.4 \text{ fb}^{-1}$  of data collected by the ALEPH, DELPHI, L3, and OPAL detectors at LEP at  $\sqrt{s} = 189\text{-}209 \text{ GeV}$ . The process  $e^+e^- \rightarrow tc(u) \rightarrow bWc(u)$  has been searched for, with the W decaying into leptonic or hadronic final states. No evidence for a FCNC process is observed. Upper limits at the 95% confidence level on the single top production cross-section as a function of the centre-of-mass energies are derived. Limits on the anomalous couplings  $\kappa_\gamma$  and  $\kappa_Z$  are determined from those results.

## 1 Introduction

In the mid-1990's, the LEP collider at CERN entered a new phase of operation, LEP2, with the first  $e^+e^-$  collisions above the  $W^+W^-$  threshold. Between 1998 and 2000, with the installation of additional super-conducting radio-frequency accelerating cavities, the centre-of-mass energy of the LEP collider was further increased. The LEP2 data accumulated at centre-of-mass energies between 189 GeV and 209 GeV have opened up a new kinematic domain for particle searches.

There are stringent experimental limits on flavour changing neutral currents (FCNC) between the first two generations of quarks. This is not the case for the third generation quarks, where interesting new phenomena can occur. New physics can appear in FCNC vertices, such as  $Z \rightarrow tq$ . The FCNC coupling  $Ztq$ <sup>b</sup> is forbidden at tree level and highly suppressed at loop level in the standard model (SM). Extensions of the SM or new physics beyond the SM could allow FCNC for the top quark at tree level. Any observation of such vertices would signal new physics.

At the Tevatron, the CDF Collaboration performed a search for FCNC in the top decays  $t \rightarrow \gamma c(u)$  and  $t \rightarrow Z c(u)$  in  $p\bar{p}$  collisions at a centre-of-mass energy of 1.8 TeV. They obtained upper limits at the 95% confidence level (CL) on the branching fractions [1]:  $\text{Br}(t \rightarrow c\gamma) + \text{Br}(t \rightarrow u\gamma) < 3.2\%$  and  $\text{Br}(t \rightarrow cZ) + \text{Br}(t \rightarrow uZ) < 33\%$ .

At LEP such FCNC vertices can appear in the single top-quark production in the process  $e^+e^- \rightarrow tc(u) \rightarrow bWc(u)$  at center-of-mass energies  $\sqrt{s} \geq 180 \text{ GeV}$ . The standard model predictions for this process are  $\mathcal{O}(10^{-9}) \text{ fb}$  [2].

A FCNC transition can be described with the parameters  $\kappa_\gamma$  and  $\kappa_Z$  which represent the tree-level  $\gamma$  and  $Z$  exchange contributions to  $e^+e^- \rightarrow \bar{t}c(u)$ . Thus, the Born-level cross-section for single top production in  $e^+e^-$  collisions for  $\sqrt{s} > (m_t + m_q)$  can be written as [3]:

$$\sigma[e^+e^- \rightarrow \bar{t}c(u)] = \frac{\pi\alpha^2}{s} \left(1 - \frac{m_t^2}{s}\right)^2 \left[ \kappa_\gamma^2 e_q^2 \frac{s}{m_t^2} \left(1 + \frac{2m_t^2}{s}\right) \right]$$

<sup>a</sup>e-mail: Axel.Leins@cern.ch

<sup>b</sup>q is a light up-type quark

$$+ \left[ \frac{\kappa_Z^2(1+a_w^2)(2+\frac{m_t^2}{s})}{4\sin^4 2\vartheta_W(1-\frac{m_Z^2}{s})^2} + 3\kappa_\gamma\kappa_Z \frac{a_w e_q}{\sin^2 2\vartheta_W(1-\frac{m_Z^2}{s})} \right], \quad (1)$$

where  $s$  is the centre-of-mass energy squared,  $\alpha$  is the fine structure constant,  $e_q$  and  $m_t$  are the charge and mass of the top quark,  $m_Z$  is the Z boson mass, and  $a_w = 1 - 4\sin^2 \vartheta_W$  with  $\vartheta_W$  being the weak-mixing angle. Using the published limits of CDF on FCNC and the above parametrisation one can derive the following 95% CL limits:  $\kappa_\gamma^2 < 0.176$  and  $\kappa_Z^2 < 0.533$ . The ZEUS and H1 Collaborations also performed a search for FCNC in  $e p$  collisions at HERA. ZEUS reports  $\kappa_{tu\gamma} < 0.19$  [4] and H1 reports  $\kappa_{tu\gamma} < 0.305$  [5]. It should be stressed that the HERA experiments are only sensitive to the  $\gamma \rightarrow tu$  coupling.

## 2 Analysis Strategy

Due to the large mass of the top quark of  $174.3 \pm 5.1$  GeV/ $c^2$  [6, 7], it is produced at LEP2 close to its threshold ( $\sqrt{s} \approx m_t$ ) and decays before hadronizing, thus leaving a characteristic signal signature: a high energetic b-jet, as well as a low energetic c(u)-jet have nearly fixed values of energies. The W-boson is almost mono-energetic and decays in 67% into  $\bar{q}q'$  (hadronic channel) and in 33% into  $l\nu$  (leptonic channel). The hadronic analysis looks for four jet events, produced by the b-,c-quark and the two quarks coming from the W-boson. The leptonic channel is characterized by one isolated lepton and some missing energy (from W-boson decay). Details about the analyses of the four LEP Collaborations on single top quark production are described in References [8–11].

In principle, a large FCNC coupling could not only lead to the associated production of a top plus a light quark at LEP2, but also to sizable branching ratios of the top quark into  $\gamma c(u)$  or  $Z c(u)$ . This analysis uses only the  $t \rightarrow bW$  channel. The reduction of the branching ratio  $\text{Br}(t \rightarrow bW)$  due to possible FCNC decays is taken into account in the results section.

## 3 Data Samples

The combined results are based on data collected by the ALEPH, DELPHI, L3, and OPAL experiment from 1998 to 2000 at centre-of-mass energies between 189 GeV and 209 GeV. The data sets correspond to a total integrated luminosity of approximately  $600 \text{ pb}^{-1}$  per experiment. The data samples recorded in 1998 at  $\sqrt{s} \simeq 189$  GeV is analysed in one sample, while the data from 1999 are divided into four samples at 192, 196, 200 and 202 GeV. The data collected in 2000 is analysed in two samples of mean centre-of-mass energies of about 205 and 207 GeV.

## 4 Combination Procedure

Limits on the single top cross-section are derived at the 95% CL from the number of observed events, the number of expected events from SM backgrounds, the reconstruction efficiencies, and the integrated luminosities.

The statistical procedure adopted for the combination of the different channels<sup>c</sup> is stated in Reference [12]. This method is referred to as the likelihood ratio method and has been used extensively in the Higgs boson searches at LEP2. The main sources of systematic errors affecting the signal and background rate predictions are included in the limit derivation with an extension of the method of Cousins and Highland [13]. The effects of including these uncertainties on the limits are small.

Label (GeV)	$m_t = 169 \text{ GeV}/c^2$		$m_t = 174 \text{ GeV}/c^2$		$m_t = 179 \text{ GeV}/c^2$	
	$\sigma_{95}^{\text{obs.}}$	$\sigma_{95}^{\text{exp.}}$	$\sigma_{95}^{\text{obs.}}$	$\sigma_{95}^{\text{exp.}}$	$\sigma_{95}^{\text{obs.}}$	$\sigma_{95}^{\text{exp.}}$
<b>Combination of the 4 LEP Experiments</b>						
189	0.15	0.14	0.11	0.11	0.13	0.13
192	0.41	0.39	0.38	0.33	0.42	0.36
196	0.38	0.24	0.36	0.20	0.39	0.22
200	0.26	0.24	0.21	0.21	0.24	0.20
202	0.31	0.40	0.30	0.35	0.27	0.35
205	0.27	0.28	0.22	0.25	0.23	0.24
207	0.19	0.20	0.17	0.18	0.15	0.17

Table 1: The overall expected ( $\sigma_{95}^{\text{exp.}}$ ) and measured 95% CL upper limits on single top production cross-section ( $\sigma_{95}^{\text{obs.}}$ ) are reported. The statistical and systematic uncertainties are included in the calculation of the upper limits. The results in this table assume a 100% branching fraction of the top quark into bW. Cross-section limits are in pb.

## 5 Results

No excess of events is observed. Model-independent upper limits on the single top quark cross-section have been derived at the 95 % CL from the LEP measurement assuming a 100% branching ratio of top into bW and  $m_t = 169, 174$ , and  $179 \text{ GeV}/c^2$ , including statistical and systematic uncertainties. The largest systematic uncertainty comes from the variation of the top quark mass. The cross-section limits are summarised in Table 1.

Finally, the combination of all the data can be used to determine limits on the anomalous coupling parameters  $\kappa_\gamma$  and  $\kappa_Z$  using the Born-level cross-section of Equation 1. Using additional QCD and the ISR corrections [14] modify the Born-level cross-section from Equation 1 slightly and are taken into account. These limits are obtained with the likelihood ratio method [12]. Each individual measurement of all the LEP experiments at each centre-of-mass energy for the leptonic and the hadronic channel has been used as an independent channel. Taking the statistical and systematic errors into account the limit on the anomalous coupling parameters in the  $\kappa_\gamma - \kappa_Z$  plane has been derived at the 95% CL. The reduction of the branching ratio  $\text{Br}(t \rightarrow bW)$  due to possible FCNC decays derived at each point in the  $\kappa_\gamma - \kappa_Z$  plane is taken into account in this limit calculation. To compare our results with the limits from Tevatron and HERA, exclusion regions for  $m_t = 169, 174$  and  $179 \text{ GeV}/c^2$

<sup>c</sup>Data have been grouped into channels distinguished by topology (leptonic or hadronic decay of the W), centre-of-mass energy, and experiment.

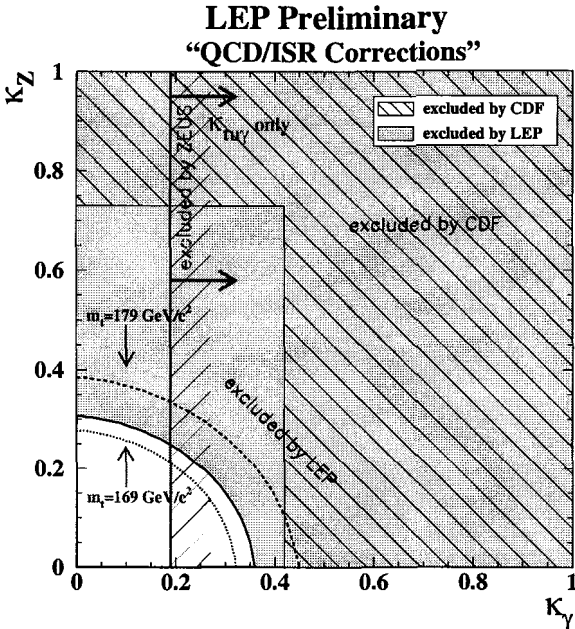


Figure 1: The light grey region shows the LEP exclusion region at 95% CL in the  $\kappa_\gamma - \kappa_Z$  plane for  $m_t = 174 \text{ GeV}/c^2$  with QCD and ISR corrections. The exclusion curves for different values of top quark masses are also shown. The reduction of the branching ratio  $\text{Br}(t \rightarrow bW)$  due to possible FCNC decays derived at each point in the  $\kappa_\gamma - \kappa_Z$  plane is taken into account in the LEP limit calculation. The hatched area shows the CDF  $\kappa_\gamma - \kappa_Z$  exclusion region [1] and the green arrow shows the ZEUS  $\kappa_{tu\gamma}$  exclusion region [4]. H1 reports  $\kappa_{tu\gamma} < 0.305$  [5].

in the  $\kappa_\gamma - \kappa_Z$  plane were derived. The exclusion curves with the inclusion of the QCD and ISR corrections are depicted in Figure 1. It corresponds to 95 % CL upper limits of  $\kappa_\gamma < 0.36$  and  $\kappa_Z < 0.31$  for a top quark mass of  $m_t = 174 \text{ GeV}/c^2$ , which become  $\kappa_\gamma < 0.32$  (0.45) and  $\kappa_Z < 0.28$  (0.38) for  $m_t = 169$  (179)  $\text{GeV}/c^2$ . This exclusion translates into branching fraction limits  $\text{Br}(t \rightarrow Zc) + \text{Br}(t \rightarrow Zu) < 6.7, 8.1$  and 12.2% for  $\kappa_\gamma = 0$  and  $m_t = 169, 174$  and  $179 \text{ GeV}/c^2$ . The result for  $\text{Br}(t \rightarrow Zq)$  versus  $\text{Br}(t \rightarrow \gamma q)$  is shown in Figure 2 for  $m_t = 174 \text{ GeV}/c^2$ .

## 6 Summary

A search for single top quark production via FCNC has been performed with approximately  $600 \text{ pb}^{-1}$  of data collected per LEP experiment in  $e^+e^-$  collision at  $\sqrt{s} = 189 - 209 \text{ GeV}$ . Limits on single top quark cross-sections with QCD and ISR corrections have been derived at the 95% CL. This leads to 95 % CL upper limits of  $\kappa_\gamma < 0.36$  and  $\kappa_Z < 0.31$  for a top quark mass of  $m_t = 174 \text{ GeV}/c^2$ . The limits become  $\kappa_\gamma < 0.32$  (0.45) and  $\kappa_Z < 0.28$  (0.38) for  $m_t = 169$  (179)  $\text{GeV}/c^2$ . It corresponds to

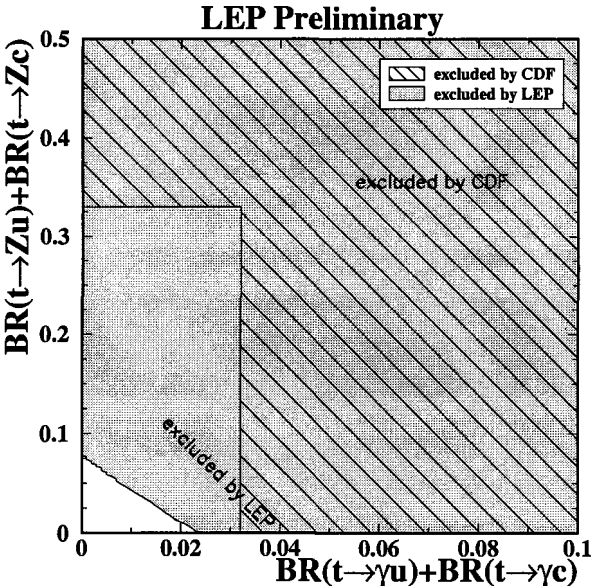


Figure 2: The light grey region shows the LEP exclusion region at 95% CL for  $\text{Br}(t \rightarrow Zc) + \text{Br}(t \rightarrow Zu)$  versus  $\text{Br}(t \rightarrow \gamma c) + \text{Br}(t \rightarrow \gamma u)$  for  $m_t = 174 \text{ GeV}/c^2$  with QCD and ISR corrections. Here, the reduction of the branching ratio  $\text{Br}(t \rightarrow bW)$  due to possible FCNC decays is taken into account. The hatched area shows the CDF exclusion region [1]. ZEUS and H1 limits on  $\kappa_{tu\gamma}$  yield  $\text{Br}(t \rightarrow \gamma u) < 0.004$  [4] and  $\text{Br}(t \rightarrow \gamma u) < 0.009$  [5], respectively.

an upper limit of  $\text{Br}(t \rightarrow Zc) + \text{Br}(t \rightarrow Zu) < 6.7, 8.1$  and  $12.2\%$  for  $\kappa_\gamma = 0$  and  $m_t = 169, 174$  and  $179 \text{ GeV}/c^2$ , which improves on the previous CDF result.

### Acknowledgments

I would like to thank the organizers for the kind invitation to participate at this conference, and thank the local organizing committee for their efforts to make this event pleasant for everybody. I would also express my gratitude to all those who contributed to the LEP Exotica Working Group and acknowledge the fruitful cooperation between all four collaborations.

### References

- [1] CDF Collaboration, F. Abe *et al.*, Phys. Rev. Lett. **80** (1998) 2525.
- [2] C. S. Huang, X. H. Wu and S. H. Zhu, Phys. Lett. **B452** (1999) 143.
- [3] J.F. Obraztsov, S. Slabospitsky, O. Yushchenko, Phys. Lett. **B426** (1998) 393.

- [4] ZEUS Collaboration, *Search for single-top production in ep collisions at HERA*, in preparation, abstract 650, EPS HEP 2001, Budapest, 2001.
- [5] H1 Collaboration, *Search for Single Top Production in ep collisions at HERA*, H1prelim-01-163, abstract 824, EPS HEP 2001, Budapest, 2001.
- [6] CDF Collaboration, F. Abe *et al.*, Phys. Rev. Lett. **82** (1999) 271;  
D0 Collaboration, B. Abbott *et al.*, Phys. Rev. **D60** (1999) 012001;
- [7] Particle Data Group, D.E. Groom *et al.*, Eur. Phys. J. **C15** (2000) 1.
- [8] ALEPH Collaboration, *Searches for Single Top Production in  $e^+e^-$  Collision at  $\sqrt{s}$  up to 208 GeV*, ALEPH 2001-054 CONF 2001-034, 2001.
- [9] DELPHI Collaboration, *Search for Single Top Production at LEP via FCNC at  $\sqrt{s} = 189\text{--}208\text{ GeV}$* , DELPHI 2001-088 CONF 516, 2001.
- [10] L3 Collaboration, *Search for Single Top Production at LEPII*, L3 note 2694, 2001.
- [11] OPAL Collaboration, *Search for Single Top Quark Production at LEP2*, Phys. Lett. **B521** (2001) 181.
- [12] T. Junk, Nucl. Inst. and Meth. **A434** (1999) 435.
- [13] R.D. Cousins and V.L. Highland, Nucl. Instr. Methods **A320** (1992) 331.
- [14] L.J. Reinders *et al.*, Physics Reports, **127**, (1985), 1.

# HEAVY ION COLLISIONS AT CMS EXPERIMENT (LHC)

L.I.Sarycheva <sup>a</sup>

*Skobeltsyn Institute of Nuclear Physics,  
Moscow State University,  
119899 Moscow, Russia*

*Abstract.* The Compact Muon Solenoid (CMS) is the general purpose detector designed to run at the LHC and optimized mainly for the search of the Higgs boson in proton-proton collisions. However, a good muon system and electromagnetic and hadron calorimeters with fine granularity gives the possibility to cover several important aspects of the heavy ion physics. The production of heavy quarkonia  $\Upsilon$ ,  $\Upsilon'$ ,  $\Upsilon''$  through their muon decay channel and the energy loss of hard jets, are valuable processes for studying the phase transition from the hadronic matter to the plasma of deconfined quarks and gluons.

## 1 Introduction

The experimental study of ultrarelativistic nuclear collisions offers the unique possibility of studying the properties of strongly interacting matter at the high energy density at which it is expected that hadronic matter becomes deconfined and a gas of asymptotically free quarks and gluons is formed, the so-called quark-gluon plasma (QGP), in which the colour interactions between partons is screened owing to collective effects (see reviews [1] and references therein).

In recent years, a great deal of attention has been devoted to the study of "hard" probes of QGP — heavy quarkonia and hard partonic jets, which do not appear as constituents of the thermalized system, but which can carry information about the earliest stages of its evolution. In particular, the strong suppression of yield of heavy quark vector mesons as  $J/\psi$ ,  $\psi'$  ( $c\bar{c}$  states) and  $\Upsilon$ ,  $\Upsilon'$ ,  $\Upsilon''$  ( $b\bar{b}$  states) is one of the promising signatures of the quark-gluon plasma formation in heavy ion collisions. It is important to study the mechanisms that governs this effect: the screening  $q\bar{q}$  potential by the surrounding colour charges [2], and the dynamical dissociation of bound resonances by semi-hard deconfined gluons [3]. An intriguing phenomenon is the "anomalously" small yield of  $\psi$ -resonances, observed in Pb-Pb collisions in the NA50 experiment (CERN-SPS) [4] and inconsistent with the conventional model of pre-resonance absorption in cold nuclear matter. For heavier ( $b\bar{b}$ ) systems, a similar suppression effect in super-dense strongly interacting matter is expected at higher temperatures than for  $c\bar{c}$ , which are expected to be reached in central collisions of heavy ions at the RHIC at BNL and LHC at CERN colliders. Here the degrees of suppression of the  $\Upsilon$ ,  $\Upsilon'$  and  $\Upsilon''$  quarkonia, which have different bound-state radii and binding energies, will differ.

Along with the suppression of heavy quarkonia, one of the processes which may give information about the earliest stages of evolution of the dense matter formed in ultrarelativistic nuclear collisions is the passage through the matter of hard jets of colour-charged partons, pairs of which are created at the very beginning of the collision process (typically, at  $\leq 0.01$  fm/c) as a result of individual initial hard nucleon-nucleon (parton-parton) scatterings. Such jets pass through the dense parton matter

---

<sup>a</sup>e-mail: lis@alex.sinp.msu.ru.

formed due to mini-jet production at larger time scales ( $\sim 0.1$  fm/c), and interact strongly with the comoving constituents in the medium, changing its original properties as a result of additional rescatterings. In a search for experimental evidences in favour of the medium-induced energy losses a significant dijet quenching [5] and a monojet-to-dijet ratio enhancement [6] were proposed as possible signals of dense matter formation in ultrarelativistic collisions of nuclei. Other possible signatures that could directly measure the energy losses involve tagging the hard jet opposite a particle that does not interact strongly as a  $Z$ -boson [7] ( $q + g \rightarrow q + Z (\rightarrow \mu^+ + \mu^-)$ ) or a photon [8] ( $q + g \rightarrow q + \gamma$ ). The possibility that the high-mass dilepton spectra are modified due to suppression of correlated semileptonic charm and bottom decays,  $D\bar{D}(B\bar{B}) \rightarrow l^+l^-$ , was recently also investigated [9] as a sign of in-medium energy losses experienced by  $c$  and  $b$  quarks.

All the above hard probes (heavy quarkonia, dijets and monojets,  $Z+jet$  and  $\gamma+jet$  channels, high mass dimuons) are important for extracting information about the properties of super-dense matter to be studied in ultrarelativistic heavy ion collisions with CMS detector at LHC collider [10].

## 2 Heavy Ion Collisions (HIC) at High Energy

There are different types of the models developed for description of hadronic and partonic matter evolution in high energy nuclear interactions: QCD for high parton densities, hydrodynamics, microscopic Monte-Carlo generators (HIJING, Venus, MQGS and others) [1].

Lattice QCD calculations predict that, above a certain temperature of density, strongly interacting matter should undergo a phase transition from hadronic gas to a deconfined state of quarks and gluons — the QGP. The critical temperature ( $T_c$ ) and the energy density ( $\varepsilon_c(T_c)$ ) for the phase transition to QGP are of order  $T_c \sim 170$  MeV, and  $\varepsilon_c(T_c) \sim 1$  GeV/fm<sup>3</sup>. Another important lattice result is that QGP can be described as the ideal gas by Stefan-Boltzmann equation at high enough temperatures  $T \geq (250 \div 350)$  MeV [11]. This temperature can be reached at LHC.

## 3 The Compact Muon Solenoid

At Large Hadron Collider (LHC) ions will be accelerated up to the energies  $E = E_p \times (2Z/A)$  per nucleon pair, where  $E_p = 7$  TeV is the proton beam energy for LHC. In the case of Pb nuclei the energy per nucleon pair will be 5.5 TeV and the expected average luminosity for a single experiment is  $L \approx 1.0 \times 10^{27}$  cm<sup>-2</sup>s<sup>-1</sup>. The interaction cross-section for Pb-Pb collisions is about 8 b, which leads to an event rate of 8 kHz.

The Compact Muon Solenoid (CMS) is the general purpose detector designed to run at the LHC and optimized mainly for the search of the Higgs boson in proton-proton collisions. Accordingly, the detector is optimized for the accurate measurement of the characteristics of high-energy muons, photons, electrons, and hadronic jets, which makes it useful also for studying hard probes of the QGP in heavy ion collisions. A schematic longitudinal view of the CMS detector is presented in Fig. 1. The  $4\pi$  detector consists of a 6 m long and 1.3 m radius central tracker and

electromagnetic (ECAL) and hadronic (HCAL) calorimeters located in a strong 4T uniform magnetic field, which is generated by a 13 m long and 6 m diameter solenoid. The electromagnetic calorimeter is made of 80000 PbWO<sub>4</sub> crystals, and the hadronic calorimeter consists of scintillator inserted between copper absorber plates. The CMS muon stations consist of drift tubes in the barrel, cathode strip chambers in the end-caps, and resistive plate chambers.

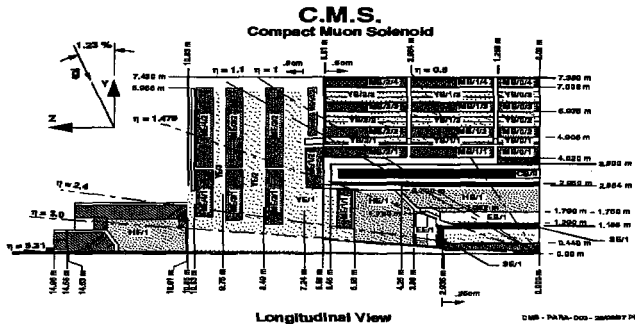


Fig. 1. The longitudinal view of CMS detector.

For studying heavy quarkonium, hard jet and high-mass dimuon production processes in heavy ion collisions, it is extremely important to perform measurements for different centrality of the events. The transverse energy deposition in the CMS calorimeters are expected to be correlated with decreasing impact parameter of nucleus-nucleus collision, thus giving us a tool to measure the centrality of the collision [10].

#### 4 Heavy Quarkonium Production

The important feature of CMS detector is excellent mass resolution ( $\sigma_M \approx 50$  MeV at  $\Upsilon$  mass) which made possible to distinguish different states of  $\Upsilon$ -family in large acceptance  $|\eta| < 2.4$ . The efficiency of dimuon reconstruction with the algorithm developed [10] depends on the multiplicity: in the "central" barrel ( $|\eta| < 0.8$ ) from 66% — for the multiplicity reduced by a factor 3. The signal-to-background ratio in  $\Upsilon$  mass region is 6 times higher than we have without the algorithm using.

In order to estimate the heavy quarkonium rates and signal-to-background ratio [10] in the barrel part  $|\eta| < 0.8$ , the  $\Upsilon$ -family production cross-section and spectra were extrapolated from the CDF experimental data at  $\sqrt{s} = 1.8$  TeV. The  $\Upsilon$  acceptance was calculated by a full GEANT simulation of the CMS detector response. The different background sources are the random decay muons from pions and kaons, and also dimuons from semileptonic open charm and bottom decays. The scaling of the hard process cross-section with the size  $A$  of the colliding nuclei was taken as  $\sigma_{AA} = A^{2\alpha} \times \sigma_{pp}$ , where  $\sigma_{pp}$  is the corresponding cross section in  $pp$  collisions evaluated using the PYTHIA model. The value  $\alpha$  was taken 0.9 for the  $J/\psi$ ,  $\alpha = 0.95$  for the  $\Upsilon$ , and  $\alpha = 1.0$  for open charm and bottom production. The background due to the random decay muons from pions and kaons has been generated for maximal estimated multiplicity of charged particles per rapidity unit 8000. The Table 1 gives

the main contributions to the dimuon mass spectrum in the  $\Upsilon$  mass interval ( $M_\Upsilon \pm 50$  MeV), the rows and the columns indicate the origin of each muon in the pair. The uncorrelated part of the background can be estimated from the  $\mu^+\mu^+$  and  $\mu^-\mu^-$  events samples and subtracted from the total  $\mu^+\mu^-$  distribution.

Table 1: Main contributions (%) to the dimuon mass spectrum in the mass region  $M_\Upsilon \pm 50$  MeV/c<sup>2</sup> for Pb-Pb collisions (left) and Ca-Ca collisions (right).

	$\Upsilon$	$\pi, K$	$b\bar{b}$	$c\bar{c}$
$\Upsilon$	61.8	0.0	0.0	0.0
$\pi, K$		13.4	12.8	2.6
$b\bar{b}$			7.2	0.0
$c\bar{c}$				0.0

	$\Upsilon$	$\pi, K$	$b\bar{b}$	$c\bar{c}$
$\Upsilon$	94.3	0.0	0.0	0.0
$\pi, K$		2.7	1.8	0.1
$b\bar{b}$			0.5	0.0
$c\bar{c}$				0.0

The mass  $\mu^+\mu^-$ -spectra in the mass range from 8.5 to 11 GeV/c<sup>2</sup> for 1 month of Pb beams with half of the time devoted for data taking ( $1.3 \times 10^6$  s) at the luminosity of  $S = 10^{27}$  cm<sup>-2</sup>s<sup>-1</sup> are shown in Fig. 2.

## 5 High Mass Dimuon Production

The spectra of dimuons originating from semileptonic open charm and bottom meson decays are sensitive to the rescattering and energy losses of massive  $b$  and  $c$  quarks propagating through the dense medium. The other process of particular interest is Drell-Yan and Z-boson production, which are unaffected by final state interactions and can be used as reference process for normalization of heavy quarkonium and hard jet

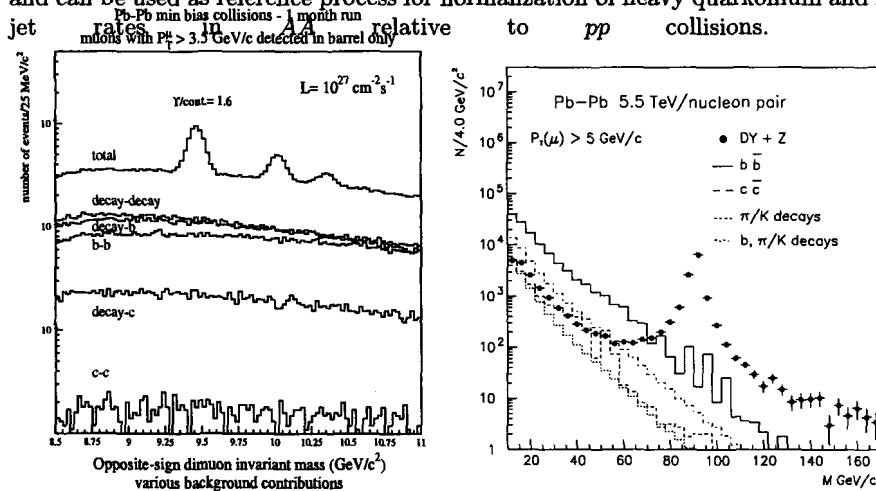


Fig. 2. Opposite-sign dimuon mass spectra for Pb-Pb collisions in one month.

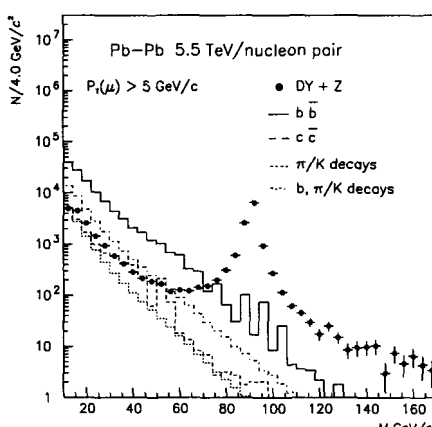


Fig. 3. Invariant mass distribution of  $\mu^+\mu^-$  pairs for muons with  $p_T > 5$  GeV/c in one month for Pb beams.

Fig. 3 present invariant  $\mu^+\mu^-$  mass spectra [10] for muons with  $p_T > 5$  GeV/c in one month of Pb beams. A clear signal from  $Z \rightarrow \mu^+\mu^-$  decays is seen with a background within  $M_Z \pm 10$  GeV/c $^2$  lower than 5%. For two weeks of LHC running time at the luminosity  $L = 10^{27}$  cm $^{-2}$ s $^{-1}$ , CMS detector will be able to detect about 11000 events of  $Z \rightarrow \mu^+\mu^-$  in full rapidity range  $10$  GeV/c $^2 \leq M \leq 70$  GeV/c $^2$  the dominant contribution comes from  $b\bar{b}$  fragmentation ( $\approx 54\%$ ). However, while traveling through the dense matter,  $b$  quarks may be subject to significant energy losses, which will result in the softening of the muon spectra and suppression of high mass dimuon rates from this source. The mixed origin contribution, when one muon is from  $b \rightarrow B$  fragmentation and the other from  $\pi/K$  decays is about 16%. The contribution from  $c\bar{c}$  fragmentation and  $\pi/K$  decays are 6% and 5% respectively. Note that the uncorrelated part of the background from  $\pi/K$  decays and from mixed origin pairs can be subtracted using like-sign dimuons, as long as the contributions of opposite-sign and like-sign muon pairs are equal. The production rates of dimuons from another sources ( $t\bar{t}$ ,  $WW$ ,  $WZ$ ,  $ZZ$ ) are very low and can be neglected at all available invariant masses.

## 6 Hard Jet Production

Study of jet characteristics in heavy ion collisions is complicated due to "false" jet background — fluctuations of the transverse energy flow arising from a huge multiplicity of "thermal" secondary particles. Applying modified window-type jet finding algorithm [10] and taking into account also the internal structure of jets, allow us to reconstruct jets beginning from  $E_T^{jet} = 100$  GeV with efficiency close to 1 and background-to-signal ratio on the level of a few percents [10]. The precision in the reconstruction of the  $\eta$  and  $\varphi$  position of jets is better than for the transverse energy:  $\sigma(E_T)/E_T \approx 20\%$ ,  $\sigma(\eta)/R \approx \sigma(\phi)/R \approx 10\%$ . The average detected fraction of initial energy is less than 1 due to influence of the magnetic field and the calibration procedure.

As example, illustrating capability of CMS to measure jet quenching effect, we consider the dependence of *jet + jet* rates on impact parameter of Pb-Pb collisions at  $\sqrt{s} = 5.5$  A TeV. It was studied in work [10] for different mechanisms of medium-induced energy loss. Fig. 4 shows dijet rates ( $E_T^{jet} > 100$  GeV,  $|y^{jet}| < 2.5$ ) in different impact parameter bins for three cases: without energy loss, with collisional loss only, with collisional and radiative loss. The rates are normalized to the expected number of events produced in Pb-Pb collisions during two weeks ( $1.2 \times 10^6$  s) of LHC run time, assuming luminosity  $L = 10^{27}$  cm $^{-2}$ s $^{-1}$ . Since jet quenching is stronger in central collisions than in per-

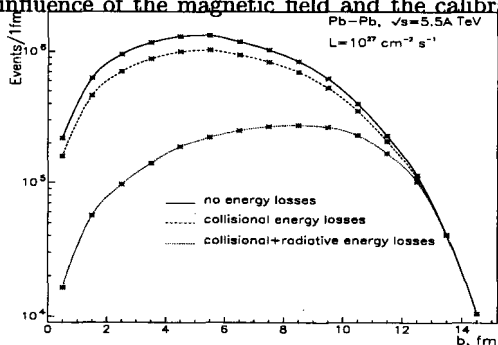


Fig. 4. Dijet rate for two running weeks, for events/1 fm different impact parameter  $b$ .

ipheral one's, the maximum and mean values of  $dN^{dijet}/db$  distribution get shifted towards the larger  $b$  as compared to what is expected from independent nucleon-nucleon interactions pattern.

## 7 Conclusions

Monte-Carlo study shows that CMS detector is well suited for the detection of dimuons and hard jets, production of which are important for extracting information about properties of dense matter created in heavy ion collisions at LHC.

The reconstruction of the  $\Upsilon$  resonances from their decay dimuons is feasible with a 66% efficiency in central Pb-Pb collisions with 8000 charged particles per rapidity unit. The total number of  $\Upsilon$  events reconstructed in one month of Pb-Pb data taking amounts to 22000 and the signal-to-background ratio is 1.6 in the most pessimistic case. The main contribution to high invariant mass ( $M > 10 \text{ GeV}/c^2$ )  $\mu^+ \mu^-$  spectra comes from semileptonic  $B\bar{B}$  meson decays and prompt dimuon (Drell-Yan) and  $Z$  production. The energy losses of  $b$  quarks traveling through the dense matter should result in the observed softening of the muon spectra and suppression of dimuon rates.  $Z(\rightarrow \mu^+ \mu^-)$  can be used as reference process for normalization of hard probes rates in  $AA$  relative to  $pp$  collisions.

The resolution in jet transverse energy has been found better than 20% at  $E_T \geq 70 \text{ GeV}$ . The expected statistics will be large enough to study dijet rates as a function of impact parameter of the collision. The suppression of dijet yield due to in-medium energy losses expected to be much stronger at central collisions in comparison with the peripheral one's. Other possibility directly to observe the energy losses involves tagging the hard jet opposite a particle that does not interact strongly. The estimated statistics is satisfactory for  $\gamma + \text{jet}$  production, but it is rather low for  $Z(\rightarrow \mu^+ \mu^-) + \text{jet}$  channel.

Transverse energy deposition in the CMS calorimeters strongly depends on the impact parameter of nucleus-nucleus collision. This will allow one to measure the centrality of events and to study the dependence of hard production processes (heavy quarkonia, high mass dimuons,  $\text{jet} + \text{jet}$ ,  $\gamma + \text{jet}$  and  $Z + \text{jet}$  channels) on the impact parameter.

The work has been supported by RF Minpromnauka.

I thank Igor Lokhtin and Natalia Karpinskaya for help in preparation of the article.

## References

- [1] J.W. Harris and B. Müller: Ann. Rev. Nucl. Part. Sci. **46** (1996) 71;  
I.P. Lokhtin, L.I. Sarycheva, A.M. Snigirev: Phys. Part. Nucl. **30** (1999) 279.
- [2] T. Matsui, H. Satz: Phys. Lett. B **178** (1986) 416.
- [3] D. Kharzeev, H. Satz: Phys. Lett. B **334** (1994) 155.
- [4] M. Gonin et al. (NA50 Coll.) Nucl. Phys. A **610** (1996) 404.
- [5] M. Gyulassy, M. Plumer: Phys. Lett. B **234** (1990) 432.
- [6] M. Plumer, M. Gyulassy, X.-N. Wang: Nucl. Phys. A **590** (1995) 511.
- [7] V. Kartvelishvili, R. Kvavadze, R. Shanidze: Phys. Lett. B **356** (1995) 589.

- [8] X.-N. Wang, Z. Huang, I. Sarcevic: Phys. Rev. Lett. **231** (1996) 77.
- [9] Z. Lin and R. Vogt: Nucl. Phys. B **544** (1999) 339;  
I.P. Lokhtin and A.M. Snigirev: C **21** (2001) 155.
- [10] M. Bedjidian et al., "Heavy Ion Physics Programme in CMS", CERN CMS Note 2000/060
- [11] E. Laermann: Phys. Part. Nucl. **30** (1999) 304.

# THE MAIN TASK OF $B$ -MESON TRIGGER AT THE LHC

N.Nikitine <sup>a</sup>, L.Smirnova <sup>b</sup>

*Skobeltsyn Institute of Nuclear Physics, Lomonosov Moscow State University,  
Moscow 119899, Russia*

*Abstract.* In this paper we presented some conceptions of the  $B$ -meson trigger performance at the ATLAS detector, which will work at CERN Large Hadron Collider (LHC).

## 1 Introduction

$B$  physics is one of the major parts of modern high energy particle physics studies. It includes analysis of CP violation, heavy meson oscillations, precision tests of the Standard Model (SM) at high orders of perturbative theory and basic questions of the strong interaction theories.

Today experimental  $B$  physics studies are carried out at large experimental facilities. Some of them, where  $B$  physics is a major task, are named " $B$  factories". Such examples are BaBar [1] and Belle [2] experiments. Others have no  $B$  physics as a main task, but contribute essentially to that. All LEP detectors [3], for example, can be considered as such type of experiments.

The Large Hadron Collider (LHC) [4], which is in construction phase now at CERN, includes both types of experiments. As LHCb is a typical  $B$  factory, the main LHC experiments ATLAS and CMS have the goals of Higgs bosons and Super Symmetry discovery. However the  $B$  physics potential of the ATLAS and CMS experiments is high. The comparison of  $B$  physics potentials for different experiments is presented in Table 1. It can be seen from the table that at the LHC one can detect  $B^0 \pm$  meson decays with the branching ratios about  $10^{-11} - 10^{-12}$  after 3 year's run at low luminosity and study the  $B_s^0$ -meson decays, which could not be even observed at  $B$  factories.

## 2 Main trigger task at the LHC

Enormous proton-proton collision rate at the LHC (40 MHz) produces 90 MHz data flow rate. It requires to make selection of "interesting" events before than put in memory complete information about event. Specifications for selection should provide registration both "interesting", or signal, events and some similar events within the windows of selection criteria, called as background events, with common rate about 100 Hz. Significant reduction of the event rate for the complete analysis is the main task of trigger systems of the LHC experiments. We consider trigger options with the ATLAS experiment.

The ATLAS trigger is a complicate electronic and computer system. It consists of three operational levels: LVL1, LVL2 and Event Filter (EF) [5]. The first one, LVL1, provides the most essential reduction of event rate. It identifies and calculate

---

<sup>a</sup>e-mail: Nikolai.Nikitine@cern.ch

<sup>b</sup>e-mail: Lidia.Smirnova@cern.ch

Table 1: Today  $B$ -physics potential

Experiment	$\sqrt{s}$ (GeV)	$\sigma_{bb}$ (mb)	$L$ (1/cm <sup>2</sup> s)	$bb$ (pairs/year)
<b>LHC-detectors at the low luminosity</b>				
ATLAS	$1.4 \times 10^4$	$10^{-1}$	$10^{33}$	$5 \times 10^{12}$
CMS	$1.4 \times 10^4$	$10^{-1}$	$10^{33}$	$5 \times 10^{12}$
LHCb	$1.4 \times 10^4$	$10^{-1}$	$2 \times 10^{32} *$	$10^{12}$
<b>B factory</b>				
<i>a) Hadronic:</i>				
B-TeV (FNAL)	$2 \times 10^3$	$10^{-1}$	$2 \times 10^{32}$	$2 \times 10^{11}$
HERA-b (DESY)	43	$1.2 \times 10^{-5}$	$3.5 \times 10^{33}$	$4 \times 10^8$
<i>b) <math>e^+e^-</math>:</i>				
Belle (KEK)	10.6	$1.1 \times 10^{-6}$	$10^{34}$	$10^8$
BaBar (SLAC)	10.6	$1.1 \times 10^{-6}$	$3 \times 10^{33}$	$3 \times 10^7$

multiplicities of the main signatures of "interesting" events. They are muons, electromagnetic clusters, narrow jets, jets and global objects as missing transvers energy, total scalar transvers energy with different transvers momentum cuts. For  $B$  physics the LVL1 trigger uses the muons with  $p_t > 6$  GeV/c. These muons originate from  $b$ -quarks semilepton decays, but also from  $c$ - and light quarks. Rate reduction at LVL1 is up to 100 kHz, or  $10^{-3}$ . The second level trigger LVL2 and EF for  $B$  physics base on kinematical parameters of  $b$ -hadron decays, measured in the ATLAS Inner Detector. LVL2 and EF are usually combined in High Level Trigger (HLT). The fast operation at LVL2 limited time for particle identification algorithms, so the algorithms used at this level are rather simple and have wide windows for reconstructed parameters. The event rate after LVL2 is expected to be 1 kHz. EF should provide additional  $10^{-1}$  rate reduction up to 100 kHz. It is achieved with using more complicate algorithms: vertex algorithm, combined track fit with vertex, angular and effective mass analysis of secondary particles with more narrow windows for fitted parameters compare to LVL2. At HLT the effective selection of exclusive  $b$ -hadron decay channels is provided also by using addition special features, or signatures, of these channels.

MSU group is involved in working out of trigger criteria for selection of rare semileptonic and leptonic  $B$ -meson decays. We demonstrate here the efficiency of the HLT for selection these events and corresponding background (BG) suppression.

### 3 Rare leptonic and semileptonic $B$ -meson decays. Physics overview

Rare leptonic  $B_{d,s}^0 \rightarrow \mu^+\mu^-$  and semileptonic  $B_d^0 \rightarrow K^{0*}(\rho^0)\mu^+\mu^-$ ,  $B_s^0 \rightarrow \phi\mu^+\mu^-$  decays correspond to  $b \rightarrow s(d)$  quark transitions, which are forbidden at tree level in the SM. These decays provide the precision test of the SM, open the way to study the physics beyond the SM (2H, SUSY, SUGRA, LR) and to estimate the Cabibbo-Kobayashi-Maskawa matrix elements  $|V_{ts}|$  and  $|V_{td}|$  [6], describing quark transitions.

The branching ratios of  $B$ -meson decays are presented in the Table 2. The rare

Table 2: Radiative, muonic and semimuonic rare B-meson decays

Decay	BR in the SM	LHC experiment
$B_d^0 \rightarrow K^{*0} \gamma$	$(4.9 \pm 2.0) \times 10^{-5}$	LHCb
$B_d^0 \rightarrow K \mu^+ \mu^-$	$(0.99^{+0.39}_{-0.32} {}^{+0.13}_{-0.15}) \times 10^{-6}$	LHCb
$B_d^0 \rightarrow K^{*0} \mu^+ \mu^-$	$1.5 \times 10^{-6}$	All exp.
$B_s^0 \rightarrow \phi \mu^+ \mu^-$	$\sim 10^{-6}$	All exp.
$B_d^0 \rightarrow \rho^0 \mu^+ \mu^-$	$\sim 10^{-7}$	All exp.
$B_s^0 \rightarrow \mu^+ \mu^-$	$3.5 \times 10^{-9}$	All exp.
$B_d^0 \rightarrow \mu^+ \mu^-$	$1.5 \times 10^{-10}$	All exp.

radiative decay  $B_d^0 \rightarrow K^{*0} \gamma$  was discovered by CLEO Collaboration at 1993 [7]. The decay  $B_d^0 \rightarrow K \mu^+ \mu^-$  was observed by Belle Collaboration at the current 2001 year [8].

As follows from the tables 1 and 2, at the LHC one can observe the decay channels  $B_{d,s}^0 \rightarrow \mu^+ \mu^-$  and  $B_s^0 \rightarrow \phi \mu^+ \mu^-$ , which could not be detected with other experiments.

#### 4 ATLAS HLT algorithms for rare leptonic $B_{d,s}^0 \rightarrow \mu^+ \mu^-$ decays

About 1500 signal events for  $B_{d,s}^0 \rightarrow \mu^+ \mu^-$  channels were simulated in each channel using PYTHIA Monte Carlo generator and programs for full ATLAS Inner Detector simulation. The structure of one typical event is presented as following:

$$\begin{array}{lcl} \bar{b} b & \rightarrow & X \text{ including } b \rightarrow (c, u) \mu^- \bar{\nu}_\mu, p_T(\mu) > 6 \text{ GeV and } \epsilon_\mu = 0.85 \\ | & & \text{for LVL1 Trigger} \\ | & & \\ \rightarrow & B_{s,d}^0 & \rightarrow \mu^+ \mu^-, p_T(\mu^\pm) > 6 \text{ GeV, } |\eta(\mu^\pm)| < 2.5 \text{ and } \epsilon_{\mu^\pm} = 0.95 \end{array}$$

where  $\epsilon_\mu$  is the muon reconstruction efficiency for the LVL1 trigger and  $\epsilon_{\mu^\pm}$  is reconstruction efficiency for second muon,  $p_T$  is transversal momentum of particle and  $\eta(\mu)$  is pseudorapidity.

The 9000 BG events were generated using the PYTHIA and ATLFAST (the program for the fast simulation of the ATLAS detector) packadges. The structure of the main BG channels contains both muons from the semileptonic decays of one or both  $b$ -quarks, presented in diagrams:

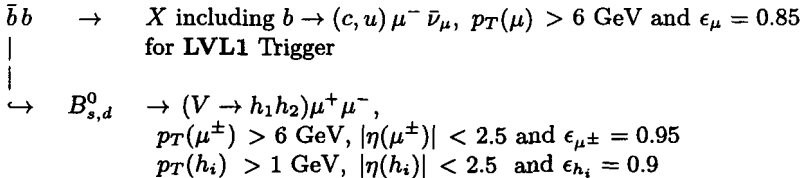
$$\begin{array}{ccc} \bar{b} b & \rightarrow & X \\ \rightarrow & X \nu_\mu \mu \bar{c} \rightarrow & \nu_\mu \nu_\mu \mu \mu \bar{s} X \end{array} \qquad \begin{array}{ccc} \bar{b} b & \rightarrow & \mu X \\ \rightarrow & \mu X & \end{array}$$

To reject the BG the following cuts have been used:

1. Decay length of  $B_{s,d}^0 > 0.7$  mm,  $\chi^2/\text{dof} < 3$ ;
2. Angle between  $p_T$  of reconstructed  $B_{s,d}^0$  and line joining primary and  $B_{s,d}^0$  decay vertices  $< 1^\circ$ ;
3. Isolation cut:  $n_{ch}(p_T > 0.8 \text{ GeV}) = 0$  in a cone  $\theta < 20^\circ$ ;
4. The mass window for  $B_{s,d}^0$ -mesons  $[-\sigma, +2\sigma]$ , where  $\sigma = 68$  MeV.

## 5 ATLAS HLT algorithms for rare semileptonic $B$ -meson decays

1500 signal events were simulated and reconstructed in the Inner Detector with minimum bias events. The typical event structure is following:



where  $V$  – is the one of the vector mesons ( $K^{*0}$  or  $\rho^0$ ) in the final state,  $h_1$  and  $h_2$  the charge products of the vector meson decays. For example,  $\rho^0 \rightarrow \pi^+ \pi^-$ .

The main BG contribution (13000 events) contains the cascade semileptonic decays of one of  $b$ -quarks and non rare semileptonic decays of both  $b$ -quarks. To reject BG the following cuts have been used:

1. The mass windows  $m(h_1 h_2) = M(K^{*0} \text{ or } \phi) \pm 2\sigma$ , where  $\sigma(K^{*0}) = 30$  MeV,  $\sigma(\phi) = 3$  MeV or  $m(\pi^+ \pi^- \rightarrow \rho^0) \in [0.60; 0.94]$  GeV;
2. Decay length of  $B_{s,d}^0 > 0.8$  mm,  $\chi^2/\text{ndf} < 10$ ;
3. Angle between  $p_T$  of reconstructed  $B_{s,d}^0$  and line joining primary and  $B_{s,d}^0$  decay vertices  $< 3^\circ$ ;  $m(\mu^+ \mu^-) \notin M(J/\psi \text{ or } \psi')$ ;
4. Isolation cut:  $n_{ch}(p_T > 0.8 \text{ GeV}) = 0$  in a cone  $\theta < 5^\circ$ ;
5. For  $B_d^0 \rightarrow K^{*0} \mu^+ \mu^-$ :  $p_T(K^{*0}) > 5$  GeV;
6. The mass window for  $B_{s,d}^0$ -mesons  $[-\sigma, +2\sigma]$ , where  $\sigma \sim 50$  MeV.

## 6 Expected results

Numbers of expected events for muonic and semimuonic rare  $B$ -meson decays after using all cuts, presented in sections 4 and 5, for 3 years of LHC running at low ( $30 \text{ fb}^{-1}$ ) and high ( $100 \text{ fb}^{-1}$ ) luminosity with the ATLAS detector have been shown in Table 3. From this table one may see, that the ATLAS can detect rare leptonic and semileptonic decays of the  $B_d^0$  and  $B_s^0$  mesons at reasonable level.

In Fig.1 the mass distributions for  $B_{d,s}^0$ -mesons signal and BG  $B_d^0 \rightarrow K^{*0} \mu^+ \mu^-$  (left),  $B_d^0 \rightarrow \rho^0 \mu^+ \mu^-$  (centre) and  $B_s^0 \rightarrow \phi \mu^+ \mu^-$  (right) are presented. The cross-hatched histogram shows the  $B_d^0 \rightarrow \rho^0 \mu^+ \mu^-$  signal, and the horizontally hatched one the reflection of  $B_d^0 \rightarrow K^{*0} \mu^+ \mu^-$  to  $B_d^0 \rightarrow \rho^0 \mu^+ \mu^-$ .

## 7 Conclusions

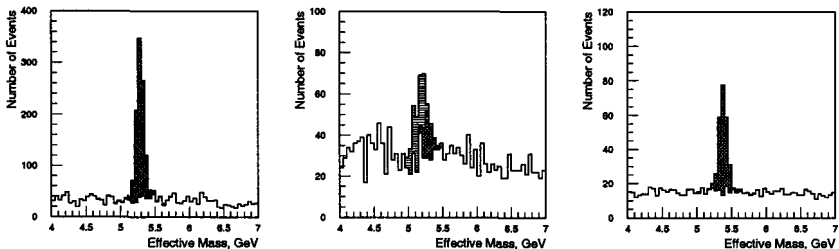
1. The main task of  $B$ -physics trigger at the LHC could be realized with fast detectors and reconstruction software and the precise simulation of special physics features of  $B$ -decays of interest.

2. Rare muonic and semimuonic  $B$ -meson decays provide the important test of the SM or its extensions and open the way for estimation the values of  $|V_{ts}|$  and  $|V_{td}|$ .

Table 3: The expected signal and BG for rare leptonic and semileptonic  $B$ -meson decays after 3 years of LHC running at low and high luminosity

$L$	Decay	Signal	BG
low	$B_d^0 \rightarrow \mu^+ \mu^-$	4	93
	$B_s^0 \rightarrow \mu^+ \mu^-$	27	93
high	$B_d^0 \rightarrow \mu^+ \mu^-$	14	660
	$B_s^0 \rightarrow \mu^+ \mu^-$	92	660
low	$B_d^0 \rightarrow K^{*0} \mu^+ \mu^-$	1995	290
	$B_d^0 \rightarrow \rho \mu^+ \mu^-$	222	950
	$B_s^0 \rightarrow \phi \mu^+ \mu^-$	411	140

Figure 1: The signal and BG mass distributions for rare semileptonic  $B$ -meson decays.



3. All of these decays could be observed with the ATLAS detector. Furthermore, the decays  $B_{s,d}^0 \rightarrow \mu^+ \mu^-$  and  $B_s^0 \rightarrow \phi \mu^+ \mu^-$  can be observed only at the LHC detectors.

### Acknowledgments

We are grateful to J.Baines, P.Eerola, N.Ellis, I.Gavrilenko, D.Melikhov, F.Rizatdinova, S.Sivoklokov and M.Smizanska for helpful and useful discussions.

### References

- [1] "The BaBar Physics Book. Physics at an Asymmetric  $B$  Factory", Edited by P.F.Harrison and H.R.Quinn, SLAC-R-504, October 1998.
- [2] "Belle Technical Design Report", KEK Reprint 95-1, 1995; K.Miyabayashi, *Acta Phys.Polon.* **B** 32, 1663 (2001).
- [3] "Physics at LEP", Edited by J.Ellis and R.Peccei, Vol.1, CERN 86-01, Geneve 1986; Vol.2 CERN 86-02, Geneve 1986;  
"Physics at LEP II", Edited by G.Altarelli, T.Sjöstrand and F.Zwirner, Vol.1, CERN 96-01, Geneve 1996; Vol.2 CERN 96-02, Geneve 1996.

- [4] "*Proceedings of the Workshop on Standard Model Physics (and more) at the LHC*", Edited by G.Altarelli and M.L.Mangano, CERN 2000-004, May 2000;  
"*ATLAS Detector and Physics Performance*", CERN/LHCC 99-14/15, ATLAS TDR 14/15, May 1999.
- [5] "*ATLAS Trigger Performance*", CERN/LHCC 98-15, August 1998.
- [6] A.Ali et al., *Z.Phys. C* 63, 437 (1994); *Phys.Rev. D* 61, 074024 (2000);  
D.Melikhov et al., *Phys.Rev. D* 57, 6814 (1998).
- [7] R.Ammar et al., *Phys.Rev.Lett.* 71, 674 (1993).
- [8] R.Abe et al., e-Print Archive hep-ex/0107072.

# TOWARDS A SIMULTANEOUS RESOLUTION OF THE COSMOLOGICAL CONSTANT AND FERMION FAMILIES PROBLEMS

E.Guendelman <sup>a</sup>, A.Kaganovich <sup>b</sup>

*Physics Department, Ben Gurion University of the Negev, Beer Sheva 84105, Israel*

*Abstract.* A spontaneously broken  $SU(2) \times U(1)$  gauge theory with just one "primordial" generation of fermions is formulated in the context of a generally covariant theory which contains two measures of integration in the action: the standard  $\sqrt{-g}d^4x$  and a new one  $\Phi d^4x$ , where  $\Phi$  is a density built out of degrees of freedom independent of the metric. Such type of models are known to produce a satisfactory answer to the cosmological constant problem. Global scale invariance is implemented. After SSB of scale invariance and gauge symmetry it is found that with the conditions appropriate to laboratory particle physics experiments, to each primordial fermion field corresponds three physical fermionic states. Two of them correspond to particles with constant masses and they are identified with the first two generations of the electro-weak theory. The third fermionic states at the classical level get non-polynomial interactions which indicate the existence of fermionic condensate and fermionic mass generation.

## 1 Introduction

One of the most perplexing questions that have arisen in the theory of elementary particles is the origin of the families (generations) of elementary fermions: electrons and quarks. Indeed, each fermion is replicated three times: instead of having one electron, we observe in addition the muon and the tau lepton; instead of one quark doublet we have three doublets of quarks. All these replications exhibit the same charge, spin, etc. but they differ in their masses.

In this paper we will follow a geometric approach to the family problem of particle physics. Basic ideas and methods of this approach have been developed in previous papers [1–5] where the emphasis was on cosmological questions, in special the question of the cosmological constant problem. It was noticed however [5] that a natural solution to the family problem could be given along these lines as well. Here we generalize the results of the toy model [5] to the  $SU(2) \times U(1)$  gauge theory.

The geometric approach of Refs. [1–5] consists of using an alternative volume element  $\Phi d^4x$ , in addition to the standard one  $\sqrt{-g}d^4x$ . So a general action of the form

$$S = \int L_1 \Phi d^4x + \int L_2 \sqrt{-g}d^4x \quad (1)$$

is considered. In order that  $\Phi d^4x$  be an invariant volume element, it is necessary that  $\Phi$  transforms as a density, i.e. just like  $\sqrt{-g}$ . This can be realized if we

---

<sup>a</sup>e-mail: guendel@bgumail.bgu.ac.il

<sup>b</sup>e-mail: alexk@bgumail.bgu.ac.il

choose  $\Phi$  to be the composite of 4 scalars  $\varphi_a$  ( $a = 1, 2, 3, 4$ )

$$\Phi = \varepsilon^{\mu\nu\alpha\beta} \varepsilon_{abcd} \partial_\mu \varphi_a \partial_\nu \varphi_b \partial_\alpha \varphi_c \partial_\beta \varphi_d. \quad (2)$$

Since  $\Phi$  is a total derivative, a shift of  $L_1$  by a constant,  $L_1 \rightarrow L_1 + const$ , has the effect of adding to S the integral of a total derivative, which does not change equations of motion. This is why the introduction of a new volume element has consequences on the way we think about the cosmological constant problem [2].

In Eq. (1),  $L_1$  and  $L_2$  are Lagrangian which are functions of the matter fields, the metric, the connection (or spin-connection) but not of the "measure fields"  $\varphi_a$ . In such a case the action (1) has the infinite dimensional symmetry [2]:  $\varphi_a \rightarrow \varphi_a + f_a(L_1)$ , where  $f_a(L_1)$  is an arbitrary function of  $L_1$ .

It may appear at first sight strange to think that geometry (measure, connections, metric) are relevant to particle physics. This is because we are used to think that these geometrical objects can be only related to gravity. However, as we will see, the consistency condition of equations of motion determines the ratio of two measures

$$\zeta \equiv \frac{\Phi}{\sqrt{-g}} \quad (3)$$

as a function of matter fields. The surprising feature of the theory is that neither Newton constant nor curvature appears in this constraint which means that the *geometrical scalar field*  $\zeta(x)$  is determined by the matter fields configuration locally and straightforward (that is without gravitational interaction). As we will see,  $\zeta(x)$  has a decisive influence in the determination of particle masses and in the "families birth effect". Therefore "Geometry" will be of importance, beyond what was known so far, i. e. that the geometrical objects which enter into the field theory are restricted by the metric associated to the gravitational field.

## 2 The model

To see how the theory works, let us consider a model containing the  $SU(2) \times U(1)$  gauge structure (the color  $SU(3)$  can be added without changing our results), as in the standard model with standard content of the bosonic sector (gauge vector fields  $A_\mu$  and  $B_\mu$  and Higgs doublet  $H$ ). But in contrast to the standard model, in our model *we start from only one family of the so called "primordial" fermionic fields*: the primordial up and down quarks  $U$  and  $D$  and the primordial electron  $E$  and neutrino  $N$ . Similar to the standard model, we will proceed with the following independent fermionic degrees of freedom:

- a) one primordial left quark  $SU(2)$  doublet  $Q_L$

$$Q_L = \begin{pmatrix} U_L \\ D_L \end{pmatrix}$$

and right primordial singlets  $U_R$  and  $D_R$ ;

b) one primordial left lepton SU(2) doublet  $L_L$ :

$$L_L = \begin{pmatrix} N_L \\ E_L \end{pmatrix}$$

and right primordial singlet  $E_R$ .

A dilaton field  $\phi$  is needed in order to achieve global scale invariance [3].

According to the general prescriptions of the two measures theory, we have to start from studying the selfconsistent system of gravity and matter fields proceeding in the first order formalism. In the model including fermions in curved space-time, this means that the independent dynamical degrees of freedom are: all matter fields, vierbein  $e_a^\mu$ , spin-connection  $\omega_{\mu}^{ab}$  and the measure  $\Phi$  degrees of freedom, i.e. four scalar fields  $\varphi_a$ . We postulate that in addition to  $SU(2) \times U(1)$  gauge symmetry, the theory is invariant under the global scale transformations:

$$\begin{aligned} e_\mu^a &\rightarrow e^{\theta/2} e_\mu^a, \quad \omega_{ab}^\mu \rightarrow \omega_{ab}^\mu, \quad \varphi_a \rightarrow \lambda_a \varphi_a \quad \text{where} \quad \Pi \lambda_a = e^{2\theta}, \\ \phi &\rightarrow \phi - \frac{M_p}{\alpha} \theta, \quad H \rightarrow H, \quad \Psi \rightarrow e^{-\theta/4} \Psi, \quad \bar{\Psi} \rightarrow e^{-\theta/4} \bar{\Psi}; \quad \theta = \text{const.} \end{aligned} \quad (4)$$

The global scale invariance is important for cosmological applications [3–5].

The action of the model has the general structure given by Eq. (1) which is convenient to represent in the following form:

$$\begin{aligned} S = & \int d^4x e^{\frac{\alpha\phi}{M_p}} (\Phi + b\sqrt{-g}) \left[ \frac{1}{2} g^{\mu\nu} \phi_{,\mu} \phi_{,\nu} + \frac{1}{2} g^{\mu\nu} (D_\mu H)^\dagger D_\nu H - \frac{1}{\kappa} R(\omega, e) \right] \\ & - \int d^4x \sqrt{-g} \left( \frac{1}{4} g^{\alpha\beta} g^{\mu\nu} B_{\alpha\mu} B_{\beta\nu} + \frac{1}{2} g^{\alpha\beta} g^{\mu\nu} \text{Tr } A_{\alpha\mu} A_{\beta\nu} \right) \\ & - \int d^4x e^{2\alpha\phi/M_p} [\Phi V_1(H) + \sqrt{-g} V_2(H)] + \int d^4x e^{\alpha\phi/M_p} (\Phi + k\sqrt{-g}) L_{fk} \\ & - \int d^4x e^{\frac{3}{2}\alpha\phi/M_p} \left[ (\Phi + h_U \sqrt{-g}) f_U \overline{Q_L} \tilde{H} U_R + (\Phi + h_D \sqrt{-g}) f_D \overline{Q_L} H D_R \right. \\ & \left. + H.c.] - \int d^4x e^{\frac{3\alpha\phi}{M_p}} (\Phi + h_E \sqrt{-g}) [f_E \overline{L_L} H e_R + H.c.] \right] \end{aligned} \quad (5)$$

The notations in (5) are the following:  $g^{\mu\nu} = e_a^\mu e_b^\nu \eta^{ab}$ ; the scalar curvature is  $R(\omega, V) = V^{a\mu} V^{b\nu} R_{\mu\nu ab}(\omega)$  where  $R_{\mu\nu ab}(\omega) = \partial_\mu \omega_{\nu ab} + \omega_{\mu a}^c \omega_{\nu cb} - (\mu \leftrightarrow \nu)$ ;  $L_{fk} = \frac{i}{2} [\overline{L}_L \not{D}^{(L)} L_L + \overline{E}_R \not{D}^{(R)} E_R + \overline{Q}_L \not{D}^{(L)} Q_L + \overline{U}_R \not{D}^{(R)} U_R + \overline{D}_R \not{D}^{(R)} D_R]$ ;  $D_\mu H \equiv \left( \partial_\mu - \frac{i}{2} g^{\vec{r}} \cdot \vec{A}_\mu - \frac{i}{2} \tilde{g}' B_\mu \right) H$ ;

$$\begin{aligned}
D^{(R)} &\equiv e_a^\mu \gamma^a \left( \vec{\partial}_\mu + \frac{1}{2} \omega_\mu^{cd} \sigma_{cd} + ig' B_\mu \right) - \left( \overleftrightarrow{\partial}_\mu - \frac{1}{2} \omega_\mu^{cd} \sigma_{cd} - ig' B_\mu \right) \gamma^a e_a^\mu; \\
D^{(L)} &\equiv e_a^\mu \gamma^a \left( \vec{\partial}_\mu + \frac{1}{2} \omega_\mu^{cd} \sigma_{cd} I - \frac{i}{2} g \vec{\tau} \cdot \vec{A}_\mu + \frac{i}{2} g' B_\mu \right) \\
&\quad - \left( \overleftrightarrow{\partial}_\mu - \frac{1}{2} \omega_\mu^{cd} \sigma_{cd} I + \frac{i}{2} g \vec{\tau} \cdot \vec{A}_\mu - \frac{i}{2} g' B_\mu \right) \gamma^a e_a^\mu; \tag{6}
\end{aligned}$$

and finally  $B_{\mu\nu} \equiv \partial_\mu B_\nu - \partial_\nu B_\mu$ ,  $A_{\mu\nu} \equiv \partial_\mu A_\nu - \partial_\nu A_\mu - ig[A_\mu A_\nu - A_\nu A_\mu]$  where  $A_\mu = \frac{1}{2} \vec{A}_\mu \cdot \vec{\tau}$ ;  $I$  is  $2 \times 2$  unit matrix in the isospin space.

A few explanations concerning our choice of the action (5) are in necessary:

1) In order to avoid a possibility of negative energy contribution from the space-time derivatives of the dilaton  $\phi$  and Higgs  $H$  fields (see Ref. [5]) we have chosen the coefficient  $b$  in front of  $\sqrt{-g}$  in the first integral of (5) to be a common factor of the gravitational term  $-\frac{1}{\kappa} R(\omega, e)$  and of the kinetic terms for  $\phi$  and  $H$ . This guarantees that this item can not be an origin of ghosts in quantum theory.

2) For the same reasons we choose the kinetic terms of the gauge bosons in the conformal invariant form which is possible only if these terms are coupled to the measure  $\sqrt{-g}$ . Introducing the coupling of these terms to the measure  $\Phi$  would lead to the nonlinear equations and non positivity of the energy.

3) For simplicity, we have taken the coupling of the kinetic terms of the fermions to the measures to be universal (see the forth integral in Eq.(5)).

Except for these three items, Eq.(5) describes the most general action of the two measures theory satisfying the formulated above symmetries.

### 3 Classical equations of motion

After SSB of scale and gauge symmetries, proceeding in the unitary gauge, the Higgs field can be represented in the standard form

$$H = \begin{pmatrix} 0 \\ \frac{1}{\sqrt{2}}(v + \chi) \end{pmatrix}$$

Varying the measure fields  $\varphi_a$ , we get  $A_a^\mu \partial_\mu L_1 = 0$  where  $L_1$  is defined, according to Eq. (1), as the part of the integrand of the action (5) coupled to the measure  $\Phi$  and  $A_a^\mu = \epsilon^{\mu\nu\alpha\beta} \epsilon_{abcd} \partial_\nu \varphi_b \partial_\alpha \varphi_c \partial_\beta \varphi_d$ .

Since  $\text{Det}(A_a^\mu) = \frac{4^{-4}}{4!} \Phi^3$  it follows that if  $\Phi \neq 0$ ,

$$L_1 = s M^4 = \text{const} \tag{7}$$

Here  $s = \pm 1$  and the appearance of a nonzero integration constant  $M^4$  of the dimension of mass spontaneously breaks the scale invariance (4).

Complete system of equations corresponding to the action (5) is very bulky. Variation of  $S$  with respect to vierbein  $e_a^\mu$  yields the gravitational equation linear both in the curvature and in the scalar field  $\zeta$ , defined by Eq. (3). Contracting this equation with  $e_a^\mu$ , solving for the curvature scalar  $R$  and replacing in Eq. (7) we obtain the following consistency condition of the theory:

$$\begin{aligned} & (\zeta - b) \left[ sM^4 e^{-\alpha\phi/M_p} + V_1 e^{\alpha\phi/M_p} - L_{fk} + \frac{v + \chi}{\sqrt{2}} e^{\frac{1}{2}\alpha\phi/M_p} \sum_i f_i \bar{\Psi}_i \Psi_i \right] + \\ & + 2V_2 e^{-\alpha\phi/M_p} + \frac{1}{2}(\zeta - 3k)L_{fk} + \sqrt{2}(v + \chi)e^{\frac{1}{2}\alpha\phi/M_p} \sum_i f_i h_i \bar{\Psi}_i \Psi_i = 0 \quad (8) \end{aligned}$$

where  $i = E, U, D$ ,  $\Psi_i$  labels  $E$ ,  $U$  and  $D$  fermion fields and  $L_{fk}$  was defined in Sec.2. Using equations of motion for all the fermion fields, it is easy to check that the following relation is true

$$\begin{aligned} L_{fk} = & \frac{e^{\frac{1}{2}\alpha\phi/M_p}}{\zeta + k} \left[ (\zeta + h_E) f_E \overline{L} \overline{L} H e_R + (\zeta + h_U) f_U \overline{Q} \overline{L} \tilde{H} U_R \right. \\ & \left. + (\zeta + h_D) f_D \overline{Q} \overline{L} H D_R + H.c. \right] \quad (9) \end{aligned}$$

Due to this relation, the consistency condition (8) becomes a constraint having a fundamental role for the theory.

In order to get the physical content of the theory it is required to express it in terms of variables where all equations of motion acquire a canonical form in an Einstein-Cartan space-time (for detail see Ref. [?]). This is possible after performing the following redefinitions of the vierbein (and metric) and all fermion fields:

$$\tilde{g}_{\mu\nu} = e^{\frac{\alpha\phi}{M_p}} (\zeta + b) g_{\mu\nu}; \tilde{e}_{a\mu} = e^{\frac{\alpha\phi}{2M_p}} (\zeta + b)^{1/2} e_{a\mu}; \Psi'_i = e^{-\frac{\alpha\phi}{4M_p}} \frac{(\zeta + k)^{1/2}}{(\zeta + b)^{3/4}} \Psi_i. \quad (10)$$

With these variables, the spin-connections become those of the Einstein-Cartan space-time. Since  $\tilde{e}_{a\mu}$  and  $\Psi'$  are invariant under the scale transformations (4), spontaneous breaking of the scale symmetry (4) (by means of Eq. (7)) is reduced in the new variables to the spontaneous breaking of the shift symmetry  $\phi \rightarrow \phi + const$  for the dilaton field.

One can check that equations of motion for the gauge fields in the new variables are canonical and after the Higgs develops VEV, the gauge bosons mass generation is standard, that is exactly the same as it is in the Weinberg-Salam electroweak theory: photon,  $W^\pm$  and  $Z$  bosons as well as the Weinberg angle appear as the result of the standard procedure of the Weinberg-Salam theory.

The gravitational equations of motion in the new variables take the form

$$G_{\mu\nu}(\tilde{g}_{\alpha\beta}) = \frac{\kappa}{2} T_{\mu\nu}^{eff} \quad (11)$$

$$\begin{aligned} T_{\mu\nu}^{eff} &= \phi_{,\mu}\phi_{,\nu} - K_\phi \tilde{g}_{\mu\nu} + \chi_{,\mu}\chi_{,\nu} - K_\chi \tilde{g}_{\mu\nu} + \tilde{g}_{\mu\nu} V_{eff} \\ &+ T_{\mu\nu}^{(gauge,can)} + T_{\mu\nu}^{(ferm,can)} - \tilde{g}_{\mu\nu} \sum_i F_i(\zeta, v+\chi) \bar{\Psi}'_i \Psi'_i, \end{aligned} \quad (12)$$

Here  $G_{\mu\nu}(\tilde{g}_{\alpha\beta})$  is the Einstein tensor in the Riemannian (or, more exactly, Einstein-Cartan) space-time with metric  $\tilde{g}_{\mu\nu}$ ;  $K_\phi \equiv \frac{1}{2}\tilde{g}^{\alpha\beta}\phi_{,\alpha}\phi_{,\beta}$ ;

$K_\chi \equiv \frac{1}{2}\tilde{g}^{\alpha\beta}\chi_{,\alpha}\chi_{,\beta}$ ;  $T_{\mu\nu}^{(gauge,can)}$  is the canonical energy momentum tensor for gauge bosons, including mass terms of  $W^\pm$  and  $Z$  bosons.  $T_{\mu\nu}^{(ferm,can)}$  is the canonical energy momentum tensor for (primordial) fermions  $E'$ ,  $U'$  and  $D'$  in curved space-time including also their standard electromagnetic and weak interactions with gauge bosons. Functions  $V_{eff}$  and  $F_i(\zeta, v+\chi)$  ( $i = E', U', D'$ ) are defined by equations

$$V_{eff} = \frac{b(sM^4 e^{-2\alpha\phi/M_p} + V_1) - V_2}{(\zeta + b)^2} \quad (13)$$

$$F_i \equiv \frac{(v + \chi)f_i}{2\sqrt{2}(\zeta + k)^2(\zeta + b)^{1/2}} [\zeta^2 + (3h_i - k)\zeta + 2b(h_i - k) + kh_i]; \quad i = E', U', D' \quad (14)$$

The scalar field  $\zeta$  in the above equations is defined by the constraint determined by means of Eqs. (8) and (9). In the new variables (10) this constraint takes the form

$$(\zeta - b) \left[ sM^4 e^{-\frac{2d\phi}{M_p}} + V_1(v + \chi) \right] + 2V_2(v + \chi) + (\zeta + b)^2 \sum_i F_i(\zeta, v + \chi) \bar{\Psi}'_i \Psi'_i = 0 \quad (15)$$

The dilaton  $\phi$  and Higgs  $\chi$  field equations in the new variables are the following

$$\square\phi - \frac{\alpha}{M_p(\zeta + b)} \left[ sM^4 e^{-2\alpha\phi/M_p} - \frac{(\zeta - b)V_1 + 2V_2}{\zeta + b} \right] = -\frac{\alpha}{M_p} \sum_i F_i \bar{\Psi}'_i \Psi'_i, \quad (16)$$

$$\square\chi + \frac{\zeta V'_1 + V'_2}{(\zeta + b)^2} = -\frac{v + \chi}{\sqrt{2}(\zeta + b)^{1/2}(\zeta + k)} \sum_i (\zeta + h_i) f_i \bar{\Psi}'_i \Psi'_i, \quad (17)$$

where  $\square\phi = (-\tilde{g})^{-1/2} \partial_\mu (\sqrt{-\tilde{g}} \tilde{g}^{\mu\nu} \partial_\nu \phi)$  and similarly for  $\square\chi$ .

Equations for the primordial fermions  $E'$ ,  $U'$  and  $D'$  in terms of the variables (10) take the standard form of fermionic equations in the Einstein-Cartan space-time where the standard interactions to the gauge fields present also. All the novelty consists of the form of the  $\zeta$  depending "masses"  $m_i(\zeta)$  of the primordial fermions:

$$m_i(\zeta) = \frac{f_i v(\zeta + h_i)}{\sqrt{2}(\zeta + k)(\zeta + b)^{1/2}} \quad i = E', U', D'. \quad (18)$$

#### 4 Vacuum and families birth effect

Let us consider the following two limiting cases:

(i) **In the absence of massive fermions**, solving  $\zeta$  from the constraint (15)

$$\frac{1}{\zeta + b} = \frac{sM^4 e^{-2\alpha\phi/M_p} + V_1}{2 [b (sM^4 e^{-2\alpha\phi/M_p} + V_1(v + \chi)) - V_2(v + \chi)]} \quad (19)$$

one can check that in this case the dilaton and Higgs fields equations (16) and (17) take the form of the canonical scalar fields equations with the effective potential

$$V_{eff}(\phi, v + \chi) = \frac{[sM^4 e^{-2\alpha\phi/M_p} + V_1(v + \chi))]^2}{4 [b (sM^4 e^{-2\alpha\phi/M_p} + V_1(v + \chi)) - V_2(v + \chi)]} \quad (20)$$

From this we immediately conclude that the stable vacuum of the scalar fields ( $\langle \phi \rangle \equiv \bar{\phi}$  and  $v$ ) is realized as a manifold determined by the equation

$$sM^4 e^{-2\alpha\bar{\phi}/M_p} + V_1(v) = 0 \quad (21)$$

provided that  $V_2(v) < 0$  in this degenerate vacuum. The masses of the dilaton and Higgs fields excitations above this degenerate vacuum are respectively

$$m_{dilat}^2 = \frac{\alpha^2 M^8}{M_p^2 |V_2(v)|} e^{-4\alpha\bar{\phi}/M_p}; \quad m_{higgs}^2 = \frac{(V'_1(v))^2}{|V_2(v)|}. \quad (22)$$

Notice that we did not assume any specific properties of  $V_1$  and  $V_2$  so far. If we wish to provide conditions for a big Higgs mass we see from the second equation in (22) that there is no need for big "pre-potentials"  $V_1(v)$  and  $V_2(v)$  but rather they both can be small as compared to a typical energy scale of particle physics, however  $V_2(v)$  must be very small.

An important feature of the degenerate vacuum (21) is that the effective vacuum energy density of the scalar fields is equal to zero without any sort of fine tuning regardless of the detailed shape of the potentials  $V_1$  and  $V_2$  as well as of the initial conditions. This fact has been very extensively explored as a way to solve the cosmological constant problem [2]. In this paper, however, we will concentrate our attention on the applications of the theory to particle physics.

Notice that according to Eq. (19),  $\zeta = \infty$  in the degenerate vacuum (21). However, in the presence of any small "contamination" by massive fermions, it follows from the constraint (15) that  $\zeta$  is large but finite. Therefore we must return to the general form of the effective potential (13) which will be small but non zero. This means that zero vacuum energy is practically unachievable, and there must be a correlation between the fermion content of the universe

and the vacuum energy. This correlation might be a possible mechanism for the explanation of the "cosmic coincidence" problem [6].

(ii) **Case where fermion densities are of the typical laboratory particle physics scales.** Assuming as it was done before that  $M^4 e^{-2\alpha\phi/M_p}$ ,  $V_1$  and  $V_2$  are small as compared to the typical particle physics energy densities of fermions, we see from the constraint (15) that now there are no reasons for  $\zeta$  to be large. On the contrary, it has to be of the same order as the dimensionless parameters of the theory ( $b$ ,  $k$  and  $h_i$ ) which we assume are of order one. So, for the case when fermion densities are of the typical laboratory particle physics scales,  $\zeta$  has to satisfy the simplified form of the constraint(15):

$$(\zeta + b)[F_E(\zeta)\overline{E}'E' + F_U\overline{U}'U' + F_D\overline{D}'D'] = 0. \quad (23)$$

To see the meaning of the constraint in this case, let us take one single primordial fermionic state: or  $E'$ , or  $U'$ , or  $D'$ . Then we have three solutions for each of  $\zeta^{(i)}$ , ( $i = E', U', D'$ ): two constant solutions are defined by the condition  $F_i(\zeta) = 0$

$$\zeta_{1,2}^{(i)} = \frac{1}{2} \left[ k - 3h_i \pm \sqrt{(k - 3h_i)^2 + 8b(k - h_i) - 4kh_i} \right], \quad i = E', U', D' \quad (24)$$

and the third solution  $\zeta + b = 0$ .

The first two solutions correspond to two different states of the  $i$ 's primordial fermion with different masses determined by Eq.(18) where we have to substitute  $\zeta_{1,2}^{(i)}$  instead of  $\zeta$ . These two states can be identified with *the first two generations of the physical leptons and quarks*.

Surprisingly that the same combination that we see in the l.h.s. of the constraint (23) appears in the last terms of Eqs. (16) and (12) (we assume here that  $\zeta + b \neq 0$ ). Therefore, in the regime where the regular fermionic matter (i.e.  $u$  and  $d$  quarks,  $e^-$  and  $\nu_e$ ) dominates, the last terms of Eqs. (16) and (12) automatically vanish. In Eq. (16), this means that *the fermion densities are not a source for the dilaton and thus the long-range forces disappear automatically*. Notice that there is no need to require no interactions of the dilaton with fermionic matter at all to have agreement with observations but it is rather enough that these interactions vanish in the appropriate regime where regular fermionic matter has the typical laboratory particle physics density. In Eq. (12), the condition (23) means that in the region where the regular fermionic matter dominates, the fermion energy-momentum tensor becomes equal to the canonical energy-momentum tensor of fermion fields in GR (see also Ref. [5]).

The third solution  $\zeta + b = 0$  is singular one as we see from equations of motion. This means that one can not neglect the first two terms in the constraint (15). Then instead of  $\zeta + b = 0$  we have to take the solution  $\zeta + b \approx 0$  by solving  $\zeta + b$  in terms of the dilaton and Higgs fields and the primordial fermionic fields

themselves.

$$\frac{1}{\sqrt{\zeta_3 + b}} \approx \left[ \frac{v [f_E(b - h_E)\bar{E}'E' + f_U(b - h_U)\bar{U}'U' + f_D(b - h_D)\bar{D}'D']}{4\sqrt{2}(b - k) [b(sM^4e^{-2\alpha\phi/M_p} + V_1) - V_2]} \right]^{1/3} \quad (25)$$

This leads to non-polynomial fermion interactions. A full treatment of the third family requires the study of quantum corrections and fermion condensates which will give the third family appropriate masses. Interestingly enough that the effective coupling constants of the non-polynomial interactions are dimensionless, which suggests that the quantum corrections of this theory may be meaningful.

Finally, it is important to notice that the theory explained here allows for transitions from a certain family to another. One can indeed notice from the constraint itself that the three distinct values of  $\zeta$  (again, for the fermion densities corresponding to laboratory conditions) can coincide when several types of fermions are present at the same space-time point. Once one reaches these "unification points", it is clear that transitions from family to family are possible. The calculation of the amplitudes of these transitions appear to be technically complicated but are in principle calculable. Therefore the parameters of the Kobayashi-Maskawa mass matrix should be indeed calculable as a function of the parameters of the theory. In this report we have ignored the question of a possible neutrino mass. but there is no problem to incorporate it in our formalism. In this case the physics of neutrino mixing will have some resemblance to the situation with quarks. It would be very important to see how the phenomenon of neutrino oscillations could appear in the context of this theory.

## References

- [1] E.I. Guendelman and A.B. Kaganovich, Phys. Rev. **D 53** (1996) 7020; ibid. **D 55** (1997) 5970; Mod. Phys. Lett. **A 12** (1997) 2421.
- [2] E.I. Guendelman and A.B. Kaganovich, Phys. Rev. **D 56** (1997) 3548; ibid. **D 55** (1997) 5970; ibid. **D 57** (1998) 7200; ibid. **D 60** (1999) 065004; Mod. Phys. Lett. **A 12** (1997) 2421 (1997); ibid. **A 13** (1998) 1583.
- [3] E.I. Guendelman, Mod. Phys. Lett. **A 14** (1999) 1043; Class. Quant. Grav. **17** (2000) 361; gr-qc/0004011; Mod. Phys. Lett. **A 14** (1999) 1397; gr-qc/9901067; hep-th/0106085; Found. Phys. **31** (2001) 1019.
- [4] A.B. Kaganovich, Phys. Rev. **D 63** (2001) 025022.
- [5] E.I. Guendelman and A.B. Kaganovich, "SSB of scale symmetry, fermion families and quintessence without the long-range force problem", hep-th/0110040.
- [6] P. Steinhardt, L Wang and I. Zlatev, Phys. Rev. **D 59** (1999) 123504.

# THE SHAPE OF THE $K_{\alpha}$ LINE AS A POSSIBLE INDICATION OF THE BLACK HOLE EXISTENCE

A.F. Zakharov<sup>1a</sup>, S.V. Repin<sup>2b</sup>

<sup>1</sup>*Institute of Theoretical and Experimental Physics,  
25, B.Cheremushkinskaya st., Moscow, 117259, Russia*

<sup>2</sup>*Space Research Institute, 84/32, Profsoyuznaya st.,  
Moscow, 117810, Russia*

**Abstract.** Observations of Seyfert galaxies in X-ray region reveal the wide emissive lines in their spectra, which can arise in inner parts of accretion disks, where the effects of General Relativity (GR) must be counted. A spectrum of a solitary emission line of a hot spot in Kerr accretion disk is simulated, depending on the radial coordinate  $r$  and the angular momentum  $a = J/M$  of a black hole, under the assumption of equatorial circular motion of a hot spot. It is shown that the characteristic two-peak line profile with the sharp edges arises at a large distance, (about  $r \approx (3 - 10) r_g$ ). The inner regions emit the line, which is observed with one maximum and extremely wide red wing. High accuracy future spectral observations, being carried out, could detect the angular momentum  $a$  of the black hole.

## 1 Introduction

The general status of black holes described in a number of papers (see, for example [1–3] and references therein). As it was emphasized in these reviews the most solid evidence for an existence of black holes comes from observations of some Seyfert galaxies because we need a strong gravitational field approximation to interpret these observational data, so probably we observe manifestations radiation processes from the vicinity of the black hole horizon (these regions are located inside the Schwarzschild black hole horizon, but outside the Kerr black hole horizon, thus we should conclude that we have manifestations of rotational black holes).

Recent observations of Seyfert galaxies in X-ray band [4–9] reveal the existence of wide iron  $K_{\alpha}$  line (6.4 keV) in their spectra along with a number of other weaker lines (Ne X, Si XIII,XIV, S XIV-XVI, Ar XVII,XVIII, Ca XIX, etc.). The line width corresponds to the velocity of the matter motion of tens of thousands kilometers per second, reaching the maximum value  $v \approx 80000 - 100000$  km/s [5] for the galaxy MCG-6-30-15 and  $v \approx 48000$  km/s [10] for MCG-5-23-16. In some cases the line has characteristic two-peak profile [5, 11] with a high “blue” maximum and the low “red” one and the long red wing, which gradually drops to the background level.

For individual objects, where the existence of the black holes is assumed, a strong variability of X-ray brightness was registered [12], as well as the rapid changes of the line profile (Yaqoob et al. [11], NGC 7413) and the quasiperiodic oscillations ([13], GRC 1915+105).

The large amount of observational data requires its comprehension, theoretical simulation and interpretation. The numerical simulations of the accretion disk spectrum under GR assumptions has been reported in the paper [14]. In the paper [15] the

---

<sup>a</sup>e-mail: zakharov@vitep5.itep.ru

<sup>b</sup>e-mail: repin@mx.iki.rssi.ru

observational manifestations of GR effects are considered in X-ray binaries. Different physical models of the origin of a wide emissive iron  $K_{\alpha}$  line in the nuclei of Seyfert galaxies are analyzed in the paper [16]. Non-geodesic motion of the emitting hot spot, representing the magnetic field loop, is simulated in the paper [17] in the framework of the magnetohydrodynamics approach.

The numerical approach, applied here based on the method, described earlier in papers [18–21].

## 2 The particles motion in a Kerr metric

Many astrophysical processes, where the great energy release is observed, are assumed to be connected with the black holes. Because the main part of the astronomical objects, such as the stars and galaxies, possesses the proper rotation, then there are no doubts that the black holes, both stellar and supermassive, possess the intrinsic proper rotation too.

The stationary black holes are described by the Kerr metric [22]:

$$ds^2 = -\frac{\Delta}{\rho^2} (dt - a \sin^2 \theta d\phi)^2 + \frac{\sin^2 \theta}{\rho^2} [(r^2 + a^2) d\phi - adt]^2 + \frac{\rho^2}{\Delta} dr^2 + \rho^2 d\theta^2, \quad (1)$$

where

$$\rho^2 = r^2 + a^2 \cos^2 \theta, \quad \Delta = r^2 - 2Mr + a^2. \quad (2)$$

The equations geodesics however can be simplified if we will use the complete set of the first integrals which were found by Carter [23]:  $E = p_t$  is the particle energy at infinity,  $L_z = p_{\phi}$  is  $z$ -component of its angular momentum,  $m = p_i p^i$  is the particle mass and  $Q$  is the Carter's separation constant [23]:

$$Q = p_{\theta}^2 + \cos^2 \theta [a^2 (m^2 - E^2) + L_z^2 / \sin^2 \theta]. \quad (3)$$

As shown by Zakharov [18, 24], the equations of photon motion can be reduced to

$$\frac{dt'}{d\sigma} = -a (\sin^2 \theta - \xi) + \frac{r^2 + a^2}{\Delta} (r^2 + a^2 - \xi a), \quad (4)$$

$$\frac{dr}{d\sigma} = r_1, \quad (5)$$

$$\frac{dr_1}{d\sigma} = 2r^3 + (a^2 - \xi^2 - \eta) r + (a - \xi) + \eta, \quad (6)$$

$$\frac{d\theta}{d\sigma} = \theta_1, \quad (7)$$

$$\frac{d\theta_1}{d\sigma} = \cos \theta \left( \frac{\xi^2}{\sin^3 \theta} - a^2 \sin \theta \right), \quad (8)$$

$$\frac{d\phi}{d\sigma} = - \left( a - \frac{\xi}{\sin^2 \theta} \right) + \frac{a}{\Delta} (r^2 + a^2 - \xi a), \quad (9)$$

where  $\eta = Q/M^2 E^2$  and  $\xi = L_z/ME$  are the Chandrasekhar's constants [25], which should be derived from the initial conditions in the disk plane;  $r$  and  $a$  are the appropriate dimensionless variables. The system (4)-(9) has also two integrals,

$$\epsilon_1 \equiv r_1^2 - r^4 - (a^2 - \xi^2 - \eta) r^2 - 2 [(a - \xi)^2 + \eta] r + a^2 \eta = 0, \quad (10)$$

$$\epsilon_2 \equiv \theta_1^2 - \eta - \cos^2 \theta \left( a^2 - \frac{\xi^2}{\sin^2 \theta} \right) = 0, \quad (11)$$

which can be used for the precision control. This method differs from the approach which was developed in papers [26–29].

We assume that the hot spot emits isotropically distributed quanta in the local frame. First, one should define the Chandrasekhar's constants for each quantum and then integrate the system (4)-(9) to either the infinity or the events horizon, depending on the constants values.

The trajectories classification, depending on the Chandrasekhar's constants can be found in the papers [30, 31]. The details of simulation and initial conditions can be found in papers [18, 21].

### 3 Simulation results

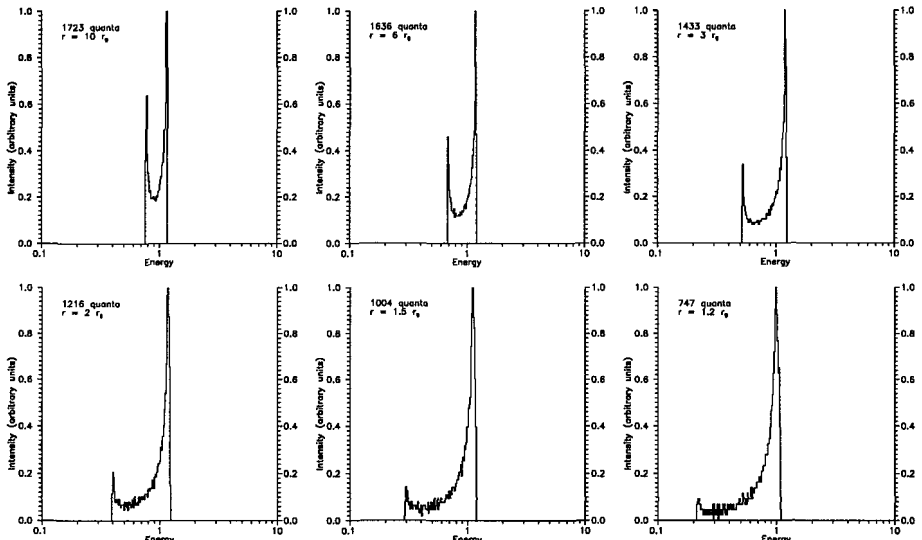


Figure 1: Spectrum of a hot spot for  $a = 0.9$ ,  $\theta = 60^\circ$  and different values of the radial coordinate. The marginally stable orbit lays at  $r = 1.16r_g$ .

The simulated spectrum of a hot spot for  $a = 0.9$ ,  $\theta = 60^\circ$  and different radius values is shown in Fig. 1. The proper quantum energy (in co-moving frame) is set to unity. The observer at infinity registers then the characteristic two-peak profile, where the “blue” peak is higher than the “red” one and the center is shifted to the left. Some

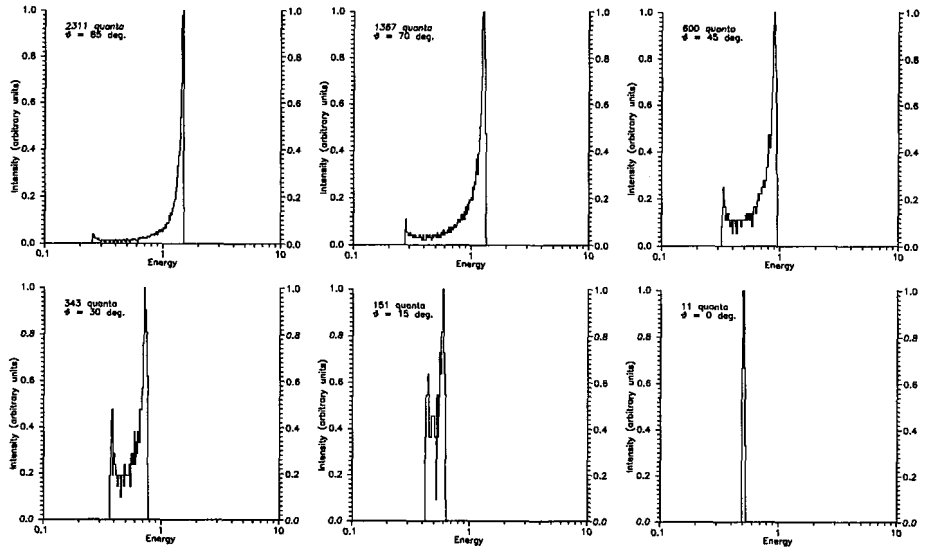


Figure 2: Spectrum of a hot spot for  $a = 0.9$ ,  $r = 1.5r_g$  and different  $\theta$  angle values.

spectrum juggling near its minimum is explained by pure statistical reasons and has no the physical nature.

As far as the radius diminishes the spectrum is enhanced, i.e. increases the residual between the maximum and minimum quanta energy, registered by far observer. For example, for  $a = 0.9$ ,  $r = 1.2r_g$  and  $\theta = 60^\circ$ , where  $r_g$  has its standard form  $r_g = 2kM/c^2$ , i.e. in the vicinity of the marginally stable orbit, the quanta, flown out to the distant observer, may differ 5 times in their energy. The red maximum decreases its height with diminishing the radius and at  $r < 2r_g$  becomes almost undistinguishable. It is interesting to note that the spectrum has very sharp edges, both red and blue. Thus, for  $a = 0.9$ ,  $r = 3r_g$ ,  $\theta = 60^\circ$  the distant observer has registered 1433 quanta of 20417 isotropically emitted; 127 of them ( $\approx 9\%$ ) drop to the interval  $1.184 < E < 1.202$  (blue maximum) and 43 quanta drop to  $0.525 < E < 0.533$  (red maximum), whereas no one quantum has the energy  $E < 0.518$  or  $E > 1.236$ .

A spectrum of a hot spot for  $a = 0.9$ ,  $r = 1.5r_g$  and different  $\theta$  values is shown on Fig. 2. The spectrum for  $\theta = 60^\circ$  and the same  $a$  and  $r$  values is included in Fig. 1 and should be added to the current figure too. As it follows from the figure, the spectrum critically depends on the disk inclination angle. For large  $\theta$  values, when the line of sight slips almost along the disk plane, the spectrum is strongly stretched, its red maximum is essentially absent, but the blue one appears narrow and very high. The red wing is strongly stretched because of the Doppler effect, so that the observer registers the quanta with 5 times energy difference. As far as the  $\theta$  angle diminishes the spectrum grows narrow and changes the shape: its red maximum first appears and then gradually increases its height. At  $\theta = 0^\circ$  both maxima merge to each other and the spectrum looks like the  $\delta$ -function. It is evident since all the

points of the emitting ring are equal in their conditions with respect to the observer. The frequency of registered quanta in that case is 2 time lower than the frequency of the emitted ones. A fall in frequency consists here in two effects, acting in the same direction: the transversal Doppler effect and the gravitational red shift.

#### 4 Discussion and conclusions

The strong variability of Seyfert galaxies in X-ray does not contradict the assumption, that we observe the emission of the hot spots from the inner region of accretion disk, which can decay or grow dim, going towards a horizon as time passes. The spectrum dynamics is understood qualitatively by reference to Fig. 1, considered sequentially from top to bottom. The exact time characteristics of this process depend critically on the disk model [32, 33] and on the physical nature of a hot spot and are not discussed here.

The assumption can be checked out in long-term systematic X-ray observations with high time resolution of such Seyfert galaxies as NGC 1068, NCG 2110, MCG-6-30-15, NGC 4507, etc., where  $K_{\alpha}$  line is sharply defined. The observations could confirm the existence of multiple spots, which motion and dynamics lead to X-ray variability in intensity and spectrum.

#### Acknowledgements

This work was supported in part by Russian Foundation for Basic Research (project N 00-02-16108).

#### References

- [1] A.F. Zakharov, in "*Fundamental problems of high energy physics and field theory*" (Proceedings of the XXIII Workshop on High Energy Physics and Field Theory), ed. by I.V. Filimonova and V.A. Petrov, Institute for High Energy Physics, Protvino, 169, 2000.
- [2] V.P. Frolov, I.D. Novikov, *Physics - Uspekhi* **44**, 291 (2001).
- [3] E.P. Liang, *Physics Reports* **302**, 69 (1998).
- [4] A.C. Fabian *et al.*, *MNRAS* **277**, L11 (1995).
- [5] Y. Tanaka, *et al.*, *Nature* **375**, 659 (1995).
- [6] K. Nandra *et al.*, *ApJ* **476**, 70 (1997).
- [7] K. Nandra *et al.*, *ApJ* **477**, 602 (1997).
- [8] A. Malizia *et al.*, *ApJSS* **113**, 311 (1997).
- [9] R.M. Sambruna *et al.*, *ApJ* **495**, 749 (1998).
- [10] K.A. Weaver, J.H. Krolik, E.A. Pier, *ApJ* **498**, 213 (1998).
- [11] T. Yaqoob *et al.*, *ApJ* **490**, L25 (1997).
- [12] J.W. Sulentic, P. Marziani, M. Calvani, *ApJ* **497**, L65 (1998).
- [13] B. Paul *et al.*, *ApJ* **492**, L63 (1998).
- [14] B.C. Bromley, K. Chen, W.A. Miller, *ApJ* **475**, 57 (1997).
- [15] W. Cui, S.N. Zhang, W. Chen, *ApJ* **492**, L53 (1998).
- [16] J.M. Sulentic *et al.*, *ApJ* **501**, 54 (1998).

- [17] M.M. Romanova *et al.*, *ApJ* **500**, 703 (1998).
- [18] A.F. Zakharov, *MNRAS* **269**, 283 (1994).
- [19] A.F. Zakharov, Preprint MPA **755**, 1993.
- [20] A.F. Zakharov, in "Annals for the 17th Texas Symposium on Relativistic Astrophysics", The New York Academy of Sciences, **759**, 550, 1995.
- [21] A.F. Zakharov, S.V. Repin, *AZh* **76**, 803 (1999).
- [22] C.W. Misner, K.S. Thorne, J.A. Wheeler, "Gravitation" W.H.Freeman and Company, San Francisco, 1973.
- [23] B. Carter, *Phys. Rev.* **D174**, 1559 (1968).
- [24] A.F. Zakharov, *AZh* 1991, **35**, 145 (1991).
- [25] S. Chandrasekhar, "Mathematical Theory of Black Holes" Clarendon Press, Oxford, 1983.
- [26] C.T. Cunningham, *ApJ* **202**, 788 (1975).
- [27] C.T. Cunningham, J.M. Bardeen, *ApJ* **183**, 237 (1973).
- [28] V. Karas, D. Vokrouhlický, A.G. Polnarev, *MNRAS* **259**, 569 (1992).
- [29] K.P. Rauch, R.D. Blandford, *Caltech Preprint*, GRP-334, 1993.
- [30] A.F. Zakharov, *ZhETPh* **91**, 3 (1986).
- [31] A.F. Zakharov, *ZhETPh* **95**, 385 (1989).
- [32] I.D. Novikov, K.S.Thorne, in "Black Holes", ed. by C. De Witt & B.S. De Witt, Gordon & Breach, New York, 334, 1973.
- [33] N.I. Shakura, R.A. Sunyaev, *Astron. & Astroph.* **24**, 337 (1973).

# QUANTUM COSMOLOGICAL MODEL WITH ROTATION

M.Fil'chenkov <sup>a</sup>,

*Peoples' Friendship University of Russia, 6 Miklukho-Maklaya Street, Moscow  
117198, Russia*

*Abstract.* The birth of a universe with rotation is regarded as a quantum tunnelling. An angular momentum of the universe proves to diminish its tunnelling probability. The upper limit for the angular velocity of the Universe's rotation allows the rotation of spiral galaxies to be due to cosmological effects.

## 1 Slow Rotation

Of importance is the question of rotation of the early Universe despite the observable angular velocity is now negligible if exists [1–4]. Friedmann's equations slightly perturbed by a slow rotation satisfying the condition  $\omega^2 \ll \frac{8\pi G\varepsilon}{3c^2}$ , where  $\omega$  is the angular velocity and  $\varepsilon$  is the energy density, are modified as follows:

$$\frac{\dot{a}^2}{2} + \frac{\omega^2 a^2}{2} - \frac{4\pi G a^2 \varepsilon}{3c^2} = -\frac{kc^2}{2}, \quad (1)$$

$$\ddot{a} = -\frac{4\pi G}{3c^2} (\varepsilon + 3p)a, \quad (2)$$

where the equation of state

$$p = \alpha\varepsilon. \quad (3)$$

The momentum conservation law for each kind of matter is [3]

$$\frac{p + \varepsilon}{c^2} a^5 \omega = J, \quad (4)$$

where  $J$  is the angular momentum.

For multicomponent matter we have [5]

$$\varepsilon = \varepsilon_0 \sum_{n=0}^6 B_n \left( \frac{r_0}{a} \right)^n, \quad (5)$$

$$\omega^2 = \frac{9J^2 c^4}{\varepsilon_0^2 r_0^{10}} \sum_{n=1}^6 \frac{1}{n^2 B_n^2} \left( \frac{r_0}{a} \right)^{2(5-n)}, \quad (6)$$

where  $n = 3(1 + \alpha)$ . In the latter we neglected the term corresponding to  $n = 0$  ( $\alpha = -1$ ,  $p = -\varepsilon$ ) since it corresponds to  $J = 0$ . The coefficients  $B_n$  are normalized by the condition

$$\sum_{n=0}^6 B_n = 1 \quad (7)$$

since they are contributions of different kinds of matter to the total energy density on the de Sitter horizon  $r_0$  satisfying the relation

$$\frac{8\pi G \varepsilon_0}{3c^4} = \frac{1}{r_0^2}. \quad (8)$$

---

<sup>a</sup>e-mail: fil@crozna.net

In the conformal time  $\eta$ , defined as  $cdt = ad\eta$ , the Lagrangian is

$$L = \frac{1}{2} \left( \frac{da}{d\eta} \right)^2 + \frac{\omega^2 a^2}{2} + \frac{4\pi G a^2 \varepsilon}{3c^2} - \frac{ka^2}{2}. \quad (9)$$

## 2 Quantization

The corresponding Hamiltonian  $H = 0$  after substituting the generalized momentum

$$P = \frac{\partial L}{\partial(\frac{da}{d\eta})} = \frac{da}{d\eta} \quad (10)$$

by the operator

$$\hat{P} = \frac{1}{i} l_{pl}^2 \frac{d}{da} \quad (11)$$

gives Wheeler-DeWitt's equation as follows

$$\frac{d^2\psi}{da^2} - V(a)\psi = 0, \quad (12)$$

where

$$V(a) = \frac{1}{l_{pl}^4} \left[ ka^2 - \left( \frac{8\pi G \varepsilon}{3c^4} - \frac{\omega^2}{c^2} \right) a^4 \right]. \quad (13)$$

Reducing it to Schrödinger's form, we have

$$\frac{\hbar^2}{2m_{pl}} \frac{d^2\psi}{da^2} - [U(a) - E]\psi = 0 \quad (14)$$

with

$$V(a) = \frac{2m_{pl}}{\hbar^2} [U(a) - E]. \quad (15)$$

In case Friedmann's unperturbed world contains only de Sitter's vacuum, strings and radiation, for a slow rotation we have

$$E = \frac{m_{pl} c^2}{2} \left( \frac{r_0}{l_{pl}} \right)^2 \left( B_4 - \frac{J^2 c^2}{\varepsilon_0^2 r_0^8 B_3^2} \right), \quad (16)$$

$$U(a) = \frac{m_{pl} c^2 a^2}{2l_{pl}^2} \left[ k - B_2 + \frac{9J^2 c^2}{16\varepsilon_0^2 r_0^8 B_4^2} - \frac{a^2}{r_0^2} \left( B_0 - \frac{9J^2 c^2}{25\varepsilon_0^2 r_0^8 B_5^2} \right) \right], \quad (17)$$

where  $B_4 \gg \frac{J^2 c^2}{\varepsilon_0^2 r_0^8 B_3^2}$ ;  $B_2 \gg \frac{9J^2 c^2}{16\varepsilon_0^2 r_0^8 B_4^2}$ ;  $B_0 \gg \frac{9J^2 c^2}{25\varepsilon_0^2 r_0^8 B_5^2}$ .

The tunnelling factor (a universe's birth probability) is given by Gamow's formula

$$D = \exp\left\{-\frac{2}{\hbar} \left| \int_{a_1}^{a_2} \sqrt{2m[E - U(a)]} da \right| \right\}, \quad (18)$$

where  $m = m_{pl}$ ,  $U(a_1) = U(a_2) = E$ . Calculating the integral in (18) near the maximum of  $U(a)$ , we have [6]

$$D = \exp \left\{ -\pi \left( \frac{r_0}{l_{pl}} \right)^2 \frac{\left| \frac{\left( k - B_2 + \frac{9J^2c^2}{16\varepsilon_0^2 r_0^8 B_4^2} \right)^2}{4 \left( B_0 - \frac{9J^2c^2}{25\varepsilon_0^2 r_0^8 B_5^2} \right)} - B_4 + \frac{J^2c^2}{25\varepsilon_0^2 r_0^8 B_5^2} \right|}{\sqrt{2 \left( k - B_2 + \frac{9J^2c^2}{16\varepsilon_0^2 r_0^8 B_4^2} \right)}} \right\}. \quad (19)$$

For  $k - B_2 \ll \frac{9J^2c^2}{16\varepsilon_0^2 r_0^8 B_4^2}$  and  $B_4 \ll \frac{3Jc}{4\varepsilon_0 r_0^4} \sqrt{\frac{\pi}{B_0}}$  we have

$$D = \exp \left\{ -\frac{27\pi J^3 c^3}{256\sqrt{2}\varepsilon_0^2 r_0^{12} B_4^2 B_0} \left( \frac{r_0}{l_{pl}} \right)^2 \right\}. \quad (20)$$

Thus the primordial rotation results in lowering Friedmann's energy levels under the barrier and diminishing the tunnelling factor.

### 3 Fast Rotation

In the case of a fast rotation the energy density  $\varepsilon$  is connected with the angular velocity  $\omega$  by the relation

$$\frac{4\pi G\varepsilon}{c^2} = \omega^2 \quad (21)$$

being characteristic of Gödel's metric for dust ( $p = 0$ ) [7]. Friedmann's equation (1) should be replaced by Raychaudhuri's equation, which after quantization gives the following expression for the potential instead of (13)

$$V(a) = \frac{1}{l_{pl}^4} \left[ ka^2 - \left( \frac{8\pi G\varepsilon}{3c^4} - \frac{2\omega^2}{3} \right) a^4 \right]. \quad (22)$$

Substituting (21) into (22) and (22) into (12), we obtain Wheeler-DeWitt's equation as follows

$$\frac{d^2\psi}{da^2} - \frac{ka^2}{l_{pl}^4} \psi = 0. \quad (23)$$

Its solution is a cylindrical function

$$\psi = C\sqrt{a}Z_{\frac{1}{4}} \left( \frac{i\sqrt{k}}{2l_{pl}^2} a^2 \right). \quad (24)$$

For a closed model ( $k=1$ ) the solution reduces to Bessel functions for imaginary argument

$$\psi = \sqrt{a} \left[ C_1 I_{\frac{1}{4}} \left( \frac{a^2}{2l_{pl}^2} \right) + C_2 K_{\frac{1}{4}} \left( \frac{a^2}{2l_{pl}^2} \right) \right]. \quad (25)$$

For an open model ( $k=-1$ ) we have Bessel functions for real argument

$$\psi = \sqrt{a} \left[ C_1 J_{\frac{1}{4}} \left( \frac{a^2}{2l_{pl}^2} \right) + C_2 Y_{\frac{1}{4}} \left( \frac{a^2}{2l_{pl}^2} \right) \right]. \quad (26)$$

For a flat model ( $k=0$ )

$$\psi = C_1 a + C_2. \quad (27)$$

As seen from the form of the potential, it is impossible for a fast rotating universe to be born either due to the absence of a barrier (for  $k = 0, -1$ ) or due to the latter is infinite (for  $k = 1$ ).

#### 4 Specific Angular Momenta

The quantum-cosmological consideration may provide initial conditions for quantum-field models which explain generation of initial perturbations necessary for constructing evolutionary models of galaxy rotation [8, 9].

Really, the upper limit for the angular velocity of the Universe's rotation [4]

$$\omega_{max} < 10^{-13} \text{ rad} \cdot \text{yr}^{-1}.$$

The specific angular momentum of the Universe

$$\frac{J}{M} < \omega_{max} R^2, \quad (28)$$

where  $R \sim 10^{28} \text{ cm}$  is the Universe's horizon, i.e.

$$\frac{J}{M} < 3 \cdot 10^{35} \text{ cm}^2 \cdot \text{s}^{-1}.$$

For example, specific angular momenta for spiral galaxies

$$\frac{J}{M} \sim 10^{29} \text{ cm}^2 \cdot \text{s}^{-1}.$$

Thus the Universe may serve as a source of lesser angular momenta for galaxies after isotropization of their rotation.

#### Acknowledgments

I am grateful to A.I. Studenikin for providing me the possibility of participating in the 10th Lomonosov Conference on Elementary Particle Physics.

#### References

- [1] J. Ellis, K.A. Olive, *Nature* 303, 679 (1983).
- [2] T. Rothman, G.F.R. Ellis, *Phys. Lett. B* 180, 19 (1986).
- [3] Ö. Grön, H.H. Soleng, *Nature* 328, 501 (1987).
- [4] Li-Xin Li, . *Gen. Relat. Grav.* 30, 497 (1998).
- [5] M.L. Fil'chenkov, *Grav. & Cosmol.* 6, Suppl., 37 (2000).

- [6] I. Dymnikova, M.L. Fil'chenkov, "*Quantum birth of a hot universe*", (gr-qc/0009025) 2000.
- [7] S.W. Hawking, G.F.R. Ellis, "*The large-scale structure of space-time*", (Cambridge University Press, Cambridge) 1973.
- [8] L.E. Gurevich, A.D. Chernin, "*Introduction to cosmogony*" (Nauka Publishers, Moscow) 1978.
- [9] M.L. Fil'chenkov, *Astron. Astrophys. Transac.* 19, 115 (2000).

# ON THE INFLUENCE OF EINSTEIN-PODOLSKY-ROSEN EFFECT ON THE DOMAIN WALL FORMATION DURING THE COSMOLOGICAL PHASE TRANSITIONS

Yu.V.Dumin<sup>a</sup>

*IZMIRAN, Russian Academy of Sciences,  
Troitsk, Moscow region, 142190 Russia*

*Abstract.* Search for the mechanisms suppressing formation of Higgs field defects (e.g. domain walls) during the cosmological phase transitions is one of key problems in explanation of the observed large-scale uniformity of the space-time. One of the possible solutions can be based on accounting for Einstein-Podolsky-Rosen (EPR) correlations. Namely, if a coherent quantum state of the Higgs field was formed in the course of its previous evolution, then reduction to the state with broken symmetry during the phase transition should be correlated even at the scales exceeding the local cosmological horizons. Detailed consideration of the simplest one-dimensional cosmological model with  $Z_2$  Higgs field demonstrates that, at certain parameters of the Lagrangian, EPR-correlations really result in a substantial suppression of spontaneous formation of the domain walls.

## 1 History and Present-Day Status of the Domain Wall Problem in Cosmology

The first mention about the problem of domain walls in field theories with spontaneous symmetry breaking was done by Bogoliubov at the conference held in Pisa (Italy) in 1964. As was written later in his report [1], “it is hard to admit, for example, that the ‘phases’ are the same everywhere in the space. So it appears necessary to consider such things as ‘domain structure’ of the vacuum.”

The next important step was done about 10 years later by Zel'dovich, Kobzarev, and Okun [2], who presented a first detailed consideration of the role of domain walls in the astrophysical context and pointed both to the positive aspects and difficulties arising in the cosmological models involving spontaneous symmetry breaking.

At last, the problem of domain walls and other Higgs field defects became one of the central topics of cosmology in the early 1980s, after appearance of the inflationary models, whose first versions were substantially based on the dynamics of Higgs fields in the course of their phase transitions. One of the principal difficulties of such models was associated with the fact that the observed region of the Universe consists of a large number of subregions that were causally-disconnected during the phase transition. Their stable vacuum states, in general, should be different and, therefore, separated by the domain walls, involving considerable energy density. But subsequent evolution and decay of these domain walls should result in dramatic irregularity of the space-time, contradicting to observational data.

Even after development of the “new” and “chaotic” inflation scenarios [3], which avoid the domain wall formation at the earliest stages of cosmological evolution, this problem still remains important for the phase transitions occurring at the later times and less energies.

---

<sup>a</sup>e-mail: dumin@cityline.ru, dumin@yahoo.com

Moreover, the problem of domain walls became even more pressing in the late 1990s, when detailed measurements of fluctuations in the cosmic microwave background radiation (CMBR) pointed to the absence of contribution to the large-scale structure from the processes of disintegration of Higgs field defects.<sup>b</sup>

There is a quite large number of works aimed at solving the above-mentioned problem. Unfortunately, their most objectionable feature is introduction of some arbitrary modifications to the theory of elementary particles, having no experimental (laboratory) confirmations. The main aim of the present report is to describe an alternative approach, which is based on accounting for EPR correlations and can be justified by, at least, some indirect laboratory experiments.

## **2 EPR Correlations and Macroscopic Quantum Phenomena: Their Probable Role in Cosmology**

In the general case, Einstein–Podolsky–Rosen (EPR) effect [4] can be defined as a correlated character of quantum processes in the “causally-disconnected” (i.e., separated by a space-like interval) regions provided that they refer to a single (coherent) quantum state of the system.<sup>c</sup> The simplest and most well-known example is a correlated measurement of the polarization states of two photons emitted by the same source, as shown in the left panel of Fig. 1.

Moreover, there are some indirect experimental evidences (the most remarkable of which were obtained in the recent years) pointing to a possibility of EPR correlations even in macroscopic systems. Particularly, we should mention

- (1) the quantum-optical experiments, confirming a presence of EPR correlations of photon pairs at considerable ( $\sim 10$  km) distances;
- (2) the experiments with ultra-cooled gases, demonstrating that Bose condensate of a macroscopic number of particles behaves exactly as a single coherent state, according to all predictions of quantum mechanics; and, especially,
- (3) the experiments on propagation of ultra-short laser pulses through amplifying media, showing a superluminal reduction of macroscopic coherent photon states, caused by a stimulated emission (e.g. see review [5]).

On the basis of the above-listed facts, it is reasonable to assume that EPR correlations can also manifest themselves in Bose condensate of Higgs fields at the early stages of cosmological evolution.

---

<sup>b</sup>In fact, the most realistic Higgs defects in the modern theories of elementary particles are cosmic strings and monopoles, associated with breaking of continuous symmetries. Nevertheless, consideration of the domain walls (related to a discrete symmetry breaking) is still of importance as a simplest model.

<sup>c</sup>It should be emphasized that EPR effect implies no violation of the “causality principle”: despite a correlated character, the quantum processes in causally-disconnected regions are random; so that no information can be transmitted by using them.

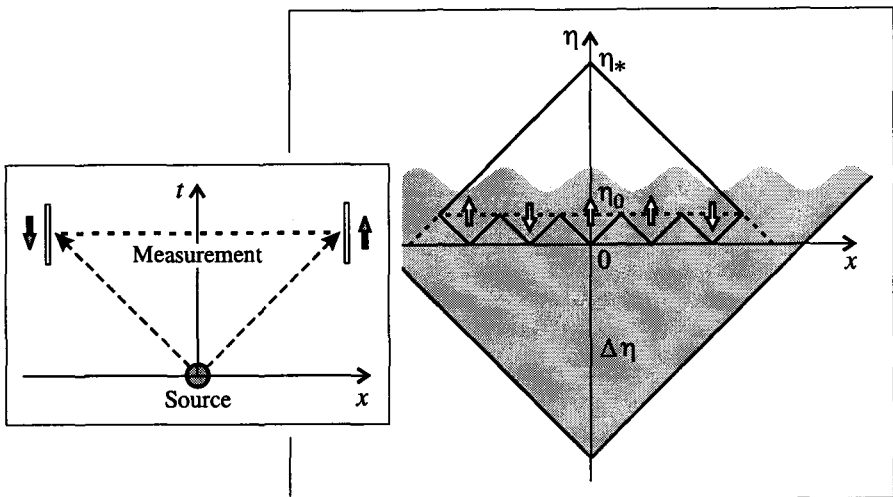


Figure 1: A scheme of laboratory EPR experiment (left panel) and conformal diagram of the space-time involving a phase transition of Higgs field (right panel).

### 3 One-Dimensional Cosmological Model Involving a Phase Transition

To estimate efficiency of EPR effect, we shall consider a simplest one-dimensional Friedmann–Robertson–Walker (FRW) cosmological model with metric

$$ds^2 = dt^2 - a^2(t) dx^2 \quad (1)$$

and Higgs field whose Lagrangian possesses  $Z_2$  symmetry group

$$\mathcal{L}(x, t) = \frac{1}{2} [(\partial_t \varphi)^2 - (\partial_x \varphi)^2] - \frac{\lambda}{4} [\varphi^2 - (\mu^2/\lambda)]^2. \quad (2)$$

As is known, the stable vacuum states of the field (2) are

$$\varphi_0 = \pm \mu / \sqrt{\lambda}, \quad (3)$$

and the structure of a domain wall between them is described as<sup>d</sup>

$$\varphi(x) = \pm \varphi_0 \tanh \left[ \frac{\mu}{\sqrt{2}} (x - x_0) \right]; \quad (4)$$

so that the energy concentrated in the domain wall (4) equals

$$E = \frac{2\sqrt{2}}{3} \frac{\mu^3}{\lambda}. \quad (5)$$

<sup>d</sup>From here on, it will be assumed that thickness of the wall  $\sim 1/\mu$  is small in comparison with a characteristic domain size.

Next, by introduction of the conformal time  $\eta = \int dt/a(t)$ , the space-time metric (1) can be reduced to the conformally flat form (e.g. [6]):

$$ds^2 = a^2(t) [d\eta^2 - dx^2]; \quad (6)$$

so that the light rays ( $ds^2 = 0$ ) will be described by the straight lines inclined at  $\pm\pi/4$ :  $x = \pm\eta + \text{const}$ .

If  $\eta = 0$  and  $\eta = \eta_0$  are the beginning and end of the phase transition, respectively, and  $\eta = \eta_*$  is the instant of observation, then, as is seen in the conformal diagram drawn in the right panel of Fig. 1,

$$N = (\eta_* - \eta_0)/\eta_0 \approx \eta_*/\eta_0 \quad (\text{at large } N) \quad (7)$$

is the number of spatial subregions causally-disconnected during the phase transition. (Their final vacuum states are arbitrarily marked by the arrows.)

A probability of phase transition without formation of the domain walls is usually estimated as a ratio of the number of Higgs field configurations without domain walls to the total number of field configurations:

$$P_N^0 = 2 / 2^N, \quad (8)$$

and this quantity tends to zero very sharply at  $N \rightarrow \infty$ .

On the other hand, if a sufficiently long interval of the conformal time

$$\Delta\eta \geq \eta_* \quad (9)$$

preceded the phase transition, then a coherent state of the Higgs field (shown by the lower dashed triangle) will be formed by the instant  $\eta = 0$  in the entire region observable at  $\eta_*$  (which is shown by the upper triangle).

The inequality (9) can be satisfied, particularly, in the case of sufficiently long de Sitter stage (which is typical for an overcooled state of the Higgs field just before its phase transition). Really, if  $a(t) = \exp(At)$ , then

$$\eta = -\frac{1}{H} e^{-At} + \text{const} \rightarrow -\infty \quad \text{at} \quad t \rightarrow -\infty; \quad (10)$$

so that  $\Delta\eta$  can be quite large.

Next, if condition (9) is satisfied, it is reasonable to assume that EPR correlations may occur between the all  $N$  subregions. In such case, the probability  $P_N^0$  should be calculated with an account of Gibbs factors for the field configurations involving domain walls:

$$P_N^0 = 2 / Z, \quad (11)$$

where

$$Z = \sum_{i=1}^N \sum_{s_i=\pm 1} \exp \left\{ -\frac{E}{T} \sum_{j=1}^N \frac{1}{2} (1 - s_j s_{j+1}) \right\}. \quad (12)$$

Here,  $s_j$  is the spin-like variable describing a sign of vacuum state in  $j$ -th subregion,  $E$  is the domain wall energy, given by (5), and  $T$  is some characteristic temperature of the phase transition.

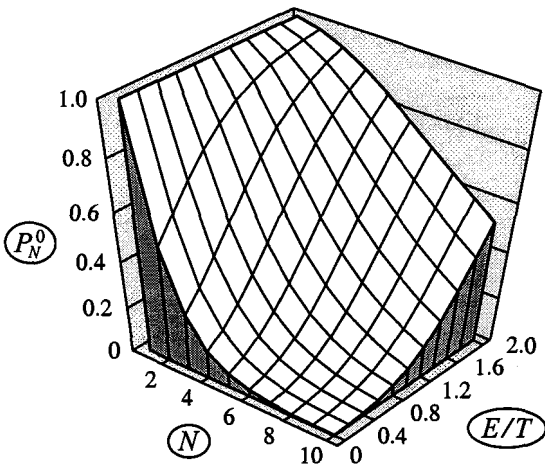


Figure 2: A probability of phase transition without formation of domain walls  $P_N^0$  as function of the number of disconnected subregions  $N$  and the ratio of the domain wall energy to the phase transition temperature  $E/T$ .

From a formal point of view, statistical sum (12) is exactly the same as in the Ising model, well studied in the condensed matter physics. By using the respective formulas (e.g. from [7]), a final result can be written in the form:<sup>e</sup>

$$P_N^0 = \frac{2}{[1 + e^{-E/T}]^N + [1 - e^{-E/T}]^N}. \quad (13)$$

As can be easily shown by analyzing (13), when  $E/T$  increases,  $P_N^0$  becomes a very gently decreasing function of  $N$ . Therefore, just the large energy concentrated in the domain walls turns out to be the factor substantially suppressing the probability of their formation. This fact is pictorially illustrated in Fig. 2 ( $E/T = 0$  refers to the case when there are no EPR correlations at all).

The probability of absence of the domain walls becomes on the order of unity (for example, 1/2) if  $E/T \geq \ln N$ , or, with an account of (5) and (7),

$$\frac{\mu^3}{\lambda T} \geq \ln \frac{\eta_*}{\eta_0}. \quad (14)$$

Because of a very weak logarithmic dependence in the right-hand side of inequality (14), this condition can be satisfied for some particular kinds of the Lagrangians. Therefore, EPR correlations may be an efficient mechanism of the domain wall suppression in a certain class of field theories.

<sup>e</sup>Yet another method for calculating this quantity, based on explicit expressions for the probabilities of field configurations with various numbers of the domain walls, was described in our article [8].

In conclusion, it should be emphasized that the same approach, based on accounting for EPR correlations, can be used to refine a concentration of other Higgs field defects (e.g., magnetic monopoles), which is one of key aspects of the modern astroparticle physics [9]. The refined concentrations, in general, should be less than the commonly accepted ones, and therefore the cosmological constraints on the parameters of the respective field theories will be less tight.

### Acknowledgments

I am grateful to I.B.Khriplovich, V.N.Lukash, L.B.Okun, A.I.Rez, M.Sasaki, A.A.Starobinsky, A.V.Toporensky, and G.E.Volovik for valuable discussions, consultations, and critical comments.

### References

- [1] N.N.Bogoliubov, *Suppl. Nuovo Cimento (Ser. prima)* 4, 346 (1966).
- [2] Ya.B.Zel'dovich, I.Yu.Kobzarev, and L.B.Okun, *Zh.Eksp.Teor.Fiz.* 67, 3 (1974) [*Sov.Phys.—JETP* 40, 1 (1975)].
- [3] A.D.Linde, *Usp.Fiz.Nauk* 144, 177 (1984) [*Rep.Prog.Phys.* 47, 925 (1984)].
- [4] A.Einstein, B.Podolsky, and N.Rosen, *Phys.Rev.* 47, 777 (1935).
- [5] A.N.Oraevsky, *Usp.Fiz.Nauk* 168, 1311 (1998) [*Phys.—Usp.* 41, 1199 (1998)].
- [6] C.W.Misner, *Phys.Rev.Lett.* 22, 1071 (1969).
- [7] A.Ishihara, “*Statistical Physics*” (Academic Press, NY), 1971.
- [8] Yu.V.Dumin, in “*Hot Points in Astrophysics*” (Proceedings of the International Workshop), JINR, Dubna, 114, 2000.
- [9] H.V.Klapdor-Kleingrothaus and K.Zuber, “*Particle Astrophysics*” (Inst. Phys.Publ., Bristol), 1997.

# POSSIBLE EPR EXPERIMENT WITH NEUTRAL PSEUDO-SCALAR MESON-ANTIMESON CORRELATED PAIRS

A.Pompili <sup>a</sup>, F.Selleri <sup>b</sup>

*Università di Bari and INFN Bari, via Amendola 173, I-70126 Bari, Italia*

*Abstract.* Local realism and quantum theory can be discriminated by means of EPR tests with correlated  $K^0\bar{K}^0$  or  $B_d^0\bar{B}_d^0$  pairs produced in  $\Phi$  or  $B$ -factories: the local realistic asymmetry for observing pairs with like and unlike flavour at different proper times remarkably differs from the quantum mechanical prediction. The experimental feasibility of the EPR test for  $B$ -mesons is discussed: asymmetric  $B$ -factories provide a powerful tool for the discrimination between the two theories.

## 1 Historical view and EPR tests in particle physics

In 1935 Einstein, Podolsky and Rosen (EPR) [1] pointed out for the first time the strange nature of quantum correlation between separated system. In 1965 Bell proved [2] that a wide class of local hidden-variable models satisfies an inequality violated by QM. The experimental check of Bell's inequality could have provided evidence of the incompatibility between quantum mechanics (QM) and local realism (LR) at the empirical level.

In 1969 Clauser, Holt, Shimony and Horne (CHSH) stressed that Bell's inequality could be experimentally checked with atomic cascade photon pairs emitted by single atoms [3]. In terms of detection probabilities, Bell's inequality becomes a double limitation on

$$\Gamma \equiv \omega(a, b) - \omega(a, b') + \omega(a', b) + \omega(a', b') \quad (1)$$

and reads

$$-1 + \omega_1(a') + \omega_2(b) \leq \Gamma \leq \omega_1(a') + \omega_2(b) \quad (2)$$

where:  $\omega(x, y)$  is the joint probability that both photons are detected by two photomultipliers placed on their paths after crossing polarisers with axes  $x$  and  $y$  ( $x = a, a'$  referred to the first photon,  $y = b, b'$  referred to the second one);  $\omega_1(a')$  [ $\omega_2(b)$ ] is the probability that the first [second] photon is transmitted by the polariser with axes  $a'$  [ $b$ ] and detected. Inequality (2) was not violated by the quantum mechanical predictions for experiments on atomic cascade photon pairs. However CHSH pointed out that meaningful experiments were possible, even with the available low efficiency photon counters, if the following *additional assumption* was made: *Given that a pair of photons emerges from two regions of space where two polarisers can be located, the probability of their joint detection by two photomultipliers is independent of the presence and orientation of the polarisers.* This assumption allowed CHSH to deduce a different inequality

$$-1 + \omega(a', \infty) + \omega(\infty, b) \leq \Gamma \leq \omega(a', \infty) + \omega(\infty, b) \quad (3)$$

---

<sup>a</sup>e-mail: pompili@ba.infn.it

<sup>b</sup>e-mail: selleri@ba.infn.it

where  $\omega(a', \infty)$  [ $\omega(\infty, b)$ ] is the joint probability that both photons are detected when the polariser is not present on the trajectory of the second [first] one, and  $\Gamma$  is given by 1 again. This shift from (2) to (3) was crucial in producing a disagreement with QM.

In 1972 experiment by Freedman and Clauser [4] the inequality (3) was violated, differently from (2). In 1974 Clauser and Horne [5] proposed a slightly different additional assumption and built an explicit model of LR reproducing the results of the Freedman-Clauser experiment within errors.

In the 1981 Orsay experiments [6] the measured value of  $\Gamma$  was found in agreement with the prediction of QM and was slightly above the upper limit of (3) but well below the upper limit of (2). Thus the inequality (2) was not violated and the meaning of the Orsay experiments is therefore totally dependent on the meaning of the inequality (3) and the underlying additional assumption.

In 1983 Marshall et al. [7] showed that a consistently local and realistic picture of atomic cascades could fit the Orsay data as closely as QM. They identified in the low efficiency of photodetectors the reason for the compatibility between QM and LR in the case of all performed EPR experiments.

During the eighties several papers [8] continued to stress the inequivalence of the inequalities (2) and (3) and in 1990 a general derivation of the two types of Bell's inequalities, those deduced from LR alone and those obtained with the essential help of an additional assumption, was given [9]. The two types of inequalities, (2) and (3), were called "weak" and "strong" respectively, since the latter gives much stronger restrictions on  $\Gamma$ .

In spite of these unequivocal developments there still are papers (like that in reference [10]) which conclude that LR is experimentally violated without examining carefully the underlying assumptions. As argued by Garuccio [11] and by Cabello and Santos [12] in different ways, the experiment carried out by the Rochester group [10] is not able to distinguish QM and LR without supplementary assumptions.

Because of low detection efficiency the same considerations apply both to the Orsay experiments and to the recent Zeilinger's experiment [13]. Thus the comparison between LR and QM is still completely open.

The behaviour of a pair of neutral pseudo-scalar mesons (e.g.  $K^0 - \bar{K}^0$  or  $B_d^0 - \bar{B}_d^0$ ), anti-correlated in flavour if produced by the decay of a  $J^{PC}=1^{--}$  state (e.g. the  $\Phi$  or the  $\Upsilon(4S)$  resonances, produced respectively at  $\Phi$ -factories and  $B$ -factories) fully exhibits the EPR paradox.

Since particle physics detectors are much more efficient than those for optical photons and the distinction between "strong" and "weak" formulations of LR becomes much less important, both conceptually and numerically, we stress that hopes of a final resolution of the EPR paradox lie in the study of these meson pairs.

A critical discussion of the EPR paradox for  $K^0\bar{K}^0$  pairs and of the earlier attempts to check Bell's inequality in  $\Phi$  decays was made by Ghirardi, Grassi and Weber [14]. The main argument was that Bell's inequality, written in terms of four different times of flight of the Kaons, is not violated by the quantum-mechanical two-time joint probability for correlated strangeness, due to the specific values of kaon masses and decay widths. It can be easily shown in the same way that an analogous argument holds for  $B_d^0$  mesons. We agree that Bell's inequality is not violated for pairs of  $K^0$

and  $B_d^0$  mesons, but LR has many other consequences.

Recently further Bell-type tests involving new Bell-like inequalities for correlated neutral meson-anti meson pairs have been proposed and discussed [15] (most of them consider the  $K^0 - \bar{K}^0$  system). However, some of them would probe only a restricted class of local realistic theories whereas others avoid this difficulty but require experimental set-ups not available in the near future [16].

One of the few works on EPR tests with the  $B_d^0 - \bar{B}_d^0$  system [17] deduces a clear indication in favour of QM combining already published data (from *CLEO* and *Argus* and from LEP experiments). However this is an expected conclusion: a *decoherence parameter*  $\zeta$  (such that the QM interference term is multiplied by a factor  $(1-\zeta)$ ) is used to measure deviations from QM but the falsification of  $\zeta = 1$  implies simply a falsification of the spontaneous factorization hypothesis (SFH). SFH was already falsified with gamma ray pairs from  $e^- - e^+$  annihilations [18], with atomic photon pairs [4] [6] and recently with Kaons pairs produced in  $p - \bar{p}$  annihilations [19]. Moreover it is possible to reproduce within the local realistic approach all non paradoxical predictions of QM, including anti-correlations in *strangeness* and *CP* (or *beauty* and *mass*), which are absent in SFH; thus SFH violation is also predicted by any reasonable approach based on LR.

Bell's inequality is only one of the many consequences of LR: EPR correlations can provide tests sensitive to possible deviations from QM. Meaningful tests of LR, not of the Bell-type, have been proposed for the  $K^0 - \bar{K}^0$  system [20, 21] and for the  $B_d^0 - \bar{B}_d^0$  system [22].

## 2 Pseudo-scalar meson pair correlations and probabilities within QM and LR

Let us consider EPR-correlated  $K^0\bar{K}^0$  and  $B_d^0\bar{B}_d^0$  pairs produced in the strong decays of  $\Phi$  and  $\Upsilon(4S)$  resonances respectively. The created  $M^0\bar{M}^0$  pairs ( $M = K, B_d$ ) inherits the resonances quantum numbers  $J^{PC} = 1^{--}$ . Since the mesons are spinless,  $J^P = 1^-$  implies that the  $M^0\bar{M}^0$  pair is in a *p-wave* angular momentum state.  $C = -1$  implies that the flavour part of the pair wavefunction is antisymmetric. Therefore immediately after the decay (namely at  $t=0$ ) the  $M^0\bar{M}^0$  state vector is given, in the resonance-frame, by

$$\begin{aligned} |\psi(0,0)\rangle &= \frac{1}{\sqrt{2}}\{|M^0\rangle_l|\bar{M}^0\rangle_r - |\bar{M}^0\rangle_l|M^0\rangle_r\} \\ &= \frac{1}{\sqrt{2}}\{|M_1\rangle_l|M_2\rangle_r - |M_2\rangle_l|M_1\rangle_r\} \end{aligned} \tag{4}$$

where  $l(r)$  denote the mesons motion directions “left” (“right”);  $|M^0\rangle$ ,  $|\bar{M}^0\rangle$  are *quark (strangeness or beauty) eigenstates*, whereas  $|M_1\rangle$ ,  $|M_2\rangle$  are *CP eigenstates*.

Small effects due to CP-violation can be neglected here since they cannot appreciably modify the large difference between LR and QM predictions that will be found. Thus  $|M_1\rangle$  and  $|M_2\rangle$  represent *short-lived* and *long-lived* Kaons or *heavy* and *light* B-mesons.

The time evolution operator for state given in 4 is the product of the time evolution operators for single mesons states, so that, at proper times  $t_l$  and  $t_r$ , the time evolved state for the  $M^0\bar{M}^0$  pair can be written as

$$|\psi(t_l, t_r)\rangle = \frac{1}{\sqrt{2}} \{ |M_1\rangle_l |M_2\rangle_r e^{-\alpha_1 t_l - \alpha_2 t_r} - |M_2\rangle_l |M_1\rangle_r e^{-\alpha_2 t_l - \alpha_1 t_r} \} \quad (5)$$

with

$$\alpha_1 = \frac{1}{2}\Gamma_1 + im_1 \quad , \quad \alpha_2 = \frac{1}{2}\Gamma_2 + im_2 \quad (6)$$

where, for *long* and *short-lived* Kaons,  $\Gamma_1 \equiv \Gamma_S$  and  $\Gamma_2 \equiv \Gamma_L$  respectively, whereas  $\Gamma_1 \equiv \Gamma_H = \Gamma_2 \equiv \Gamma_L$  since the two neutral B-mesons are expected to have a negligible difference in lifetime.

The different exponentials in (5) generate  $M^0 M^0$  and  $\bar{M}^0 \bar{M}^0$  components. Indeed the time evolution of  $M^0$  and  $\bar{M}^0$  is governed by a weak interaction that does not conserve flavour and thus allows  $M^0 - \bar{M}^0$  oscillations to take place between the flavour eigenstates.

From (5) the probabilities of  $M^0 \bar{M}^0$ ,  $M^0 M^0$  and  $\bar{M}^0 \bar{M}^0$  observations can be obtained. For  $t_l = t_r$ , the probability of having like flavours is zero. This flavour anti-correlation means that the two neutral mesons evolve in phase so that at equal proper times, until one of them decays, there are always a  $M^0$  and a  $\bar{M}^0$  present.

Let us consider the following flavour asymmetry

$$A(t_l, t_r) = \frac{P[M^0(t_l); \bar{M}^0(t_r)] - P[\bar{M}^0(t_l); \bar{M}^0(t_r)]}{P[M^0(t_l); \bar{M}^0(t_r)] + P[\bar{M}^0(t_l); \bar{M}^0(t_r)]} \quad (7)$$

that is the fundamental parameter for the comparison between quantum theory and the local realistic predictions in references [21, 22]. Experimentally the advantage of considering ratios of probabilities or number of events is that systematic errors tend to cancel out.

In QM the asymmetry in (7) is predicted to be a very simple function of  $t_r - t_l$  only; for Kaons:

$$A^{QM}(t_l, t_r) = \frac{2\sqrt{E_L(t_r - t_l)E_S(t_r - t_l)}}{E_L(t_r - t_l) + E_S(t_r - t_l)} \cos(\Delta m (t_r - t_l)) \quad (8)$$

with  $E_{1,2}(t_{l,r}) \equiv e^{-\Gamma_{1,2} t_{l,r}}$ , whereas for B-mesons ( $E_1 = E_2$ ) it reduces to:

$$A^{QM}(t_l, t_r) = \cos(\Delta m (t_r - t_l)) \quad (9)$$

The asymmetry predicted by LR results to be quite different from (8) and (9) as explained in detail in references [21, 22] for Kaons and B-mesons respectively.

The local realism can be expressed by the following three assumptions:

(I) If, without in any way disturbing a system, we can predict with certainty the value of a physical quantity, then there exists an element of physical reality corresponding to this physical quantity (*EPR reality criterion*).

(II) If two physical systems (e.g. the two neutral mesons) are separated by a large distance, an element of reality belonging to one of them cannot have been created by a measurement performed on the other one (*separability*).

(III) If at a given time  $t$  a physical system has an element of reality, the latter cannot be created by measurements performed on the same system at time  $t' > t$  (*no retroactive causality*).

Local realism can be applied to the meson pairs described quantum mechanically by the state vector in (5), by considering only those predictions of (5) to which EPR reality criterion can be applied. These are *flavour* and *mass* or *CP* anti-correlations.

According to the exposition in references [21, 22] the  $M^0 \bar{M}^0$  pair is local-realistically described by means of two hidden variables:

a) each meson of every pair has an associated element of reality  $\lambda_1$  which determines a well defined value of mass or CP eigenvalue ( $\lambda_1 = +1, -1$  corresponds to  $m_H, m_L$ , respectively);

$$\begin{aligned} M_1 &= K_S [B_H] : \text{state with } s[b] = +1 \text{ and } CP = +1 [m = m_H] \\ M_2 &= \bar{K}_S [\bar{B}_H] : \text{state with } s[b] = -1 \text{ and } CP = +1 [m = m_H] \\ M_3 &= K_L [B_L] : \text{state with } s[b] = +1 \text{ and } CP = -1 [m = m_L] \\ M_4 &= \bar{K}_L [\bar{B}_L] : \text{state with } s[b] = -1 \text{ and } CP = -1 [m = m_L] \end{aligned} \quad (10)$$

b) each meson of every pair has an associated element of reality  $\lambda_2$  which determines a well defined value of flavour ( $\lambda_2 = +1, -1$  corresponds to  $q = +1, -1$ , respectively). Furthermore  $q$  is not a stable property: it has sudden jumps, from  $+1$  to  $-1$  and vice-versa, that are simultaneous for the two mesons of every pair but happen at random times in a statistical ensemble of many pairs.

The application of LR to the physical situation described by (5) leads outside the quantum theory: no quantum mechanical state vector exists which can describe a meson as having simultaneously well defined *CP* (or mass) and flavour values. Thus four meson basic states can be introduced:

The first two concern *short-living* Kaons (*heavy* B-mesons), the other two the *long-living* (*light*) ones.

The treatment given in references [21, 22] provides the asymmetry parameter in 7 for LR. It turns out to have maximum and minimum values given by

$$\begin{cases} A_{max}^{LR}(t_l; t_r) = 1 - 2 |Q_+^l - Q_+^r| \\ A_{min}^{LR}(t_l; t_r) = 1 - 2 \text{Min}[(Q_+^l + Q_+^r); (Q_-^l + Q_-^r)] \end{cases} \quad (11)$$

where, for Kaons,

$$Q_{\pm}^{l,r} \equiv \frac{1}{2} [1 \pm \frac{2\sqrt{E_L(t_{l,r})E_S(t_{l,r})}}{E_L(t_{l,r}) + E_S(t_{l,r})} \cos(\Delta m t_{l,r})] \quad (12)$$

whereas for B-mesons

$$Q_{\pm}^{l,r}(t) \equiv \frac{1}{2} [1 \pm \cos(\Delta m t_{l,r})] \quad (13)$$

so that in both cases  $Q_+(t) + Q_-(t) = 1$ .

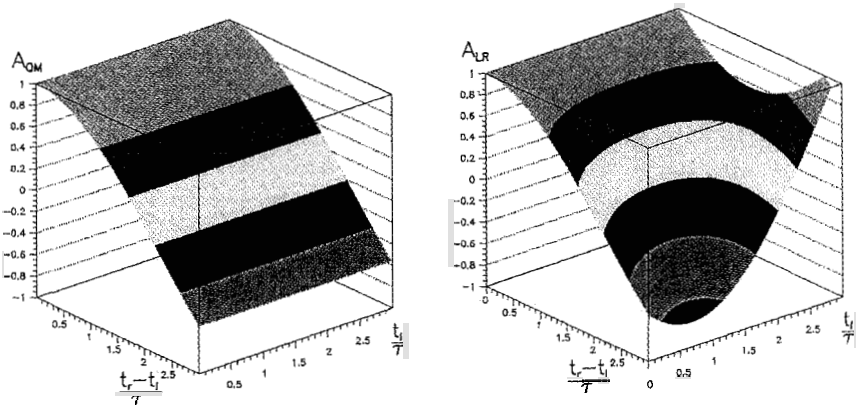


Figure 1:  $B_d^0\overline{B_d^0}$  flavour asymmetry predicted by QM (left) and LR (right; maximum values).

In fig. 1 the behaviour of (9) and (11) for B-mesons is shown.

$A^{QM}$  depends only on the difference of the two proper times and remains unchanged under the  $t_l \leftrightarrow t_r$  exchange. Therefore with  $t_l > t_r$ , the study of  $A^{QM}$  is reduced to the case  $t_r > t_l$ . On the other hand  $A^{LR}$  depends not only on this difference but also on one given absolute proper time. However, under the  $t_l \leftrightarrow t_r$  exchange  $A^{LR}$  is symmetric as can be easily shown and as should be expected from the conventionality of  $l$  and  $r$  tags. Thus the study of  $A^{LR}$  can be limited to the case  $t_r \geq t_l$  establishing, by convention, the dependence of  $A^{LR}$  on the shorter absolute time.

To appreciate the difference between the prediction of QM and the maximum prediction of LR it is useful to represent the asymmetry parameter as a function of  $(t_r - t_l)/\tau$  for some given values of  $t_l/\tau$  as in fig. 2 (where  $\tau \equiv \tau_S$  for Kaons).

The comparison of the whole LR prediction with the MQ one, for two representative values of  $t_l$ , is given in fig. 3 for B-mesons.

### 3 EPR test performed by mixing measurement method

It is interesting to notice that the difference between the predictions of QM and LR is higher in the  $B^0 - \overline{B^0}$  system than in the  $K^0 - \overline{K^0}$  system. From an experimental point of view B-mesons require measuring smaller decay times that is more challenging.

The asymmetric B-factories (high luminosity asymmetric  $e^+e^-$  colliders operating at the  $\Upsilon(4S)$  resonance), i.e. the PEP-II storage ring instrumented with *BaBar* detector at SLAC [23], and the KEK-B storage ring with *Belle* detector at KEK [24], can provide a powerful tool to perform the EPR test just proposed. The asymmetric machine configuration and the high performance in B vertexing allow time-dependent measurements.

A way to experimentally obtain the asymmetry in (7), in order to check the quantum mechanical and local realistic predictions ((9) and (11) respectively), can be based on the measurement of the time-dependent mixing (namely of the mixing parameter  $\Delta m_B$ ) that are performed by *BaBar* [25, 26] and *Belle* [27].

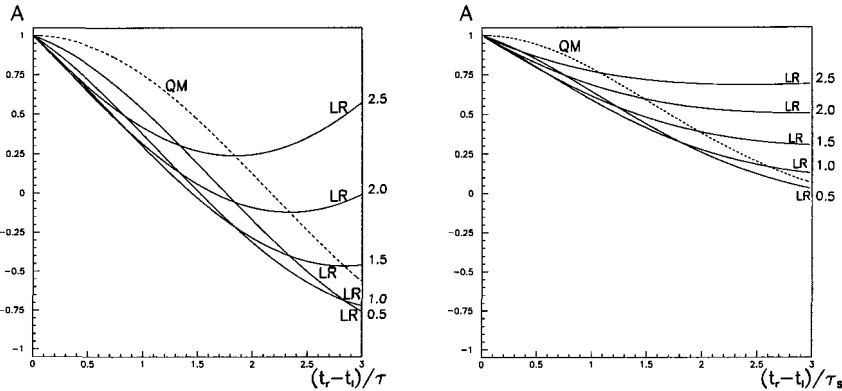


Figure 2:  $B_d^0 \overline{B_d^0}$  (left) and  $K^0 \overline{K^0}$  (right) flavour asymmetry predicted by QM and LR (maximum values) for some fixed  $t_l/\tau$  values.

$P[B^0(t_l); \overline{B^0}(t_r)] = P[\overline{B^0}(t_l); B^0(t_r)], P[\overline{B^0}(t_l); \overline{B^0}(t_r)] = P[B^0(t_l); B^0(t_r)]$  hold both in QM and in LR; thus the asymmetry (9) can be written as

$$A(t_l, t_r) = \frac{P[B^0(t_l); \overline{B^0}(t_r)] + P[\overline{B^0}(t_l); B^0(t_r)] - P[\overline{B^0}(t_l); \overline{B^0}(t_r)] - P[B^0(t_l); B^0(t_r)]}{P[B^0(t_l); \overline{B^0}(t_r)] + P[\overline{B^0}(t_l); B^0(t_r)] + P[\overline{B^0}(t_l); \overline{B^0}(t_r)] + P[B^0(t_l); B^0(t_r)]} \quad (14)$$

and also as

$$A(t_l, t_r) = \frac{N(B^0, \overline{B^0})(t_l, t_r) - N(\overline{B^0}, \overline{B^0})(t_l, t_r) - N(B^0, B^0)(t_l, t_r)}{N(B^0, \overline{B^0})(t_l, t_r) + N(\overline{B^0}, \overline{B^0})(t_l, t_r) + N(B^0, B^0)(t_l, t_r)} \quad (15)$$

where  $N(B^0, \overline{B^0})$  represents the number of unlike-flavour events.

In LR the asymmetry depends not only on  $\Delta t$ , as in QM, but also on one given absolute proper time (the shorter by previous convention). However the local realistic time dependence on  $\Delta t$  could be directly compared to that of QM, for instance by performing a partial time integration, namely an integration on  $t_l/\tau$  for  $t_l/\tau < 2$  with the constraint  $\Delta t/\tau \leq 2$ . Moreover, considering that a very large fraction of the events (double B-decays) is included in the double requirement ( $t_l/\tau < 3$  and  $t_r/\tau < 3$ ), for a given  $t_l/\tau < 3$  these events are characterized by values of  $\Delta t$  belonging to the time interval  $[0, 3 - (t_l/\tau)]$ , for which the local realistic prediction is always below the quantum mechanical one. Thus a total integration on  $t_l/\tau$  is clearly allowed. This allows one to consider the following quantity with simplified time dependence:

$$A(\Delta t) = \frac{N(B^0, \overline{B^0})(\Delta t) - N(\overline{B^0}, \overline{B^0})(\Delta t) - N(B^0, B^0)(\Delta t)}{N(B^0, \overline{B^0})(\Delta t) + N(\overline{B^0}, \overline{B^0})(\Delta t) + N(B^0, B^0)(\Delta t)} \quad (16)$$

Therefore, considering a dilepton tagging approach to obtain experimentally the asymmetry in (16), one can measure the asymmetry

$$A(|\Delta t|) = \frac{N(l^+l^-) - N(l^+l^+) - N(l^-l^-)}{N(l^+l^-) + N(l^+l^+) + N(l^-l^-)} \quad (17)$$

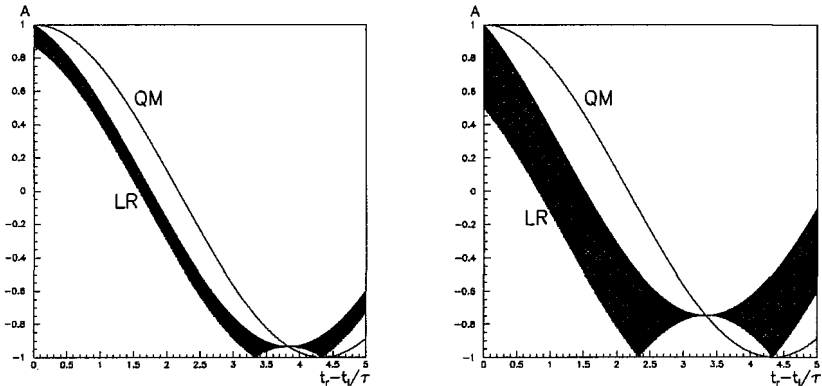


Figure 3:  $B_d^0\overline{B_d^0}$  flavour asymmetry predicted by QM and LR for  $t_l/\tau=0.5$  (left) and  $t_l/\tau=1.0$  (right). The prediction of all local realistic theories must fall in the dark area.

by counting the number of *like-sign* and *unlike-sign* events ( $N(l^\pm l^\pm)$  and  $N(l^+l^-)$ , as a function of  $|\Delta t|$ .

As argued in reference [22], where the experimental feasibility of this EPR test is discussed for B-mesons with more details, the technique for time-dependent di-lepton mixing measurement, properly adapted, seems to be suitable to provide a separation of several standard deviations between QM and LR predictions, with an integrated luminosity of  $30 \text{ fb}^{-1}$  that has already been collected by *BaBar* and *Belle*.

#### 4 Conclusions

Developing a very general local realistic theory of correlated  $M^0\overline{M^0}$  ( $M = K, B_d$ ) a not-of-Bell-type EPR test was proposed in references [21,22] to discriminate between quantum mechanics and local realism. Indeed the asymmetry for observing neutral pseudo-scalar meson pairs with like and unlike flavour predicted by local realism is significantly different from the quantum mechanical prediction.

At the asymmetric B-factories the technique for time-dependent di-lepton mixing measurement developed by *BaBar* and *Belle*, properly adapted, seems to be suitable to provide a separation of several standard deviations between QM and LR predictions, with an integrated luminosity of  $30 \text{ fb}^{-1}$  that has already been collected. The same EPR test can be performed with Kaons at the DaΦne Φ-factory when higher luminosities will be reached.

#### References

- [1] A.Einstein, B.Podolsky, and N.Rosen, *Phys.Rev.* **A** **47**, 777 (1935).
- [2] J.S.Bell, *Physics* **1**, 195 (1965).
- [3] J.F.Clauser, M.A.Horne, A.Shimony, and R.A.Holt, *Phys.Rev.Lett.* **23**, 880 (1969).
- [4] S.J.Freedman and J.F.Clauser, *Phys.Rev.Lett.* **28**, 938 (1972).
- [5] J.F.Clauser and M.A.Horne, *Phys.Rev.* **D** **10**, 526 (1974).

- [6] A.Aspect, P.Grangier and G.Roger, *Phys.Rev.Lett.* **47**, 460 (1981); **49**, 91 (1982); A.Aspect, P.Dalibard and G.Roger, *Phys.Rev.Lett.* **49**, 1804 (1982).
- [7] T.W.Marshall, E.Santos and F.Selleri, *Phys.Lett.* **98 A**, 5 (1983).
- [8] F.Selleri, *Phys.Lett.* **108 A**, 197 (1985); D.Home and T.W.Marshall, *Phys.Lett.* **113 A**, 183 (1985); M.Ferraro and E.Santos, *Phys.Lett.* **116 A**, 356 (1986); F.Selleri and A.Zeilinger, *Found.Phys.* **18**, 1141 (1988); E.Santos, *Phys.Lett.* **139 A**, 431 (1989).
- [9] V.L.Lepore and F.Selleri, *Found.Phys.Lett.* **3**, 203 (1990).
- [10] J.R.Torgenson, D.Branning, C.H.Monken and L.Mandel, *Phys.Lett.* **A 204**, 323, (1995).
- [11] A.Garuccio, *Phys.Rev.* **A 52**, 2535 (1995).
- [12] A.Cabello and E.Santos, *Phys.Lett.* **214 A**, 316 (1996).
- [13] G.Weih, T.Jennewein, C.Simon, H.Weinfurter and A.Zeilinger, *Phys.Rev.Lett.* **81**, 5039 (1998).
- [14] G.C.Ghirardi, R.Grassi and T.Weber, in "*The DAΦNE Physics Handbook*", vol I, ed. by L.Maiani, G.Panzeri and N.Paver, INFN, Frascati, 1992.
- [15] Most of them are relative to  $K^0\bar{K}^0$  pairs and  $\Phi$ -factories. Among them: P.H.Eberhard, *Nucl.Phys.* **B 398**, 155 (1993); A.Di Domenico, *Nucl.Phys.* **B 450**, 293 (1995); B.Ancochea, A.Bramon and M.Nowakowski, *Phys. Rev.* **D 60**, 094008 (1999); F.Benatti and R.Flooreanini, *Phys. Rev.* **D 57**, 1332 (1998). With regard to  $B^0\bar{B}^0$  pairs: A.Datta, in "*Proceedings of the Workshop on High Energy Physics Phenomenology*", Calcutta, 1996.
- [16] A.Afriat and F.Selleri, "*The Einstein, Podolsky and Rosen paradox in atomic, nuclear and particle physics*", (Plenum, London and New York), 1998.
- [17] R.A.Bertlmann and W.Grimus, *Phys.Lett.* **B 392**, 426 (1997); G.V.Dass and K.V.L.Sarma, *Eur.Phys.J.* **C5** (2), 283 (1998); R.A.Bertlmann and W.Grimus, *Phys.Rev.* **D 58**, 034014 (1998).
- [18] D.Bohm and Y.Aharonov, *Phys.Rev.* **108**, 1070 (1957).
- [19] CPLEAR Collaboration, *Phys.Lett.* **B 422**, 339 (1998).
- [20] F.Selleri, *Phys.Rev.* **A 56**, 3493 (1997).
- [21] R.Foadi and F.Selleri, *Phys.Lett.* **B 461**, 123 (1999).
- [22] A.Pompili and F.Selleri, *Eur.Phys.J.* **C 14**, 469 (2000).
- [23] BaBar Collaboration, "*BaBar Physics Book*", SLAC-R-504, 1998.
- [24] BELLE Collaboration, "*Technical Design Report*", KEK-R-95-1, 1995.
- [25] BaBar Collaboration, in "*ICHEP 2000*" (Proceedings of the 30th International Conference on High Energy Physics), ed. by C.S.Lim and T.Yamanaka, World Scientific , 2001.
- [26] BaBar Collaboration, SLAC-PUB-01-22 submitted to *Phys.Rev.Lett.*, hep-ex/0112045.
- [27] BELLE Collaboration, *Phys.Rev.Lett.* **86**, 3228 (2001).

# VIOLATION OF PARITY IN SPACE-TIME OF DIMENSION N+1

S. V. Kopylov

STE "Brainstorm", 26-9 Konstantinov St.,  
129278 Moscow, Russia

*Abstract.* In the work is shown, that in space-time of dimension  $(2m) + 1$  massless objects do not break parity, and massive, which could it break, do not exist, as well as the corresponding interaction. At the same time, in space-time of dimension  $(2m+1) + 1$  massless objects breaking parity can exist, as well as the corresponding interaction.

## 1 Introduction

Even Ehrenfest's first examinations [1,2] have shown that the properties of physical objects, in spaces with dimension not equal to three are essentially distinct from properties of these objects in space of dimension three ( $n=3$ ). A further development of the multidimensional theories is mainly related to the theories of Kaluza-Klein's type [3,4]. In these theories to additional dimensions the properties are ascribed distinguishing them from the properties of the usual three-dimensional space remaining not modified. At the same time, the study of properties of physical objects in spaces with dimension distinct from three without modification of properties of dimensions was also continued [5]. In the present work a violation of parity in spaces of various dimension is considered assuming equal status of spatial coordinates.

## 2 Equation of motion in the absence of interaction

### 2.1 Form of the equations

A massive and massless Dirac equation in space-time 2+1 will take the form:  $(\gamma_\alpha \partial_\alpha + Mc/\hbar)\Phi_M = 0$ ,  $(\gamma_\alpha \partial_\alpha)\Phi_0 = 0$ , where  $\alpha = 0, 1, 2$ , and  $\gamma_0 = \gamma_{ict}$ . Here, as distinct from the case 3+1, there appears a "free"  $\gamma$ -matrix:  $\gamma_3$ , earlier at  $\partial_3$ . Applying a unitary transformation  $U = (1 + i\gamma_3)/\sqrt{2}$  the massive Dirac equations reduce to the form:  $(\gamma_\alpha \partial_\alpha + \gamma_3 iMc/\hbar)\Phi_M = 0$ . Now, both in the case of  $M = 0$  and at  $M \neq 0$ , if  $\Phi$  is a solution of the reduced equations, then  $(1 \pm \gamma_5)\Phi$  is a solution as well.

### 2.2 Massless equation

In the case of the massless Dirac equation the solution generally takes the form  $(1 + A\gamma_3 + B\gamma_5 + Ci\gamma_3\gamma_5)\Phi$ , where  $A^2 + B^2 + C^2 = 1$ , and by a unitary transformation  $U = a\gamma_3 + b\gamma_5 + ci\gamma_3\gamma_5$ ,  $(a^2 + b^2 + c^2 = 1)$  due to variation of two of the three parameters:  $a, b, c$ , can be reduced to the form  $(1 \pm \gamma_5)\Phi$ . However, now, in the case of spatial inversion, the solutions  $(1 \pm \gamma_5)\Phi_0$  do not correspond (any more) to various equations of motion, as was in space 3+1. Really, in the spatial inversion the solution  $(1 + \gamma_5)\Phi_0$  transforms into a solution  $(1 - \gamma_5)\Phi_0$ , but by a unitary transformation  $U = \gamma_3$  it is possible to transform one solution to another, thus these two equations describe physically equivalent objects, and there do not take place a violation of parity.

### 2.3 Massive equation

For the massive Dirac equation solutions with different signs correspond to physically different objects, since these equations cannot be unitary transformed into each other. In the inversion of space these objects transform into each other, and since they are different, the spatial parity is broken. However, for a massive object, always there will be an inertial frame of reference moving with a velocity exceeding that of the object in an initial frame. In a new frame of reference the direction of momentum, in the direction of motion, will undergo inversion, and by that the object under consideration will transform into another object described by another equation of motion. The situation becomes inconsistent, while moving a frame of reference with a velocity of the object itself (that cannot be in space 3+1, due to a zero rest-mass of the corresponding object). The object in this case should be described by both equations simultaneously, but they describe different objects, hence such solutions are not realised. Thus a violation of parity does not occur here as well.

## 3 Parity in the presence of interaction

In space 3+1, the interaction of the form  $(1 - \gamma_5)$  after spatial inversion is transformed to the form  $(1 + \gamma_5)$ . In space 2+1, the interaction  $(1 - \gamma_5)$  after a spatial inversion also transforms into  $(1 + \gamma_5)$ . However, due to the unitary transformation  $\gamma_3$  it can be transformed to the form  $(1 - \gamma_5)$ . In so doing the sign at a massive term in the Lagrangian changes, that is the systems described by such Lagrangians should be considered different. That is the distinction of a physical situation in inverted systems has transferred from interaction to the massive sector, that is on the object. However, as shown above, the massive objects in spaces 2+1 are P-invariant. Thus, the interaction cannot have the form  $(1 - \gamma_5)$ , and hence the spatial parity is not broken. The common conclusion thus consists in the absence of violation of the parity in space-time of dimension 2+1.

## 4 Space 1+1

Such a space is, in the sense of parity violation, an analogue of space 3+1. Really, the massive equation of motion in this case can be written as  $(\sigma_1 \partial_{ict} + \sigma_2 \partial_x + Mc/\hbar) \phi_M = 0$ , and the massless one is:  $(\sigma_1 \partial_{ict} + \sigma_2 \partial_x) \phi_0 = 0$ . In the massless case the solution can also have the form:  $(1 \pm \sigma_3) \phi_0$ . This can be told about the form of interaction as well.

## 5 Space 4+1

This a space, in the sense of parity violation is an analogue of space 2+1. In such a space we are forced to use the  $\gamma_5$  a matrix at the  $\partial_4$ . However, more clearly to use instead of  $\gamma$ -matrices, the matrices constructed like  $\gamma$ -matrices as a direct product of  $\sigma$ -matrices ( $\gamma = \sigma \otimes \sigma$ ), but to consider a direct product of not two  $\sigma$ -matrices but three. Using five anticommuting  $\gamma$ -matrices as a basis, it is possible to construct only seven matrices anticommuting between one another of the form  $\Gamma = \sigma \otimes \sigma \otimes \sigma$ . Then the massive equation in such a space may again be written, like in space 2+1,

as a matrix at a massive term. Thus there also remains one free matrix. In the massless case, as well as in 2+1 there will be two "free" matrices. Later on, in 4+1, all considerations are repeated as in 2+1.

It is necessary to note that the direct product of three  $\sigma$ -matrices generates 64 Hermitian matrices forming a basis in space of  $8 \times 8$  Hermitian matrices, as well as the direct product of two  $\sigma$ -matrices generates base  $4 \times 4$  Hermitian matrices. This means that four  $\sigma$ -matrices are used, that is including the unit one. In space  $8 \times 8$  Hermitian of matrices, by construction, there exist seven anticommuting matrices and also, by construction, there is no eighth matrix. Various representations of these of seven matrices, are only possible:  $\Gamma_\alpha = i\Gamma_0\Gamma_\alpha$ ,  $\alpha = 1, \dots, 6$ .

## 6 Conclusion

Since the procedure of construction anticommuting matrices, as a direct product  $\sigma$ -matrices, will add each time two matrices to the set of anticommuting matrices, while adding each factor in a direct product of  $\sigma$ -matrices, then the scheme of parity violation will be reproduced in spaces 1+1, 2+1, 3+1, 4+1, ... considered above in the general case as well. Thus, we may say, that in space - time the form  $((2n) + 1)$ , the violation of parity in the fermion sector of the Lagrangian is impossible. In spaces of odd spatial dimension of the form  $((2n+1) + 1)$  the violation considered can take place.

## References

- [1] P. Ehrenfest, *Proc. Amsterdam Acad.* 20, 200 (1917).
- [2] G.E. Gorelik, "Space dimension", (Moscow University Publishers, Moscow), 1983.
- [3] T. Kaluza, *Sitzungsber. d. Berl. Acad.* 966 (1921).
- [4] Y.S. Vladimirov, "Dimension of physical space - time and unification of interactions", (Moscow University Publishers, Moscow), 1987.
- [5] Y.S. Vladimirov, "Frame of reference in the theory of gravitation", (Energoizdat, Moscow), 1982.

# RENORMALIZATION-GROUP FLOW IN THE 3D GEORGI-GLASHOW MODEL

D.Antonov <sup>a</sup>

*INFN-Sezione di Pisa, Universitá degli studi di Pisa, Dipartimento di Fisica, Via  
Buonarroti, 2 - Ed. B - I-56127 Pisa, Italy  
and*

*Institute of Theoretical and Experimental Physics, B. Cheremushkinskaya 25,  
RU-117 218 Moscow, Russia*

**Abstract.** The renormalization-group (RG) flow in the finite-temperature (2+1)-dimensional Georgi-Glashow model is explored. This is done in the limit when the squared electric coupling constant is much larger than the mass of the Higgs field. The novel equation describing the evolution of the Higgs mass is derived and integrated along the separatrices of the RG flow in the limit when the original theory reduces to the 2D XY model. In particular, it is checked that in the vicinity of the phase-transition point, the Higgs mass evolved along some of these separatrices is still much smaller than the squared electric coupling constant.

## 1 The model

(2+1)D Georgi-Glashow model is known to be the famous example of a theory allowing for an analytical description of confinement [1]. However, the finite-temperature effects in this theory were addressed only recently. Namely, first in ref. [2] the phase transition associated with the binding of monopoles into molecules has been studied and then in ref. [3], there has been explored another phase transition corresponding to the deconfinement of charged W-bosons. In this talk, we shall concentrate ourselves at the first of these two phase transitions, but account also for the effects brought about by the Higgs field. In this way, we shall follow the analysis performed in ref. [4].

The Euclidean action of the (2+1)D Georgi-Glashow model has the following form

$$S = \int d^3x \left[ \frac{1}{4g^2} (F_{\mu\nu}^a)^2 + \frac{1}{2} (D_\mu \Phi^a)^2 + \frac{\lambda}{4} ((\Phi^a)^2 - \eta^2)^2 \right], \quad (1)$$

where the Higgs field  $\Phi^a$  transforms by the adjoint representation, and  $D_\mu \Phi^a \equiv \partial_\mu \Phi^a + \epsilon^{abc} A_\mu^b \Phi^c$ . In the one-loop approximation, the partition function of this theory reads [5]

$$\begin{aligned} Z &= 1 + \sum_{N=1}^{\infty} \frac{\zeta^N}{N!} \left[ \prod_{i=1}^N \int d^3 z_i \sum_{q_i=\pm 1} \right] \times \\ &\times \exp \left\{ -\frac{g_m^2}{2} \left[ \int d^3x d^3y \rho_{\text{gas}}(\mathbf{x}) D_0(\mathbf{x} - \mathbf{y}) \rho_{\text{gas}}(\mathbf{y}) - \sum_{\substack{a,b=1 \\ a \neq b}}^N D_m(\mathbf{z}_a - \mathbf{z}_b) \right] \right\}. \end{aligned} \quad (2)$$

---

<sup>a</sup>e-mail: antonov@df.unipi.it

Here,  $g_m$  is the magnetic coupling constant of dimensionality [length]<sup>1/2</sup> related to the electric one  $g$  according to the equation  $gg_m = 4\pi$ ,  $\rho_{\text{gas}}(\mathbf{x}) = \sum_{a=1}^N q_a \delta(\mathbf{x} - \mathbf{z}_a)$  is the density of monopole gas with  $q_a$ 's standing for the monopole charges in the units of  $g_m$ . Next, in Eq. (2),  $m = \eta\sqrt{2\lambda}$  is the mass of the Higgs boson and

$$\zeta = \frac{m_W^{7/2}}{g} \delta\left(\frac{\lambda}{g^2}\right) e^{-(4\pi/g^2)m_W\epsilon(\lambda/g^2)} \quad (3)$$

is the statistical weight of a single monopole (else called fugacity) with  $m_W = g\eta$  being the mass of the  $W$ -boson. Here,  $\epsilon$  is a slowly varying function equal to unity at the origin (*i.e.* in the Bogomolny-Prasad-Sommerfield limit [6]) and  $1.787\dots$  at infinity [7], whereas the function  $\delta$  is determined by the loop corrections. Finally, in eq. (2),  $D_0(\mathbf{x}) \equiv 1/(4\pi|\mathbf{x}|)$  is the Coulomb propagator, and  $D_m(\mathbf{x}) \equiv e^{-m|\mathbf{x}|}/(4\pi|\mathbf{x}|)$  is the propagator of the Higgs boson.

Notice that as it follows from eq. (2), in the Bogomolny-Prasad-Sommerfield limit, the interaction of two monopoles doubles for opposite and vanishes for equal charges. As far as the opposite limit,  $m \rightarrow \infty$ , is concerned, we apparently arrive there at the standard compact-QED result [1].

The effective field theory describing the grand canonical partition function (2) can easily be obtained and its action reads [5]

$$S = \int d^3x \left[ \frac{1}{2}(\nabla\chi)^2 + \frac{1}{2}(\nabla\psi)^2 + \frac{m^2}{2}\psi^2 - 2\zeta e^{g_m\psi} \cos(g_m\chi) \right], \quad (4)$$

where  $\chi$  is the dual photon field, whereas the field  $\psi$  is an additional one. The latter field can be integrated out in the limit  $g \gg \sqrt{m}$ , when the exponent in the last term on the r.h.s. of eq. (4) can be shown [4] to be approximated by the terms not higher than the linear one. (Note that the above inequality is implied only in the polynomial and not in the exponential sense.)

In such a limit, Gaussian integration over the field  $\psi$  yields the following action of the dual photon field:

$$S = \int d^3x \left[ \frac{1}{2}(\nabla\chi)^2 - 2\zeta \cos(g_m\chi) \right] + \\ + 2(g_m\zeta)^2 \int d^3x d^3y \cos(g_m\chi(\mathbf{x})) D_m(\mathbf{x} - \mathbf{y}) \cos(g_m\chi(\mathbf{y})). \quad (5)$$

The last term here represents the correction to the standard result [1]. It stems from the fact that the mass of the Higgs field was considered to be not infinitely large compared to the standard Debye mass of the dual photon,  $m_D = g_m\sqrt{2\zeta}$ . The respective correction to  $m_D$  is positive, and the square of the full mass reads:  $M^2 = m_D^2 \left(1 + \frac{m_D^2}{m^2}\right)$ . Clearly, this result is valid at  $m_D \ll m$  and reproduces  $m_D^2$  in the limit  $m \rightarrow \infty$ .

Another relation between the dimensionful parameters in the model (1), we shall adapt for our analysis, is  $g \ll \eta$ . [Clearly, this inequality parallels the requirement that  $\eta$  should be large enough to ensure the spontaneous symmetry breaking from

$SU(2)$  to  $U(1)$ .] In particular, from this relation and the inequality  $g \gg \sqrt{m}$  we immediately obtain:  $\frac{\lambda}{g^2} \sim \left(\frac{m}{m_W}\right)^2 \ll \left(\frac{g}{\eta}\right)^2 \ll 1$ . This means that we are working in the regime of the Georgi-Glashow model close to the Bogomolny-Prasad-Sommerfield limit.

Note further that in the limit  $g \gg \sqrt{m}$ , the dilute gas approximation holds perfectly. Indeed, this approximation implies that the mean distance between monopoles, equal to  $\zeta^{-1/3}$ , should be much larger than the inverse mass of the  $W$ -boson. By virtue of eq. (3) and the fact that the function  $\epsilon$  is of the order of unity, we obtain that this requirement is equivalent to the following one:  $\sqrt{\frac{\pi}{g}} \delta \left(\frac{\lambda}{g^2}\right) e^{-4\pi\eta/g} \ll 1$ . Although at  $\lambda \ll g^2$ , the function  $\delta$  grows, the speed of this growth is so that at  $g \ll \eta$ , the l.h.s. of the last inequality remains exponentially small [8]. Another consequence of this fact is that in the regime of the Georgi-Glashow model under discussion, the Debye mass of the dual photon,  $m_D$ , remains exponentially small as well. In particular, the inequality  $m_D \ll m$ , under which the full mass  $M$  was derived, holds due to this smallness. Also, due to the same reason, the mean field approximation, under which the effective field theory (4) is applicable, remains valid as well with the exponential accuracy. This approximation means that one can disregard the fluctuations of individual monopoles only provided that in the Debye volume  $m_D^{-3}$  there contained a lot of them. This condition can formally be written as

$$\left[ \text{average density} = \frac{\partial \ln Z}{V \partial \ln \zeta} \simeq 2\zeta \right] \times m_D^{-3} \gg 1,$$

where  $V$  is the 3D volume of observation. This yields the inequality  $g^3 \gg \zeta$ , which is really satisfied owing to the above-discussed exponential smallness of  $\zeta$ .

## 2 The RG flow

At finite temperature  $T \equiv 1/\beta$ , one should supply all the fields in the model (1) with the periodic boundary conditions in the time direction, with the period equal to  $\beta$ . The lines of the magnetic field of a monopole thus cannot cross the boundary of the one-period region in the time direction and should go parallel to this boundary at the distances larger than  $\beta$ . Therefore, monopoles separated by such distances interact via the 2D Coulomb potential, rather than the 3D one. Recalling that the average distance between monopoles is equal to  $\zeta^{-1/3}$ , we conclude that at  $T \geq \zeta^{1/3}$ , the monopole ensemble becomes two-dimensional.

This result can also be obtained formally by computing the following sum over Matsubara frequencies:

$$\frac{1}{|\vec{x}|} \equiv \sum_{n=-\infty}^{+\infty} \frac{1}{\sqrt{\vec{x}^2 + (\beta n)^2}} = 2T \sum_{n=-\infty}^{+\infty} K_0(2\pi T |\vec{x}| n) \simeq -2T \ln(\mu |\vec{x}|).$$

Here,  $\mu$  denotes the IR momentum cutoff,  $\vec{x} \equiv (x^1, x^2)$ , and without the loss of generality we have considered the case  $x_0 = 0$ . Next,  $K_0$  stands for the modified Bessel function, which is rapidly decreasing. Owing to this fact, the term with  $n = 0$

(zero Matsubara mode) dominates in the whole sum, which yields the last equality. In the same way, we obtain for the Yukawa propagator:

$$\begin{aligned} \frac{e^{-m|\mathbf{x}|}}{|\mathbf{x}|} &\equiv \sum_{n=-\infty}^{+\infty} \frac{e^{-m\sqrt{\vec{x}^2 + (\beta n)^2}}}{\sqrt{\vec{x}^2 + (\beta n)^2}} = \\ &= 2T \sum_{n=-\infty}^{+\infty} K_0 \left( m|\vec{x}| \sqrt{1 + \left( \frac{2\pi T n}{m} \right)^2} \right) \simeq 2T K_0(m|\vec{x}|). \end{aligned}$$

These equations mean that the strength of the monopole-antimonopole interaction, stemming from eq. (2) at finite temperature, is proportional itself to the temperature. Owing to this fact, at low temperatures the interaction is weak, *i.e.* monopoles exist in the plasma phase, whereas at the temperatures higher than some critical one,  $T_c$ , they form monopole-antimonopole molecules. This situation is reversed with respect to the standard Berezinskii-Kosterlitz-Thouless (BKT) phase transition in the 2D XY model [9]. There, the strength of the interaction is  $T$ -independent, which leads to the molecular phase at low temperatures and to the plasma phase at high temperatures. In our model, the critical temperature of the phase transition is then the one, below which the mean squared separation of a monopole and an antimonopole in the molecule diverges. According to the above formulae, this separation reads

$$\langle L^2 \rangle \propto \int d^2x |\vec{x}|^{2-\frac{8\pi T}{g^2}} \exp \left[ \frac{4\pi T}{g^2} K_0(m|\vec{x}|) \right].$$

This yields  $T_c = g^2/(2\pi)$ , which coincides with the result obtained in ref. [2] without accounting for the Higgs field. Clearly,  $T_c \gg \zeta^{1/3}$ , which means that there exists a broad range of temperatures where the monopole ensemble (plasma) is two-dimensional.

Let us now proceed with the formal RG analysis of the leading ( $m_D/m$ )-part of the action (5), which has been performed in ref. [4]. This part of the action can be written as

$$S = \int d^3x \left[ \frac{1}{2} (\partial_x^2 + \partial_y^2 + a_1 \partial_t^2) \chi + 2\zeta a_2 \cos(g_m \chi) + \left( \frac{g_m \zeta a_3}{m} \right)^2 \cos(2g_m \chi) \right], \quad (6)$$

where  $a_1 = a_2 = a_3 = 1$ . The idea of derivation of the RG equations [10] is to split the cutoff field into two pieces,  $\chi_\Lambda = \chi_{\Lambda'} + h$ . Here, the field  $h$  includes the modes with the momenta lying in the range between  $\Lambda'$  and  $\Lambda$  and all possible Matsubara frequencies. After that, the field  $h$  should be integrated out, which yields the same action, but with another values of parameters  $a_i$ 's. The RG equations can then be derived by performing the infinitesimal transformation  $\Lambda' = \Lambda - \delta\Lambda$  and comparing the deviation of the values of  $a_i$ 's from unity. In this way, we arrive at the following system of RG equations (see ref. [4] for some details of the derivation):

$$dx = -x^3 z^2 dt, \quad dz^2 = -2z^2 \left( \pi x \frac{\tau}{2} \coth \frac{\tau}{2} - 2 \right) dt,$$

$$d\ln u = \left( \frac{3}{4} - \pi x \frac{\tau}{2} \coth \frac{\tau}{2} \right) dt, \quad d\ln \tau = -2dt.$$

Here,  $t = -\ln(\Lambda/T)$ ,  $x = Tg_m^2/(4\pi^2)$ ,  $u = \Lambda^{-3/4}\sqrt{g_m\zeta m^{-1}}$ ,  $\tau = A\Lambda/T$ ,  $z = B\zeta/(\Lambda^2 T)$  with  $A$  and  $B$  standing for some inessential constants.

The above-presented equation for the dimensionless  $m$ -dependent parameter  $u$  is a new one with respect to the other equations. Those can be derived independently [10] in the limit when the Debye mass of the dual photon is considered to be negligibly small with respect to the Higgs one. In the limit  $t \rightarrow \infty$  (or, equivalently,  $\tau \rightarrow 0$ ) the RG flow for the quantities  $x$  and  $z$  becomes that of the 2D XY model with the  $T$ -dependent strength of the interaction. In particular, we straightforwardly obtain the BKT phase transition point  $z_c = 0$ ,  $x_c = 2/\pi$ , which reproduces the critical temperature  $T_c$ , derived above heuristically. In the vicinity of the BKT transition point, the RG trajectories stemming from the integration of the equations for  $x$  and  $z$  are typical hyperbolae of the XY model. They are defined by the equation  $(x - x_c)^2 - (2/\pi)^4 z^2 = \text{const}$ .

In the same XY-model limit, the RG equation for  $u$  becomes remarkably simple,  $d\ln u = (\frac{3}{4} - \pi x) dt$ , and can be integrated along the separatrices  $T = T_c$ , which yields

$$\ln u = -\frac{5}{2\pi(x - x_c)} + \frac{7}{4} \ln \frac{2x}{\pi|x - x_c|} + \frac{3}{2\pi^2 x^2} - \frac{1}{\pi x} + \text{const.}$$

This equation means that at  $x \rightarrow x_c$ ,  $u$  vanishes exponentially along the separatrices. By virtue of eq. (3) with  $\epsilon \sim 1$ , this fact can formally be written as

$$\frac{\eta}{g} \delta^2 \left( \frac{\lambda}{g^2} \right) e^{-8\pi\eta/g} \ll \left( \frac{m}{g^2} \right)^2 \left( \frac{\Lambda}{\eta^2} \right)^3.$$

Clearly, owing to the exponential smallness of its l.h.s., this inequality is satisfied at sufficiently large  $(\eta/g)$  even in the limit  $m \ll g^2$  under study. This fact means that the theory (6) reduced by the RG flow to the 2D XY model stays within the original approximation  $g \gg \sqrt{m}$  when the flow drives this theory in the vicinity of the critical point along the separatrices  $T = T_c$ .

### Acknowledgments

The author is grateful to Prof. A. Di Giacomo for useful discussions and to Dr. N. Agasian, in collaboration with whom the paper [4] has been written. This work has been supported by INFN and partially by the INTAS grant Open Call 2000, project No. 110. And last but not least, the author acknowledges the organizers of the Tenth Lomonosov Conference on Elementary Particle Physics (Moscow, 23-29 August, 2001) for an opportunity to present the above-discussed results in a very stimulating atmosphere.

### References

- [1] A.M. Polyakov, *Nucl.Phys.* **B** 120, 429 (1977).

- [2] N.O. Agasian and K. Zarembo, *Phys.Rev.* **D** 57, 2475 (1998).
- [3] G. Dunne, I.I. Kogan, A. Kovner, and B. Tekin, *JHEP* 01, 032 (2001).
- [4] N. Agasian and D. Antonov, *JHEP* 06, 058 (2001).
- [5] K. Dietz and Th. Filk, *Nucl.Phys.* **B** 164, 536 (1980).
- [6] M.K. Prasad and C.M. Sommerfield, *Phys.Rev.Lett.* 35, 760 (1975); E.B. Bogomolny, *Sov.J.Nucl.Phys.* 24, 449 (1976).
- [7] T.W. Kirkman and C.K. Zachos, *Phys.Rev.* **D** 24, 999 (1981).
- [8] V.G. Kiselev and K.G. Selivanov, *Phys.Lett.* **B** 213, 165 (1988).
- [9] V.L. Berezinskii, *Sov.Phys.-JETP* 32, 493 (1971); J.M. Kosterlitz and D.J. Thouless, *J.Phys.* **C** 6, 1181 (1973); J.M. Kosterlitz, *J.Phys.* **C** 7, 1046 (1974).
- [10] B. Svetitsky and L.G. Yaffe, *Nucl.Phys.* **B** 210, 423 (1982).

# NONCOMMUTATIVE FIELD THEORIES AND UV/IR PROBLEM <sup>a</sup>

A.S.Koshelev<sup>b</sup>

*Steklov Mathematical Institute, Russian Academy of Sciences, Gubkin st. 8, 117966  
Moscow, Russia*

*Abstract.* We consider noncommutative quantum field theories emphasizing an issue of their renormalizability and discussing an UV/IR mixing.

## 1 Introduction

In this talk the main results obtained in our papers [1, 2] are presented (for a review and a comprehensive list of references see [3]). In those papers we study perturbative aspects of the noncommutative fields theories, or field theories on a noncommutative space-time [4–6], emphasizing an issue of their renormalizability and draw a special attention to the problem of an UV/IR mixing found initially in [7] and [1].

It was found by Seiberg and Witten [6] that for the string in the background of constant B-field there is a special limit in which the entire string dynamics is described by a supersymmetric gauge theory on a noncommutative space. Also, an equivalence between ordinary gauge fields and noncommutative gauge fields was established.

One of the earlier motivations to consider noncommutative field theories was a hope that it would be possible to avoid quantum field theory divergences. Now there are some reasons to think that a theory on a noncommutative space is renormalizable if (and only if) the corresponding commutative theory is renormalizable. However, most of the models suffer from IR divergencies resulting from so-called UV/IR mixing.

In the present talk the most important aspects of perturbative analysis of noncommutative field theories are discussed. Several noncommutative field theory models are considered:  $\varphi_4^4$  theory, complex scalar field, scalar electrodynamics and  $\mathcal{N} = 2$  SYM. In the last section an appearance of IR singularities even in the massive models is shown on examples and discussed.

## 2 Noncommutative $\varphi^4$ -model.

The simplest nontrivial model which can demonstrate the most important properties of the noncommutative field theories is a non-commutative  $\varphi^4$ -model.

The theory is defined by the action

$$S = S_0 + S_{int} = \int d^d x \left( \frac{1}{2} (\partial_\mu \varphi)^2 + \frac{1}{2} m^2 \varphi^2 + \frac{g}{4!} (\varphi \star \varphi \star \varphi \star \varphi)(x) \right), \quad (1)$$

where  $\star$  is a Moyal product

$$(f \star g)(x) = e^{i\xi \theta^{\mu\nu} \partial_\mu \otimes \partial_\nu} f(x) \otimes g(x),$$

---

<sup>a</sup>This work is based on the papers [1, 2] in the co-authorship with I. Ya. Aref'eva, D. M. Belov and O. A. Rytchkov.

<sup>b</sup>e-mail: koshel@orc.ru

$\xi$  is a deformation parameter,  $\theta^{\mu\nu}$  is a non-degenerate anti-symmetric real constant matrix,  $\theta^2 = -1$ ,  $d$  is even. Hereafter in the talk we deal with four dimensional Euclidean space. Also, we introduce the convenient notation  $p_1 \wedge p_2 \equiv \xi p_1 \theta p_2$ . Rewriting the interaction term in the Fourier representation

$$S_{int} = \frac{g}{4!(2\pi)^d} \int \prod dp_i e^{-ip_1 \wedge p_2 - ip_3 \wedge p_4} \varphi(p_1) \varphi(p_2) \varphi(p_3) \varphi(p_4) \delta(\sum p_i). \quad (2)$$

we see the following distinguished properties of the deformed theory as compared with the standard local  $\varphi_d^4$  model:

- There are non-local phase factors in the vertex.
- These factors provide regularization for some loop integrals but not for all.
- To have renormalizability the sum of divergences in each order of perturbation theory must have a phase factor already present in the action.

To single out phase factors it is useful to use the 't Hooft double-line graphs and a notion of planar graphs [8]. While phase factors provide a regularization to integrals over loop momenta it is not obvious that these factors are combined after calculation to the expressions already present in the action. This effect could be, for example, in the graph with a divergent nonplanar subgraph. This issue gave us a reason to consider explicitly the two-loop renormalization of the theory (1). It turned out that there is a renormalizability at two-loop level. However, there is an UV/IR mixing to be discussed below.

In explicit calculations we use single-line graphs and symmetric vertices. After the symmetrization of (2) we get

$$S_{int} = \frac{g}{3 \cdot 4!} \frac{1}{(2\pi)^d} \int \prod dp_i \varphi(p_1) \varphi(p_2) \varphi(p_3) \varphi(p_4) \delta(\sum p_i) \times \\ \times (\cos(p_1 \wedge p_2) \cos(p_3 \wedge p_4) + (1 \leftrightarrow 3) + (1 \leftrightarrow 4)).$$

We compute explicitly one-loop counterterms using dimensional regularization  $d = 4 - 2\epsilon$ .



Figure 1:  $\Gamma_1^{(2)} - \Delta\Gamma_1^{(2)}$ .

The only graph 1a contributes to  $\Gamma_1^{(2)}$  and

$$\Gamma_1^{(2)} = -\frac{g(\mu^2)^\epsilon}{6(2\pi)^d} \int dk \frac{2 + \cos 2p \wedge k}{k^2 + m^2}.$$

Here we have introduced a new parameter  $\mu$  of dimension of mass to leave the action dimensionless in  $4 - 2\epsilon$  dimensions.

Performing integration we find

$$\Gamma_1^{(2)} = \frac{g}{32\pi^2} \frac{2}{3} m^2 \left( \frac{1}{\epsilon} + \psi(2) - \ln \frac{m^2}{4\pi\mu^2} + O(\epsilon) - \sqrt{\frac{m^2}{\xi^2 p^2}} K_1(2m\xi|p|) \right) \quad (3)$$

The divergent part is subtracted by the counterterm 1b which is equal to

$$\Delta\Gamma_{1l}^{(2)} = \frac{g}{48\pi^2} \frac{m^2}{\epsilon}.$$

However, there is an unusual last term in the expression (3) which contains modified Bessel function. It comes from the nonplanar part of the graph. Moreover, this term has a pole with respect to momentum  $p$  in the point  $p = 0$ . This phenomenon is of the main concern of the UV/IR mixing discussion.

$\Gamma_2^{(4)}$  is a sum of s-, t- and u-channel graphs. Skipping detailed calculations we present the result:

$$\Delta\Gamma_{1l}^{(4)} = \frac{g^2}{16\pi^2} \frac{1}{9\epsilon} (\cos(p_1 \wedge p_2) \cos(p_3 \wedge p_4) + (1 \leftrightarrow 3) + (1 \leftrightarrow 4)).$$

Therefore, we see that the counterterms have the same structure as in the initial action for the 2- and 4-point one-loop corrections.

### 3 More involved noncommutative models

We proceed with the noncommutative quantum field theory of the complex scalar field [9] whose commutative analogue  $(\phi^* \phi)^2$  is renormalizable in four-dimensional case. There are two different noncommutative structures that generalize a commutative quartic interaction  $(\phi^* \phi)^2$ :  $\phi^* \star \phi \star \phi^* \star \phi$  and  $\phi^* \star \phi^* \star \phi \star \phi$ .

In the commutative case the quartic interaction  $(\phi^* \phi)^2$  is invariant under local  $U(1)$ -transformations. In the noncommutative theory we can consider a "deformed"  $U(1)$ -symmetry ( $U \star U^* = 1$ ). One sees that only the first structure is invariant under these transformations. We can construct an interaction

$$V(\phi^*, \phi) = A\phi^* \star \phi \star \phi^* \star \phi + B\phi^* \star \phi^* \star \phi \star \phi$$

Repeating all steps described in the previous section (see relevant graphs on Fig.2) we can prove one-loop renormalizability of this model. Furthermore, if we impose condition of the *one* coupling constant renormalizability, there are only two solutions at one loop:  $A = B$  and  $B = 0$ . In the first case we have the potential to be anticommutator squared. This is surprising because we have commutator squared of scalar fields in the supersymmetric theories. In the second case we avoid nonanalytic behavior of the one-loop corrections to the propagator in the IR region.

Now we are going to consider noncommutative gauge theories. Explicit calculations [10]- [13] show that pure noncommutative  $U(1)$  gauge theory is renormalizable at one-loop.

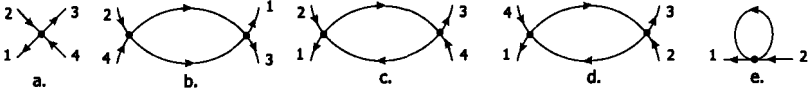


Figure 2: The vertex and one-loop graphs.

We examine the noncommutative scalar electrodynamics in Euclidean space. The classical action is given by

$$S = \int d^4x \left( -\frac{1}{4}F_{\mu\nu} \star F^{\mu\nu} + (\mathcal{D}_\mu \phi^*) \star (\mathcal{D}_\mu \phi) + V(\phi^*, \phi) \right),$$

$$V(\phi^*, \phi) = \lambda^2(a\phi^* \star \phi \star \phi^* \star \phi + b\phi^* \star \phi \star \phi^* \star \phi), \quad (4)$$

where the covariant derivative is defined by  $\mathcal{D}_\mu \phi = \partial_\mu \phi - ig[A_\mu, \phi]_*$ .  $g$  and  $\lambda$  are coupling constants and  $a$  and  $b$  are fixed real numbers. It can be proved explicitly performing loop calculation that there is only one solution to the constants  $a$  and  $b$  which gives one-loop renormalizability of the theory (4):  $a = b$ . As compared with the case of the complex scalar field we lost solution  $b = 0$ . Moreover, we still have anticommutator but not commutator squared for the potential of the scalar field.

The last model is the Euclidean noncommutative  $\mathcal{N} = 2$  SUSY Yang-Mills theory with the action

$$S = \int d^4x \left( -\frac{1}{4}F_{\mu\nu} \star F^{\mu\nu} + (\mathcal{D}_\mu \phi_-) \star (\mathcal{D}_\mu \phi_+) - i\chi^* \star \hat{\mathcal{D}}\chi \right. \\ \left. - g\sqrt{2}\chi^* \star (R[\chi, \phi_+]_* + L[\chi, \phi_-]_*) - \frac{g^2}{2}([\phi_-, \phi_+]_*)^2 \right), \quad (5)$$

where  $\mathcal{D}_\mu = \partial_\mu - ig[A_\mu, \cdot]_*$ ,  $L, R = \frac{1}{2}(1 \pm \Gamma^5)$ ,  $\phi_\pm$  are real scalar fields,  $\chi$  is a complex four-component spinor<sup>c</sup>.

Note that the scalar electrodynamics can be considered as a bosonic part of  $\mathcal{N} = 2$  NCSYM if we identify  $\phi$  and  $\phi^*$  with  $\phi_+$  and  $\phi_-$ , respectively and put  $\lambda = g$  and  $a = -b = -1$  (last condition gives commutator in the potential of the scalar fields). Fortunately, in spite of the anticommutator structure of the potential in the scalar electrodynamics it is turned out that the contribution of the loops with internal fermion lines is enough to make this model renormalizable.

#### 4 UV/IR Problem

Now we would like to consider in more details UV/IR mixing mentioned in the above. For instance, we examine one-loop correction to the propagator in the  $\varphi_4^4$  theory. The answer is given by (3). The behavior of (3) in the limit  $p^2 \rightarrow 0$  (the same as the limit  $\xi \rightarrow 0$ ) is the following

$$\Gamma_{1,f,p.}^{(2)} \underset{p^2 \rightarrow 0}{\sim} \frac{c}{(\xi|p|)^2}.$$

<sup>c</sup>Note that  $\mathcal{N} = 2$  SYM in Minkowski space contains a complex scalar field.

This result can be easily obtained from the series expansion of the modified Bessel function  $K_1(z)$

$$K_1(z) = 1/z + \frac{1}{2}z \ln(z) + \left(\frac{1}{2}C - \frac{1}{4} - \frac{1}{2}\ln(2)\right)z + O(z^3)$$

where  $C$  is Euler constant. Caused by this asymptotic there are problems with an IR behavior of graphs with tadpoles. They produce divergence in the IR region if the number of insertions is three or more. Thus, theories with a real scalar field have problems with infrared behavior originated in multi one-loop insertions.

As already mentioned, such an IR pole in the complex scalar field theory is proportional to  $B$  and can be eliminated, if we consider the solution  $B = 0$  which is in the agreement with UV renormalizability.

In the case of scalar electrodynamics we also can avoid IR poles by imposing the additional condition on the constants of the theory, namely:  $\lambda^2 a = -3g^2$ .

Computing a one-loop correction to the scalar field propagator in the  $\mathcal{N} = 2$   $d = 4$  NC SYM (5) we have no IR poles. There are only logarithmic divergencies which are integrable in the origin.

Let us note that these results concerning the UV/IR mixing and IR divergencies are independent of the regularization scheme. We refer reader to [3] where sample calculations using Pauli-Villars regularization and regularization via cut-off are performed. These methods give the same answer. The issue of such a strange mixing even in the massive theories makes the self-consistency of noncommutative theories rather questionable.

## Acknowledgments

This work was supported in part by RFBR grant 99-01-00166, RFBR grant for leading scientific schools and INTAS grant 99-0590.

## References

- [1] I.Ya. Aref'eva, D.M. Belov, A.S. Koshelev, *Phys.Lett.* **B** 476, 431 (2000), hep-th/9912075.
- [2] I.Ya. Arefeva, D.M. Belov, A.S. Koshelev, O.A. Rychkov, *Phys.Lett.* **B** 487, 357 (2000), hep-th/0001215;  
I.Ya. Aref'eva, D.M. Belov, A.S. Koshelev, O.A. Rytchkov, *Nucl.Phys.Proc.Suppl.* 102, 11 (2001), hep-th/0003176.
- [3] I.Y. Arefeva, D.M. Belov, A.A. Giryavets, A.S. Koshelev, P.B. Medvedev, hep-th/0111208.
- [4] A.Connes, "Noncommutative Geometry", (Academic Press), 1994.
- [5] J.Madore, "An Introduction to Noncommutative Differential Geometry and its Physical Applications", (Cambridge University Press), 2nd Ed., 1999.
- [6] N.Seiberg and E.Witten, *JHEP* 9909, 032 (1999), hep-th/9908142.
- [7] S. Minwalla, M. Raamsdonk and N. Seiberg, *JHEP* 0002, 020 (2000), hep-th/9912072.

- [8] G.'t Hooft, *Comm.Math.Phys.* 88, 1 (1983).
- [9] I.Ya. Aref'eva and I.V. Volovich, in "New Symmetries and Integrable Models", eds. A. Frydryszak, J. Lukierski, Z. Popowicz, World.Scien., 2000, hep-th/9907114.
- [10] C.P. Martin, D. Sanchez-Ruiz, *Phys.Rev.Lett.* 83, 476 (1999).
- [11] M.M. Sheikh-Jabbari, *J. High Energy Phys.* 9906, 105 (1999).
- [12] T. Krajewski and R. Wulkenhaar, *Int.J.Mod.Phys.* **A** 15, 1011 (2000), hep-th/9903187.
- [13] M. Hayakawa, *Phys.Lett.* **B** 478, 394 (2000), hep-th/9912094, hep-th/9912167, hep-th/0009098.

# EXACTLY SOLVABLE POTENTIALS FOR THE ONE-DIMENSIONAL STATIONARY DIRAC EQUATION

V.G. Bagrov<sup>a</sup>, A.A. Pecheritsyn<sup>b</sup>, B.F. Samsonov<sup>c</sup>

*Physics Faculty of Tomsk State University, 634050 Tomsk, Russia*

*Abstract.* The Darboux transformation operator method is extended to the one-dimensional stationary Dirac equation. This permits one, starting from an exactly solvable Dirac equation, to obtain a family of matrix-valued exactly solvable Dirac potentials. New potentials can be isospectral with the initial one or their spectra differ by one or two levels. Special cases of scalar and pseudoscalar potentials for which the Dirac equation is equivalent to a supersymmetric pair of Schrödinger equations are analyzed in details. An interrelation between Schrödinger and Dirac transformation operators is found. It is shown that the Dirac case induces the transformations of either supersymmetric Schrödinger partners.

## 1 Darboux transformation for the one-dimensional stationary Dirac equation

Recall that the Darboux transformation for the Schrödinger equation is defined as a differential operator  $L$  which satisfies the intertwining relation [1]

$$LH_0 = H_1 L \quad (1)$$

between two Schrödinger Hamiltonians

$$H_i = -\partial_x^2 + U_i(x), \quad i = 0, 1. \quad (2)$$

If the operator  $L$  is found then the eigenfunctions of  $H_1$  can be obtained by applying  $L$  to the eigenfunctions of  $H_0$ . The operator  $L$  and the potential difference  $U_1 - U_0$  have the form

$$L = \partial_x - (\ln u)', \quad (3)$$

$$U_1 - U_0 = -2(\ln u)'' \quad (4)$$

where  $u$  is a solution to the equation

$$H_0 u = \alpha u$$

with a real eigenvalue  $\alpha \leq E_0$  with  $E_0$  being the lower bound of  $H_0$  (it is supposed to be bounded from below). The function  $u$  is called *transformation function*.

Expression (1) is a general relation which is suitable not only for Schrödinger Hamiltonians but also for any linear operators  $H_0$  and  $H_1$ . For instance, authors of [2] apply this relation to the Dirac equation, but  $L$  is supposed to be an integral operator. We also use this relation for the Dirac equation, but suppose  $L$  to be a differential operator.

---

<sup>a</sup>e-mail: bagrov@phys.tsu.ru

<sup>b</sup>e-mail: pecher@ido.tsu.ru

<sup>c</sup>e-mail: samsonov@phys.tsu.ru

So, we will find an operator  $L$  which intertwines two Dirac Hamiltonians  $h_0$  and  $h_1$ ,  $h_i = \gamma\partial_x + V_i$ ,  $i = 0, 1$ . Here  $\gamma = i\sigma_y$  with  $\sigma_y$  being the standard Pauli matrix and  $V_i$  are self-adjoint matrix-valued potentials.

Suppose that the solutions of the Dirac equation

$$h_0\psi(x) = E\psi(x), \quad x \in (a, b) \quad (5)$$

are known for all real values of the parameter  $E$ . The function  $\psi$  here is a two-component spinor:  $\psi = (\psi_1, \psi_2)^t$ .

The Hamiltonians  $h_0$  and  $h_1$  are matrix operators, hence  $L$  should have a differential-matrix nature. Let us make the *Ansatz* that  $L$  is a first-order differential operator

$$L = A\partial_x + B \quad (6)$$

where  $A$  and  $B$  are  $2 \times 2$  matrices with  $x$ -dependent elements.

Inserting (6) into the intertwining relation for the Hamiltonians  $h_0$  and  $h_1$  we obtain a system of equations for the matrices  $A$  and  $B$  and for the transformed potential  $V_1$ :

$$A\gamma - \gamma A = 0, \quad (7)$$

$$AV_0 - V_1A + B\gamma - \gamma B - \gamma A_x = 0, \quad (8)$$

$$AV_{0x} + BV_0 - \gamma B_x - V_1B = 0. \quad (9)$$

Equation (8) gives us an expression for  $V_1$  in terms of  $A$  and  $B$ . After inserting it in Eq. (9) and using the substitution  $B = -Au_xu^{-1}$ , where  $u$  is an unknown non-degenerate second-order matrix, Eq. (9) becomes

$$[u^{-1}(\gamma u_x + V_0u)]_x = 0 \quad \Rightarrow \quad \gamma u_x + V_0u = u\lambda. \quad (10)$$

Here  $\lambda$  is a constant  $2 \times 2$  matrix. If we take  $\lambda$  to be a diagonal matrix with real non-zero elements  $\lambda_1$  and  $\lambda_2$  ( $\lambda_1 \neq \lambda_2$ ), then, comparing (10) and (5), we find that the columns of  $u$  are two different solutions of the original equation (5) with the eigenvalues  $E = \lambda_1$  and  $E = \lambda_2$ , respectively. These solutions should be chosen such that the matrix  $u$  be non-degenerate for all  $x$  from the interval  $(a, b)$ .

Now, using (7) – (9), the operator  $L$  and the potential  $V_1$  are expressed in terms of  $u$ :

$$L = A(\partial_x - u_xu^{-1}), \quad (11)$$

$$V_1 = A(V_0 + \sigma\gamma - \gamma\sigma - \gamma A^{-1}A_x)A^{-1} \quad (12)$$

where  $\sigma = -u_xu^{-1}$ . No constraint should be imposed on  $A$  except for (7). In particular,  $A$  may be the unit matrix. We thus obtain simpler expressions for  $L$  and  $V_1$

$$L = \partial_x - u_xu^{-1}, \quad (13)$$

$$V_1 = V_0 + \sigma\gamma - \gamma\sigma, \quad (14)$$

It is seen from (13) and (14) that the transformation operator  $L$  and the new potential  $V_1$  are completely defined by the function  $u$ . Therefore, we call it *transformation function*.

Since the Dirac equation is a first-order differential equation, one can express  $u_x$  with the help of Eq. (10) in terms of  $u$ . Then (14) becomes

$$V_1 = -\gamma V_0 \gamma + d_1 \sigma_z + d_2 \sigma_x \quad (15)$$

where  $d_1 = (\lambda_1 - \lambda_2)(u_{11}u_{22} + u_{12}u_{21})/\det u$ ,  $d_2 = (\lambda_1 - \lambda_2)(u_{21}u_{22} - u_{11}u_{12})/\det u$ , and  $u_{ij}$  are the elements of the matrix  $u$ .

One can see from (11) that the operator  $L$  has a non-trivial kernel:  $\ker L = u$ . From here it follows that, applying  $L$  to the general solution of Eq. (5) with  $E \neq \lambda_{1,2}$ , one obtains the general solution of the equation

$$h_1 \varphi = E \varphi \quad (16)$$

with the same value of  $E$ . Solutions of Eq. (16) with  $E = \lambda_1$  and  $E = \lambda_2$  have to be found by other means. In particular, it can be shown by direct calculations that the function  $v = (u^+)^{-1}$  satisfies the equation  $h_1 v = v\lambda$ . Hence, its columns  $v_1 = (v_{11}, v_{21})^t$  and  $v_2 = (v_{12}, v_{22})^t$  are the solutions of the equation (16) with  $E = \lambda_1$  and  $E = \lambda_2$  respectively.

It can be shown that the operator (13) transforms all square integrable solutions of Eq. (5) into square integrable solutions of Eq. (16). Hence, if  $\lambda_{1,2}$  do not belong to the spectrum of  $h_0$  then all energy levels of Eq. (5) are the energy levels of Eq. (16) as well. If  $\lambda_1$  and/or  $\lambda_2$  belong to the spectrum of  $h_0$ , the corresponding levels are absent in the spectrum of  $h_1$ . Furthermore, if one or two columns of the matrix  $v = (u^+)^{-1}$  are square integrable, the corresponding levels belong to the spectrum of  $h_1$ . So, the new Hamiltonian  $h_1$  may be either isospectral with the original Hamiltonian  $h_0$  or their spectra differ by one or two levels.

## 2 Special cases

If the matrix-valued potential  $V$  is scalar or pseudoscalar, the one-dimensional stationary Dirac equation is equivalent to the supersymmetric pair of Schrödinger equations [4, 5]. Suppose that the original potential  $V_0$  belongs to one of these two types. It is interesting to consider the following questions:

1. When the transformed potential  $V_1$  (15) is a potential of the same structure as the original one?
2. What are the interrelations between the Schrödinger Hamiltonians corresponding to the original and the transformed Dirac equation?

### 2.1 Pseudoscalar potential

Suppose that the original potential is pseudoscalar. Then it has the form [5]

$$V_0 = m \sigma_z + v_0(x) \sigma_x \quad (17)$$

where  $m$  is a constant and  $v_0(x)$  is a real function which is regular for all  $x \in (a, b)$ . Equation (5) with the potential (17) can be written as follows:

$$\begin{aligned} -\psi'_1 + v_0 \psi_1 &= (E + m) \psi_2, \\ \psi'_2 + v_0 \psi_2 &= (E - m) \psi_1. \end{aligned} \quad (18)$$

Consider expression (15) for the transformed potential  $V_1$ . If  $V_0$  is given by (17), then  $\gamma V_0 \gamma = V_0$ . It can readily be seen that if one of the elements of the matrix  $u$  is zero, then  $d_1 = \text{const}$  and  $V_1$  is a pseudoscalar potential as well. However, if we put in (18)  $\psi_2 = 0$ , ( $\psi_1 = 0$ ) then  $\psi_1 \neq 0$  ( $\psi_2 \neq 0$ ) if and only if  $E = m$  ( $E = -m$ ). Therefore, one of the columns of the matrix  $u$  (e. g.  $u_1 = (u_{11}, u_{21})^t$ ) must be a solution of the system (18) with  $E = \lambda_1 = \pm m$ .

Let  $\lambda_1 = m$  then  $u_{21} = 0$ . In this case, we obtain the following expressions for the transformation operator  $L$  and the transformed potential  $V_1$ :

$$L = \partial_x - \begin{pmatrix} (\ln u_{11})' & -(\lambda_2 + m) \\ 0 & (\ln u_{22})' \end{pmatrix}, \quad (19)$$

$$V_1 = -\lambda_2 \sigma_z + v_1 \sigma_x, \quad v_1 = (\ln u_{22})'. \quad (20)$$

So, the transformed potential is defined by a single component of the matrix  $u$  only. Note that the transformed Dirac equation corresponds to the mass equal to  $-\lambda_2$ .

It is well known that the system (18) is equivalent to the supersymmetric pair of Schrödinger equations [6]

$$\begin{aligned} -\psi_1'' + U_0^{(+)} \psi_1 &= \varepsilon \psi_1, \\ -\psi_2'' + U_0^{(-)} \psi_2 &= \varepsilon \psi_2 \end{aligned} \quad (21)$$

where  $U_0^{(\pm)} = v_0^2 \pm v'_0$  and  $\varepsilon = E^2 - m^2$ . Then the transformed equation corresponds to the pair of Schrödinger equations with the potentials  $U_1^{(\pm)} = v_1^2 \pm v'_1$ . Using the expression (20) for  $v_1$ , it can be shown that

$$\begin{aligned} U_1^{(+)} - U_0^{(+)} &= -2(\ln u_{11})'' - (\lambda_2^2 - m^2), \\ U_1^{(-)} - U_0^{(-)} &= -2(\ln u_{22})'' - (\lambda_2^2 - m^2). \end{aligned} \quad (22)$$

These expressions agree with formulae (4) for the potential differences generated by the transformation functions  $u_{11}$  and  $u_{22}$ . The constant  $\lambda_2^2 - m^2$  appears in Eq. (22) due to the fact that the original and transformed equations correspond to different masses.

In the case where  $\lambda_1 = -m$  the formulae for the operator  $L$  and the new potential  $V_1$  are similar to (19) and (20) [3].

## 2.2 Scalar potential

Now let the potential  $V_0$  be scalar [4]

$$V_0 = (m + S_0(x))\sigma_z. \quad (23)$$

Here  $S_0(x)$  is a real function which is regular for all  $x \in (a, b)$ . It is convenient to make the transformation  $\tilde{\psi}_1 = \psi_1 - \psi_2$ ,  $\tilde{\psi}_2 = \psi_1 + \psi_2$ . Then the potential  $V_0$  transforms to  $\tilde{V}_0 = (m + S_0(x))\sigma_x$ . The Dirac equation with the potential  $\tilde{V}_0$  then becomes

$$\begin{aligned} -\tilde{\psi}_1' + (m + S_0)\tilde{\psi}_1 &= E\tilde{\psi}_2, \\ \tilde{\psi}_2' + (m + S_0)\tilde{\psi}_2 &= E\tilde{\psi}_1. \end{aligned} \quad (24)$$

This system is similar to (18) with  $m = 0$  and  $v_0 = m + S_0$ .

It is not difficult to show that if the spinor  $\tilde{u}_1 = (\tilde{u}_{11}, \tilde{u}_{21})^t$  is a solution to the system (24) with  $E = \lambda$ , then the spinor  $\tilde{u}_2 = (-\tilde{u}_{11}, \tilde{u}_{21})^t$  is a solution to the same system with  $E = -\lambda$ .

Build up the transformation function  $\tilde{u}$  from the spinors  $\tilde{u}_1$  and  $\tilde{u}_2$ . Consider now expression (15). One has  $\gamma \tilde{V}_0 \gamma = \tilde{V}_0$  and  $d_1 = 0$ . Thus, the transformed potential  $\tilde{V}_1$  has the form  $\tilde{V}_1 = (m + S_1(x))\sigma_x$ , i. e., it is a scalar potential.

The expressions for the operator  $\tilde{L}$  and the new potential  $\tilde{V}_1$  can be found by direct calculations:

$$\tilde{L} = \partial_x - \begin{pmatrix} (\ln \tilde{u}_{11})' & 0 \\ 0 & (\ln \tilde{u}_{21})' \end{pmatrix}, \quad (25)$$

$$\tilde{V}_1 = (m + S_1(x))\sigma_x, \quad S_1 = S_0 + (\ln \tilde{u}_{21})' - (\ln \tilde{u}_{11})'. \quad (26)$$

Thus the operator  $\tilde{L}$  is represented by a diagonal matrix whose elements are the non-relativistic Darboux transformation operators (3) generated by the functions  $\tilde{u}_{11}$  and  $\tilde{u}_{21}$ .

The Dirac equation with the potential  $\tilde{V} = (m + S(x))\sigma_x$  corresponds to the pair of Schrödinger equations with the potentials  $U^{(\pm)} = (m + S)^2 \pm S'$  [4]. It can be shown using relation (26) that

$$\begin{aligned} U_1^{(+)} - U_0^{(+)} &= -2(\ln \tilde{u}_{11})'', \\ U_1^{(-)} - U_0^{(-)} &= -2(\ln \tilde{u}_{21})'' \end{aligned} \quad (27)$$

These expressions are exactly the transformations (4) of the Schrödinger potentials generated by the functions  $\tilde{u}_{11}$  and  $\tilde{u}_{21}$ .

So, the Darboux transformation which preserves the type of the potential to be scalar (pseudoscalar) induces Darboux transformations of the corresponding Schrödinger equations.

### 3 Examples

**Example 1.** Let the initial potential be pseudoscalar potential of "Dirac oscillator" [6]

$$V_0 = m\sigma_z + \frac{x}{2}\sigma_x. \quad (28)$$

The Schrödinger equations potentials  $U_0^{(\pm)}$  (see Eq. (21)) correspond to the harmonic oscillator  $U_0^{(\pm)} = x^2/4 \pm 1/2$ . Build up the transformation function  $u$  from the spinors

$$u_1 = (e^{x^2/2}, 0)^t, \quad \lambda_1 = m \quad (29)$$

$$u_2 = \left( -\frac{i}{\varepsilon_n - m} e^{x^2/4} \text{He}_n(ix), e^{x^2/4} \text{He}_{n-1}(ix) \right)^t, \quad (30)$$

$$\lambda_2 = \varepsilon_n = (m^2 - n)^{1/2}$$

where  $\text{He}_n(z) = 2^{-n/2} H_n(z/\sqrt{2})$  and  $H_n(z)$  are Hermite polynomials [8].

The transformed potential can be obtain with Eq. (20)

$$V_1 = -\varepsilon_n \sigma_z + \left( \frac{x}{2} + (n-1) \frac{q_{n-2}(x)}{q_{n-1}(x)} \right) \sigma_x \quad (31)$$

where  $q_n(x) = (-i)^n \text{He}_n(ix)$ . Fig. 1. shows the behavior of the initial potential (curve 1) together with the transformed one (curve 2) given by the formula (31) with  $n = 3$ .

Potential of the corresponding Schrödinger equation is

$$U_{2k+1}^{(-)} = \frac{x^2}{4} + 2k - \frac{1}{2} - 4k(2k-1) \frac{q_{2k-2}(x)}{q_{2k}(x)} + 8k^2 \left[ \frac{q_{2k-1}(x)}{q_{2k}(x)} \right]^2 \quad (32)$$

where  $n = 2k+1$ ,  $k = 1, 2, \dots$ . For  $k = 1$  this potential is plotted in the Fig. 2., curve 2.

**Example 2.** Now build up the transformation function  $u$  from the spinors  $u_1$  (29) and

$$u_2 = \left( \frac{1}{\varepsilon_0 - m} (xQ_1(x)e^{x^2/4} + e^{-x^2/4}), Q_1(x)e^{x^2/4} \right)^t \quad (33)$$

where  $\lambda_2 = \varepsilon_0 = (m^2 - 1)^{1/2}$  and  $Q_1(x) = \sqrt{\pi/2}(B + \text{erf}(x/\sqrt{2}))$ ,  $|B| > 1$ . The new potential have the form

$$V_1 = -\lambda_2 \sigma_z + \left( \frac{x}{2} + e^{-x^2/2}/Q_1(x) \right) \sigma_x. \quad (34)$$

Potential of the corresponding Schrödinger equation is

$$\hat{U}^{(-)} = \frac{x^2}{4} - \frac{1}{2} + 2xQ_1^{-1}e^{-x^2/2} + 2Q_1^{-2}e^{-x^2}. \quad (35)$$

Fig. 3 (curve 2) shows the potential (34) with  $B = 2$ , Fig. 5 (curve 2) shows the same with  $B = 1 + 10^{-10}$ . The corresponding potentials of the Schrödinger equation (35) are shown on the Fig. 4 and Fig. 6 (curve 2).

## References

- [1] V. G. Bagrov, B. F. Samsonov, in "Lecture Notes in Theoretical and Mathematical Physics". (Kazan State University Publishing House, Kazan), 2000.
- [2] B. M. Levitan, I. S. Sargsian, "Introduction into spectral theory". (Nauka, Moscow), 1970.
- [3] B. F. Samsonov, A. A. Pecheritsyn, *Izv. VUZov, Fizika* 43, N. 7, 48, (2000).
- [4] Y. Nogami, F. M. Toyama, *Phys. Rev. A* 47, 1708, (1993).
- [5] Y. Nogami, F. M. Toyama, *Phys. Rev. A* 57, 93, (1998).
- [6] Y. Nogami, F. M. Toyama *J. Phys. A* 30, 2585, (1997).
- [7] V.G. Bagrov, B.F. Samsonov, *Phys. Element. Particle Nucl.* **28**, 951, (1997).
- [8] I. S. Gradshteyn, I. M. Ryzhik, "Tables of Integrals, Series and Products". (Academic Press, New York), 1980.

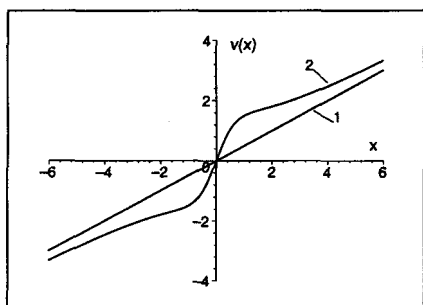


Figure 1: Potentials of Dirac equation. 1 — potential of "Dirac oscillator", 2 — potential (31) with  $n = 3$ .

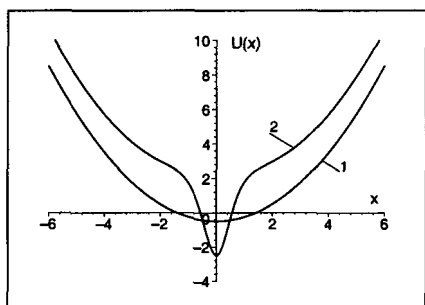


Figure 2: Potentials of Schrödinger equations. 1 — potential of harmonic oscillator, 2 — potential (32) with  $k = 1$ .

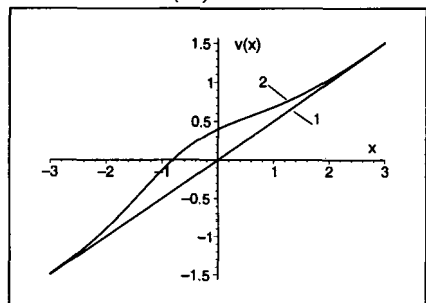


Figure 3: Potentials of Dirac equation. 1 — potential of "Dirac oscillator", 2 — potential (34) with  $B = 2$ .

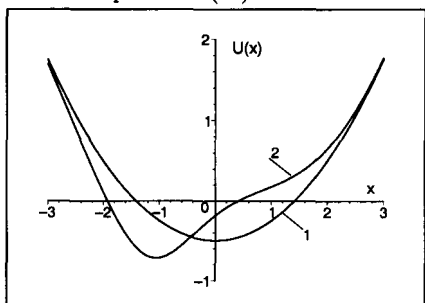


Figure 4: Potentials of Schrödinger equations. 1 — potential of harmonic oscillator, 2 — potential (35) with  $B = 2$ .

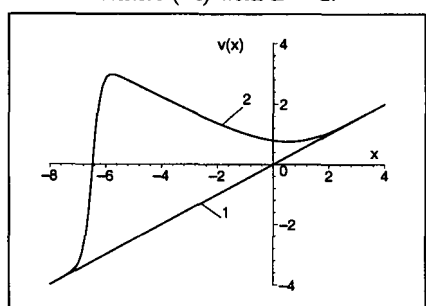


Figure 5: Potentials of Dirac equation. 1 — potential of "Dirac oscillator", 2 — potential (34) with  $B = 1 + 10^{-10}$ .

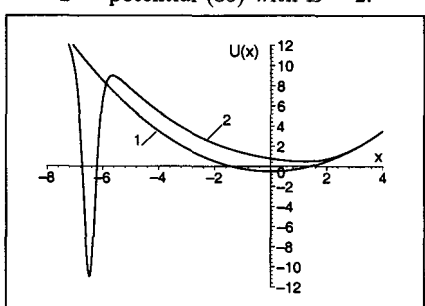


Figure 6: Potentials of Schrödinger equations. 1 — potential of harmonic oscillator, 2 — potential (35) with  $B = 1 + 10^{-10}$ .

## INTELLIGENTSIA: SINGULAR OR PLURAL

John Kuhn Bleimaier<sup>a</sup>

*15 Witherspoon Street, Princeton, New Jersey 08542 USA*

*Abstract.* A healthy society is lead by thinking people. Positive leadership can never be exercised by individuals or institutions alone. It requires a cadre of intellectually acute and orally unified persons to direct the evolution of the social unit. This is the role of the intelligentsia. Leadership in this sense is distinct from governance. Presidents, legislators and jurists administer a bureaucracy, but it is writers, artists and scholars who collaborate in pointing the way to the future. Thus it is that the vigor of the intelligentsia is critical to the life of each individual sovereign unit and of the international community at large.

Historically a definition of the intelligentsia has seemed illusive. It is neither an organization nor a formal unit. The boundaries of its membership are fluid. The intelligentsia was neither founded on a particular day nor can it be disbanded by any formal decree. It is a group of people characterized by intellectual acuity and unified by a sense of shared moral imperative. The requisite intellectual acuity is not gauged by academic attainments alone. The unity of moral purpose subsumes within itself a substantial diversity of opinions and beliefs.

### 1

The intelligentsia is not merely the educated class. It represents the intellectual, moral and spiritual elite within society. To exist within the social structure the intelligentsia must possess a common language. Here the term is not used in its philological sense. The requisite common language is a cultural framework; a shared literary and scientific awareness which makes meaningful dialogue possible. It is also necessary for the members of the intelligentsia to possess common values. This does not mean that the intellectual elite is a monolithic entity. Far from it. The members of the intelligentsia will inevitable represent a broad spectrum of opinions on a multiplicity of subjects. However, for an intelligentsia to exist and to have meaning it is imperative that the members of this grouping share a fundamental moral consciousness.

The intelligentsia which we postulate serves a useful purpose in the social structure. It facilitates the development of an interdisciplinary dialogue. This is the prerequisite for progress in society. When chemists and architects; artists and lawyers; physicists and painters can interact on the playing field of intellectual discourse creativity is the end result. It is this creativity which allows for the scientific breakthrough; for the emergence of aesthetic beauty; and for the attainment of spiritual enlightenment.

---

<sup>a</sup>B.A., M.I.A., J.D.: member of the New York, New Jersey & United States Supreme Court bars.

## 2

Is there but a single intelligentsia, or are there many of these entities to be found in various countries and communities around the world? The answer to this question has great potential importance. If there are indeed many intelligentsias representing various national groups and distinct communities, then the intelligentsia can represent a significant centrifugal force in the world at large. The separate intelligentsias may facilitate the balkanization of mankind through the spin-off of ever smaller cultural units. On the other hand, if there be only one intelligentsia it must of necessity constitute a mighty centripetal force, bringing peoples together.

## 3

Historically the term intelligentsia had its genesis in 19th Century Russia, that hot bed of intellectual foment at the dawning of the modern era. The emergence of Russia as an important player on the international scene after the Napoleonic wars and the contemporaneous attainment of literary, artistic and scientific triumphs by a heretofore insular people created a unique self consciousness among the elite class of the old Russian Empire. The collegial nature of Russia's intellectual leadership resulted in the emergence of the concept: intelligentsia. In the modern world it is perhaps inevitable that there should exist a gulf between the creative elements in society and the broad populace of functionaries. The existence of the intelligentsia was first discovered in Russia, the precocious youngest child of the European intellectual community.

Indeed, there have historically been precursors for the entity which we know as the intelligentsia. Let us consider but a few. The sophists who engaged in philosophical repartee with the Apostle Paul on Athens' Mars Hill, these were a community of intellectuals well schooled in the wisdom of their time. The medieval scholastics who preserved the classical heritage of the west during the Dark Ages; they too have elements in common with the archetypal intelligentsia. And, of course, the Renaissance men with their universal curiosity and rapacious appetite for knowledge; what intelligentsia would not be proud to claim them as spiritual forbearers?

Contemplation of these historic analogies for the institution of the intelligentsia provides us with a hint as to the answer to our question: intelligentsia... singular or plural? The philosophers of the classic era were universal in their approach to the quest for understanding. There was nothing parochial about the sweep of their conceptions. Indeed, when Saint Paul took Christianity to the Greeks and Romans he laid the foundation for the first universal battle of ideas. The medieval scholars were very much in keeping with this revolutionary multilateralism. With the Latin language is their lingua franca the

churchmen of the Middle Ages forged a broad based culture across the innumerable boundaries of a world enfeoffed. And surely the men of the Renaissance formed a sparkling intellectual cadre athwart all Christendom.

#### 4

It was the age of nationalism, from 1848 forward, to which we may trace the notion that the bastion of western culture is but an agglomeration of distinct and disharmonious sub-units. The fallacies of romanticism lead to false faction and the assumption of hopeless diversity. However, while the exponents of division expounded their paen of fractiousness their creative actions put the lie to their words. At the height of the age of nationalism the world of music literature and scientific inquiry continued to break down national barriers. What Polish composer was not influenced by Beethoven? What German writer was deaf to the poetry of Shakespeare? What Italian chemist could disregard Mendeleev's periodic table?

To the extent that some may still argue for the existence of diverse intelligentsias, this represents but the echo of a bygone era. The intelligentsia is one.

#### 5

Nevertheless, the intelligentsia was and remains a western phenomenon. The product of the universal Christian church with its distinct morality and its unshakable faith in the improbability of the human condition, Christendom is the home of the intelligentsia. Eastern philosophies look inward with the ultimate goal being self realization through contemplation. The west, on the other hand, has always stood for societal action and has staked its all on the concept of progress. The east is static and seeks to engender satisfaction through resignation and acceptance of the immutable. The west finds solace in development, joy in evolution and change.

The dialogue which is at the heart of the idea of the intelligentsia is rooted on the assumption that progress is possible, desirable and inevitable. Thus the institution of the intelligentsia can be greater than the sum of its parts. Its aggregate moral conscience can change the world.

Christianity has served to free the human spirit, first from the bonds of superstition and secondly from the tyranny of selfishness. The vice of heathen superstition is self evident. However, the corrosive and stultifying nature of self centered tribalism must not be underestimated. When each people has its own gods or God the unification of humanity is impossible. With the revelation that one God cares for all peoples the revolution of progress becomes attainable. Thus Christian values are at the core of the intelligentsia. It is not ironic to

recognize that without Christianity humanism is unthinkable. The Christian spiritual conception of the value of each individual soul places man and his species in a position of central importance.

The intellectuals who accept this fundamental premise, who share this morality, constitute the intelligentsia. Curiously enough, this does not mean that all the members of the intelligentsia profess the Christian faith. The path to spiritual development and salvation as expounded by the Church is distinct from the moral and ethical values which Christianity has set at large in the society. It has become self-evident that a person not believing in the Christian religion may yet fully espouse the value system which is premised on Christ's Sermon on the Mount.

This notion may be controversial in some quarters. The institutional churches have over the centuries accumulated many enemies who consider themselves to be at odds with Christianity. However, a dispassionate examination of the personal ethics of such persons or groups will reveal the extent to which many are unconsciously anchored in fundamental Christian morality.

Christianity, with its emphasis on the value of the individual and the importance of personal conduct, has laid the groundwork for the freedom of conscience, indeed the supremacy of conscience. This personal moral responsibility is independent of, and greater than, the practical strictures of the law. A shared moral consciousness gives substance to the very fabric of the intelligentsia.

When we conclude that the intelligentsia is a western concept, the product of Christian culture, we are not establishing its geographic boundaries for the contemporary world community. For Christian intellectual influence has spread around the world. We need only look to the nonviolence of Ghandi or the egalitarianism of Mao to see that the western world view has come to exercise a pivotal influence at the epicenter of the east. Thus, in the Twenty-first Century the intelligentsia has grown to be truly a global institution.

## 6

Of course, as the intelligentsia broadens its geographic base there arises the danger that what is broadly unified community of intellectuals will gradually disintegrate, losing its character of moral cohesion. Were that to occur, by our definition, the intelligentsia would cease to exist as such. This would be a tragedy of enormous proportions. The demise of our intelligentsia would bring with it the close of the interdisciplinary dialogue essential to the continuation of progress. However, we can insure that this will not happen if we recognize the importance of fundamental unity within the intelligentsia.

We must rededicate ourselves to the maintenance of the common cultural language of the intelligentsia, and most importantly to its common system of values. Keeping alive the concept of our unified intelligentsia insures that

the vital interdisciplinary dialogue will continue. The continued progress of humanity is at stake.

As we begin a new century and a new millennium the intelligentsia faces critical challenges. In many countries highly specialized professional education has failed to impart the cultural ingredients required for interdisciplinary thought and has not engendered the requisite sense of shared moral purpose. Broad general education is necessary for creative thinking in every individual field of endeavor. The fundamental assumptions as to what is good and what is evil; what is desirable and what is undesirable; must be shared by its members in order for there to exist an intelligentsia. Without a common language of shared culture the concept of an intelligentsia becomes meaningless. In an age of ever more narrow academic specialization intellectual development requires the ability to see the big picture. Furthermore, a shared moral compass is needed for cohesion within the ever changing social unit.

## 7

Let us examine our intellectual antecedents. In the classic world the patrician citizenry formed the leadership cadre of the first modern state. We have no doubt idealized the Greek and Roman predecessors of our societal organization on the basis of the literature, art and architecture which they have left behind. However, classical civilization witnessed the genesis of participatory democracy. Self government requires the existence of a class of citizens with the intelligence to lead an informed populace and the moral purpose to eschew despotism and seek the common weal. Was it not the ultimate intellectual and moral decline of the Roman citizen which made possible the triumph of the barbarians and the commencement of the dark Ages?

Let us next take up the thread of our precursors in the faltering candle glow of medieval cloistered monasticism. After the fall of Rome and the retreat of organized civilization, the spark of intellectualism and the moral tenets of civilization came into the care of isolated Christian religious communities where scholarship and a dedication to moral ideals continued in a sheltered environment protected from a turbulent and uncertain macrocosm. But we cannot consider the medieval monks to have constituted an intelligentsia. They were a mighty intellectual force and a bastion of moral authority, but their isolation from the world of social interaction disqualifies them from the appellation, intelligentsia. Their significance lies in their having sheltered the sputtering flame which burst forth in the Renaissance.

Ever since his appearance at the terminus of the Middle Ages, the "Renaissance Man" has represented an ideal of intellectual development and moral courage. The Renaissance Man is educationally complete and well rounded. Yet he is ever studying and striving to expand his horizons. He is morally

anchored in the spiritual and ethical verities of western civilization, yet keenly aware of the ambiguities and imponderables of the human condition. The Renaissance Man is a master of arts and literature while being devoted to the scientific analysis of his physical environment. He knows right from wrong in the context of an elaborated system of values, just as he is ever challenged by their equitable application to the complexities of life in society. The Renaissance was a blossoming forth of individuals, an unprecedented simultaneous personal evolution of deep thinkers and great souls. They are the models for the individual components of the intelligentsia to this day.

The concepts of the Renaissance spread more deeply and broadly throughout western society giving birth to the Enlightenment. The concept of freedom of conscience with their roots in the Reformation penetrated the entire fabric of the western world, Catholic, Protestant and Orthodox, with the resultant proliferation of experimentation in the natural and social sciences. Parallel to the exposition of Newtonian physics the exponents of innovative statecraft in the persons of John Locke and Jean Jacques Rousseau set the stage for social experiment.

## 8

It is in the 19th Century that we first see the emergence of an identifiable social group assuming of the name, intelligentsia. During this period liberal education and sensitive social conscience became widely diffused throughout Christendom. The word, "Intelligentsia," was first coined in Russia. Because the full impact of the cornucopia of western thought came late to Russia, after the petrine reforms, its impact was the more dramatic. When Peter the Great opened the Russian state to the world of post Enlightenment Europe the effect was overpowering. The immense natural resources of the Russian land provided the economic base for the development of a leisure class. The contemplative Russian mind seemed ideally suited for insightful intellectual activity. It was in the 19th Century that the Russian novelists and composers burst forth upon the stage of Europe. With the virility of a young culture and the zeal of new converts to the intellectual life they coined the term and epitomized the concept of "intelligentsia."

The intelligentsia as we know it developed in parallel fashion in central Europe. The prosperity of the German mercantile classes characterized by the celebrated Biedermeier Period fueled an interest in the arts and sciences. The Germans excelled in nurturing philosophers, poets and scientific investigators. The intellectual curiosity of Humbolt and the moral passion of Goethe set the stage for a century of accomplishment for the German intelligentsia.

The high water mark of British colonialism coupled with the flowering of the industrial revolution, as well as the Yankee prosperity born of expansion across

the American continent, contributed to the formation of a substantial prosperous and educated class in the English speaking world. Here too a contemplative intelligentsia took root.

Indeed, the development of our intelligentsia must be seen as the product of prosperous and peaceful times following the establishment of a general European political order by the Congress of Vienna. Perhaps historians in the 21st Century will come to view the 19th as one of the high points of European civilization. With leisure time available to a substantial number there arose the possibility for the development of a large cadre of creative and contemplative intellectuals. With greater attention paid to the philosophical and ethical underpinnings of society, social conscience waxed in proportion.

## 9

If we view the 19th Century intelligentsia as an intellectually advanced and morally unified social group then the conclusion is inescapable that these people constituted an extraordinary assemblage of amateurs. The men and women of the 19th Century intelligentsia were by and large dilettantes and dabblers. People possessed of classical education, wide ranging intellectual curiosity and dedication to a systematic exploration of their intellectual, spiritual and physical environment. Amateur scientists made startling discoveries. Gentleman explorers filled in all the blanks on the map. Men and women of studied leisure wrote great books and composed innovative music. Is it any wonder that the cult of the amateur was born during this fabled period?

Before the birth of specialized education a class of intellectuals set to work harnessing the forces of the natural environment and directing the moral development of the society at large. Unschooled but in the classics of their civilization and dedicated to the concepts of the scientific method, they sallied forth to physically and spiritually conquer an entire planet. Theirs was a missionary zeal born of the conviction that progress is possible and that the human condition is infinitely improvable. In their home countries these amateurs of the intelligentsia opened museums, libraries and botanical gardens so as to spread the bounty of their discovery. In the distant corners of the world they planted the seeds of their culture and forever influenced the moral development of mankind and his value systems. From Darwin to Stanley; from Marx to Nietzsche; from Brahms to Mendelsohn; from Mendeleev to Edison the heroes of the 19th Century intelligentsia made their mark for all time.

Progress was the watchword of the intelligentsia, its lodestar and battle cry. And in the wake of scientific discovery came plodding technology. The discovery of fundamental principles leads inescapably to their application to everyday life in the form of engineering. Thus the faith of the intelligentsia in the possibility of real progress seemed to have been justified by the advances of practical

automation which promised to improve the lot of all mankind.

## 10

All of the intellectual constructs of the intelligentsia were shaken to the core by the coming of the Great War. Who could have predicted the conflagration of the First World War? The intelligentsia had extrapolated the doctrines of Christianity into the pacifism of Tolstoy and the utopian socialism of Fourier. The powers of Europe, under the guidance of their intellectual jurisprudents conceived the Permanent Court of International Justice in the Netherlands for the peaceful resolution of international conflicts. How ironic that the Hague court should be born simultaneously with the century which was destined to be one of mankind's most violent!

The Great War brought into question the fundamental assumptions of the intelligentsia. The belief in progress was shattered by the empirical finding that technical and organizational development had resulted the most effective mass destruction of men and the trappings of civilization. The period from 1914 to 1918 witnessed the disenchantment of the intelligentsia and its gradual eclipse as the dominant social force. For a time the world was to turn from the leadership of thoughtful, classically trained amateurs to the soulless administration of specialists, experts and bureaucrats. The intelligentsia was at bay.

The Great War spawned the excesses of Russian Revolution. The economic dislocations of the war and its aftermath impoverished central Europe. The unbridled world of capitalism shorn of its moral anchorage made the Great Depression inevitable. All these tragic occurrences of the first third of the 20th Century worked strongly against the continuing viability of the intelligentsia. Where is the place for wide ranging, liberal education or moral conscience in a world of savage revolution and uninhibited laissez-faire?

## 11

The classic intelligentsia of the 19th Century had consisted of individuals who spoke the same language of western civilization and shared the bedrock values of Christian morality. Musicians and scientific investigators, poets and explorers could commune together and share their insights. It is impossible to measure the value of this interdisciplinary cross fertilization. In the 20th Century intensive and early specialization has substantially eroded the common bonds which joined the members of the earlier intelligentsia. A vast industrial complex of great technological complexity has demanded a corps of engineers and specialists in exceedingly narrow fields who are thought not to need broad interdisciplinary understanding. Professional education has started early and continued long, divorced from classical instruction. The ever narrowing sub-

jects of academic research have developed their own highly specialized jargon which serves more to exclude the uninitiated than to serve the cause of precise expression.

The professions have been debased and been turned into trades. Architecture the most fundamental of the practical arts has been compartmentalized to the extinguishment of overall creativity. The clergy have turned from the elaboration of a morally based world view and have busied themselves with theosophical minutia. The law, formerly presumed to be known by all sentient humans, has been transformed into a morass of politically motivated legislated verbiage. Medicine, the most humane science, has become mired in diagnostic technology, precluding a view of the patient as a whole person.

Ah, and how the fine arts and literature have suffered in a time of specialized professionalism. Serious music has become inaccessible to the layman. The heirs of the classic tradition compose works which are merely academically interesting in a formulaic sense or for its exoticism. Painting and sculpture similarly require a specialist's training in order for the viewer to derive any satisfaction from them whatsoever. Belles Lettres and poetry also have come to constitute academic puzzles to be unraveled and appreciated only by those possessed of highly advanced training.

At the terminus of the 20th Century would an educated amateur design his own house? Read poetry in his leisure time for casual elevation and entertainment? Go to an exhibit of serious art in search of inspiration. Can a layman defend his cause before the courts or expound on the doctrines of his faith? Can an educated person realistically set about trying to personally unravel a particular discreet scientific phenomenon? If the answer to these questions is in the negative then what has become of the intelligentsia. Where are those educated men and women who can engage in reasoned discourse on a variety of subjects and hope to obtain enlightenment?

## 12

While academic degrees do not a member of the intelligentsia make, the key to membership in this gallant company is indeed education. But by education we here comprehend general acquaintance with the classics of western arts and letters coupled with at least a passing familiarity with mathematics and the scientific method. We do not impose an unwanted burden when we suggest that budding scientists must read Shakespeare or that aspiring poets understand Euclidean geometry. The scientist with a facility for language will the more successfully express his findings. While the creative humanist's art will be enriched by his scientific understanding. Independently of its practical applications broad based general education is an endless source of personal entertainment and satisfaction.

The pedagogic profession is thus pivotal. Teaching is a calling not a mere occupation. Teachers should be the missionaries of enlightenment. Historically, those periods when vast segments of the population have first been exposed to education and when illiteracy has been eradicated, have been periods when teachers were motivated by religious, nationalistic or ideological zeal. In the realm of today's higher education the roll of the teacher should also involve a burning desire to open up new horizons and nurture a new generation of members of the intelligentsia.

A specialist's exhaustive knowledge of his chosen discipline is not inconsistent with the wide ranging intellectual curiosity of the generalist. Today's expert who also aspires to membership in the intelligentsia must cultivate the intellectual curiosity of the proverbial Renaissance man.

At the beginning of the Third Millennium the greatest threat to the continued life of the intelligentsia is posed by what appears to be an information medium but is in fact a dalliant circus: television. Television, conceived as mass communication but evolved as a sorry substitute for information. Television, the tool of economic forces who would artificially manipulate the demand for what they are prepared to dearly supply. Television, the propagandist's dream and the analytical person's nightmare. Ah, and the worst part of television is that it gives the uneducated the illusion of knowledge.

"Seeing is believing," says the old adage. Perhaps it was inevitable that a powerful visual medium should be flagrantly exploited by the cynical aspirants for economic or political dominance. Mass communication has brought forth mass culture and in the process stifled both national cultures and western civilization. However, television and its attendant cult of the superficial does not present the first challenge to civilization. Western man as either repelled or co-opted previous barbarian onslaughts. The battle must be entrusted to the intelligentsia. From at least one perspective the odds are in our favor. After all this is a contest of the thoughtful against the trivial; of the well schooled against the unlettered; of the ethical against the unscrupulous; of those who propagate ideas against those whose stock in trade is a virtual image.. This is epic combat.

May our unified intelligentsia long survive and ever perpetuate itself. May intellectual analysis and moral courage ever carry the day.

## INTERNATIONAL SCIENTIFIC COLLABORATION AND RUSSIAN PHYSICAL SOCIETY

V. Mikhailin <sup>a</sup>

*Physics Faculty of Moscow State University, 119992 Moscow, Russia*

The first natural scientific societies appeared in Russia at the end of the XVIIIth century and at the beginning of the XIXth century due to the changes in the system of public education and expansion of the network of universities. The most famous were the Moscow Physical-Medical Society in Moscow University (1804) and the Moscow Society of the Explorers of Nature (1805). Both societies published journals and proceedings. While the Academy of Sciences and universities were run by the state, scientific societies were really independent.

Originally societies on natural sciences united different scientific fields, physics section was among them. The peak of the activity in the organizing of dedicated societies by physicists, mathematicians and chemists falls to the second half of the XIXth century when Kharkov Physical-Chemical Society (1872), Kiev Physical-Mathematical Society (1890) and Kazan Physical- Mathematical Society (1890) were founded. A special role in the development of physics in Russia was played by the Russian Physical Society founded in 1872. Its goal was the promotion and dissemination of physical knowledge in Russia. As N.Gesekhus wrote "it may be said without any exaggeration that the history of the Russian Physical Society is at the same time the history of physics in Russia..." [1]. The initiative of the creation of this society belonged to the Russian physicists E.H.Lenz and B.S.Jacoby supported by D.I.Mendeleev. After his suggestion in 1878 the Physical society was united with the Russian Chemical Society to form a joint Russian Physical-Chemical Society. Its members were outstanding Russian physicists F.F.Petrushevsky, V.V.Lermantov, O.D.Khwolson, N.A.Umov, A.G.Stoletov, A.S.Popov, A.F.Ioffe, V.A.Fock and many others. From the very beginning, there was close co-operation between RPS and European Physical Societies. These were the first steps of the International collaboration of the Russian scientists with world scientific community.

The Russian Physical Society (Physical section of the RPCS after 1878) used to organize lectures with the demonstration of new discoveries and inventions, e.g. at its session in 1895 A.S.Popov presented his wireless telegraph. Much attention was paid to the publishing of "The Journal of the Russian Physical-Chemical Society (Physics)" which at that time was the main scientific journal in physics. Later on, in 1930 the title was changed into the Journal of Experimental and Theoretical Physics (famous JETP).

In 1911 Moscow Physical Society was organized in the Moscow University,

---

<sup>a</sup>e-mail: mikh@opts.phys.msu.ru

this society in 1912 was named after P.N.Lebedev. Due to its activity it soon became one of the leading societies in Russia.

In 1912 another society, namely the Society of Research and Dissemination of the Physical Knowledge, was organized in Moscow. Its founder, honorary member and the first president was N.A.Umov.

Similar to the present situation, more and more new societies were emerging both in the capital and in the province, which finally united in 1924 to form the Russian Association of Physicists.

Starting with 1919 till 1930 annual congresses of Russian physicists were held. At this time there were halls big enough to house all the Russian physicists. In 1930 many Russian public institutions were banned with the Russian Physical-Chemical Society among them.

In 1946 there was an appeal of an initiative group (N.N.Andreev, S.I.Vavilov, D.D.Ivanenko) to the governing body of the country to renew the activity of the Physical Society, but the reply was to keep to their business. In November, 1989 the Physical Society was revived, this time in USSR. About 900 scientists from all over the country attended the meeting which took place in the Grand Hall of the Moscow State University. The Charter of the Society was approved and 50 members of the Council were elected, as well as the President (S. Kapitza) and Vice-President (Yu.Novozhilov). The society was sponsored by the Academy of Sciences of the USSR, the Ministry of Education and the Union of Scientific and Engineering Societies. This event has bridged the gap of nearly 60 years after 1930 when together with most of the other professional societies the activity of the Russian Physical-Chemical society was banned.

In November, 1991 the Congress of the Russian Physical Society (RPS) took place. The founders of the revived RPS were the Physical Society of the USSR, the Union of the Engineering Societies, the Academy of Natural Sciences as well as local and regional physical institutions. The Congress was attended by 120 delegates from different parts of Russia. The Congress adopted a new charter of the RPS and elected the administrative board and myself to be the President.

In 1992 the USSR Physical Society was transformed into the Euro-Asian Physical Society. One of its founders and members was the Russian Physical Society. The Russian Physical Society is aiming at bringing together all scientists who are engaged in fundamental and applied research and are teaching physics at universities and schools. Members are elected on merit of their work by the regional branches of the society. Local societies are based on large institutions or research centres or can unite physicists of a large town.

One of the activities of the RPS is the sponsorship of scientific conferences, RPS supports about 10 conferences per year. The recent examples are the 5th International Conference on Inorganic Scintillators and Their Applications and Physics and Industry. The society also tries to do what has not been done earlier. For example, over the last 70 years we did not have a general conference

of physicists of Russia (the last one was in 1930). Here the experience of the General Assembly of the EPS may be helpful. We plan to organize such General Assembly of Russian physicists. Besides the scientific tasks, the aim of such an Assembly is to unite individual Russian physicists and their numerous unions.

Of high priority are recognition and protection of professional rights of scientists. At present it's first of all the survival in a complicated social and financial situation. We see the role of the RPS in the dialogue with the Government, Ministry of Science and Duma. The splitting of the FSU caused migration and looking for employment for many scientists, which RPS tries to assist. We also try to promote the integration of Russian science and education into the world association, to overcome the barriers, both internal and external, in international exchange. Here co-operation with the physical societies of the world can be helpful.

Today the fate of physics is especially difficult, there will be the redefinition of priorities, on the new stage one has to conclude that social treaty with the society on which depends the progress of science. A greater meaning than earlier is gained by creation of natural connections between science and high school, where, in particular, especially physics can play an important role in the progress of high engineering education [2].

A few words about "international affairs" of the RPS. Contacts with the APS started from the very first day of the USSR PS. Originally there was an agreement with the APS about the joint membership. Due to the reorganizations undergone by the Russian society the agreement at the moment requires a renewal. We are very grateful for the support of the American physicists via the APS by the individual grants to the physicists of the former Soviet Union. Another action very important for all of us was free subscription to scientific journals and other means helping to overcome the "information blockade". We appreciate very much the help from the Japanese, German, European Physical Societies and International Science Foundation. Our individual foreign members from the UK (Profs. Ph.Duke, I.H.Munro, and D. Norman) help us with scientific journals.

Following the long-lasting traditions, publishing is an important aspect of our activity. We interact with the American Institute of Physics, they have published a book "Sakharov Remembered" (Eds. S.Drell and S.Kapitza). We are publishing the Bulletin of the Physical Societies (4 issues per year), conference proceedings, prepared for publication scientific books. We have also published a popular among Russian scientists book of the series "Physicists joking". The RPS promotes the improvement of the secondary and university education in physics, training courses and tries to assist the perfection of the certification procedure of scientific personnel. We try to attract talented youth into physics and to support the creative growth of young scientists. The RPS supports student scientific conferences in physics.

The RPS has founded not only the Euro-Asian Physical Society but also the Russian Astronomical Society, the Association of Medical Physicists, the Russian Gravitational Society and the Russian Society of Synchrotron Radiation. Promotion of researches and applications of synchrotron radiation is one of the important issues in the RPS activity.

The Collaboration in Synchrotron Radiation Research may serve as an example of a fruitful international scientific programme. In 1944 Soviet physicists Ivanenko and Pomeranchuk established a theory of this radiation [3]. It was experimentally observed by American scientists Blewett and Haber (1947) as light from electrons accelerated in a synchrotron and therefore was given the name synchrotron radiation (SR). The first book on the theory of SR was written by Sokolov and Ternov in 1966 and translated into English in 1968 [4]. Beginning in the 1960s, synchrotron radiation found wide use in various fields of science and technology [5].

At that very time synchrotron radiation investigations were also started in Russia. They were carried at the synchrotron S-60 by scientists of FIAN (Lebedev Physics Institute) and Moscow State University and at the VEPP storage rings in the Institute of Nuclear Physics in Novosibirsk.

In the late 1970s and early 1980s special electron storage facilities built solely for SR activities were put into operation one after another. This synchrotron boom extended to entire branches of science and technology, such as physics, molecular biology, chemistry, medicine, electronic industry, and ecology.

Physicists of the Moscow State University are carrying out joint investigations on Synchrotron Radiation Applications to various fields of material science and medicine. They have joint projects supported by different foundations such as DFG-RFBR, INTAS, ISTC, NATO etc. We are very glad that recently the General Director of DESY (German Electron Synchrotron) A. Wagner, who has also made an important contribution to broadening the synchrotron international collaboration, became the Honorary Doctor of Lomonosov Moscow University.

The nearest plans for the future are to organize the Conference devoted to the 130 anniversary of the Russian Physical Society, Russian Conference on the VUV-spectroscopy and Interaction of Radiation with Matter. Together with the EAPS we are preparing the next conference "Physics and Industry". And of course preparations have started for the General Assembly of Physicists of Russia.

To conclude with, the main aim of the RPS at the moment is the preservation of the scientific community in Russia in the time of social and economic crisis. This is not for the first time in our history. We also have a strong feeling that we are a part of a big world community. Both these facts make us hope.

## References

- [1] N.Gesekhus, A historical sketch of the 10-year activity of the Physical society, Moscow, 1882.
- [2] S. P. Kapitza, *Bull.Phys.Soc.* No 2, 3 (1992).
- [3] D. D. Ivanenko, I. Pomeranchuk *Phys.Rev.* **65**, 343 (1944).
- [4] A.A. Sokolov, I.M. Ternov *Synchrotron Radiation*, Academie - Verlag, Berlin, 1968.
- [5] I.M. Ternov, V.V. Mikhailin, and V.R. Khalilov *Synchrotron Radiation and Its Applications*, (Harwood Academic Publishers, NY) 1985.

**Programme of X Lomonosov Conference on  
Elementary Particle Physics  
and  
IV International Meeting on Problems of Intelligentsia**

**23 August, THU**

<b>08.30 - 10.00</b>	<b>Registration</b> (Auditorium 1-31, Faculty of Physics, Moscow State University)
<b>10.00 - 10.15</b>	<b>Opening</b> (Conference Hall)
A.Sudenikin, MSU and ICAS	
P.Kashkarov, Vice Dean of Faculty of Physics of Moscow State University	
A.Slavnov, Head of Department of Theoretical Physics of MSU	
V.Matveev, Director of Institute for Nuclear Research of Russian Academy of Sciences	

**10.15 - 13.30 MORNING SESSION** (Conference Hall)

Chairman: V.Savrin

**10.15** E.Shabalin (ITEP) Situation with test of CP, T, CPT and C invariance (*40 min*)  
**10.55** P.Watkins (Univ. of Birmingham & CERN) General LEP2 physics review (without Higgs) (*40 min*)

**11.35 - 12.05** Tea break

Chairman: V.Matveev

**12.05** D.Shirkov (JINR) Analitic perturbation theory in QCD (*45 min*)  
**12.50** A.Slavnov (MSU) Renormalization by enforcing a symmetry (*40 min*)

**13.30 - 15.30** Lunch

**15.30 - 17.50** **AFTERNOON SESSION** (Conference Hall)

Chairman: E.Shabalin

**15.30** M.Cirilli (INFN-Pisa & CERN) The precise determination of the  $\epsilon'/\epsilon$  (*40 min*)

**16.10 - 16.40** Tea break

**16.40** A.Bizzeti (Univ. of Florence & CERN) Rare decays of K0L(S) and the future experimental programme of N48 collaboration at CERN (*40 min*)  
**17.20** M.Martemyanov (ITEP & INFN-LNF) Study of charge kaon decays with the KLOE detector at DAFNE (*30 min*)

**18.00 - 22.30 SPECIAL SESSION**

Reception banquet will be held on board of a ship that will stream along the river across central part of Moscow

**24 August, FRI**

Chairman: V.Semikoz

**9.00 - 13.40 MORNING SESSION (Conference Hall)**

**9.00** Y.Fukuda (Univ. of Tokyo) Neutrino oscillation measurements at Super-Kamiokande (*40 min*)

**9.40** V.Gavrin (INR) The Russian-American solar neutrino gallium experiment SAGE (*40 min*)

**10.20** S.Mikheev (INR) Solar neutrino problem. Summer 2001 (*40 min*)

**11.20 - 11.40** Tea break

**11.40** V.Lobashov (INR) Direct search for mass of neutrino in beta-decay of tritium (*40 min*)

**12.20** V.Tioukov (INFN-Naples) (( appearance experiments with the emulsion technique: CHORUS at CERN and OPERA on the long baseline neutrino beam from CERN to Gran Sasso (*40 min*)

**13.00 - 15.00** Lunch

**15.00 - 19.00 AFTERNOON SESSION (Conference Hall)**

Chairman: S.Mikheev

**15.00** P.Spillantini (INFN-Florence) From the 'Extreme Universe Space Observatory' (EUSO) to the extreme energy neutrino observatory (*20min*)

**15.20** M.Skorohvatov (Kurchatov Inst.) Search for new physics with reactor antineutrinos (*20 min*)

**15.40** V.Berezinsky (LNGS,Gran Sasso), V.Dokuchaev (INR) High-energy neutrino from a nascent massive black hole (*20 min*)

**16.00** V.Tsarev (Lebedev Phys. Inst.) Detection of UHE cosmic rays with space solar sail (*20 min*)

**16.20 - 16.40** Tea break

Chairman: A.Zakharov

**16.40** A.Ali (Desy), A.Borisov, N.Zamorin (MSU) Majorana neutrinos and same-sign dilepton production at LHC and in rare meson decays (*20 min*)

**17.00** M.Dvornikov, A.Grigoriev, A.Lobanov, A.Studenikin (MSU) Suppression of MSW effect in moving and polarized matter (*20 min*)

**17.20** V.Semikoz (IZMIRAN)Neutrino flux propagation in a magnetized plasma(*20 min*)

**17.40** T.Rashba (IZMIRAN) Resonant and non-resonant neutrino spin-flavor conversion in static solar magnetic field (*20 min*)

**18.00** S.Mayburov (Lebedev Phys. Inst.) Quantum space-time, causality and restrictions for gravity quantization (*20 min*)

**19.00 - 22.00** Sight-seeing bus excursion in Moscow

**25 August, SAT**

**9.00-13.30**

**MORNING SESSION** (Conference Hall)

Chairman: A.Kaidalov

**9.00** Yu.Simonov (ITEP) New developments in non-perturbative QCD: microscopic structure of QCD vacuum and spectrum of QCD (*45 min*)

**9.45** K.Seth (Northwestern Univ.) Status and prospects for onium spectroscopy (*45 min*)

**10.30** T.Barnes (Univ. of Tennessee) Exotics-hybrids and glueballs (*40 min*)

**11.10 - 11.30** Tea break

Chairman: K.Seth

**11.30** A.Badalian (ITEP) Spin structure of heavy quarkonia (*20 min*)

**11.50** V.Kiselev, A.Likhoded, O.Pakhomova, V.Saleev (IHEP) Leptonic constants of heavy quarkonia in potential approach of NRQCD (*20 min*)

**12.10** A.Pivovarov (INR) Heavy quark production near threshold in QCD (*20 min*)

**12.30** S.Alekhin (IHEP) High-twist contribution to the structure function  $xF_3(N)$  (*20 min*)

**12.50** E.Shabalin (ITEP) Pragmatic approach to description of  $\pi\pi$  scattering (*20 min*)

**13.10 - 15.00** Lunch

**15.00-18.30** **AFTERNOON SESSION** (Conference Hall)

Chairman: Yu.Simonov

**15.00** A.Kaidalov (ITEP) From small-x physics to heavy ion collisions (*30 min*)

**15.30** J.Manjavidze, A.Sissakian (JINR, Dubna) Physics of hadronic production at very high multiplicities (*20 min*)

**15.50** A.Nefediev (IST, Lisbon & ITEP) QCD2 in the axial gauge revisited (*20 min*)

**16.10** N.Agasian , S.Fedorov (ITEP) Instantons in the nonperturbative QCD (*20 min*)

**16.30** V.Kopeliovich (INR, Moscow) Characteristic predictions of topological soliton models (*20 min*)

**16.50 - 17.10** Tea break.

Chairman: A.Borisov

**17.10** T.Aibergenov, A.Koltsov, A.Kravtsov, A.Lvov, L.Pavlyuchenko, G.Sokol (Lebedev Phys. Inst.) Discovery of the eta-mesic nuclei (*20 min*)

**17.30** D.Antonov (INFN-Pisa & ITEP) Confining strings and RG flow in the Georgi-Glashow model (*20 min*)

**17.50** A.M.Safronov, A.A.Safronov (INP MSU) Relativistic mode of hadron-hadron interaction at low and intermediate energies (*20 min*)

**18.10** A.Nesterenko (MSU) New analytic running coupling in QCD (*20 min*)

**26 August, SUN**

**9.00 - 19.00** Bus tour to Sergiev Posad (75 km away from Moscow, visit to the Abbey, historical and icon museums, lunch at the Russian Orthodox Academy)

**27 August, MON****9.30-13.45 MORNING SESSION** (Conference Hall)

Chairman: P.Spillantini

**9.30** C.Heusch (SLAC) TeV linear collider physics in the electron-electron mode (*40 min*)

**10.10** F.Selleri (Univ. of Bari) EPR paradox in particle physics (*40 min*)

**10.50** G.Diambrini-Palazzi (Univ. of Rome) An experiment for detecting macroscopic quantum coherence: last results (*30 min*)

**11.20 - 11.50** Tea break

Chairman: P.Watkins

**11.50** P.Colas (Saclay & CERN) Twelve years of Higgs hunting at LEP (*40 min*)

**12.30** Ph.Bambade (Univ. of Paris & CERN) Flavour independent Higgs searches at LEP2 (*25 min*)

**12.55** D.Fayolle (LPC Clermont II & CERN) Search for anomalous gauge couplings (*25 min*)

**13.20** A.Leins (Univ. of Munich & CERN) Single top production on behalf of OPAL (*25 min*)

**13.45 - 15.15** Lunch**15.15 - 19.10** AFTERNOON SESSION (Conference Hall)

Chairman: P.Bambade

**15.15** N.Nikitin, F.Rizatdinova, L.Smirnova (MSU) The main task of B-meson trigger at LHC(*20*)

**15.35** L.Sarycheva (MSU) Status of CMS LHC (CERN) experiment (*20 min*)

**15.55** V.Korotkikh (INP MSU) Exotic mesons in E852 experiment (BNL-MSU) (*20 min*)

**16.15** M.Osipenko (MSU-INFN) The studies of nucleon and N\* structure (*20 min*)

**16.35** V.Zamiralov (INP MSU) Magnetic moments of the charm baryons in chiral perturbation theory (*20 min*)

**16.55 - 17.15** Tea break

**17.15** A.Nikishov (Lebedev Phys. Inst.) Vector boson in constant electromagnetic field (*25 min*)

**17.40** A.Milstein (INP, Novosibirsk) Multiple e+e- productions in relativistic heavy ion collisions (*25 min*)

**18.10** V.Belov, V.Maksimov (MSIEM, Moscow), Semiclassical spectrum of helium atom in external magnetic field (*20 min*)

**18.30** V.Bagrov, A.Pecheritsyn, B.Samsonov (Univ. of Tomsk) Darboux transformation for the one-dimensional stationary Dirac equation (*20 min*)

**18.50** V.Popov (ITEP), On Schwinger mechanizm of e+e- pair production from vacuum by optical and Roentgen-lasers (*20 min*)

**28 August, TUE**

**9.00-13.30 MORNING SESSION (Conference Hall)**

Chairman: A.Kaganovich

**9.00** V.Lukash (Astro-Space Centre & Lebedev Phys. Inst.) Cosmological model of the Universe from CMB and LSS observational data (*40 min*)

**9.40** A.Zakharov, S.Repin (ITEP) The shape of the iron K( lines as an evidence of the BH's existence (*20 min*)

**10.00** Yu.Grats, A.Rossikhin (MSU) Renormalization in the effective action for classical string (*20 min*)

**10.20** Yu.Dumin (IZMIRAN) On the influence of Einstein-Podolsky-Rosen effect on the domain wall formation during the cosmological phase transitions (*20 min*)

**10.40 - 11.20** Tea break

**11.20** I.Arefeva (Steklov Math. Inst.) Non-perturbative effects in superstring theory (*40 min*)

**12.00** M.Katanaev (Steklov Math. Inst.) Global solutions in gravity (*30 min*)

**12.30** E. Guendelman, A. Kaganovich (Ben Gurion Univ.) Towards simultaneous resolution of the cosmological constant and fermion family problems (*30min*)

**13.00** M.Fil'chenkov (Peoples' Friendship University of Russia) Quantum cosmological model with rotation (*20 min*)

**13.20** D.Belov, Koshelev (Steklov Math. Inst.) UV and IR behaviour of non-commutative field theories (*20 min*)

**13.40 - 15.00** Lunch

**15.00 - 18.45 AFTERNOON SESSION (Conference Hall)**

Chairman: A.Milstein

**15.00** V.Burdyuzha (Astro-Space Centre) The Cosmological and physical consequences of the next structural level of matter (*30 min*)

**15.30** B.Kerimov, M.Safin (MSU) Spin phenomena and standard model (*30 min*)

**16.00** F.Mazzucato (Geneva University & CERN) Search for supersymmetry (*25 min*)

**16.25 - 16.45** Tea break

**16.45** G.Fedotovich (NPI, Novosibirsk) Precise measurements of the hadronic cross sections with CMD-2 and (g-2)( *30 min*)

**17.15** P.Nowosad (Univ. of San Paolo) Proclus and foundations of theory of everything (*20 min*)

**17.35** O.Khrustalev , M.Tchitchikina, O.Timofeevskaya (MSU) Quantum gravity on the classical background-group analysis (*20 min*)

**17.55** G.Kravtsova, A.Mandel, V.Rodionov (MSU) The threshold processes in strong electromagnetic fields (*20 min*)

**18.15** S.Kopylov (STE "Brainstorm") Physical objects in spaces of different dimensions (*20 min*)

**29 August, WED**

**9.00 -10.20        MORNING SESSION (Conference Hall)**

Chairman: Y.Fukuda

**9.00 I.Royzen (Lebedev Phys. Inst.) Quark-gluon plasma: pro and contra (40 min)**

**9.40 I.Dremin (Lebedev Phys. Inst.) Wavelets and their uses (40 min)**

**10.20 - 10.50      Tea break**

**10.50 - 13.40        FOURTH INTERNATIONAL MEETING ON  
                          PROBLEMS OF INTELLIGENTSIA:  
                          "INTERNATIONAL CO-OPERATION OF INTELLECTUALS"**

Chairman: A.Studenikin

**11.00 A.Yagola (Department of Physics of MSU) (10 min)**

**11.10 S.Kapitza (Russian Academy of Sciences) Responsibility of intelligentsia (40 min)**

**11.50 V.Mikhailin (MSU) International synchrotron radiation collaboration supported by INTAS, DFG and RFBR (20 min)**

**12.10 G.Diambrini-Palazzi (Univ. of Rome) On meaning and features of scientific development and the human condition (30 min)**

**12.40 J.Bleimaier (Princeton) Intelligentsia - Singular or Plural (20 min)**

**13.00 P.Nowosad (San Paolo) Collapse of societies: self-defeating price of success and its mechanisms of prevention (20 min.)**

**13.20-14.00 Discussion (S.Kapitza , J.Bleimaier , P.Nowosad , A.Studenikin, P.Bashindzhagyan)**

**14.00 Closing banquet**

**List of participants of the 10<sup>th</sup> Lomonosov Conference  
on Elementary Particle Physics and the 4<sup>th</sup> International Meeting on Problems  
of Intelligentsia**

Agasian N.	ITEP	<a href="mailto:fedorov@heron.itep.ru">fedorov@heron.itep.ru</a>
Aibergenov T.	FIAN	<a href="mailto:pavl@pluton.lpi.troitsk.ru">pavl@pluton.lpi.troitsk.ru</a>
Alekhin Sergey	IHEP	<a href="mailto:alekhin@mx.ihep.su">alekhin@mx.ihep.su</a>
Antonov Dmitri	INFN-Pisa & ITEP	<a href="mailto:antonov@df.unipi.it">antonov@df.unipi.it</a>
Arefeva Irina	Steklov Math. Inst.	<a href="mailto:arefeva@mi.ras.ru">arefeva@mi.ras.ru</a>
Badalian Alla	ITEP	
Bagrov Vladislav	Univ. of Tomsk	<a href="mailto:pecher@ido.tsu.ru">pecher@ido.tsu.ru</a>
Bambade Philip	Univ. of Paris & CERN	<a href="mailto:bambade@lal.in2p3.fr">bambade@lal.in2p3.fr</a>
Barnes Ted	Univ. of Tennessee	<a href="mailto:barnes@bethe.phy.ornl.gov">barnes@bethe.phy.ornl.gov</a>
Belokurov Vladimir	MSU	<a href="mailto:Belokur@rector.msu.ru">Belokur@rector.msu.ru</a>
Belov Dmitri	Steklov Math. Inst.	
Belov Vladimir	MSIEM, Moscow	<a href="mailto:belov@amat.msk.ru">belov@amat.msk.ru</a>
Bizzeti Andrea	Univ. of Florence & CERN	<a href="mailto:Andrea.Bizzeti@fi.infn.it">Andrea.Bizzeti@fi.infn.it</a>
Bleimaier John	Princeton	<a href="mailto:BLEIMAIER@aol.com">BLEIMAIER@aol.com</a>
Bogolubsky Igor	JINR	<a href="mailto:bogolubs@cv.jinr.ru">bogolubs@cv.jinr.ru</a>
Borisov Anatoly	MSU	<a href="mailto:Borisov@ave.phys.msu.su">Borisov@ave.phys.msu.su</a>
Burdyuzha Vladimir	Astro-Space Centre	<a href="mailto:burdyuzh@ASC.rssi.ru">burdyuzh@ASC.rssi.ru</a>
Cherdnikov Igor	JINR	<a href="mailto:igor@thsun1.jinr.ru">igor@thsun1.jinr.ru</a>
Chichikina Margarita	MSU	
Cirilli Manuela	INFN-Pisa & CERN	<a href="mailto:Manuela.Cirilli@cern.ch">Manuela.Cirilli@cern.ch</a>
Colas Paul	Sacley & CERN	<a href="mailto:Paul.Colas@cea.fr">Paul.Colas@cea.fr</a>
Diambrini-Palazzi Giordano	Univ. of Rome	<a href="mailto:Diambrini@Roma1.infn.it">Diambrini@Roma1.infn.it</a>
Dobrovolskaya Anna	France	
Dokuchaev Vladislav	INR	<a href="mailto:Dokuchaev@inr.npd.ac.ru">Dokuchaev@inr.npd.ac.ru</a>
Domogatskiy Grigory	INR	<a href="mailto:Domogats@pcbai10.inr.ruhep.ru">Domogats@pcbai10.inr.ruhep.ru</a>
Dremin Igor	FIAN	<a href="mailto:dremin@lpi.ru">dremin@lpi.ru</a>
Dumin Yurii	IZMIRAN	<a href="mailto:dumin@cityline.ru">dumin@cityline.ru</a>
Dvornikov Maxim	MSU	<a href="mailto:maxim_dvornikov@aport.ru">maxim_dvornikov@aport.ru</a>
Egorov Andrey	ICAS, Moscow	<a href="mailto:Ane@srdlan.npi.msu.su">Ane@srdlan.npi.msu.su</a>
Evseevichev Nikolay	Russian Physical Society	
Fayolle David	LPC Clermont II & CERN	<a href="mailto:david.fayolle@cern.ch">david.fayolle@cern.ch</a>
Fedorov S.	ITEP	<a href="mailto:fedorov@heron.itep.ru">fedorov@heron.itep.ru</a>
Fedotovich G.	NPI, Novosibirsk	<a href="mailto:G.V.Fedotovich@inp.nsk.su">G.V.Fedotovich@inp.nsk.su</a>
Fil'chenkov Mikhail	Peoples' Friendship University of Russia	<a href="mailto:Fil@crosna.net">Fil@crosna.net</a>
Fukuda Yoshiyuki	Univ. of Tokyo	<a href="mailto:fukuda@icrr.u-tokyo.ac.jp">fukuda@icrr.u-tokyo.ac.jp</a>
Gavrin Vladimir	INR	<a href="mailto:gavrin@dionis.iasnet.ru">gavrin@dionis.iasnet.ru</a>
Gay Igor	MSU	
Grats Yuri	MSU	<a href="mailto:grats@string.phys.msu.su">grats@string.phys.msu.su</a>
Grigoriev Alexander	MSU	
Heusch Clemens	SLAC	<a href="mailto:heusch@slac.stanford.edu">heusch@slac.stanford.edu</a>
Illarionov Alexei	JINR	
Ishhanov Boris	NPI-MSU	

Kaganovich Alexander	Ben Gurion Univ.	<a href="mailto:alexk@bgumail.bgu.ac.il"><u>alexk@bgumail.bgu.ac.il</u></a>
Kaganovich Faina	Ben Gurion Univ.	
Kaidalov Alexey	ITEP	<a href="mailto:kaidalov@vitep5.itep.ru"><u>kaidalov@vitep5.itep.ru</u></a>
Kapitza Serguey	Russian Academy of Sciences (Moscow)	<a href="mailto:Sergey@kapitza.ras.ru"><u>Sergey@kapitza.ras.ru</u></a>
Kravtsova Galina	MSU	
Kashkarov Pavel	MSU	
Katanaev Michael	Steklov Math. Inst.	<a href="mailto:Katanaev@mi.ras.ru"><u>Katanaev@mi.ras.ru</u></a>
Kerimov Burkhan	MSU	
Kiselev Valeri	IHEP	<a href="mailto:kiselev@th1.ihep.su"><u>kiselev@th1.ihep.su</u></a>
Koltsov A.	FIAN	<a href="mailto:pavl@pluton.lpi.troitsk.ru"><u>pavl@pluton.lpi.troitsk.ru</u></a>
Konjushko	MSU	
Kopeliovich Vladimir	INR, Moscow	<a href="mailto:kopelio@al20.inr.troitsk.ru"><u>kopelio@al20.inr.troitsk.ru</u></a>
Kopylov Sergey	STE "Brainstorm"	
Korotkikh Vladimir	INP MSU	<a href="mailto:ylk@lav01.sinp.msu.ru"><u>ylk@lav01.sinp.msu.ru</u></a>
Kravtsov A.	FIAN	<a href="mailto:pavl@pluton.lpi.troitsk.ru"><u>pavl@pluton.lpi.troitsk.ru</u></a>
Leins Axel	Univ. of Munich & CERN	<a href="mailto:Axel.Leins@cern.ch"><u>Axel.Leins@cern.ch</u></a>
Likhoded Anatoly	IHEP	
Lobanov Andrey	MSU	
Lobashov Vladimir	INR	<a href="mailto:Lobashev@al20.inr.troitsk.ru"><u>Lobashev@al20.inr.troitsk.ru</u></a>
Loznikov Vladimir	Space Research Inst.	<a href="mailto:vlozniko@cgrsmx.iki.rssi.ru"><u>vlozniko@cgrsmx.iki.rssi.ru</u></a>
Lukash Vladimir	Astro-Space Centre & Lebedev Phys. Inst.	<a href="mailto:Vladimir@lukash.asc.rssi.ru"><u>Vladimir@lukash.asc.rssi.ru</u></a>
Lvov A.	FIAN	
Martemianov Maxim	ITEP & LNF-INFN	<a href="mailto:Maxim.Martemianov@lnf.infn.it"><u>Maxim.Martemianov@lnf.infn.it</u></a>
Maksimov Vladimir	MSIEM, Moscow	<a href="mailto:Pm@miem.edu.ru"><u>Pm@miem.edu.ru</u></a>
Matveev Victor	INR	<a href="mailto:matveev@ms2.inr.ac.ru"><u>matveev@ms2.inr.ac.ru</u></a>
Mayburov Sergey	FIAN	<a href="mailto:Mayburov@sci.lebedev.ru"><u>Mayburov@sci.lebedev.ru</u></a>
Mazzucato Federica	Geneva Univ. & CERN	<a href="mailto:Federica.Mazzucato@cern.ch"><u>Federica.Mazzucato@cern.ch</u></a>
Mikhailin Vitaly	MSU	
Mikheev Stanislav	INR	<a href="mailto:Mikheyev@pcbai10.inr.ruhep.ru"><u>Mikheyev@pcbai10.inr.ruhep.ru</u></a>
Milstein Alexander	INP, Novosibirsk	<a href="mailto:A.I.Milstein@inp.nsk.su"><u>A.I.Milstein@inp.nsk.su</u></a>
Narodetskii Ilya	ITEP	<a href="mailto:naro@heron.itep.ru"><u>naro@heron.itep.ru</u></a>
Nedossekin Alexandre	INFN-LNF	<a href="mailto nedosekin@lnf.infn.it"><u>nedosekin@lnf.infn.it</u></a>
Nefediev Alexey	IST, Lisbon & ITEP	<a href="mailto:Nefediev@gtac2.ist.utl.pt"><u>Nefediev@gtac2.ist.utl.pt</u></a>
Nesterenko Alexander	MSU	<a href="mailto:Nesterav@thsun1.jinr.ru"><u>Nesterav@thsun1.jinr.ru</u></a>
Nikiforova Nataliya	MSU	<a href="mailto:inter@phys.msu.su"><u>inter@phys.msu.su</u></a>
Nikishov Anatoly	Lebedev Phys. Inst.	<a href="mailto:Nikishov@lpi.ru"><u>Nikishov@lpi.ru</u></a>
Nikitin N.	MSU	
Nowosad Noemi	Univ. Of San Paulo	
Nowosad Pedro	Univ. Of San Paulo	<a href="mailto:Nowoped@usp.br"><u>Nowoped@usp.br</u></a>
Osipenko Mikhail	MSU-INFN	<a href="mailto:Osipenko@ge.infn.it"><u>Osipenko@ge.infn.it</u></a>
Pakhomova O.	IHEP	
Pavlyuchenko Larisa	FIAN	<a href="mailto:pavl@pluton.lpi.troitsk.ru"><u>pavl@pluton.lpi.troitsk.ru</u></a>
Pechekhonov Dmitri	JINR	<a href="mailto:Peshehon@sunse.jinr.ru"><u>Peshehon@sunse.jinr.ru</u></a>
Piotti Enrico	CERN	
Pivovarov Alexei	INR	<a href="mailto:Aapiv@ms2.inr.ac.ru"><u>Aapiv@ms2.inr.ac.ru</u></a>
Popov V.	ITEP	

Popov Yurii	MSU	Popov@srdlan.npi.msu.su
Proskurin Denis	JINR	Proskurin@thsun1.jinr.ru
Pukhaeva Nelli	CERN/JINR/UIA	N.Pukhaeva@cern.ch
Rashba Timur	IZMIRAN	Rashba@izmiran.rssi.ru
Repin S.	ITEP	Repin@mx.iki.rssi.ru
Rizatdinova F.	MSU	
Rossikhin A.	MSU	
Rodionov Vasily	MSU	
Royzen Ilya	FIAN	Royzen@lpi.ru
Safronov Alexander A.	INP MSU	
Safronov Arkady M.	INP MSU	Safron@srđ.sinp.msu.ru
Saleev V.	IHEP	
Samsonov B.	Univ. of Tomsk	<u>Pecher@ido.tsu.ru</u>
Sarycheva Ludmila	MSU	<u>Lis@lav01.sinp.msu.ru</u>
Safin Mikhail	MSU	Safin@veb.ru
Selleri Franco	Univ. of Bari	<u>Selleri@ba.infn.it</u>
Semikoz Victor	IZMIRAN	<u>Semikoz@orc.ru</u>
Seth Kamal	Nothwestern Univ.	Seth@bach.phys.nwu.edu
Shabalin Evgeny	ITEP	Shabalin@vxitep.itep.ru
Shatsky Alexander	MSU	Bruk@lpi.ru
Shirkov Dmitry	JINR	Shirkovd@thsun1.jinr.ru
Sidorov Alexander	BLTR & JINR	<u>Sidorov@thsun1.jinr.ru</u>
Simonov Yury	ITEP	<u>Simonov@heron.itep.ru</u>
Sissakian Alexey	JINR, Dubna	<u>sisakian@jinr.ru</u>
Skorohvatov Mikhail	Kurchatov Inst.	Skoro@polyn.kiae.su
Slavnov Andrey	MSU& Steklov Math. Inst.	Slavnov@mi.ras.ru
Shlyk Ivan	MSU	
Smirnova Lidia	MSU	Lsmirnov@mail.cern.ch
Sokol G.	FIAN	pavl@pluton.lpi.troitsk.ru
Soloviev Anton	MSU	Anton@spin.phys.msu.su
Spillantini Piero	INFN-Florence	<u>Piero.Spillantini@fi.infn.it</u>
Studenikin Alexander	MSU	<u>Studenik@srđ.sinp.msu.ru</u>
Terfous Myriam	France	
Tioukov Valeri	INFN-Naples	Valeri.Tioukov@na.infn.it
Trukhin Vladimir	MSU	
Trusov Michael	ITEP	trusov@heron.itep.ru
Tsarev Vladimir	Lebedev Phys. Inst.	<u>Tsarev@x4u.lpi.ruhep.ru</u>
Tsipenyuk Dmitry	General Physics Inst.	tsip@kapella.gpi.ru
Volkov Serguey	MSU	
Vydrov Vladimir	Kurchatov Inst.	<u>vyrodov@dnuc.polyn.kiae.su</u>
Watkins Peter	Univ. of Birmingham &	<u>pmw@hep.ph.bham.ac.uk</u>
Zakharov Alexander	CERN	
Zamiralov Valery	ITEP	<u>Zakharov@vitep5.itep.ru</u>
Zamorin N.	INP MSU	<u>zamir@depni.npi.msu.su</u>
Zinoviev Alexander	MSU	

**World Scientific**  
[www.worldscientific.com](http://www.worldscientific.com)  
5234 hc

ISBN 981-238-319-0



9 789812 383198